

ABSTRACT

LUNIYA, SONALI R. Transient Electrothermal Modeling of Digital and Radio Frequency Circuits. (Under the direction of Professor Michael B. Steer).

Simulator technology for the high dynamic range, electrothermal modeling of electronic circuits is developed and applied to digital, radio frequency (RF) and microwave circuits. High-dynamic range is achieved using a combination of device models based on state-variables and utilizing automatic differentiation, precise error determination, and time step control. State-variables enable simpler and faster development of models less prone to implementation error. Automatic differentiation yields error free evaluation of the derivatives of circuit quantities with respect to each other and so removes any uncertainty in establishing the precise circuit condition. In transient analysis precise error determination and time step control is achieved by comparing two nonlinear solutions at each time point. A two-tone test of an X-band GaAs MESFET MMIC (Gallium Arsenide, Metal Semiconductor Field Effect Transistor Monolithic Microwave Integrated Circuit) was used to investigate and validate dynamic range. In the determination of the third-order intermodulation product in a two tone test a dynamic range of 165 dB was demonstrated. This high dynamic range was achieved through precise evaluation of the derivatives, accurate time step control and the circuit state, which is important in long electrothermal transient simulations. This minimization of accumulated numerical error is especially important in long electrothermal transient simulations. The 3D compact thermal models of the X-band MMIC LNA developed were verified with thermal images of the MMIC LNA taken with an infra red camera. The thermal models predict the temperature rise on various spots of the MMIC with less than 5% error. To perform an coupled electrothermal simulation at RF frequencies, a linear RC network based thermal macromodel of the MMIC was developed. The high dynamic range capability helped detect the small changes in the output voltage of the MMIC, at elevated temperatures. This thermal macromodel was applied to electrothermal simulations of an 3D thermal test chip designed with a 0.18 μm Fully Depleted Silicon on Insulator (FDSOI) MOSFET (Metal Oxide Semiconductor Field Effect Transistor) technology. An experimentally validated state-variable based electrothermal model of a 0.18 μm FDSOI MOSFET is implemented.

**Transient Electrothermal Modeling of Digital and
Radio Frequency Circuits**

by

Sonali R. Luniya

A dissertation submitted to the Graduate Faculty of
North Carolina State University
in partial fulfillment of the
requirements for the Degree of
Doctor of Philosophy

Electrical and Computer Engineering

Raleigh

2006

Approved By:

Dr. Rhett Davis

Dr. Kevin G. Gard

Dr. Michael B. Steer
Chair of Advisory Committee

Dr. Paul D. Franzon

Dedicated to my husband, Abhi, my child to be and my family . . .

Biography

Sonali R. Luniya received a degree in Computer Engineering in 2000 from the Pune Institute of Computer Technology in Pune, India. From June 1999 to May 2000 she worked as an intern with Parametric Technologies, Pune, India. She was admitted to North Carolina State University in Spring 2001 in the Master of Computer Engineering program. She received a Master degree in Computer engineering in 2002 North Carolina State University. Her interests are in the fields of analog circuit design and computer-aided analysis of circuits.

Acknowledgements

I would like to express my sincere gratitude to my advisor, Dr. Michael Steer, for giving me an opportunity to work in his research group. It was a great privilege to be a part of his NeoCAD and 3DIC research programs. I would also like to thank Dr. Paul Franzon, Dr. Rhett Davis and Dr. Kevin Gard for serving on my P.h.D. committee.

My special thanks to Dr. Carlos Christofferson for helped me understand *fREEDA*[™]. His knowledge of *fREEDA*[™] provided me lots of tips along the way. Special thanks to Dr. William Batty to help me understand the thermal model. I would also like to thank the mixed-signal design team at the Air Force Research Lab, Wright Patterson Air Force Base, Ohio, who helped me develop the FDSOI electrothermal model and the X-band LNA. A very big thanks to all my graduate colleagues and friends and to everyone else in MRC 410 and MRC 438.

I would also like to thank, Mikael Garcia and Vincent Caccamesi, at Raytheon, for capturing the infra-red thermal images of the X-band MMIC LNA. Also, I would like to thank, Alan Victor and his colleagues at Harris Corporation, for assembling the X-band GaAs MMIC LNA dice onto carriers, which greatly facilitated laboratory measurements.

My special thanks to my parents whose foresight and sacrifice have put me in a position to succeed. Last but not the least, I would like to thank my loving husband, Abhi, for all his support, encouragement and care.

Contents

List of Tables	viii
List of Figures	x
1 Introduction	1
1.1 Original Contribution	3
1.2 Organization	5
1.3 Publications	5
1.3.1 Journals	6
1.3.2 Conferences	6
1.3.3 Book Chapter	7
2 Literature Review	8
2.1 Introduction	8
2.2 Sources of Error in Transient Circuit Analysis Techniques	9
2.2.1 SPICE Transient Analysis	10
2.2.2 Numerical Integration Techniques	11
2.2.3 Predictors	18
2.2.4 Fourier Transformation Techniques	20
2.3 Sources of Error in Steady-State Transient Analysis	22
2.4 Thermal Modeling	23
2.4.1 Thermal Impedance Matrix	25
2.4.2 Transformations to Linearize the Heat Diffusion Equation	28
2.4.3 Analytical Solutions	29
2.4.4 Heat Sink Mounted Thermal Subvolume	33
2.4.5 Vertically Matched Thermal Subvolume	34
2.4.6 Embedded Subvolumes	34
2.5 Compact Electrothermal Modeling	36
2.5.1 The Chain Rule in Derivative Evaluation	37
2.5.2 Simplified Device Model Development Approach	37
2.6 Summary	40

3	High Dynamic Range Transient Circuit Simulation	42
3.1	Introduction	42
3.2	Time Step Control	43
3.2.1	Conventional Time Step Control in SPICE	43
3.2.2	New Time Step Control Technique	44
3.3	Implementation of the New Time Step Control Technique in <i>fREEDA</i> TM	45
3.3.1	Nonlinear Equation Formulation in <i>fREEDA</i> TM	45
3.4	Algorithm of the New Time Step Control Technique	50
3.5	Accuracy Test With A Simple RC Network	53
3.6	Dynamic Range Test On An X-band MMIC LNA	56
3.6.1	Comparison With Harmonic Balance	78
3.6.2	Classic Two Tone Test	81
3.7	Summary	83
4	X-band MMIC Electrothermal model	85
4.1	Introduction	85
4.2	Thermal Impedance Model	86
4.3	Electrothermal Model Of The Mounted and Metallized MMIC	88
4.3.1	GaAs Die	88
4.3.2	DIE-MAT Epoxy Layer	90
4.3.3	Kovar Substrate Layer	90
4.3.4	Vias	91
4.3.5	Via Capacitors	91
4.4	Electrothermal MESFET Model	92
4.5	Thermal Nonlinearity	94
4.6	Thermal Camera Calibration	98
4.7	Electrothermal Simulations of the X-band MMIC Structure	102
4.8	Surface Discretization	104
4.9	Surface Metallization	107
4.9.1	Thermal Model Verification	108
4.10	Summary	114
5	Thermal Macromodel	116
5.1	Introduction	116
5.2	Thermal Macromodel	118
5.3	Thermal Macromodel of the X-band MMIC LNA	121
5.3.1	Temperature Rise at Steady-State	121
5.3.2	Coupled Electrothermal Simulations at RF Frequencies	126
5.4	Why 3DIC?	130
5.5	Simulations of the 3DIC Thermal Macromodel	133
5.6	Summary	145

6	BSIMSOI Electrothermal model	147
6.1	SOI Model Formulation	148
6.2	Implementation Of The BSIMSOI Model In <i>fREEDA</i> TM	150
6.2.1	BSIMSOI Model Code In <i>fREEDA</i> TM	154
6.3	BSIMSOI Model Validation	159
6.4	Electrothermal BSIMSOI Model	163
6.5	Electrothermal BSIMSOI Model Validation	166
6.6	Summary	168
7	Conclusions and Future Work	175
7.1	Conclusions	175
7.2	Future Work	177
	Bibliography	180
A		192
B		195
B.1	Simple RC Network Netlist	195
B.2	Netlist for the LP6836 pHEMT	195
B.3	Curtice Cubic Model Parameters for X-band GaAs MMIC LNA pHEMTs	196
B.4	Dynamic Range Test Netlist of the X-band GaAs MMIC LNA	196
B.5	Test Netlist for X-band GaAs MMIC LNA with Harmonic Balance Analysis.	200
B.6	Dynamic Range Test Measurements of the MMIC LNA	202
B.7	Netlist To Test The Thermal Nonlinearity In The Thermal Compact Model	207
B.8	Netlist Of The X-band GaAs MMIC LNA Thermal Model	207
B.9	Netlist For The Thermal Macromodel of the X-band GaAs MMIC LNA	214
B.10	Netlist For The Thermal Macromodel of the 3DIC	253
B.11	BSIMSOI Extracted Model Parameters	302
B.12	Netlist To Verify The BSIMSOI Model	302
B.13	Measured BSIMSOI I/V Curves	305
B.14	BSIMSOI Model Parameters	307
B.15	BSIMSOI Model Equations	323
B.16	BSIMSOI <i>fREEDA</i> TM Model Code	353

List of Tables

2.1	MOSFET model implementation in University of California, Berkeley, UCB SPICE3f5 [69].	36
3.1	Comparison of the number of time points in a transient simulation for a specified relative tolerance (<i>RELTOL</i>)	53
4.1	Thermal constant (<i>b</i>) and Thermal Conductivity of Si, GaAs, SiO ₂ at room temperature.	94
4.2	Description of various spots in the thermal image of the MMIC structure.	101
4.3	Camera error at various spots on the MMIC at 35°C. See Table 4.2 for description of the various spots on the MMIC structure.	102
4.4	Time required to simulate the MMIC structure at various surface discretization levels.	107
4.5	Number of nodes in the MMIC structure at various surface discretization levels.	107
4.6	Simulated temperature (°C) at various spots on the MMIC with different layers of surface metallization. See Table 4.2 for description of the various spots on the MMIC structure. Spot 1 - DC PAD, Spot 2 - Transistor 2, Spot 3 - Transistor 1.	108
4.7	Measured and corrected temperatures at various spots on the MMIC at various base temperatures with DC power applied. See Table 4.2 for description of the various spots on the MMIC structure.	109
4.8	Simulated and measured temperatures at various spots on the MMIC at 35°C. See Table 4.2 for description of the various spots on the MMIC structure. Spot 1 - DC PAD, Spot 2 - Transistor 2, Spot 3 - Transistor 1.	111
4.9	Simulated temperature with Kirchhoff's transformation applied and without Kirchhoff's transformation applied, at various spots on the MMIC structure at 35°C. See Table 4.2 for description of the various spots on the MMIC structure. Spot 1 - DC PAD, Spot 2 - Transistor 2, Spot 3 - Transistor 1.	111
5.1	Measured and simulated temperatures with the compact thermal model and the thermal macromodel at various spots on the MMIC structure at a base temperature of 35°C.	125

5.2	Values of thermal resistances in the RC network of the macromodel.	138
6.1	MOSFET model implementation in University of California, Berkeley, SPICE3f5 and <i>f</i> REEDA™.	159
A.1	Thermal macromodel Input Parameters.	192
B.1	TYPICAL CURTICE MODELS FOR 0.25 μm DHPHEMT WITH 1000Å NITRIDE (MD1A).	197
B.2	Measurements used in dynamic range test of the new time step control technique. Input power (Pin) at 11 GHz is varied from -10 dBm to -80 dBm. Input power (Pin) at 10 GHz is kept constant at -10 dBm.	203
B.3	Model parameters of the FDSOI MOSFET from MIT Lincoln Labs.	303
B.4	Measured drain current (A) of the FDSOI MOSFET.	306
B.5	BSIMSOI Built-In Potential Lowering (ΔV_{bi}) Model Parameters	308
B.6	BSIMSOI BSIMPD Model Control Parameters	309
B.7	Process Parameters	310
B.8	DC Parameters	311
B.9	Gate-to-body Tunneling Parameters	317
B.10	AC and Capacitance Parameters	318
B.11	Temperature Parameters	321
B.12	RF Parameters	322

List of Figures

2.1	A sine wave integrated using Forward Euler Formula, Backward Euler Formula and Trapezoidal Rule with a time step of 1.	16
2.2	A sine wave integrated using Forward Euler Formula, Backward Euler Formula and Trapezoidal Rule with a time step of 0.25.	17
2.3	Layout of LMA411 X-band GaAs MMIC LNA.	24
2.4	Generic thermal subvolume for analytical construction of the thermal impedance matrix. This is the structure of the compact thermal model with a 6×6 surface discretization. Each of the blocks has a thermal terminal and the heat flow at each of these terminals is treated as being uniformly applied across the area of each surface discretization.	31
2.5	Automatic Differentiation in <i>fREEDA</i> TM . After [52].	39
3.1	Network with nonlinear elements. After [15]. (Copyright IEEE 2006)	45
3.2	General flow diagram of the new time step control technique.	51
3.3	Simple RC circuit with a sinusoidal signal source.	53
3.4	Comparison of voltage across the capacitor for the conventional and new time step control technique and the expected result derived from analytical calculations.	54
3.5	Comparison of absolute error in the voltage across the capacitor as a function of relative tolerance.	55
3.6	Layout of the X-band MMIC LNA.	58
3.7	CUT 1. This image shows the 2 corner gate fingers of pHEMT2, the drain metal coming in from the top and the source metal coming in from the right hand side. This cut can be used to extract the gate-gate width, drain and source metal thickness.	59
3.8	CUT 1. A zoomed image of the mushroom gate metal (light gray area). Ohmic metal contacts of the drain and source (light gray area). Thickness of the ohmic contacts can be extracted.	60
3.9	CUT 1. A zoomed image of the drain metal. Thickness of the drain metal layer can be extracted.	61
3.10	CUT 1. A zoomed image of the ohmic metal contact.	62
3.11	CUT 1. A zoomed image of the mushroom gate metal (light gray area). . .	63

3.12	CUT 1. A zoomed image of the mushroom gate metal.	64
3.13	CUT 2. Image of two adjacent microstrip lines.	65
3.14	CUT 2. Zoomed image of the ohmic contacts.	66
3.15	CUT 2. Zoomed image of the ohmic contacts. Thickness of the Silicon Nitride (dark black layer) can be extracted.	67
3.16	CUT 2. Zoomed image of the ohmic contacts to see processing effects.	68
3.17	CUT 3. Image of the air bridge over the spiral inductor. Image shows the underpass metal layer and the overpass metal layer of the air bridge.	69
3.18	CUT 3. Zoomed image of the air bridge, showing the overpass metal layer. Thickness of the overpass metal layer (light gray layer) can be extracted.	70
3.19	CUT 3. Zoomed image of the left hand side footing of the air bridge.	71
3.20	CUT 3. Zoomed image of the right hand side footing of the air bridge.	72
3.21	Measured and simulated I/V curves of the Filtronic Solid State pHEMT – LP6836.	73
3.22	Simulated I/V curves of pHEMT1 of the LMA411 MMIC.	74
3.23	Simulated I/V curves of pHEMT2 of the LMA411 MMIC.	75
3.24	Comparison of the measured IM3 output power levels for the LMA411 MMIC and simulated levels using the new time step control technique and a commercial harmonic balance simulator.	79
3.25	Comparison of the calculated linear IM3 output power levels at 12 GHz for the LMA411 MMIC with the simulated power level using the new time step control technique.	80
3.26	Comparison between the simulated output voltage of the LMA411 MMIC obtained using harmonic balance and the new time step control technique.	81
3.27	Simulated output power levels of the fundamental and IM3 products of a classic two tone test of the LMA411 MMIC.	82
4.1	Thermal N-port generated directly from analytical solution of the heat diffusion equation, and represented by thermal impedance matrix, $R_{TH_{ij}}(s)$. After [61]. (Copyright IEEE 2006)	91
4.2	An electrothermal element connected to linear and thermal networks.	93
4.3	Temperature rise of a GaAs die with and without thermal nonlinearity. Thermal nonlinearity is considered when the Kirchhoff's transformation is applied (dashed line). Temperature plotted is T. Thermal nonlinearity is ignored when the Kirchhoff's transformation is applied but its inverse is not applied (solid line). Temperature plotted is θ	95
4.4	Temperature rise of a Si die with and without thermal nonlinearity. Thermal nonlinearity is considered when the Kirchhoff's transformation is applied (dashed line). Temperature plotted is T. Thermal nonlinearity is ignored when the Kirchhoff's transformation is applied but its inverse is not applied (solid line). Temperature plotted is θ	96

4.5	Temperature rise of a SiO ₂ die with and without thermal nonlinearity. Thermal nonlinearity is considered when the Kirchhoff's transformation is applied (dashed line). Temperature plotted is T. Thermal nonlinearity is ignored when the Kirchhoff's transformation is applied but its inverse is not applied (solid line). Temperature plotted is θ	97
4.6	MMIC die (A) Mounted die before inking. (B) Mounted die after inking. (C) Zoomed in image of the mounted die before inking. (D) Zoomed in image of the mounted die after inking.	99
4.7	Calibration image at 35°C with no DC and no RF power. See Table 4.2 for description of the various spots on the MMIC structure.	100
4.8	Calibration image at 45°C with no DC and no RF power. See Table 4.2 for description of the various spots on the MMIC structure.	101
4.9	<i>f</i> REEDA™ electrothermal model of the MMIC structure.	103
4.10	Temperatures simulated in <i>f</i> REEDA™ at different surface discretization levels.	105
4.11	Percentage error in the simulated temperatures in <i>f</i> REEDA™ at different surface discretization levels.	106
4.12	Thermal image of the X-band MMIC with DC power applied at 35°C. See Table 4.2 for description of the various spots on the MMIC structure.	109
4.13	Temperatures of the transistor fingers simulated in <i>f</i> REEDA™ at 35°C.	110
4.14	Simulated output voltage at elevated temperatures.	113
5.1	Schematic of the thermal macromodel of each grid block.	117
5.2	Schematic of 4 horizontally adjacent grid blocks in the X-Y direction of a layer.	120
5.3	Three-dimensional view of the MMIC structure.	122
5.4	Transient temperature of the grid blocks of the MMIC thermal macromodel with the 4 heat generating sources: Resistor 1, Resistor 2, Transistor 1 and Transistor 2.	124
5.5	Simulated output voltage of the MMIC at $t_{base} = 35^{\circ}\text{C}$ in an electrical and a coupled electrothermal simulation.	127
5.6	Simulated output voltage of the MMIC in a coupled electrothermal simulation at $t_{base} = 35^{\circ}\text{C}$, $t_{base} = 45^{\circ}\text{C}$ and $t_{base} = 60^{\circ}\text{C}$	128
5.7	Simulated dissipated power by the stage 2 transistor of the MMIC in a coupled electrothermal simulation at $t_{base} = 35^{\circ}\text{C}$, $t_{base} = 45^{\circ}\text{C}$ and $t_{base} = 60^{\circ}\text{C}$	129
5.8	Schematic representation of 3-D integration with multilevel wiring network and VILICs. T1: first active layer device, T2: second active layer device, Optical I/O device: third active layer I/O device. M1 and M2 are for T1, M1 and M2 are for T2. M3 and M4 are shared by T1, T2, and the I/O device. After [77]. (Copyright IEEE 2006)	131
5.9	Schematic of a 3-D chip showing integrated heterogeneous technologies. After [77]. (Copyright IEEE 2006)	132
5.10	Three-dimensional view of the 3DIC thermal chip. The thick boundary is the topmost layer. Each tier is discretized into a 10×10 grid.	134
5.11	Two-dimensional vertical cross section of the 3DIC thermal chip (Not to scale).	135

5.12 (A) Vertical cross section of the 3DIC thermal chip with 3D vias and metal layers. (B) A 3D representation of the 3D vias, metal layers and active islands in the tiers.	136
5.13 Temperature Map of Tier A.	138
5.14 Temperature Map of Tier B.	139
5.15 Temperature Map of Tier C.	140
5.16 Maximum temperature on Tier A with vertical metal density of all grid blocks on Tier A varied. A factor of 1 on the x-axis corresponds to the vertical metal density extracted by the thermal extractor. The extracted metal density of all the blocks on this tier is less than 0.2	141
5.17 Vertical thermal conductivity of the hottest block on Tier A with vertical metal density of all grid blocks varied. A factor of 1 on the x-axis corresponds to the vertical metal density extracted by the thermal extractor. The extracted metal density of all the blocks on this tier is less than 0.2	142
5.18 Maximum temperature on Tier A with power dissipation of all the grid blocks varied. A factor of 1 on the x-axis corresponds to the power dissipation extracted by the thermal extractor.	143
5.19 Maximum temperature on Tier A with the thermal conductivity of the epoxy varied.	144
6.1 Circuit representation of the floating body in BSIMPD.	149
6.2 Comparison between simulated and measured IV curves of a FDSOI MOSFET at gate bias levels (V_{gs}) of 0.0 V to 0.6 V at 0.2 V intervals. The simulated curves were simulated with the <i>f</i> REEDA™ model and the SPICE model.	161
6.3 Comparison between simulated and measured IV curves of a FDSOI MOSFET at gate bias levels (V_{gs}) of 0.8 V to 2.0 V at 0.2 V intervals. The simulated curves were simulated with the <i>f</i> REEDA™ model and the SPICE model.	162
6.4 Circuit representation of the electrothermal BSIMSOI model.	163
6.5 Comparison of measured and simulated with no self heating IV curves of a FDSOI MOSFET with self heating turned on at $V_{gs} = 1.0$ V. The curves between the $T = 300^\circ\text{K}$ (second curve from the top) and $T = 400^\circ\text{K}$ (bottom curve) were done at 10°K ambient temperature intervals.	169
6.6 Device temperature with self heating turned on, $V_{ds} = 2.0$ V, $V_{gs} = 1.0$ V, at $T = 300^\circ\text{K}$	170
6.7 Comparison of measured and simulated with no self heating IV curves of a FDSOI MOSFET with self heating turned on at $V_{gs} = 1.8$ V. The curves between the $T = 300^\circ\text{K}$ (second curve from the top) and $T = 400^\circ\text{K}$ (bottom curve) were done at 10°K ambient temperature intervals.	171
6.8 Comparison between IV curves of a FDSOI MOSFET with self heating turned on, $V_{gs} = 1.8$ V, $R_{th} = 350 \Omega$ and $R_{th} = 250 \Omega$, at $T = 300^\circ\text{K}$	172
6.9 Device temperature with self heating turned on, $V_{ds} = 2.0$ V, $V_{gs} = 1.8$ V, at $T = 300^\circ\text{K}$	173

Chapter 1

Introduction

Rapid design of complex communication hardware with new circuit integration techniques demand full chip modeling with incorporation of multiple physical effects. The work reported in this dissertation has the premise that transient analysis based on circuit simulation paradigms is required to achieve fully predictive modeling capabilities. In addition multiple physical effects like transient thermal effects during the initial turn-on transient are important in full modeling of an electronic circuit. This capability of capturing transient thermal effects can be added to a circuit simulator. This requires three capabilities to be developed. The small variations in the output signal due to the addition of thermal effects, should be detected during simulation. This requires a simulator with a high dynamic range and numerical robustness including very low accumulated numerical error. These small variations in the output signal levels can be detected correctly if the temperature rise in the electronic circuit is predicted accurately. The accurate prediction of the temperature rise requires a good thermal model. The temperature rise in an electronic circuit is dependent on the structural information of the electronic circuit. To simulate the variations in the output signal due to this temperature rise, the electronic devices in a circuit should incorporate temperature dependent functionalities. Hence an accurate electrothermal device model is necessary.

In this work the three aspects of the goal to perform long electrothermal transient simulations are addressed. Techniques to add these capabilities to a circuit simulator are discussed.

The high dynamic range of the simulator is defined here as the ability to detect a small signal such a sinusoidal wave in the presence of a large signal. For example this large signal could be an interfering signal at the input of the complex communication hardware with multiple functionalities. This interfering signal could cause in-band or out-of-band distortion. The receivers in a communication system are sometimes expected to detect signals as small as $1 \mu\text{V}$. In this work the reasons for limited dynamic range in existing time-domain analysis techniques are explored. The error estimation in numerical integration techniques used by existing time-domain analysis techniques limit the dynamic range of the simulator. A new time-domain analysis technique, which uses a predictor-corrector integration technique is developed and implemented. Key to the new transient analysis technique is a good estimation of error. The dynamic range of the new technique is verified with a two-tone test on an X-band Monolithic Microwave Integrated Circuit (MMIC) Low Noise Amplifier (LNA). The new technique achieved a dynamic range of 165 dB.

With this ability to detect small signals, the next aspect of the goal is addressed. In electrothermal simulations, the transient temperature rise in an electronic circuit has an impact on the circuit performance. Traditional numerical techniques solve the heat diffusion partial differential equation with spatial and time discretization. These techniques are compute intensive, since they require a surface or volume mesh with a large number of nodes. In this work, a compact thermal model is developed and implemented in a general purpose circuit simulator. In the compact thermal model, the partial differential heat diffusion equations of the complex thermal subsystem are represented by coupled algebraic equations, which can be easily implemented in a circuit simulator. The model is in effect an ‘interface element’ equivalent of a volumetric model. It discretises only interfaces between subvolumes and hence goes beyond the typical boundary-element formulation, which discretises whole surfaces. Transformations enable the nonlinear volume to be described by an analytical thermal impedance matrix model while still capturing full thermal transient behavior. Thermal nonlinearity of the material properties are also captured. Complex MMIC features such as surface metallization and via holes, and package and mounting configurations, such as epoxy or solder attach to lead-frame paddle or carrier are also considered. This model matches temperatures only at the surface interfaces. Since only the surface interfaces are discretized, the aspect ratio limitation suffered by numerical techniques is removed in this model. The temperature rise predicted by this thermal model is verified with thermal images of the X-band MMIC LNA taken with an infra red camera. As will be

seen the thermal model can predict temperature rise within 5% error. The electrothermal transient simulation of the compact thermal model is limited to a time step as small as 2 ns. For time steps smaller than 2 ns (as required in coupled electrothermal simulations at Radio Frequencies (RF)) a simple linear RC network based thermal macromodel was developed. This macromodel is based on the structural information and the metal density information of the thermal volume. Such a thermal macromodel of the X-band MMIC LNA is developed in this work. This model was used to perform coupled electrothermal simulations at RF frequencies.

Variations of the output voltages due to the addition of thermal effects depends on the temperature dependent effects in the semiconductor devices. The accuracy by which these effects can be captured depends on the accuracy of the temperature rise predicted by the thermal model used. As some parameters of the semiconductor device model have exponential dependencies on temperature. The utilized thermal model plays a significant role in the accuracy of the semiconductor device model predictions. It is also shown how dynamic temperature dependencies can be implemented in a semiconductor device model. In this work an electrothermal model of a Fully Depleted Silicon on Insulator (FDSOI) Metal Oxide Semiconductor Field Effect Transistor (MOSFET) is developed and verified. The use of state-variables and automatic differentiation enabled the temperature dependence to be incorporated in two days. The use of automatic differentiation eliminates the error-prone process of manually evaluating and coding derivatives. The automatic evaluation of derivatives from the model equations written in a standard format reduced the code size to one-tenth compared to the implementation of an electrical only model in Berkeley SPICE, the Simulation Program With Integrated Circuit Emphasis. This device model was verified with experimental data of a FDSOI MOSFET with self heating. The accuracy of the simulated device model with self heating effects was found to depend on the thermal model parameters extracted during measurements, making a good thermal model important.

1.1 Original Contribution

The motivation for this work was the development of a high dynamic range analysis technique so that transient thermal effects in an electronic circuit could be captured. The techniques and models developed in this work are implemented in the multi-domain multi-

physics circuit simulator *fREEDA*TM.

The underlying cause for the limited dynamic range in traditional simulators and other circuit analyses techniques is examined. This limited dynamic range problem is solved with the new time step control technique described in Chapter 3. This new time step control using state-variables and sparse matrices in the multi-physics multi-domain circuit simulator, *fREEDA*TM is an original contribution. The accuracy of this new technique was verified with the analytical solution of a simple RC circuit. The better initial guess prediction capability of the new technique helped achieve higher accuracy compared to the conventional time step control technique 29% fewer simulation time points. The dynamic range of the analysis was tested with a two tone test of a X-band GaAs MMIC LNA. A dynamic range of 165 dB was achieved indicating the ability to accurately calculate a small signal 165 dB below that of a large signal.

This high dynamic range analysis technique was applied to the study of electrothermal effects on the performance of an X-band GaAs MMIC LNA. Thermal effects are modeled based on a 3D quasi-analytical thermal model developed by Dr. William Batty of the University of Leeds. This analysis was encapsulated in thermal elements implemented in the *fREEDA*TM circuit simulator used to model various primitives of the MMIC an X-band GaAs MMIC LNA. The implementation of the 3D quasi-analytical model into *fREEDA*TM, described in Chapter 5, is an original contribution. This implementation enabled the thermal modeling of the different layers, i.e. the GaAs die, Epoxy layer and the Kovar substrate of the MMIC. Surface metallization features like vias, metal layers of via capacitors were also incorporated. The steady-state temperature rise at various spots on the MMIC, were verified with thermal images of the MMIC taken with an infra-red camera. The thermal models can predict the temperature rise with less than 5% error.

Another original contribution is the development of a 3D thermal macromodel in *fREEDA*TM. The macromodel is used to perform coupled electrothermal simulations of the MMIC at RF frequencies. This model is based on structural and metal density information of the MMIC. The steady-state temperature rise predicted by the thermal macromodel of the MMIC, agrees within 10% error of the measured temperatures.

The *fREEDA*TM development of the University of Berkeley's and implementation BSIMSOI model of a FDSOI (Fully Depleted Silicon on Insulator) MOSFET is an original contribution. A state-variable based model with thermal effects was developed and implemented in *fREEDA*TM. This model described in Chapter 6 was verified with measurements

of a 0.2 μm FDSOI MOSFET. This represents the first integrated electrothermal model of a FDSOI transistor.

The thermal macromodel was applied to study the thermal effects in the 3DIC, where the thermal problem is exacerbated due to stacking of chips. This model helped examine the various hot spots in a 3DIC. This study also showed that, in a 3DIC the epoxy used to glue the chips, acts as the bottleneck for heat removal and spreading. Using an epoxy with better thermal conductivity can help alleviate this problem. Another solution for heat removal is the addition of thermal 3D vias.

1.2 Organization

Chapter 2 is a review of the literature on transient analysis techniques and of analytical thermal models. Chapter 3 focuses on improving the dynamic range of a transient simulator. Validation is achieved through a comparison between simulated and measured dynamic range of an X-band MMIC. Chapter 4 elaborates the 3D analytical thermal solution implemented in *fREEDA*TM. A thermal network for the X-band MMIC is developed. The temperature on various spots of the X-band MMIC is verified with thermal images captured using a thermal infra-red camera. Chapter 5 introduces a 3D thermal macromodel for an electronic circuit. This macromodel was used to perform coupled electrothermal simulations at RF frequencies on the X-band MMIC LNA discussed in Chapter 3. This model was also applied to study the thermal problems in a 3DIC. The results in this chapter predict the thermal hot spots in a 3DIC. Chapter 6 illustrates a state-variable universal electrothermal modeling approach of a FDSOI MOSFET. The model is validated with experimental results of a 0.2 μm FDSOI MOSFET from MIT Lincoln Labs. Chapter 7 summarizes this work and provides an outline for future work in the area of electrothermal modeling for a electronic circuit.

1.3 Publications

The work described in this dissertation resulted in the following publications:

1.3.1 Journals

- Sonali Luniya, Kevin G. Gard, and Michael B. Steer, “Modeling Nonlinear Distortion of Ultra Wideband Signals at X-Band,” *IEEE Microwave and Wireless Components Letters*, 2006, In Press.
- F. Hart, S. Luniya, J. Nath, D. Ghosh, J.-P. Maria, “Discrete-time filter synthesis and implementation in a circuit simulator,” *International Journal of Microwave and Millimeter Wave Computer Aided Engineering*, 2006, In Press.

1.3.2 Conferences

- S. Luniya, M. B. Steer and C. Christoffersen, “High dynamic range transient simulation of microwave circuits,” *2004 IEEE Radio and Wireless Conference*, 19-22 Sept. 2004 pp. 487-490.
- F. Hart, N. Kriplani, S. Luniya, C. Christoffersen and M. B. Steer, “Streamlined Circuit Device Model Development with fREEDA and Adol-C,” *Fourth International Workshop on Automatic Differentiation - AD 2004*, July 2004.
- Sonali Luniya, William Batty, Vincent Caccamesi, Mikael Garcia, Carlos Christoffersen, Samson Melamed, W. Rhett Davis, and Michael Steer, “Compact Electrothermal Modeling of an X-band MMIC,” *2006 IEEE International Microwave Symposium*, June 11 2006.
- M. Steer, P. Franzon, A. Cangellaris, A. Verma, S. Luniya, N. Kriplani, G. Manetas, H. Li, C. Christoffersen, “Simulation and Modeling of Substrate Coupling – Workshop on Substrate Effects In Si Rfic Interconnect,” *2006 IEEE International Microwave Symposium*, June 11 2006 pp. WFG.D.1-WFG.D.27.
- M. B. Steer, N. Kriplani, S. Luniya, C. E. Christofferson, “Strategies for uncompromising accuracy in modeling mixed signal circuits,” *Proceedings of International Conference on Mixed Design of Integrated Circuit and Systems*, Gdynia, Poland, 2224 June 2006.
- M. B. Steer, N. M. Kriplani, S. Luniya, F. Hart, J. Lowry and C. E. Christoffersen, “fREEDA: an open source circuit simulator,” *Proceedings of International Workshop*

on Integrated Nonlinear Microwave and Millimeter-wave Circuits, Jan. 2006.

1.3.3 Book Chapter

F. P. Hart, N. Kriplani, S. R. Luniya, C. E. Christoffersen and M. B. Steer, “Streamlined Circuit and Device Model Development with fREEDA and ADOL-C,” in *Automatic Differentiation: Applications, Theory, and Implementations*, edited by H. M. Bücker, G. F. Corliss, P. Hovland, U. Naumann and B. Norris, Series: Lecture Notes in Computational Science and Engineering, Vol. 50, Springer, New York, NY, 2005.

Chapter 2

Literature Review

2.1 Introduction

In this chapter a concise literature review of the techniques that will be used to achieve our goal of performing long electrothermal transient simulations is presented. A review of the three aspects of the perceived goal mentioned in the previous chapter: high dynamic range, a good thermal model, and a good semiconductor electrothermal device model is presented.

Integration techniques play an important role in achieving high dynamic range in a circuit simulator. A predictor-corrector integration technique must be used to achieve high dynamic range. To estimate the dynamic range of the transient circuit simulator, the time-domain waveform obtained from the transient analysis must be viewed in the frequency domain. The time-domain data is Fourier transformed to frequency domain. The Fourier transform technique used also affects the dynamic range of the circuit simulator. The dynamic range of the transient analysis is defined as the ability to detect small sinusoidal signals in the presence of large sinusoidal signals. Sources of errors which limit the dynamic range of current transient analysis techniques are presented in Section 2.2. Various integration techniques and predictors are discussed in Section 2.2.2. The different techniques to perform the Fourier transform are discussed in Section 2.2.4. The new time step control technique for transient analysis developed in this work focuses on precisely

estimating the error introduced by the numerical integration technique. The new time step control technique uses the integration and prediction techniques discussed in these sections.

The next aspect of the goal, the choice a good thermal model, is discussed in Section 2.4. A thermal model that can be used in circuit simulators should be compact and easily implementable in a circuit simulator. A compact thermal model is a reduced-order model where a complex thermal dynamic system modelled by differential equations is reduced to a set of coupled first-order differential equations and a set of algebraic equations. The model reduction procedure is based on a rigorous mathematical background and reduces a high dimensional model of a dynamic system to a low dimensional model. This reduced-order low dimensional model being represented by algebraic equations can be implemented in a suitable simulator. A suitable reduced-order thermal model, developed and implemented as a compact model in the work presented in this dissertation is based on the thermal modeling work by Dr. William Batty of the University of Leeds. Section 2.4 is a review of the model theory relevant to the work presented here

A review of the last aspect of the goal, a good semiconductor electrothermal device model is presented in Section 2.5. A brief discussion of the cumbersome approach of model development and the errors associated with it, in conventional simulators is presented. In this work the approach used to develop a semiconductor and thermal device model is a simplified process by the use of state-variables and automatic differentiation. A review of the background of this approach is presented in Section 2.5.2.

2.2 Sources of Error in Transient Circuit Analysis Techniques

In this section the sources of error in the conventional transient circuit analysis technique used in SPICE-like simulators are described. Transient circuit analysis use numerical integration techniques to discretize a model in time. The nonlinear equations in a transient analysis are typically solved using the Newton Raphson technique. The local truncation error introduced by the numerical integration technique used is discussed. In addition errors are introduced by an incorrect estimate of error. It is essential that the estimation of error be correct so that iterations are not terminated prematurely and the time step used is not too short introducing numerical round off errors, nor too long introducing quantization errors. In communication systems many of the performance parameters are

specified in the frequency domain and to view the time-domain signal in the frequency domain the time-domain data must be Fourier transformed. The Fourier transforms require uniformly spaced time-domain data points. In variable time step transient analysis techniques, the time data points are interpolated to present uniformly spaced data points to the Fourier transforms. The effect of the error introduced into the data set by the interpolation on the Fourier transform is discussed. Different Fourier transform techniques used to reduce the effect of this error are also discussed.

2.2.1 SPICE Transient Analysis

SPICE, the Simulation Program With Integrated Circuit Emphasis, is a general purpose circuit simulator developed at the University of California, Berkeley in 1973. It is used for nonlinear dc, nonlinear transient, and linear ac analyses. Circuits may contain resistors, capacitors, inductors, mutual inductors, independent voltage and current sources, four types of dependent sources, lossless and lossy transmission lines (two separate implementations), switches, uniform distributed RC lines, and the many types of semiconductor devices such as: diodes, BJTs, JFETs, MESFETs, and MOSFETs.

SPICE is most commonly used to simulate circuits in the time-domain. In transient analysis it linearizes the nonlinear device equations at every time point and solves them using Newton Raphson iterative methods. It uses various time-domain integration techniques to evaluate time-domain derivatives. The choice of the time step is critical in the management of error. If the time step is too short numerical errors accumulate and the simulation takes too long. Longer time steps result in more efficient simulation but also approximate errors. The error at each time point is used in determining if the time step is appropriate. If the error estimate is larger than the specified tolerance the current solution is abandoned and the problem is solved again with a smaller time step. If the error estimation is less than a threshold, it is used in calculating the next time step. Using the maximum allowable time step reduces overall computation time. These non-uniformly time points, reduce the time required to complete the simulation. Various numerical integration techniques used in a transient analysis are discussed in the next section.

2.2.2 Numerical Integration Techniques

The general procedure for the transient analysis of a nonlinear circuit is to evaluate the state of the circuit at a given point in time and then to extrapolate ahead to a new time point. The computation time required for such an analysis program is directly proportional to the number of time increments or time steps required. The step of the time steps indirectly depends on the circuit activity. It dynamically changes according to the rate of transitions of the circuit voltages and currents. During low circuit activity or when a signal is changing slowly, the difference between the solutions at two consecutive equilibrium time points is small, allowing an increase in the time step. The error introduced due to the large time steps is very small since either the signal has not changed during the duration of the large time step or it has changed insignificantly. Whereas in a rapidly changing signal the time step should be small to capture the rapid changes. The small time steps captures sudden or large changes in the device model relations during the duration of the time step. This ensures accuracy and convergence for circuits with large and rapid voltage and current transitions. Also for an accurate numerical integration of the sudden or rapid changes in the signal the time step should be small. For low circuit activities, the time step can be large for numerical integration and reduce simulation time [5]. Numerical integration helps determine the circuit response at the next time step given the circuit's response at the previous time steps. They are used to discretize the relations in device models in time. The various integration techniques used in circuit simulators are explained in the book, *Simulation and Modeling for Analog, RF and Mixed Mode Design*, [10]. The development in this book is used here for error estimation. This development is repeated here for convenience.

In general any device model relation can be expressed in the form of a first-order differential equation [10],

$$\mathbf{x}' = \mathbf{f}(\mathbf{x}, t) \quad (2.1)$$

where \mathbf{x} is an unknown variable, t is time, $\mathbf{f}(\mathbf{x}, t)$ is a given function and \mathbf{x}' is the first derivative of \mathbf{x} with respect to time. If \mathbf{x}_0 is the state-variable at time t_0 , \mathbf{x}_1 is the state-variable at time $t_1 = t_0 + h$, where h is the time step. Numerical integration is used to predict the future value of a quantity from the current or previous value of the quantity. The equivalent integral function of Equation 2.1 is

$$\mathbf{x}(t_1) = \mathbf{x}(t_0) + \int_{t_0}^{t_1} \mathbf{f}(\mathbf{x}, t) dt \quad (2.2)$$

where t_0 and t_1 are two time points as defined above. Since the difference between the two time steps is very small, $\mathbf{f}(\mathbf{x}, t)$ is almost constant. Therefore the integral equation can be discretized as

$$\mathbf{x}_1 = \mathbf{x}(t_1) = \mathbf{x}(t_0) + \mathbf{x}' * (t_1 - t_0). \quad (2.3)$$

With $\mathbf{x}_0 = \mathbf{x}(t_0)$, the generic expression for the Equation 2.3 is

$$\mathbf{x}_n = \mathbf{x}_{n-1} + h * x', \quad (2.4)$$

where \mathbf{x}_n and \mathbf{x}_{n-1} are the values of the state-variable at time $t_n = t_{n-1} + h$ and at time t_{n-1} respectively, indicating that the future value can be computed based on the current value. The discretized integral equation of Equation 2.4 is the basic numerical integration step in time-domain analysis. The inherent assumption is that there is a straight line of slope \mathbf{x}' between the points (\mathbf{x}_0, t_0) and (\mathbf{x}_1, t_1) . The main issue of this section is discussing the calculation of \mathbf{x}' to minimize error and obtain a stable solution. Different integration methods differ in the method used to estimate \mathbf{x}' . Three major low order numerical integration formulas are commonly used: the Forward Euler formula, the Backward Euler formula, and the Trapezoidal Rule. The formulas differ by the method used to estimate \mathbf{x}' . The generalization to higher order is called the weighted integration formula from which a fourth method, the Gear Two method, is derived. These are discussed below.

FORWARD EULER FORMULA In the Forward Euler Formula we approximate \mathbf{x}' as \mathbf{x}'_0 . Now the basic numerical integration step, Equation 2.4, becomes

$$\mathbf{x}_1 = \mathbf{x}_0 + h\mathbf{x}'_0 \quad (2.5)$$

Numerical integration using the Forward Euler formula is called a predictor method as information about the behavior of the waveform at time t_0 , (\mathbf{x}'_0) is used to predict the waveform at t_1 .

BACKWARD EULER FORMULA Setting $\mathbf{x}' = \mathbf{x}'_1$ the discretized numerical integration equation becomes

$$\mathbf{x}_1 = \mathbf{x}_0 + h\mathbf{x}'_1. \quad (2.6)$$

The obvious problem here is how to determine \mathbf{x}'_1 when \mathbf{x}_1 is not known. The solution is to iterate as follows: 1) assume some initial value for \mathbf{x}_1 (e.g. using the Forward Euler formula); and 2) now iterate to satisfy the requirement $\mathbf{x}'_1 = \mathbf{f}(\mathbf{x}_1, t)$. Integration using the Backward Euler formula is therefore called a predictor-corrector method.

TRAPEZOIDAL RULE Setting $\mathbf{x}' = (\mathbf{x}'_0 + \mathbf{x}'_1)/2$ the discretized numerical integration equation becomes

$$\mathbf{x}_1 = \mathbf{x}_0 + \frac{h}{2}\mathbf{x}'_0 + \mathbf{x}'_1. \quad (2.7)$$

So the essence of the Trapezoidal Rule is that the slope of the waveform is taken as the average of the slope at the beginning of the time step and the slope at the end of the time step determined using the Backward Euler formula. This is also a predictor-corrector method.

The Euler formulas and the Trapezoidal Rule above used \mathbf{x}'_0 and/or \mathbf{x}'_1 , that is the derivatives at two times, to estimate the slope of the waveform between \mathbf{x}_0 and \mathbf{x}_1 . A generalization of these approaches is to use higher order derivatives, or equivalently the function at many past times. The rationale for considering a generalization of the discretized integration formula is that it may be possible to take longer times steps and so reduce computation. The generalization also allows the properties of the integration schemes to be discussed and to evaluate the truncation error introduced by each technique.

WEIGHTED INTEGRATION FORMULAE A generalized weighting of the basic integration equation is

$$a_1\mathbf{x}_1 = -a_0\mathbf{x}_0 + h[b_1\mathbf{x}'_1 + b_0\mathbf{x}'_0] \quad (2.8)$$

rearranging and using $t_1 = t_0 + h$ this becomes

$$a_1\mathbf{x}_1 = a_1\mathbf{x}(t_0 + h) = -a_0\mathbf{x}(t_0) + h[b_1\mathbf{x}'(t_0 + h) + b_0\mathbf{x}'(t_0)] = 0 \quad (2.9)$$

Expanding $\mathbf{x}(t_0 + h)$ and $\mathbf{x}(t_0)$ into a Taylor series yields

$$c_0\mathbf{x}(t_0) + c_1\mathbf{x}'(t_0) = -c_2\mathbf{x}''(t_0) - c_3\mathbf{x}'''(t_0) - \dots \quad (2.10)$$

or

$$\mathbf{x}(t_0)[a_1 + a_0] + h\mathbf{x}'(t_0)[a_1 - b_1 - b_0] = -h^2\mathbf{x}''(t_0)\left[\frac{a_1}{2!} - b_1\right] - h^3\mathbf{x}'''(t_0)\left[\frac{a_1}{3!} - \frac{b_1}{2!}\right] - \dots \quad (2.11)$$

where

$$c_0 = a_1 + a_0 \quad (2.12)$$

$$c_1 = a_1 - b_1 - b_0 \quad (2.13)$$

$$c_2 = a_1/2 - b_1 \quad (2.14)$$

$$c_3 = a_1/6 - b_1/2. \quad (2.15)$$

For a well behaved analytic function $c_3 < c_2 < c_1 < c_0$ and generally $\mathbf{x}'''(t_0) < \mathbf{x}''(t_0) < \mathbf{x}'(t_0)$. Minimizing the error due to ignoring higher order terms leads to the requirement

$$c_0 = c_1 = c_2 = c_3 = 0. \quad (2.16)$$

That is,

$$a_1 + a_0 = 0 \quad (2.17)$$

$$a_1 - b_1 - b_0 = 0 \quad (2.18)$$

$$\frac{a_1}{2} + b_1 = 0 \quad (2.19)$$

$$\frac{a_1}{6} - \frac{b_1}{2} = 0. \quad (2.20)$$

The lower order integration formulas can now be expressed in terms of the weighted integration as follows for the one dimensional situation.

The *Forward Euler Formula* has $a_1 = 1$, $a_0 = -1$, $b_1 = 0$ and $b_0 = 1$. The upper bound on the truncation error is $|h^2 c_2 x''(t_0)|$ and $c_2 = -\frac{1}{2}$.

The *Backward Euler Formula* has $a_1 = 1$, $a_0 = -1$, $b_1 = 1$ and $b_0 = 0$. The upper bound on the truncation error is $|h^2 c_2 x''(t_0)|$ and $c_2 = \frac{1}{2}$.

The *Trapezoidal Rule* has $a_1 = 1$, $a_0 = -1$, $b_1 = \frac{1}{2}$ and $b_0 = \frac{1}{2}$ and the upper bound on the truncation error is $|h^3 c_3 x'''(t_0)|$ and $c_3 = \frac{1}{12}$.

Note that:

- The truncation error in each method is reduced by reducing h .
- The reduction in error with reduction in h is significant with the Trapezoidal Rule.
- The error coefficient, c_n , is small for the Trapezoidal Rule.
- Numerical integration and the analysis performed here can be extended to multi dimensions (i.e. for \mathbf{x} instead of x).
- The methods can be extended to several time steps.

Due to the difference in the integration formulas, each method will produce a different result when used to discretize a given function. The performance of a method is determined by its accuracy and stability. Since the numerical integration solution is only an approximation to the exact solution, a finite amount of Local Truncation Error (*LTE*)

is introduced at each time point. With a well behaved function (with $c_3 < c_2 < c_1 < c_0$ and $\mathbf{x}'''(t_0) < \mathbf{x}''(t_0) < \mathbf{x}'(t_0)$) the error would be reduced by considering the second or third or higher order derivatives. The error introduced by considering only low order derivatives is called local truncation error. Errors result when the function is not well behaved in addition to the *LTE*. How the error accumulates over a large number of time points is a measure of the stability of an integration method. If a method is unstable it will diverge from the exact solution over a large number of time points. However a method can be stable and still lead to significant accumulated error. The accuracy and stability of an integration method depends on the function it is applied to and the time step used. Decreasing the step size improves the accuracy. Decreasing the time step also increases the chance of additional numerical error. Whereas a time step that is too large leads to a failure mechanism called overshoot. In particular the Trapezoidal Rule suffers from what is called trapezoidal overshoot [13]. Trapezoidal oscillation of the predicted solution around the correct solution occurs when the integration step size is too large to follow the curvature of a given function. All integration methods suffer from a failure mechanism called accumulated error, which occurs in “quasi-periodically” driven circuits and long transient simulations. Choice of the integration technique, depends on the function it is applied to. For the most functions used to express circuit signals in electronic circuits (linear, piecewise linear, sinusoidal and exponential), the Forward Euler Formula is generally inaccurate and unstable [11].

Figure 2.1 and Figure 2.2 show a sine wave calculated using the Forward Euler, Backward Euler and Trapezoidal Rule Formula with a time step of 1 and a time step of 0.25 respectively. The analytical derivative of the sine wave is used at each time step. The Forward Euler Formula overshoots the sine wave and the Backward Euler Formula undershoots the sine wave by a comparable amount. The derivatives \mathbf{x}'_0 and \mathbf{x}'_1 required by the Forward Euler (Equation 2.5) and Backward Euler Formula (Equation 2.6) respectively are known a priori and hence both the techniques suffer from the same amount of absolute local truncation error of $|h^2 c_2 x''(t_0)|$. Since the Trapezoidal Rule uses the average of the derivatives at two points, it suffers from the least local truncation error and gives the best result.

In the above example no nonlinear iteration is performed. Hence no prediction of the solution at the next time point is required and no correction is performed. In circuit simulation, the solution at the next time point is not known. This solution is calculated

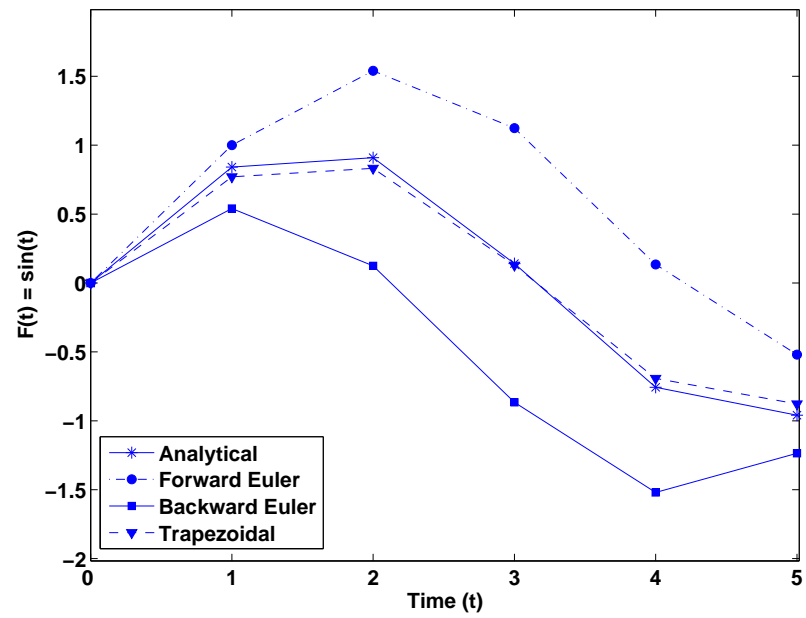


Figure 2.1: A sine wave integrated using Forward Euler Formula, Backward Euler Formula and Trapezoidal Rule with a time step of 1.

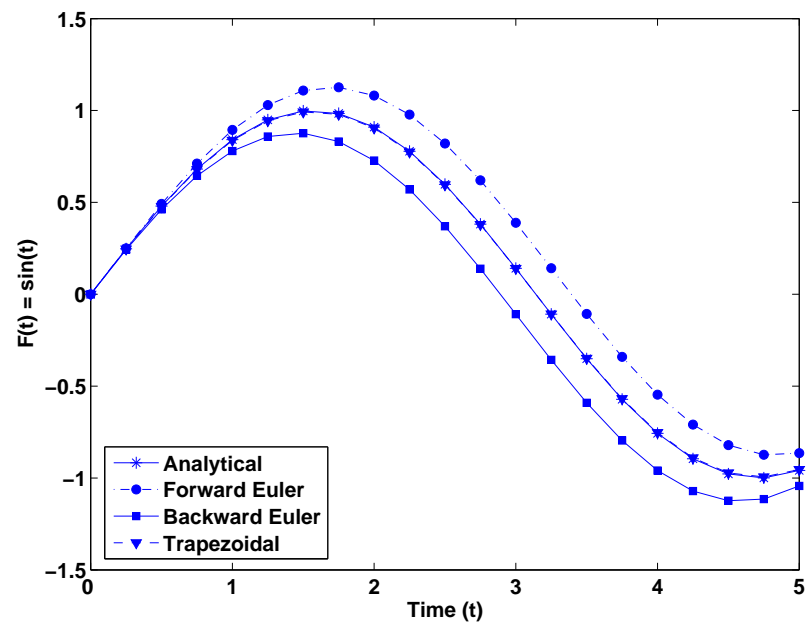


Figure 2.2: A sine wave integrated using Forward Euler Formula, Backward Euler Formula and Trapezoidal Rule with a time step of 0.25.

by a Newton Raphson iteration, which requires a good initial guess of the solution at the next time point. This solution is further corrected by the predictor-corrector integration technique used. In SPICE-like time step control techniques, this initial guess is provided by the Forward Euler Formula. If instead this initial guess is provided by the Backward Euler Formula the initial guess would suffer from the same amount of local truncation error. This is true only if the derivative values are known a priori. In circuit simulations the derivative values are not known a priori and the nonlinear iteration requires a good initial guess. In such cases a prediction using the Forward Euler Formula alone is not a good initial guess. This is due to the inherent characteristic of the Forward Euler Formula, where an initial guess is based on past history only. For highly nonlinear circuits a prediction based completely on the past history is not a good prediction of the future. The Backward Euler Formula is a predictor-corrector technique, and provides a good initial guess based on past and current information for the next time point. This initial guess which will be reiterated by the Newton Raphson technique and another integration technique like Trapezoidal Rule is a predicted-corrected solution based on past and current information. The effect of the predicted value on the estimated error at each time point and hence the time step size is discussed in the next section.

2.2.3 Predictors

The Backward Euler Formula and Trapezoidal Rule use the derivative at the next time point. In circuit analysis the value of the solution and hence its derivatives at the next time point is not known and cannot be reasonably estimated. Therefore in order to start the calculations an approximate value must be computed. In SPICE this is done in various ways, the simplest being predicting the value of the solution at the next time point as the result at the previous time step. Another possibility is to use the Forward Euler Formula, $\mathbf{x}_1 = \mathbf{x}_0 + \mathbf{h} * \mathbf{x}$ [5], to predict the value of the solution at the next time point. Once the predicted value is inserted into the corrector (say Backward Euler or Trapezoidal), iteration is performed to correct the mismatch. This iteration is usually performed using the Newton Raphson method. The convergence criterion applied in SPICE is if that the new value has changed by less than $(ABSTOL + RELTOL * \max(\text{old}, \text{new}))$, the iteration has converged. Here *ABSTOL* is the absolute difference between the old and the new value and *RELTOL* is the maximum allowable percentage change in the old value. As discussed in the previous

section, each of the integrating formula suffer from some finite amount of *LTE*. The *LTE* in each technique is reduced by reducing the time step h . In SPICE the total *LTE* at each time point is calculated as the difference between the converged value obtained from the Newton Raphson iteration and the predicted value obtained from the Forward Euler Formula. From Equation 2.5, the predicted value using the Forward Euler Formula is a linear extrapolation. The new time step is predicted by:

$$t_{\mathbf{f}} = t_{\mathbf{old}} * \frac{\sqrt{TRTOL * (\max(|\mathbf{new}|, |\mathbf{predicted}|) * RELTOL + ABSTOL)}}{LTE} \quad (2.21)$$

where, $t_{\mathbf{f}}$ is the new time step, $t_{\mathbf{old}}$ is the old time step and $TRTOL$ is a *LTE* correction factor. The new time step is inversely proportional to the calculated *LTE*.

The *LTE* in SPICE is estimated as the difference between the linearly extrapolated value and the converged solution after the nonlinear iteration works well for digital circuits, where the output voltage levels are constant for a portion of the duration of the pulse period. This effectively resets the accumulated numerical error. During this low circuit activity duration, a prediction based on past history works well. In highly nonlinear circuits with sinusoidal signals where the voltage levels are changing continuously and rapidly, a prediction based on only past history will be in large error. Especially at troughs and crests of the sinusoid a linear extrapolation does not work well as it does not follow the curves. It over shoots the curves as seen in Figure 2.1. Hence the *LTE* estimated as difference between the linearly extrapolated value and the final predicted-corrected value is large. From Equation 2.21, this leads to unnecessary reductions in time step h , to meet the *RELTOL* limits and result in bunching of time points along the curves. The error in a prediction based on the past and current information will be small effectively precisely estimating the *LTE*. A prediction based on past and current history works better for sinusoidal circuits as the voltage levels are changing continuously. A better prediction hence a more accurate solution at every time point will reduce the accumulated error in a continuously changing signal where it tends to accumulate indefinitely.

Estimation of error and consequently appropriate choice of step size is critical in controlling the accumulation of error. If the time step is too small numerical round-off errors will accumulate. If the error is underestimated the time step will be too large with additional accumulation of error. A new scheme for accurate estimation of error is developed in Chapter 3.

2.2.4 Fourier Transformation Techniques

After performing the time-domain analysis to view the spectrum of time-domain signal in the frequency domain, a Fourier analysis must be performed on the time-domain data points of the signal. The dynamic range is affected by the Fourier transform technique used to view the frequency spectrum. Several techniques can be used to calculate the Fourier coefficients at the frequency harmonics of interest. For e.g. Discrete Fourier Transform (DFT), Fast Fourier Transform (FFT) or a Fourier integral can be used to calculate the Fourier coefficients. The characteristics of these techniques are discussed below.

DISCRETE FOURIER TRANSFORM: To obtain an accurate Discrete Fourier Transform (DFT), the waveform should be uniformly sampled, forcing SPICE to compute the solution at each of the sample points. This uniform sampling is done in SPICE using interpolation. The Discrete Fourier transform suffers from errors introduced by interpolation. The number of Fourier coefficients computed is equal to number of data time points and the DFT suffers from aliasing. There are several reasons why interpolation can lead to unacceptable error:

- Interpolation introduces significant error to hamper the accuracy of small signals.
- The Fourier analysis in SPICE is a post processing activity and does not bound the time step to assure reasonable accuracy.
- SPICE controls the time-step to assure that second order interpolation is accurate on capacitor charge and inductor flux waveforms, not to assure accurate Fourier analysis. Fourier analysis is performed on the nodal voltages and voltage source currents rather than the charge and flux waveforms. Thus SPICE is not choosing the time steps to control error in the signals being Fourier analyzed. If the circuit contains only small capacitors, *CHGTOL* effectively loosens the local truncation error criterion, allowing the simulator to take large time steps even though the Fourier analysis requires smaller steps.

If a DFT is performed on this interpolated data it can resolve harmonics that are 60 dB or 80 dB below the carrier [7]. Interpolation error can be eliminated by forcing SPICE to place a time point everywhere a sample is needed for the Fourier analysis. This dramatically improves the frequency resolution at the expense of long simulation times. The long simulation times is not a major overhead if the waveform being analyzed has low distortion.

However for a broad spectrum signal with very fast transitions between two equilibrium points, the DFT's will need very small time steps in the fast transition region and the condition of equally spaced time points will make the simulator unnecessarily compute small time-steps during the flat portions of the waveforms between the transitions. To overcome the problem of equally spaced time points, some SPICE-like simulators, like PSPICE, use variable time steps, but forces the analysis to calculate waveforms at the beginning and the end of the Fourier transform intervals. However, several commercial versions of SPICE do solve for the state of a circuit at uniformly spaced time points.

FOURIER INTEGRAL: Another technique to reduce the effect of the errors introduced by interpolation in a variable time step analysis and the need for uniformly spaced time points required in a DFT is to perform the Fourier transform using the Fourier integral [7]. This technique is used in the commercial simulator, SPECTRE. For a periodic waveform x of period T , the Fourier coefficient is computed with the following,

$$a_k = \frac{2}{T} \int_t^{(t+T)} x(\tau) \cos \frac{(2\pi k\tau)}{T} d\tau \quad (2.22)$$

where $k = 1, 2, \dots$. The circuit simulator discretizes time and solves the system of equations that describe the circuit at $N + 1$ time points, t_0, t_1, \dots, t_N . Equation 2.22 is rewritten as a sum of integrals over each time step,

$$a_k = \frac{2}{T} \sum_{n=1}^N \int_{t_{n-1}}^{(t_n)} x(\tau) \cos \frac{(2\pi k\tau)}{T} d\tau \quad (2.23)$$

where $t_N - t_0 = T$. Between time-points, x is approximated with a low-order polynomial,

$$x(\tau) = \sum_{m=0}^M C_{mn} \tau^m \quad (2.24)$$

for $t_{n-1} \leq \tau \leq t_n$, where M is the order of the approximating polynomial. This approximation is substituted in Equation 2.23 to calculate the Fourier coefficients approximately as,

$$a_k \approx \frac{2}{T} \sum_{n=1}^N \sum_{m=0}^M C_{mn} \int_{t_{n-1}}^{(t_n)} \tau^m \cos \frac{(2\pi k\tau)}{T} d\tau. \quad (2.25)$$

Also in SPECTRE, to reduce interpolation error, the Fourier analyzer forces SPECTRE to place a time point at both the beginning and the end of the Fourier transform intervals (using SPECTRE breakpoints). The Fourier coefficients of the specified frequency harmonics only

are calculated using the Fourier integral [7]. In this technique the time points are non-uniformly spaced and it does not suffer from aliasing. This method reduces the numerical noise floor to -160 dBm. To calculate a large number of Fourier coefficients for a broad bandwidth signal, this technique is too slow.

FAST FOURIER TRANSFORM: To perform a Fourier transform on a broad bandwidth signal quickly and eliminate the noise introduced in the data set due to interpolation, a Fast Fourier Transform with time-domain window weight functions techniques can be used. This noise, simulator inaccuracies and transient response of the circuit are sources of spectral leakage in the Fourier transform. The spectral leakage increases the FFT noise floor of the simulation and thus degrades the dynamic range of the simulation [8]. Use of a time-domain window (having a weighting function) reduces the detrimental effects of the spectral leakage with a small loss in frequency resolution. Many windowing techniques can be used. The Hanning window with a Hanning constant of 2 shows the best tradeoff between frequency resolution and dynamic range. It can detect signals 100 dB below the carrier [8]. However this technique suffers from aliasing.

In summary to resolve the small signals in the time-domain data a good Fourier transform technique should be used. Tradeoffs between frequency resolution, dynamic range and computation time must be made.

2.3 Sources of Error in Steady-State Transient Analysis

One of the methods to perform a steady-state transient analysis in electronic circuits is the Harmonic Balance method. While the focus of this work is the enhancement of the transient analysis comparison must be made with the Harmonic Balance (HB) method. Harmonic Balance is the preferred simulation method for microwave circuits as it is not necessary to calculate the initial transient response. Harmonic Balance techniques are generally more efficient at solving nonlinear circuits with periodic and quasi-periodic excitation signals [9]. Harmonic balance formulates the circuit equations and their solution in the frequency domain. The solution is written as a Fourier series that cannot represent transient behavior, and so harmonic balance directly finds the steady-state solution. Harmonic balance works best when the circuit is behaving in a near linear fashion. To simulate a strong nonlinearity large number of harmonics must be considered, making the simulation equa-

tions intractable. To make the numerical solution tractable only the first K harmonics are considered. It is in general difficult to formulate models for the nonlinear components in the frequency domain. To overcome this problem, nonlinear components are usually evaluated in the time-domain and converted to the frequency domain using the Fourier transform, demanding tighter error control strategies. There are two sources of error that are of interest in the harmonic balance. The first results from truncating the harmonics considered to a finite number, and the second results from not completely converging the iteration used to solve the nonlinear system of algebraic equations [6]. Simulator inaccuracies are sources of spectral leakage when transforming the time-domain waveforms to frequency domain using Fourier transform [8]. The frequency domain representation of a signal allows resolution of small signals in the presence of large signals, with dynamic range sometimes reaching 120 dB [6]. There are also limitation is the types of models that can be incorporated. A further limitation is that transient effects, including thermal transient effects, cannot be captured.

2.4 Thermal Modeling

In this section, a brief review of the mathematical formulation of the thermal models is presented. The models are implemented in *fREEDA*TM and are used to model the mounted and metallized X-band GaAs MMIC LNA, Figure 2.3. The X-band GaAs MMIC LNA is further discussed in chapter 4. The theory presented in this section is based on two publications :

- W. Batty, C. E. Christoffersen, S. David, A. J. Panks, R. G. Johnson, C. M. Snowden and M. B. Steer, “Electrothermal CAD of power devices and circuits with fully physical time-dependent thermal modelling of complex 3-d systems,” *IEEE Transactions on Component and Packaging Technologies, Part A: Packaging Technologies*, vol. 24, Issue 4, Dec. 2001, pp. 566-590.
- W. B. Batty, C. E. Christoffersen, S. David, A. J. Panks, R. G. Johnson, C. M. Snowden, and M. B. Steer, “Fully physical time-dependent compact thermal modeling of complex nonlinear 3-dimensional systems for device and circuit level electrothermal CAD,” *Seventeenth IEEE Semiconductor Thermal Measurement and Management Symposium*, 2001, pp. 71-84

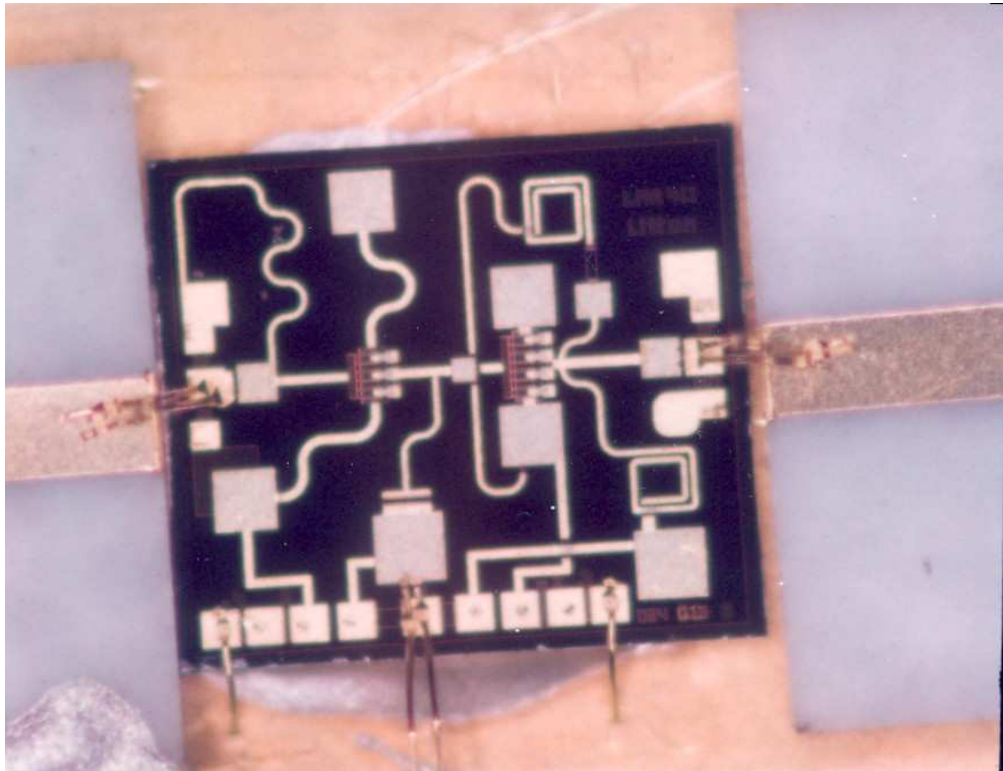


Figure 2.3: Layout of LMA411 X-band GaAs MMIC LNA.

One way of incorporating thermal effects in a circuit simulator [58] is to render the thermal model as an electrical circuit. The thermal and electrical circuits are then solved simultaneously as if they were one large electrical circuit. Power dissipated in the active devices is represented as a heat current source referenced to thermal ground. One problem with this strategy is providing separate circuits for the electrical and thermal parts. This has been addressed by the concept of local reference nodes [50]. The use of local reference nodes guarantees that there is no mixing of electric and thermal currents.

To represent the thermal model in the form of an electrical circuit in a circuit simulator, the thermal model should be in compact model form. A compact model represents the partial differential heat diffusion equation as a set of first-order differential equations and coupled algebraic equations. This form is easily implementable in a general purpose circuit simulator. This form enables easy interfacing of the electrical and thermal networks for electrothermal simulations. Both networks can be solved simultaneously to simulate coupled electrothermal effects which embodies all thermal manifestations in the electronic circuits. Conventional numerical techniques use finite element, finite volume, finite difference or boundary element techniques to represent the thermal network as an electric circuit. All these techniques must construct a surface or volume mesh. The computation requirements due to the large number of mesh-nodes in these techniques limits their use for coupled electrothermal simulations at CAD timescales. Also these techniques are inherently approximate due to finite differentiation. Faster accurate analytical compact thermal models must be developed to capture the effects of temperature on circuit performance. Representing the compact thermal model developed in this work as an electric circuit, it requires that it be described by a thermal impedance matrix. This matrix is the impedance matrix of a N -port element. This model reduces the partial differential heat diffusion equation to a set of coupled algebraic equations with rigorous mathematics. The formulation and the mathematics of the thermal impedance matrix is explained in the following sections.

2.4.1 Thermal Impedance Matrix

The thermal modeling of complex 3D structures can be achieved by standard numerical techniques [60], and solutions of the heat diffusion equation for complex 3D systems are commonly based on finite volume, finite element, finite difference or boundary element methods. All of these approaches require construction of a volume or surface mesh.

They are computationally intensive and therefore generally too slow for direct coupling to electronic device and circuit simulators. Recently, numerical solutions optimized to model thermal effects of electronic devices which are based on hierarchical nesting and adaptive grid refinement have been introduced in [59]. This technique handles the wide ranges of spatial and temporal scales have reduced computational requirements and are two orders of magnitude faster. This improvement makes it possible to simultaneously perform electrical and thermal analysis of real world electronic circuits. Hefner *et. al* developed techniques based on spatial discretization using finite difference [25] to generate thermal networks for time-independent and time-dependent electrothermal co-simulation in the electrothermal simulator SABER. SABER has thermal models for individual circuit components, devices, heat sinks, packages. The thermal system is represented by an interconnection of these individual thermal components. These components are parameterized with user defined structural and material information. These models were verified for a Silicon Insulated Gate Bipolar Transistor (IGBT) [26]. Three thermal component models were developed — the silicon chip thermal model, the chip package model, and the heat sink model. The silicon chip thermal model is based on one-dimensional rectangular coordinate heat diffusion equation and include nonlinear thermal conductivity of silicon. Using spatial and time discretization a logarithmic grid is constructed for the silicon chip model. As the thermal gradients in the silicon chip disperse through the chip, a logarithmic grid will require a minimum number of thermal nodes to describe temperature distribution for the range of applicable power dissipation levels. The thermal resistance and capacitance is calculated at each node of the grid. The chip model also includes a distributed heat source, where the power density is a function of the depth into the chip. The power distribution at each node and node thermal capacitance are precomputed as they do not depend on simulator system variables. The thermal resistance at each node is a function of thermal conductivity and must be calculated during simulation to capture the temperature dependence of the thermal conductivity. The package model describes the two-dimensional lateral heat spreading and the heat capacity of the periphery of the package. The lateral heat spreading in the package results in an effective heat flow area that increases with the depth into the package. The heat sink model describes the heat spreading beneath the package-heat sink interface, the semicylindrical heat flow from the package towards the heat sink fins, and nonlinear forced and natural convection heat transfer at the heat sink fins. This model includes temperature dependence of the physical properties of Silicon and gives the dynamic temperature distri-

bution within the thermal network. This model can capture self-heating thermal effects on the device, but it does not capture the mutual heating effects in multiple power dissipating sources. This model and in general the numerical techniques are inherently approximate due to the use of finite difference and their networks contain large number of nodes. Also, the finite difference method simplifies the 3-D thermal solution, by solving the heat equation in only in a reduced dimensional form. Also these techniques were applied to only power devices and did not include structural details like surface metallization.

Considerable effort has been expended in developing faster compact thermal models. Fast analytical solutions to avoid the approximations introduced by the numerical methods have been proposed. The simplest thermal model uses simple arrangements of thermal resistances and capacitances together with a circuit-based thermal source, typically a controlled voltage or current source, whose amplitude is proportional to the power dissipated in electrical devices. But to describe complex structures, the fast analytical models get complicated and hence have been limited to a simple rectangular multilayer structure. An analytical thermal impedance model for SOI MOSFETs has been proposed by [62]. Vejiola *et al.* [63], developed an analytical heat dissipating spheres approach in the circuit simulator, APLAC, to develop the thermal impedance. Rizzoli developed a thermal resistance calculation technique using Green's functions for harmonic balance and transient simulations, with the thermal capacitances described using simple enthalpy formulation [64]. Szekely *et al.*, developed thermal RC-ladder from simulated and measured time constant spectra. Various thermal resistance calculation techniques using Fourier series, conformal mapping, extraction using deconvolution from numerically generated and measured thermal responses, and numerical techniques have been applied to individual circuit components, devices, heat sinks, packages.

The thermal approach implemented in *fREEDA*TM has been presented in [60] and [61]. It is a new fully physical and analytical spectral domain decomposition technique, suitable for electrothermal co-simulation at CAD timescales. This model linearizes the nonlinear time dependent heat diffusion equations using transformations and domain decomposition. This transformed linear equation is solved analytically with a double Fourier series solution using separation of variables in the complex frequency space, s . This approach is called the *Leeds thermal impedance matrix model*. It is modular and it can describe simultaneously all device details, from surface metalization, bias and substrate thinning in power FETs and MMICs, through (actively cooled) MMIC on substrate arrays, up to MCMs and circuit

board level. The various steps of this approach are described below.

2.4.2 Transformations to Linearize the Heat Diffusion Equation

The time dependent heat diffusion equation is given by

$$\nabla \cdot [\kappa(T) \nabla T] + g = \rho C \partial T / \partial t, \quad (2.26)$$

where T is temperature, t is time, $\kappa(T)$ is temperature dependent thermal conductivity, $g(x, y, z, t)$ is the rate of heat generation, ρ is material density and C is specific heat. This equation is nonlinear through the temperature dependent $\kappa(T)$. The temperature dependence of the thermal conductivity is given by:

$$\kappa = \kappa_s * (T/T_s)^{-b}, \quad (2.27)$$

where κ_s is the thermal conductivity at temperature T_s and $-b$ is a constant.

The nonlinear thermal problem is converted into a linear problem by means of two transformations [60], the Kirchhoff transformation and the time variable transformation. The Kirchhoff transformation is used to correct the steady-state error of the thermal response and a time transformation is used to obtain accurate modeling of the time constants.

Kirchhoff Transformation:

The temperature dependence of the thermal conductivity given by Equation 2.27, can be linearized using Kirchhoff's transformation [53], given by:

$$\theta = T_s + \frac{1}{\kappa_s} \int_{T_s}^T \kappa(T) dT \quad (2.28)$$

where $\kappa_s = \kappa(T_s)$ and T_s is the heatsink mount temperature. This transformation transforms the temperature T to a transformed temperature θ . The diffusion equation for this transformed temperature θ is:

$$\nabla^2 \theta - \frac{1}{k(\theta)} \frac{\partial \theta}{\partial t} = -\frac{g}{\kappa_s} \quad (2.29)$$

where diffusivity $k = \kappa/\rho C$. This transformation removes only the temperature dependence of the thermal conductivity. An inverse Kirchhoff's transformation must be applied *a posteriori* to the solution of the linear heat diffusion equation, to obtain 'physical' temperature T .

Time Variable Transformation:

The above equation is still nonlinear due to the dependence of diffusivity k on θ . To remove the dependence of diffusivity on θ , a time variable transformation must be applied. This transformation defines a new time variable τ .

$$k_{s\tau} = \int_0^t k(\theta) dt. \quad (2.30)$$

Approximating the Laplacian by its conventional rectangular Cartesian form, the time-dependent heat diffusion equation becomes finally

$$\nabla^2 \theta - \frac{1}{k_s} \frac{\partial \theta}{\partial \tau} = -\frac{g}{\kappa_s}. \quad (2.31)$$

For semiconductor electrothermal simulations, diffusivity is assumed constant. In such situations the time variable transformation need not be applied. In this work the diffusivity is assumed constant and hence the time variable transformation is not applied. Even though the rest of the equations are in the τ domain, for this work it is safe to assume the real time $t = \tau$. This fully linearized heat diffusion equation, Equation 2.31, can now be solved exactly with general linear boundary conditions.

2.4.3 Analytical Solutions

The analytical solution to the fully linearized heat diffusion equation in terms of thermal impedance matrices is described in this section.

To derive the thermal impedance matrix, the solution to Equation 2.31 is assumed to be of the form:

$$\Delta\theta_i = \sum \mathbf{R}_{\text{TH}_{ij}}(\mathbf{s}) \mathbf{P}_j \quad (2.32)$$

where $\Delta\theta_i$ is the Laplace transformed temperature rise of the element i above its initial temperature, $\sum \mathbf{R}_{\text{TH}_{ij}}$ is the thermal impedance matrix in the Laplace s -space and the \mathbf{P}_j are the transformed time-dependent fluxes due to power dissipation elements $j = 1, 2, \dots, M$.

Formulation of the thermal impedance matrix approach in the Laplace transform s -space, rather than in the time-domain, is chosen for a number of reasons. Firstly, the s -space formulation is a natural development of the thermal resistance matrix approach for the time independent case, described by the authors in [54] – [56]. All of the advantageous features of the thermal resistance matrix approach for the coupled electrothermal description of complex systems, carry over to the time dependent case in s -space. Secondly, the s -space formulation of the thermal impedance matrix allows immediate incorporation

as a multi-port distributed thermal network in circuit level harmonic balance simulators. Finally, Laplace inversion also allows use in circuit level transient simulations, and analytical inversion of s -space expressions readily gives rise to both small-time and large-time results for the thermal response, which are not easily obtained using a direct time-domain formulation. However, the thermal impedance matrix approach can also be developed in the time-domain using Green's function techniques, as described in [57].

In the thermal impedance matrix approach presented here, $\mathbf{R}_{\text{TH}_{ij}}(\mathbf{s})$ is determined in explicit analytical form, purely from structural information. It is independent of temperature and power dissipation, and hence of device bias. Its order is determined only by the number of heat dissipating and temperature sensitive elements, independent of the level of the complexity of the device structure, so is already minimal without any explicit model reduction. Thermal updates in the coupled electrothermal problem reduce to small matrix multiplications, Equation 2.32. This approach therefore offers orders of magnitude speed-up compared to numerical thermal solutions.

An adiabatic boundary condition and a generalized radiation boundary condition is imposed. This is written as:

$$\alpha_{0,D}\kappa_s\frac{\partial\theta}{\partial z} + H_{0,D}(\theta - \theta_{0,D}(x, y, \tau)) + p_{0,D}(x, y, \tau) = 0. \quad (2.33)$$

Here, imposed flux densities $p_{0,D}(x, y, \tau)$ are time dependent. Coefficients $H_{0,D}$ describe surfaces fluxes due to radiation and convection. The $\alpha_{0,D}$ equal zero for imposed temperature boundary conditions and unity for imposed flux boundary conditions. The respective ambient temperatures $\alpha_{0,D} \neq 0$, or heat sink mount temperatures $\alpha_{0,D} = 0$, are also dependent on time, $\theta_{0,D}(x, y, \tau)$. The generality of this boundary condition allows vertical matching of thermal subsystems, by interface discretisation and thermal impedance matrix manipulation, as well as integral treatment of surface fluxes.

Equation 2.31 is solved in the Laplace domain, hence a Laplace transform of this equation is constructed. An analytical double Fourier series solution to this equation in the Laplace domain is obtained using separation of variables. This solution is explained in [61] and in the general form is given by,

$$\mathbf{R}_{\text{TH}_{ij}}(\mathbf{s}) = \sum_{mn} \left\{ \begin{array}{c} \coth(\gamma_{mn}D) \\ \operatorname{cosech}(\gamma_{mn}D) \end{array} \right\} \times \frac{-4/(\kappa LW \gamma_{mn})}{(1 + \delta_{m0})(1 + \delta_{n0})} \frac{I_{mn}^i I_{mn}^j}{I_{00}^i I_{00}^j}, \quad (2.34)$$

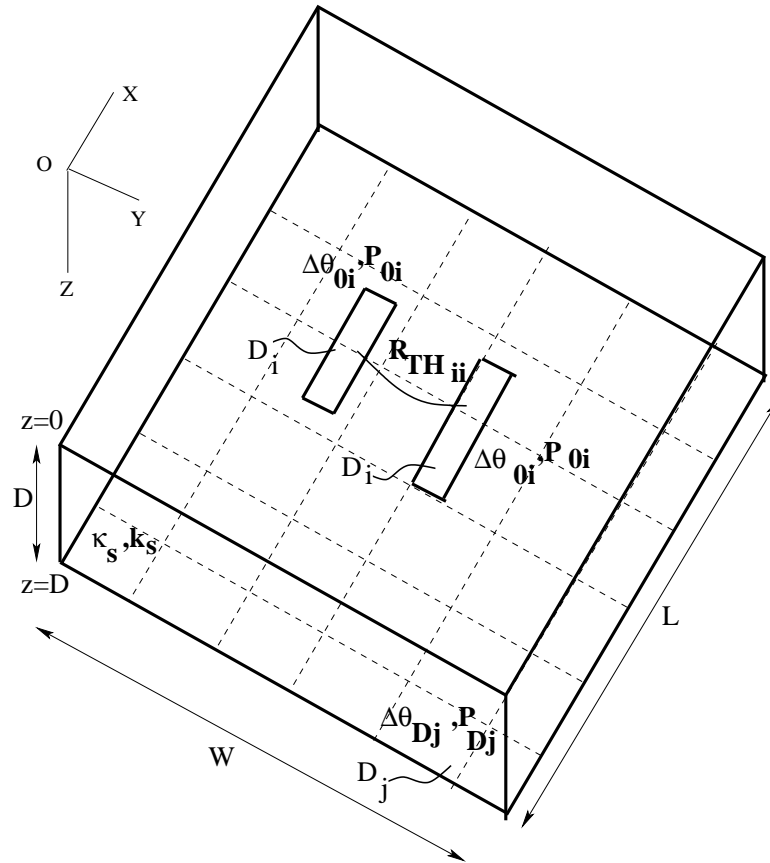


Figure 2.4: Generic thermal subvolume for analytical construction of the thermal impedance matrix. This is the structure of the compact thermal model with a 6×6 surface discretization. Each of the blocks has a thermal terminal and the heat flow at each of these terminals is treated as being uniformly applied across the area of each surface discretization.

where $m, n = 0, 1, 2, \dots$,

$$\lambda_m = \frac{m\pi}{L}, \mu_n = \frac{n\pi}{W}, \gamma_{mn} = \left(\lambda_m^2 + \mu_n^2 + \frac{s}{k} \right)^{1/2}, \quad (2.35)$$

L, W, D are the subvolume dimensions in the x, y and z directions respectively; the subvolume has thermal conductivity, κ , diffusivity, k ; and I_{mn}^i are area integrals over the heating element and discretised interface element areas D_i , see Figure 2.4, so that

$$I_{mn}^i = \iint_{D_i} \cos \lambda_m x \cos \mu_n y \, dx dy. \quad (2.36)$$

Note: D in the above equation is height or depth of thermal subvolume in the z direction, and D_i is discretised interface element surface areas in the $x - y$ plane.

The subvolume solutions, relate the transformed temperature rises of the heating elements and discretised interface elements, to corresponding power dissipations, as described in Equation 2.32. The nonlinear, volumetric thermal problem is thus reduced to the discretised interfaces between thermal subvolumes (for example the interface between the GaAs die and the Epoxy layer) and the interface with the already nonlinear electrical model, the power dissipating elements.

In Equation 2.35 the elements of the thermal impedance matrix at every simulation time point is completely based only on the structural information of the thermal subvolume. The area integral I_{mn}^i can be computed as the summation over a finite number of ms and ns . These elements can be precomputed at every time point.

Now the heat diffusion equation is completely linear and solved in the s -space with the separation of variables method. Each $\mathbf{R}_{\text{TH}_{ij}}(\mathbf{s})$ is calculated in the s -space, and is inverted with a Laplace inversion, to evaluate the time-dependent $\mathbf{R}_{\text{TH}_{ij}}(\tau)$, at the time τ . Here if \mathbf{P}_j is assumed to be the transformed time dependent fluxes of simple step inputs of magnitudes P_j , the Laplace inverted $\mathbf{R}_{\text{TH}_{ij}}(\tau)$ can be calculated. This Laplace inversion, is performed by a Stehfest's numerical inversion rather than analytical inversion, since the numerical inversion is simple to implement.

Also, in Equation 2.32, for a coupled electrothermal simulation, the Laplace transformed \mathbf{P}_j are not known explicitly and must be obtained self consistently. To perform the electrothermal simulation, the corresponding Laplace inverted $\mathbf{P}_j(\tau)$ must be discretized in time into subintervals of length $\delta\tau$. These subintervals are the time steps at which the electrical simulation is performed. Assuming that $\mathbf{P}_j(\tau)$ takes the piecewise constant form

in these subintervals,

$$\mathbf{P}_j(\tau) = \mathbf{P}_j^{(n)} \text{ for } (n-1)\delta\tau < \tau \leq n\delta\tau, n = 1, \dots, N \quad (2.37)$$

then gives

$$\mathbf{P}_j(s) = \sum_n \frac{1}{s} (1 - e^{-s\delta\tau}) (1 - e^{-(n-1)s\delta\tau}) \mathbf{P}_j^{(n)}. \quad (2.38)$$

Laplace inverting Equation 2.32, the temperature rise $\Delta\theta_i^{(m)}$ at each element i at time $t = m\delta\tau$ is a function of the piecewise constant $\mathbf{P}_j^{(n)}$. Thus,

$$\Delta\theta_i^{(m)} = \Delta\theta_i^{(m)}(P_i^{(m)}) = L^{-1}\{R_{TH_{ij}}(s)\mathbf{P}_j(s)_{\tau=m\delta\tau}\}, \quad (2.39)$$

$$= \sum_n \sum_j [u(m-n+1)R_{TH_{ij}}((m-n+1)\delta\tau) - u(m-n)R_{TH_{ij}}((m-n)\delta\tau)] \mathbf{P}_j^{(n)}, \quad (2.40)$$

where $u(\tau)$ is the unit step function. This corresponds to N systems of equations in M unknowns, where N is the number of discretised time points in the time interval under consideration, and M is the number of power dissipating or temperature sensitive elements. The Laplace inversion, with piecewise constant power dissipation, avoids any explicit convolution operation. The calculated temperature is in the ‘transformed’ time variable domain i.e. the τ domain. An inverse time variable transformation must be applied. In this work, however, since the diffusivity is assumed constant and no time variable transformation is applied, an inverse time variable transformation is not applied either. Only an inverse Kirchhoff’s transformation is applied. The inverse Kirchhoff’s transformation is applied to transform the ‘transformed’ temperature θ back to the ‘physical’ temperature T . This final temperature after the Kirchhoff’s transformation is in the real time-domain.

2.4.4 Heat Sink Mounted Thermal Subvolume

For a heat sink mounted thermal subvolume, in the general boundary condition, Equation 2.33, put $\alpha_D = 0$, $H_D = 1$, $p_D(x, y, \tau) = 0$ and $\theta_D(x, y, \tau) = \theta(\tau = 0)$ (uniform temperature at the bottom surface, $z = D$, corresponding to heat sink mounting at ambient temperature). Also put $\alpha_0 = 1$ and $H_0 = 0$ for no radiation from the top surface $z = 0$. The corresponding thermal impedance matrix is given by:

$$\mathbf{R}_{TH_{ij}}(s) = \frac{1}{\kappa_s LW} \sum_{mn} \frac{4 \tanh \gamma_{mn} D}{(1 + \delta_{m0})(1 + \delta_{n0}) \gamma_{mn}} \frac{I_{mn}^i I_{mn}^j}{I_{00}^i I_{00}^j} \quad (2.41)$$

where the I_{mn}^i area integrals over the areas D_i , and are given by Equation 2.36.

2.4.5 Vertically Matched Thermal Subvolume

For a vertically matched element, the temperature at the top and the bottom surface of the thermal subvolume vary and must be matched. In this case the specifying flux on top and bottom surfaces, $z = 0, D$, and assuming no radiative or convective surface losses, ($\alpha_{0,D} = 1, H_{0,D} = 0$), the following relations are obtained for temperatures, θ_{0av_i} and θ_{Dav_i} , averaged over elementary areas, D_i , and D_j , on faces $z = 0$ and $z = D$, respectively,. The corresponding equations, of the form Equation 2.32, are given by:

$$\theta_{0av_i} - \frac{\theta(\tau = 0)}{s} = \sum_{i'} \mathbf{R}_{\text{TH}_{ii'}}^{\text{00}} \mathbf{P}_{0i'} + \sum_j \mathbf{R}_{\text{TH}_{ij}}^{\text{0D}} \mathbf{P}_{Dj'} \quad (2.42)$$

$$\theta_{Dav_i} - \frac{\theta(\tau = 0)}{s} = \sum_i \mathbf{R}_{\text{TH}_{ji}}^{\text{D0}} \mathbf{P}_{0i'} + \sum_{j'} \mathbf{R}_{\text{TH}_{jj'}}^{\text{DD}} \mathbf{P}_{Dj'}. \quad (2.43)$$

Here, \mathbf{P}_{0i} and \mathbf{P}_{Dj} are respective imposed fluxes in elementary areas, D_i , and D_j . The thermal impedance matrices are obtained in the explicit form

$$\mathbf{R}_{\text{TH}_{ii'}}^{\text{00}} = \frac{1}{\kappa_s LW} \sum_{mn} \frac{4 \coth \gamma_{mn} D}{(1 + \delta_{m0})(1 + \delta_{n0}) \gamma_{mn}} \frac{I_{mn}^{0i} I_{mn}^{0i'}}{I_{00}^{0i} I_{00}^{0i'}} \quad (2.44)$$

$$\mathbf{R}_{\text{TH}_{ij}}^{\text{0D}} = \frac{1}{\kappa_s LW} \sum_{mn} \frac{-4 \operatorname{cosech} \gamma_{mn} D}{(1 + \delta_{m0})(1 + \delta_{n0}) \gamma_{mn}} \frac{I_{mn}^{0i} I_{mn}^{Dj}}{I_{00}^{0i} I_{00}^{Dj}} \quad (2.45)$$

$$\mathbf{R}_{\text{TH}_{ji}}^{\text{D0}} = \frac{1}{\kappa_s LW} \sum_{mn} \frac{4 \operatorname{cosech} \gamma_{mn} D}{(1 + \delta_{m0})(1 + \delta_{n0}) \gamma_{mn}} \frac{I_{mn}^{Dj} I_{mn}^{0i}}{I_{00}^{Dj} I_{00}^{0i}} \quad (2.46)$$

$$\mathbf{R}_{\text{TH}_{jj'}}^{\text{DD}} = \frac{1}{\kappa_s LW} \sum_{mn} \frac{-4 \coth \gamma_{mn} D}{(1 + \delta_{m0})(1 + \delta_{n0}) \gamma_{mn}} \frac{I_{mn}^{Dj} I_{mn}^{Dj'}}{I_{00}^{Dj} I_{00}^{Dj'}} \quad (2.47)$$

where the I_{mn}^{0i} and I_{mn}^{Dj} are area integrals over the areas D_i , and D_j , and are given by Equation 2.36.

This vertically matched thermal subvolume enables the inclusion of surface metalization and air bridges, and other vertical geometries such as through vias. These features can be modeled as separate thermal subvolumes, and the temperature and the flux at the discretized interfaces of these subvolumes is matched.

2.4.6 Embedded Subvolumes

In the above sections all subvolumes are considered homogenous. A homogenous subvolume is a good assumption for a MMIC. For more complex electronic circuits, with

embedded interconnects and metal layers, the thermal subvolume is non-homogenous. In such situations thermal subvolumes must be embedded and these subvolumes must be horizontally and vertically matched. In this case the adiabatic sidewall boundary in the general boundary condition, Equation 2.33, must be removed to allow horizontal matching and subvolume embedding. The solution of the heat diffusion equation with this boundary condition and volume heat sources/sinks requires the solution of the Helmholtz's equation in the Laplace transform s – *space*. A double Fourier series solution, describing arbitrarily distributed volume heat sources and sinks, without the use of Green's function is described in detail in [61]. In this work all subvolumes were considered homogenous hence this formulation is not explained here.

Thus this model represents the partial differential heat diffusion of a dynamic complex thermal subsystem with a set of coupled algebraic equations. The solution of each thermal subvolume takes the form of a s -space thermal impedance matrix, relating the transformed temperature rises of the heating elements and discretised interface elements, to corresponding power dissipations, by an algebraic equation described in Equation 2.32. Each element of the matrix can be calculated with algebraic equations, Equation 2.41 and Equations 2.44 — Equation 2.47. As temperature rises only at heating elements and at the discretized interfaces between thermal subvolumes are calculated, no redundant temperature rises within the thermal subvolume are calculated. This minimizes the required number of nodes and thus reduces computation time. The nonlinear volumetric thermal problem is reduced only to the discretised interfaces between subvolumes and the interface with the already non linear electrical model. The transformations and the domain decompositions allow the precomputation of the thermal impedance matrix which considers the temperature dependent thermal conductivity. This thermal impedance matrix can be stored and reused, hence reducing computation time in multiple simulations. Thus the thermal network, i.e. the thermal impedance matrix represented by the impedance of a N -port element is set up before simulation like an electrical network. Now the thermal and electrical network can be solved simultaneously, where the relation of the thermal network is given by Equation 2.32. Thus the nonlinear dynamic thermal subsystem is represented by a reduced-order compact thermal model with a set of algebraic equations.

Prior to this work a customized thermal impedance matrix for a homogenous subvolume in a homogenous thermal subsystem was implemented in *fREEDA*TM. In this work the generic thermal impedance matrix for the homogenous subvolume in a heterogenous

Table 2.1: MOSFET model implementation in University of California, Berkeley, UCB SPICE3f5 [69].

Number	Level 1	Level 2	BSIM3	BSIM4	BSIMSOI
If Statements	501	609	822	1495	1757
Parameters in Code	32	38	399	610	615
Intermediate Variables	56	56	430	811	972
Total Lines of Code	7,673	8,634	12,348	20,113	20,664

thermal subsystem was implemented in *fREEDA*TM. Surface metallization features and vertically matched thermal subvolumes were implemented and verified for the first time in *fREEDA*TM, a general purpose circuit simulator.

2.5 Compact Electrothermal Modeling

This section discusses the difficulties involved in the cumbersome device model development strategies in conventional circuit simulators. In this work, a simplified approach to develop an electrothermal device model is used. The key features of this approach are presented here.

The most significant building block to designing mixed-signal integrated circuits (ICs) is the availability of well tested and high accuracy semiconductor device models for various IC processes. At present BSIM3 remains an industry standard, but the enormous amount of time spent on research and development of the model, has developed a need for standard model development techniques and sophisticated modeling tools. Table 2.1 shows the level of difficulty and complexity involved in the developing various MOSFETs models in cumbersome and an error-prone strategy of model development in SPICE-like simulators [69].

Complete manual implementation of the model has become increasingly difficult. Along with the difficulties in model development, difficulties in model debugging, testing, profiling and maintaining have exacerbated too. Compact modeling tools like automatic model generators, compact model compilers, or tools which use symbolic or automatic differentiation seem to be the solution to this problem [73]. Compact model compilers like MCAST [69] and ADMS [70] have shown promising results. These tools accept high-level behavioral descriptions in the VHDL-AMS or Verilog-AMS languages, apply several auto-

matic code generation processes to develop low-level C/C++ device source code for the requested device model. This model can then be compiled and linked to a target simulator. If the target simulator uses standard model development techniques or standard formats to code the device equations, the compact model compilers can develop efficient and optimized device model source codes for the target simulator. The use of state-variables and automatic differentiation in *fREEDA*TM greatly facilitates this standard format to code the device equations and hence tools like Paragon can capture the high level model description of the device model. This model description is processed by the compact model compiler ADMS, to generate low-level C++ device model source code for *fREEDA*TM [70]. This process lowers the barrier of introducing a new device model into the circuit simulator.

2.5.1 The Chain Rule in Derivative Evaluation

One of the biggest error prone step of manually evaluating and hand coding the derivatives is eliminated with the use of automatic differentiation. Many device equations in a model are dependent on a variable, which is in turn dependent on many other variables. For example in the BSIM3 model many equations are dependent on V_{gsteff} , which itself is dependent on V_{gs} , V_{ds} and V_{bs} . Hence any equation dependent on V_{gsteff} should have three partial derivatives evaluated. Sometimes all these three derivatives are not calculated upfront and are forgotten leading to an model with errors. The chain rule is then completed at the end of the source code after few debugging rounds. Each time any of these dependent equations must be modified to add a new parameter, all the necessary partial derivatives must be evaluated and hand coded. These derivatives are harder to verify and effectively almost every compact model has a derivative error in its first release [71].

2.5.2 Simplified Device Model Development Approach

The two key features of the simplified approach used in this work to develop the electrothermal device model are: a state-variable based device model and the use of automatic differentiation.

State-Variable Based Device Model

The concept of state-variable used in this work is the one defined in [52]. The nonlinear device models are parameterized, allowing the same implementation of device equations to be used in different analysis types. The parameterized device equations are written as:

$$\mathbf{v}_{NL}(t) = u[\mathbf{x}(t), \frac{d\mathbf{x}}{dt}, \dots, \frac{d^m\mathbf{x}}{dt^m}, \mathbf{x}_D(t)] \quad (2.48)$$

$$\mathbf{i}_{NL}(t) = w[\mathbf{x}(t), \frac{d\mathbf{x}}{dt}, \dots, \frac{d^m\mathbf{x}}{dt^m}, \mathbf{x}_D(t)]. \quad (2.49)$$

These device equations translate well understood device physics into controlled charge and current sources and provide the circuit designer all manifestations of device design. After selecting the state-variables, the model developer must code the nonlinear device voltage and nonlinear device current equations in the above format. In the circuit analysis technique formulation, the above equation is linearized using the Newton Raphson technique. The Newton Raphson technique requires the Jacobian of the nonlinear device voltages and nonlinear device currents to be computed. These Jacobians are computed by automatic differentiation. The model developer does not need to linearize the device model to develop the equivalent linear circuit stamp. Hence no internal device nodes need to be added.

Automatic Differentiation

In *fREEDA*TM the analytic Jacobian is calculated using Adol-C [74]. This is a software package written in C and C++ and performs automatic differentiation. The numerical values of the derivative vectors (required to fill the Jacobians) are obtained free of truncation errors at a small multiple of the run time required to evaluate the original function with little additional memory required. The implementation of automatic differentiation in *fREEDA*TM is shown in Figure 2.5. The `eval()` method of the nonlinear element class is executed at initialization time and so the operations to calculate the currents and voltages of each element are recorded by Adol-C in a tape which is actually an internal buffer. After that, each time that the values or the derivatives of the nonlinear elements are required, an Adol-C function is called and the values are calculated using the tapes. This implementation is efficient because the taping process is done only once (this almost

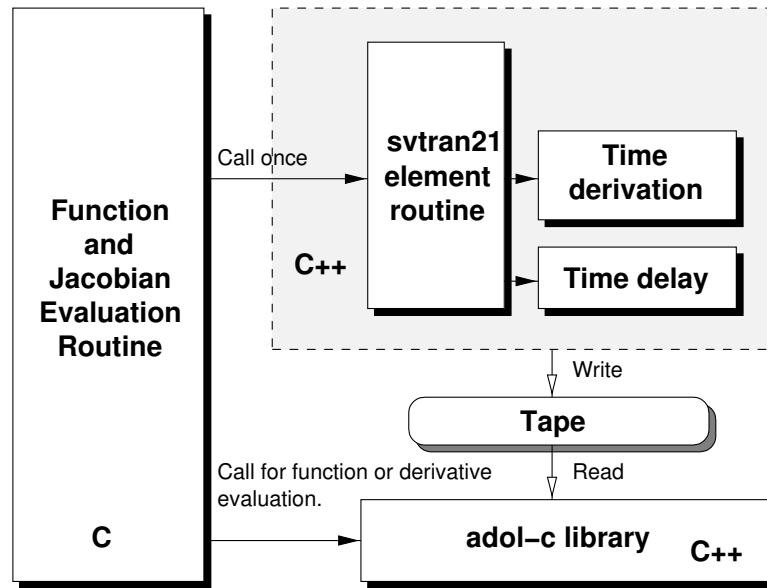


Figure 2.5: Automatic Differentiation in *fREEDA*[™]. After [52].

doubles the speed of the calculation compared to the case where the functions are taped each time they are needed). The advantage in terms of rapid model development is significant. The majority of the development time in implementing models in simulators, is in the manual development of the derivative equations. Unfortunately the determination of derivatives using numerical differences is not sufficiently accurate for any but the simplest circuits. With Adol-C, full analytic accuracy is obtained and the implementation of non-linear device models is dramatically simplified. Note that time differentiation, time delay and transformations are left outside the automatic differentiation block. The calculation speed achieved is approximately ten times faster than the speed achieved by including time differentiation, time delay and transformations inside the block.

These two key features of the simplified approach for device model development reduces the burden of the model developer of handling the various implementation details specific to the simulator. The model developer does not have worry about numerous things, like matrix stamping, loading the Jacobian-matrix and the right-hand-side, evaluating and manually hand coding the derivatives of the various dependent variables. Every flavor of the SPICE-like simulators, would implement the above items slightly differently, forcing the model developer to gain knowledge about the intricacies of the simulators. This approach,

automatically computes the Jacobian values and inserts them into the Jacobian matrix, so that the model developer can concentrate on developing the model equations and model behavior, since finally the accuracy of the model is determined by the accuracy of the equations used to capture the model behavior.

The automatic differentiation library keeps track of all the dependent equations, the parameters they depend on, and evaluates the necessary partial derivatives. This results in a model free of derivative errors, and making addition of new parameters is greatly simplified. This helps in rapid development of electrothermal models, since adding the effects of temperature is easy. Temperature can be added as an independent parameter or a state-variable and equations dependent on temperature are evaluated at each time step. No extra partial derivatives with respect to temperature must be evaluated or hand coded. A good example is: self-heating effects were added to a Verilog-A model implementation of BSIM3 in two days, whereas the same addition took two weeks in a native C code [71].

The advantages of this approach can be listed as:

- The model development time is dramatically reduced facilitating rapid model prototyping
- The model source code is easier to maintain and modify.
- Human errors introduced by manually evaluating and coding complex derivatives are eliminated.

2.6 Summary

In this chapter an outline of the circuit analysis techniques used in circuit simulators is presented. A discussion of the sources of errors in the simulated results using these techniques, which limit the dynamic range of a circuit simulator is presented. The aspects of the transient analysis techniques which can be improved to increase the dynamic range of the transient analysis are also discussed. These improvements and its usage is further discussed in the Chapter 3. This high dynamic range transient analysis will be applied to study the thermal effects of an electronic circuit.

Conventional numerical thermal modeling techniques were briefly reviewed in this chapter. These techniques are too slow to be in coupled electrothermal simulations. The

theory of the faster analytical compact thermal model developed in this work was reviewed in this chapter. This thermal model will be used to build an electrothermal model of an X-band MMIC discussed in Chapter 4.

Coupled electrothermal circuit modeling is possible only with well tested compact electrothermal device models. The importance of compact electrothermal device models is presented in this chapter. Also the sources of error in a device model built with all manual coding is also presented. To eliminate these errors, automated model development is a solution. The simplified device model development approach used in this work is described in the chapter. This approach helps rapid model development and is used to develop an electrothermal BSIMSOI MOSFET model, discussed in Chapter 6.

Chapter 3

High Dynamic Range Transient Circuit Simulation

3.1 Introduction

One of the goals this chapter is presenting a method for precise transient simulation of circuits. One of the measures that can be used to define the precision of a circuit simulator is to use the dynamic range defined as the ability to resolve small sinusoidal signal in the presence of a much larger sinusoidal signal. With high dynamic range small variations of a signal from one time step to the next can be captured. In electrothermal simulations the signal variations that must be captured should be as small as $1 \mu\text{V}$ while the total signal level is 10 V or so. In addition to being a requirement for transient electrothermal simulation, high dynamic range is a requirement if transient circuit simulation is to be used in the design of communication and radar circuits.

As mentioned in the previous chapter, the accurate error estimation is critical in achieving a high dynamic range transient simulator. Imprecise estimation of error results in both early termination of iterations and improper time step selection.

The new time step control technique described in this chapter accurately provides good estimation of the error at each time point. Section 3.2 presents the formulation of the

new time step control technique. Section 3.3 presents the implementation of the new time step control in *fREEDA*TM. The accuracy of this technique is tested by a comparison of the simulated results of a simple RC circuit with an analytical solution of the simple RC circuit. The details and the results of this test are presented in Section 3.5. The dynamic range of the new technique is tested with a two-tone test performed on an X-band Gallium Arsenide (GaAs) Monolithic Microwave Integrated Circuit (MMIC) Low Noise Amplifier (LNA). The simulated results of this test are verified with electrical measurements in Section 3.6. To illustrate the advantage of the new technique over harmonic balance, a comparison between the simulated results of output voltage of the MMIC obtained by using the two techniques with a single tone input at -110 dBm is done in Section 3.6.

3.2 Time Step Control

3.2.1 Conventional Time Step Control in SPICE

As discussed in the previous chapter, numerical integration techniques used in circuit simulators introduce *LTE*. The *LTE* can be reduced by reducing the time step, h , in a transient analysis. However there are limits as using a small timestep introduces round-off errors. It is important to use the largest time step compatible with the acceptable tolerance on error. Some of the numerical integration techniques are predictor-corrector techniques, which need the derivative of solution at the next time point to predict the solution at the next time point. Such techniques use an educated initial guess at the next time point as the predicted value of the solution at the next time point and solve the nonlinear equation iteratively until convergence is achieved. This prediction is made based on the information known so far. SPICE uses the Forward Euler Formula to predict the solution at the next time point. As discussed in the previous chapter the Forward Euler Formula is a linear extrapolation and does not provide a good initial guess for highly nonlinear RF circuits since it is based purely on past history [11]. The *LTE* estimated as the difference between the linearly extrapolated initial guess and the solution following the Newton iteration is large and results in unnecessary cuts in the time step, h .

3.2.2 New Time Step Control Technique

The unnecessary reductions in the time step, h in the conventional time step control technique can be eliminated if the initial guess at the new time point is predicted better.

The Backward Euler Formula is a predictor-corrector method. It uses information at the previous time point and the current time point to find the solution at the current time point. In the new time step control technique the converged solution of the previous time point is used as the initial guess for its next time point. A Backward Euler Formula is applied to this value to calculate the derivative at the next time point. On convergence of the nonlinear iteration the solution obtained is the new predicted initial guess for the Trapezoidal Rule. The derivatives are calculated again with the Trapezoidal Rule followed by the nonlinear iteration until convergence is achieved. The solution obtained from this nonlinear iteration is the final solution at the time point. The difference between the final Trapezoidal Rule solution and the Backward Euler solution is the estimated *LTE*. The value of the next time step, is predicted by:

$$t_{\mathbf{f}} = t_{\mathbf{old}} * \frac{\sqrt{TRTOL * (\mathbf{max}(|x_{tr}|, |x_{be}|) * RELTOL + ABSTOL)}}{LTE} \quad (3.1)$$

where, $t_{\mathbf{f}}$ is the new time step, $t_{\mathbf{old}}$ is the old time step, x_{be} is the voltage/current predicted by Backward Euler Integration and x_{tr} is the voltage/current calculated using Trapezoidal Rule. The predicted value between the nonlinear iterations cannot change more than *RELTOL* percent of the final value. *ABSTOL* complements *RELTOL* at zero crossings, where the relative tolerance goes to zero, making the solution to be infinitely accurate. The new time step is inversely proportional to the current *LTE*.

The Backward Euler and Trapezoidal Integrations are both predictor-corrector techniques. In this approach the prediction-correction steps are applied twice. The accuracy of the Newton Raphson iteration depends on the initial guess. Since Backward Euler Formula does not entirely depend on past history, its solution is more accurate than Forward Euler Formula in highly nonlinear circuits where the voltage levels are changing rapidly. At troughs and crests of the sinusoid the Backward Euler Formula uses the information at the current and past time points, hence it makes a better prediction than a linear extrapolation. This solution if used as the initial guess for the Trapezoidal Rule, a more accurate initial guess than the Forward Euler Formula is provided. As the initial guess and the final solution

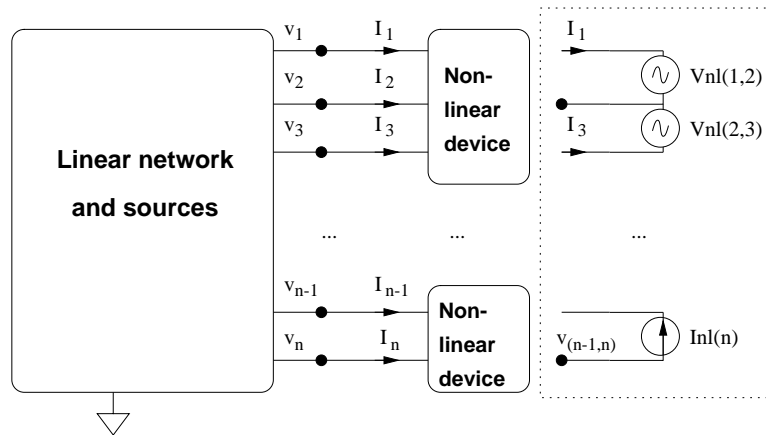


Figure 3.1: Network with nonlinear elements. After [15]. (Copyright IEEE 2006)

are predicted and corrected, the estimated *LTE* is precise and smaller. The smaller value of *LTE* eliminates the unnecessary cut in time steps. In sinusoidal circuits this technique results in larger and fewer time steps without any loss in accuracy. The predicted-corrected initial guess of the this algorithm helps it follow curves with less time points.

3.3 Implementation of the New Time Step Control Technique in *fREEDA*TM

This section describes the general formulation of the nonlinear equations used by the new time step control technique in *fREEDA*TM. Details of the implementation of the new time step control technique are explained in Section 3.4.

3.3.1 Nonlinear Equation Formulation *fREEDA*TM

The new time step control technique explained in the previous section was implemented in a state-variable based multi-domain circuit simulator *fREEDA*TM. The formulation of the system equations begins with the partitioned network of Figure 3.1 with the nonlinear elements replaced by variable voltage or current sources [15]. For each nonlinear element one terminal is taken as the reference and the element is replaced by a set

of sources connected to the reference terminal. Both voltage and current sources are valid replacements for the nonlinear elements, but current sources are more convenient because they yield a smaller modified nodal admittance matrix (MNAM).

Linear Network

The MNAM of the linear subcircuit is formulated as follows. Define two matrices \mathbf{G} and \mathbf{C} of equal size n_m , where n_m is equal to the number of non-reference nodes in the circuit plus number of additional required variables [13]. Define a vector \mathbf{s} of size n_m for the right hand side of the system. The contributions of the fixed sources and the nonlinear elements (which depend on the time t) will be entered in this vector. All conductors and frequency dependent MNAM stamps arising in the formulation will be entered in \mathbf{G} , whereas capacitors and inductor values and other values that are associated with dynamic elements will be stored in matrix \mathbf{C} . The linear system obtained is the following:

$$\mathbf{G}\mathbf{u}(t) + \mathbf{C}\frac{d\mathbf{u}(t)}{dt} = \mathbf{s}(t), \quad (3.2)$$

where \mathbf{u} is the vector of the nodal voltages and required currents, and \mathbf{s} is composed of an independent component s_f and a component s_v that depends on the state-variables, as in the Harmonic Balance case [15]. Now,

$$\mathbf{s}(t) = s_f(t) + s_v(t). \quad (3.3)$$

where the s_f vector is due to the independent sources in the circuit. The s_v vector is the contribution of the currents injected into the linear circuit by the nonlinear network.

Nonlinear Network

The concept of state-variable used in this work is the one defined in [52]. The equations are rewritten here for convenience:

$$\mathbf{v}_{NL}(t) = u[\mathbf{x}(t), \frac{d\mathbf{x}}{dt}, \dots, \frac{d^m\mathbf{x}}{dt^m}, \mathbf{x}_D(t)] \quad (3.4)$$

$$\mathbf{i}_{NL}(t) = w[\mathbf{x}(t), \frac{d\mathbf{x}}{dt}, \dots, \frac{d^m\mathbf{x}}{dt^m}, \mathbf{x}_D(t)]. \quad (3.5)$$

where $\mathbf{v}_{NL}(t)$, $\mathbf{i}_{NL}(t)$ are vectors of voltages and currents at the common ports, $\mathbf{x}(t)$ is a vector of state-variables and $\mathbf{x}_D(t)$ a vector of time-delayed state-variables, i.e., $\mathbf{x}_{D_i}(t) = x_i(t - \tau_i)$. The time delays τ_i may be functions of the state-variables. The error function of an arbitrary circuit is developed using connectivity information (described by an incidence matrix and constitutive relations describing the nonlinear elements). The incidence matrix, \mathbf{T} , is built as follows. The number of columns is n_m , and the number of rows is equal to the number of state-variables, n_s . In each row, enter “+1” in the column corresponding to the positive terminal of the row nonlinear element port and “-1” in the column corresponding to the negative terminal (the local reference of the port). Then, each row of \mathbf{T} has at most 2 nonzero elements and the number of nonzero elements is at most $2n_s$.

The following equations are true for all t :

$$\mathbf{v}_L(t) = \mathbf{T}\mathbf{u}(t) \quad (3.6)$$

$$\mathbf{s}_v(t) = \mathbf{T}^T \mathbf{i}_{NL}(t) \quad (3.7)$$

where $\mathbf{v}_L(t)$ is the vector of the port voltages of the nonlinear elements calculated from the nodal voltages of the linear network.

Error Function Formulation

Now we have all the equations necessary to build a nonlinear error function for the entire circuit. Combining Equations (3.2), (3.3) and (3.7), the general equation for the linear network is obtained:

$$\mathbf{G}\mathbf{u}(t) + \mathbf{C} \frac{d\mathbf{u}(t)}{dt} = \mathbf{s}_f(t) + \mathbf{T}^T \mathbf{i}_{NL}(t). \quad (3.8)$$

The reduced error function $\mathbf{f}(t)$ is defined as follows

$$\mathbf{f}(t) = \mathbf{v}_L(t) - \mathbf{v}_{NL}(t) = 0. \quad (3.9)$$

Replacing $\mathbf{v}_L(t)$ from Equation (3.6)

$$\mathbf{f}(t) = \mathbf{T}\mathbf{u}(t) - \mathbf{v}_{NL}(t) = 0. \quad (3.10)$$

Equations (3.4), (3.5), (3.8) and (3.9) confirm the generalized state-variable reduction formulation. The error function in Equation (3.9) only depends on the state-variables and the time derivatives:

$$\mathbf{f} \left[\mathbf{x}(t), \frac{d\mathbf{x}}{dt}, \dots, \frac{d^m \mathbf{x}}{dt^m}, \mathbf{x}_D(t) \right] = 0. \quad (3.11)$$

The dimension of the error function and the number of unknowns are equal to n_s , and this number is the minimum necessary to solve the equations of a circuit without any loss of information. To reduce the error function formulation the differential equations in an algebraic system of nonlinear equations are converted to nonlinear algebraic systems using time marching integration methods.

First Equations (3.4) and (3.5) are expressed using discretized time

$$\mathbf{v}_{NL}(\mathbf{x}_n) = u[\mathbf{x}_n, \mathbf{x}'_n, \dots, \mathbf{x}_n^{(m)}, \mathbf{x}_{D,n}] \quad (3.12)$$

$$\mathbf{i}_{NL}(\mathbf{x}_n) = w[\mathbf{x}_n, \mathbf{x}'_n, \dots, \mathbf{x}_n^{(m)}, \mathbf{x}_{D,n}] \quad (3.13)$$

where $\mathbf{x}_n = \mathbf{x}(t_n)$, $\mathbf{x}'_n = \mathbf{x}'(t_n)$, $(\mathbf{x}_{D,n})_i = \mathbf{x}_i(t_n - \tau_i)$ and t_n is the current time. Discretization of Equation (3.8) yields

$$\mathbf{G}\mathbf{u}_n + \mathbf{C}\mathbf{u}'_n = s_{f,n} + \mathbf{T}^T \mathbf{i}_{NL}(\mathbf{x}_n). \quad (3.14)$$

The time marching integration approximation used is given by,

$$x'_n = ax_n + b_{n-1} \quad (3.15)$$

where a is a constant and b_{n-1} depends on previous history of x . Applying this equation to calculate the \mathbf{u}'_n vector gives,

$$\mathbf{u}'_n = a\mathbf{u}_n + \mathbf{b}_{n-1} \quad (3.16)$$

where \mathbf{b}_{n-1} has the same dimension as \mathbf{u}_n . Replacing \mathbf{u}'_n in Equation (3.14),

$$\mathbf{G}\mathbf{u}_n + \mathbf{C}[a\mathbf{u}_n + \mathbf{b}_{n-1}] = s_{f,n} + \mathbf{T}^T \mathbf{i}_{NL}(\mathbf{x}_n). \quad (3.17)$$

The size of the resulting algebraic system of nonlinear equation is n_s .

Sparse Matrix Formulation

The solution to these nonlinear algebraic equations is transformed in the successive solution of a sequence of linear circuits. This successive solution to calculate the $\mathbf{i}_{NL}(\mathbf{x}_n)$ vector and the $\mathbf{v}_{NL}(\mathbf{x}_n)$ is introduced by applying Newton Raphson technique,

$$x^{j+1} = x^j - [\mathbf{J}(x^j)]^{-1} f(x^j) \quad (3.18)$$

where $\mathbf{J}(x)$ is the Jacobian of $f(\mathbf{x})$. Hence

$$\mathbf{i}_{NL}(\mathbf{x}_n^{(j+1)}) = \mathbf{i}_{NL}(\mathbf{x}_n^j) + \mathbf{J}_i[\mathbf{x}_n^{(j+1)} - \mathbf{x}_n^j] \quad (3.19)$$

$$\mathbf{v}_{NL}(\mathbf{x}_n^{(j+1)}) = \mathbf{v}_{NL}(\mathbf{x}_n^j) + \mathbf{J}_v[\mathbf{x}_n^{(j+1)} - \mathbf{x}_n^j]. \quad (3.20)$$

Replacing $\mathbf{i}_{NL}(\mathbf{x}_n)$ in Equation (3.17) results in,

$$[\mathbf{G} + \mathbf{C}a]\mathbf{u}_n^{(j+1)} - \mathbf{T}^T \mathbf{J}_i \mathbf{x}_n^{(j+1)} = [s_{f,n} - \mathbf{C}a\mathbf{b}_{n-1}] + \mathbf{T}^T [\mathbf{i}_{NL}(\mathbf{x}_n^j) - \mathbf{J}_i \mathbf{x}_n^j]. \quad (3.21)$$

Replacing $\mathbf{v}_{NL}(\mathbf{x}_n)$ in Equation (3.10) results in,

$$\mathbf{T}\mathbf{u}_n^{(j+1)} - \mathbf{v}_{NL}(\mathbf{x}_n^j) - \mathbf{J}_v[\mathbf{x}_n^{(j+1)} - \mathbf{x}_n^j] = 0. \quad (3.22)$$

From Equation (3.21) and Equation (3.22) it can be seen that there are two equations and two unknowns, $\mathbf{u}_n^{(j+1)}$ and $\mathbf{x}_n^{(j+1)}$. These equations can be solved simultaneously. Since all the quantities in the two equations are vectors or matrices, they can be put together giving a matrix equation of the form $\mathbf{A}\mathbf{x} = \mathbf{B}$, where \mathbf{A} is the coefficient matrix, \mathbf{x} is the vector of unknown quantities and \mathbf{B} is the right hand side matrix.

Combining Equation (3.21) and Equation (3.22) results in,

$$\begin{pmatrix} [\mathbf{G} + \mathbf{C}a] & -[\mathbf{T}^T \mathbf{J}_i] \\ \mathbf{T} & -\mathbf{J}_v \end{pmatrix} \begin{pmatrix} \mathbf{u}_n^{(j+1)} \\ \mathbf{x}_n^{(j+1)} \end{pmatrix} = \begin{pmatrix} [s_{f,n} - \mathbf{C}a\mathbf{b}_{n-1}] & +\mathbf{T}^T [\mathbf{i}_{NL}(\mathbf{x}_n^j) - \mathbf{J}_i \mathbf{x}_n^j] \\ \mathbf{v}_{NL}(\mathbf{x}_n^j) & -\mathbf{J}_v \mathbf{x}_n^j \end{pmatrix} \quad (3.23)$$

From the above Equation it can be seen that an equivalent linear circuit is formed for every nonlinear element. The circuit is only equivalent to the nonlinear element at the j^{th} iteration because its element values (but not its topology) change by discrete amounts at every iteration. This circuit is repeatedly solved with updated element values till convergence is achieved.

In the above Equation the following observations can be made:

- Matrix $\mathbf{G} + \mathbf{C}a$ is sparse
- Matrix \mathbf{T} is sparse
- Matrices \mathbf{J}_i and \mathbf{J}_v are sparse and block diagonal

Hence the matrix \mathbf{A} thus formed is sparse. The above Equation can be solved using LU factorization technique [16]. After solving Equation (3.23), the value of the state-variable vector and \mathbf{u}_n is known, so finding v_{NL} and i_{NL} is straightforward.

The size of the resulting algebraic system of linear equations is $(n_m+n_s) \times (n_m+n_s)$. $\mathbf{G} + \mathbf{C}a$ is constant as long as the time step h is constant. \mathbf{T} is constant. The right hand side vectors, \mathbf{J}_i and \mathbf{J}_v change at every Newton iteration and every time step. Thus with every iteration the equivalent circuit of every element remains same, as the topology remains the same, but the values of the elements in the equivalent circuit change by discrete amounts at every iteration.

This formulation of the linear algebraic equations is used by the new time step control technique described in the next section.

3.4 Algorithm of the New Time Step Control Technique

The previous section described the general formulation of the linear algebraic equations solved at every time step and every Newton iteration. The matrices in Equation (3.23) must be updated depending on whether a Newton Raphson iteration is performed or the time step has changed. The general flow of the new time step control technique is shown in Figure 3.2 and was implemented in *fREEDA*TM.

Step 1: After the netlist is parsed and the incidence matrix \mathbf{T} , is created, the Time-Domain MNAM ($\mathbf{G} + \mathbf{aC}$) in Equation (3.23), of the linear network is created using the package *Sparse 1.3* [16]. This MNAM is constant as far as the time step h is constant. If the time step h has changed, this matrix must be updated since $a = \frac{1}{h}$ has changed.

Step 2: The initial guess of the state-variable vector x is set to the final solution at the previous accepted time point. If $t = 1 \times h$, x is set to zero.

Step 3: The nonlinear voltage vector v_{NL} is evaluated using the value of the state-variable vector x . After that, the Jacobians \mathbf{J}_i and \mathbf{J}_v are created for every nonlinear element. The Jacobians are calculated using the package *Adol-C*. To calculate the Jacobians different

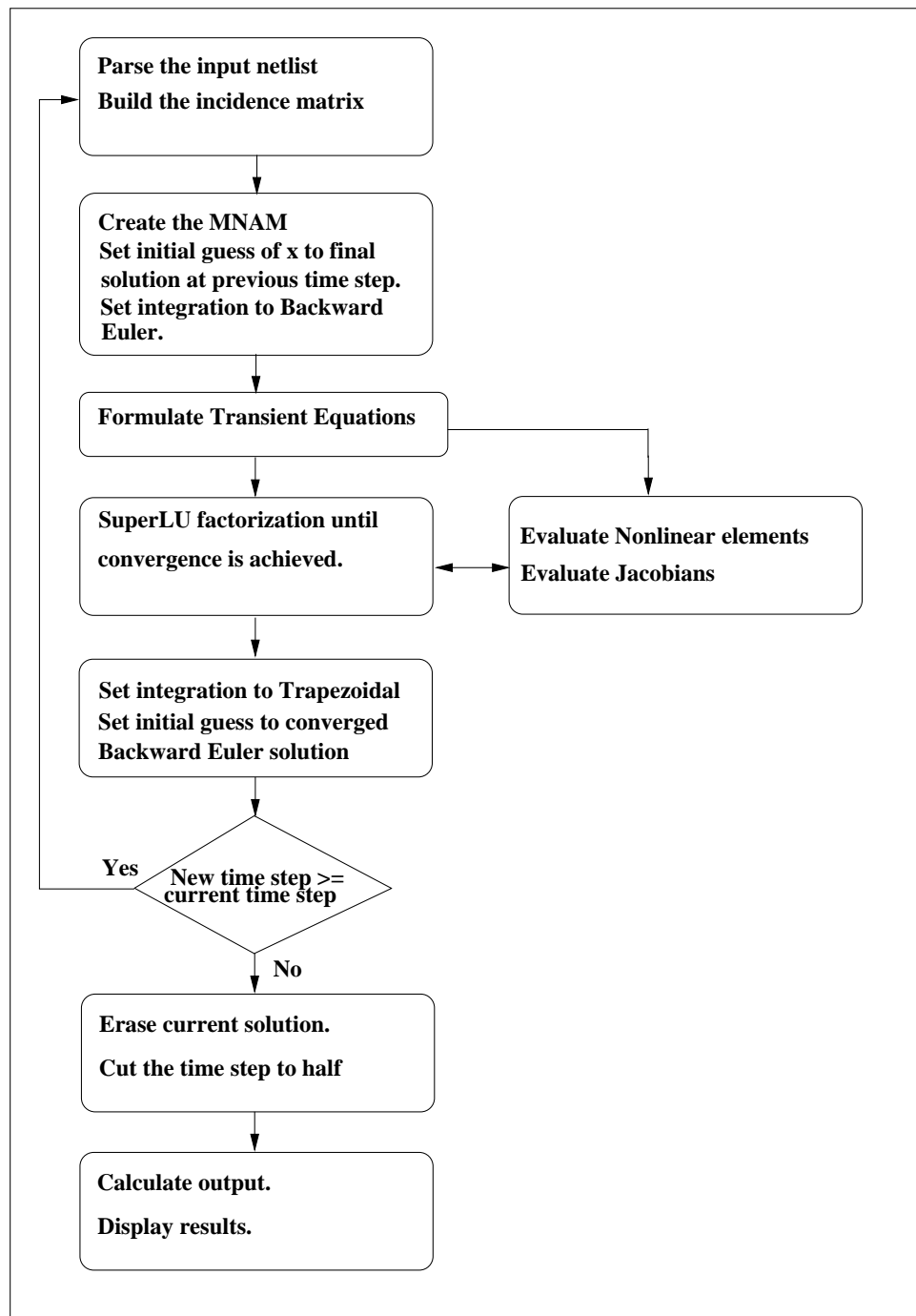


Figure 3.2: General flow diagram of the new time step control technique.

integration methods to calculate the time derivatives can be used. There is an interface class that links the analysis class to the ADOL-C library. This interface class is notified about which integration method, i.e. Backward Euler or Trapezoidal rule, must be used to calculate the time derivatives. For the first time the Backward Euler Formula is used.

Step 4: The external sources' vector s_f is then formulated for the current time step. With all these vectors the left hand side and the right hand side matrices in Equation (3.23) are formulated. This system is solved using the LU factorization package *SuperLU*¹.

Step 5: The values of the state-variables \mathbf{x}_n and nodal voltages \mathbf{u}_n are compared to those obtained from the previous Newton iteration, to check for convergence. If convergence is not achieved Steps 3 to 5 are repeated with these new values of state-variables \mathbf{x}_n and nodal voltages \mathbf{u}_n .

Step 6: If convergence is achieved, the integration technique is changed to Trapezoidal rule. The state-variable vector x is set to the converged solution obtained using the Backward Euler formula. Steps 3 to 5 are repeated with the Trapezoidal Rule until convergence is achieved.

Step 7: If convergence is achieved from the Trapezoidal rule the new time step is calculated by Equation 3.1.

Step 8: If the new time step is more than or equal to the current time step, the converged solution at the current time point is saved and this time point is accepted. The time step h is changed to this new time step. The simulation time point is incremented by h from the current time point. If the time step h has changed Steps 1 to 7 are repeated or else Steps 2 to 7 are repeated.

Step 9: If the new time step is less than 90% of the current time step, the time step h is cut into half. The converged solution at the current time point is erased. The simulation time point is incremented by this cut time step h , from the previous time step. Steps 1 to 8 are repeated with this new time step at this time point.

Once the equations are solved for all time steps, the requested currents and voltages are saved in files. The results are displayed using *gnuplot*. All the graphs requested in the input netlist are plotted.

¹<http://crd.lbl.gov/xiaoye/SuperLU/>

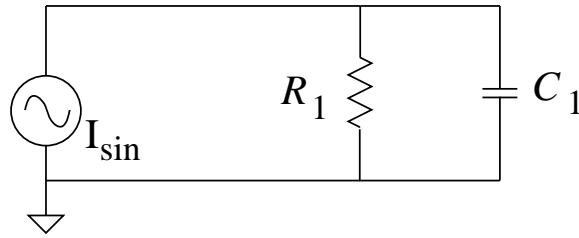


Figure 3.3: Simple RC circuit with a sinusoidal signal source.

Table 3.1: Comparison of the number of time points in a transient simulation for a specified relative tolerance ($RELTOL$) .

% $RELTOL$	Conventional Approach	New Approach	% Reduction
0.1	224	159	29.01
0.01	493	350	29.00
0.001	668	476	28.7

3.5 Accuracy Test With A Simple RC Network

The goal of the new time step control algorithm was to precisely estimate the error at each time point and to provide a more accurate initial guess at each time point. To test the effect of a more accurate initial guess on the accuracy of the new time step control technique, the simulated output voltage of a simple RC network was compared to analytical solution of the simple RC network. The input was a sinusoidal current source, and the simple RC network was simulated with a maximum time step of $0.1 \mu s$ and $10 \mu s$ simulation time [2]. The test netlist of the RC network is provided in Appendix B, Section B.1.

Figure 3.4 compares the voltage across the capacitor using the the two time step control techniques, and are in excellent agreement with the analytical solution. As expected the absolute error (difference between the analytical solution and simulated solution) introduced in the final solution reduces with the relative tolerance, $RELTOL$, as shown in Figure 3.5.

As mentioned in Section 2.2.2, if the derivatives of the solutions at every time point were known a priori, the Forward Euler Formula and the Backward Euler Formula would suffer from the same amount of LTE . But in circuit simulation, the solution at every

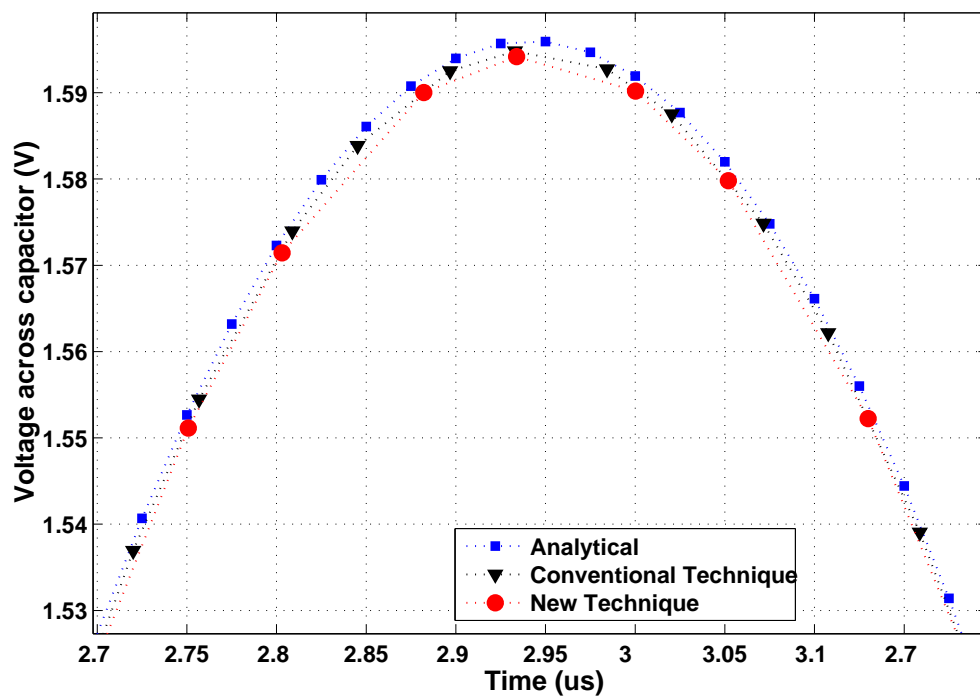


Figure 3.4: Comparison of voltage across the capacitor for the conventional and new time step control technique and the expected result derived from analytical calculations.

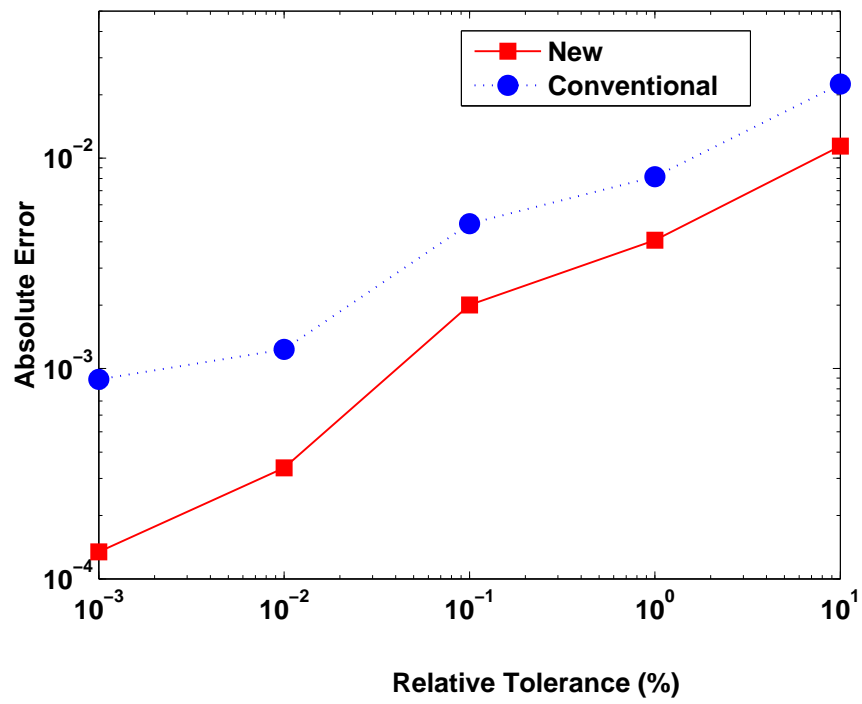


Figure 3.5: Comparison of absolute error in the voltage across the capacitor as a function of relative tolerance.

time point and so its derivative is not known a priori and must be solved. The accuracy and number of iterations of the nonlinear iterations depend on the initial guess provided. As seen in Figure 3.4, the error at every time point of the conventional technique is higher than the new time step control technique. The conventional technique uses the Forward Euler Formula to predict the initial guess at the next time point, whereas the new technique uses the Backward Euler Formula to predict the initial guess at the next time point. This predicted-corrected initial guess improves the accuracy of the solution at each time point in the sinusoidal signal. The comparison of the final solution obtained using the Trapezoidal Rule to the predicted-corrected Backward Euler initial guess reduces the local truncation error at each time point and hence eliminates the unnecessary reduction in the time step, h . Hence the new technique does not show bunching of data points at the peak of the sine wave.

At high relative tolerance the absolute error introduced by the conventional technique is approximately two times that of the new technique. At lower relative tolerance levels to maintain similar amount of tolerance as the new time step control technique, the conventional approach shows bunching of data points at the peak of the sinusoidal signal. Table 3.1 compares the total number of time points required by the two methods. The straight line extrapolation overshoots the sinusoid at every time point, resulting in a bigger *LTE*, effectively reducing the predicted time step. Whereas in the new approach, at the peak of sinusoid the predicted-corrected initial guess reduces the *LTE* and increasing the time step. The overall reduction in the number of time points is approximately 29.0%. The new time step control technique achieves better accuracy with fewer number of time points compared to the conventional time step control technique used in SPICE.

3.6 Dynamic Range Test On An X-band MMIC LNA

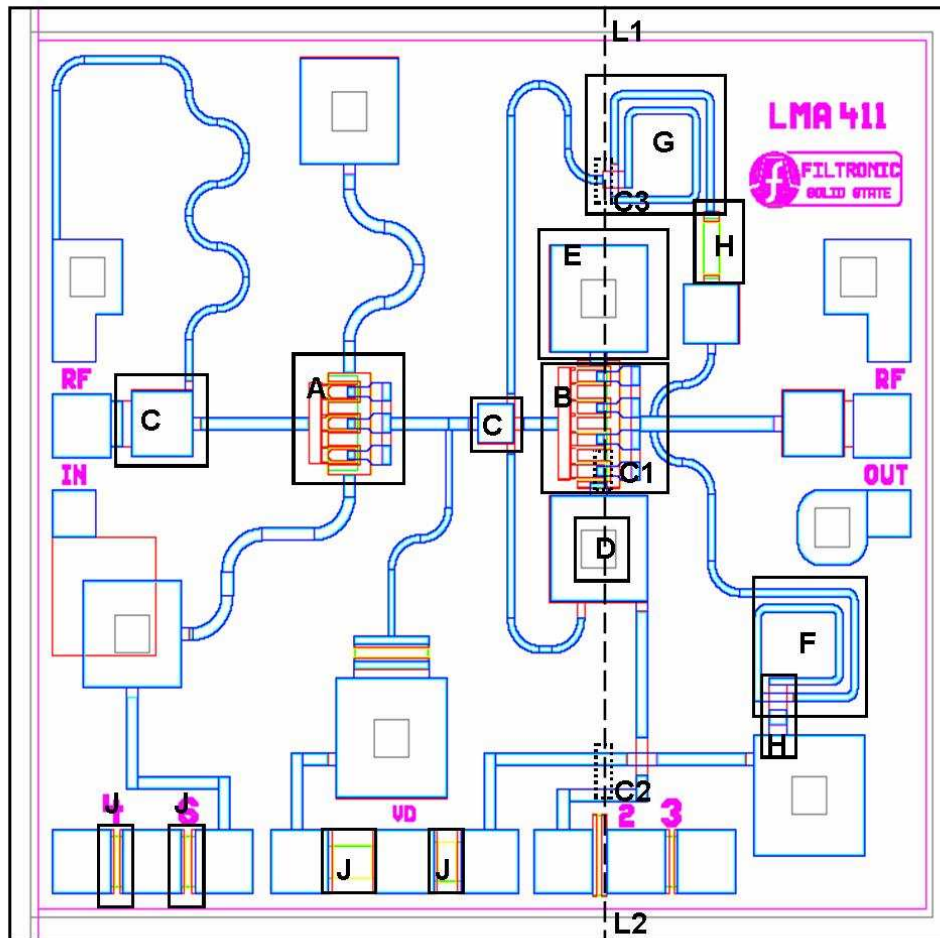
In this section the two-tone test performed on a X-band GaAs MMIC LNA to verify the dynamic range of the new time step control technique is described. A long transient simulation is performed on the MMIC to verify the time step selection criteria and the numerical robustness of the new technique. In modern communication hardware receivers are expected to be sensitive to signals as small as $1 \mu\text{V}$ at the input in the presence of a large interfering signal. Receivers are narrow band circuits and so the nonlinearity is quantified

by measuring the intermodulation distortion. This involves driving the input with two sinusoids that are in band and close to each other in frequency and then measuring the intermodulation products. In this section in the two-tone test the input power level of one of the tones is varied from -10 dBm to -110 dBm. The intermodulation products are expected to be well below -110 dBm. The ability to detect these small intermodulation products will test the dynamic range of the transient analysis.

The X-band GaAs MMIC LNA (LMA411 MMIC) used in this test was built by Filtronic Solid State. It is a high dynamic range LNA and operates from 8.5 GHz to 14 GHz. The amplifier is reactively matched at the two ports which provides a 18 dB nominal gain with a 1-dB gain compression power output of +17 dBm. It can be used as a pre-driver amplifier for phased array radar as well as in commercial communications applications.

The die is $1624 \mu\text{m} \times 1470 \mu\text{m} \times 100 \mu\text{m}$ in size. All bond pads are $100 \mu\text{m} \times 100 \mu\text{m}$. A DC supply voltage of 6 V, is applied to the MMIC. The two stage LNA consists of 2 $0.25 \mu\text{m}$ pHEMTs. Each finger of the pHEMT is $50 \mu\text{m}$ wide. Stage 1 pHEMT has 6 fingers and stage 2 pHEMT has 8 fingers. The backside of the die is gold plated. It acts a ground plane for the through vias. The die consists of two metal layers. The first metal layer is mostly Gold and is 10,750 Angstroms thick, while the second metal layer is also mostly Gold and is $3 \mu\text{m}$ thick. The capacitors use standard Silicon Nitride Si_3N_4 thickness and are nominally $600\text{pF}/\text{mm}^2$. The nitride layer was deposited after the first metal layer, and before the second metal layer, and thus the second metal layer would form the top contacts of the Metal-Insulator-Metal capacitors. There are features that require a connection between first and second metal, which is the “footing”, sort of like the foundation or support for an air bridge. After first metal layer and nitride layer have been deposited, openings are etched where the footings need to be, and second metal is then plated up over the openings and everywhere else (it is then removed where is needs to be removed). So a footing would be 1,000 Angstroms high typically (the thickness of the nitride layer). The TaN thin film resistors are 50 Ohms/square nominal. The die is passivated with a standard layer of 1,000 Angstroms of Silicon Nitride ($\epsilon_r = 7.5$).

Figure 3.6 shows a detailed layout of the X-band MMIC LNA. The physical dimensions of each of the components in the LNA were extracted from this layout [17]. Figures 3.7 – 3.20 show the images of the cuts made on the MMIC die with a Focused Ion Beam (FIB) along the line L1-L2 in Figure 3.6. These images were taken with a Scanning Electron Microscope (SEM). Three cuts were made at a 30° vertical angle along the line A-B. The



A pHEMT1 B pHEMT2 C COUPLING CAPACITORS
D VIA TO BACKSIDE METAL E VIA CAPACITORS F RF CHOKE INDUCTOR
G RF FEEDBACK SPIRAL INDUCTOR H AIR BRIDGE
I FEEDBACK NETWORK RESISTOR J DC BIAS TaN RESISTORS
L1-L2 FIB LINE C1 CUT 1 C2 CUT 2 C3 CUT 3

Figure 3.6: Layout of the X-band MMIC LNA.

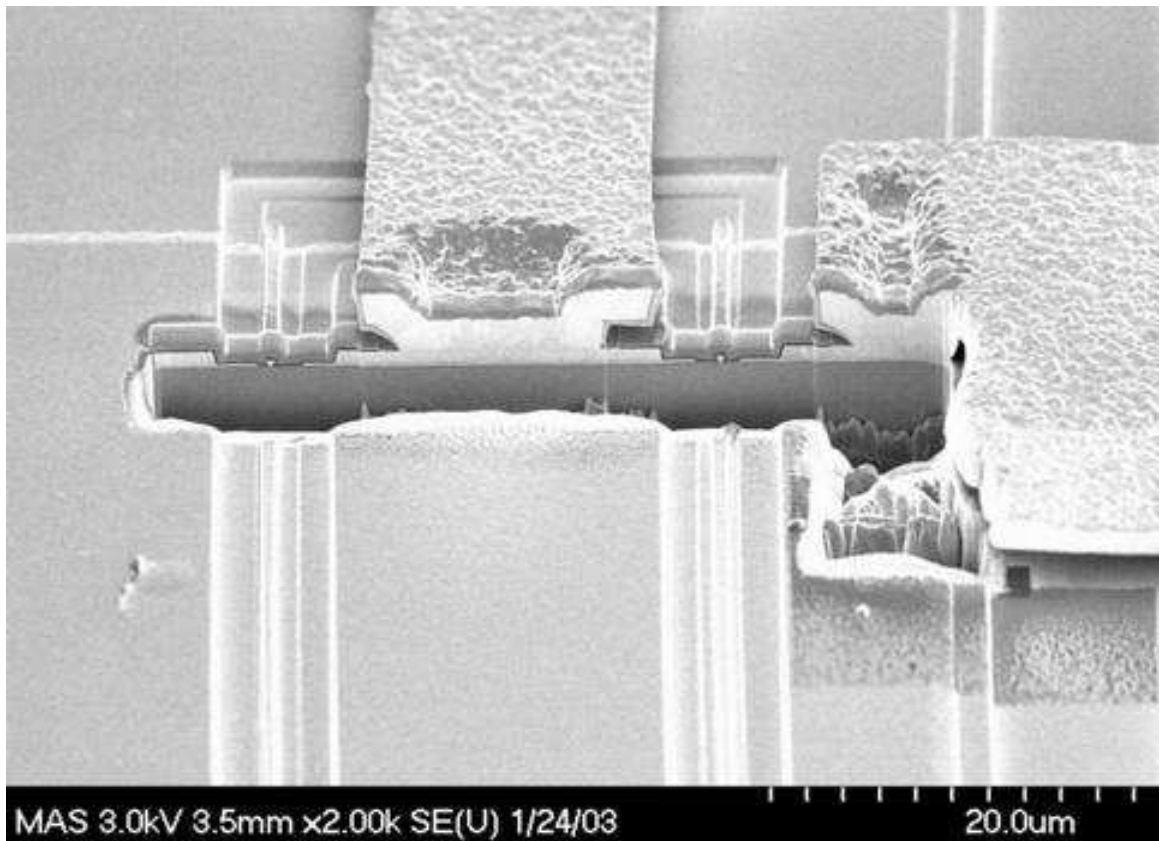


Figure 3.7: CUT 1. This image shows the 2 corner gate fingers of pHEMT2, the drain metal coming in from the top and the source metal coming in from the right hand side. This cut can be used to extract the gate-gate width, drain and source metal thickness.

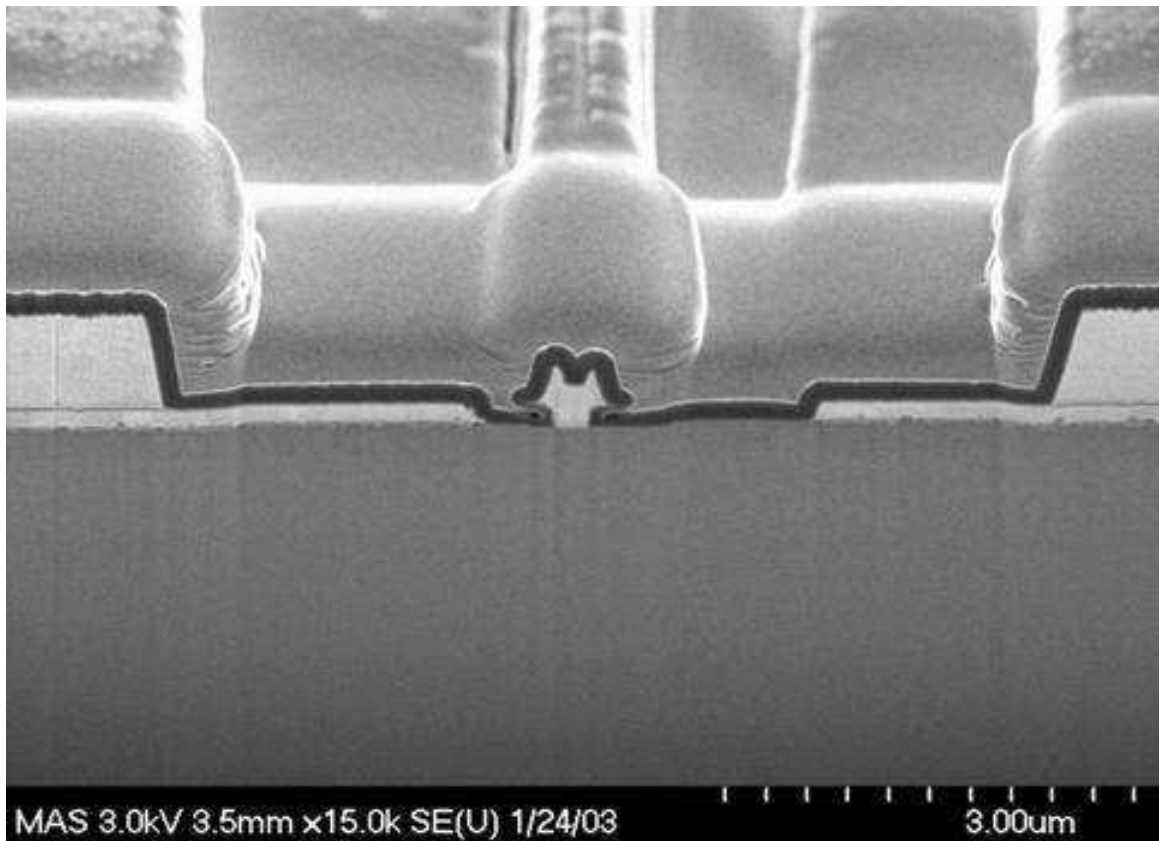


Figure 3.8: CUT 1. A zoomed image of the mushroom gate metal (light gray area). Ohmic metal contacts of the drain and source (light gray area). Thickness of the ohmic contacts can be extracted.

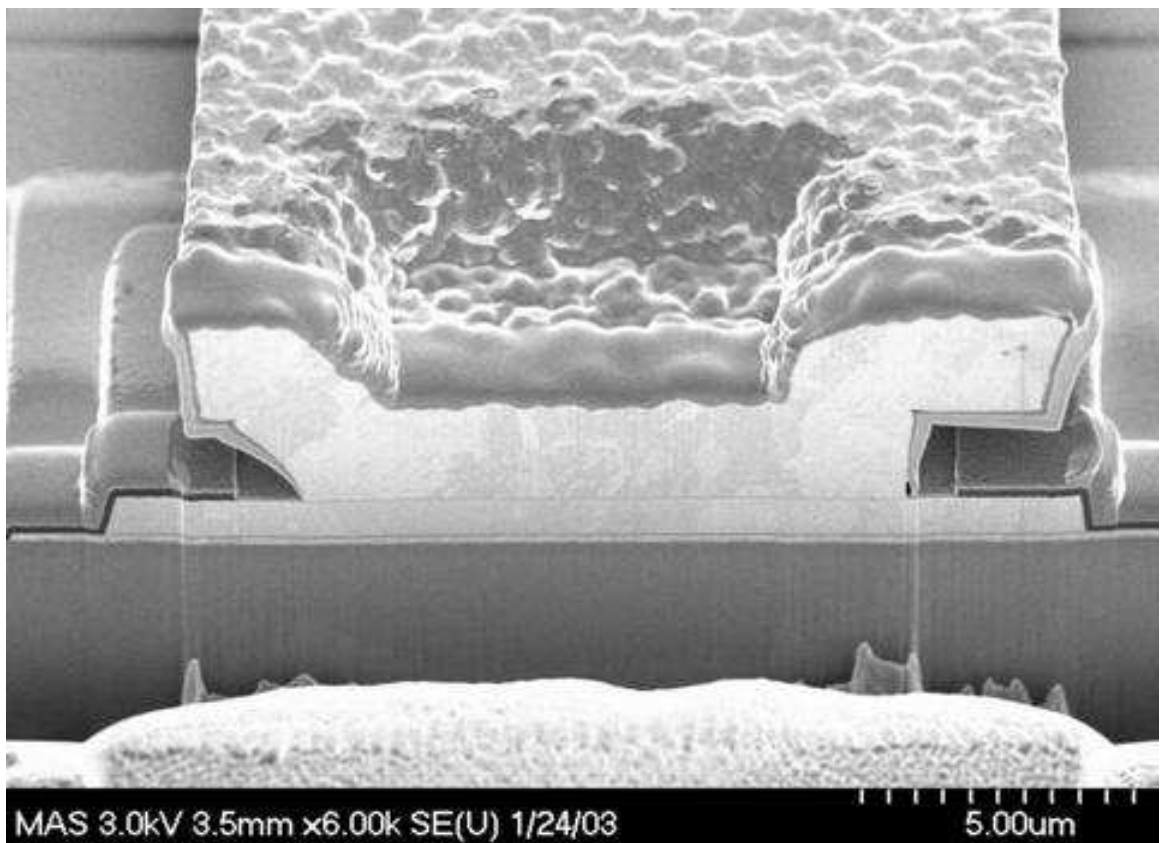


Figure 3.9: CUT 1. A zoomed image of the drain metal. Thickness of the drain metal layer can be extracted.

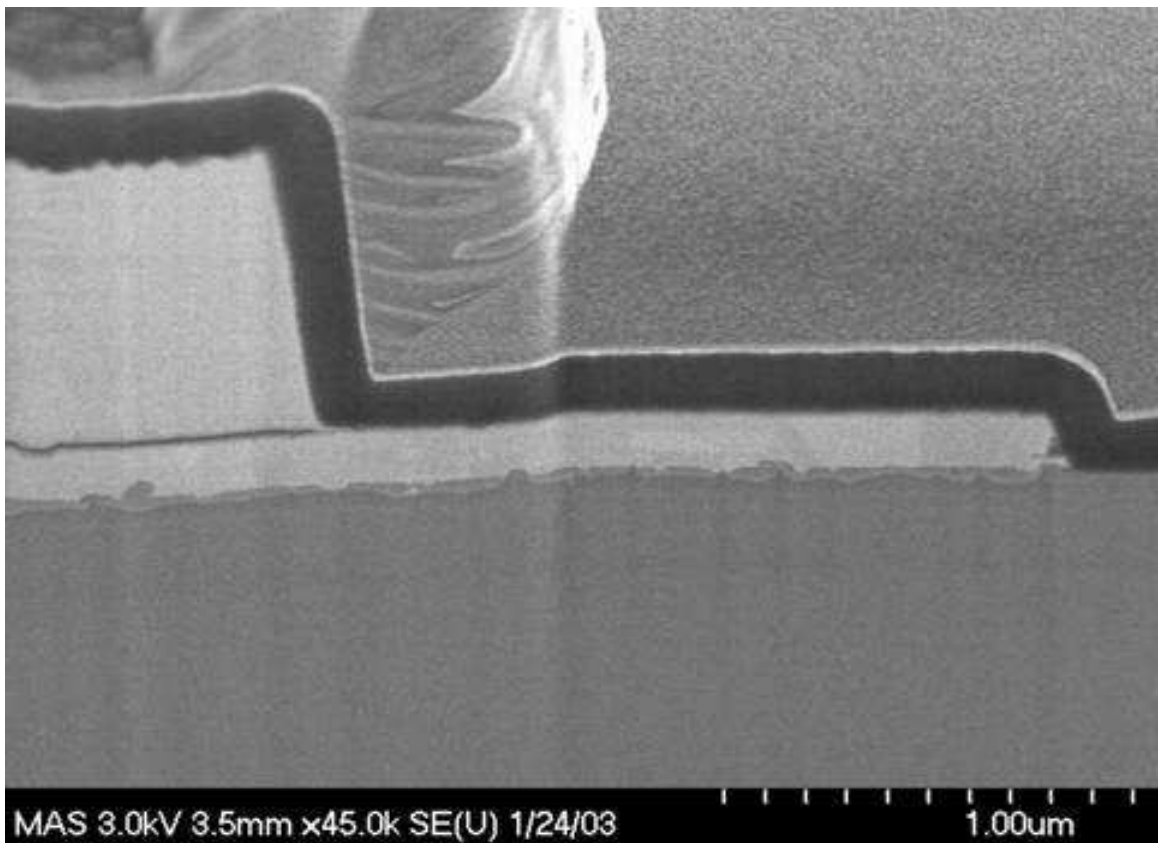


Figure 3.10: CUT 1. A zoomed image of the ohmic metal contact.

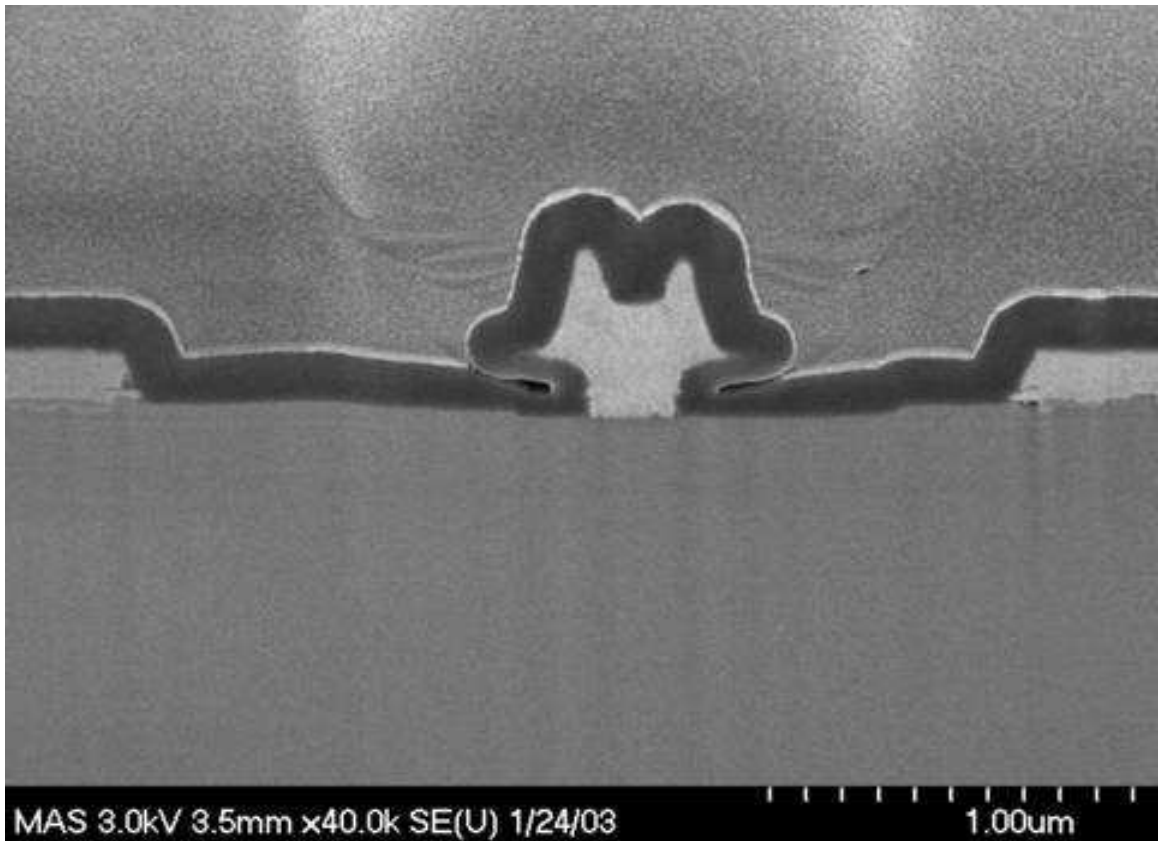


Figure 3.11: CUT 1. A zoomed image of the mushroom gate metal (light gray area).

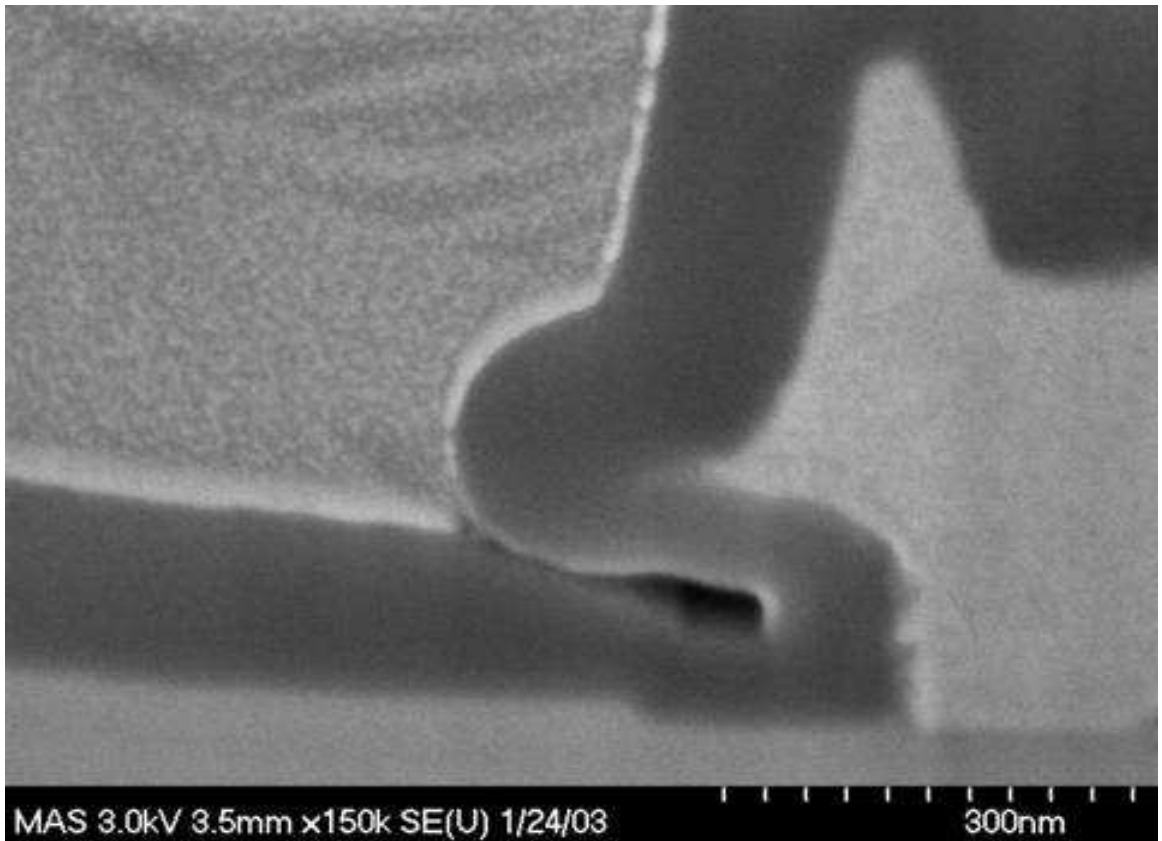


Figure 3.12: CUT 1. A zoomed image of the mushroom gate metal.

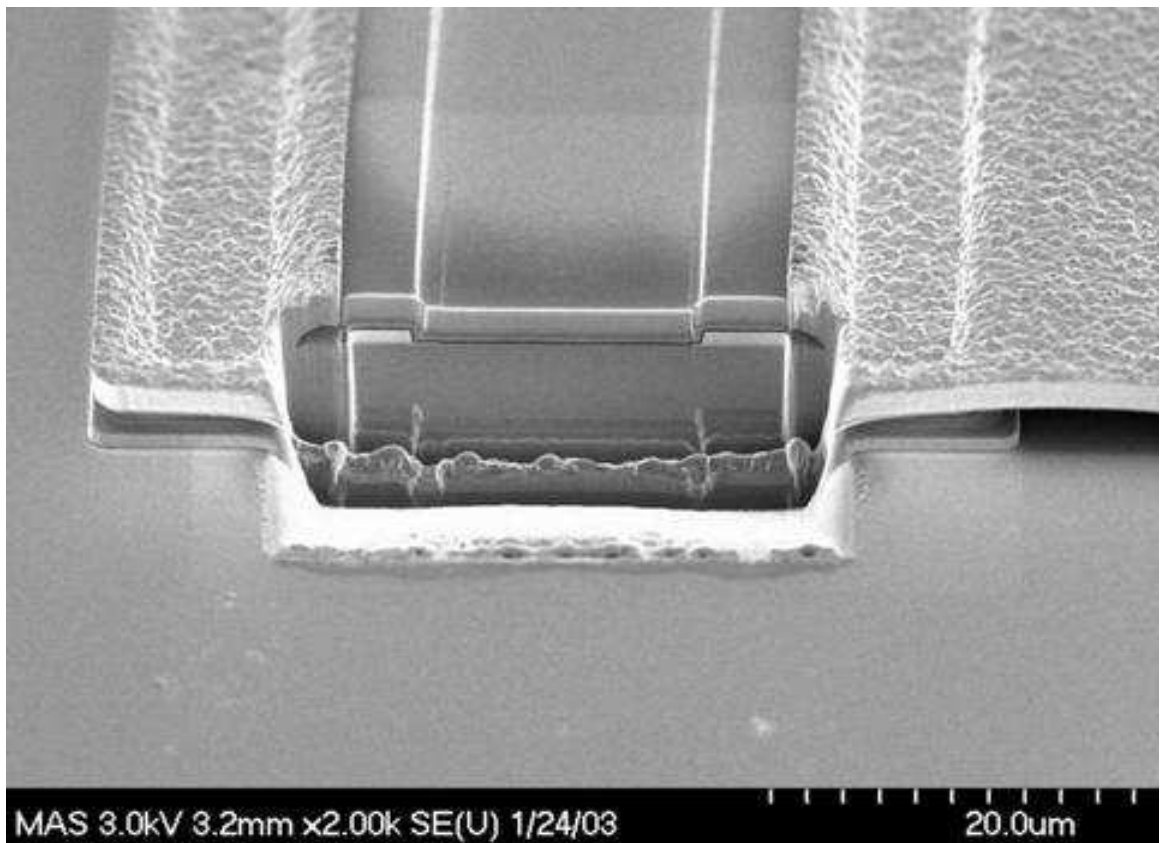


Figure 3.13: CUT 2. Image of two adjacent microstrip lines.

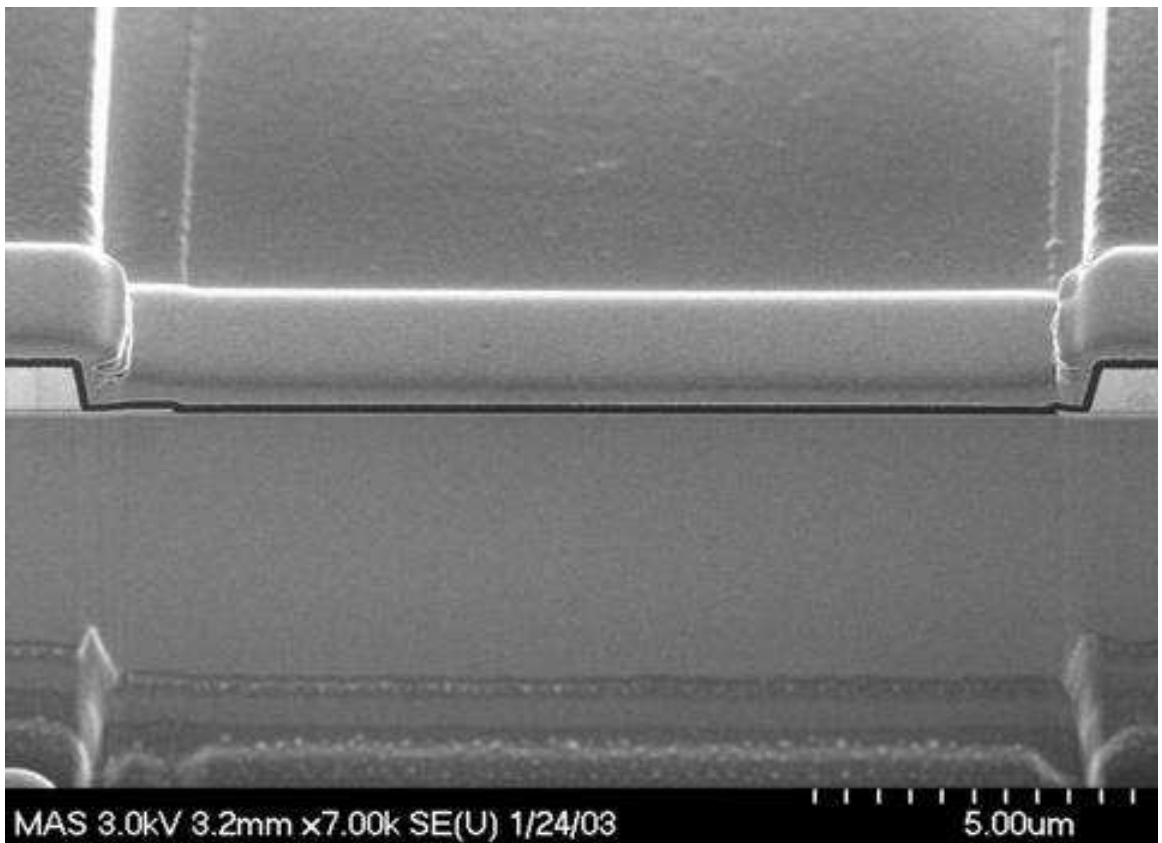


Figure 3.14: CUT 2. Zoomed image of the ohmic contacts.

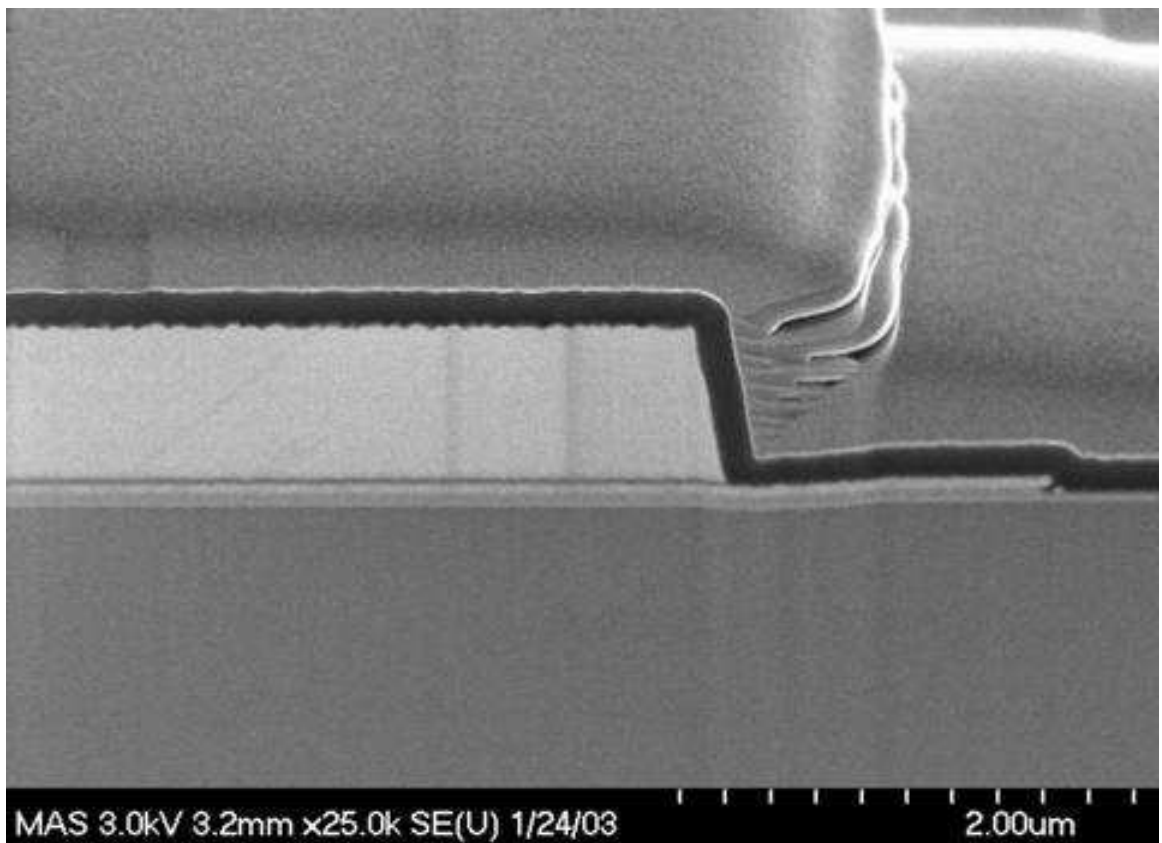


Figure 3.15: CUT 2. Zoomed image of the ohmic contacts. Thickness of the Silicon Nitride (dark black layer) can be extracted.

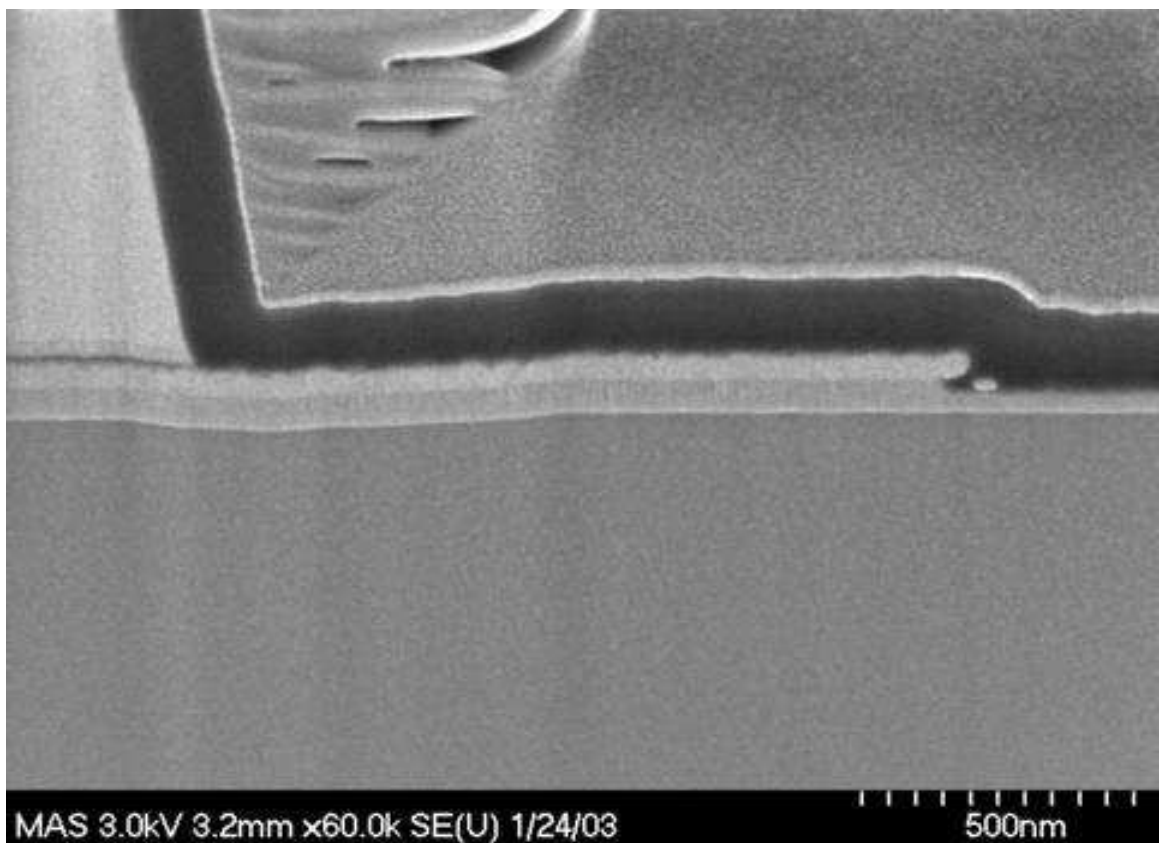


Figure 3.16: CUT 2. Zoomed image of the ohmic contacts to see processing effects.

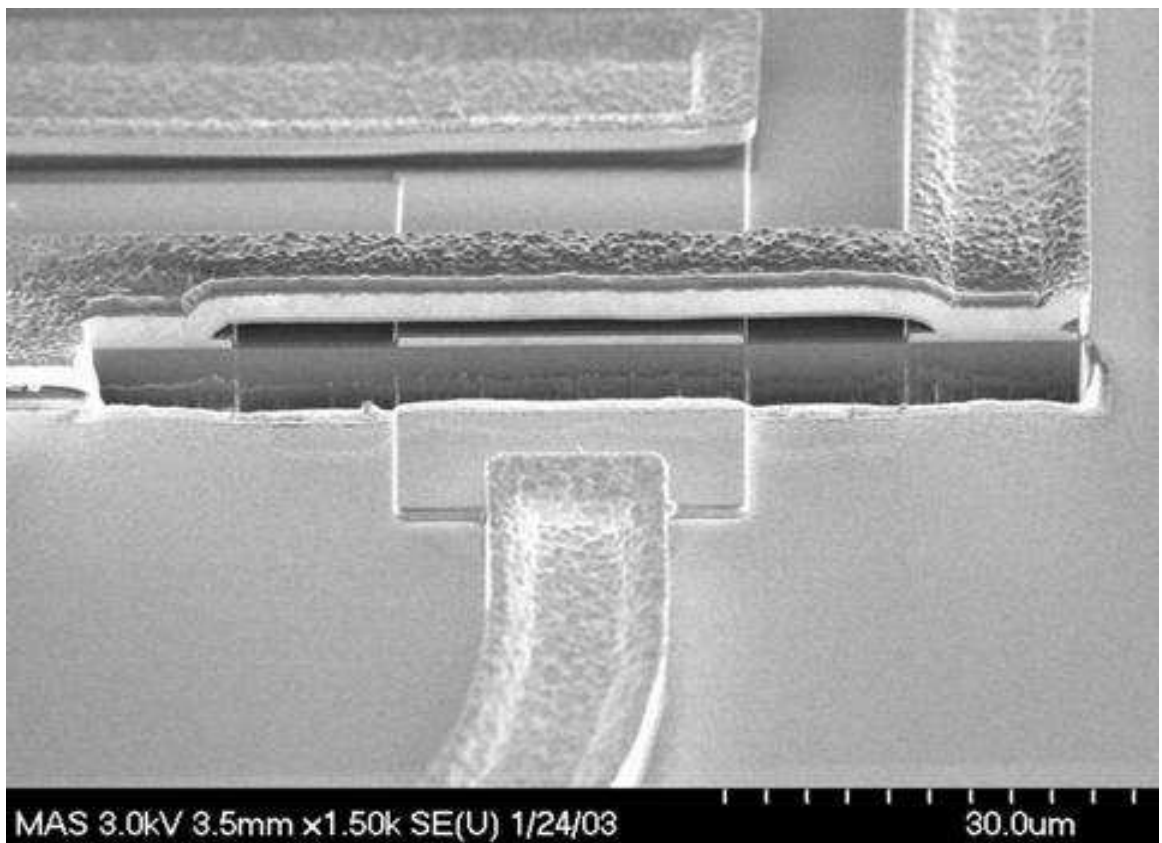


Figure 3.17: CUT 3. Image of the air bridge over the spiral inductor. Image shows the underpass metal layer and the overpass metal layer of the air bridge.

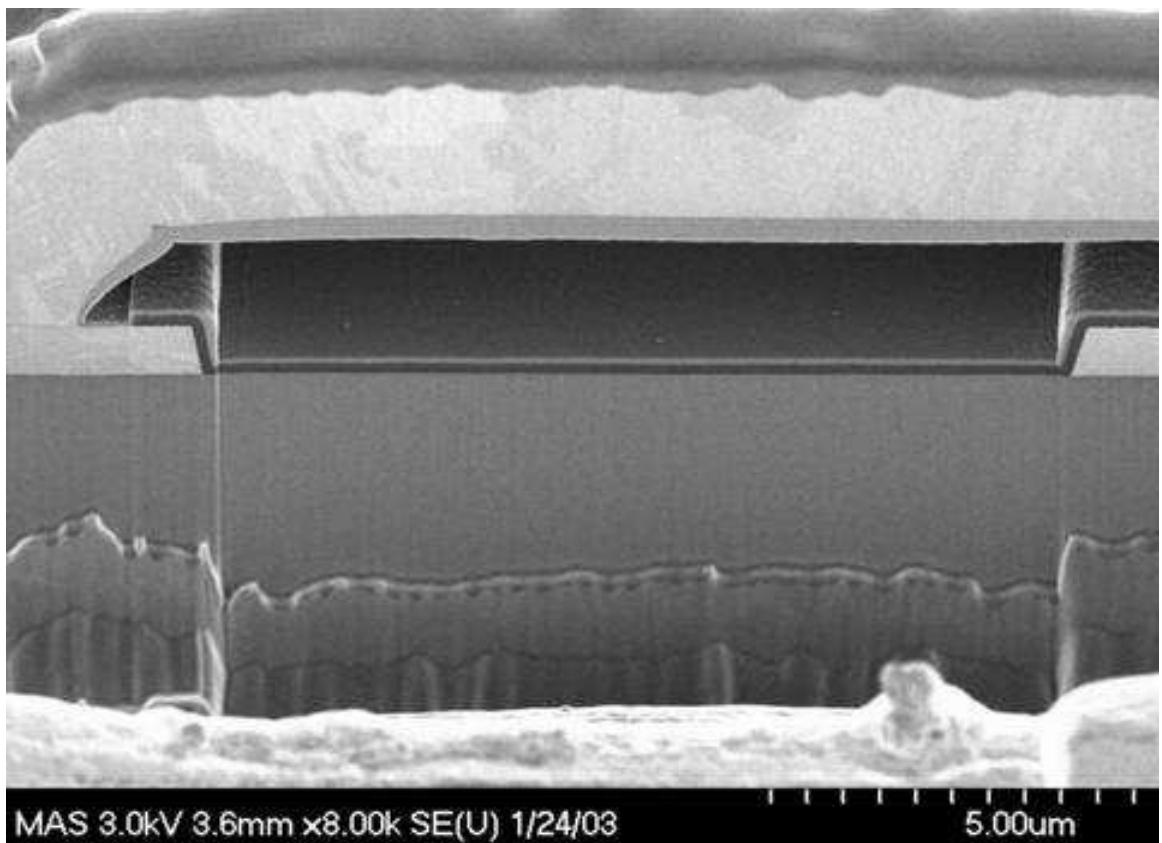


Figure 3.18: CUT 3. Zoomed image of the air bridge, showing the overpass metal layer. Thickness of the overpass metal layer (light gray layer) can be extracted.

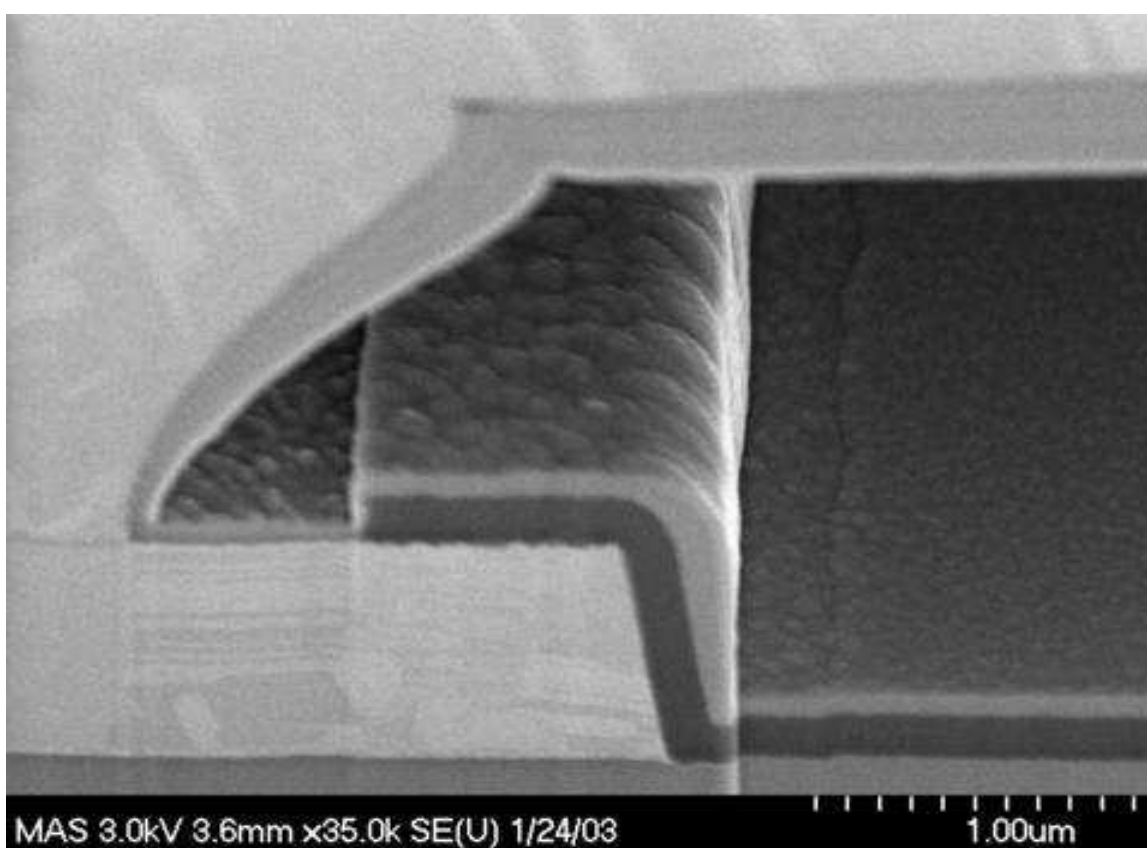


Figure 3.19: CUT 3. Zoomed image of the left hand side footing of the air bridge.

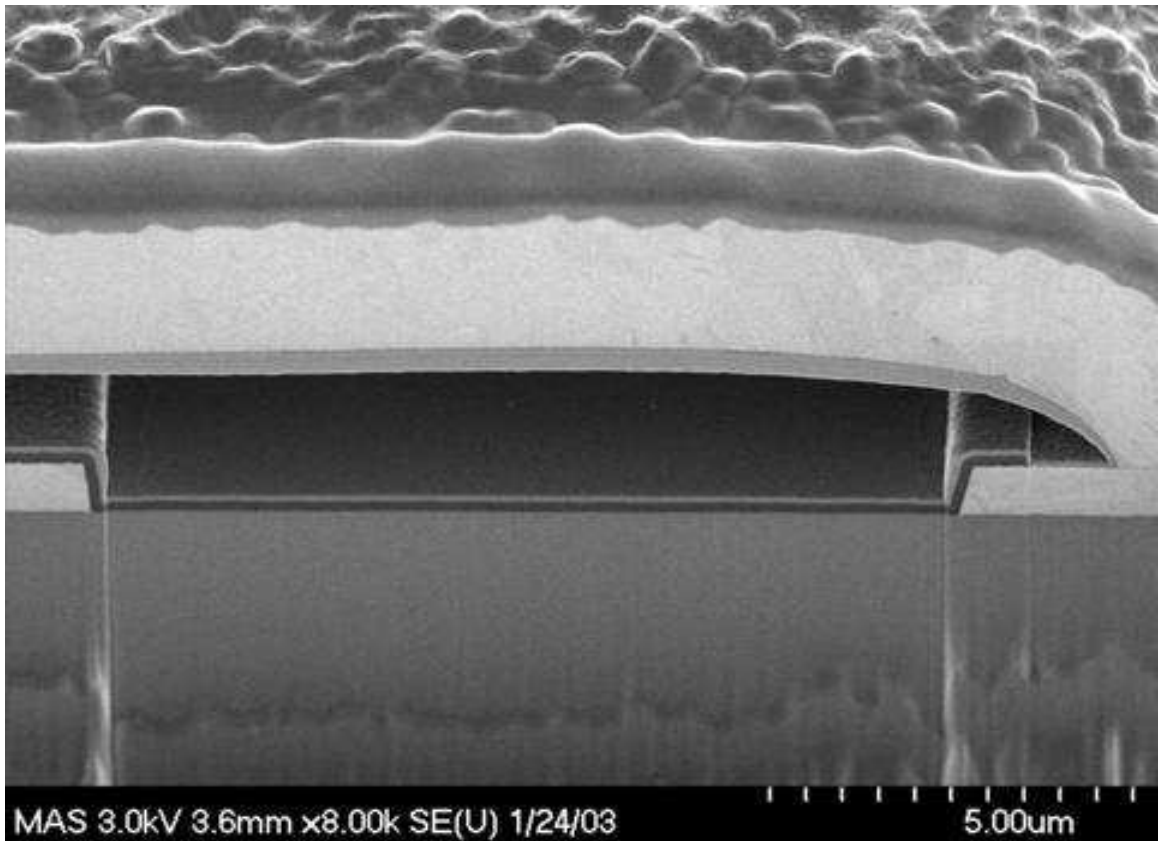


Figure 3.20: CUT 3. Zoomed image of the right hand side footing of the air bridge.

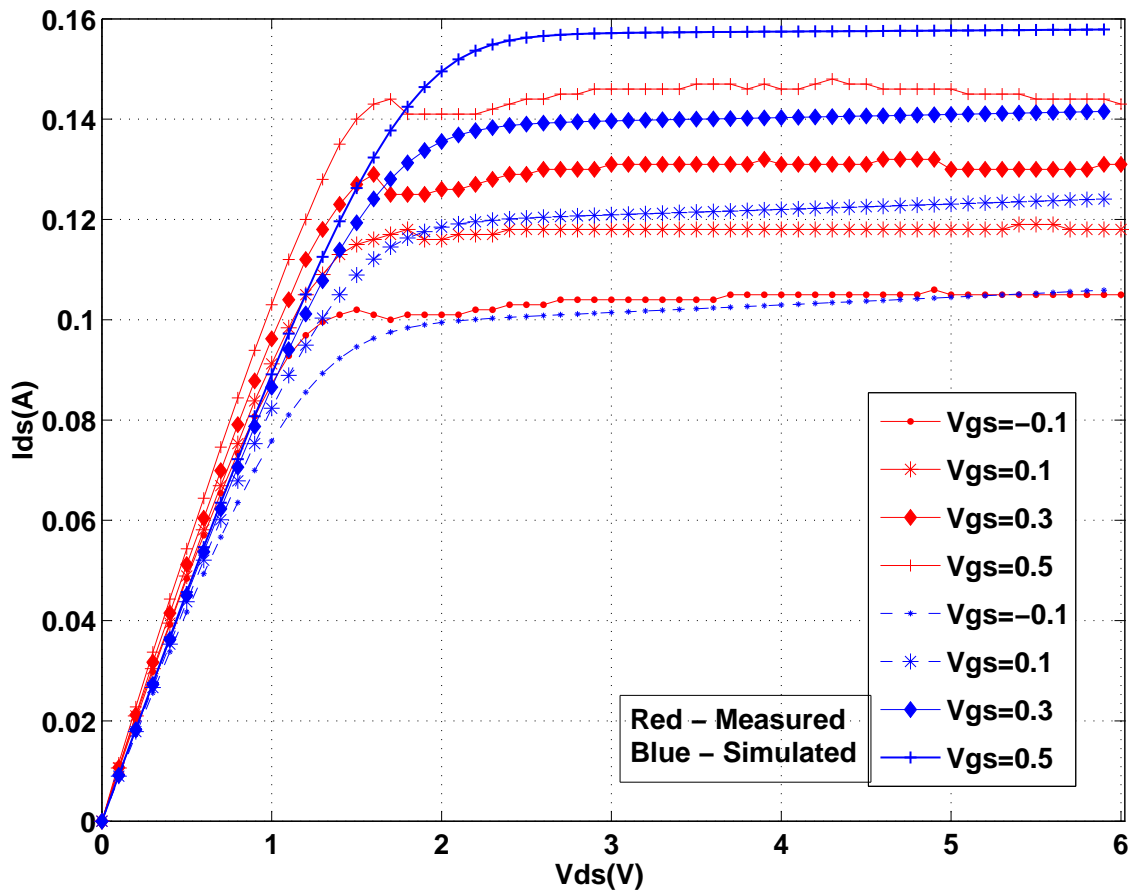


Figure 3.21: Measured and simulated I/V curves of the Filtronic Solid State pHEMT – LP6836.

first cut was made along the 2 corner fingers of pHEMT2. The second cut was made along a microstrip line. The third cut was made along the air bridge of the spiral inductor. These images can be used to determine the physical dimensions of some of the features of the MMIC.

Here the pHEMTs of the LNA were modeled using the Curtice-Cubic model of a MESFET. The transmission lines were modeled as generalized transmission lines. As this was a time-domain analysis the transmission lines were modeled as RLGC elements. To verify the Curtice-Cubic model, Figure 3.21 shows the I/V curves of a GaAs pHEMT (LP6836) from Filtronic Solid State. The LP6836 is $0.25 \mu\text{m} \times 360 \mu\text{m}$ pHEMT, utilizing an

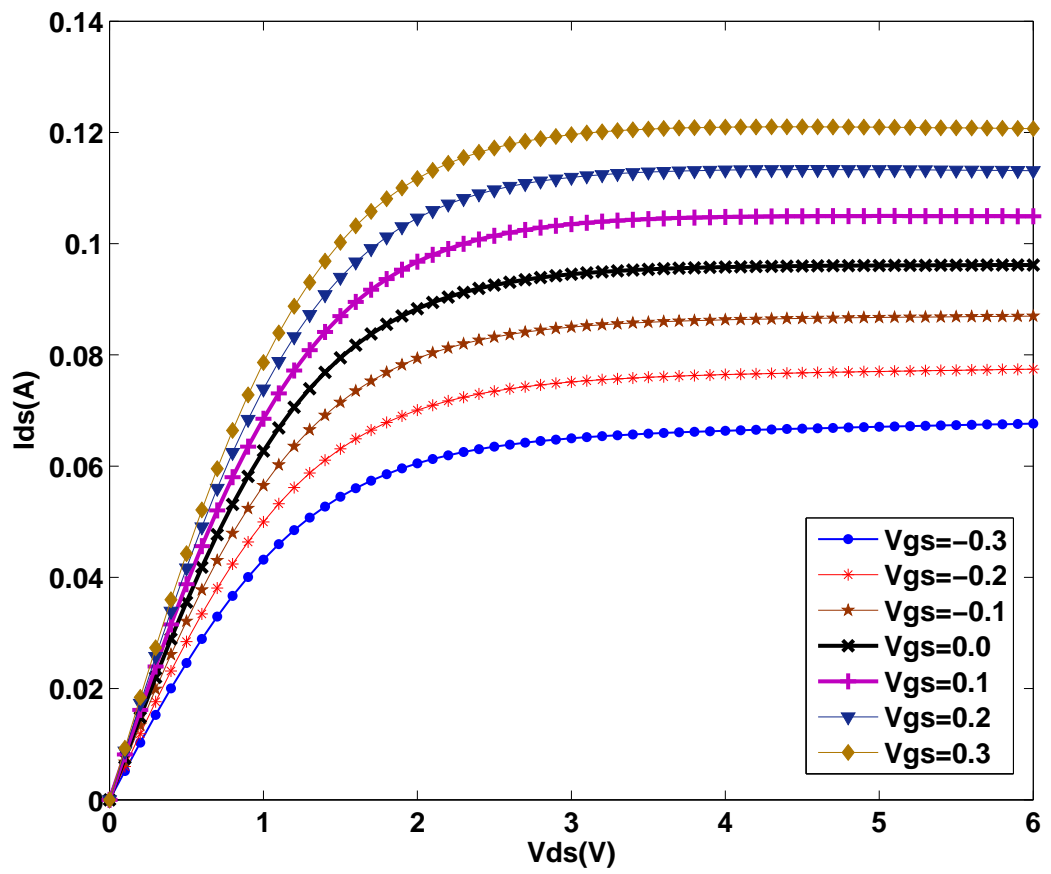


Figure 3.22: Simulated I/V curves of pHEMT1 of the LMA411 MMIC.

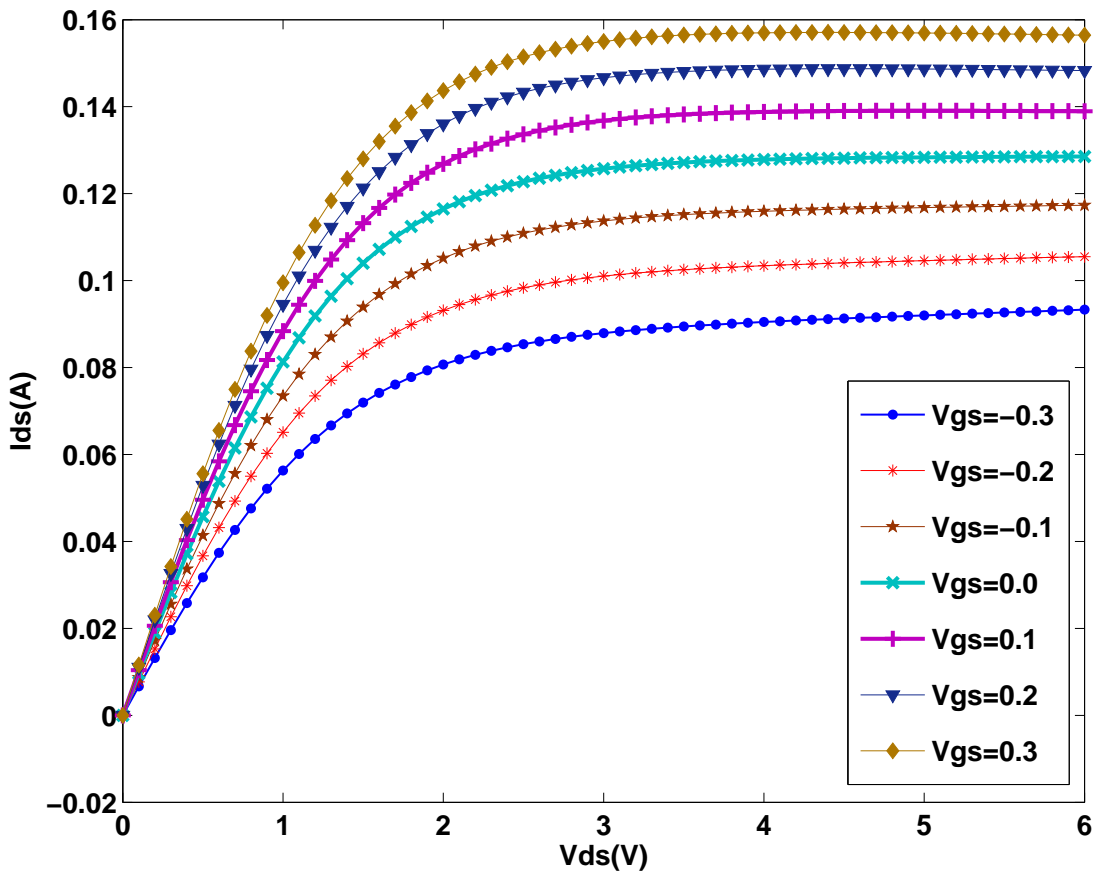


Figure 3.23: Simulated I/V curves of pHEMT2 of the LMA411 MMIC.

Electron-Beam direct-write Schottky barrier gate. The recessed “mushroom” gate structure minimizes parasitic gate-source and gate resistances. The epitaxial structure and processing have been optimized for high dynamic range. The Curtice Cubic model parameters for the LP6836 pHEMT were extracted by Filtronic Solid State. The *fREEDA*TM netlist for this test is provided in Appendix B, Section B.2. At $V_{gs} = -0.1$ V and $V_{gs} = 0.1$ V, the measured and simulated I/V show good agreement. At higher gate bias levels, the simulated I/V curves deviate substantially from the measured I/V curves. Figures 3.22 and 3.23 show the I/V curves of the stage 1 pHEMT and stage 2 pHEMT of the LMA411 MMIC, with Curtice Cubic model parameters extracted by Filtronic Solid State. At $V_{gs} = 0$ V and $V_{ds} = 6$ V, the simulated drain current of pHEMT 1 is 96.1 mA and that of pHEMT 2 is 128.5 mA.

In the two-tone test a 6 V drain DC bias and a 0 V gate DC bias was applied to the MMIC. The MMIC was biased at 50% I_{dss} bias, by including the resistor ladder network between the DC ground pads. These resistors are shown by label J (the first two labels J on the left), in Figure 3.6. The input power level of the first sinusoidal tone at 10 GHz was held constant at -10 dBm and the input power level of the second sinusoidal tone at 11 GHz was varied from -10 dBm to -110 dBm. The two tones will produce third order intermodulation products at the output due to the third order nonlinearity of the LNA devices – the pHEMTs. A second tone 100 dB below the carrier, will have a IM3 product more than 100 dB below the carrier, which will help to test the maximum possible dynamic range of the new technique. A transient simulation with new time step control technique was performed with a maximum time step of 3 ps for a simulation time of 29.6 ns. The netlist for this test is provided in Appendix B, Section B.4 . The input voltage of the voltage source at 11 GHz in the netlist should be varied to simulate the necessary data points. The Curtice Cubic model parameters used in this netlist are also provided in Appendix B, Section B.3. The measured output power levels at 9 GHz, 10 GHz , 11 GHz and 12 GHz are also provided in Appendix B, Section B.6. The measured losses in the components used during measurements are also provided. The total loss at each frequency is added to the respective measured output power level. As desired, a gain of 16 dB was seen at the output of the two tones. Figure 3.24 compares the measured output power levels of the IM3 products at 9 GHz and 12 GHz with those obtained using different analysis techniques. The different analysis techniques were, the new time step control technique for transient analysis implemented in *fREEDA*TM, the transient analysis technique used in a commercial simulator, and the harmonic balance technique. Since the commercial simulator

used a FFT to view the time-domain data in the frequency domain, a FFT was used to transform the time-domain data obtained from the new time step control technique. The output power level at 9 GHz (2×10 GHz–11 GHz), has a slope of 1, whereas the output power level at 12 GHz (2×11 GHz–10 GHz) has a slope of 2. Also the linear calculated power at 12 GHz with a slope of 2 is plotted in the figure for comparisons.

At the second tone input power levels below -50 dBm, the IM3 product at 12 GHz is below -100 dBm. The measurements of the IM3 product at 12 GHz at or below these power levels hit the noise floor of the spectrum analyzer. There is good agreement between the measurements and all other techniques, till an input power level of -50 dBm at 11 GHz. Below -50 dBm, a successful comparison between measured and simulated results could not be made, since the IM3 product at 12 GHz hits the noise floor of the spectrum analyzer. Comparisons between the simulated results below -50 dBm input power at 11 GHz were made. Harmonic balance simulation can detect signals as low as approximately -110 dBm. Below -110 dBm, harmonic balance hits its numerical noise floor of -120 dBm. Since the carrier output power at 10 GHz is 5 dBm, the maximum achievable dynamic range of a harmonic balance simulation is 125 dB.

As mentioned above, the figure also compares the simulated results using the transient analysis technique in a commercial simulator and new time step control transient analysis technique implemented in *fREEDA*TM. In *fREEDA*TM, the new time step control used a *RELTOL* of 0.001. The simulated results are in good agreement at higher power levels. But at lower power levels, the commercial transient analysis technique starts to deviate away from the expected linear power. At point B, this deviation is approximately 3 dB in the commercial transient simulator, whereas it is approximately 1.75 dB in the new technique implemented in *fREEDA*TM. A zoomed in comparison between the linear power and the simulated results obtained from the new technique in *fREEDA*TM from point A to point B in Figure 3.24 on the 12 GHz curve is shown in Figure 3.25. The new technique in *fREEDA*TM deviates slightly from the linear power below input power levels of -58 dBm at 11 GHz, and at input power of -70 dBm this deviation is approximately 1.75 dB. The new technique in *fREEDA*TM hits its numerical noise floor of -160 dBm. Since the carrier output power at 10 GHz is 5 dBm, the maximum achievable dynamic range of the new technique is 165 dB. The improved accuracy of the new technique as seen from the simple RC network test is maintained in the long transient simulations of the MMIC. A precise estimation of error and a predicted-corrected initial guess at every time point helps maintain

the improved accuracy and a low value of the accumulated error in the nonlinear RF output waveform of the MMIC. The low accumulated error and the precise estimation of error helps achieve the high dynamic range of the transient analysis. It also results in the new technique being numerically robust.

3.6.1 Comparison With Harmonic Balance

To better illustrate the low dynamic range of harmonic balance, a single tone simulation at a very low input power was performed on the MMIC. Figure 3.26 compares the output voltage of the MMIC, obtained from a transient simulation using the new time step control technique implemented in *fREEDA*TM and the harmonic balance analysis technique with 20 harmonics of the fundamental at 10 GHz. The netlist for this single tone simulation with harmonic balance analysis is provided in Appendix B, Section B.5. With the appropriate analysis type, the same netlist can be used for a single tone simulation using the new time step control technique. The output voltage obtained from the new technique is compared with the output voltage obtained from harmonic balance only after steady-state is reached. This simulation was done with an input power of -110 dBm at 10 GHz. The new time step control technique used a *RELTOL* of 0.001. The peak output voltage obtained by the new technique is 0.07 mV, whereas the peak output voltage obtained by the harmonic balance technique is 0.061 mV. Harmonic balance fails to detect very small levels of voltage below $10 \mu\text{V}$ i.e. -110 dBm for a 50Ω system. Hence in Figure 3.24, harmonic balance hits its numerical noise floor of approximately -120 dBm for signal levels below -110 dBm.

In harmonic balance, the nonlinear elements are solved in time-domain and the linear elements are solved purely in the frequency domain. This time-domain result is transformed to frequency domain at every time step, limiting the accuracy of the spectrum to the accuracy of the Fourier transform technique used. Another source of error in harmonic balance is the truncation of the number of the harmonics used to represent the signal in the frequency domain. Hence the error in harmonic balance analysis consists of the Fourier transform error, error due to truncation of number of harmonics to a finite number and convergence error introduced during solving the nonlinear algebraic equations. Now, since the new technique follows sinusoidal curves better, it can detect very small signals, as the *LTE* is small enough not to encapsulate tiny signals, as seen in Figure 3.26. At the troughs

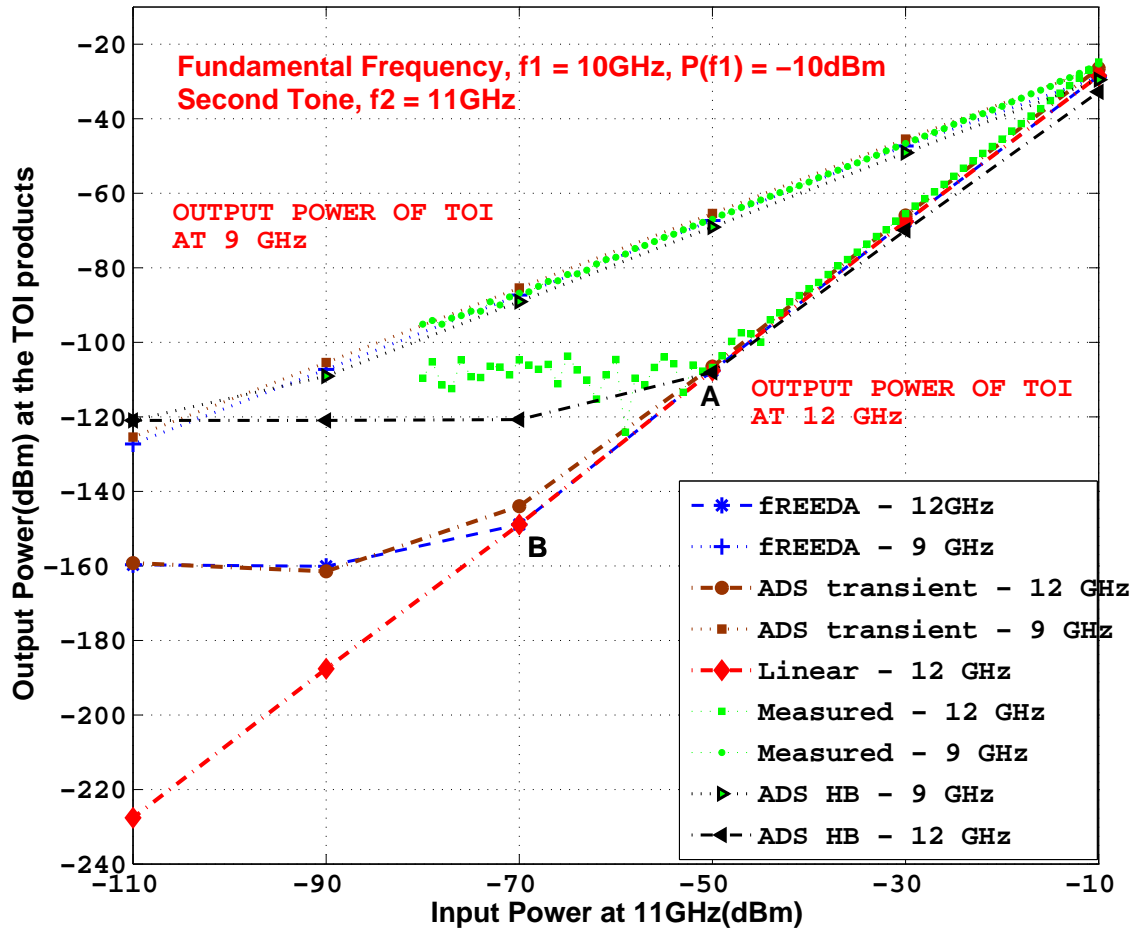


Figure 3.24: Comparison of the measured IM3 output power levels for the LMA411 MMIC and simulated levels using the new time step control technique and a commercial harmonic balance simulator.

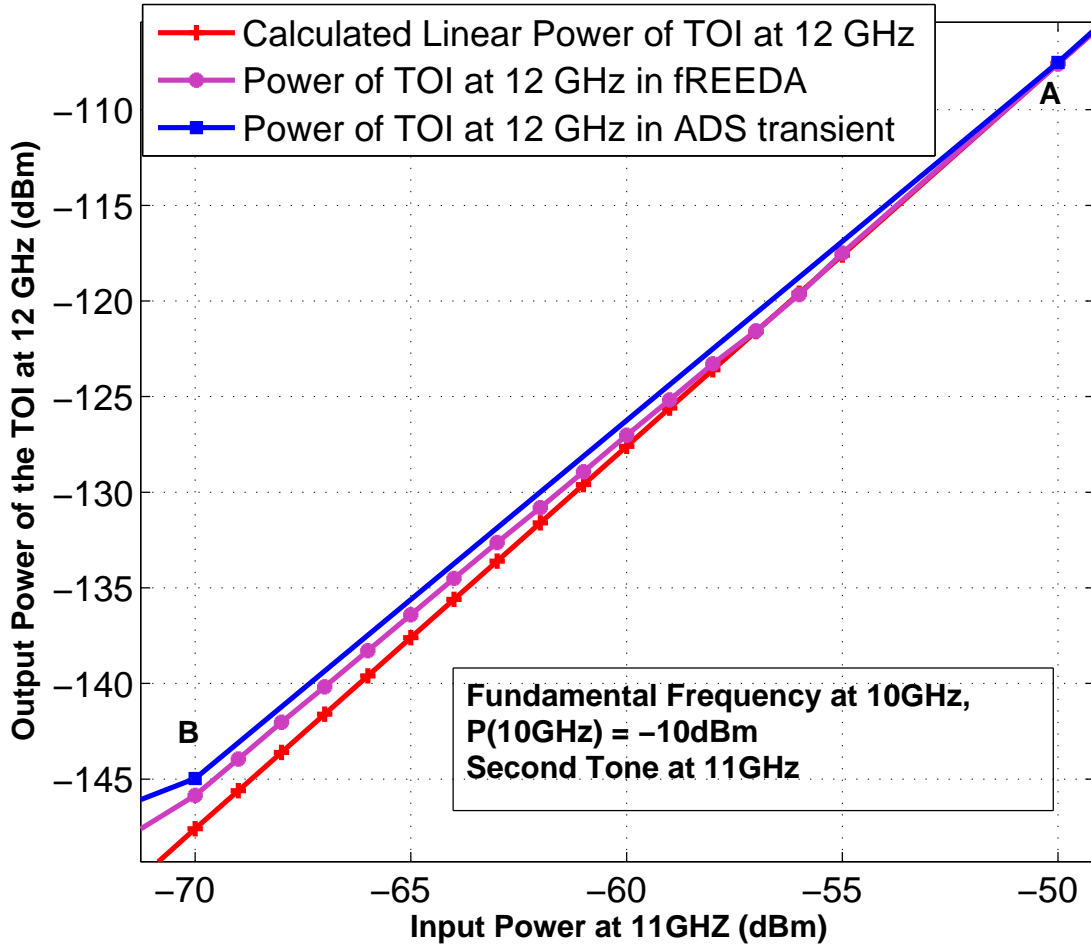


Figure 3.25: Comparison of the calculated linear IM3 output power levels at 12 GHz for the LMA411 MMIC with the simulated power level using the new time step control technique.

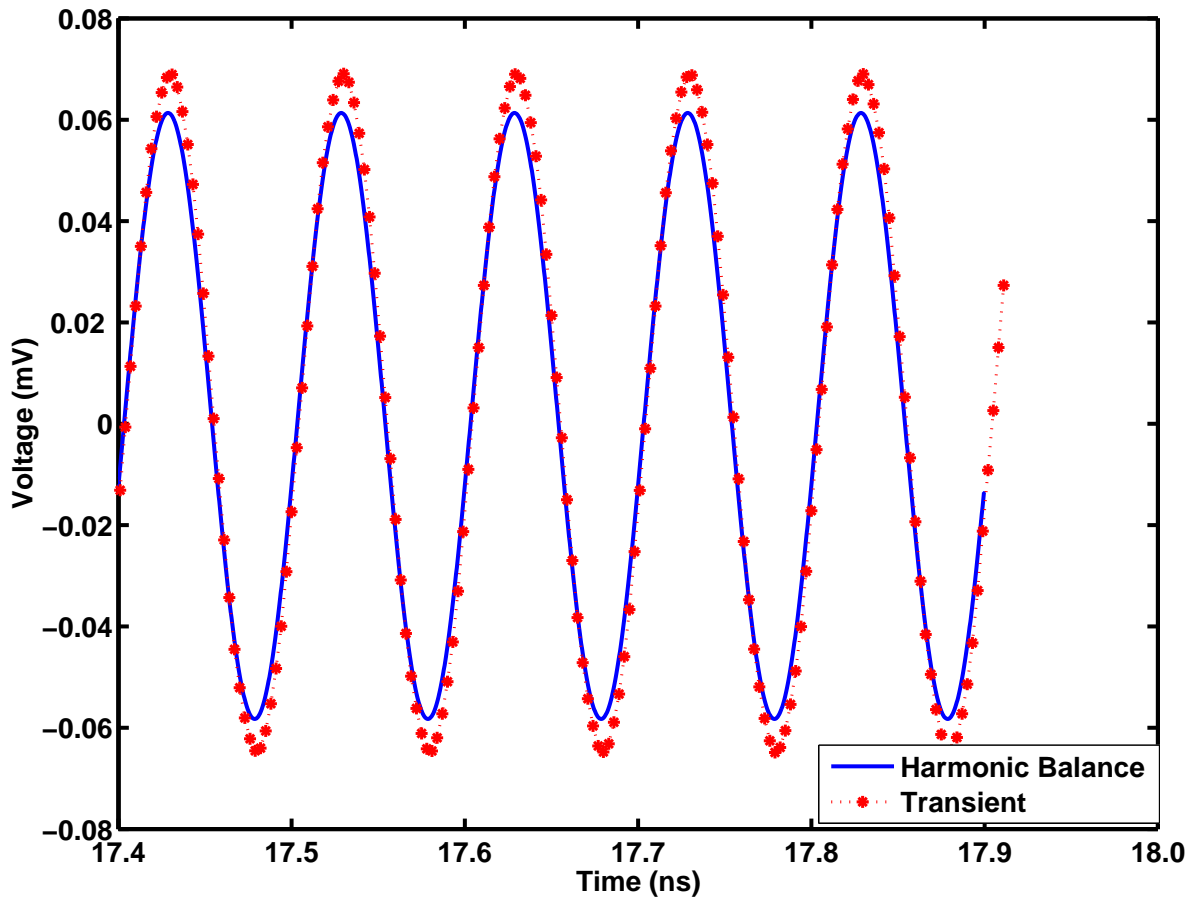


Figure 3.26: Comparison between the simulated output voltage of the LMA411 MMIC obtained using harmonic balance and the new time step control technique.

and the crests of the sinusoidal signal, the transient analysis overshoots and undershoots the harmonic balance output. Consequently the new technique has a numerical noise floor of approximately -160 dBm.

3.6.2 Classic Two Tone Test

To test accuracy and robustness of the new technique with nonlinear signals a classic two tone test was simulated on the LNA. The input power level of the two tones at 10 GHz and 11 GHz was varied from -70 dBm to 6 dBm. At 6 dBm the amplifier is well

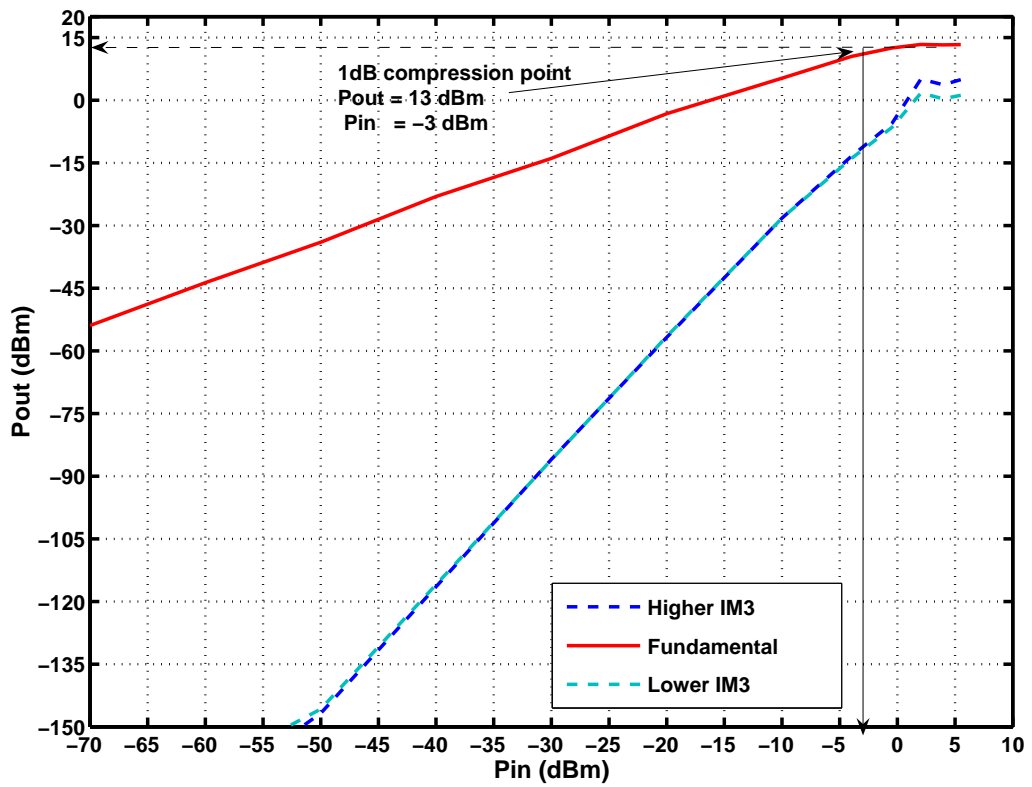


Figure 3.27: Simulated output power levels of the fundamental and IM3 products of a classic two tone test of the LMA411 MMIC.

into compression. The netlist used to verify the dynamic range of the new time step control technique is used for this test. In the netlist, the input voltage of the voltage sources at 10 GHz and 11 GHz is varied to simulate the necessary data points. In Figure 3.27 the output power levels of the fundamental at 10 GHz and that of the two IM3 products are shown. The new time step control technique captures the nonlinear characteristics of the LNA very well. As expected the slope of the output power curve of the fundamental is 1 and that of the IM3 products is 3. The IM3 products differ from each other by approximately 1 dB. The simulated results show a 1 dB compression point at output power of +13 dBm. The deviation from the specification of +17 dBm can be accounted for the approximations in the transistor model. At higher input power levels, where the transistors are well into saturation the IM3 curve deviates substantially from the linear IM3 curve, since at higher power levels the fifth and higher order nonlinearities play a significant role.

3.7 Summary

In this chapter, a new time step control technique which achieves unprecedented dynamic range is described. This technique was implemented in a multi-domain simulator, *fREEDA*TM. This technique precisely estimates local truncation error at every simulation time point. This eliminates the reduction of the time step unnecessarily, when following the crests and troughs of the sinusoid. This method allows the time step size to be as large as possible without reducing the accuracy of the simulated result. The accuracy of the technique was verified with a comparison of the simulated output voltage of a simple RC circuit with the analytical output voltage of the simple RC circuit. To achieve the same amount of accuracy, like a conventional time step technique, the new technique required approximately 29% fewer time points.

The dynamic range of the new technique was verified with measurements of a two tone simulation of a X-band GaAs MMIC LNA. The new technique can capture signals as small -150 dBm before it hits its numerical noise floor of -160 dBm. The dynamic range of the new technique is 165 dB. The improved accuracy, precise estimation of error, a predicted-corrected initial guess at every time point and a low value of accumulated error helps achieve the high dynamic range of the transient analysis. A comparison between the output voltage of the MMIC obtained from a harmonic balance simulation and the

new technique with very small input power levels was made. Harmonic balance cannot successfully detect very small voltage levels of $10\ \mu\text{V}$ or below, hence limiting its dynamic range to 125 dB.

This capability to detect small input signals after a long transient analysis can be used to capture the effects of temperature on the operation of an electronic circuits, in a full chip level simulation. Long thermal transients can have significant effects on the second order intermodulation product or adjacent channel distortion. At the fundamental frequency, this change in temperature is rapid and small. Hence the change in voltage levels due to the change in device operating temperature, is also very tiny. The tiny voltage levels can be detected, if the dynamic range of the simulator is high. In this chapter, a new technique to improve the dynamic range of a transient analysis is developed in *fREEDA*TM.

Chapter 4

X-band MMIC Electrothermal model

4.1 Introduction

In the previous chapter a new time step control technique with high dynamic range was developed in *fREEDA*TM. This technique can detect signal levels as small as -150 dBm. In this chapter this capability will be used to capture the small variations in the output signals due to transient electrothermal effects. These small variations have an effect on circuit performance. Long thermal transients also have a significant effect on second order intermodulation distortion or adjacent channel distortion [67],[68]. Such intermodulation distortion and small variations should be captured during simulation, for rapid prototyping. The thermal models should be fast, accurate and compact to be easily implemented in a circuit simulator to perform coupled electrothermal simulations at CAD timescales. Such a reduced-order compact thermal model is developed and implemented in a general purpose circuit simulator, *fREEDA*TM.

The compact thermal model of a MMIC body developed is in effect a boundary element equivalent of a volumetric model, since the approach presented discretizes only the surface interfaces, the power dissipating areas and the temperature sensitive areas. The

model solves the nonlinear, time dependent heat diffusion equation by transformation of the equation to linear form, domain decomposition, and analytical solution of the transformed equation in regular subvolumes in complex frequency s -space. The solutions of these regular subvolumes are double Fourier series solutions. The global solution for the complex system is constructed by matching the temperature and flux at the subsystem interfaces using algebraic equations.

Different thermal models were developed in *fREEDA*TM to model the complex heat sink mounted and metallized MMIC structure. Each of these models is described in Section 4.3. In Section 4.5 the importance of considering thermal nonlinearity is shown in an example by a heat generating source in thermal subvolumes with different material properties. Section 4.7 verifies the steady-state temperature rise on various spots of the MMIC predicted using the compact thermal model with thermal images taken with an infra-red camera.

4.2 Thermal Impedance Model

As explained in Chapter 2, the compact thermal model developed in *fREEDA*TM is based on the *Leeds thermal impedance matrix model*, described in [60] and [61]. The thermal impedance matrix is developed in the s -space. The top and bottom surface of each 3D structure is discretized into a regular grid to form the elementary areas D_i and D_j . Also each surface heating element is also considered as either an elementary area D_i or D_j depending on its location. Each element $\mathbf{R}_{\text{TH}_{ij}}(\mathbf{s})$ of the thermal impedance matrix is the average thermal impedance between elementary area D_i and D_j . Since it is a thermal impedance it includes the thermal transient effects due to the thermal heat capacity. Each $\mathbf{R}_{\text{TH}_{ij}}(\mathbf{s})$ element is precomputed at the required simulation time points. The temperature dependent thermal nonlinearity of the thermal conductivity is linearized with the Kirchhoff's transformation. It transforms the time dependent heat diffusion equation to another temperature θ . This transformation calculates the thermal conductivity at this transformed temperature θ . This transformed heat diffusion equation is still nonlinear, due to the dependence of the diffusivity $k = \kappa/\rho C$ on θ . It is linearized with another transformation, by defining a new time variable, τ , which calculates the thermal diffusivity at temperature rise θ at time τ . In *fREEDA*TM the diffusivity is assumed constant, and hence the time variable

transformation is not applied. Even though the following equations are in the τ domain, it can be assumed that the real time $t = \tau$.

In *fREEDA*TM thermal elements are considered as nonlinear elements in the time-domain. The power dissipation \mathbf{P}_j of each elementary area D_j is a state-variable for the thermal elements. The thermal impedance matrix approach [60] is used to calculate the resulting temperature at each iteration to solve the nonlinear system. This calculated temperature is fed back to the heat generating electrothermal devices, to calculate the temperature dependent power. This feedback helps perform a fully-coupled electrothermal simulation of a circuit.

In *fREEDA*TM two types of Thermal-Nport elements are implemented. One of the Thermal-Nport elements is a vertically matched thermal subvolume. The temperature on top ($z = 0$) and bottom ($z = D$) surfaces of the element are evaluated. The boundary condition in Equation 2.33 is applied to the top and bottom surface. The top and bottom surfaces are discretized into elementary area D_i and D_j respectively. Heat generating elements are assumed on the top surface and are also considered as elementary areas D_i . This element generates 4 thermal impedance matrices solved at ($z = 0$) and ($z = D$), given by Equation 2.44 - Equation 2.47. The 4 matrices are explained below:

- Matrix $\mathbf{R}_{\text{TH}}^{00}$ has matrix elements which are the thermal impedances between an elementary area D_i on the top surface and all other elementary areas D_i on the top surface.
- Matrix $\mathbf{R}_{\text{TH}}^{0D}$ has matrix elements which are the thermal impedances between an elementary area D_i on the top surface and all other elementary areas D_j on the bottom surface.
- Matrix $\mathbf{R}_{\text{TH}}^{D0}$ has matrix elements which are the thermal impedances between an elementary area D_j on the bottom surface and all other elementary areas D_i on the top surface.
- Matrix $\mathbf{R}_{\text{TH}}^{DD}$ has matrix elements which are the thermal impedances between an elementary area D_j on the bottom surface and all other elementary areas D_j on the bottom surface.

The average temperature rise over each of the elementary areas D_i and D_j is calculated and matched.

The other Thermal-Nport element is a heat sink mounted thermal subvolume. The bottom surface is connected to a heat sink. Now, only the top surface of the element is discretized into elementary areas D_i . This element generates only a single thermal impedance matrix, solved at $z = 0$, given by Equation 2.41. This matrix has elements which are thermal impedances between an elementary area D_i on the top surface and all other elementary areas D_i on the top surface. The average temperature rise over each of the elementary areas D_i is calculated and matched.

These two types of elements are used to model subsystems of the X-band GaAs MMIC LNA structure, discussed in Chapter 3.

4.3 Electrothermal Model Of The Mounted and Metallized MMIC

The 3D thermal model of the X-band GaAs MMIC LNA explained in Chapter 3 was developed with the two Thermal-Nport elements discussed in the previous section. The bare GaAs die was attached with DIE-MAT epoxy to a Kovar substrate, which was screwed to a block of Aluminum. The Kovar substrate acts a good heat spreader, to spread out the heat from the GaAs die. The block of Aluminum acts as the thermal heat sink. These layers/tiers makes the MMIC a complex structure. To achieve good thermal accuracy, each layer/tier of the MMIC should be modeled. Hence, this complex structure was divided into subsystems- the GaAs die, the DIE-MAT epoxy, the Kovar substrate and the heat sink. The GaAs die consists of heat generating elements, the transistors and also heat removal and heat spreading elements, like through vias and metallized surface of via-capacitors. This surface metallization should also be considered to develop a precise thermal model. The vias and the via-capacitors of the MMIC were modeled as separate subsystems. Detailed model explanation of each subsystem is described in the following sections.

4.3.1 GaAs Die

The GaAs die ($1624 \mu\text{m} \times 1470 \mu\text{m} \times 100 \mu\text{m}$) of the MMIC, shown in Figure 2.3, consists of 2 heat generating transistors, and 2 heat generating TaN resistors between the DC pads. The first stage transistor consists of 6 fingers and the second stage stage transistor

consists of 8 fingers. To mimic the resolution of the infra-red thermal imaging camera of $50\mu\text{m}$, 3 ‘pixel’ ($50\mu\text{m} \times 50\mu\text{m}$) elements were constructed and placed over transistor 1 ($50\mu\text{m} \times 150\mu\text{m}$), transistor 2 ($50\mu\text{m} \times 200\mu\text{m}$) and between the 2 TaN resistors ($66.5\mu\text{m} \times 54\mu\text{m}$ and $31.9\mu\text{m} \times 64\mu\text{m}$). These pixel elements received zero power but delivered the temperature response over $50\mu\text{m} \times 50\mu\text{m}$ ‘pixel’ areas. The rest of the GaAs die acts as a heat sink or heat dissipator for the heat generating elements. Since this thermal model is an ‘interface element’ model, only the interfacing surfaces are discretized. Here the bottom surface of the GaAs die interfaces with the top surface of the DIE-MAT Epoxy, hence only the bottom surface of the GaAs die should be discretized. But since this is a generalized vertically matched element, the top and bottom surfaces of the GaAs die were discretized into a 5×5 grid. The blocks on the top surface of the grid received zero power, but they act as heat sinks for the heat generating sources on the GaAs die. The blocks on the bottom surface grid are connected to the blocks on the top surface of the underlying DIE-MAT epoxy layer. The GaAs die also interfaces with the metal layer of the via-capacitors. This interface patch on the top layer of the GaAs die is also discretized into a 4×4 grid.

This GaAs die, with the all heat generating and heat dissipating elements mentioned above, was modeled as a vertically matched thermal subvolume with an Thermal-Nport element, Figure 4.1. To generate the thermal impedance matrix, the heat diffusion equations are solved analytically and the temperatures at the top and bottom discretized surfaces are matched. As described in [60] adiabatic boundary conditions were assumed on the sidewalls, and the small radiation and convection losses at the top and bottom surfaces of the die were neglected. With these boundary conditions the average temperatures, θ_{0av_i} , θ_{Dav_i} averaged over elementary areas, D_i , and D_j , on the top ($z=0$) and bottom ($z=D$) surfaces, respectively, are obtained by:

$$\theta_{0av_i} - \frac{\theta(\tau=0)}{s} = \sum_{i'} \mathbf{R}_{\text{TH}_{ii'}}^{\text{00}} \mathbf{P}_{0i'} + \sum_j \mathbf{R}_{\text{TH}_{ij}}^{\text{0D}} \mathbf{P}_{Dj'} \quad (4.1)$$

$$\theta_{Dav_i} - \frac{\theta(\tau=0)}{s} = \sum_i \mathbf{R}_{\text{TH}_{ji}}^{\text{D0}} \mathbf{P}_{0i'} + \sum_{j'} \mathbf{R}_{\text{TH}_{jj'}}^{\text{DD}} \mathbf{P}_{Dj'}. \quad (4.2)$$

Here, \mathbf{P}_{0i} and \mathbf{P}_{Dj} are respective imposed fluxes in elementary areas, D_i , and D_j . The thermal impedance matrices are obtained in the explicit form

$$\mathbf{R}_{\text{TH}_{ii'}}^{\text{00}} = \frac{1}{\kappa_s LW} \sum_{mn} \frac{4 \coth \gamma_{mn} D}{(1 + \delta_{m0})(1 + \delta_{n0}) \gamma_{mn}} \frac{I_{mn}^{0i}}{I_{00}^{0i}} \frac{I_{mn}^{0i'}}{I_{00}^{0j'}} \quad (4.3)$$

$$\mathbf{R}_{\text{TH}_{ij}}^{\text{OD}} = \frac{1}{\kappa_s LW} \sum_{mn} \frac{-4 \text{cosech} \gamma_{mn} D}{(1 + \delta_{m0})(1 + \delta_{n0}) \gamma_{mn}} \frac{I_{mn}^{0i} I_{mn}^{Dj}}{I_{00}^{0i} I_{00}^{Dj}} \quad (4.4)$$

$$\mathbf{R}_{\text{TH}_{ji}}^{\text{DO}} = \frac{1}{\kappa_s LW} \sum_{mn} \frac{4 \text{cosech} \gamma_{mn} D}{(1 + \delta_{m0})(1 + \delta_{n0}) \gamma_{mn}} \frac{I_{mn}^{Dj} I_{mn}^{0i}}{I_{00}^{Dj} I_{00}^{0i}} \quad (4.5)$$

$$\mathbf{R}_{\text{TH}_{ij}'}^{\text{DD}} = \frac{1}{\kappa_s LW} \sum_{mn} \frac{-4 \text{coth} \gamma_{mn} D}{(1 + \delta_{m0})(1 + \delta_{n0}) \gamma_{mn}} \frac{I_{mn}^{Dj} I_{mn}^{Dj'}}{I_{00}^{Dj} I_{00}^{Dj'}} \quad (4.6)$$

where the I_{mn}^{0i} and I_{mn}^{Dj} are area integrals over the areas D_i , and D_j , and are given by:

$$I_{mn}^i = \iint_{D_i} \cos \lambda_m x \cos \mu_n y \, dx dy. \quad (4.7)$$

4.3.2 DIE-MAT Epoxy Layer

The DIE-MAT epoxy layer ($1624 \mu\text{m} \times 1470 \mu\text{m} \times 100 \mu\text{m}$) was modeled as a vertically matched Thermal-Nport element, like the GaAs die layer explained above, but with no heat generating sources. The blocks on the bottom discretized surface of the epoxy layer were connected to the blocks of the top discretized surface of the underlying Kovar substrate. The heat diffusion equations are solved analytically and the temperatures at the top and bottom discretized surfaces are matched.

4.3.3 Kovar Substrate Layer

The Kovar substrate layer ($5 \text{ cm} \times 2.5 \text{ cm} \times 381 \mu\text{m}$) was modeled as a heat sink mounted Thermal-Nport element, with only the top surface discretized, since it is mounted on the Aluminum block which acts as a heat sink. The bottom surface of the Kovar substrate layer was assumed to be at constant temperature. The GaAs die was attached at the center of the Kovar substrate. Only the ‘interfacing area’ ($1624 \mu\text{m} \times 1470 \mu\text{m} \times 381 \mu\text{m}$) between the DIE-MAT Epoxy and the Kovar substrate was discretized into a 5×5 grid. These grid blocks of the Kovar substrate were connected to the bottom layer blocks of the DIE-MAT Epoxy. With no heat generating sources the average temperatures over the elementary areas are given by Equation 2.32, where

$$\mathbf{R}_{\text{TH}_{ij}}(\mathbf{s}) = \frac{1}{\kappa_s LW} \sum_{mn} \frac{4 \tanh \gamma_{mn} D}{(1 + \delta_{m0})(1 + \delta_{n0}) \gamma_{mn}} \frac{I_{mn}^i I_{mn}^j}{I_{00}^i I_{00}^j} \quad (4.8)$$

where the I_{mn}^i area integrals over the areas D_i , and are given by Equation 2.36.

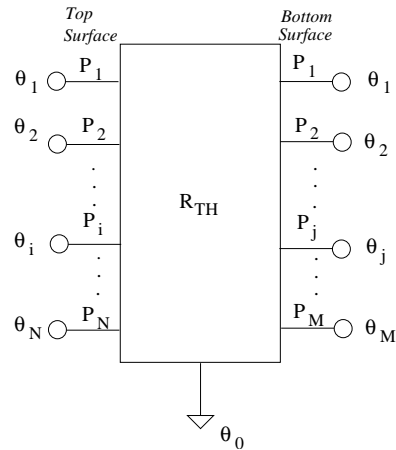


Figure 4.1: Thermal N-port generated directly from analytical solution of the heat diffusion equation, and represented by thermal impedance matrix, $R_{THij}(s)$. After [61]. (Copyright IEEE 2006)

4.3.4 Vias

The two vertical through vias near transistor 2, were modeled as two separate subsystems. They were modeled as vertically matched thermal subvolumes. These vias were assumed Gold filled. This $50\mu\text{m} \times 50\mu\text{m} \times 100\mu\text{m}$ Gold 3D structure was modeled as a 2-port vertically matched thermal subvolume, and temperatures at the 2 ports are matched. The vertical vias provide a path parallel to the vertical heat conduction path of the GaAs die. Hence they are connected in parallel to the GaAs die, and are connected to the GaAs die grid blocks located in the via vicinity. The thermal impedance matrices of the vias are given by equations in section 4.3.1, with only one elementary area D_i and D_j , on the top and bottom surface respectively.

4.3.5 Via Capacitors

The top metallized layer of the via capacitors near transistor 2 act as heat spreaders. This metallized layer provides a path parallel to the lateral heat conduction path of the top surface of the GaAs die. This $150\mu\text{m} \times 150\mu\text{m} \times 7\mu\text{m}$ Gold metal layer of the via capacitors, was modeled as a vertically matched Thermal-Nport element, with no heat generating sources. The top and bottom surfaces of this element were discretized into a 4×4 grid. To connect this metal layer to the top surface of the GaAs die, a similar size

interface patch on the top surface of the GaAs die was discretized into a 4×4 grid. The bottom surface grid blocks of the Gold metal layer were connected to the grid blocks of this patch. The top surface grid blocks of the metal layer were connected to zero power sources. The heat diffusion equations are solved analytically and the temperatures at interfacing nodes are matched. The thermal impedance matrices are obtained by equations given in Section 4.3.1.

4.4 Electrothermal MESFET MODEL

The electrothermal modeling approach in *fREEDA*TM, uses state-variables to model various nonlinear devices. The state-variable based parameterized nonlinear devices can be described with the following set of equations:

$$\mathbf{v}_{NL}(t) = u[\mathbf{x}(t), \frac{d\mathbf{x}}{dt}, \dots, \frac{d^m\mathbf{x}}{dt^m}, \mathbf{x}_D(t)] \quad (4.9)$$

$$\mathbf{i}_{NL}(t) = w[\mathbf{x}(t), \frac{d\mathbf{x}}{dt}, \dots, \frac{d^m\mathbf{x}}{dt^m}, \mathbf{x}_D(t)] \quad (4.10)$$

where $\mathbf{v}_{NL}(t)$, $\mathbf{i}_{NL}(t)$ are vectors of voltages and currents at the common ports, $\mathbf{x}(t)$ is a vector of state-variables and $\mathbf{x}_D(t)$ a vector of time-delayed state-variables, i.e., $\mathbf{x}_{Di}(t) = x_i(t - \tau_i)$. The time delays τ_i may be functions of the state-variables. All the vectors in Equation 4.9 and Equation 4.10 have the same size n_d equal to the number of common (device) ports. The general formulation to solve the system of linear and nonlinear devices is described in [52]. To incorporate the thermal effects into the circuit simulator, the thermal model is made to look like an electrical circuit. The thermal and electrical circuits are then solved simultaneously as if they were one large electrical circuit. The concept of local reference groups [50] helps to integrate the thermal network and guarantees no mixing of the electric and thermal currents. A general integration of an electrothermal network is shown in Fig. 4.2. Power dissipated in the active devices are represented as a heat current sources referenced to thermal ground. The thermal ground is taken as 0 K, and is treated in the circuit simulator as a local reference node. Thus, the entire thermal network is treated by the circuit simulator as a single local reference group. At the interface between the thermal component and thermal network are temperature, \mathbf{T} 's, and heat flow, \mathbf{P} 's, variables. The error function at the thermal network interface is $P = 0$, which is equivalent to the error function of $I = 0$ in the electrical network. The temperature rise of thermal network can

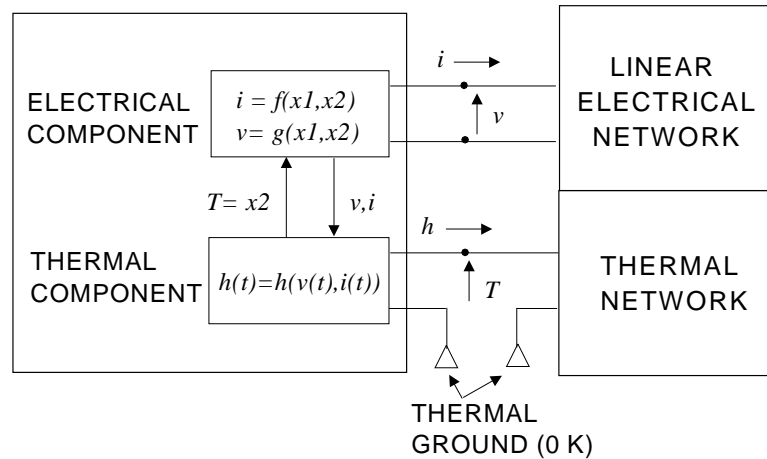


Figure 4.2: An electrothermal element connected to linear and thermal networks.

be described by Equation 2.32. The thermal network is connected to the electrical network through a temperature terminal. The temperature at this terminal is a state-variable of the device model. The temperature at this terminal captures the effects of temperature on mobility and threshold voltage through the temperature coefficient parameters of the device model. In a regular electrical model, the device temperature is an input parameter, and the temperature effects are calculated based on this parameter. Dynamic thermal effects cannot be captured in this model. In an electrothermal model the device temperature is dynamically calculated with the help of the thermal impedance network connected to the temperature terminal. Due to the use of automatic differentiation and state-variables, no equations evaluating derivatives with respect to temperature had to be added. An equation calculating the power dissipated by the device was added. This approach of model development helped develop the electrothermal MESFET device model within one week. Also, the same model can be used in the frequency and time-domain.

The thermal impedance matrix for all thermal elements are precomputed and can be stored in a file for reuse. The Equation 2.32 is solved within the thermal model, with the power dissipated by each source/sink as the state-variables. The calculated temperature rise from the thermal model is matched at the electrical and thermal network interface.

Table 4.1: Thermal constant (b) and Thermal Conductivity of Si, GaAs, SiO₂ at room temperature.

Material	constant (b)	Thermal Conductivity (W/mK)
Si	1.342	142
GaAs	1.22	46
SiO ₂	0.0342	1.1

4.5 Thermal Nonlinearity

This section discusses the importance of considering the nonlinearity of the material thermal conductivity, for thermal modeling. As mentioned in Section 2.4, the thermal conductivity of materials is temperature dependent. The thermal conductivity constant $-b$ for some materials is given in Table 4.1. In this compact model this nonlinearity is linearized using Kirchhoff's transformation. This transformation and its inverse is applied in the thermal compact models implemented in *fREEDA*TM. The temperature, T , is predicted by the model when the Kirchhoff's transformation and its inverse is applied. The temperature, θ , is predicted by the model when the Kirchhoff's transformation is applied but its inverse is not applied. In this case the thermal nonlinearity is ignored.

To illustrate the effects of thermal nonlinearity on various materials, this model was used to describe the response to a step power input of 0.4W, over a central square of 40 $\mu\text{m} \times 40 \mu\text{m}$, at the surface of a heat sink mounted cubic die with each side = 400 μm . This configuration can illustrate a multi-finger power FET. The netlist with the thermal compact model of this setup is provided in Appendix B, Section B.7. The material parameters of the thermal compact model are set accordingly. Figures 4.3, 4.4 and 4.5 show temperature rise for GaAs, Si and SiO₂ respectively. Although the thermal constant ($-b$) of Si is larger than that of GaAs Si [75], for the similar structural and heat supplied conditions, the good thermal conductivity of Si (approximately 3 \times of that of GaAs), leads to a small temperature rise compared to GaAs at any instance in time. If thermal nonlinearity is completely ignored, from Figures 4.3, 4.4, it was found that neglecting the thermal nonlinearity totally (solid line) the temperature rise at time = 10^{-3} s, was underestimated by 20°C in a temperature rise of 120°C for the GaAs die and by 3°C in a temperature rise of 37°C for Si die. The error in temperature rise for Si is 10% and for GaAs the error was approximately 20%. For SiO₂ although, the temperature constant ($-b$)

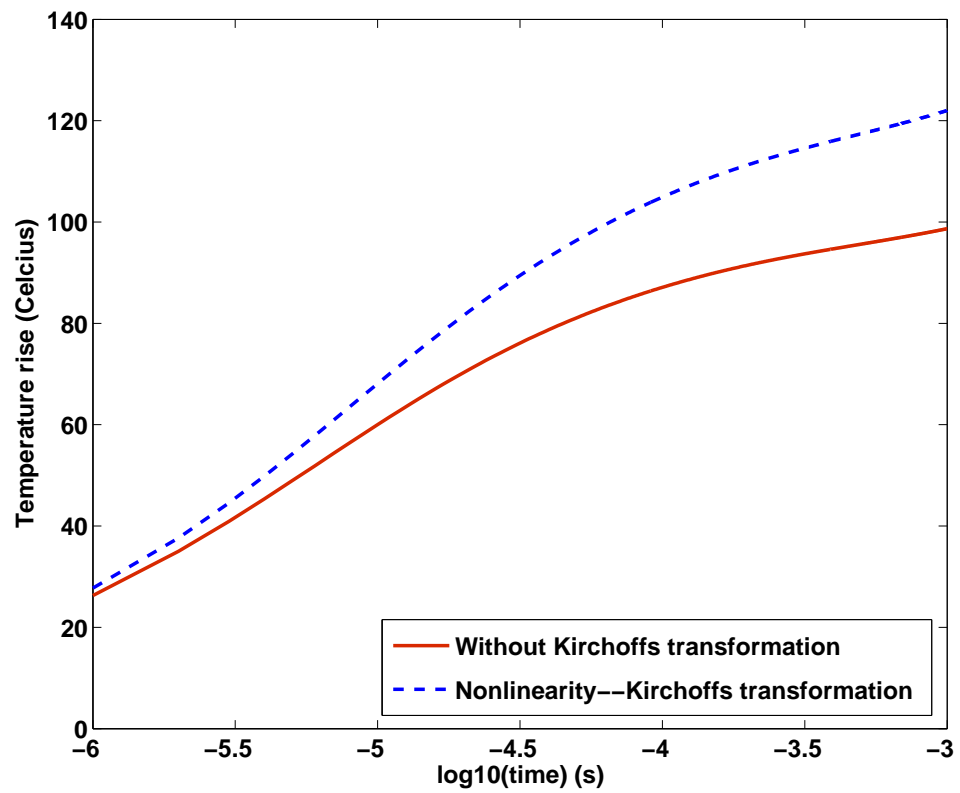


Figure 4.3: Temperature rise of a GaAs die with and without thermal nonlinearity. Thermal nonlinearity is considered when the Kirchoff's transformation is applied (dashed line). Temperature plotted is T . Thermal nonlinearity is ignored when the Kirchoff's transformation is applied but its inverse is not applied (solid line). Temperature plotted is θ .

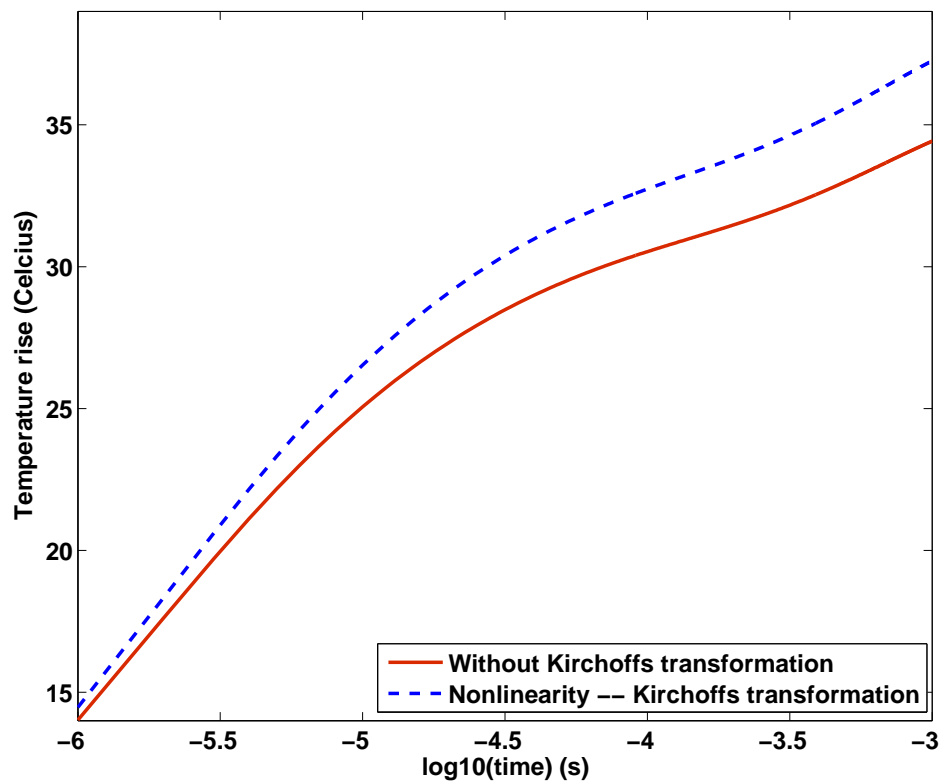


Figure 4.4: Temperature rise of a Si die with and without thermal nonlinearity. Thermal nonlinearity is considered when the Kirchoff's transformation is applied (dashed line). Temperature plotted is T . Thermal nonlinearity is ignored when the Kirchoff's transformation is applied but its inverse is not applied (solid line). Temperature plotted is θ .

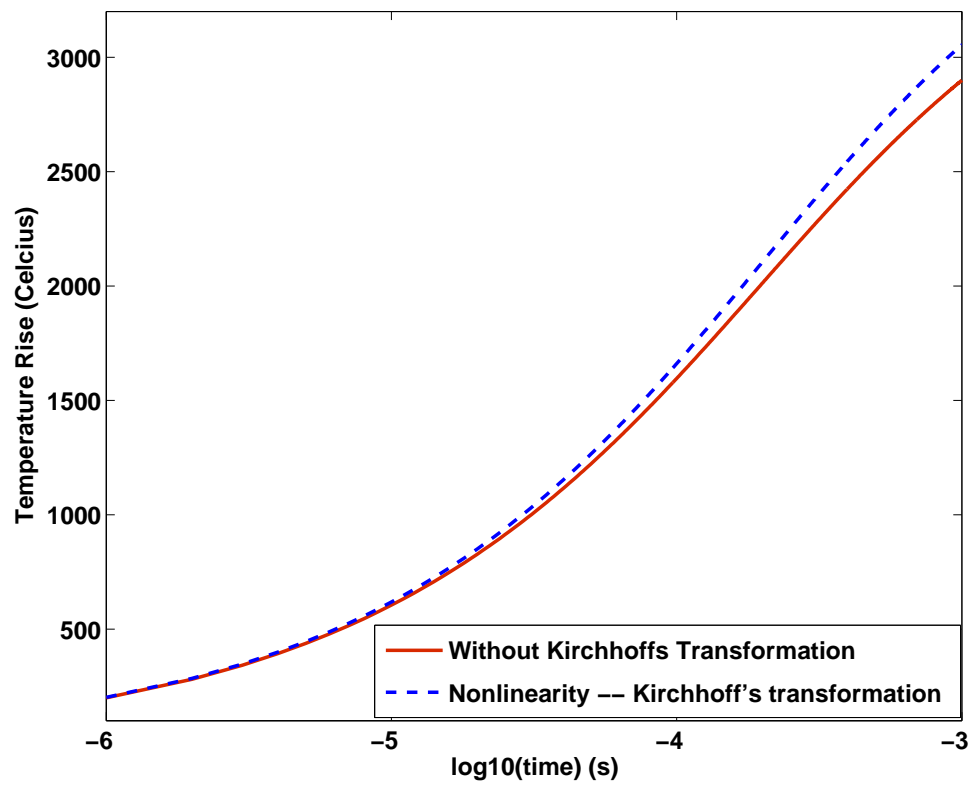


Figure 4.5: Temperature rise of a SiO_2 die with and without thermal nonlinearity. Thermal nonlinearity is considered when the Kirchhoff's transformation is applied (dashed line). Temperature plotted is T . Thermal nonlinearity is ignored when the Kirchhoff's transformation is applied but its inverse is not applied (solid line). Temperature plotted is θ .

is smaller, making the temperature dependence of material properties less pronounced and ignorable. In Figure 4.5, the two SiO₂ temperature rise curves are very close to each other even after long periods of time, allowing the temperature dependence of thermal conductivity to be ignored.

The nonlinearity of the thermal conductivity in the heat diffusion equation is linearized using the Kirchhoff's transformation. This transformed equation is still nonlinear due to the dependence of diffusivity on the transformed temperature, θ . This nonlinearity is linearized using the time variable transformation. But for semiconductors this nonlinearity can be ignored and the diffusivity is assumed constant [60]. In *fREEDA*TM the diffusivity is assumed constant and hence the time variable transformation described in Section 2.4 is not applied. However Batty *et. al* have shown that this assumption of constant diffusivity results in an error in estimation of the temperature rise [60]. For the GaAs die example the assumption of constant diffusivity can lead to overestimate the temperature rise by 4% at any given instant, or, equivalently, to underestimate the rise time required to reach a given temperature by as much as 35% [60]. The amount of error is not only dependent on the material properties, it is also dependent on the die size [60]. The correct handling of thermal transients is left as future work.

4.6 Thermal Camera Calibration

The thermal images of the MMIC were captured using an infra red AFEMA Thermovision 900 SW/TE camera with a pixel size of 50 μm^1 . The MMIC was painted with a specially prepared black ink with known emissivity. Figure 4.6 shows the MMIC before and after the black ink was painted. The zoomed in inked picture, Figure 4.6, shows that the black ink was unevenly sprayed on the MMIC, since some spots on this die are brighter than the others. The bright spots have an emissivity less than the known emissivity of the black ink. Hence a calibration process was applied to eliminate the error introduced due to uneven emissivity through out the surface of the MMIC. Figure 4.7 shows the temperature across the MMIC surface with no DC power and RF power supplied i.e. no heat is generated in the measured body. The temperature on the top of the Kovar substrate was measured using a thermocouple. This temperature was measured as 35°C. The temperature

¹http://www.thermotec-es.de/Dienstleistung_Messen_Agema_e.html

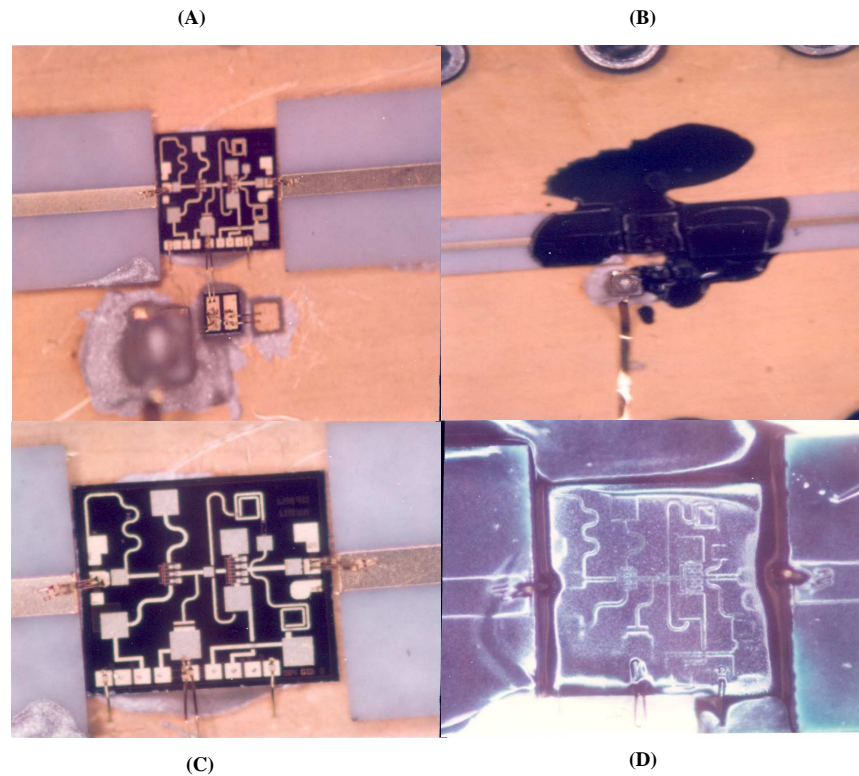


Figure 4.6: MMIC die (A) Mounted die before inking. (B) Mounted die after inking. (C) Zoomed in image of the mounted die before inking. (D) Zoomed in image of the mounted die after inking.

at various spots of interest on the MMIC were measured. Table 4.2 gives the description of the 12 spots on the MMIC structure whose temperature was measured by placing a marker on them. Table 4.3 shows the measured temperature at these spots. Due to the even heat spreading across the body of the MMIC, the expected temperature at each of these spots is 35°C . The variations in emissivity through out the surface of the MMIC results in variations in temperature values from the expected value of 35°C across the surface. The error at each spot is calculated as the difference between the measured value and the expected value of 35°C . Table 4.3 shows the calculated error at each spot. This error was subtracted from the measured temperatures when the DC power and RF power were supplied i.e. when heat is generated in the measured body. A similar correction procedure was applied to the measured temperatures at the various Kovar substrate temperatures. Figure 4.8 shows the temperature across the MMIC surface with no DC and RF power with the Kovar substrate temperature set to 45°C .

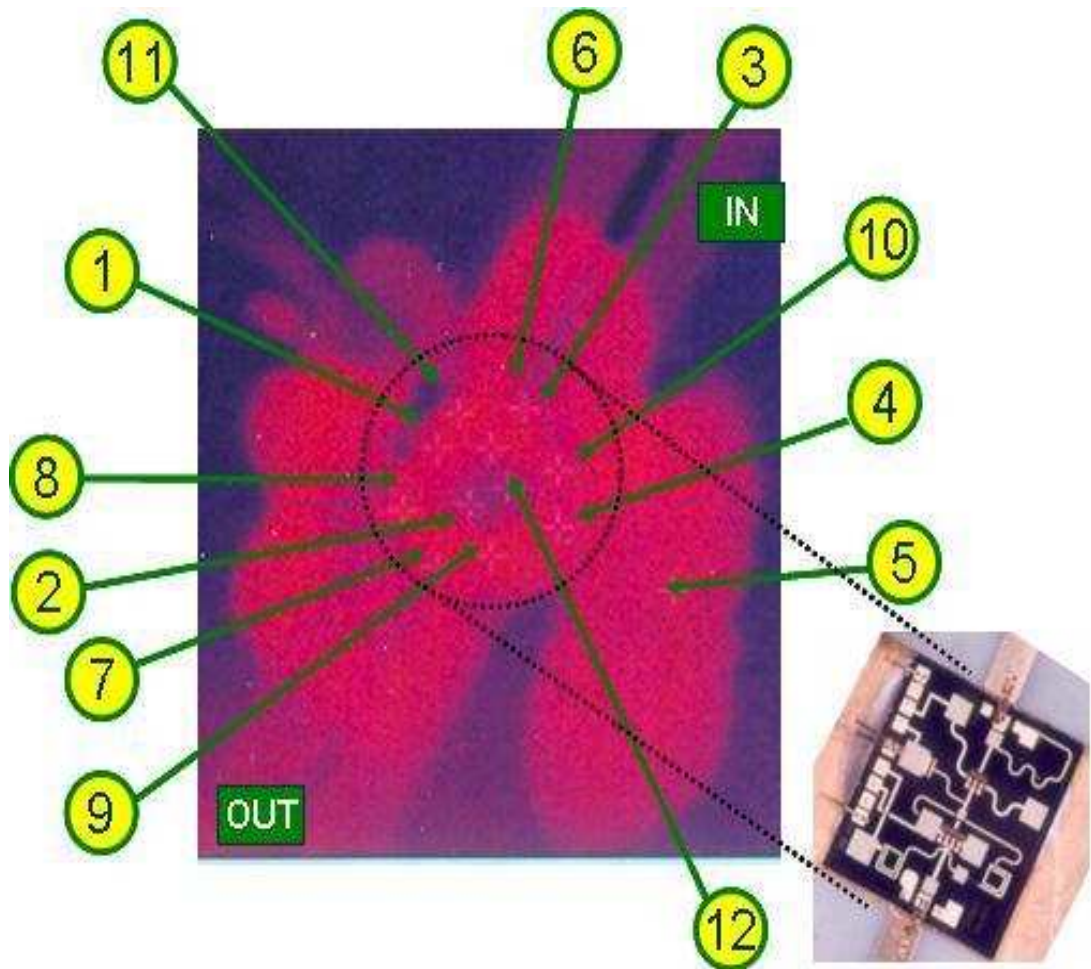


Figure 4.7: Calibration image at 35°C with no DC and no RF power. See Table 4.2 for description of the various spots on the MMIC structure.

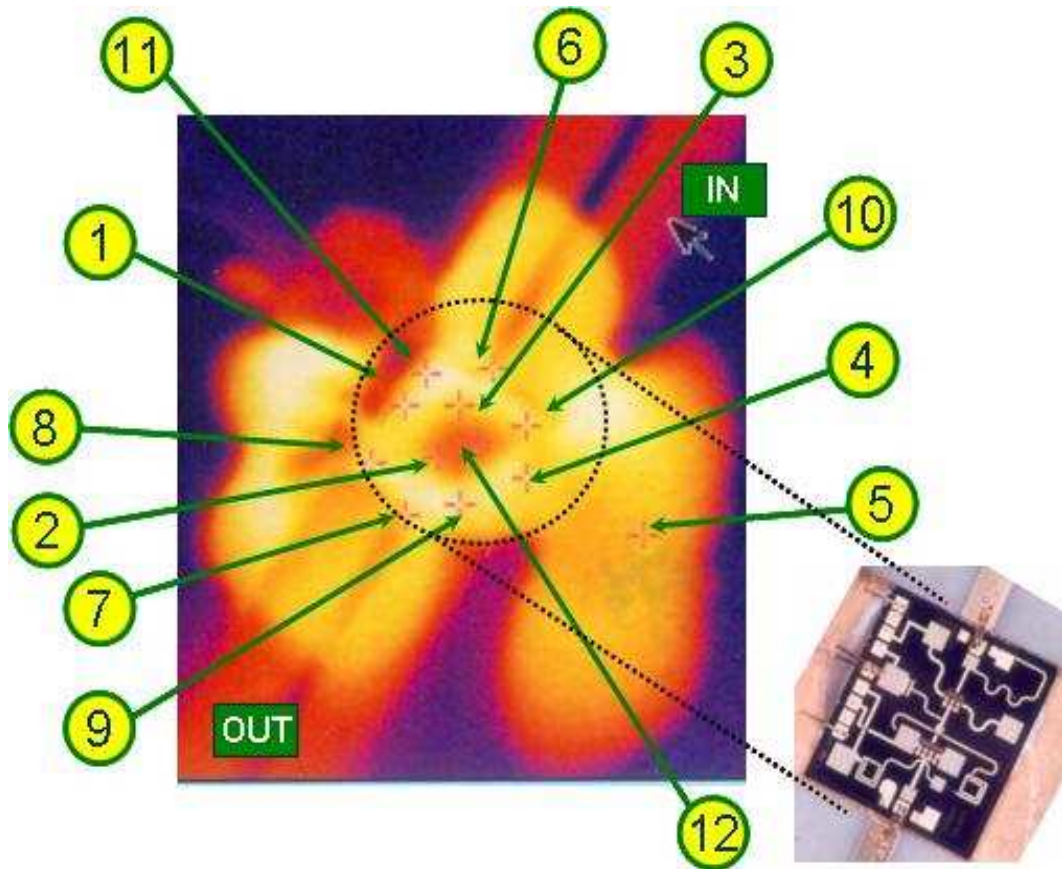


Figure 4.8: Calibration image at 45°C with no DC and no RF power. See Table 4.2 for description of the various spots on the MMIC structure.

Table 4.2: Description of various spots in the thermal image of the MMIC structure.

SPOT Number	Description
1	DC PAD on the GaAs die
2	Transistor 2 on the GaAs die
3	Transistor 1 on the GaAs die
4	Kovar substrate just near the edge of the GaAs die
5	Kovar substrate far away from the edge of the GaAs die
6	RF input external bond wire
7	RF output external bond wire
8	Lower right hand corner of the GaAs die
9	Upper right hand corner of the GaAs die
10	Upper left hand corner of the GaAs die
11	Lower left hand corner of the GaAs die
12	Between the two transistors on the GaAs die

Table 4.3: Camera error at various spots on the MMIC at 35°C. See Table 4.2 for description of the various spots on the MMIC structure.

SPOT	Measured Temperature(°C) at 35°C	Error at 35°C	Measured Temperature(°C) at 45°C	Error at 45°C
1	41.1	6.1	49.3	4.3
2	39.4	4.4	46.5	1.5
3	40.7	5.7	48.3	3.3
4	40.7	5.7	48.7	3.7
5	40.7	5.7	48.1	3.1
6	40.8	5.8	48.8	3.8
7	40.9	5.9	48.6	3.6
8	41.4	6.4	49.4	4.4
9	41.5	6.5	49.9	4.9
10	40.9	5.9	49.1	4.1
11	41.6	6.6	49.6	4.6
12	39.1	4.1	45.4	0.4

4.7 Electrothermal Simulations of the X-band MMIC Structure

The electrothermal model of MMIC structure described in the above sections was verified with thermal images X-band MMIC under DC power and without RF drive. The thermal images of the MMIC were captured using the infra red AFEMA Thermovision 900 SW/TE camera with a pixel size of 50 μm . The temperature measured by the camera is the average temperature over each pixel area. A temperature over any pixel area can be read by placing a marker on it. The MMIC was painted with a Raytheon proprietary black ink with known emissivity. The 19 heating elements were 6 fingers of transistor 1, 8 fingers of transistor 2, 2 TaN resistors and 3 pixel elements. These pixel elements were added to the thermal model to mimic the camera pixels whose temperature was measured. The 3 camera pixels and model pixel elements were placed on transistor 1, transistor 2 and between the 2 TaN resistor. Metallization of the through vias was also modeled. The heat dissipation of the spiral inductors and other surface metallization was ignored. The electrothermal network of the MMIC structure is shown in Figure 4.9. In this figure, in each element the ‘white’ terminals are connected to the 19 heat generating sources explained above. These terminals are connected to the temperature terminal of the electrothermal device model.

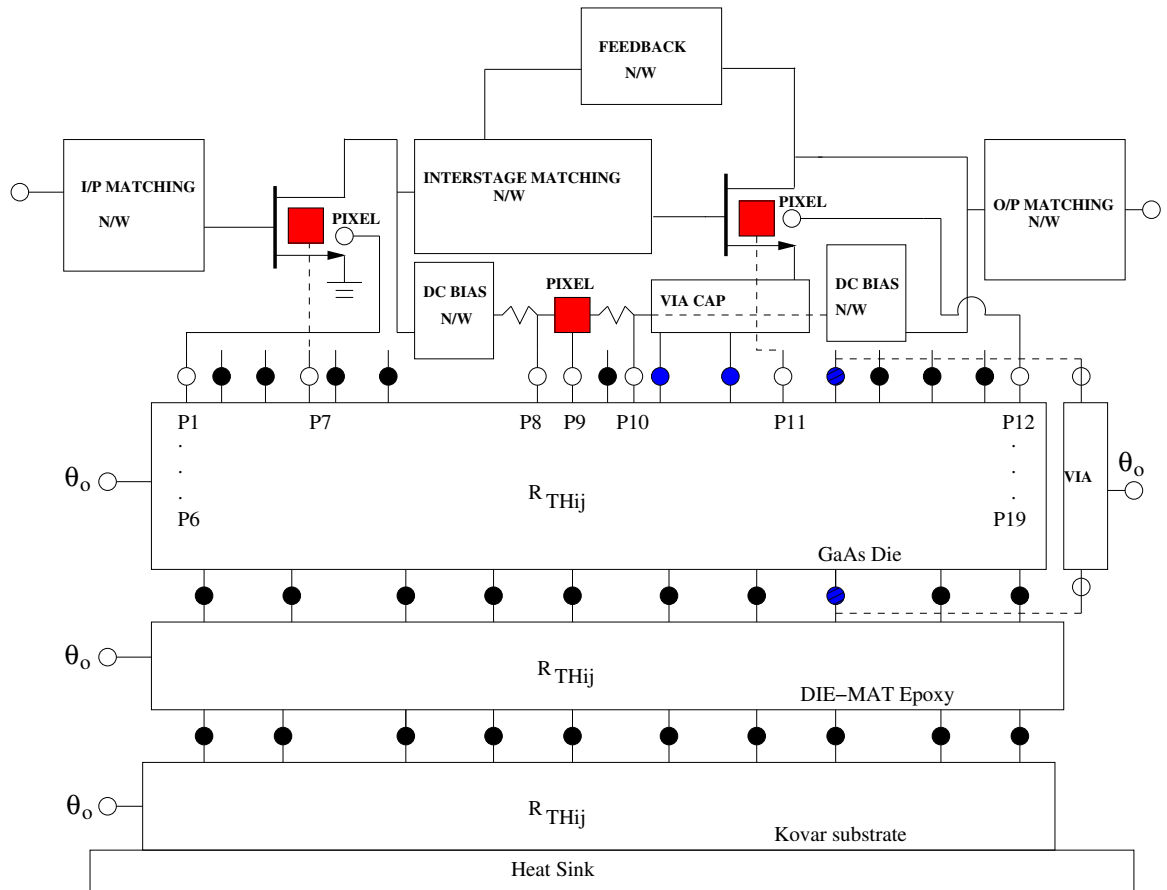


Figure 4.9: fREEDA™ electrothermal model of the MMIC structure.

The temperature at this terminal is fed back to the electrothermal device model as the device temperature. The ‘black’ terminals are the terminals over the discretized surface at each interface. The temperatures at these terminals are matched. The ‘blue’ terminals in the GaAs die element are connected to the surface metallization features including the via capacitors and the through vias. Each thermal element has a thermal ground, θ_0 . The *fREEDA*TM netlist for this set up is provided in Appendix B, Section B.8. The netlist includes the 19 heat sources, the thermal compact model for the GaAs die, Epoxy layer, Kovar substrate, vias and via capacitors. The surface and patch discretization parameter “msubstrate” and “ppatch” can be varied to see the effect of surface discretization. The same netlist with no surface metallization elements i.e. vias and via capacitors is used to see the effect of surface metallization.

4.8 Surface Discretization

Models of all layers or tiers of the MMIC structure used surface discretization at the interfacing surfaces, see Figure 2.4. The blocks of the grid formed due to surface discretization used in the model act as heat sinks or heat dissipating areas for the power sources. The temperature calculated over each block is the average temperature over the entire block. Similarly the thermal impedance is calculated for the entire block. To achieve better accuracy in calculating the thermal impedance and hence temperature, the surface should be discretized into a fine grid. Simulations were performed at different levels of surface discretization to achieve finer grid sizes.

Figure 4.10 shows the temperature rise of transistor 1, transistor 2 and DC pad, at different surface discretization levels. At higher surface discretization levels, the simulated temperature rise is in very good agreement with the measured temperature rise. Figure 4.11 shows the improvement in accuracy at various surface discretization levels. At a surface discretization level of 2, all the models of the MMIC structure, i.e. the GaAs die, the via capacitors metal layer, the patches on the GaAs Die for the via capacitors, the epoxy layer and the Kovar substrate layer, use a 2×2 surface discretization. For the surface discretization level 5, a surface discretization of only 4 was used by the via capacitors’ metal layer and the patches for via capacitors on the GaAs die. There is a $2\times$ improvement in accuracy when the surface discretization level is increased from 2 to 3 and from 3 to 4. At

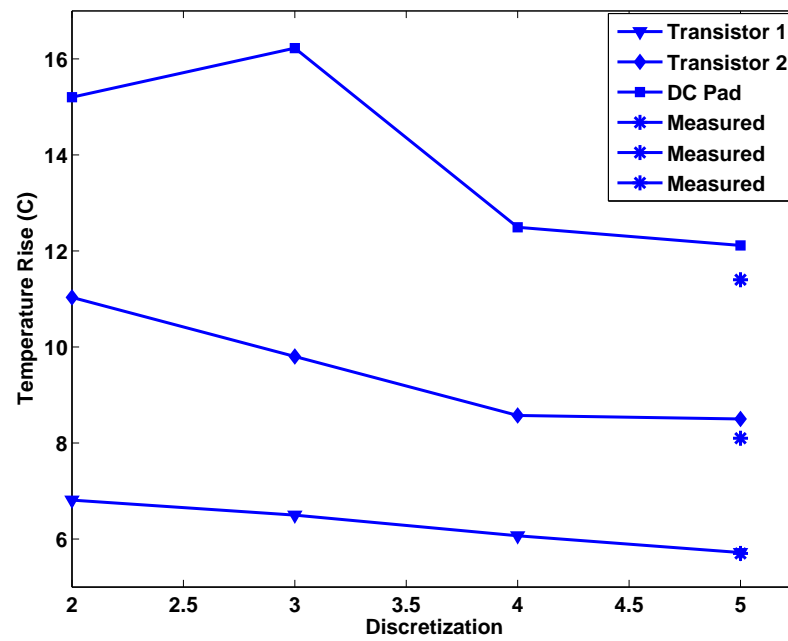


Figure 4.10: Temperatures simulated in *fREEDA*TM at different surface discretization levels.

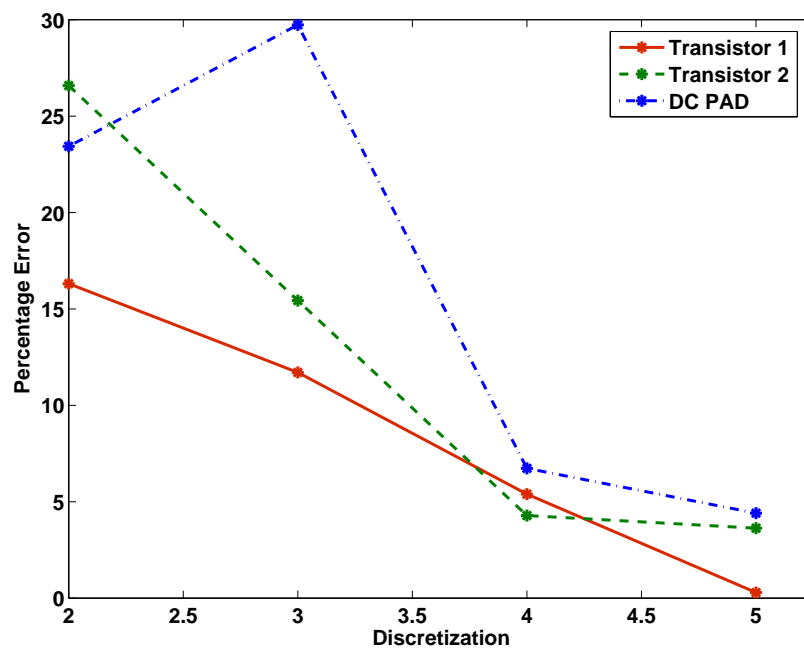


Figure 4.11: Percentage error in the simulated temperatures in *f*REEDA™ at different surface discretization levels.

Table 4.4: Time required to simulate the MMIC structure at various surface discretization levels.

Surface Discretization Level	Simulation Time(s)
2	143
3	377
4	985
5	1383

Table 4.5: Number of nodes in the MMIC structure at various surface discretization levels.

Surface Discretization Level	Number of Nodes
2	47
3	82
4	110
5	158

levels higher than 4, the percentage error flattens out. At levels higher than 5, there is no significant improvement in the accuracy. At this level, the percentage error in the measured and simulated temperature rise of transistor 1, is less than 1%. Also, the percentage error in the temperature rise of transistor 2 and the DC PAD, is less than 5%. Table 4.4 shows the time required for simulation at various surface discretization levels. For higher accuracies the computation time is $10\times$, but the number of nodes to simulate the entire the MMIC structure increases only by a factor of 3.

4.9 Surface Metallization

The developed compact thermal model includes surface metallization. Surface metallization is found to have significant impact due to heat spreading effects. Thus heat spreading must be considered to achieve highly accurate thermal simulations. The vias and the via capacitors on the MMIC act as good heat spreaders. Also the surface metallization on the fingers of transistor 1 and transistor 2 act as good heat spreaders. Table 4.6 shows the improvement in accuracy when the metallization due to the through vias and the via capacitors were considered. The vias and the via capacitors close to transistor 2 only were considered. Other vias and via capacitors were not considered since they were far away

Table 4.6: Simulated temperature ($^{\circ}\text{C}$) at various spots on the MMIC with different layers of surface metallization. See Table 4.2 for description of the various spots on the MMIC structure. Spot 1 - DC PAD, Spot 2 - Transistor 2, Spot 3 - Transistor 1.

SPOT	No metallization	Via	Via and Via Caps	Via and extended via caps
Transistor 1	41.47	41.45	41.44	41.41
Transistor 2	46.92	46.74	46.25	44.9
DC PAD	47.65	47.63	47.62	47.2

from the heat generating transistors. Heat spreading effects due to the other vias and via capacitors is negligible and is ignored. Addition of the vias and via capacitors decreases the temperature rise of transistor 2 only marginally, making the inclusion of the finger surface metallization important. The surface area of the two via capacitor elements were extended to meet at the center of transistor 2, to mimic the finger surface metallization of transistor 2. This is the weakest approximation of the finger metal. Alternatively metal layer over each finger was explicitly modeled as a separate thermal element. But this was not done here. The inclusion of the extended via capacitors, improves the accuracy of the transistor 2 temperature rise by 20%. The finger surface metallization acts as a very good heat spreader, and cannot be ignored to achieve highly accurate thermal simulations.

4.9.1 Thermal Model Verification

The thermal images captured by the infra-red camera show the steady-state temperature of the MMIC, see Figure 4.12. To verify the model the temperatures predicted by the model at time = 0.04 s, corresponding to steady-state, with only DC power supplied were compared to the measured temperature. The netlist used to verify the thermal model of the MMIC is provide in Appendix B, Section B.8. A surface discretization of 5 was used by all elements and extended via capacitors as explained in the previous section were used. Figure 4.12 shows the thermal image of the MMIC, with the temperature of the heat sink set to 35°C . The thermal camera error in Table 4.3 was used to calculate the corrected measured temperature readings of the various spots on the MMIC in Table 4.7. Table 4.8 compares the measured temperatures and simulated temperatures of the ‘pixel’ elements at a heat sink temperature of 35°C . The simulated temperatures are in good agreement with

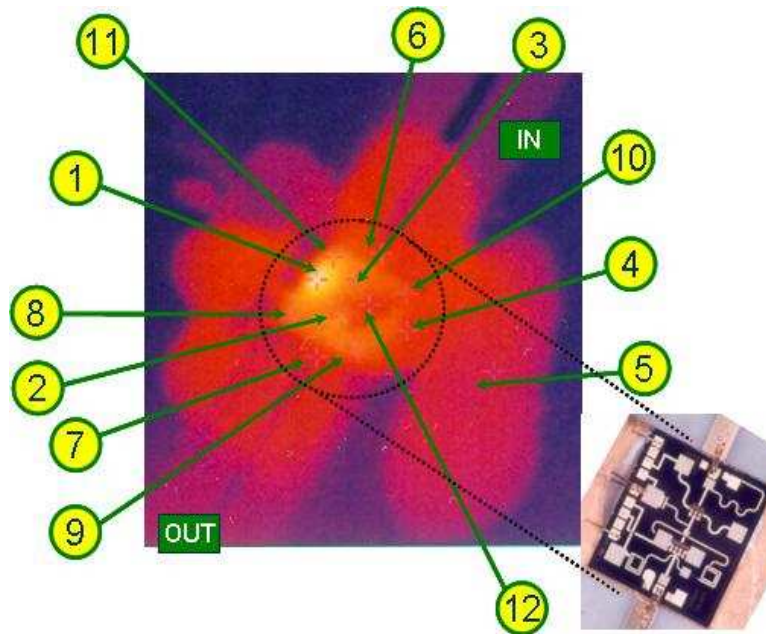


Figure 4.12: Thermal image of the X-band MMIC with DC power applied at 35°C. See Table 4.2 for description of the various spots on the MMIC structure.

Table 4.7: Measured and corrected temperatures at various spots on the MMIC at various base temperatures with DC power applied. See Table 4.2 for description of the various spots on the MMIC structure.

SPOT	Measured at 35°C	Corrected at 35°C	Measured at 45°C	Corrected at 45°C	Measured at 60°C	Corrected at 60°C
1	52.5	46.4	61.8	57.5	74.5	72.6
2	47.5	43.1	55.8	54.3	67.1	68.5
3	46.4	40.7	55.6	52.3	65.5	67.4
4	43.9	38.2	52.3	48.6	65.5	64.2
5	41.8	36.1	49.3	46.2	59.6	61.5
6	43.8	38.0	52.5	48.7	64.1	63.8
7	43.4	37.5	51.5	47.9	62.4	62.7
8	46.5	40.1	55.3	50.9	67.2	65.9
9	46.7	40.2	55.4	50.5	67.7	65.7
10	44.3	38.4	53.2	49.1	65.3	64.7
11	48.2	41.6	57.1	52.5	70.2	67.6
12	43.9	39.8	51.6	51.5	61.2	66.2

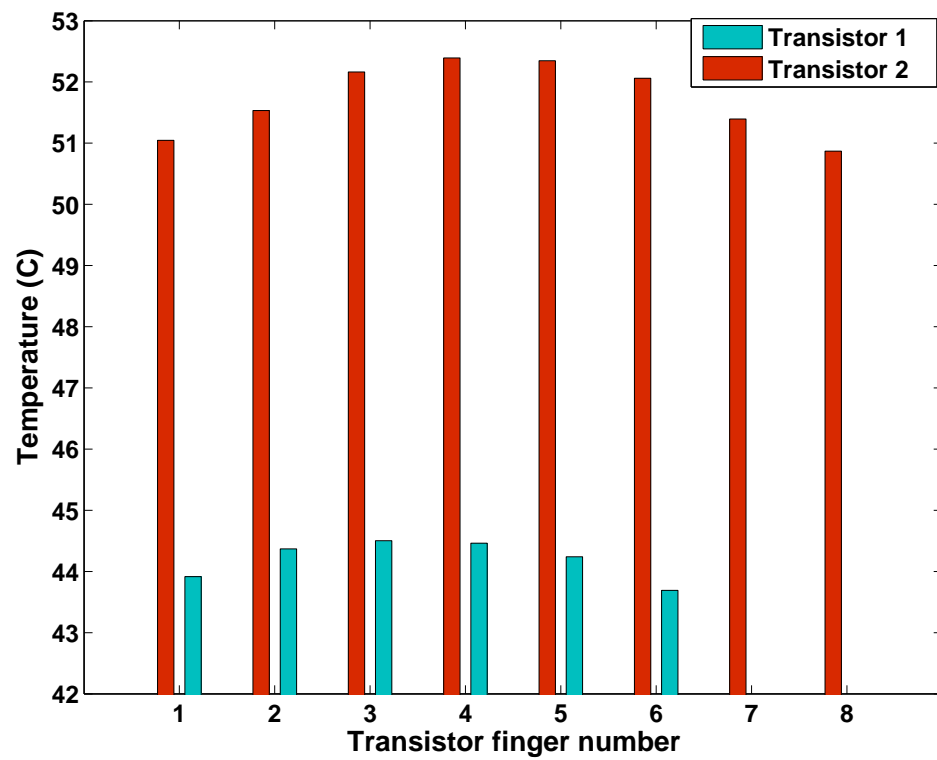


Figure 4.13: Temperatures of the transistor fingers simulated in *f*REEDA™ at 35°C.

Table 4.8: Simulated and measured temperatures at various spots on the MMIC at 35°C. See Table 4.2 for description of the various spots on the MMIC structure. Spot 1 - DC PAD, Spot 2 - Transistor 2, Spot 3 - Transistor 1.

SPOT	Simulated Temperature(°C)	Measured Temperature(°C)
DC PAD	47.2	46.4
Transistor 1	41.4	40.7
Transistor 2	44.9	43.1

Table 4.9: Simulated temperature with Kirchhoff's transformation applied and without Kirchhoff's transformation applied, at various spots on the MMIC structure at 35°C. See Table 4.2 for description of the various spots on the MMIC structure. Spot 1 - DC PAD, Spot 2 - Transistor 2, Spot 3 - Transistor 1.

SPOT	Simulated Temperature(°C) without Kirchhoff's transformation	Simulated Temperature(°C) with Kirchhoff's transformation
DC PAD	46.9	47.2
Transistor 1	41.3	41.4
Transistor 2	44.7	44.9

the measured temperatures. As seen in Figure 4.13, individual transistor finger temperatures are higher than the 'pixel' element temperatures. The 'pixel' elements of the model calculate the average temperature over the resolution or 'pixel' size of the thermal camera. Each pixel of $50 \mu\text{m} \times 50 \mu\text{m}$ is bigger than the individual fingers of $0.5 \mu\text{m} \times 50 \mu\text{m}$. The average temperature over the larger surface area of the pixel would be lower than the temperature over the smaller surface area of individual fingers, due to heat spreading effects. Also it can be seen in Figure 4.13 that all the fingers do not show the same temperature rise. The fingers between the other fingers are at a higher temperature, compared to ones at the ends, due to the limited area available to the middle fingers for heat spreading and the mutual thermal interactions is maximum at these fingers.

The above simulations were done with the forward and inverse Kirchhoff's transformation applied with all metallization features. To see the importance of thermal nonlinearity on this particular MMIC die size and layout, simulations were performed with the inverse Kirchhoff's transformation ignored. All metallization features were included in all the simulations. Table 4.9 compares the simulated temperature at various spots on the MMIC with the inverse Kirchhoff transformation applied and without the inverse Kirchhoff

transformation applied. Kirchhoff's transformation linearizes the thermal nonlinearity in the heat diffusion equation. The temperature predicted by this linearized heat diffusion equation is a transformed temperature, θ . By not applying the inverse Kirchhoff's transformation the thermal nonlinearity is partially ignored and the temperature predicted is the transformed temperature, θ . As expected, by neglecting partially the thermal nonlinearity by not performing the inverse Kirchhoff transformation, underestimates the temperature rise by less than 0.3°C . The error introduced in the temperature rise due to the neglect of the thermal nonlinearity is less than 2% in a temperature rise of 12°C . As shown in Chapter 2 this error is 20% for GaAs. But Batty *et al.* have shown that this error is not constant for all ranges of temperature and depends on the size of the die [60]. It appears from Tables 4.7 and 4.9 that the error between the measured and simulated temperature without the inverse Kirchhoff transformation is smaller than the error between the measured and simulated temperature with the inverse Kirchhoff transformation. As mentioned in the previous section, the neglect of the inverse Kirchhoff transformation or thermal nonlinearity underestimates the temperature rise, similar results are seen in the simulations in Table 4.9. The error in the predicted temperature is due to a number of reasons. One of the sources of errors arises because the measured pixel elements are not exactly at the center of the transistors as assumed in the simulation. Another source of error is the variations in the thickness of the GaAs die is ignored. In simulations a uniform thickness was assumed. Finally in simulation the heat sink is assumed to be at a constant temperature at all points. Due to these unavoidable errors the predicted temperature rise cannot have infinite accuracy.

The effect of temperature on device performance is shown in Figure 4.14. Here the predicted output voltage of the MMIC with an electrical model at room temperature, and an electrothermal model using the temperature provided by the thermal model. If self-heating and mutual thermal interactions are ignored the output voltage is overestimated. Hence self-heating and mutual thermal interactions cannot be ignored in evaluating the performance of the MMIC. Another observation can be made from the above experiment, at all base temperatures the DC pad is the hottest. In an Low Noise Amplifier (LNA) design, to minimize thermal noise the DC pad should be as far away from the first stage. This is because the first stage plays a dominant role in the noise characteristics of the amplifier.

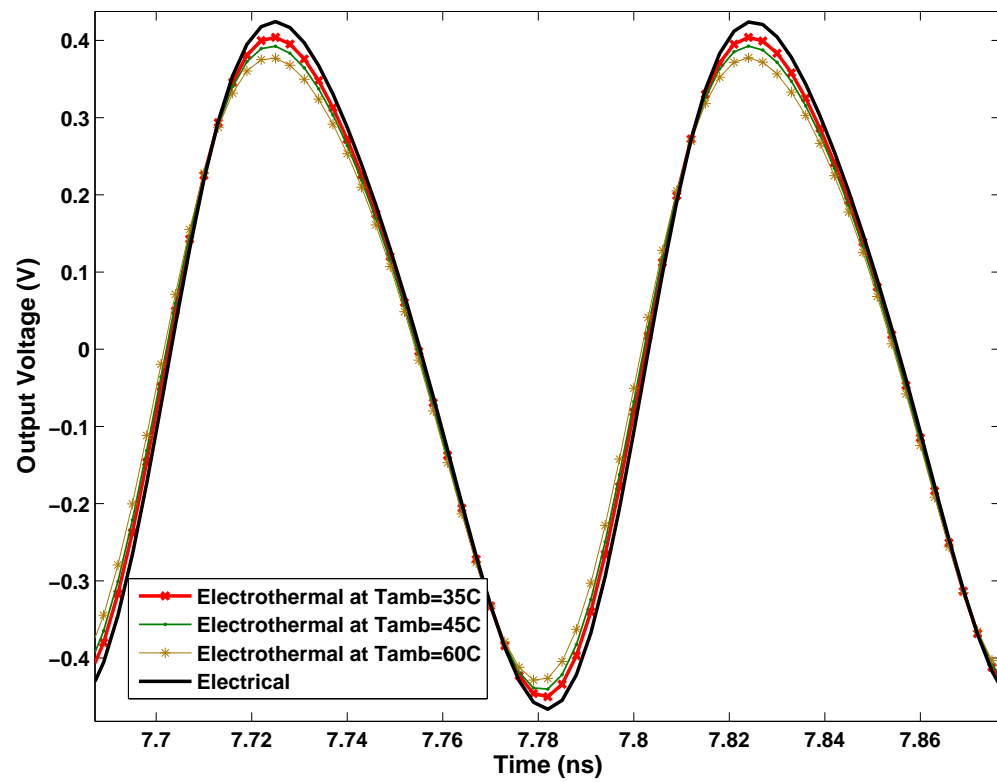


Figure 4.14: Simulated output voltage at elevated temperatures.

4.10 Summary

In this chapter a reduced-order compact thermal model of an X-band MMIC was implemented and validated in, *fREEDA*TM, the general purpose circuit simulator. The model predicts the steady-state temperature rise on various spots of the MMIC with high accuracy. This model solves the nonlinear time-dependent heat diffusion equation of the MMIC structure by transformation of the equation to linear form and domain decomposition. These transformations are applied to every thermal subvolume or layer, i.e. the GaAs die, vias, epoxy layer etc., considered in modeling the MMIC structure. For each subvolume or layer, the transformed equations are solved, to obtain the *s*-space thermal impedance matrices for each subvolume. These thermal impedance matrices accurately describe the thermal interactions between thermal subvolumes by algebraic equations. Temperatures at only the interfaces of these subvolumes are calculated thus requiring minimum number of nodes as temperature rises within the thermal subvolume are not calculated. The algebraic equations and minimization of the number of thermal nodes makes the model a reduced-order compact model which is easily implemented in *fREEDA*TM.

The steady-state thermal simulations of the MMIC structure were validated with thermal images taken with an infra-red thermal imaging camera. Accuracy better than 5% error was achieved. The accuracy of the temperature calculations is significantly improved with the inclusion of complex MMIC features such as via and surface metallization of via capacitors and the transistors fingers. The temperatures obtained from the thermal simulations were used to perform an electrical simulation at RF frequencies at elevated device temperatures. If the temperature rise in a device due to self-heating and mutual thermal interactions is ignored, the output voltage of the MMIC is overestimated. Hence thermal effects are important considerations in the performance evaluation of the MMIC.

The thermal effects must be considered during the chip design process. To design a good integrated circuit, thermal simulations must be done as a part of the design cycle. Also, at elevated temperatures, power dissipation of individual devices is reduced, due to current reduction. This reduced power dissipation must be fed back to the thermal simulations, for better temperature calculations. This type of feedback can be obtained by a fully-coupled electrothermal simulation.

The thermal model developed in this chapter, can be used to perform a fully-coupled electrothermal simulation with DC power sources applied. The long thermal tran-

sient of the MMIC, and its electrothermal effects, can be simulated with an electrothermal time-domain co-simulation. To include these effects at RF frequencies, the electrothermal co-simulation must be performed at very small time steps, since the electrical simulation must be done at these small time steps. The time steps required are as small as 3ps. At these small time steps, the time dependent s -space thermal impedance matrices, change very gradually, due to the long thermal constants. The thermal compact model is limited to time steps as small as 2 ns. For simulations with time steps smaller than 2 ns a multi time step transient analysis, where the electrical domain uses a small time step for RF simulations, and the thermal domain uses a large time step for thermal transient simulations can be used. At time points between the large thermal time step, the thermal solution can be interpolated. This type of analysis is under development in *fREEDA*TM.

Chapter 5

Thermal Macromodel

5.1 Introduction

In the previous chapter a reduced-order compact thermal model of the MMIC structure based on analytical solutions of the linearized partial differential heat diffusion equation was developed. The simulated steady-state temperature rise of the MMIC was verified using the experimental thermal images of the MMIC. To perform a fully-coupled electrothermal simulation at RF frequencies, however the time step for the simulation must be as small as 3 ps. Unfortunately the compact thermal model is limited to a time step of about 2 ns. For time steps smaller than 2 ns the accumulated numerical error in the compact thermal model is too large for an accurate simulation. To perform a fully-coupled electrothermal simulation of the X-band MMIC LNA a different approach was adopted. A 3D thermal macromodel of the MMIC was developed. This macromodel is based on structural and metal density information in each direction. It is compatible with the small time steps of the transient RF simulations. The volume discretization used in the model uses the effective thermal conductivity in each direction. The effective thermal conductivity is a function of the metal density in the dielectric in each direction. It is a good first-order approximation for electronic circuits with several metal layers and large number of through vias. The model helps predict the average temperature rise on various spots on the layer. Section 5.2 describes the linear RC network used to build thermal macromodel in detail.

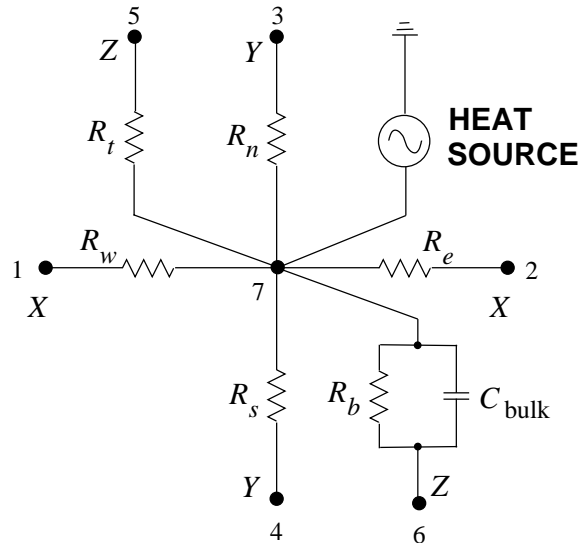


Figure 5.1: Schematic of the thermal macromodel of each grid block.

This macromodel and high dynamic range capability of the new time step control developed in Chapter 3 were used to capture the small variations in the output voltage levels due to the thermal effects in a coupled electrothermal simulation at RF frequencies. The coupled electrothermal simulation for the X-band GaAs MMIC LNA is discussed in Section 5.3.2.

The effective thermal conductivity used in the thermal macromodel is a good first-order approximation to study the thermal effects in a 3DIC, which has several metal layers and large number of through vias. In a 3DIC the thermal problem is exacerbated due to the stacking of chips. The finite number of objects handling capacity in traditional numerical thermal analyses techniques cannot simulate huge number of transistors, metal layers and vias in a 3DIC. To study the hot spots in a 3DIC the thermal macromodel was used. The large number of metal interconnects and metal vias in the 3D architecture, will provide the metal density of the layer/tier in each direction. This macromodel was used to simulate maximum temperature rise in a 3DIC, when various parameters of the 3DIC are varied. These results are presented in Section 5.5.

5.2 Thermal Macromodel

The thermal macromodel developed in this work is a linear RC network and is used to estimate the temperature in a thermal subvolume with each of the thermal subvolumes confined to a single layer or tier. The layer or tier is divided into smaller blocks. Each block is modeled by the thermal macromodel. Each block has zero or more active devices. It has been shown experimentally that the introduction of intermetallic vias reduces the effective thermal resistance between metallization layers [78]. Also, the impact on thermal resistances at the boundaries between silicon dioxide and metallization is negligible [78]. If the intermetallic vias cover 20% of the area, the intermetallic thermal resistance is reduced by approximately 35%. Of this reduction 90% originates from the effective reduction of the thermal resistance by the intermetallic vias. Based on these findings, the vertical thermal resistance of a dielectric layer with vertical vias, can be approximated as the parallel combination of the vertical dielectric thermal resistance and the thermal resistance of the vertical vias. This finding can be applied in each direction of the macromodel to evaluate the thermal resistance in that direction. The thermal macromodel consists of a RC network shown in Figure 5.1. The information required by the thermal macromodel, is the metal density, the thermal conductivities of the dielectric material and the thermal conductivities of the metal in the X, Y and Z direction of each block. In the thermal macromodel the X, Y and Z direction is further divided into east, west, north, south, top and bottom directions. The X direction is the east-west direction, the Y direction is the north-south direction and the Z direction is the top-bottom direction. Metal density here is calculated as the percentage cross sectional area of the material the metal is embedded in occupied by the metal. The metal layers embedded in the material act as the paths of heat removal. Based on the material information and the structural information of each block, the macromodel calculates the thermal resistance in each direction, using the one-dimensional heat equation. The one dimensional heat equation is given by [79], assuming uniform thermal conductivity,

$$\frac{d}{dx}\left(\kappa \frac{dT}{dx}\right) = 0. \quad (5.1)$$

On solving this equation and using Fouriers first law, the thermal resistance of heat conduction is given by,

$$R_{th} = \frac{L}{\kappa A} \quad (5.2)$$

where L is the length of the block in the x-direction and A is the area of cross section. The above equation is used to calculate the thermal resistance of the dielectric and the metal in east, west, north, south, top and bottom direction of Figure 5.1. In this figure the suffix of the thermal resistance indicates its direction. For example the thermal resistance R_n in Figure 5.1 is calculated as:

$$R_{N-metal} = \frac{l_x}{2 * k_{mx} * A_{N-metal}} \quad (5.3)$$

$$R_{N-die} = \frac{l_x}{2 * k_{bulk} * A_{N-die}} \quad (5.4)$$

$$R_n = \frac{R_{N-metal} * R_{N-die}}{R_{N-metal} + R_{N-die}} \quad (5.5)$$

where $A_{N-metal}$ is the cross sectional area of the metal in the north direction, A_{N-die} is the cross sectional area of the die in the north direction, l_x is the length of block in X direction, k_{mx} is the thermal conductivity of metal in X direction, k_{bulk} is the thermal conductivity of bulk material, $R_{N-metal}$ is the thermal resistance of metal in north direction, R_{N-die} is the thermal resistance of die in north direction and R_n is the thermal resistance in north direction.

Similarly the thermal resistance in each direction is a parallel combination of thermal resistance of the dielectric and the metal in that direction. The capacitor models the heat capacity of the dielectric material. The total power dissipated in the block is modeled as a single heat source connected to the central node of the macromodel. The formulae used to calculate the RC values are explained in Appendix A. The boundary conditions applied to each layer or tier are:

- The four sidewalls are adiabatic.
- The bottom wall is connected to the heat sink and is isothermal.

Each block of each layer is modeled by the thermal macromodel shown in Figure 5.1. These blocks are connected to each other through the external nodes, NODES 1, 2, 3, 4, 5 and 6 in Figure 5.1, making this model extensively scalable. Figure 5.2 shows 4 horizontally adjacent grid blocks in the X-Y direction of a layer. To connect the layers vertically the Node 6 of the top layer is connected to Node 5 of the bottom layer. Thus each layer and stack of layers are modeled by connecting the thermal macromodel of each block appropriately. This forms a large linear RC network. The thermal macromodel of the chip is a linear

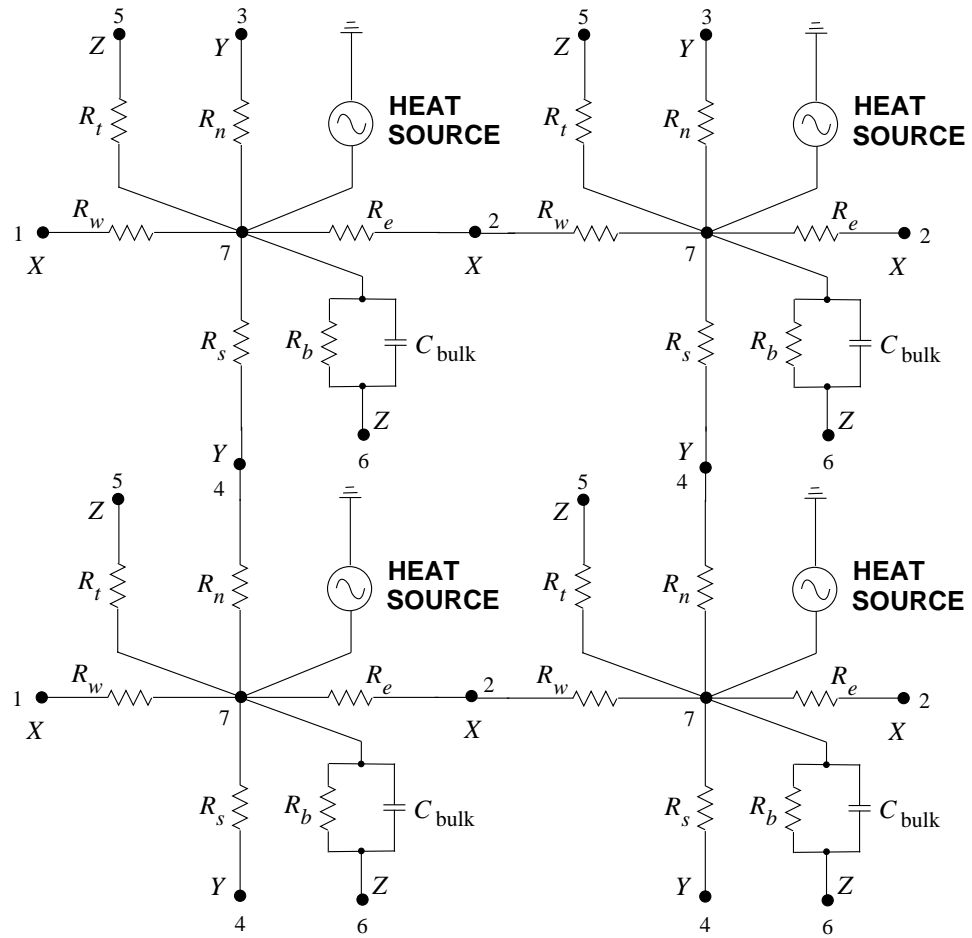


Figure 5.2: Schematic of 4 horizontally adjacent grid blocks in the X-Y direction of a layer.

RC network, and the temperature is found by solving nodal equations, numerically. The macromodel uses geometry, grid, boundary conditions and material properties. This model gives the temperature rise averaged over the surface area of the block, which is used to plot a temperature profile of the entire tier and the whole chip at large. The whole chip can be modeled with an RC network, which can be solved numerically to find the nodal temperatures. This model can be scaled down to a microlevel by reducing the physical size of each block.

5.3 Thermal Macromodel of the X-band MMIC LNA

5.3.1 Temperature Rise at Steady-State

The macromodel described in the above section is used here to perform a coupled electrothermal simulation of the X-band MMIC LNA. The steady-state temperature predicted by the thermal macromodel were verified with steady-state thermal images taken with an infra red camera. The macromodel is a linear RC network and does not account for the thermal nonlinearity of the thermal conductivity of GaAs. In Chapter 4, in Table 4.9, it was shown, that the neglect of thermal nonlinearity for this X-band MMIC LNA, introduced an error of less than 2% in the temperature rise. Hence using a linear RC model to predict the steady-state temperature rise of the X-band MMIC LNA, would have less than 2% error due to the neglect of thermal nonlinearity. Figure 3.6 shows the layout of the X-band MMIC LNA. This MMIC was attached by DIE-MAT epoxy to a Kovar substrate. The Kovar substrate was screwed to a block of Aluminum, which acted as the heat sink. All these layers of the mounted MMIC were modeled using the thermal macromodel described in Section 5.2.

Figure 5.3 shows the three-dimensional view of the MMIC structure. The black shaded area is the DIE-MAT epoxy used to attach the GaAs die to the Kovar substrate. The Kovar substrate is screwed to the heat sink. The three layers of the MMIC, i.e. the GaAs die ($1624 \mu\text{m} \times 1470 \mu\text{m} \times 100 \mu\text{m}$), the DIE-MAT epoxy ($1624 \mu\text{m} \times 1470 \mu\text{m} \times 100 \mu\text{m}$) and the Kovar substrate ($5 \text{ cm} \times 2.5 \text{ cm} \times 381 \mu\text{m}$) were discretized into a 10×10 grid. Only the surface area of the Kovar substrate covered by the attached GaAs die was discretized ($1624 \mu\text{m} \times 1470 \mu\text{m} \times 381 \mu\text{m}$) into a 10×10 grid. Each grid block

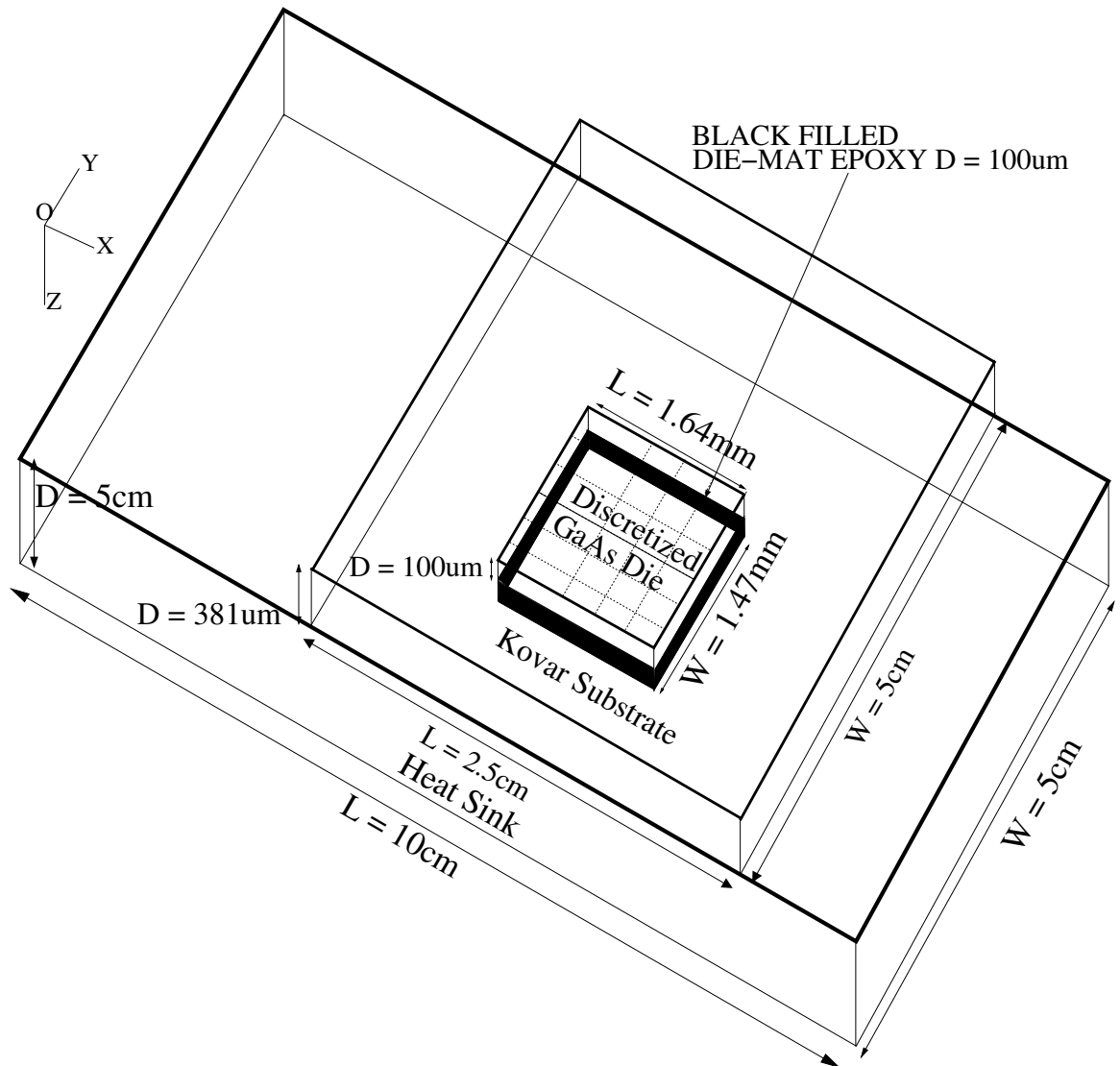


Figure 5.3: Three-dimensional view of the MMIC structure.

was modeled using the RC network shown in Figure 5.1. These blocks are connected to each other as shown in Figure 5.2. The values of the RC network were calculated using the formulae in Appendix A. The four heat generating sources considered were, the 2 transistors shown by the labels A and B and the 2 TaN resistors shown by the labels J, in Figure 3.6. Here resistor 1, refers to the left hand side resistor of the two resistors labelled with J in Figure 3.6 and resistor 2 refers to the right hand side resistor. The metal density of all the blocks of the GaAs die was taken as zero. The exceptions are for the blocks with the two vias and via capacitors near transistor 2. The vias ($50 \mu\text{m} \times 50 \mu\text{m} \times 100 \mu\text{m}$), shown by the label D, to the backside metal plane, were modeled using a nonzero vertical metal density. The top metal layer ($150 \mu\text{m} \times 282 \mu\text{m} \times 7 \mu\text{m}$) of the via capacitors act as good heat spreaders. They were modeled with nonzero horizontal metal density of the grid blocks they are located in. For example the vertical metal density of the grid block ($162.4 \mu\text{m} \times 147 \mu\text{m}$) with a via ($50 \mu\text{m} \times 50 \mu\text{m}$) is 10.4%.

The DIE-MAT epoxy and the Kovar substrate were also modeled using the thermal macromodel. These layers were connected vertically. To connect the layers vertically, Node 6 of each block of the GaAs die is connected to Node 5 of each block of the DIE-MAT Epoxy. Similarly the DIE-MAT Epoxy is connected to the Kovar substrate. The bottom terminals, Terminal 6 in Figure 5.1, of the Kovar substrate blocks were connected to the heat sink at a constant base temperature of 35°C . The top terminal, Terminal 5, of the GaAs die blocks, were connected to zero power sources. All grid blocks on all the layers had zero heat sources at Terminal 7, except for the blocks on the GaAs die where the 2 transistors and 2 TaN resistors are located. To verify the steady-state temperature a coupled electrothermal transient analysis, with only the DC power supplied, was performed on this thermal macromodel connected to the electrical model of the MMIC LNA. The netlist for the coupled electrothermal simulation at RF frequency is provided in Appendix B, Section B.9. This netlist with no RF power supplied is used to predict the steady-state temperature. Figure 5.4 shows the temperature of the grid blocks with the 4 heat generating sources. The temperature reaches steady-state at 180 ms. In the compact thermal model of the MMIC structure described in Chapter 4, the temperature reaches steady-state at 40 ms. The various transformations and the 3D analytical formulation of the compact thermal model makes it precise in predicting the thermal time constant [60]. The compact thermal model also includes the thermal nonlinearity effects. These effects are ignored in the thermal macromodel. Also in the thermal macromodel the 3D heat diffusion equation is

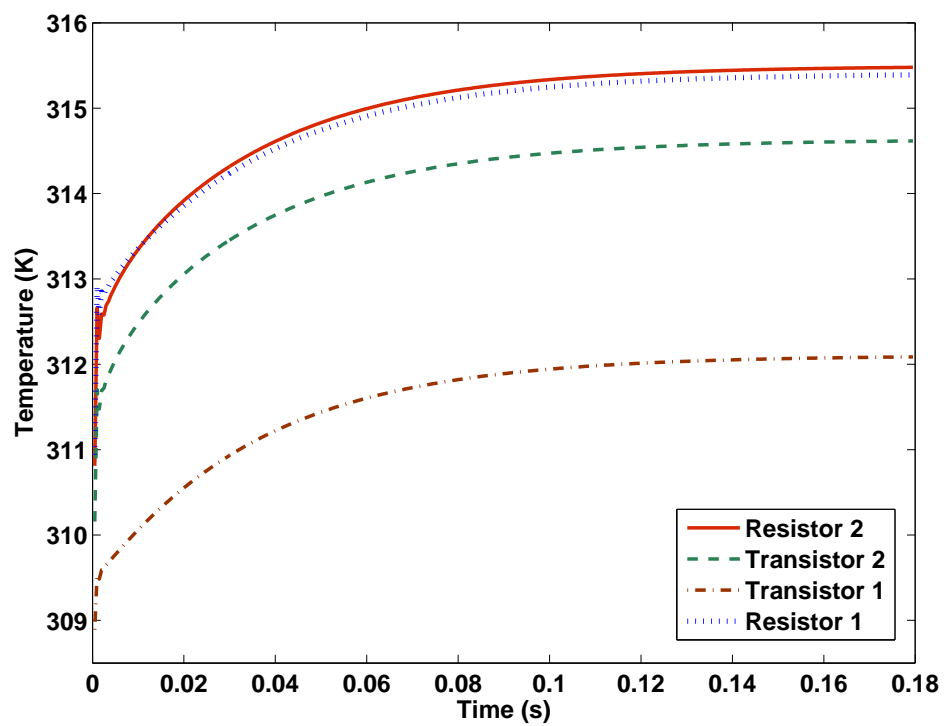


Figure 5.4: Transient temperature of the grid blocks of the MMIC thermal macromodel with the 4 heat generating sources: Resistor 1, Resistor 2 , Transistor 1 and Transistor 2.

Table 5.1: Measured and simulated temperatures with the compact thermal model and the thermal macromodel at various spots on the MMIC structure at a base temperature of 35°C.

SPOT	Simulated Temperature(°C) Compact Thermal Model	Simulated Temperature Macromodel(°C)	Measured Temperature(°C)
DC PAD	47.2	-	46.4
Resistor 1	57.16	42.4	-
Resistor 2	59.75	41.6	-
Transistor 1	41.4	39.0	40.7
Transistor 2	44.9	42.3	43.1

essentially reduced to 1D heat diffusion equation in all three directions. Hence the thermal time constant predicted by the thermal macromodel is overestimated by more than 4 times. But the predicted steady-state temperature rise, is in pretty good agreement with that predicted by the compact thermal model and the thermal measurements.

As explained in the previous chapter the resolution of infra-red thermal camera is 50 μm . During measurements the temperature of a pixel (50 $\mu\text{m} \times 50 \mu\text{m}$) on the DC pad was measured. In the compact thermal model such an ‘pixel element’ (50 $\mu\text{m} \times 50 \mu\text{m}$) was placed on the DC pad to mimic the pixel of the infra-red camera. Hence it could predict the temperature of the pixel on the DC pad in the thermal image. In the thermal macromodel such pixel elements cannot be added since it does not need information about the physical size of the heat dissipating source. Also in this model all heat sources in a single grid block are modeled as a single heat source. The heat dissipated by this single source is the total heat dissipated by all the sources in that block. The predicted temperature rise is the temperature rise averaged over the total surface area of that block. It is not the temperature rise over the individual heat sources. In the compact thermal model the predicted temperature rise is the average temperature rise over the total surface area of the heat source. In the compact model it is average temperature rise over the individual heat sources. The temperatures of the 2 transistors predicted by the macromodel agree with the measurements within 5% error. In Table 5.1 this error is larger for the resistors. The predicted temperature of the transistors agrees better with the compact thermal model than that of the two resistors. This is due to the larger surface area occupied by the transistors

in a grid block. The heat generating surface areas occupied by the 2 transistors are $50 \mu\text{m} \times 150 \mu\text{m}$ and $50 \mu\text{m} \times 200 \mu\text{m}$, respectively. They are approximately 30% and 40% of the surface area of each grid block ($162.4 \mu\text{m} \times 147.0 \mu\text{m}$) of the GaAs die. The heat generating surface areas occupied by the 2 TaN resistors were, $66.5 \mu\text{m} \times 54 \mu\text{m}$ and $31.9 \mu\text{m} \times 64 \mu\text{m}$, respectively. They are approximately 14% and 8% of the surface area of their respective grid blocks in ($162.4 \mu\text{m} \times 147.0 \mu\text{m}$) the 10×10 grid of the GaAs die. Since the 2 transistors occupy a larger surface area of the grid block compared to the resistors and the temperature is averaged over the total surface area of the grid block, the average temperatures predicted by the thermal macromodel of the grid blocks with the transistors agree better with the measured temperatures and temperatures predicted using the compact thermal model. Due to the small percentage area occupied by the 2 resistors, their predicted temperatures do not agree well with those predicted by the compact thermal model. To achieve better accuracy, the GaAs die can be discretized into a finer grid, at the expense of more compute time since the number of nodes will increase.

5.3.2 Coupled Electrothermal Simulations at RF Frequencies

As discussed in the previous section, the steady-state temperature predicted by the thermal macromodel of the MMIC agrees within 10% error of the measured temperature. This model can be used to perform coupled electrothermal simulations at RF frequencies. A coupled electrothermal simulation at 10 GHz was performed on the MMIC with the thermal macromodel. The new time step control technique developed in Chapter 3 was used to perform the coupled electrothermal simulation. The netlist for the coupled electrothermal simulation at RF frequency is provided in Appendix B, Section B.9 The high dynamic range and the numerical robustness of the new time step control technique will help capture the small variations in the output voltage in the electrothermal simulation.

Figure 5.5 shows the simulated output voltage of the MMIC in an electrical transient simulation and a coupled electrothermal transient simulation. These simulations were performed with a -90 dBm sinusoidal input at 10 GHz. In the electrical simulation the device temperature is set to the base temperature. It remains at this temperature throughout the simulation. In an electrothermal simulation the device temperature is not constant. The rise in the device temperature due to self heating is calculated in the electrothermal simulation. This rise in temperature results in a reduction in the output current and volt-

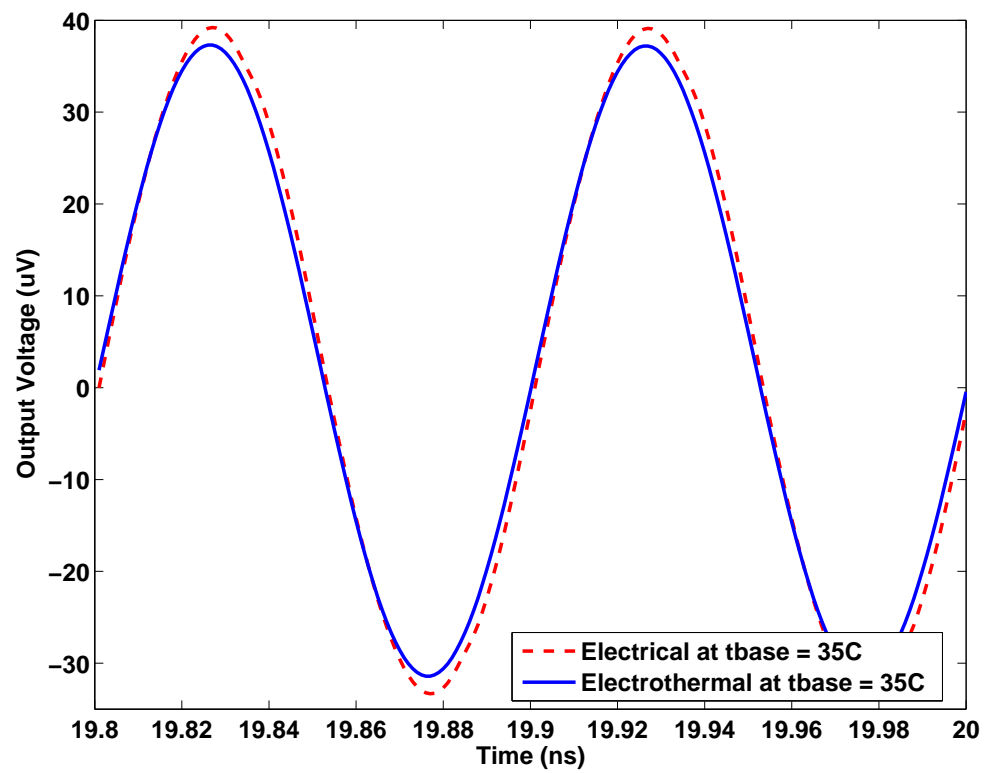


Figure 5.5: Simulated output voltage of the MMIC at $t_{base} = 35^{\circ}\text{C}$ in an electrical and a coupled electrothermal simulation.

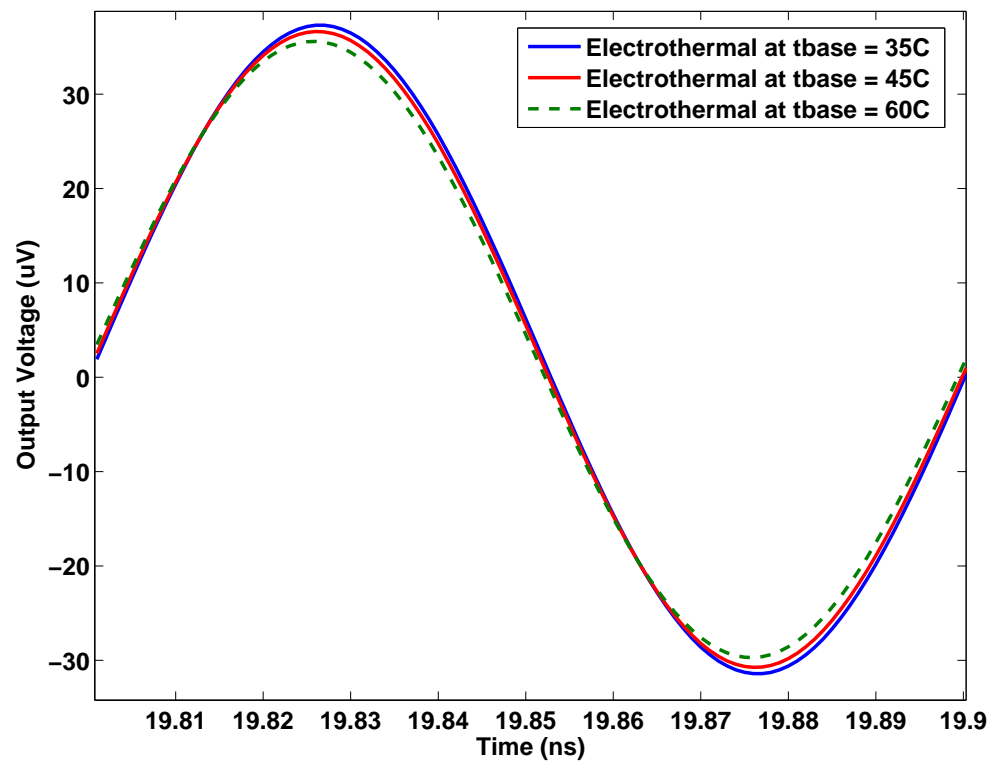


Figure 5.6: Simulated output voltage of the MMIC in a coupled electrothermal simulation at tbase = 35°C, tbase = 45°C and tbase = 60°C.

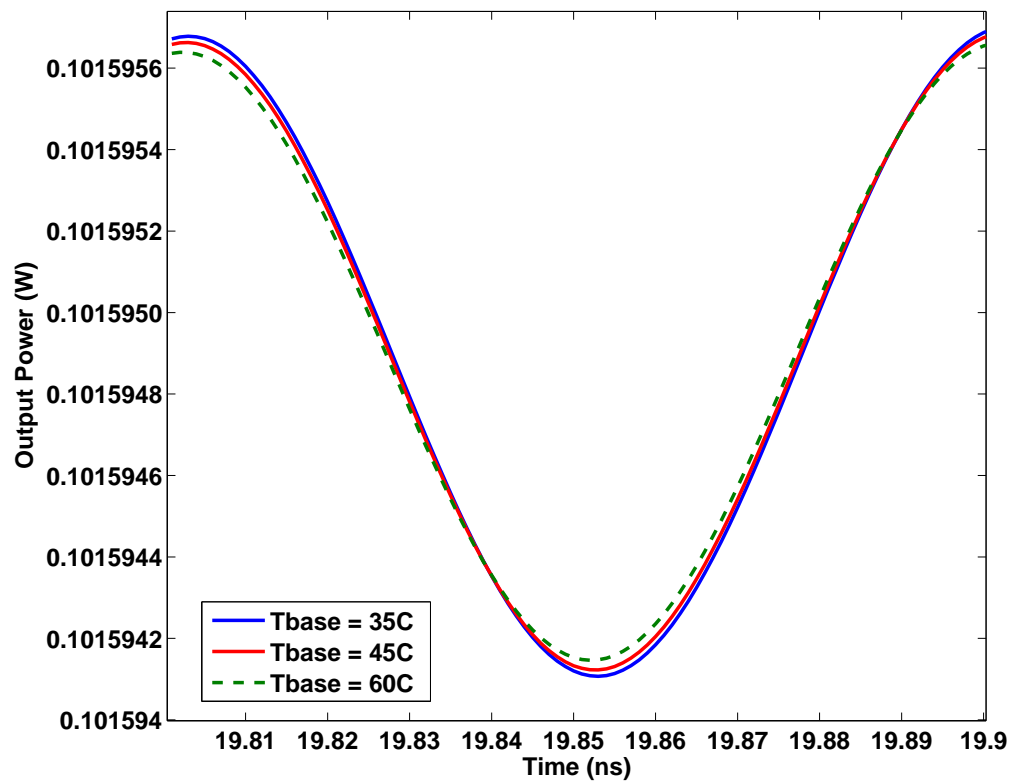


Figure 5.7: Simulated dissipated power by the stage 2 transistor of the MMIC in a coupled electrothermal simulation at $t_{base} = 35^{\circ}\text{C}$, $t_{base} = 45^{\circ}\text{C}$ and $t_{base} = 60^{\circ}\text{C}$.

age. In a purely electrical simulation this reduction is ignored and hence the output voltage of the MMIC is overestimated. Here it is overestimated by $2 \mu\text{V}$ at the peak of the sinusoid. The better initial guess prediction and the precise estimation of error in the new time step control technique helped detect these small variations in sinusoidal output voltage due to thermal effects. Similar simulations were carried out at base temperatures of 35°C , 45°C and 60°C . The output voltage at these base temperatures is shown in Figure 5.6. At higher base temperatures, and so at higher device temperatures, the reduction in the output voltage is larger. A small reduction of less than $1 \mu\text{V}$ in the output voltage could also be detected, due to the high dynamic range capability. The reduction in the output voltage and current effectively reduces the power dissipated. Figure 5.7 shows the reduction in the power dissipated by the stage 2 transistor at the various base temperatures. The output voltage of the MMIC is overestimated if the thermal effects are ignored, making them important considerations in the MMIC performance evaluation.

From the above results it can be concluded that, the macromodel can be used to predict temperature rise in an electronic circuit, if a reasonable amount of surface discretization is used. To achieve more than 5% accuracy the surface discretization must be such that the heat sources in each grid block occupy at least 40% of its surface area. The high dynamic range capability of the new time-domain technique developed in Chapter 3, helped capture the small changes in the output voltage levels in electrothermal simulations. With these capabilities the macromodel can be used to predict hot spots and thermal bottle necks in a 3DIC. This is discussed in the next section.

5.4 Why 3DIC?

In recent years reliability has gained focus in advanced integrated circuit technologies such as SOI, copper metallization and low-K insulators. In spite of continuous device scaling circuit performance and reliability are increasingly determined by the interconnects instead of the devices, making designers use interconnect-centric design flows [35]. Thermal effects are one of the key components in determining interconnect reliability. Thermal conduction is a characteristic of the material and physical structure of a component, making thermal effects an increasingly complex issue with new IC technologies. Studies by Gill *et al* have shown that the thermal conductance of thin insulators is less than that predicted

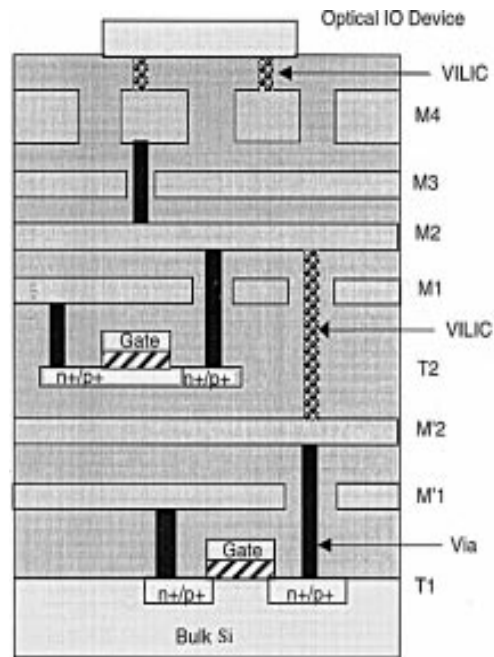


Figure 5.8: Schematic representation of 3-D integration with multilevel wiring network and VILICs. T1: first active layer device, T2: second active layer device, Optical I/O device: third active layer I/O device. M1 and M2 are for T1, M1 and M2 are for T2. M3 and M4 are shared by T1, T2, and the I/O device. After [77]. (Copyright IEEE 2006)

due to the localized substrate heating in interconnects [32],[33]. To study these effects they used an ‘effective conductivity’ quasi-analytical model based on Schwarz-Christoffel transforms.

The delay in these interconnects is limiting the performance improvement in new technologies [39],[40],[41],[42]. According to the ITRS’97 Road Map [38], there is a trend of a growing gap between device delays and interconnect delays. This gap can be narrowed with the use of new interconnect materials and low dielectric constant materials etc. The ITRS’99 Road Map [39] predicts that beyond the 130-nm technology node, performance improvement advances will require some paradigm shift in the architecture of IC’s. One of the architectures being investigated is a three dimensional integrated circuit 3DIC (a simplified schematic is shown in Figure 5.8). This architecture still a concept, can significantly improve the interconnect performance, packaging density, reduce chip area and power dissipation [76]. In this architecture the 2-D planar chips are stacked on top of each other. Each

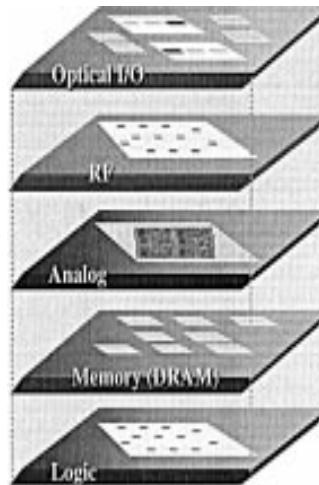


Figure 5.9: Schematic of a 3-D chip showing integrated heterogeneous technologies. After [77]. (Copyright IEEE 2006)

2-D chip can have multiple layers of interconnects and these layers can be connected to each other with Vertical Interlayer Interconnects (VILIC). Due to this stacking two of the important issues in a 3DIC architecture are the heat dissipation and thermal conduction [43]. Heat dissipation is shown to impact the performance of interconnects and devices [43]. In a 3D architecture the thermal problem is severe since the same amount of heat is dissipated in a smaller area, which may result in a sharp temperature rise. Furthermore, all the active layers or each individual chip will be either attached or isolated from the other layers using epoxy. Epoxy has a thermal conductivity that is lower than Si, making thermal conduction a severe problem and causing degradation in device performance and reliability. To explore the feasibility of this technology tools must be developed to study coupled electrothermal effects in a 3DIC. Models must be developed to estimate the temperature at each layer in the chip. Package thermal resistance models for 2D and 3DICs are developed which assume only one-dimensional heat flow [43]. Analytical die temperature models enabling full chip thermal analysis have been developed by Banerjee [44]. This model shows that interconnect joule heating and low thermal conductivities of dielectrics will impact the temperature rise in a 3DIC. Banerjee *et. al* also developed compact models to study the effect of interconnect joule heating and propose that thermal vias can be used to reduce the temperature rise in the interconnects. The effectiveness of these vias depends on the via separation and the dielectric material used. Tedious finite element and finite difference techniques or semi-

analytical techniques with optimization are employed to study the effects of these thermal vias [34],[36],[37],[77].

One of the motivations of a 3DIC is the integration of disparate technologies (digital, analog , RF mixed signal, SOI, SiGe etc.) A schematic of such an integration is shown in Figure 5.10. SOI technology has dominated the VLSI market and is serious contender in the high performance and low power consumption applications [46]. The dielectric isolation between the devices allows for high packaging densities and reduces the junction capacitances. This low junction capacitance allows the circuits to operate at higher speed, or operate with substantially lower power at the same speed. Due to these unique technology features, the SOI technology provides dense 3-D device and layout structures. Studies show that with a 3-D architecture, the SOI technology can have approximately a 50% reduction for 2 device layer structures over standard 2-D structures and 18% global interconnection delay gain over standard 2-D structure [47],[48], [49]. Research continues to lower the processing cost of a 3-D architecture. Recent improvements in the cutoff frequencies of the FDSOI technology makes it a promising candidate for low-power high frequency communication applications [88].

In the study presented here, a thermal macromodel for each tier of a 3DIC designed using FDSOI MOSFETs is developed. The results of the simulations using this macromodel is presented in the next section. Various parameters of the thermal macromodel were varied to see their effect on the heat removal in a 3DIC.

5.5 Simulations of the 3DIC Thermal Macromodel

To demonstrate the capability of the macromodel, the thermal profile of a 3DIC is simulated. As demonstrated Chapter 4, since thermal nonlinearity effects of SiO_2 can be ignored, this macromodel with a linear RC network can be used to perform a thermal analysis of the 3D chip. The 3DIC thermal chip is a 8-pt 32-bit floating point Winograd FFT [80] with a self-testing mechanism, designed with MIT Lincoln Labs 0.18μ FDSOI MOSFET technology [81]. The design accepts 16 32-bit floating point values (8 Real and Imaginary inputs) and similarly generates 16 32-bit floating point outputs per cycle. Synthesized with a 0.18μ SOI-based standard cell library, it has about 136,000 cells. The number of Flip-flops (all scannable) are about 2050. The floating point units used are downloaded from the

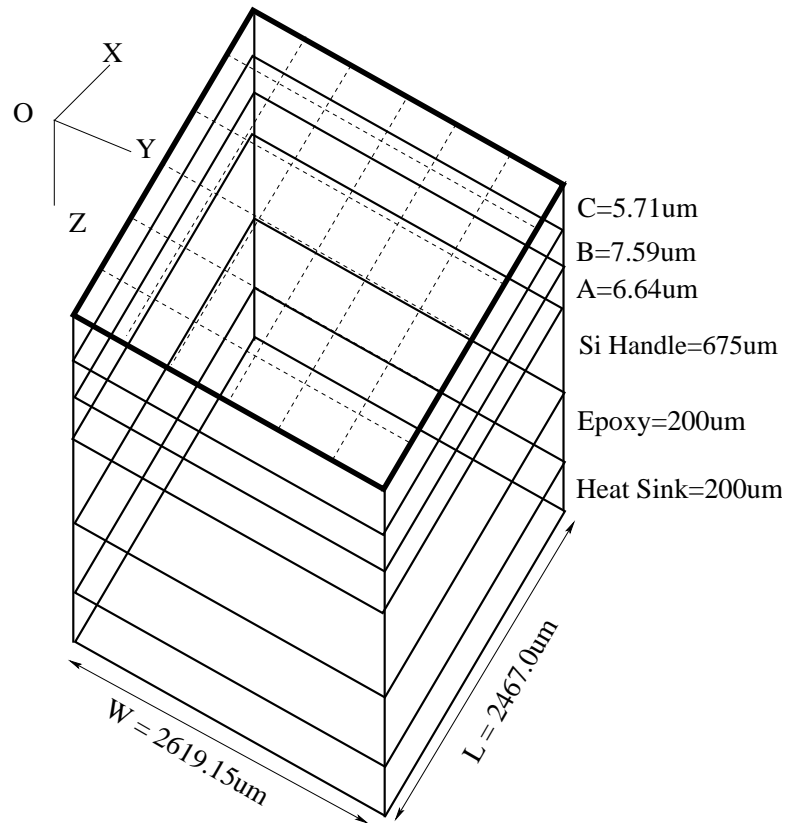


Figure 5.10: Three-dimensional view of the 3DIC thermal chip. The thick boundary is the topmost layer. Each tier is discretized into a 10×10 grid.

Free Floating Point Madness website [82]. The self-test mechanism generates a series of 16 32-bit pseudo-random inputs for 1024 consecutive cycles and feeds it to the design. It also generates a hash of the 1024 sets of outputs and compares it to a known hash value, thus validating the design. The MIT Lincoln Labs 3D Manufacturing Technology with 3 Tiers is used as the target for placing and routing the design. The Cadence First Encounter [83] place and route tool is made 3D aware by partitioning the chip into 3 tiers with the partitioner tool Metis [84]. Inter-tier vias are placed at the proper locations in all tiers and each tier is individually placed and routed. The 3D-placed and routed design is then converted into the OpenAccess [85] format for further processing. Power for each instance in the design is determined by using Synopsys PrimePower. It requires excitation data for each instance in the design over the period of simulation. Prime power calculates the average power for each instance.

The chip has three tiers, A, B and C, and a total of approximately 1 million

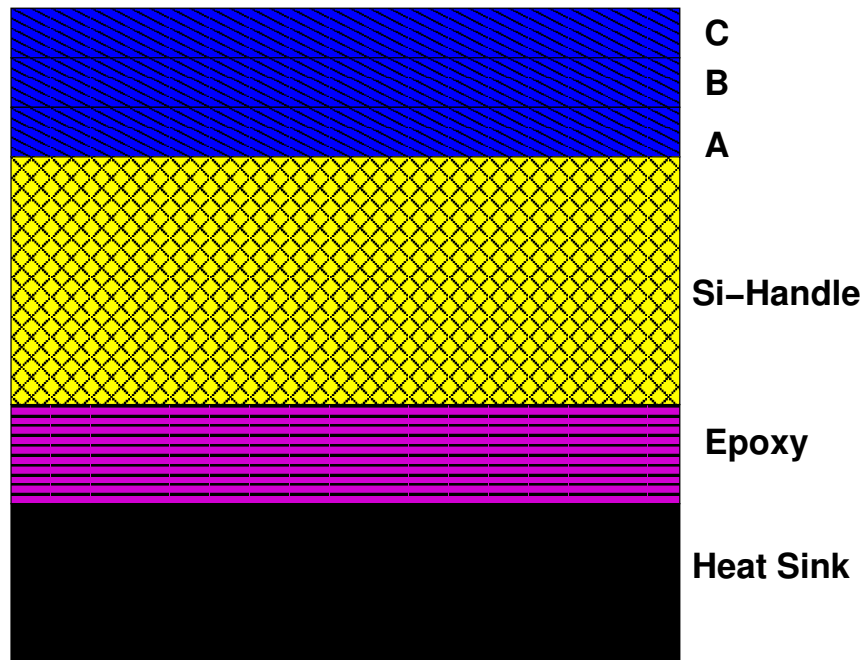


Figure 5.11: Two-dimensional vertical cross section of the 3DIC thermal chip(Not to scale).

transistors. Each tier is a separate wafer. Tier B and C are flipped chips. The Silicon handle of Tier A is not removed. The Silicon handle of Tiers B and C is removed to etch the 3D vias. The tiers are bonded to each other with low-temperature oxide wafer bond such as glass. The Silicon handle of Tier A is attached to the heat sink with epoxy. The three-dimensional view of the entire structure is shown in Figure 5.10. Each tier is $246.7 \mu\text{m} \times 261.915 \mu\text{m}$. The thickness, D , of each layer of the structure is shown in Figure 5.10. Figure 5.11 shows the vertical cross section of the stack of the system modeled. A detailed cross section of only the 3 tiers with the vertical vias, metal layers and active islands is shown in Figure 5.12.

Each tier is discretized into a 10×10 grid to form 100 uniform blocks. The power figure for each block is calculated. Each block has approximately 3000 transistors. The other parameters required by *fREEDA*TM to generate effective thermal conductivities of the thermal macromodel are described below. These parameters are extracted using a thermal parameter extractor. This parameter extractor uses a user-defined set of X and Y grid steps to divide the design into uniform pieces (in this case 100). The parameter extractor uses the information provided by the tools Cadence First Encounter, the OpenAccess database and Synopsys PrimePower. The following parameters are extracted:

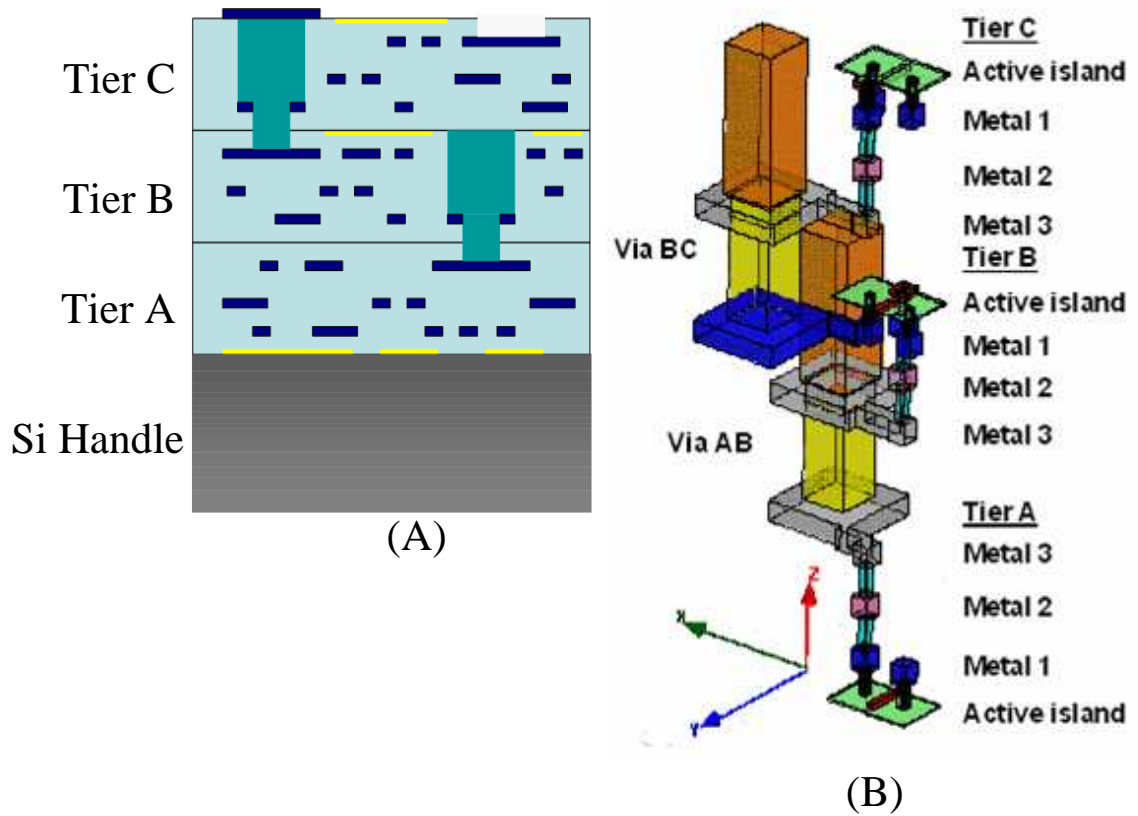


Figure 5.12: (A) Vertical cross section of the 3DIC thermal chip with 3D vias and metal layers. (B) A 3D representation of the 3D vias, metal layers and active islands in the tiers.

- **Metal Density:** The metal density of routing is extracted for each block. Numbers are calculated by taking a virtual cross-section at the grid lines, and determining the percentage surface area of the die occupied by the via metal to glass.
- **3D Via Density or Vertical Metal Density:** The 3D via density is determined by calculating the percentage surface area of the die occupied by the via metal to glass when looking down on the grid square in the z direction. For the MIT Lincoln Labs FDSOI process, each tier is split into two halves and separate 3D via densities are extracted for each half. The first density number correlates to vias on the top side of the tier that is, vias that have metal in the half of the tier without the SOI island. The second density correlates to vias that are on the bottom side of the tier and have metal on the same half of the tier that the SOI island is on.
- **Power Dissipation:** The power dissipation of all cell instances in the grid block are summed, and the total power dissipation is reported in milliwatts.

With the parameters extracted the *fREEDA*TM netlist is automatically assembled from the thermal extractors output and the boundary conditions are applied. This automatically assembled *fREEDA*TM netlist used for this study is provided in Appendix B, Section B.10. Various parameters of the thermal macromodel of each block were varied to obtain several results. These results are discussed here. First, the thermal conductivity in the x, y, and z direction for each block is derived. *fREEDA*TM additionally solves for the temperature at the center of each block. Table 5.2 shows a the RC values of the centre block on Tier A. The resistance in the vertical direction is smallest, making it the path of least thermal resistance. Figures 5.13, 5.14 and 5.15 show the temperature rise across the three layers of the chip. As can be seen from the Figures 5.13, 5.14 and 5.15 the maximum temperature rise or the hottest block is on tier B. The maximum temperature on Tier B is approximately 304.66°K. The hot spots are shown by markers ‘A’ and ‘B’. The heat dissipated in Tier C, experiences the maximum thermal resistance till the heat sink, due to the resistances of all the layers between it and the heat sink. Tier A, on the other hand, experiences the least thermal resistance, but the heat dissipated from the layers above it flow into Tier A. Tier B, experiences a mid-range thermal resistance and heat flow, which may be the reason why it has the maximum temperature rise. If the heat is flowing down into the heat sink, Tier A, has the maximum heat flux, and should have a temperature

Table 5.2: Values of thermal resistances in the RC network of the macromodel.

R_{th}	Value(Ohms)
R_n	16181.1948
R_s	19032.5796
R_e	25623.088
R_w	22742.8008
R_t	4.3839
R_b	43.8968

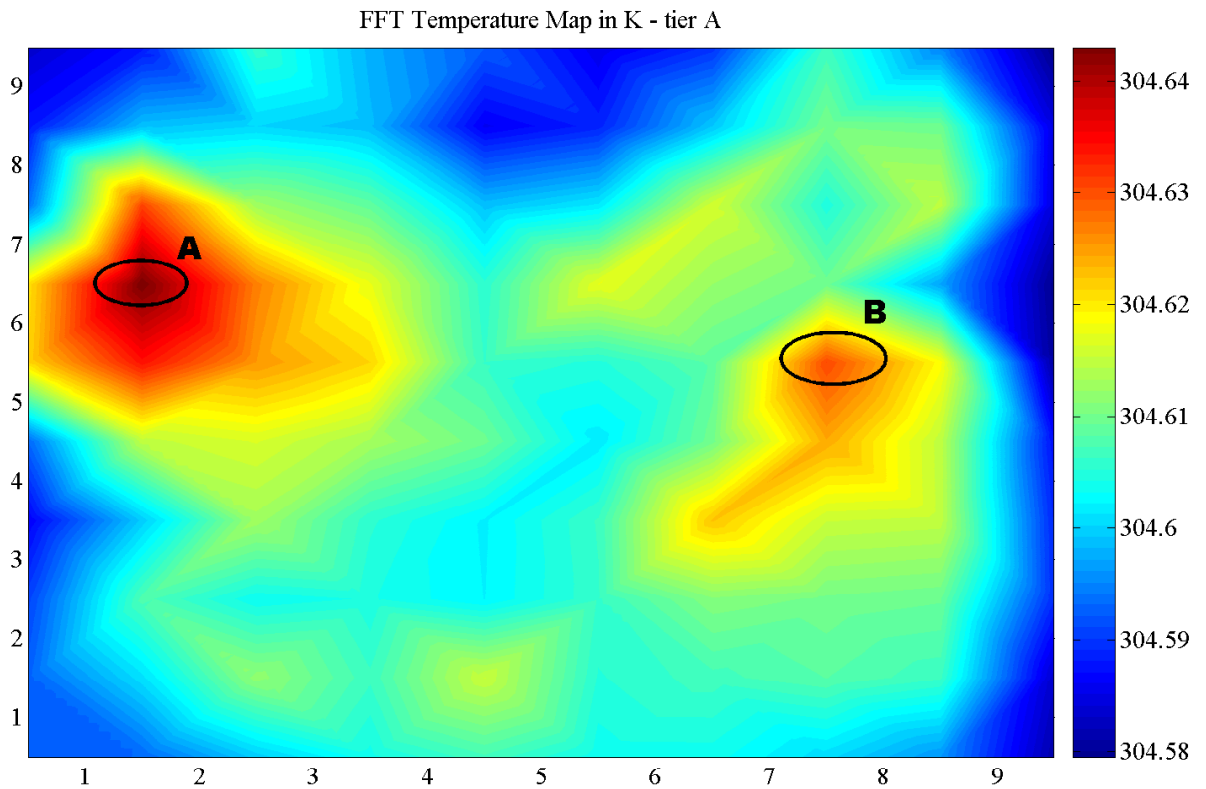


Figure 5.13: Temperature Map of Tier A.

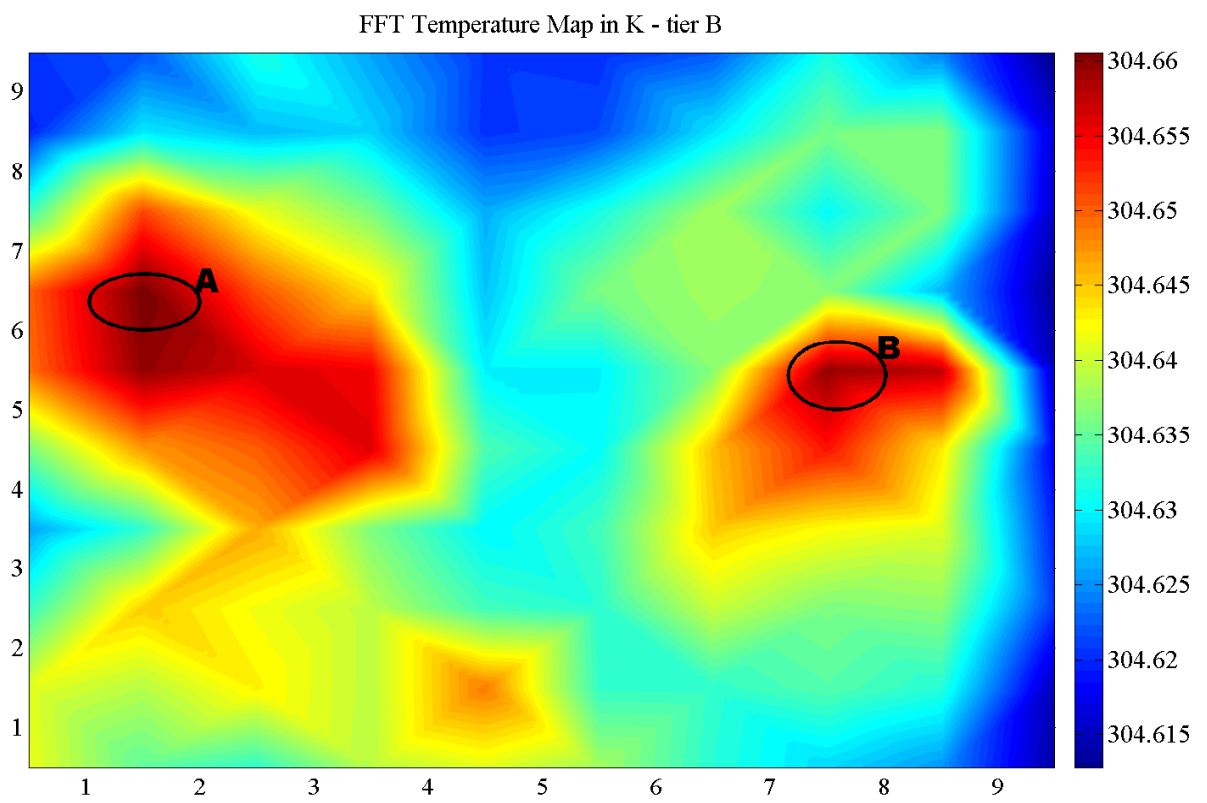


Figure 5.14: Temperature Map of Tier B.

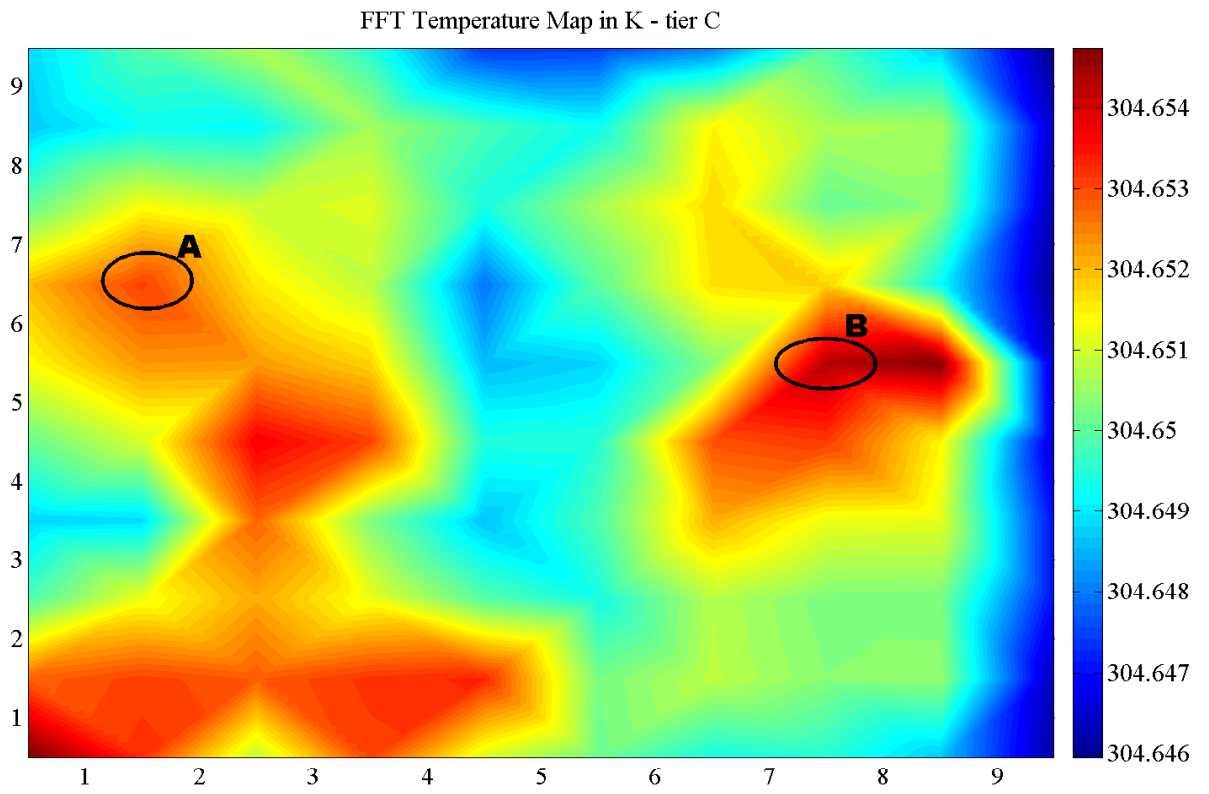


Figure 5.15: Temperature Map of Tier C.

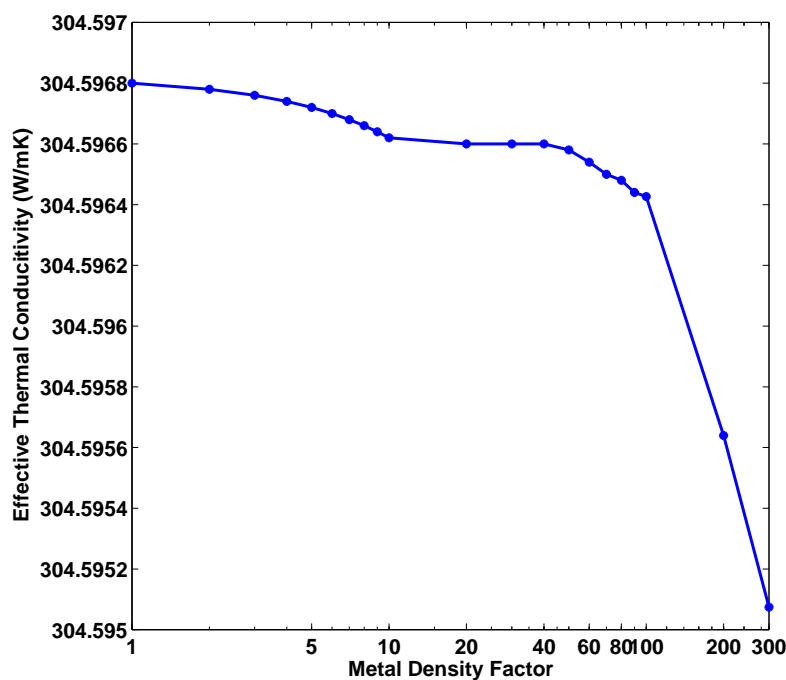


Figure 5.16: Maximum temperature on Tier A with vertical metal density of all grid blocks on Tier A varied. A factor of 1 on the x-axis corresponds to the vertical metal density extracted by the thermal extractor. The extracted metal density of all the blocks on this tier is less than 0.2 .

higher than Tier C. This can be seen at marker ‘A’ in the figures. Now marker ‘B’ shows the opposite phenomenon, Tier C has a greater temperature than Tier A. This could be due to higher localized heating and lower local metal densities. To eliminate the hot spots on each tier, these phenomenon needs to be further investigated.

The heat may be better removed if the numbers of thermal vias i.e. vertical metal density is increased. Figure 5.16 shows the simulated maximum temperature on Tier A, if the vertical metal density of all the blocks on Tier A is varied. This density is varied by a factor of 1 to 300. It can be seen that increasing the vertical metal density, reduces the maximum temperature by only 0.0029°K. Also, the vertical thermal conductivity, Figure 5.17, improves only by 18%, from 1.87 W/mK to 2.21 W/mK. From these two simulations, it can be concluded that increasing the number of thermal vias or the vertical metal density, will improve heat removal only marginally.

Figure 5.18 shows the maximum temperature as the power dissipation of the chip

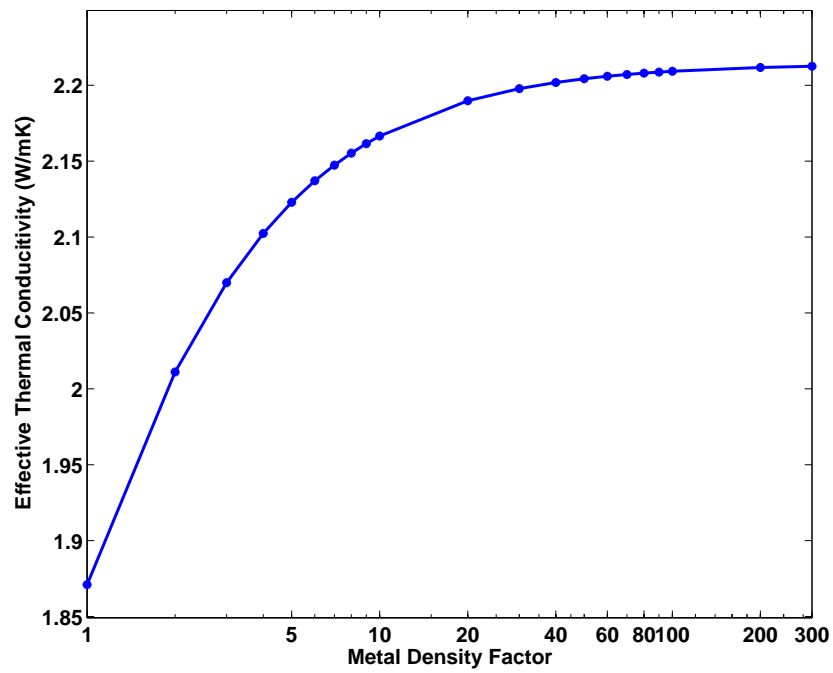


Figure 5.17: Vertical thermal conductivity of the hottest block on Tier A with vertical metal density of all grid blocks varied. A factor of 1 on the x-axis corresponds to the vertical metal density extracted by the thermal extractor. The extracted metal density of all the blocks on this tier is less than 0.2 .

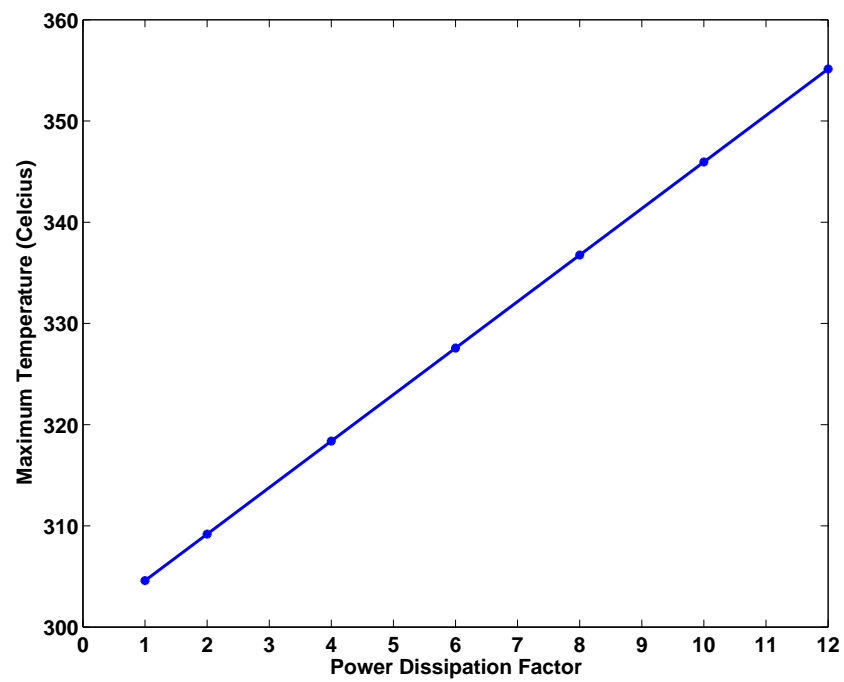


Figure 5.18: Maximum temperature on Tier A with power dissipation of all the grid blocks varied. A factor of 1 on the x-axis corresponds to the power dissipation extracted by the thermal extractor.

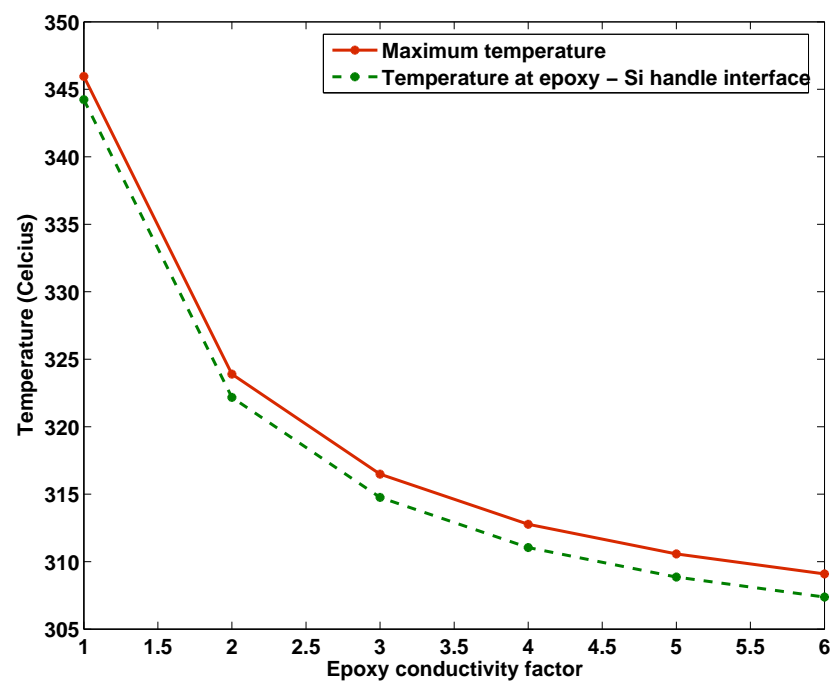


Figure 5.19: Maximum temperature on Tier A with the thermal conductivity of the epoxy varied.

is varied from a factor of 2 to 12. The extracted power dissipated by each block on Tier A is varied from a factor of 2 to 12. The maximum temperature on Tier A, varies linearly with power dissipation.

The heat dissipated by the three tiers is trapped at the Si-handle and epoxy interface. The epoxy has a thermal conductivity 1 W/mK and is 200 μ m thick, effectively has a high thermal resistance. This high thermal resistance between the tiers and the heat sink, inhibits the heat removal from the tiers. If an epoxy with a better thermal conductivity is used, the maximum temperature on Tier A can be reduced significantly, as shown in Figure 5.19. If the thermal conductivity of the epoxy is improved from 1 W/mK to 6 W/mK, the maximum temperature on Tier A, can be reduced from 345.95 $^{\circ}$ K to 309.08 $^{\circ}$ K. Hence it can be concluded that to reduce the temperature rise, in a 3DIC, thermal vias and a good thermally conducting epoxy should be used.

5.6 Summary

The thermal compact model developed in Chapter 4, can perform coupled electrothermal simulations for time steps as small as 2 ns. For smaller time steps the accumulated numerical error in the compact thermal model is too large to perform an accurate simulation. For time steps smaller than 2 ns, as required in modeling the X-band GaAs MMIC LNA, a thermal macromodel of the different layers in the MMIC structure was developed. This thermal macromodel is a linear RC network based on metal density information in each direction. This model was described in this chapter. The macromodel of the MMIC had a 10 \times 10 grid. Metal density of the surface metallization features such as vias and the top metal layer of the via capacitors were added to the appropriate grid blocks. The temperature rise predicted by this model agreed with measured temperature rise within 10% error. This model was used to perform a coupled electrothermal simulation of the MMIC at 10 GHz. A comparison between the electrical and electrothermal simulated output voltage of the MMIC showed that the output voltage is overestimated if the thermal effects are ignored. At very small input power levels, the output voltage in a purely electrical simulation is overestimated by few μ V. The high dynamic range capability of the new time step control technique developed in *f*REEDATM detected this small overestimation. At elevated temperatures due to current reduction, the power dissipated is reduced. This

reduction is accounted for in the coupled electrothermal simulation. Hence in the performance evaluation of a MMIC thermal effects are important considerations and cannot be ignored.

With these capabilities the thermal macromodel was used to predict the hot spots and the thermal bottlenecks in a 3DIC, where the thermal problem is exacerbated due to the stacking of chips. This macromodel for a 3DIC is developed and implemented in *fREEDA*TM. Since SiO₂ is not very thermally nonlinear, this model can be used to model the thermal effects a 3DIC designed with Silicon on Insulator technology. This model was used to evaluate the temperature rise in a 3DIC thermal test chip, designed with MIT Lincoln Labs 0.18 μm FDSOI MOSFET technology. The 3DIC thermal test chip had approximately a million transistors and 3 tiers. The thermal macromodel used a 10×10 discretization. Various parameters of 3DIC thermal chip were varied, to see their effect on the heat removal problem. It was seen that thermal vias and an epoxy with good thermal conductivity can be used to reduce the temperature rise in a 3DIC.

Chapter 6

BSIMSOI Electrothermal model

Two aspects of the goal of this work were presented in Chapters 3 — 5. The last aspect of the goal development of a rapid and accurate semiconductor electrothermal device model is presented in this chapter. Fully-coupled electrothermal modeling of an electronic circuit needs electrothermal device models. The accuracy of a simulation is largely dependent on the accuracy of the semiconductor device models. Device model development is too cumbersome in traditional SPICE-like simulators. The model developer spends a lot of efforts in coding the device models into the simulator and understanding the intricacies of the simulator. Since all the derivatives are manually coded, human errors are unavoidably introduced in the model code. If device modeling is automated the model developer can concentrate on developing the equations of the model. Also automation enables rapid model development. Since all device models will follow a standard approach of model code development, model debugging and maintenance will be simpler.

The use of state-variables and automatic differentiation in *fREEDA*TM, helps rapid model development. The use of state-variables aids all the device models to follow a standard model code development approach. This makes model development simple and less cumbersome. Automatic differentiation eliminates the need to manually code the derivatives, and hence eliminates human errors. These features were applied to develop an electrothermal model of a Fully Depleted Silicon on Insulator MOSFET. The use of automatic differentiation and state-variables, helped develop the the device model in a couple of weeks. The addition of thermal effects took only a couple of days.

This chapter provides the details of the *fREEDA*TM implementation of the Fully Depleted Silicon on Insulator model, based on the University of Berkeley's - BSIMSOI model. The *fREEDA*TM model is validated with experimental data of a $0.18\mu\text{m} \times 200\mu\text{m}$ FDSOI MOSFET from MIT Lincoln Labs. Section 6.4 presents the formulation of the electrothermal model in *fREEDA*TM. The effects of self heating in a FDSOI MOSFET are presented in Section 6.4.

6.1 SOI Model Formulation

Silicon on Insulator (SOI) CMOS technology has many advantages over bulk-Si. SOI CMOS could offer upto 25-30% gain over bulk CMOS technology [86]. To name a few advantages the SOI technology has reduced parasitic capacitance and high transconductance due to the buried- oxide. SOI technology also shows suppressed short channel effects and has a simplified fabrication process. Due to these advantages and its high packing density, the high-speed, low-power FDSOI [87] is ideal for CMOS system on a chip (SoC) integration. Due to these advantages and its excellent cutoff frequency [88],[89] FDSOI technology is explored as an alternate technology for SoC and 3DIC architectures. It is promising for RF integrated circuits with low power consumption and low supply voltage [90]. As the technology advances extensive scaling of the SOI thickness must be done to achieve low junction capacitances and good device performance. Also the buried-oxide underneath the Si film gives rise to self-heating effect(SHE). Self-heating effects change the transistor characteristics due to device temperature rise. At elevated temperatures the carrier mobility and saturation velocity decrease, resulting in a negative output conductance or in general lower drain currents. To explore the advantages of this technology in RF applications a good model which can handle all these effects and features must be developed. Hence a FDSOI model for RF applications was developed at University of California, Berkeley [91]. This model is based on the key that the index for degree of full depletion is the *body-source built-in potential lowering* ΔV_{bi} . A general circuit representation of the BSIMPD floating body model is shown in Figure 6.1. The unified SOI model is a generalized BSIMPD model, wherein ΔV_{bi} is incorporated into the body-source diode current model (I_{BS}) which counter balances the body charge injection (e.g. impact ionization) and determines the body potential (V_{BS}) and the threshold voltage (V_T) of the SOI transistor. This model

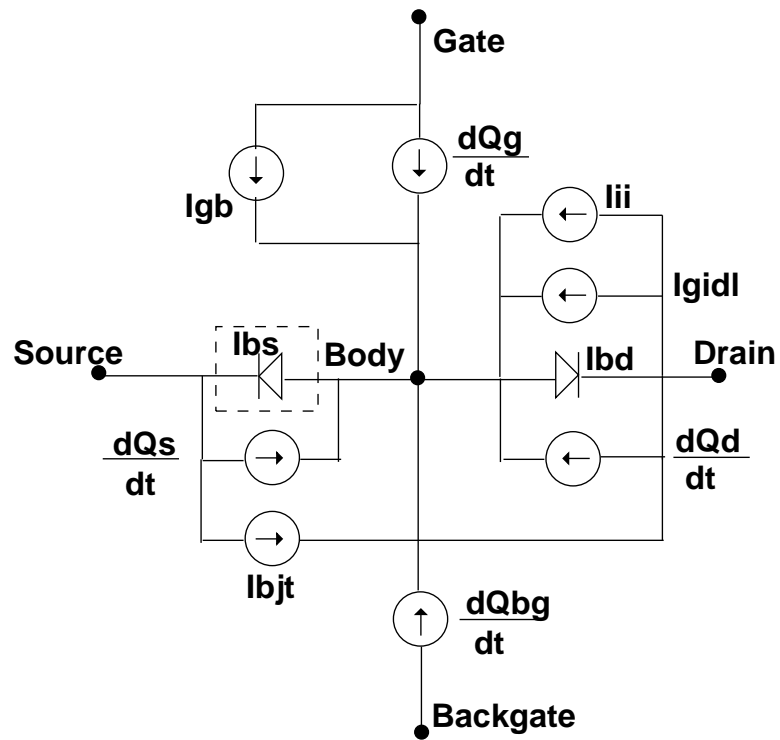


Figure 6.1: Circuit representation of the floating body in BSIMPD.

was implemented in SPICE3f5 and was validated with a FDSOI MOSFET fabricated and characterized at MIT Lincoln Lab. Since this model was developed in SPICE, the conventional model development technique of Associated Discrete Modeling [14] was used. In this approach the analysis of a nonlinear dynamic circuit is converted into successive analysis of linear resistive circuits developed from the original circuit using time discretization based on Newtons iterative method. These linear resistive circuits are solved using nodal analysis. This technique works very well, but model development is tedious and time consuming. This is primarily due to the fact that, different models must be developed for transient and harmonic balance analysis, and derivatives in the time and frequency domain must be manually coded and kept track of. These problems are eliminated in the global modeling approach [51], [52], developed in *fREEDA*TM. The global modeling approach in *fREEDA*TM uses the simplified device model development approach discussed in Chapter 2. The simplified device model development approach uses universal parameterized device models based on state-variables and automatic differentiation. The universal parameterized model does not add any internal nodes to the nonlinear device, and is a reduced-order model in its true form [3]. Automatic differentiation is used to keep track of the derivatives. The BSIMSOI FDSOI model developed in *fREEDA*TM uses this approach. The use of automatic differentiation reduces the code size to one tenth, and the use of state-variables aids the model to follow a standard model code development approach. This make the model maintenance easier since only two files must be modified to accommodate any type of change.

6.2 Implementation Of The BSIMSOI Model In *fREEDA*TM

The BSIMSOI model shown in Figure 6.1 was implemented in *fREEDA*TM using the global modeling approach [4], [52]. The characteristic nonlinear equations of this model are provided in Appendix B, Section B.15. The common port voltages and branch currents are functions of the device nodal voltages, their derivatives, time and time delays. In the global modeling approach each of these equations are parameterized and expressed as functions of state-variables, [52], [92]. The parameterized device equations are written as:

$$\mathbf{v}_{NL}(t) = u[\mathbf{x}(t), \frac{d\mathbf{x}}{dt}, \dots, \frac{d^m\mathbf{x}}{dt^m}, \mathbf{x}_D(t)] \quad (6.1)$$

$$\mathbf{i}_{NL}(t) = w[\mathbf{x}(t), \frac{d\mathbf{x}}{dt}, \dots, \frac{d^m\mathbf{x}}{dt^m}, \mathbf{x}_D(t)] \quad (6.2)$$

where $\mathbf{v}_{NL}(t)$, $\mathbf{i}_{NL}(t)$ are vectors of voltages and currents at the common ports, $\mathbf{x}(t)$ is a vector of state-variables and $\mathbf{x}_D(t)$ a vector of time-delayed state-variables, i.e., $\mathbf{x}_{Di}(t) = x_i(t - \tau_i)$. The time delays τ_i may be functions of the state-variables. All the vectors in Equation 6.1 and Equation 6.2 have a same size n_d equal to the number of common (device) ports. Adhering to the local reference node concept [50], the body terminal is selected as the local reference terminal for the model for the BSIMSOI FDSOI model. In the model the device port voltages, V_{ds} , V_{gs} , V_{sb} , are chosen as the state-variables. From Equation 6.2, the port currents, $\mathbf{i}_{NL}(t)$, are a function of the state-variables and their derivatives. In the SPICE modeling approach these derivatives are manually evaluated and kept track off. This process is tedious and can be error prone. Also, if any of the model equations are changed, the derivatives of those equations must be changed too, making model development and maintenance difficult. These problems are eliminated in the global modeling approach. In this approach these derivatives are calculated by automatic differentiation. The parametrization of all the nonlinear device equations using a standard formula helps the automatic differentiation library to read the equations from the model code and calculate the derivatives. These derivatives are calculated by this library, outside the model code. Since the derivatives are calculated outside the model code the equations for the nonlinear voltages and currents are implemented in the model code only. No derivatives are coded. The chosen state-variables define the *derivatives to be evaluated*. This makes the model independent of the circuit analysis type. The global modeling approach uses the modified nodal analysis described in [1],[52]. In this analysis the nonlinear device equations are transformed into a successive solution of a sequence of linear circuits. This successive solution is introduced by applying Newton's method [1] to calculate the $\mathbf{i}_{NL}(\mathbf{x}_n)$ vector and the $\mathbf{v}_{NL}(\mathbf{x}_n)$,

$$\mathbf{i}_{NL}(\mathbf{x}_n^{(j+1)}) = \mathbf{i}_{NL}(\mathbf{x}_n^j) + \mathbf{J}_i[\mathbf{x}_n^{(j+1)} - \mathbf{x}_n^j] \quad (6.3)$$

$$\mathbf{v}_{NL}(\mathbf{x}_n^{(j+1)}) = \mathbf{v}_{NL}(\mathbf{x}_n^j) + \mathbf{J}_v[\mathbf{x}_n^{(j+1)} - \mathbf{x}_n^j], \quad (6.4)$$

where \mathbf{J}_v and \mathbf{J}_i are the voltage and current Jacobian matrices. The elements in the voltage Jacobian matrix are the derivatives of each nonlinear voltage function $\mathbf{v}_{NL}(\mathbf{x}_n)$ with respect to every dependent variable, \mathbf{x}_n . Similarly the elements in the current Jacobian

matrix are the derivatives of each nonlinear current function $\mathbf{i}_{NL}(\mathbf{x}_n)$ with respect to every dependent variable, \mathbf{x}_n . The automatic differentiation library reads the nonlinear device equations implemented in the model code to evaluate these derivatives. These derivatives are passed to the modified nodal analysis for use. The modified nodal analysis uses the error function formulation and sparse matrix formulation explained in Section 3.3. A summary of this formulation is presented here for convenience. In the modified nodal analysis, the error function formulates the simultaneous equations to be solved to simulate the electrical network. These equations are based on Kirchoff's Current Law and Kirchoff's Voltage Law. They are given by:

$$\mathbf{G}\mathbf{u}_n + \mathbf{C}[a\mathbf{u}_n + \mathbf{b}_{n-1}] = s_{f,n} + \mathbf{T}^T \mathbf{i}_{NL}(\mathbf{x}_n) \quad (6.5)$$

and

$$\mathbf{f}(t) = \mathbf{T}\mathbf{u}(t) - \mathbf{v}_{NL}(t) = 0. \quad (6.6)$$

In these equations the equations for \mathbf{i}_{NL} and \mathbf{v}_{NL} are nonlinear. The sparse matrix formulation linearizes the nonlinear current, \mathbf{i}_{NL} , and voltage, \mathbf{v}_{NL} , equations using the Newton's method. This linearization represents the simultaneous equations, Equations 6.5 and 6.6, as a matrix equation of the form $\mathbf{A}\mathbf{x} = \mathbf{B}$, where \mathbf{A} is the coefficient matrix, \mathbf{x} is the vector of unknown quantities and \mathbf{B} is the right hand side matrix. The final matrix equation in this form is given by:

$$\begin{pmatrix} [\mathbf{G} + \mathbf{C}a] & -[\mathbf{T}^T \mathbf{J}_i] \\ \mathbf{T} & -\mathbf{J}_v \end{pmatrix} \begin{pmatrix} \mathbf{u}_n^{(j+1)} \\ \mathbf{x}_n^{(j+1)} \end{pmatrix} = \begin{pmatrix} [s_{f,n} - \mathbf{C}a\mathbf{b}_{n-1}] & +\mathbf{T}^T [\mathbf{i}_{NL}(\mathbf{x}_n^j) - \mathbf{J}_i \mathbf{x}_n^j] \\ \mathbf{v}_{NL}(\mathbf{x}_n^j) & -\mathbf{J}_v \mathbf{x}_n^j \end{pmatrix} \quad (6.7)$$

This matrix equation is repeatedly solved at every j^{th} iteration of the Newton's method. The values in this matrix are populated by the modified nodal analysis used by the circuit analysis technique. As mentioned earlier the automatic differentiation library passes the values of the Jacobians to the modified nodal analysis. Thus the model developer need not be concerned about loading and entering the values in the Jacobian matrix. Also the values of the nonlinear equations \mathbf{i}_{NL} and \mathbf{v}_{NL} are passed by the device model to the modified nodal analysis. The modified nodal analysis populates the above matrix with these values. Thus model developer does not must know the intricacies of the simulator and spend time

understanding how to load the Jacobian matrices of the device. This reduces the burden of the model developer.

To verify that all nonlinear effects in the characteristic device equations are considered an example is presented here. As shown in the Figure 6.1, the total current at the drain node can be written as:

$$I_d = Ieq_{BD} - Ieq_{GIDL} - Ieq_{II} - I_{ds} - I_c + I_{gd} + I_{gcd} \quad (6.8)$$

where:

- Ieq_{BD} = Body-drain diode current
- Ieq_{GIDL} = Gate Induced Leakage current
- Ieq_{II} = Substrate Current
- I_{ds} = Square law drain-source current
- I_c = BJT collector current
- I_{gd} and I_{gcd} are the gate channel tunneling components.

Each of these current components are nonlinear functions of the branch voltages V_{ds} , V_{gs} , V_{bs} etc. In associated discrete modeling used in SPICE, these nonlinear functions are linearized using Newton iterations. The derivatives of these functions must be calculated. For example the component Ieq_{BD} is evaluated as:

$$Ieq_{BD} = I_{BD} + (\partial I_{BD}/\partial V_{bd}) * V_{bd} + (\partial I_{BD}/\partial V_{ds}) * V_{ds}. \quad (6.9)$$

In the device model code this equation is represented as a linear circuit with a current source, I_{BD} , connected between device terminals B and D, a transconductance, $(\partial I_{BD}/\partial V_{bd})$, between device terminals B and D and a transconductance, $(\partial I_{BD}/\partial V_{ds})$, between device terminals D and S. These values of these elements are updated at every Newton iteration. The model code developer must manually evaluate these derivatives and code them in the model code as the values of the transconductances. Once this is done, the model developer also should connect these linear elements between the appropriate device terminals. This involves getting the device terminal information and populating device admittance matrix and the device Jacobian matrix. The model developer must know these intricacies of the simulator. This burden is reduced in the global modeling approach.

In the global modeling approach, applying Equations 6.3 to 6.9 gives,

$$i_{NL}(t) = I_{eqBD} = I_{BD}(V_{bd}, V_{ds}) + \left(\frac{\partial I_{BD}}{\partial V_{bd}}\right) * V_{bd} + \left(\frac{\partial I_{BD}}{\partial V_{ds}}\right) * V_{ds} \quad (6.10)$$

where:

- $V_{bd} = -V_{db}$ and $V_{ds} = V_{db} - V_{sb}$.
- $\left(\frac{\partial I_{BD}}{\partial V_{bd}}\right) = \mathbf{J}_i(V_{bd})$ and $\left(\frac{\partial I_{BD}}{\partial V_{ds}}\right) = \mathbf{J}_i(V_{ds})$

The values of the transconductances, the derivatives, represented as the Jacobians are calculated by the automatic differentiation library. These values are passed to the modified nodal analysis. The value of the current source, I_{BD} , is calculated by the device model and passed to the modified nodal analysis. The modified nodal analysis uses these values to populate the matrices in the matrix equation, Equation 6.7. Similarly all other components on the right hand side of Equation 6.8 are evaluated to calculate the total drain current of the device. The values of these components and their Jacobians are used to by modified nodal analysis to solve the matrix equation. Thus the model developer need not be concerned about connecting the linear elements and populating the appropriate matrices. The use of Object Oriented Programming, [93], makes all device models use the same implementation format of the device equations. With the standard implementation format the model is developed faster and is easy to maintain as the equations must be coded only once.

6.2.1 BSIMSOI Model Code In fREEDA™

The *f*REEDA™ code of the electrothermal BSIMSOI model is provided in Appendix B B.16. The model code is implemented in two files, a C++ file and a header file. The pseudo code of the model is shown below.

```
/*Model code for BSIMSOI*/
#include "../network/CircuitManager.h"
#include "../network/Element.h"
#include "../network/AdolcElement2.h"
#include "Bsim3nsoitestT.h"

//Static members
const unsigned Bsim3nsoitestT::n_par = 206;

//Element information
```

```

ItemInfo Bsim3nsoitestT::einfo = {
    "bsim3nsoitestt",
    "Mosfet model using Bsim3nsoitestT level, version 3.2.4",
    "Sonali Luniya and Ramya Mohan",
    DEFAULT_ADDRESS"elements/Bsim3nsoitestT.h.html",
    "2005_07_07"
};
//Parameter description
ParmInfo Bsim3nsoitestT::pinfo[] = {
    {"l", "Length (m)", TR_DOUBLE, false},
    {"w", "Width (m)", TR_DOUBLE, false},
    {"dtoxcv", "---", TR_DOUBLE, false},
    {"llc", "Length reduction parameter for CV", TR_DOUBLE, false},
    .
    .
    .
    {"shmod", "self heat - shmod", TR_DOUBLE, false}
};

//Set default values of parameters
Bsim3nsoitestT::Bsim3nsoitestT(const string& iname)
    : AdolcElement2(&einfo, pinfo, n_par, iname)
{
    //Set default parameter values
    paramvalue[0] = &(l = 0.25e-6);
    paramvalue[1] = &(w = 10.0e-6);
    paramvalue[2] = &(dtoxcv = 0);
    paramvalue[3] = &(llc = 0);
    paramvalue[206] = &(shmod = 1.0);
    .
    .
    .
    //Set flags
    setFlags(NONLINEAR | MULTI_REF | TR_TIME_DOMAIN);
}

void Bsim3nsoitestT::init() throw(string&)
{
    //Set number of terminals
    setNumTerms(6);

    //Set number of state variables
    setNumberOfStates(4);
}

```

```

//create tape
IntVector var(4);
var[0] = 0; //Vds
var[1] = 1; //temp
var[2] = 2; //Vbs
var[3] = 3; //Vgs

IntVector novar;
DoubleVector nodelay;
createTape1(var, novar, nodelay, 4, 8);
createTape2();
}

//Set local reference nodes
void Bsim3nsoitestT::getLocalRefIdx(UnsignedVector& local_ref_vec,
    TerminalVector& term_list)
{
    // Make sure the vectors are empty
    term_list.erase(term_list.begin(), term_list.end());
    local_ref_vec.erase(local_ref_vec.begin(), local_ref_vec.end());

    // Insert vector elements
    term_list.push_back(getTerminal(0));
    term_list.push_back(getTerminal(1));
    term_list.push_back(getTerminal(2));
    term_list.push_back(getTerminal(3)); // Local reference terminal
    term_list.push_back(getTerminal(4));
    term_list.push_back(getTerminal(5)); // Local reference terminal

    local_ref_vec.push_back(3); // Local reference index
    local_ref_vec.push_back(5); // Local reference index
}

//Function with device equations

void Bsim3nsoitestT::eval1(adoublev& x, adoublev& xt,
    adoublev& y1, adoublev& z1)
{
    //declare intermediate variables
    adouble Vgs_eff, Vbsmos, Vbp, Vbsh, Vbseff, Phis,
        sqrtPhis, Xdep, lt1, ltw;
    adouble DeltVthtemp, DIBL_Sft;
    adouble sqrtPhisExt, Vth, n, Vgst, VgstNVt, ExpArg,

```

```

Vgsteff, Vgst2Vtm, Weff, Rds;

//implement device equations
.
.
.
adouble Idl = gche * T9;
T9 = diffVds / Va;
T0 = 1.0 + T9;
adouble Ids = Idl * T0 / nseg;
.
.
.
y1[0] = qdrn;
y1[1] = qgate;
y1[2] = qsrc;
y1[3] = temp;

adouble Icjd = Ibd - Iii - Idgidl;
adouble Icjs = Ibs - Isgidl;

z1[0] = Ids + Ic -Icjd + Igd ;
z1[1] = Igd + Igs + Igb;
z1[2] = -Ids - Ic + -Icjs + Igs;
z1[3]= - Ids * (x[0]-x[2]);

z1[4] = x[0] - x[2];//Vdb
z1[5] = x[3] - x[2];//Vgb
z1[6] = - x[2];//Vsb
z1[7] = x[1] + temp;
}

//Function to update the final voltage and current vectors
void Bsim3nsoitestT::eval2(adoublev& dy1, adoublev& z1,
adoublev& vp, adoublev& ip)
{
    vp[0] = z1[4];
    vp[1] = z1[5];
    vp[2] = z1[6];
    vp[3] = z1[7];

    ip[0] = z1[0] + dy1[0];
    ip[1] = z1[1] + dy1[1];
    ip[2] = z1[2] + dy1[2];
}

```

```

    ip[3] = z1[3] + dy1[0];
}

```

After including the header files and updating the model name, author and version information, the description and names of the model parameters is stored in the vector **pinfo**. In the constructor of the model the default values of the parameters are set. These values are overwritten with the values provided in the netlist. The *init()* function, sets the number of device terminals (here 6) and the number of state-variables (here 4). In this model the chosen state-variables are the device port voltages, V_{ds} , V_{gs} , V_{sb} and the device temperature. The index of the variables for which the derivatives must be evaluated are stored in vector *var*. The function calls *createTape1()* and *createTape2()* pass this information to the automatic differentiation library. The *getLocalRefIdx()* updates the local reference node information. In this model there are two local reference nodes, one for the electrical network and the other for the thermal network. The local reference node for the electrical network is the body terminal and the thermal network is the global thermal ground set in the netlist. All the nonlinear voltage and current equations are implemented in the *eval1()* function. The values of the state-variables and their derivatives with respect to time are passed to this function as the parameter vector **x**. In this model the time derivatives of charge also must be evaluated. The parameter vector **y1** stores values of the device charges and the parameter vector **z1** stores the values of the nonlinear currents and voltages. All the intermediate variables to evaluate the nonlinear current and voltage equations are implemented in this function. The derivatives of the of charges, **y1**, are passed as the parameter vector **dy1** to the *eval2()* function. The vectors **dy1** and **z1** are used to calculate the final device port voltages and currents. The device port voltages are stored in the vector **vp** and the currents are stored in the vector **ip**. The *eval1()* and *eval2()* functions are called by the modified nodal analysis. All parameter vectors of these two functions are passed as pointers. Hence the values of the voltages (**vp**) and currents (**ip**) using the state-variables, **x**, evaluated in these functions are passed back to the modified nodal analysis. The automatic differentiation library tapes the *eval1()* and *eval2()* function and uses the information provided in the *createTape1()* and *createTape2()* functions to evaluate the appropriate derivatives. The voltage and current Jacobians are the derivatives of the vectors **vp** and **ip** with respect to state-variables. The relationship between state-variables and the vectors **vp** and **ip** is provided in the *eval1()* and *eval2()* function. The automatic differentiation library has taped

Table 6.1: MOSFET model implementation in University of California, Berkeley, SPICE3f5 and *fREEDA*TM.

Number	Spice	<i>fREEDA</i> TM
If Statements	1757	165
Files to be modified	25	2
Total Lines of Code	20,664	3385

these functions which is used to evaluate the Jacobians analytically. These Jacobians are then passed to the modified nodal analysis for use.

In this model only the nonlinear current and voltages equations are implemented. No derivatives are coded in the model. The model developer does not load the Jacobian and admittance matrices. This reduces the model code size drastically. Table 6.1 attempts to make an comparison between the model implementation in UCB SPICE3f5 and *fREEDA*TM. The number lines in the *fREEDA*TM model code are approximately one-tenth of the number of lines in the UCB SPICE3f5 model. The use of Object Oriented Programming in *fREEDA*TM helps implement the model code in a standard format. This standard format also makes model development easy and fast. This standard format implements the model code in only two files as compared to 25 in SPICE. This makes model maintenance easy as only 2 files must be modified and kept track off. In SPICE the default model parameter values are set in a separate file, these values are overwritten in a separate file, the actual characteristic equations are implemented in a separate file etc. These large number of files makes model maintenance and debugging difficult.

6.3 BSIMSOI Model Validation

The BSIMSOI model developed was validated with experimental data of a 0.18μ x 200μ FDSOI MOSFET fabricated at MIT Lincoln Labs. The device has 20 fingers with each finger 10μ wide. The model parameters for this device extracted by MIT Lincoln Labs are provided in Appendix B, Section B.11. The experimental data for the FDSOI MOSFET used to validate the simulated output is provided in Appendix B, Section B.13. This experimental data was provided by the Air Force Research Lab, Dayton, Ohio. The *fREEDA*TM netlist for the simulations discussed here is also included in Appendix

B, Section B.12. Figures 6.2 and 6.3 show a comparison between IV curves obtained from SPICE, *fREEDA*TM and the experimental data. From the comparison it can be seen that all nonlinear effects captured by the SPICE model are also captured by the *fREEDA*TM model. In the lower gate bias voltage region, Figure 6.2, the SPICE model cannot capture all the nonlinear effects in the measured data. But the *fREEDA*TM model agrees with the measured data better. The maximum difference between the simulated drain current with the *fREEDA*TM model at a V_{gs} of 0.6V and measured drain current is approximately 2 mA. The maximum difference between the simulated drain current with the SPICE model at a V_{gs} of 0.6 V and measured drain current is approximately 4 mA. The automatic differentiation library in *fREEDA*TM calculates the derivatives of the characteristic equations of the model with analytically. All parameter dependencies are considered while evaluating the derivatives. In SPICE these derivatives are manually evaluated, verified and coded in the model. This process is prone to human error. Also only the parameter dependencies coded by the model developer are considered while evaluating the derivatives. If any parameter dependencies are ignored, the derivatives evaluated are not accurate. The BSIMSOI model equation formulation is based on dividing the bias range into bias regions. The model equations are different in the different bias regions. All parameter dependencies may be ignored in the SPICE model in the low gate bias voltage region. The use of automatic differentiation eliminates such inaccuracies introduced by the manual evaluation and coding of derivatives. This improves the accuracy of the model. At higher gate bias voltages, Figure 6.3, the accuracy of the SPICE model has improved. But the simulated drain current of the *fREEDA*TM agrees better with the measured drain current. The average error in the *fREEDA*TM model drain current is approximately 1% with a maximum absolute difference of 1.4 mA, while the average error in the SPICE model is 2% with a maximum absolute difference of 3 mA. At higher drain ($V_{ds} > 1.6$ V) and gate bias voltages ($V_{gs} > 1.4$ V) the simulated drain current is still rising, but the measured drain current has almost saturated. This is due to the self heating effects in the device model. At higher bias levels the device temperature rises significantly leading to reduction in drain current. These effects are ignored in a purely electrical model. These temperature effects must be incorporated to develop an accurate semiconductor device model. Hence an electrothermal model must be developed. Such an electrothermal model is discussed in the next section.

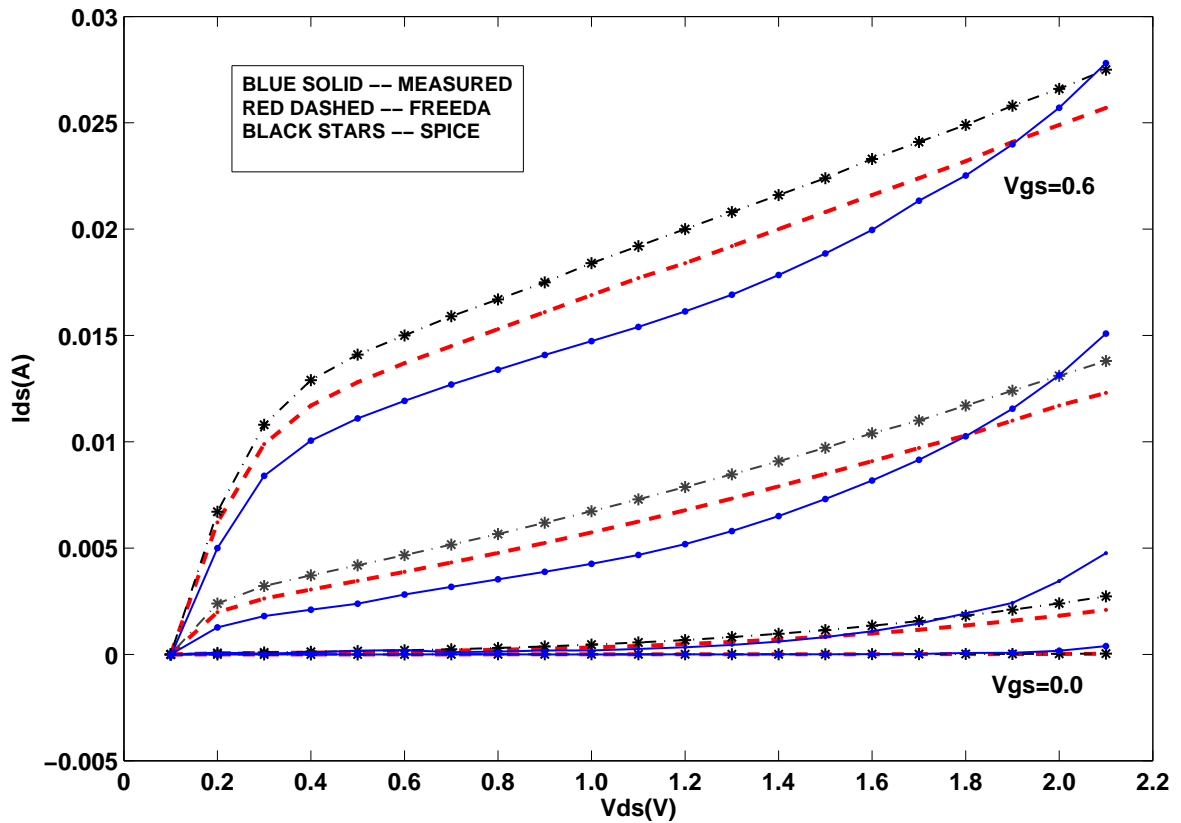


Figure 6.2: Comparison between simulated and measured IV curves of a FDSOI MOSFET at gate bias levels (V_{gs}) of 0.0 V to 0.6 V at 0.2 V intervals. The simulated curves were simulated with the *fREEDA*TM model and the SPICE model.

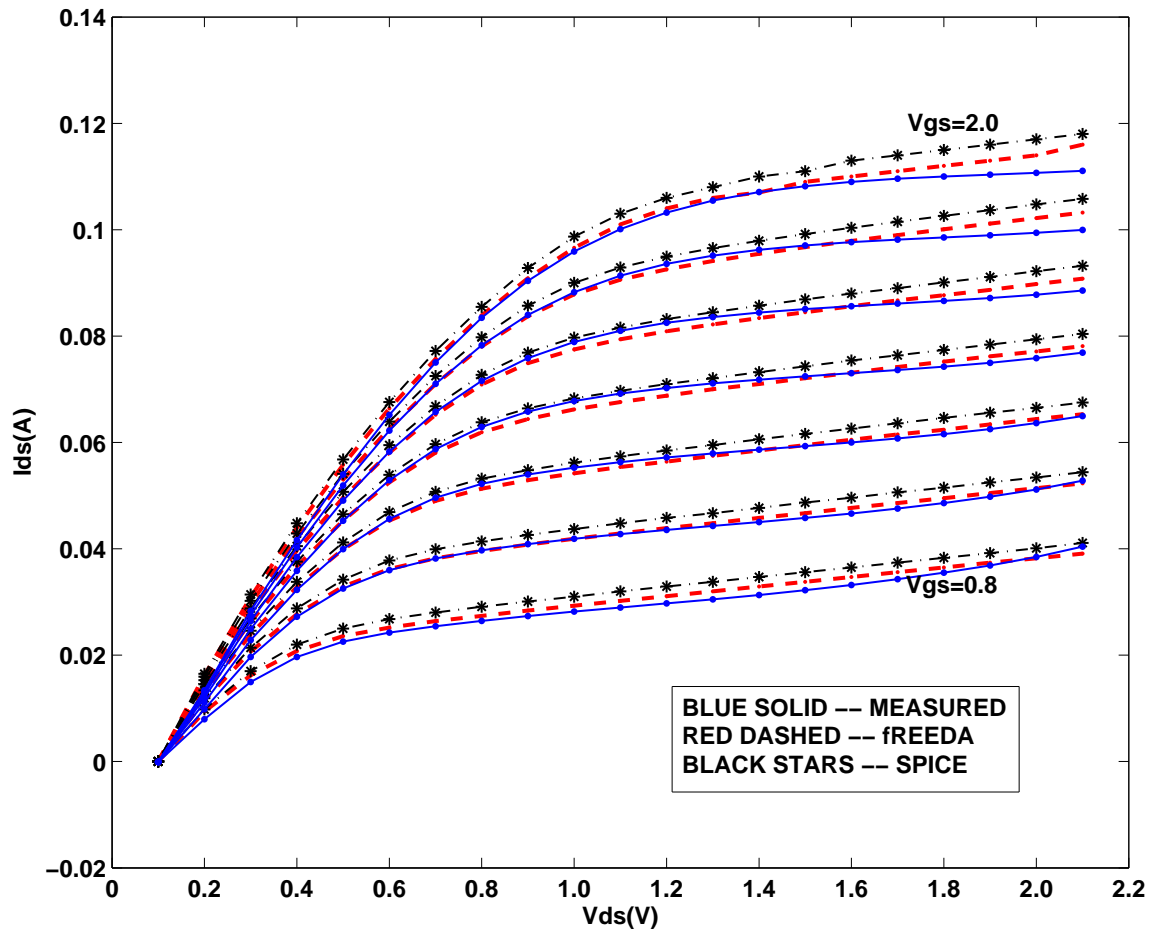


Figure 6.3: Comparison between simulated and measured IV curves of a FDSOI MOSFET at gate bias levels (V_{gs}) of 0.8 V to 2.0 V at 0.2 V intervals. The simulated curves were simulated with the *fREEDA*TM model and the SPICE model.

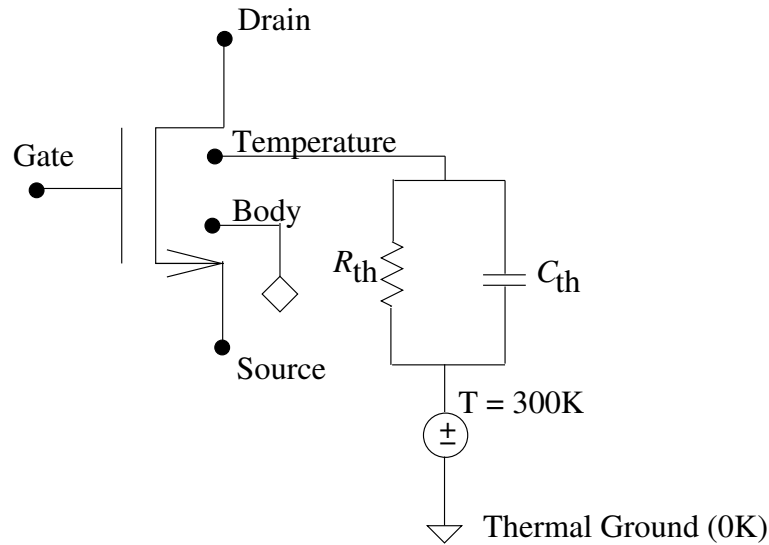


Figure 6.4: Circuit representation of the electrothermal BSIMSOI model.

6.4 Electrothermal BSIMSOI Model

To add the thermal effects, the BSIMSOI model makes use of another technology developed in *fREEDA*[™], the universal error concept. In the electrical domain Kirchhoff's laws are used to calculate the nodal voltages and branch currents. The same concept can be extended to the thermal domain, nodal temperatures and branch heat flows can be calculated. The thermal model is rendered as an electrical circuit [94],[58]. To ensure the separate circuits for the electrical and thermal subsystems, a local reference node concept is employed.

As mentioned at the beginning of this chapter, the buried oxide under the Si film in a SOI transistor gives rise to Self-Heating Effect (SHE). SHE leads to reduction in drain current. To model the SHE, an electrothermal BSIMSOI model is developed in *fREEDA*[™]. This model is based on the universal error concept. The SHE is modeled by an equivalent RC circuit [95]. Analytical model to derive R_{th} is provided in [96] and a thermal impedance extraction methodology is provided in [97]. R_{th} for this device is extracted by the technique provided in [98]. The technique in [97] is more accurate to extract C_{th} than R_{th} . Since R_{th} strongly depends on the technology it must be characterized for every technology [97], making the use of an analytical extraction model inappropriate. The electrothermal model

developed in *fREEDA*TM is based on the universal error concept and the local reference node concept. In the universal error concept, in the thermal domain the nodal temperature and branch heat flow must be calculated. In the electrothermal model two device thermal terminals are added to the electrical device model. One of the two thermal terminals is the temperature terminal and the other is the thermal ground. The temperature at the temperature terminal is the evaluated device temperature and the thermal ground is the local reference node for the thermal domain. The thermal RC network is connected between the temperature terminal and the heat sink as shown in Figure 6.4. In the device model the thermal effects are captured using an extra state-variable to model the device temperature. The value of this state-variable is the temperature at the temperature terminal. This temperature is the equivalent of voltage in the electrical domain. The heat flow into thermal RC network is the equivalent of current in the electrical domain. The heat flow into the thermal network is the total power dissipated, P , by the electrical device model. The temperature rise, ΔT at the temperature terminal is given by,

$$\Delta T = P * R_{th}. \quad (6.11)$$

In *fREEDA*TM, the device temperature is modeled as a state-variable. In the electrical model this device temperature is specified as a model parameter and is constant over all bias levels. This constant temperature is used as any other model parameter while evaluating the characteristic device equations. In an electrothermal model the device temperature rise due to self heating is calculated and depends on the operating bias levels. The temperature is no longer constant, but is an unknown to be evaluated. Hence in the *fREEDA*TM model it is modeled with a state-variable. As mentioned in the previous section in the global modeling approach model development and maintenance is easier and faster. The temperature is added as a state-variable to the state-variable vector in the parameterized device equations, Equation 6.1 and Equation 6.2. The derivatives of these equations with respect to this state-variable are calculated using automatic differentiation. These derivatives are a part of the device Jacobians. The temperature derivatives of the equations are not coded in *fREEDA*TM. In SPICE these derivatives must be manually evaluated and coded in the model code. For example in the SPICE code the drain current I_{ds} is evaluated as,

```
T0 = 1.0 + gche * Rds;
T9 = Vdseff / T0;
Idl = gche * T9;
```

```

T0 = 1.0 + T9;
if (selfheat)
    dIdl_dT = (gche * dVdseff_dT + T9 * dgche_dT
              - Idl * dRds_dT * gche) / T0;
else dIdl_dT = 0.0;
here->B3S0Iids = Ids = Idl * T0 / here->B3S0Inseg;
if (selfheat)
    GmT0 = T0 * dIdl_dT - Idl * (dVdseff_dT + T9 * dVa_dT) / Va;
else GmT0 = 0.0;

```

Here I_{ds} is dependent on V_{dseff} . V_{dseff} is dependent on V_{ds} and temperature, making I_{ds} dependent on temperature. The linearization of the device equations in the Associated Discrete Modeling technique used in SPICE requires the derivative of I_{ds} with respect to temperature. Hence this derivative, $dIdl_dT$, is manually evaluated and coded in the model code. This derivative, $dIdl_dT$, is used to evaluate the temperature dependent transconductance $GmT0$. This transconductance, $GmT0$, is connected between the drain and temperature device terminals. Similar temperature derivatives of other equations are manually evaluated and coded in the SPICE model code. This makes model development and feature enhancement cumbersome and time consuming. In *fREEDA*TM the use of the global modeling approach eliminates these steps. As explained in the previous section, the derivatives with respect to the state-variables are evaluated by the automatic differentiation library and passed to modified nodal analysis. The model developer does not spend time manually coding any derivatives or loading the Jacobian matrices. Addition of thermal effects involves only adding temperature as a state-variable and the equation for heat flow into the thermal network.

In *fREEDA*TM the heat flow in the thermal network is the power dissipated by the electrical device model, P , given by $I_{ds} * V_{ds}$. This heat flow is the equivalent of current in the electrical domain. The heat flow equation is one of the characteristic current equations i_{NL} of the device. This equation is added to the *fREEDA*TM model code as the nodal current at the temperature terminal. It is stored in variable $z1[3]$ in the *fREEDA*TM pseudo code shown in the previous section. The other equations added to develop the electrothermal model are the temperature dependence mobility and saturation velocity equations. Since no derivatives must be calculated and no matrices must be populated by the model developer, this model can be developed within a couple of days.

6.5 Electrothermal BSIMSOI Model Validation

Self heating effects in the BSIMSOI model developed in *fREEDA*TM were simulated for a $0.18\mu \times 200\mu$ FDSOI MOSFET fabricated at MIT Lincoln Labs. The device has 20 fingers with each finger 10μ wide. The model parameters for this device extracted by MIT Lincoln Labs are provided in Appendix B, Section B.11.

Device temperature rise depends on the power dissipated by the device. Self heating effects are significant at high power dissipating levels. The self heating effects in the FDSOI MOSFET were simulated at gate bias (V_{gs}) voltages of 1.0 V and 1.8 V. The drain bias (V_{ds}) voltage was swept from 0 V to 2.0 V in steps of 0.1 V. IV curves for the FDSOI MOSFET at $V_{gs} = 1.0$ and $V_{gs} = 1.8$ V are plotted in Figures 6.5 and 6.7 respectively. The *fREEDA*TM netlist used to test the self heating effects in the electrothermal BSIMSOI model is provided in Appendix B, Section B.12. These figures show a comparison between the DC IV curves with and without self heating effects. In Figure 6.5 a gate bias V_{gs} of 1.0 V was set. The simulations were performed with no self heating effects i.e. a purely electrical simulation at a constant device temperature, which is the ambient temperature T of 300°K . The other curves are drain currents with self heating effects in the electrothermal device model at different ambient temperatures. The ambient temperature T was varied from 300°K to 400°K at 10°K intervals. In the simulations with the self heating effects, the device temperature rises above the set ambient temperature. An example of device temperature at various drain bias points is shown Figure 6.6. In this figure, at an ambient temperature T of 300°K , gate bias V_{gs} of 1.0 V and drain bias V_{ds} of 2.0 V a device temperature rise above the ambient temperature due to self heating effects of approximately 45°K is seen. The device temperature is not constant at all drain points in Figure 6.5. The rise in the device temperature leads to a reduction in the drain current. This is seen in Figure 6.5. Hence at an ambient temperature T of 300°K the curves with self heating effects and with no self heating effects do not match. This reduction in drain current is ignored in a purely electrical model where self heating effects are ignored.

At higher gate bias levels the power dissipated by the device will be larger and hence a larger rise in the device temperature is expected. To see this effect DC IV curves were simulated at a gate bias of 1.8 V with self heating effects at different ambient temperatures. In Figure 6.7 a gate bias V_{gs} of 1.8 V was set. The simulations were performed with no self heating effects i.e. a purely electrical simulation at a constant device temperature,

which is the ambient temperature T of 300°K . The other curves are drain currents with self heating effects in the electrothermal device model at different ambient temperatures. The ambient temperature T was varied from 300°K to 400°K at 10°K intervals. As explained for the gate bias of 1.0 V case, the device temperature is not constant at all drain bias points. The rise in the device temperature at an ambient temperature T of 300°K and gate bias V_{gs} of 1.8 V is shown in Figure 6.7. At a drain bias of 2.0 V this rise is approximately 86°K . This larger rise in temperature than the temperature rise of 45°K at V_{gs} of 1.0 V results in a larger reduction in drain current. A reduction of approximately 7 mA with the self heating effects at an ambient temperature, T , 300°K of is seen in Figure 6.7. This reduction is ignored in a purely electrical model where no self heating effects are considered. At higher ambient temperatures and effectively at higher device temperatures the reduction in drain current is significantly large. The reduction in drain current from an ambient temperature of 300°K to 400°K is approximately 10 mA .

In Figure 6.9 the measured drain current and simulated drain current at $T = 300^\circ\text{K}$ with self heating do not match very well. The device temperature rises during measurements and hence the measured drain current includes the self heating effects. The average difference between the measured and simulated drain current is 1.53 mA with a maximum of 3.5 mA at $V_{ds} = 1.3\text{ V}$. This difference can be accounted as an overestimated extracted thermal resistance. In Figure 6.9 the thermal resistance R_{th} in the thermal network was $350\ \Omega$. This value of the thermal resistance gives a larger rise in temperature and hence a larger reduction in the drain current. If this value is reduced the device temperature rise will be smaller leading to a smaller reduction in drain current. If the thermal resistance is decreased to $250\ \Omega$ a smaller reduction in the drain current due to self heating is seen, Figure 6.8. The average difference between the simulated drain current and the measured current reduces from 1.53 mA to 0.6 mA with a maximum of 2.3 mA at $V_{ds} = 1.3\text{ V}$. This illustrates the importance of accurately modeling and extracting the thermal resistance. Here the thermal resistance was an extracted parameter and modeled as a simple linear resistor. It is also considered constant over all temperature ranges. The thermal nonlinearity is completely ignored. The thermal network of this model can be modeled using the 3D compact thermal model developed in Chapter 4. This compact model is based on structural and material properties of the die. It is a quasi-analytical model and captures the nonlinear thermal effects in the SOI die. Hence the accuracy of a semiconductor device model depends on the thermal model used to model the thermal

effects.

6.6 Summary

In this chapter an electrothermal BSIMSOI MOSFET model was successfully developed and implemented in *fREEDA*TM. The model used *fREEDA*TM's simplified model development approach. In this approach the global modeling technique is used. In the global modeling technique the characteristic device equations are parameterized using state-variables. This parameterization and Object Oriented Programming enables model code implementation in a standard format. This speeds up the model development process. Derivatives of device equations is calculated using automatic differentiation in *fREEDA*TM. In the SPICE like model development approach the derivatives of equations must be manually evaluated and coded in the model code. This process is time consuming and error prone. The use of automatic differentiation in *fREEDA*TM eliminates the need to manually evaluate and code the derivatives in the model code. This reduces the model code size to one tenth of the implementation in SPICE. Also if any model equations are changed or added their derivatives need not be changed or added. This makes model maintenance and feature enhancement easy and fast. In the SPICE like model development approach, the model developer must populate the appropriate matrices with the derivatives. This requires knowledge about the intricacies of the simulator. In the global modeling technique in *fREEDA*TM the appropriate matrices are populated by the modified nodal analysis and the model developer need to be concerned about loading and populating the matrices. This reduces the burden of the model developer and can concentrate on developing the device equations. With these features and techniques the electrical BSIMSOI model was developed within couple of weeks.

The BSIMSOI model developed in *fREEDA*TM is validated with experimental data of a $0.18\mu\text{m} \times 200\mu\text{m}$ FDSOI MOSFET. The simulated *fREEDA*TM model IV curves agreed better with the measured data than the SPICE model in all bias regions. In the gate bias region with $V_{gs} > 0.8\text{ V}$ the simulated drain current obtained from the *fREEDA*TM model was within an average error of 1% compared to 2% error in the SPICE model. Automatic differentiation used in *fREEDA*TM evaluates the derivatives of the variables analytically and hence is accurate error free. All parameter dependencies are considered while evaluating

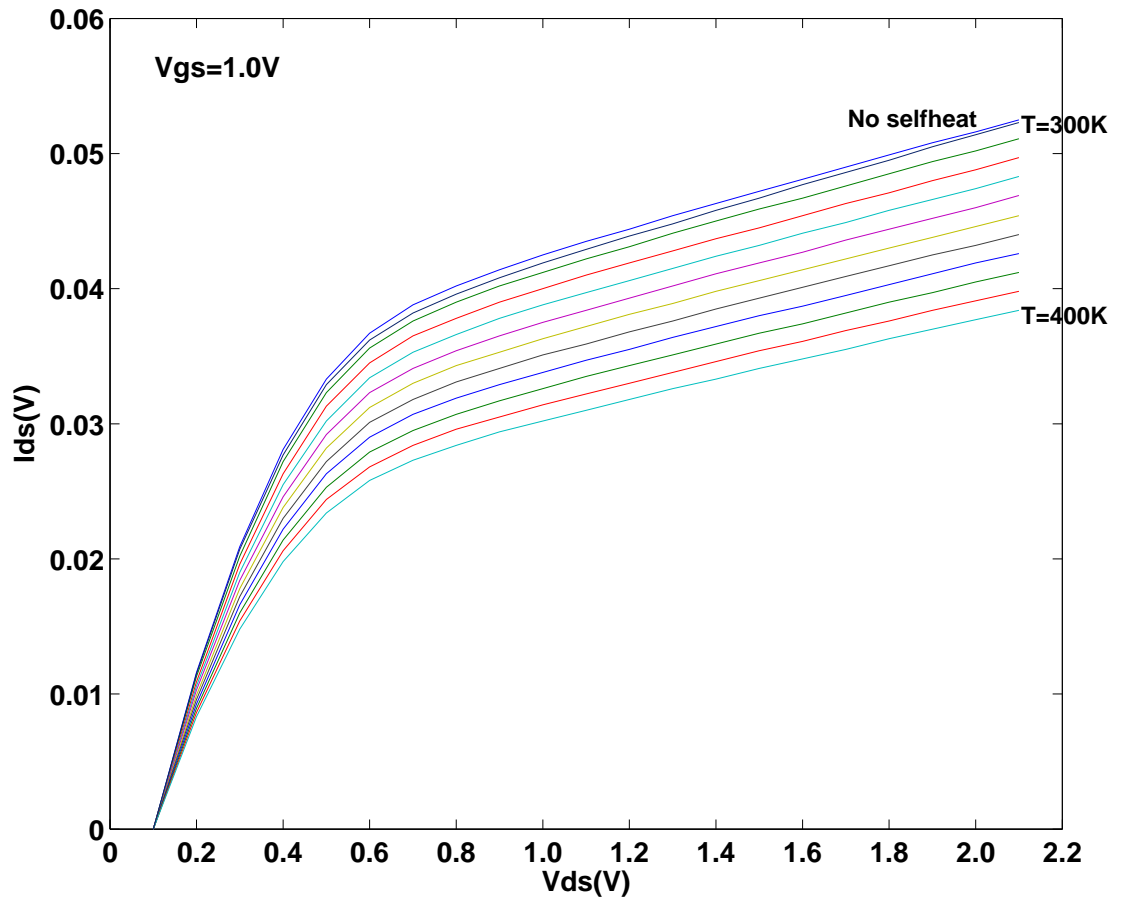


Figure 6.5: Comparison of measured and simulated with no self heating IV curves of a FDSOI MOSFET with self heating turned on at $V_{gs} = 1.0$ V. The curves between the $T = 300^{\circ}K$ (second curve from the top) and $T = 400^{\circ}K$ (bottom curve) were done at $10^{\circ}K$ ambient temperature intervals.

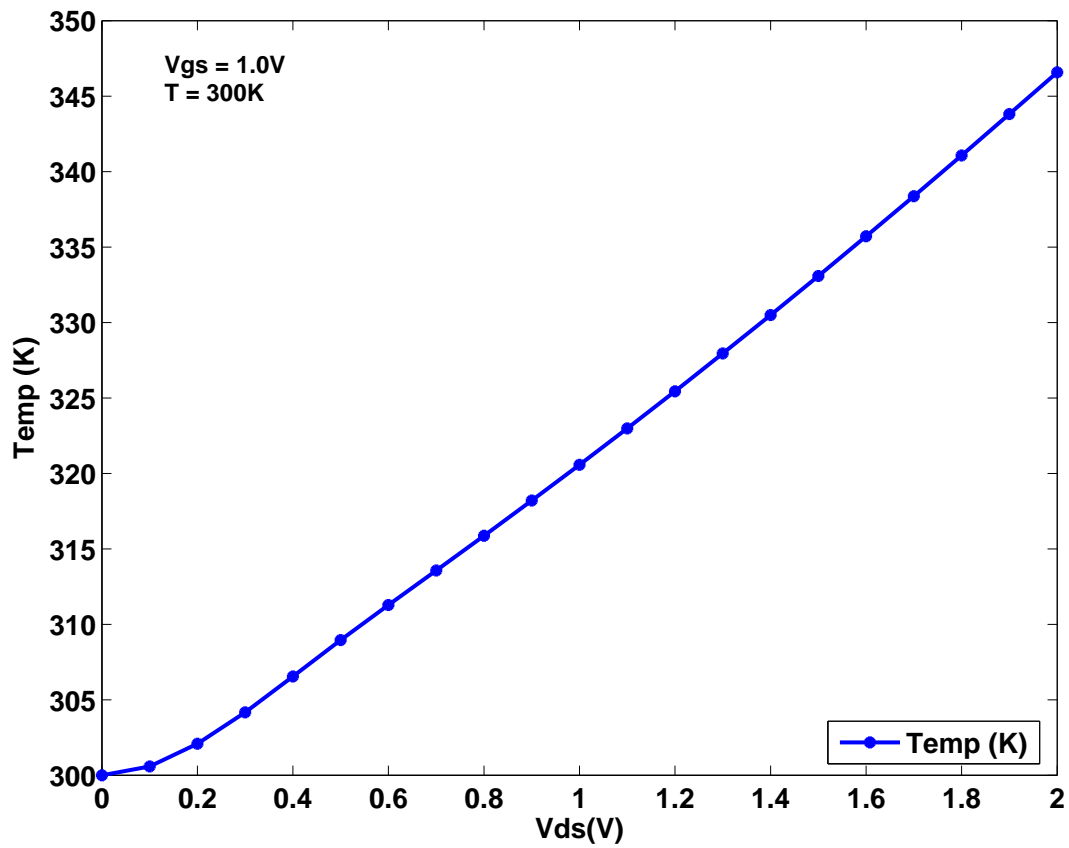


Figure 6.6: Device temperature with self heating turned on, $V_{ds} = 2.0$ V, $V_{gs} = 1.0$ V, at $T = 300^\circ\text{K}$.

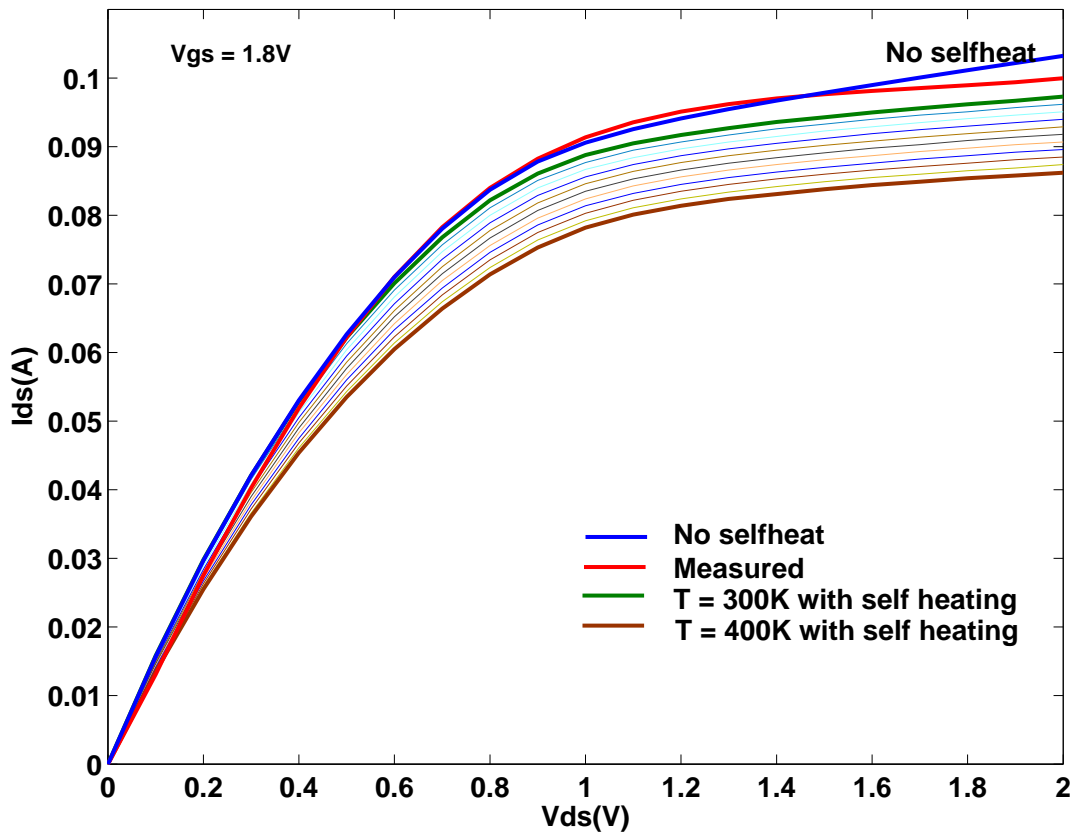


Figure 6.7: Comparison of measured and simulated with no self heating IV curves of a FDSOI MOSFET with self heating turned on at $V_{gs} = 1.8$ V. The curves between the $T = 300^{\circ}\text{K}$ (second curve from the top) and $T = 400^{\circ}\text{K}$ (bottom curve) were done at 10°K ambient temperature intervals.

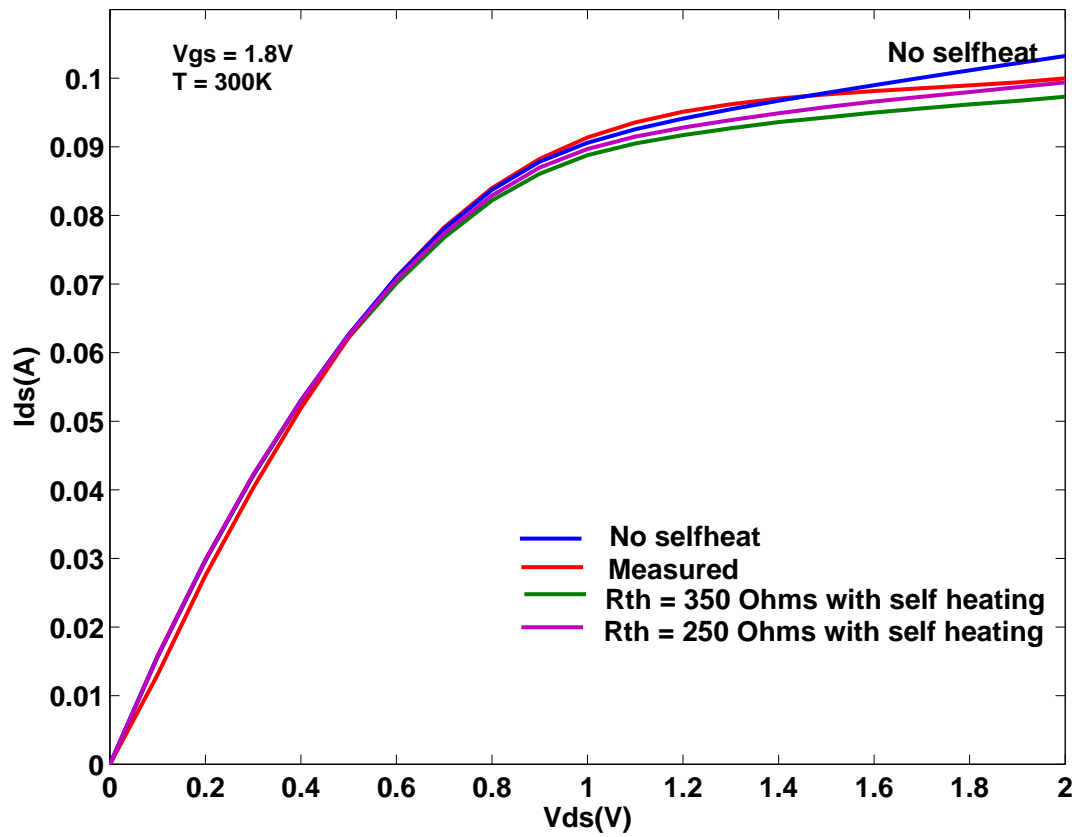


Figure 6.8: Comparison between IV curves of a FDSOI MOSFET with self heating turned on, $V_{gs} = 1.8$ V, $R_{th} = 350 \Omega$ and $R_{th} = 250 \Omega$, at $T = 300^\circ\text{K}$

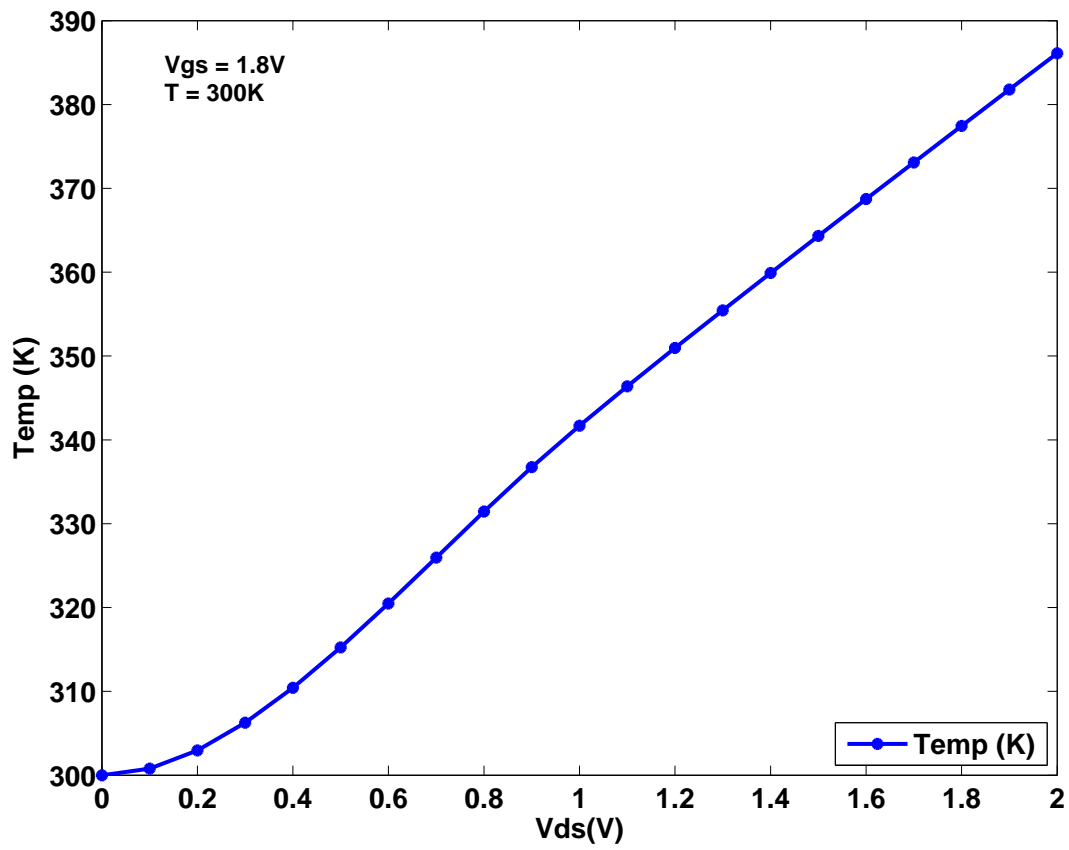


Figure 6.9: Device temperature with self heating turned on, $V_{ds} = 2.0$ V, $V_{gs} = 1.8$ V, at $T = 300^{\circ}\text{K}$

the derivatives. This improves the accuracy of the device model.

Thermal effects must be considered to develop a good and accurate semiconductor device model. An electrothermal BSIMSOI model was also developed in this chapter. With the use of automatic differentiation and global modeling technique in *fREEDA*TM the thermal effects to the electrical BSIMSOI model were added within couple of days. In the electrothermal model device temperature is modeled as a state-variable. This state-variable is added to the state-variable vector of the model. The automatic differentiation library evaluates the derivatives of the device equations with respect to temperature. Hence no temperature derivatives were coded in the model. A temperature terminal is added to the model. The thermal RC network is connected to this terminal. The voltage at this terminal is the evaluate device temperature. The equation describing the heat flow into the thermal network was added to the model. The heat flow is equivalent of current in the electrical domain. Hence this equation is added as another characteristic device equation describing the current at the temperature terminal. The addition of the temperature as a state-variable, the heat flow equation and other temperature dependent device equations required couple of days. Hence the thermal effects were added to the electrical model within couple of days.

Simulations to examine the thermal effects on the device performance were also performed. These simulations were performed on the $0.18\mu\text{m} \times 200\mu\text{m}$ FDSOI MOSFET. At high gate and drain bias levels self heating effects can raise the device temperature by approximately 90 degrees. This large rise in device temperature results in a reduction of the drain current. This reduction could be as large as few mA at high bias levels. This reduction in drain current is ignored in an electrical model where self heating effects are not considered. Thus thermal effects must be considered to develop a good and accurate semiconductor device models. The accuracy of the simulated self heating effects depends on the thermal model used to capture them. An over estimation of the thermal resistance would unnecessarily raise the device temperature resulting a reduction of drain current. Precise extraction of the thermal parameters are important to capture the thermal effects. The thermal network in the device model can also be modeled with a good compact thermal model based on structural and material properties of the device.

Hence an electrothermal device model for fully-coupled electrothermal simulations can be developed in *fREEDA*TM rapidly and is derivative error free.

Chapter 7

Conclusions and Future Work

7.1 Conclusions

This dissertation has focused on the transient analysis advances required to perform fully predictive modeling capabilities. Predictive modeling incorporating other physical effects such as transient thermal effects were developed. The goal of this work was to develop a high dynamic range transient analysis for long coupled electrothermal simulation. To achieve this goal three features were incorporated in the circuit simulator paradigm: a high dynamic range transient analysis, an accurate compact thermal model and an accurate electrothermal semiconductor device model. These three features were developed and implemented in the multi-physics, multi-domain circuit simulator, *fREEDA*TM for long electrothermal simulations.

A new transient analysis technique using state-variables was developed to achieve a high dynamic range. At every time step the precise estimate of error and the good initial guess prediction for the Newton iteration helped achieve a high dynamic range transient analysis technique. Also it eliminates the unnecessary reduction in time steps. The accuracy of the new time step control was tested with the analytical solution of a simple RC circuit. The new technique was found to be more accurate than the conventional technique and required a smaller number of simulation time points. The improvement in the number of time points was 29%. The dynamic range of the transient simulation was tested with a

two tone test performed on a X-band GaAs MMIC LNA. The new technique achieved a dynamic range of 165 dB. It can detect signals as small as approximately -160 dBm.

To incorporate the electrothermal effects in an electronic circuit, a 3D compact thermal model for the mounted and metallized X-band GaAs MMIC LNA was developed and implemented. This model is in effect an ‘interface element’ model of a volumetric model, which discretizes only interfaces of subvolumes. The heat generating elements in the thermal model of the MMIC were the transistor fingers and the DC bias TaN resistors. Surface metallization such as the top layer of the via capacitors and of the through vias were also considered. Other mounting layers such as the epoxy used to attach the die to the Kovar substrate and the Kovar substrate itself were also considered as individual subvolumes. A coupled electrothermal simulation to see the thermal transient with only the DC power applied, was performed. The steady-state temperature rise on various spots of the MMIC were verified with thermal images taken with an infra-red camera. The model can predict steady-state temperature rise on various spots of the MMIC with less than 5% error. The high dynamic range transient analysis can be applied to perform a fully-coupled electrothermal simulation at RF frequencies. This model can perform RF simulations with time steps as small as 2 ns. The X-band MMIC requires time steps as small as 3 ps to perform RF simulations. To perform the coupled electrothermal simulation of the MMIC a thermal 3D macromodel of the MMIC body was developed. This 3D macromodel is a RC network based on the structural information and metal density information in each direction of the body. This model predicted the hot spots on the MMIC die. The predicted temperature rise agreed with the measured temperature rise within 10% error. This model was used to perform a coupled electrothermal simulation at RF frequencies on the MMIC. The high dynamic range capability of the new time step control technique developed in Chapter 3, detected the small variations in the output voltage, as small as $1 \mu\text{V}$, due to thermal effects.

This thermal macromodel was also found suitable in a study of the temperature rises in a 3DIC, where the thermal problem is exacerbated due to stacking of chips. It was applied to a self-testing 3DIC thermal chip. With three tiers the thermal chip had approximately 1 million transistors. The temperature profile for each tier, showed that the middle tier of the stack, experiences the maximum temperature rise. One of the techniques used for heat removal was thermal vias. Increasing the vertical metal density i.e. the thermal vias density, reduces the the temperature rise only marginally. This improvement does not

depend on the power consumption of the chip. To reduce the temperature rise of the chip, an epoxy with good thermal conductivity should be used. If the thermal conductivity of the epoxy is increased by a factor of 6, a maximum temperature rise of 37% is achieved, whereas if the thermal conductivity of the epoxy is not improved, a maximum temperature rise of 170% is seen.

To simulate the variations in the output voltage in electrothermal simulations, temperature dependent functionalities should be incorporated in the device model. These temperature dependent functionalities were added to an electrothermal model of a FDSOI MOSFET. This model was developed and implemented in *fREEDA*TM. It was based on the BSIMSOI model from the University of Berkeley. The use of automatic differentiation to develop this model, reduces the model code size to one tenth and only two files must be modified to accommodate any changes, making model maintenance easy. This model was validated with experimental data of a FDSOI MOSFET from MIT Lincoln Labs. The self heating thermal effects of the FDSOI MOSFET were studied using the electrothermal FDSOI MOSFET model, developed in *fREEDA*TM. Simulations showed that at high drain and gate bias levels the device temperature can rise by 86 degrees, reducing the drain current. Also, the extracted thermal resistance value R_{th} used in the model was modified to fit the simulated drain current with self heating effects to the measured drain current. This illustrates, the importance to accurately model or extract the thermal resistance parameter in a device model.

7.2 Future Work

Most of the work presented in this dissertation is open to further research. As presented in this dissertation the thermal time constants in electronic circuits are large compared to the time steps required by the electrical simulation. If a small time step is used to perform the thermal simulation, the accumulated numerical error in the thermal model is large to perform an accurate fully-coupled electrothermal simulation at RF frequencies. To avoid the accumulation of the numerical error the thermal network must be simulated with large time steps and the electrical network must be simulated with small time steps. This can be performed with a multi time step transient analysis. In this analysis the electrical domain will use small time steps to resolve the electrical signals at RF frequencies,

whereas the thermal domain will use large time steps for the long thermal constants. The temperature rises at the time points between the long thermal time points is considered piecewise constant. The algorithm for this technique is presented below:

- Create MNAM for the linear elements in the electrical domain.
- Precompute the thermal impedance matrix with the thermal time step provided in the netlist.
- Set the simulation time step to the electrical domain time step provided in the netlist.
- Formulate transient equations for the electrical domain.
- Check if the current simulation time point is a integer multiple of the thermal time step. If yes formulate the transient equations for the thermal domain with the thermal impedance matrix for the current simulation time point.
- Solve the system of equations with LU factorization.
- On convergence update the time point.
- Calculate output and display results.

The 3D compact thermal solution discussed in Chapter 4 uses individual models for every subvolume. Each of these models must be connected to each other to model the entire structure. These models can be reduced using hierarchical reduction techniques to combine all subvolumes into one large subvolume represented by one global thermal impedance matrix. An introduction to these techniques is presented in [60] and [66]. This solution will form a single global matrix for a metallized and mounted MMIC. Every metallization feature or layer will not be considered as a separate subvolume with a separate thermal impedance matrix. Instead a single global matrix must be manipulated for all the metallization features and structural layers. This solution can also be applied to a multi tier 3DIC, where each tier is considered as an individual subvolume. All subvolumes are combined to form a large subvolume represented by a single global thermal impedance matrix.

Currently only vertically matched thermal subvolumes of the compact thermal model developed in Chapter 4 are implemented in *fREEDA*TM. Horizontally matched subvolumes can be implemented with embedded subvolumes. This will model lateral heat dissipation in subvolumes. For embedded subvolumes the the heat dissipating sources are

considered as volume heat sources/sinks. An original solution for volume heat sources using double Fourier series solutions is presented in [60]. This solution does not use the Green's functions. Lateral heat dissipation is an important phenomenon in a 3DIC with multiple metal layers and interconnects. This solution can be used to model lateral heat dissipation in a 3DIC. Each metal layer can be considered as an embedded subvolume. The 3D vias can be considered as vertically matched thermal subvolumes. The entire 3DIC can be modeled as a heterogenous structure.

As mentioned in Section 5.5, the reasons for the formation of hot spots of different tiers of a 3DIC, must be determined. This will help gain insight into how to eliminate the hot spots on different tiers. A surface area of 3DIC is large compared to an individual die, making heat loss due to radiation and convection significant. These heat losses can be accounted for in the thermal macromodel, with nonlinear radiation and convection thermal resistances connected to the sides of the chip.

The electrothermal FDSOI MOSFET model developed in *fREEDA*TM must be validated with experimental data at different temperature settings. The capacitance model of the FDSOI MOSFET model must be developed and verified. The temperature variations at RF frequencies in the FDSOI MOSFET must be studied with the help of the capacitance model.

Bibliography

- [1] S. Luniya, *SPICE Like Sparse Transient Analysis*, Master's Thesis, Department of Electrical and Computer Engineering, North Carolina State University, Dec. 2002.
- [2] S. Luniya, M. B. Steer and C. Christoffersen, "High dynamic range transient simulation of microwave circuits," *2004 IEEE Radio and Wireless Conference*, 19-22 Sept. 2004 pp. 487-490.
- [3] F. Hart, N. Kriplani, S. Luniya, C. Christoffersen and M. B. Steer "Streamlined Circuit Device Model Development with fREEDA and Adol-C," *AD 2004 Fourth International Workshop on Automatic Differentiation*, July 2004.
- [4] M. B. Steer and C. E. Christoffersen, "Generalized circuit formulation for the transient simulation of circuits using wavelet, convolution and timemarching techniques," *Proc. of the 15th European Conference on Circuit Theory and Design*, August 2001, pp. 205-208.
- [5] W. J. McCalla and D. O. Pederson, "Elements of Computer-Aided Circuit Analysis", *IEEE Transactions on Circuit Theory*, January 1971, pp. 14-26.
- [6] K. S. Kundert and A. Sangiovanni-Vincentelli, "Simulation of Nonlinear circuits in the Frequency Domain," *IEEE Transactions on Computer-Aided Design*, October 1986, pp. 521-535.
- [7] K. S. Kundert, "Accurate fourier analysis for circuit simulators," *IEEE Custom Integrated Circuits Conference*, 1994.
- [8] K. Gard, "FFT Windows for Intermodulation analysis of microwave circuits from

- transient simulation,” *IEEE MTT-S International Microwave Symposium Digest*, 1997, pp. 1699-1702.
- [9] K. S. Kundert, “Introduction to RF simulation and its applications,” *IEEE Journal of Solid-State Circuits*, Vol. 34, September 1999, pp.1298-1319
- [10] M. B. Steer and C. E. Christoffersen, *Simulation and Modeling for Analog, RF and Mixed Mode Design*, To be published.
- [11] Ron. M. Kielkowski, *Inside SPICE*, 2nd ed, McGraw Hill, 1998.
- [12] R. J. Schwarz and B. Freiland, *Linear Systems*, McGraw Hill, 1965.
- [13] J. Vlach and K. Singhal, *Computer Methods for Circuit Analysis and Design*, Chapman and Hall, 1994.
- [14] L.O.Chua and P.Lin, *Computer Aided Analysis of Electronic Circuits*, Englewood Cliffs, NJ, Prentice-Hall, 1975.
- [15] C. E. Christoffersen, M. B. Steer and M. A. Summers, “Harmonic balance analysis for systems with circuit-field interactions,” *1998 IEEE International Microwave Symposium Digest*, June 1998, pp. 1131-1134.
- [16] K. S. Kundert and A. Songiovanni-Vincentelli, *Sparse users guide - a sparse linear equation solver*, Dept. of Electrical Engineering and Computer Sciences, University of California, Berkeley, Calif. 94720, Version 1.3a, Apr 1988.
- [17] Richard Tong and Wendell Feres Jrn, *X-Band Low Noise Phemt Amplifier*, Master’s Degree Project Report, Department of Electrical and Computer Engineering, Lakehead University, Canada, March 2003.
- [18] D. A. Pope, “An exponential method of numerical integration of ordinary differential equations,” *Comm. ACM*, Vol. 6, pp. 491-493, August 1963.
- [19] M. E. Fowler and R. M. Warten, “A numerical technique for ordinary differential equations with widely spread eigenvalues,” *IBM J. Res. Develop.*, pp. 537-543, September 1967.

- [20] Debra L. Waller, Leslie R. Fox and R. J. Hannemann, "Analysis of surface mount thermal and thermal stress performance," *IEEE Transactions of components, hybrids and manufacturing technology*, Vol. CHMT-6, No. 3, September 1983, pp. 257-266.
- [21] Chin C. Lee, A. L. Palisoc and Y. Jay Min, "Thermal Analysis of integrated circuit devices and packages," *IEEE Transactions of components, hybrids and manufacturing technology*, Vol. 12, No. 4, December 1989, pp. 701-709.
- [22] J. Albers, "Semiconductor measurement technology: TXYZ: A program for semiconductor IC thermal analysis," NIST Special Publication Report 400-76, 1984.
- [23] Vladimir Szekely, "Identification of RC Networks by Deconvolution: Changes and Limits," *IEEE Transactions on Circuits and Systems – I: Fundamental Theory and Applications*, Vol. 45, No. 3, March 1998, pp. 244-258
- [24] Vladimir Szekely, M. Renez and B. Courtois, "Simulation, Testing, and Modeling of the Thermal Behavior and Electrothermal Interactions in ICs, MCMs, and PWBs," *1999 Southwest Symposium on Mixed-Signal Design*, pp. 168-173, April 1999.
- [25] Allen R. Hefner and D. L. Blackburn, "Thermal Component Models for Electrothermal Network Simulation," *IEEE Transactions on Components, Packaging and Manufacturing Technology*, Part A. Vol. 17, No. 3, September 1994, pp. 413-424
- [26] Allen R. Hefner and D. L. Blackburn, "An Experimentally Verified IGBT Model Implemented in the Saber Circuit Simulator," *IEEE Transactions on Power Electronics*, Vol. 9, No. 5, September 1994, pp. 532-542
- [27] Gordon N. Ellison "Extensions of the Closed Form Method for Substrate Thermal Analyzers to Include Thermal Resistances from Source-to-Substrate and Source-to-Ambient ," *IEEE Transactions of components, hybrids and manufacturing technology*, Vol. 15, No. 5, October 1992, pp. 658-666
- [28] Gordon N. Ellison "Thermal Analysis of Circuit Boards and Microelectronics Components Using An Analytical Solution to the Heat Conduction Equation," *Twelfth IEEE Semiconductor Thermal Measurement and Management Symposium*, 1996, pp. 144-150

- [29] *ANSYS Engineering Analysis Systems Users Manual.*, <http://www.ansys.com>, Canonsburg, Pennsylvania: Ansys Inc.
- [30] Xiang Gui, Paul W. Webb and Guang-bo Gao "Use of Three Dimensional TLM Method in the Thermal Simulation and Design of Semiconductor Devices," *IEEE Transactions on Electron Devices*, Vol. 39, No. 6, June 1992, pp. 1295-1302
- [31] Paul W. Webb and A. D. Russell "Application of the TLM Method to Transient Thermal Simulation of Microwave Power Transistors ," *IEEE Transactions on Electron Devices*, Vol. 42, No. 4, April 1995, pp. 624-631
- [32] J. Gill, D. Harmon, J. Furukawa and T. Sullivan "Predicting Thermal Behavior of Interconnects," *IEEE International Integrated Reliability Workshop Final Report*, 1999, pp. 54-60.
- [33] J. Gill, D. Harmon, J. Furukawa and T. Sullivan "Thermal Conductance of IC interconnects embedded in dielectrics," *IEEE International Integrated Reliability Workshop Final Report*, 1998, pp. 1-9.
- [34] R. S. Li, "Optimization of Thermal Via Design Parameters Based on an Analytical Thermal Resistance model," *IEEE Intersociety Conference on Thermal Phenomena*, 1998, pp. 475-480
- [35] Jason Cong, "An Interconnect-centric design flow for nanometer technologies," *IEEE International Symposium on VLSI Technology, Systems and Applications*, 1999, pp. 54-57.
- [36] F. Christiaens, E. Beyne and J. Berghmans, "Modeling of thermal vias in thin flim multichip modules," *1994 InterSociety Conference on Thermal Phenomena in Electronic Systems, I-THERM IV*," 1994, pp. 101-107.
- [37] S. Lee, T. F. Lemczyk and M. M. Yovanovich, "Analysis of thermal visa in high density interconnect technology," *Proceedings of the Eighth IEEE SEMITHERM Symposium*," Austin, TX, 1992, pp. 55-60.
- [38] The National Technology Roadmap for Semiconductors (*ITRS*), 1997.
- [39] The International Technology Roadmap for Semiconductors (*ITRS*), 1999.

- [40] K. C. Saraswat and F. Mohammadi, "Effect of interconnection scaling on time delay of VLSI circuits," *IEEE Transactions Electron Devices*, 1982, Vol. ED-29, pp. 645-650.
- [41] S.-Y. Oh and K.-J. Chang, "2001 needs for multi-level interconnect technology," *IEEE Circuits and Devices Magazine*, 1995, pp. 16-21.
- [42] M. T. Bohr and Y. A. El-Mansy, "Technology for advanced highperformance microprocessors," *IEEE Transactions Electron Devices*, Vol. 45, pp. 620-625, Mar. 1998.
- [43] S. A. Kuhn, M. B. Kleiner, P. Ramm, and W. Weber, "Thermal analysis of vertically integrated circuits," *International Electron Devices Meeting Technical Digest*, 1995, pp. 487-490.
- [44] Sungjun Im and Kaustav Banerjee, "Full Chip Thermal Analysis of Planar(2-D) and Vertically Integrated (3-D) High Performance ICs," *International Electron Devices Meeting Technical Digest*, 2000, pp. 727-730.
- [45] M. B. Kleiner, S. A. Kuhn, P. Ramm, and W. Weber, "Performance improvement of the memory hierarchy of RISC-systems by application of 3-D technology," *IEEE Transactions Components, Packaging, Manufacturing Technology B*, vol. 19, pp. 709-718, 1996.
- [46] C. T. Chuang, P. F. Lu, and C. J. Anderson, "SOI for digital CMOS VLSI: Design considerations and advances," *Proceedings IEEE*, vol. 86, pp. 689-720, Apr. 1998.
- [47] R. Zhang, K. Roy, and D. B. Jones, "Architecture and performance of 3-dimensional SOI circuits," *IEEE International Silicon on Insulator Conference 1999*, pp. 44-45, 1999.
- [48] M. Nakano, "3-D SOI/CMOS," *International Electron Devices Meeting Technical Digest*, 1984, pp. 792-795.
- [49] S. Kawamura, N. Sasaki, T. Iwai, M. Nakano, and M. Takagi, "Three-dimensional CMOS ICs fabricated by using beam recrystallization," *IEEE Electron Device Letters*, vol. EDL-4, pp. 366-368, Oct. 1983.

- [50] C. E. Christoffersen and M. B. Steer, "Implementation of the local reference node concept for spatially distributed circuits," *International Journal on RF and Microwave Computer Aided Engineering*, Vol. 9, No. 5, Sept. 1999, pp. 376-384.
- [51] Carlos E. Christoffersen, Senthil Velu, Michael B. Steer, "A Universal Parameterized Nonlinear Device Model Formulation for Microwave Circuit Simulation," *IEEE International Microwave Symposium Digest*, Vol.3, June 2002, pp. 2189-2192.
- [52] C. E. Christoffersen, "Global Modeling of Nonlinear Microwave circuits," Ph.D. Thesis, Department of Electrical and Computer Engineering, North Carolina State University, 2000.
- [53] W. B. Joyce, "Thermal resistance of heat sinks with temperature-dependent conductivity," *Solid State Electronics*, vol. 18, pp. 321-322, 1975.
- [54] W. Batty, A. J. Panks, and C. M. Snowden, "Fully-coupled electrothermal simulation of MMICs and MMIC arrays based on a physical model," in *IEEE MTT-S International Microwave Symposium Digest*, vol. 2, 1999, pp. 693-696.
- [55] W. Batty, A. J. Panks, R. G. Johnson, and C. M. Snowden, "Electrothermal modeling and measurement for spatial power combining at millimeter wavelengths," *IEEE Transactions Microwave Theory Technology*, vol. 47, pp. 2574-2585, Dec. 1999.
- [56] W. Batty, A. J. Panks, R. G. Johnson, and C. M. Snowden, "Electrothermal modeling of monolithic and hybrid microwave and millimeter wave ICs," *VLSI Design*, vol. 10, no. 4, pp. 355-389, 2000.
- [57] S. David, W. Batty, A. J. Panks, R. G. Johnson, and C. M. Snowden, "Fully physical coupled electrothermal modeling of transient and steady-state behavior in microwave semiconductor devices," in *2000 8th Gallium Arsenide Application Symposium (GAAS 2000)*, Paris, France, Oct. 2000.
- [58] H. Gutierrez, C. E. Christoffersen, and M. B. Steer, "An integrated environment for the simulation of electrical, thermal and electromagnetic interactions in high-performance integrated circuits," *Proc. IEEE 6th Topical Meeting Elect. Performance and Electronic Packaging*, Sept. 1999, pp. 217-220

- [59] James S. Wilson, and Peter E. Raad, "A transient self-adaptive technique for modeling thermal problems with large variations in physical scales," *International Journal of Heat and Mass Transfer*, May. 2004.
- [60] W. Batty, C. E. Christoffersen, S. David, A. J. Panks, R. G. Johnson, C. M. Snowden and M. B. Steer, "Electrothermal CAD of power devices and circuits with fully physical time-dependent thermal modelling of complex 3-d systems," *IEEE Transactions on Component and Packaging Technologies, Part A: Packaging Technologies*, vol. 24, Issue 4, Dec. 2001, pp. 566-590 .
- [61] W. B. Batty, C. E. Christoffersen, S. David, A. J. Panks, R. G. Johnson, C. M. Snowden, and M. B. Steer, "Fully physical time-dependent compact thermal modeling of complex nonlinear 3-dimensional systems for device and circuit level electrothermal CAD," *Seventeenth IEEE Semiconductor Thermal Measurement and Management Symposium*, 2001, pp. 71-84
- [62] J. S. Brodsky, R. M. Fox, D. T. Zweidinger, and S. Veeraraghavan, "A physics-based, dynamic thermal impedance model for SOI MOSFETs," *IEEE Transactions on Electron Devices*, vol. 44, pp. 957-964, June 1997.
- [63] W. Veijola, L. Costa, and M. Valtonen, "An implementation of electrothermal component models in a general purpose circuit simulation programme," *THERMINIC '97*, Cannes, France, Sept. 21-23, 1997, pp. 96-100.
- [64] V. Rizzoli, A. Lipparini, A. Costanzo, and A. Frontini, "Three-dimensional computation of the thermal parameters of multi-gate power FETs," *European Microwave Conference*, vol. 23, 1993, pp. 698-700.
- [65] W. Batty, C. E. Christoffersen, S. David, A. J. Panks, R. G. Johnson, C. M. Snowden and M. B. Steer, "Predictive microwave device design by coupled electrothermal simulation based on a fully physical thermal model," *2000 8th IEEE International Symposium on High Performance Electron Devices for Microwave and Optoelectronic Applications, Glasgow UK*, November 2000, pp. 111-116.
- [66] W. Batty, C. E. Christoffersen, S. David, A. J. Panks, R. G. Johnson, C. M. Snowden and M. B. Steer, "Steady-state and transient electrothermal simulation of power

- devices and circuits based on a fully physical thermal model,” *THERMINIC 2000 Digest, Budapest*, September 2000.
- [67] S. David, W. Batty, A. J. Panks, R. G. Johnson and C. M. Snowden, “Thermal transients in microwave active devices and their influence on intermodulation distortion,” *IEEE Microwave Theory and Techniques Symposium Digest*, 2001, pp.431-434,
- [68] K. Lu, P. M. McIntosh, C. M. Snowden, and R. D. Pollard, “Low-frequency dispersion and its influence on the intermodulation performance of AlGaAs/GaAs HBT’s,” *IEEE Microwave Theory and Techniques Symposium Digest*, 1996, pp. 1373-1376,
- [69] Bo Wan, Emrah Acar, Sani Nassif and C. -J. Richard Shi, “Design-Adaptive Device Modeling in Model Compiler for Efficient and Accurate Circuit Simulation,” *Behavioral Modeling and Simulation Conference 2004*, October 2004.
- [70] V. Chaudhary, M. Francis, W. Zheng A. Mantooth, and L. Lemaitre, “Automatic Generation of Compact Semiconductor Device Models using Paragon and ADMS,” *Behavioral Modeling and Simulation Conference 2004*, October 2004.
- [71] Geoffrey Coram, “How to (and How Not to) Write a Compact Model in Verilog-A,” *Behavioral Modeling and Simulation Conference 2004*, October 2004.
- [72] B. Troyanovsky, P. O’Halloran and M. Mierzwinski, “Analog RF Model Development with Verilog-A,” *2005 IEEE Radio Frequency Integrated Circuit Symposium Digest*, pp. 287-290, 2005.
- [73] K. Kundert, “Automatic Model Compilation - An Idea Whose Time Has Come,” *The Designers-Guide*, May 2002.
- [74] A. Griewank, D. Juedes and J. Utke, “Adol-C: A Package for the Automatic Differentiation of Algorithms Written in C/C++,” *ACM TOMS*, Vol. 22(2), pp. 131-167, June 1996.
- [75] Y. S. Touloukian et al, “Thermophysical properties of matter, The TPRC Data series,” *Thermophysical Properties Research Center, Purdue University*, vol. 10, IFI/Plenum, 1973.

- [76] S. J. Souri, K. Banerjee, A. Merhotra, and K. C. Saraswat, "Multiple Si layer ICs:motivation, performance, analysis, and design implications," *37th Design Automation Conference (DAC)*, Los Angeles, California, June 2000, pp 873-880.
- [77] K. Banerjee, S. J. Souri, P. Kapur, K. C. Saraswat, "3-D ICs: A novel chip design for improving deep submicron interconnect performance and systems-on-chip integration," *IEEE Proceedings, Special Issue on Interconnects*, May 2001, pp. 602-633.
- [78] M. B. Kleiner, S. A. Kühn, Werner Weber, "Thermal conductivity measurements of this silicon dioxide films in integrated circuits," *IEEE Transactions on electron devices*, vol. 43, No. 9, September 1996, pp.1602-1609
- [79] F. P. Incropera and D. P. DeWitt, "Fundamentals of Heat and Mass Transfer," Fourth Edition, John Wiley and Sons
- [80] S. Winograd, "On computing the discrete fourier transform. Mathematics of Computation," 32(141):175-199, 1978.
- [81] Massachusetts Institute of Technology Lincoln Labs <http://www.ll.mit.edu>.
- [82] M.E.Phair, Free Floating Point Madness arithmetic units, available at <http://www.hmc.edu/chips/index.html>.
- [83] Cadence First Encounter Physical Design Software available at, http://www.cadence.com/products/digital_ic/first_encounter
- [84] G. Karypis and V. Kumar, The METIS Serial Graph Partitioning Tool, available at <http://www-users.cs.umn.edu/karypis/metis>.
- [85] Silicon Integration Initiative OpenAccess data exchange format among IC design tools available at <http://www.si2.org/openaccess/index.html>.
- [86] G. G. Shahidi, "SOI Technology for the GHz era," *IBM J. Research and Development* Vol 46, No. 2/3, pp.121-131, 2002.
- [87] H. I. Liu, J. A. Burns, C. L. Keast and P. W. Wyatt, "Thin silicide development for fully-depleted SOI CMOS technology," *IEEE Trans. Electron Devices*, vol. 45, pp. 1099-1104, May 1998.

- [88] C. L. Chen, S. J. Spector, R. M. Blumgold, R. A. Neidhard, W. T. Beard, D.-R. Yost, J. M. Knecht, C. K. Chen, M. Fritze, C. L. Cerny, J. A. Cook, P. W. Wyatt, C. L. Keast, "High-Performance Fully Depleted SOI RF CMOS," *IEEE Transactions on Electron Devices Letters*, vol. 23, No. 1, January 2002, pp. 52-54
- [89] Sang Lam, Hui Wan, Pin Su, Peter W. Wyatt, C. L. Chen, Ali M. Niknejad, Chenming Hu, P. K. Ko, Mansun Chan, "RF Characterization of Metal T-Gate Structure in Fully-Depleted SOI CMOS Technology," *IEEE Transactions on Electron Devices Letters*, vol. 24, No. 4, April 2003, pp. 251-253
- [90] Y. Taur, "CMOS Scaling into the Nanometer regime", *Proceedings IEEE*, Vol. 85, pp. 486-504, April 1997.
- [91] Pin Su, Samuel K. H. Fung, Peter W. Wyatt, Hui Wan, Mansun Chan, Ali M. Niknejad and Chenming Hu, "A Unified Model for Partial-Depletion and Full-Depletion SOI Circuit Designs: Using BSIMPD as a Foundation," *IEEE Custom Integrated Circuits Conference 2003*, September 2003, pp. 241-244.
- [92] V. Rizzoli, A. Lipparini, A. Costanzo, F. Mastri, C. Ceccetti, A. Neri and D. Masotti, "State-of-the-Art Harmonic-Balance Simulation of Forced Nonlinear Microwave Circuits by the Piecewise Technique," *IEEE Transactions on Microwave Theory and Techniques*, Vol. 40, No. 1, Jan 1992, pp. 12-28.
- [93] C. E. Christoffersen, U. A. Mughal and M. B. Steer, "Object oriented microwave circuit simulation," *International Journal of RF and Microwave Computer-Aided Engineering*, Vol. 10, Issue 3, 2000, pp. 164-182.
- [94] V. Szekely and K. Tarnay, "Accurate algorithm for temperature calculation of devices in nonlinear-circuit-analysis programs," *Electronic Letters*, vol. 8, pp. 470-472, Dec. 1972.
- [95] BSIMSOI user's manual: <http://www-device.eecs.berkeley.edu/~bsimsoi/>
- [96] L. T. Su, J. E. Chung, D. A. Antoniadis, K. E. Goodson and M. I. Flik, "Measurement and modeling of self-heating in SOI NMOSFET's," *IEEE Transactions on Electron Devices*, Vol. 41, No. 1, pp. 67-69, 1994.

- [97] Wei Jin, W. Liu, Samuel K. H. Fung, Philip C. H. Chan and Chenming Hu, "SOI thermal impedance extraction methodology and its significance for circuit simulation," *IEEE Transactions on Electron Devices*, Vol. 48, No. 4, April 2001, pp. 730-736
- [98] Hui Wan, Pin Su, Samuel K. H. Fung, Chang-Lee Chen, P. W. Wyatt, Ali M. Niknejad and Chenming Hu, "RF Modeling for FDSOI MOSFET and Self Heating Effect on RF parameter extraction," To be published.

Appendix

Appendix A

Thermal Macromodel

The input parameters used by the formulae of the thermal macromodel developed in Chapter 5 are given in Table A.1. Formulae used to calculate the RC network values are given below.

Calculation of cross-sectional areas from % density numbers:

$$A_{N-metal} = \frac{m\rho_N}{100} * l_y * (h_{above} + h_{below}) \quad (A.1)$$

$$A_{N-die} = \frac{100 - m\rho_N}{100} * l_y * (h_{above} + h_{below}) \quad (A.2)$$

$$A_{S-metal} = \frac{m\rho_S}{100} * l_x * (h_{above} + h_{below}) \quad (A.3)$$

$$A_{S-die} = \frac{100 - m\rho_S}{100} * l_x * (h_{above} + h_{below}) \quad (A.4)$$

Table A.1: Thermal macromodel Input Parameters.

$m\rho_d$	%metal density in direction d (N/S/E/W/top/bottom)
k_{md}	Thermal conductivity of metal in direction d (x;y;z)
k_{ild}	Thermal conductivity of active layer dielectric
k_{bulk}	Thermal conductivity of bulk material
l_d	Length of block in direction d (x;y)
h_{above}	Height above SOI island (in Z direction)
h_{below}	Height below SOI island (in Z direction)
d_{md}	Metal spacing in direction d (x;y)
ρ	Material density of the bulk material
c	Heat capacity of the bulk material

$$A_{E-metal} = \frac{m\rho_E}{100} * l_x * (h_{above} + h_{below}) \quad (A.5)$$

$$A_{E-die} = \frac{100 - m\rho_E}{100} * l_x * (h_{above} + h_{below}) \quad (A.6)$$

$$A_{W-metal} = \frac{m\rho_W}{100} * l_x * (h_{above} + h_{below}) \quad (A.7)$$

$$A_{W-die} = \frac{100 - m\rho_W}{100} * l_x * (h_{above} + h_{below}) \quad (A.8)$$

$$A_{top-metal} = \frac{m\rho_{top}}{100} * l_x * l_y \quad (A.9)$$

$$A_{top-die} = \frac{100 - m\rho_{top}}{100} * l_x * l_y \quad (A.10)$$

$$A_{bottom-metal} = \frac{m\rho_{bottom}}{100} * l_x * l_y \quad (A.11)$$

$$A_{bottom-die} = \frac{100 - m\rho_{bottom}}{100} * l_x * l_y \quad (A.12)$$

Calculation of metal and die resistances:

$$R_{N-metal} = \frac{l_x}{2 * k_{mx} * A_{N-metal}} \quad (A.13)$$

$$R_{N-die} = \frac{l_x}{2 * k_{bulk} * A_{N-die}} \quad (A.14)$$

$$R_{S-metal} = \frac{l_x}{2 * k_{mx} * A_{S-metal}} \quad (A.15)$$

$$R_{S-die} = \frac{l_x}{2 * k_{bulk} * A_{S-die}} \quad (A.16)$$

$$R_{E-metal} = \frac{l_y}{2 * k_{my} * A_{E-metal}} \quad (A.17)$$

$$R_{E-die} = \frac{l_y}{2 * k_{bulk} * A_{E-die}} \quad (A.18)$$

$$R_{W-metal} = \frac{l_y}{2 * k_{my} * A_{W-metal}} \quad (A.19)$$

$$R_{W-die} = \frac{l_y}{2 * k_{bulk} * A_{W-die}} \quad (A.20)$$

$$R_{top-metal} = \frac{h_{above}}{2 * k_{mz} * A_{top-metal}} \quad (A.21)$$

$$R_{top-die} = \frac{h_{above}}{2 * k_{bulk} * A_{top-die}} \quad (A.22)$$

$$R_{below-metal} = \frac{h_{below}}{2 * k_{mz} * A_{below-metal}} \quad (A.23)$$

$$R_{below-die} = \frac{h_{below}}{2 * k_{ild} * A_{below-die}} \quad (A.24)$$

Total Thermal Resistance: If the cross-sectional area of metal is zero, the resistance is the same as the die resistance. If not the resistance is calculated as the parallel combination of the metal and die resistances:

$$R_d = \frac{R_{d-metal} * R_{d-die}}{R_{d-metal} + R_{d-die}} \quad (A.25)$$

Effective Thermal Conductivities:

$$k_{effx} = \frac{l_x / (R_N + R_S)}{l_y * (h_{above} + h_{below})} \quad (A.26)$$

$$k_{effy} = \frac{l_y / (R_E + R_W)}{l_a * (h_{above} + h_{below})} \quad (A.27)$$

$$k_{effz} = \frac{(h_{above} + h_{below}) / (R_{top} + R_{bottom})}{l_x * l_y} \quad (A.28)$$

Thermal Capacitance:

$$C_{bulk} = \rho * c * l_x * l_y * h_{above} + h_{below} \quad (A.29)$$

Appendix B

This chapter includes the various *fREEDA*TM netlists and measurements used in this work.

B.1 Simple RC Network Netlist

The simple RC network netlist used to test accuracy of the new time step control technique, discussed in Section 3.5, is given below.

```

**simple RC network****
vsource:vdc 1 0 vdc=0
isource:iin 3 1 iac=0.005 f=0.5e6
res:r2 3 0 r=1e3
cap:c1 3 0 c=1e-9
.tran3 tstep=0.1u tstop=5u cm=1 im=1 gcomp=0 reltol=0.01 abstol=0.0001
.out plot term 3 vt in "rc2_p0001_be_trap.out"
.end

```

B.2 Netlist for the LP6836 pHEMT

The Filtronic Solid State, LP6836 pHEMT, was used to test the Curtice cubic mesfet model in *fREEDA*TM. The netlist for verifying the I/V curves is given below. The Curtice Cubic model parameters were extracted by Filtronic Solid State. This netlist is used to for the results in Section 3.6.

```

**** Test netlist for mesfet models ****
**Parameters for the device were extracted by Filtronic Solid State

```

```

.options f0 = 5.1e9
*Sweep drain bias
.dc sweep="vsource:vdrain" start=0. stop=6.0 step=.1
mesfetc:m2 2 3 4 a0 = .16662 a1 = .0819 a2 = -.0465 a3 = -.01646
+gama = 2.4235 t = 2.475e-12 beta = 0.04168 rds = 800 is =1.0e-14
+vbd = 15 nr = 1 cgs0 = .723e-12 cgd0 = .0197e-12
+vt0=-1.2 vbi=1.5 +eg=1.11 xti=3.0 vds0=9.6304
r:rd 8 3 r=5.068
r:rg 6 2 r=7.21
r:rs 4 0 r=3.695
*Gate bias
vsource:vbias 6 0 vdc = 0.5
*Drain bias
vsource:vdrain 8 0 vdc = 6.0
.out plot element "mesfetc:m2" 1 it in "mesfet_id.dc_pp5"
.end

```

B.3 Curtice Cubic Model Parameters for X-band GaAs MMIC

LNA pHEMTs

The X-band GaAs MMIC LNA pHEMTs used the MD1A process. The parameters for the Curtice Cubic Mesfet model used to model the pHEMTs in the X-band GaAs MMIC LNA are given in the Figure B.1. These parameters were extracted by Filtronic Solid State. Use default value for all other elements not listed.

B.4 Dynamic Range Test Netlist of the X-band GaAs MMIC

LNA

The netlist to test the dynamic range of the new time step control technique discussed in Section 3.6 is given below. The input voltage of the second tone at 11 GHz must be varied.

```

**Netlist to test dynamic range of the Xband MMIC LNA LMA 411
**Low noise phemt lna using 0.25um technology
**First amplifier is 300um (6x50um) thick and second is 400 um thick
**DC supply of 6 volts ** Litton process
**Spiral inductor modeled as regular inductor

```

Table B.1: TYPICAL CURTICE MODELS FOR 0.25 μm DHPHEMT WITH 1000Å NI-TRIDE (MD1A).

ELEMENT	DEVICE						UNITS
	2X50	4X50	6X50	8X50	10X50	12X50	
A0	0.02620	0.06154	0.09910	0.1321	0.1767	0.2106	A
A1	0.03782	0.06570	0.08541	0.1085	0.1478	0.1538	A/V
A2	-0.002560	-0.01109	-0.02030	-0.04804	-0.08028	-0.07631	A/V ²
A3	-0.007533	-0.006795	-0.01543	-0.03821	-0.06075	-0.05092	A/V ³
BETA	0.01576	0.03776	0.01865	0.03141	0.02432	0.02535	
VDS0	2.062	2.361	6.494	5.892	2.170	6.929	V
GAMA	1.644	1.472	0.8293	0.7946	0.6657	0.5884	
VT0	-1.2	-1.2	-1.2	-1.2	-1.2	-1.2	V
CGS0	157.2	325.6	528.2	695.2	858.5	973.1	fF
CGD0	1	2	3	4	5	6	fF
IS	1	2	3	4	5	6	pA
N	1.2	1.2	1.2	1.2	1.2	1.2	
T	1	1	1	1	1	1	pA
VBI	0.8	0.8	0.8	0.8	0.8	0.8	V
VBD	12	12	12	12	12	12	V
RG	2.50	1.25	0.83	0.63	0.50	0.40	OHM
RD	2.50	1.25	0.83	0.63	0.50	0.40	OHM
RS	1	0.50	0.33	0.25	0.20	0.17	OHM
LG	20	10	7	16	13	10	pH
LD	0	0	0	11	9	7	pH
LS	11	11	11	11	11	11	pH
CDS	20	40	60	80	100	120	fF
CDSD	0.01	0.01	0.01	0.01	0.01	0.01	uF
RDSD	2000	1000	666	500	400	333	OHM
CGE	4	8	12	16	20	24	fF
CDE	5	10	15	20	25	30	fF
CGDE	10	20	30	40	50	60	fF

```

.options f0=10e9

*transmission lines models
.model m_line1 tlinp4 (z0mag = 95.7
k=7.55 fscale=10e9 alpha=773 nsect=5 fopt=10e9 tand=0.006)
.model m_line2 tlinp4 (z0mag= 81.9 k=7.73 fscale=10e9 alpha=78
nsect=5 fopt=10e9 tand=0.006)
.model m_line3 tlinp4 (z0mag = 76.2 k=7.82 fscale=10e9 alpha= 156
nsect=5 fopt=10e9 tand=0.006)

c1 2 3 6e-12
tlinp4:t1 3 0 0 0 model="m_line1" length = 1194u
tlinp4:t2 3 0 4 0 model="m_line2" length = 183u

*Stage 1 pHEMT
mesfetc:m1 42 51 62 A0=0.09910 A1=0.08541
A2=-0.02030 A3=-0.01543
+BETA=0.01865 GAMA=0.8293
+VDS0=6.494 VTO=-1.2 VBI=0.8 CGD0=3f CGS0=528.2f IS=3e-12
+NR=1.2 T=1e-12 vbd=12
res:rg1 41 42 r=0.83
res:rd1 5 51 r=0.83
res:rs1 61 62 r=0.33
l:lg1 4 41 l=7e-12
l:ls1 6 61 l=11e-12
tlinp4:t3 6 0 8 0 model="m_line2" length=391u
tlinp4:t4 6 0 7 0 model="m_line2" length=401u
c:c_via4 7 0 c=17e-12
res:r_via4 7 0 r=6
c:c_via3 8 0 c=17e-12
tlinp4:t5 5 0 9 0 model="m_line2" length=102u
tlinp4:t6 9 0 10 0 model="m_line1" length=368u
res:r1 10 11 r=10.53
res:r2 11 12 r = 24.93
c:c_s6 11 0 c=17e-12
tlinp4:t7 9 0 13 0 model="m_line2" length=33u
c:c2 13 14 c=2e-12
tlinp4:t8 14 0 15 0 model="m_line1" length=705u
tlinp4:t9 14 0 0 0 model="m_line2" length=419u
tlinp4:t10 14 0 17 0 model="m_line2" length=58u

*Stage 2 pHEMT
mesfetc:m2 172 192 182

```

```

+A0=0.1321 A1=0.1085 A2=-0.04804 A3=-0.03821
+BETA=0.03141 GAMA=0.7946 VDS0=5.892 VTO=-1.2 VBI=1.5
+CGD0=4e-15 CGS0=695.2f IS=4e-12 N=1.2 T=1e-12 vbd=12
res:rg2 171 172 r=0.63
res:rd2 191 192 r=0.63
res:rs2 181 182 r=0.25
l:lg2 17 171 l=16e-12
l:ld2 19 191 l=11e-12
l:ls2 18 181 l=11e-12
c:c_via8 18 0 c=17p
res:r_via8 18 0 r=5
tlinp4:t11 19 0 20 0 model="m_line1" length=138u
c:cfb 20 21 c=4.28e-12
res:rfb 21 22 r=237.4

*Feedback Spiral Inductor
l:lfb 22 15 l=1.268n int_res=9.55
tlinp4:t12 19 0 23 0 model="m_line1" length=313u

*RF Choke Spiral Inductor
l:lp 23 24 l=1.268n int_res=9.55
res:rpad 24 29 r=24
vsource:v2 29 0 vdc=6
c:c_via12 24 0 c=17e-12
tlinp4:t13 19 0 25 0 model="m_line3" length=229u
c:cload 25 26 c=6e-12
res:r50 26 0 r=50
vsource:vin 2 211 f=10e9 vac=0.1 phase=-90
vsource:vin2 211 0 f=11e9 vac=0.000001 phase=-90
vsource:v1 12 0 vdc=6
.tran3 tstep=3ps tstop=29.6ns out_steps=400 cm=0 reltol=0.001 im=1
.out plot term 26 vt in "mmic.out"
.out plot term 2 vt in "mmic.in"
.out plot element "mesfetc:m2" 1 it in "m2.di"
.out plot element "mesfetc:m1" 1 it in "m1.di"
.end

```

B.5 Test Netlist for X-band GaAs MMIC LNA with Harmonic Balance Analysis.

The test netlist for a single tone harmonic balance simulation of the X-band GaAs MMIC LNA discussed in Section 3.6.1 is given below.

```

**HB netlist of the Xband MMIC LNA (LMA 411)
**Low noise pHEMT lna using 0.25um technology
**First amplifier is 300um (6x50um) thick and second is 400 um thick
**DC supply of 6 volts ** Litton process
**Spiral inductor modeled as regular inductor

.options f0=10e9

*transmission lines models
.model m_line1 tlinp4 (z0mag = 95.7
k=7.55 fscale=10e9 alpha=773 nsect=5 fopt=10e9 tand=0.006)
.model m_line2 tlinp4 (z0mag= 81.9 k=7.73 fscale=10e9 alpha=78
nsect=5 fopt=10e9 tand=0.006)
.model m_line3 tlinp4 (z0mag = 76.2 k=7.82 fscale=10e9 alpha= 156
nsect=5 fopt=10e9 tand=0.006)

c1 2 3 6e-12
tlinp4:t1 3 0 0 0 model="m_line1" length = 1194u
tlinp4:t2 3 0 4 0 model="m_line2" length = 183u

*Stage 1 pHEMT
mesfetc:m1 42 51 62 A0=0.09910 A1=0.08541
A2=-0.02030 A3=-0.01543
+BETA=0.01865 GAMA=0.8293
+VDS0=6.494 VTO=-1.2 VBI=0.8 CGD0=3f CGS0=528.2f IS=3e-12
+NR=1.2 T=1e-12 vbd=12
res:rg1 41 42 r=0.83
res:rd1 5 51 r=0.83
res:rs1 61 62 r=0.33
l:lg1 4 41 l=7e-12
l:ls1 6 61 l=11e-12
tlinp4:t3 6 0 8 0 model="m_line2" length=391u
tlinp4:t4 6 0 7 0 model="m_line2" length=401u
c:c_via4 7 0 c=17e-12
res:r_via4 7 0 r=6
c:c_via3 8 0 c=17e-12
tlinp4:t5 5 0 9 0 model="m_line2" length=102u

```

```

tlinp4:t6 9 0 10 0 model="m_line1" length=368u
res:r1 10 11 r=10.53
res:r2 11 12 r = 24.93
c:c_s6 11 0 c=17e-12
tlinp4:t7 9 0 13 0 model="m_line2" length=33u
c:c2 13 14 c=2e-12
tlinp4:t8 14 0 15 0 model="m_line1" length=705u
tlinp4:t9 14 0 0 0 model="m_line2" length=419u
tlinp4:t10 14 0 17 0 model="m_line2" length=58u

```

*Stage 2 pHEMT

```

mesfetm2:m2 172 192 182
+A0=0.1321 A1=0.1085 A2=-0.04804 A3=-0.03821
+BETA=0.03141 GAMA=0.7946 VDS0=5.892 VTO=-1.2 VBI=1.5
+CGD0=4e-15 CGS0=695.2f IS=4e-12 N=1.2 T=1e-12 vbd=12
res:rg2 171 172 r=0.63
res:rd2 191 192 r=0.63
res:rs2 181 182 r=0.25
l:lg2 17 171 l=16e-12
l:ld2 19 191 l=11e-12
l:ls2 18 181 l=11e-12
c:c_via8 18 0 c=17p
res:r_via8 18 0 r=5
tlinp4:t11 19 0 20 0 model="m_line1" length=138u
c:cfb 20 21 c=4.28e-12
res:rfb 21 22 r=237.4

```

*Feedback Spiral Inductor

```

l:lfb 22 15 l=1.268n int_res=9.55
tlinp4:t12 19 0 23 0 model="m_line1" length=313u

```

*RF Choke Spiral Inductor

```

l:lp 23 24 l=1.268n int_res=9.55
res:rpad 24 29 r=24
vsource:v2 29 0 vdc=6
c:c_via12 24 0 c=17e-12
tlinp4:t13 19 0 25 0 model="m_line3" length=229u
c:cload 25 26 c=6e-12
res:r50 26 0 r=50
vsource:vin 2 211 f=10e9 vac=0.1 phase=-90
vsource:vin2 211 0 f=11e9 vac=0.000001 phase=-90
vsource:v1 12 0 vdc=6
.svhb n_freqs = 20 fundamental=10e9 steps=20 deriv=1
.out plot term 26 vf invfft 10 repeat in "mmic_hb.out"

```

.end

B.6 Dynamic Range Test Measurements of the MMIC LNA

Measurements used to in the dynamic range test of the new time step control technique discussed in Section 3.6 are given below. These measurements were done on the bare die of the MMIC LNA with DC and RF probes. A DC supply of 6V was supplied and the measurements were done at 50% Idss. Total current consumed was 96 mA.

Table B.2: Measurements used in dynamic range test of the new time step control technique. Input power (P_{in}) at 11 GHz is varied from -10 dBm to -80 dBm. Input power (P_{in}) at 10 GHz is kept constant at -10 dBm.

P_{in} (dBm)	9 GHz	P_{out} (dBm) 10 GHz	11 GHz	12 GHz
-10	-29	3.33	3.33	-30.67
-11	-30.33	3.33	2.33	-32.83
-12	-31.5	3.33	1.33	-35
-13	-32.67	3.33	0.33	-37
-14	-33.67	3.33	-0.5	-39
-15	-35	3.33	-1.5	-41
-16	-36	3.33	-2.5	-43.17
-17	-37	3.33	-3.5	-45.17
-18	-38.17	3.33	-4.5	-47.17
-19	-39.17	3.33	-5.5	-49.17
-20	-40.33	3.33	-6.5	-51.33
-21	-41.33	3.33	-7.5	-53.33
-22	-42.33	3.33	-8.33	-55.17
-23	-43.17	3.33	-9.33	-57.17
-24	-44.17	3.33	-10.33	-59.17
-25	-45.17	3.33	-11.33	-61.33
-26	-46.33	3.33	-12.5	-63.5
-27	-47.33	3.33	-13.5	-65.5
-28	-48.33	3.33	-14.33	-67.33
-29	-49.33	3.33	-15.33	-69.33
-30	-50.33	3.33	-16.33	-71.33
-31	-51.33	3.33	-17.33	-73.33
-32	-52.33	3.33	-18.33	-75.67
-33	-53.5	3.33	-19.5	-77.5
-34	-54.5	3.33	-20.5	-79.5
-35	-55.5	3.33	-21.5	-81.67
-36	-56.5	3.33	-22.5	-83.67
-37	-57.5	3.33	-23.5	-85.33
-38	-58.5	3.33	-24.5	-87.67
-39	-59.5	3.33	-25.5	-89.83
-40	-60.67	3.33	-26.5	-91.5

Table B.2 (continued)

Pin (dBm)	Pout (dBm)			
	9 GHz	10 GHz	11 GHz	12 GHz
-41	-61.67	3.33	-27.5	-93.33
-42	-62.67	3.33	-28.5	-95
-43	-63.5	3.33	-29.5	-98
-44	-64.5	3.33	-30.5	-99.83
-45	-65.5	3.33	-31.5	-105.8
-46	-66.5	3.33	-32.33	-103.6
-47	-67.5	3.33	-33.5	-103.3
-48	-68.67	3.33	-34.5	-105.6
-49	-69.5	3.33	-35.5	-109.5
-50	-70.67	3.33	-36.5	-112.6
-51	-71.5	3.33	-37.5	-113.6
-52	-72.5	3.33	-38.67	-112
-53	-73.5	3.33	-39.5	-119.3
-54	-74.67	3.33	-40.67	-111.6
-55	-75.5	3.33	-41.67	-109.8
-56	-76.67	3.33	-42.67	-112.6
-57	-77.67	3.33	-43.67	-117.3
-58	-78.5	3.33	-44.67	-115.5
-59	-80	3.33	-45.67	-130
-60	-80.83	3.33	-46.67	-110.5
-61	-81.5	3.33	-47.67	-114.6
-62	-82.67	3.33	-49	-121.1
-63	-84.33	3.33	-50.17	-116
-64	-85.33	3.33	-51.17	-113.3
-65	-85.5	3.33	-51.67	-109.6
-66	-87.17	3.33	-52.67	-117
-67	-87.33	3.33	-53.67	-111.8
-68	-88.67	3.33	-54.67	-113.1
-69	-90.17	3.33	-55.67	-112
-70	-90.5	3.33	-56.67	-110.6
-71	-91.5	3.33	-57.67	-114.6
-72	-93.67	3.33	-58.67	-112.5
-73	-92.83	3.33	-59.67	-112.3
-74	-95.33	3.33	-60.67	-115.3
-75	-95.33	3.33	-61.83	-115.1
-76	-96.5	3.33	-62.67	-110.6
-77	-97.17	3.33	-63.5	-118.3
-78	-98.83	3.33	-64.83	-117.3
-79	-97.83	3.33	-65.67	-111.1
-80	-98.83	3.33	-66.67	-115.5

Measured Losses Through All Components in the Dynamic Range Test Measurements:

The total measured loss at each frequency is added to the respective measured output power level in Table B.2.

At 9 GHz:

S11 of input Probe : 0.416dB
 S22 of output probe: 0.604 dB
 S21 of thru line : 0.639 dB
 Cable loss: 2.765 dB
 Total o/p loss: $0.604 + 0.639/2 + 2.765 = 3.6885$ dB
 Total i/p loss: $0.416 + 0.639/2 = 0.7355$ dB
 Total loss at 9 GHz = $3.6885 - 0.7355 = 2.953$ dB

At 10 GHz:

S11 of input Probe : 0.5164 dB
 S22 of output probe : 0.576 dB
 S21 of thru line : 0.764 dB
 Cable loss: 3.059 dB
 Total o/p loss: $0.576 + 0.764/2 + 3.059 = 4.017$ dB
 Total i/p loss: $0.5164 + 0.764/2 = 0.8984$ dB
 Total loss at 10 GHz= $4.017 - 0.8984 = 3.1186$ dB

At 11 GHz:

S11 of input Probe : 0.5dB
 S22 of output probe : 0.4524 dB
 S21 of thru line : 0.8352 dB
 Cable loss: 3.704 dB
 Total o/p loss: $0.4524 + 0.8352/2 + 3.704 = 3.91$ dB
 Total i/p loss: $0.5 + 0.8352/2 = 0.917$ dB
 Total loss at 11 GHz= $3.91 - 0.9176 = 3.0$ dB

At 12 GHz:

S11 of input Probe : 1.085 dB
 S22 of output probe : 1.317 dB
 S21 of thru line : 0.854 dB
 Cable loss: 4.1321 dB
 Total o/p loss: $1.3177 + 0.854/2 + 4.1321 = 5.876$ dB
 Total i/p loss: $1.085 + 0.854/2 = 1.512$ dB
 Total loss at 12 GHz= $5.876 - 1.512 = 4.364$ dB

B.7 Netlist To Test The Thermal Nonlinearity In The Thermal Compact Model

The netlist used to test the effects of nonlinearity in the thermal conductivity considered in the Thermal Compact Model of Section 4.5 is given below. With the appropriate material parameters, this netlist can be used to see the effects of thermal nonlinearity in GaAs, Si and SiO₂.

```

**Netlist used to see thermal nonlinearity with and without
**Kirchoffs transformation
.options deltat=1us nsteps=1000 temp=300.
.svtr tstop = 1000us n_freqs = 8 tstep = deltat deriv=0
**Input power source
isource:pin 1 0 idc=0.4
**with default GaAs values
**thermalmmic:test1 1 10 Ntimesteps=nsteps dt=deltat Tambient=temp
+time_d=1 nfingers = 1 kt=1
**For Silicon substrate
thermalmmic:test1 1 10 Ntimesteps=nsteps dt=deltat Tambient=temp
+time_d=1 ks = 142 b=1.342 + nfingers = 1 kt=1 rho = 2300 c = 710
**We need some resistor in parallel, otherwise the MNAM would
**be singular.
res:rdummy2 1 10 r=1e5
vsource:t1 10 0 vdc=temp
.out plot element "thermalmmic:test1" 0 it in "si.input.power"
.out plot element "thermalmmic:test1" 0 ut in
+"si_transformation.output.temperaturec"
.end

```

B.8 Netlist Of The X-band GaAs MMIC LNA Thermal Model

The netlist to verify the thermal compact model of the X-band GaAs MMIC LNA developed in Section 4.7 is given below. Thermal measurements of the MMIC were done on a mounted MMIC die with an external bias resistor of 20 Ohms. The mounting was done by Harris Corporation. This MMIC die was from a different process batch than the bare die used for the dynamic range measurements.

MMIC netlist for DC power calculation: The DC power of each of the heat dissipating elements in the MMIC LNA is calculated using the netlist below. This netlist includes the

external DC bias resistor.

```

**Netlist to calculate dc power of an Xband MMIC LNA (LMA 411)
**Low noise phemt lna using 0.25um technology
**First amplifier is 300um (6x50um) thick and second is 400 um thick
**DC supply of 6 volts
**GaAs substrate thickness 100 um, silicon nitride passivation:
**Standard thickness 1,000 ang
**Litton process
**spiral inductor modeled as regular inductor

```

```

.options f0=10e9
.model m_line1 tlinp4 (z0mag = 95.7 k=7.55 fscale=10e9 alpha=773
+nsect=20 fopt=10e9 tand=0.006)
.model m_line2 tlinp4 (z0mag= 81.9 k=7.73 fscale=10e9 alpha=78
+nsect=20 fopt=10e9 tand=0.006)
.model m_line3 tlinp4 (z0mag = 76.2 k=7.82 fscale=10e9 alpha= 156
+nsect=20 fopt=10e9 tand=0.006)
.ref 7000
c1 702 703 6e-12
tlinp4:t1 703 7000 7000 7000 model="m_line1" length = 1194u
tlinp4:t2 703 7000 704 7000 model="m_line2" length = 183u
.model hemt1 mesfetc (A0=0.09910 A1=0.08541 A2=-0.02030 A3=-0.01543
+BETA=0.01865 GAMA=0.8293 VDS0=6.494 VTO=-1.2
VBI=0.8 CGD0=3f CGS0=528.2f IS=3e-12 NR=1.2 T=1e-12 vbd=12
+area=1 tj=308)
.model hemt2 mesfetc (A0=0.1321 A1=0.1085 A2=-0.04804 A3=-0.03821
+BETA=0.03141 GAMA=1.946 VDS0=5.892 VTO=-1.2
VBI=0.8 CGD0=4e-15 CGS0=695.2f
+IS=4e-12 N=1.2 T=1e-12 vbd=12 area=1 tj=308)
mesfetc:m1 42 51 62 model="hemt1"
res:rg1 41 42 r=0.83
res:rd1 5 51 r=0.83
res:rs1 61 62 r=0.33
ind:lg1 704 41 l=7e-12
ind:ls1 706 61 l=11e-12
tlinp4:t3 706 7000 8 7000 model="m_line2" length=391u
tlinp4:t4 706 7000 7 7000 model="m_line2" length=401u
cap:c_via4 7 7000 c=17e-12
res:r_via4 7 7000 r=6
cap:c_via3 8 7000 c=17e-12
tlinp4:t5 5 7000 9 7000 model="m_line2" length=102u
tlinp4:t6 9 7000 10 7000 model="m_line1" length=368u
res:r1 10 11 r=10.53

```

```

res:rpad1 11 30 r = 61.53
cap:c_s6 11 7000 c=17e-12
tlinp4:t7 9 7000 13 7000 model="m_line2" length=33u
cap:c2 13 14 c=2e-12
tlinp4:t8 14 7000 15 7000 model="m_line1" length=705u
tlinp4:t9 14 7000 7000 7000 model="m_line2" length=419u
tlinp4:t10 14 7000 17 7000 model="m_line2" length=58u
mesfetc:m2 172 192 182 model="hemt2"
res:rg2 171 172 r=0.63
res:rd2 191 192 r=0.63
res:rs2 181 182 r=0.25
ind:lg2 17 171 l=16e-12
ind:ld2 19 191 l=11e-12
ind:ls2 18 181 l=11e-12
cap:c_via8 18 7000 c=17p
res:r_via8 18 7000 r=11
tlinp4:t11 19 7000 20 7000 model="m_line1" length=138u
cap:cfb 20 21 c=4.28e-12
res:rfb 21 22 r=237.4
ind:lfb 22 15 l=1.268n int_res=0.55
tlinp4:t12 19 7000 23 7000 model="m_line1" length=313u
ind:lp 23 24 l=1.268n int_res=0.55
res:rpad2 24 30 r=24.93

*External DC bias resistor
res:rdc 30 31 r=20
vsource:v2 31 7000 vdc=6
cap:c_via12 24 7000 c=17e-12
tlinp4:t13 19 7000 25 7000 model="m_line3" length=229u
cap:cload 25 26 c=6e-12
res:r50 26 7000 r=50
vsource:vin 702 7000 f=10e9 vac=0.00001 phase=-90
.dc
.out plot term 192 vt in "m2.d"
.out plot term 62 vt in "m1.s"
.out plot element "mesfetc:m2" 1 it in "m2.di"
.out plot term 51 vt in "m1.d"
.out plot term 182 vt in "m2.s"
.out plot element "mesfetc:m1" 1 it in "m1.di"
.end

```

X-band GaAs MMIC LNA netlist with the thermal compact models: The test netlist with thermal compact models of the MMIC LNA is given below. The power of each of the heat dissipating elements in the MMIC is calculated using the previous netlist.

```
*Purely thermal turn-on transient for the Xband MMIC LNA LMA411
*with compact thermal models
.options deltat=0.02 nsteps=2 temp=308.
.svtr tstop = 0.04 n_freqs = 8 tstep = deltat deriv=0

* Input power source
*Total power consumption of each heating element
*isource:pin1 1 0 idc=0.03696
*isource:pin2 2 0 idc=0.120
*isource:pin3 3 0 idc=0.09
*isource:pin4 4 0 idc=0.08

*Heat source fingers of pHEMT1
isource:pin1 1 0 idc=0.00616
isource:pin2 2 0 idc=0.00616
isource:pin3 3 0 idc=0.00616
isource:pin4 4 0 idc=0.00616
isource:pin5 5 0 idc=0.00616
isource:pin6 6 0 idc=0.00616
*Heat source fingers of pHEMT2
isource:pin7 7 0 idc=0.015
isource:pin8 8 0 idc=0.015
isource:pin9 9 0 idc=0.015
isource:pin10 10 0 idc=0.015
isource:pin11 11 0 idc=0.015
isource:pin12 12 0 idc=0.015
isource:pin13 13 0 idc=0.015
isource:pin14 14 0 idc=0.015
*Heat source of the DC resistors
isource:pin15 15 0 idc=0.09
isource:pin16 16 0 idc=0.08
*Pixel elements
isource:pin17 17 0 idc=0.00
isource:pin18 18 0 idc=0.00
isource:pin19 19 0 idc=0.00

*Surface discretization of the GaAs die connected to zero power
*sources
isource:pin20 101 0 idc=0.00
isource:pin21 102 0 idc=0.00
isource:pin22 103 0 idc=0.00
isource:pin23 104 0 idc=0.00
isource:pin24 105 0 idc=0.00
isource:pin25 106 0 idc=0.00
```

```
isource:pin26 107 0 idc=0.00
isource:pin27 108 0 idc=0.00
isource:pin28 109 0 idc=0.00
isource:pin29 110 0 idc=0.00
isource:pin30 111 0 idc=0.00
isource:pin31 112 0 idc=0.00
isource:pin32 113 0 idc=0.00
isource:pin33 114 0 idc=0.00
isource:pin34 115 0 idc=0.00
isource:pin35 116 0 idc=0.00
isource:pin536 517 0 idc=0.0
isource:pin537 518 0 idc=0.0
isource:pin538 519 0 idc=0.0
isource:pin539 520 0 idc=0.0
isource:pin540 521 0 idc=0.0
isource:pin541 522 0 idc=0.0
isource:pin542 523 0 idc=0.0
isource:pin543 524 0 idc=0.0
isource:pin544 525 0 idc=0.0
```

*Surface discretization of metal via caps connected to zero power

*sources

```
isource:pin36 217 0 idc=0.0
isource:pin37 218 0 idc=0.0
isource:pin38 219 0 idc=0.0
isource:pin39 220 0 idc=0.0
isource:pin40 221 0 idc=0.0
isource:pin41 222 0 idc=0.0
isource:pin42 223 0 idc=0.0
isource:pin43 224 0 idc=0.0
isource:pin44 225 0 idc=0.0
isource:pin45 226 0 idc=0.0
isource:pin50 227 0 idc=0.00
isource:pin51 228 0 idc=0.00
isource:pin52 229 0 idc=0.00
isource:pin53 230 0 idc=0.00
isource:pin54 231 0 idc=0.00
isource:pin55 232 0 idc=0.00
isource:pin60 233 0 idc=0.00
isource:pin61 234 0 idc=0.00
isource:pin62 235 0 idc=0.00
isource:pin63 236 0 idc=0.00
isource:pin64 237 0 idc=0.00
isource:pin65 238 0 idc=0.00
```

```

isource:pin66 239 0 idc=0.00
isource:pin67 240 0 idc=0.00
isource:pin68 241 0 idc=0.00
isource:pin69 242 0 idc=0.00
isource:pin70 243 0 idc=0.00
isource:pin71 244 0 idc=0.00
isource:pin72 245 0 idc=0.00
isource:pin73 246 0 idc=0.00
isource:pin74 247 0 idc=0.00
isource:pin75 248 0 idc=0.00

```

*MMIC GaAs Die element

```

thermalnportnlmmic:test1 1 2 3 4 5 6 7 8 9 10 11 12 13 14 15 16 17 18 19
+101 102 103 104 105 106 107 108 109 110 111 112 113 114 115 116
+517 518 519 520 521 522 523 524 525
+117 118 119 120 121 122 123 124 125 126 127 128 129 130 131 132
+133 134 135 136 137 138 139 140 141 142 143 144 145 146 147 148
+201 202 203 204 205 206 207 208 209 210 211 212 213 214 215 216
+617 618 619 620 621 622 623 624 625
+1002
+Ntimesteps=nsteps dt=deltat Tambient=temp time_d=1 msubstrate=5 read_input=0
+filename="Die_Rth_elements_19Devices.dat"
+l=1624e-6 w=1470e-6 d=100e-6 rho=5320 c=350 ks=46 xi=0 ndevices=19
+mmax=50 nmax=50 ppatch=4 ofilename = "Die_temperature5x5_extviacap.dat"
+b=1.22

```

*Metal of Via capacitor

```

thermalnportnlmmic:testv1cap 117 118 119 120 121 122 123 124 125 126 127 128
+129 130 131 132 217 218 219 220 221 222 223 224 225 226 227 228 229 230 231
+232 1002
+Ntimesteps=nsteps dt=deltat Tambient=temp time_d=1 msubstrate=4
+read_input=0 filename="ViaCap1_Rth_elements.dat"
+l=150e-6 w=282e-6 d=7e-6 c=128 rho=19320 ks=319 xi=0 ndevices=0
+mmax=5 nmax=5 ppatch=0 ofilename="ViaCap1_temperature5x5.dat"

```

*Metal of Via capacitor

```

thermalnportnlmmic:testv2cap 133 134 135 136 137 138 139 140 141 142 143 144
+145 146 147 148 233 234 235 236 237 238 239 240 241 242 243 244 245 246 247
+248 1002
+Ntimesteps=nsteps dt=deltat Tambient=temp time_d=1 msubstrate=4
+read_input=0 filename="ViaCap2_Rth_elements.dat"
+l=150e-6 w=282e-6 d=7e-6 c=128 rho=19320 ks=319 xi=0 ndevices=0
+mmax=5 nmax=5 ppatch=0 ofilename="ViaCap2_temperature=5x5.dat"

```

```

*Through Via
thermal2:testv1 517 617 1002 l=405e-6 w=367.5e-6 d=100e-6 xl=90e-6 xr=40e-6
+yu=263.5e-6 yd=213.5e-6
+ks=273 c=128 rho=19320 xi=0 b=0 read_input=0
+Ntimesteps=nsteps dt=deltat Tambient=temp time_d=1

*Through Via
thermal2:testv2 518 618 1002 l=405e-6 w=367.5e-6 d=100e-6 xl=90e-6 xr=40e-6
+yu=323.0e-6 yd=273.0e-6
+ks=273 c=128 rho=19320 xi=0 b=0 read_input=0
+Ntimesteps=nsteps dt=deltat Tambient=temp time_d=1

*DIE-MAT Epoxy layer
thermalnportnlmmic:test2 201 202 203 204 205 206 207 208 209 210 211 212
+213 214 215 216 617 618 619 620 621 622 623 624 625 301 302 303 304
+305 306 307 308 309 310 311 312 313 314 315 316 717 718 719 720 721
+722 723 724 725 1002
+Ntimesteps=nsteps dt=deltat Tambient=temp time_d=1 msubstrate=5
+read_input=0 filename="Epoxy_Rth_elements.dat"
+l=1624e-6 w=1470e-6 d=100e-6 rho=6700 c=500 ks=60 xi=0 ndevices=0
+mmax=50 nmax=50 ofilename="Epoxy_temperature5x5.dat"

*Kovar substrate model
thermalnportkovar:test3 301 302 303 304 305 306 307 308 309 310 311 312
+313 314 315 316 717 718 719 720 721 722 723 724 725 1002
+xl=2.4188e-2 xr=2.2564e-2 yU=1.3235e-2 yD=1.1765e-2 d=381e-6 ks=17.3
+rho=8359 c=502 time_d=1
+Ntimesteps=nsteps dt=deltat l=5.0e-2 w=2.5e-2
+Tambient=temp xi=0 narray=5 ndevices=1 read_input=0

* We need some resistor in parallel, otherwise the MNAM would
* be singular.
res:rdummy2 101 1002 r=1e5

*Heat Sink Temperature
vsource:t2 1002 0 vdc=temp

.out plot element "thermalnportnlmmic:test1" 0 it in "lnainput1.power"
*Temperature at finger of pHEMT1
.out plot element "thermalnportnlmmic:test1" 0 ut in
+"lnaoutput_mmic1_n19_wvia_wk.temperaturec"

.out plot element "thermalnportnlmmic:test1" 6 it in "lnainput2.power"

```

```

*Temperature at finger of pHEMT2
.out plot element "thermalnportnlmmic:test1" 6 ut in
+"lnaoutput_mmic2_n19_wvia_wk.temperaturec"

.out plot element "thermalnportnlmmic:test1" 14 it in "lnainput3.power"
*Temperature at DC pad resistor1
.out plot element "thermalnportnlmmic:test1" 14 ut in
+"lnaoutput_res1_n19_wvia_wk.temperaturec"

.out plot element "thermalnportnlmmic:test1" 15 it in "lnainput4.power"
*Temperature at DC pad resistor2
.out plot element "thermalnportnlmmic:test1" 15 ut in
+"lnaoutput_res2_n19_wvia_wk.temperaturec"

.out plot element "thermalnportnlmmic:test1" 16 it in "lnainput_t1.power"
*Temperature at pixel over pHEMT1
.out plot element "thermalnportnlmmic:test1" 16 ut in
+"lnaoutput_t1_n19_wvia_wk.temperaturec"

.out plot element "thermalnportnlmmic:test1" 17 it in "lnainput_t2.power"
*Temperature at pixel over pHEMT2
.out plot element "thermalnportnlmmic:test1" 17 ut in
+"lnaoutput_t2_n19_wvia_wk.temperaturec"

.out plot element "thermalnportnlmmic:test1" 18 it in "lnainput_p1.power"
*Temperature at pixel over DC Pad
.out plot element "thermalnportnlmmic:test1" 18 ut in
+"lnaoutput_p1_n19_wvia_wk.temperaturec"

.end

```

B.9 Netlist For The Thermal Macromodel of the X-band

GaAs MMIC LNA

The netlist for the coupled electrothermal RF simulation of the MMIC LNA using the thermal macromodel in Section 5.3 is given below.

```

*Netlist for the Xband MMIC LNA LMA411
*with thermal macromodel for an electrothermal coupled RF simulation
.options f0=10e9
.model m_line1 tlinp4 (z0mag = 95.7 k=7.55 fscale=10e9 alpha=773

```

```

+nsect=20 fopt=10e9 tand=0.006)
.model m_line2 tlinp4 (z0mag= 81.9 k=7.73 fscale=10e9 alpha=78
+nsect=20 fopt=10e9 tand=0.006)
.model m_line3 tlinp4 (z0mag = 76.2 k=7.82 fscale=10e9 alpha= 156
+nsect=20 fopt=10e9 tand=0.006)
.ref 7000
c1 702 703 6e-12
tlinp4:t1 703 7000 7000 7000 model="m_line1" length = 1194u
tlinp4:t2 703 7000 704 7000 model="m_line2" length = 183u
.model hemt1 mesfetct (A0=0.09910 A1=0.08541 A2=-0.02030 A3=-0.01543
+BETA=0.01865 GAMA=0.8293
+VDS0=6.494 VTO=-1.2 VBI=0.8 CGD0=3f CGS0=528.2f
+IS=3e-12 NR=1.2 T=1e-12 vbd=12 area=1)
.model hemt2 mesfetct ( A0=0.1321 A1=0.1085 A2=-0.04804 A3=-0.03821
+BETA=0.03141 GAMA=1.946 VDS0=5.892 VTO=-1.2 VBI=0.8
+CGD0=4e-15 CGS0=695.2f
+IS=4e-12 N=1.2 T=1e-12 vbd=12 area=1)
*Thermal Mesfet model
mesfetct:m1 42 51 62 3537 0 model="hemt1"
res:rg1 41 42 r=0.83
res:rd1 5 51 r=0.83
res:rs1 61 62 r=0.33
ind:lg1 704 41 l=7e-12
ind:ls1 706 61 l=11e-12
tlinp4:t3 706 7000 8 7000 model="m_line2" length=391u
tlinp4:t4 706 7000 7 7000 model="m_line2" length=401u
cap:c_via4 7 7000 c=17e-12
res:r_via4 7 7000 r=6
cap:c_via3 8 7000 c=17e-12
tlinp4:t5 5 7000 9 7000 model="m_line2" length=102u
tlinp4:t6 9 7000 10 7000 model="m_line1" length=368u
res:r1 10 11 r=10.53
*res:rpad1 11 30 r = 61.53
*Thermal DC pad resistor
rt:rpad1 11 30 3037 0 r0=61.53 tc1=0 pdr=1
cap:c_s6 11 7000 c=17e-12
tlinp4:t7 9 7000 13 7000 model="m_line2" length=33u
cap:c2 13 14 c=2e-12
tlinp4:t8 14 7000 15 7000 model="m_line1" length=705u
tlinp4:t9 14 7000 7000 7000 model="m_line2" length=419u
tlinp4:t10 14 7000 17 7000 model="m_line2" length=58u
*Thermal Mesfet model
mesfetct:m2 172 192 182 3667 0 model="hemt2"
res:rg2 171 172 r=0.63

```

```

res:rd2 191 192 r=0.63
res:rs2 181 182 r=0.25
ind:lg2 17 171 l=16e-12
ind:ld2 19 191 l=11e-12
ind:ls2 18 181 l=11e-12
cap:c_via8 18 7000 c=17p
res:r_via8 18 7000 r=11
tlinp4:t11 19 7000 20 7000 model="m_line1" length=138u
cap:cfb 20 21 c=4.28e-12
res:rfb 21 22 r=237.4
ind:lfb 22 15 l=1.268n int_res=0.55
tlinp4:t12 19 7000 23 7000 model="m_line1" length=313u
ind:lp 23 24 l=1.268n int_res=0.55
*res:rpad2 24 30 r=24.93
*Thermal DC pad resistor
rt:rpad2 24 30 3047 0 r0=24.93 tc1=0 pdr=1
*External DC bias resistor
res:rdc 30 31 r=20
vsource:v2 31 7000 vdc=6
cap:c_via12 24 7000 c=17e-12
tlinp4:t13 19 7000 25 7000 model="m_line3" length=229u
cap:cload 25 26 c=6e-12
res:r50 26 7000 r=50
vsource:vin 702 7000 f=10e9 vac=0.00001 phase=-90

ThermalBlock3:b300 3001 2 3003 4 3005 2005 3007 lx=162.4u ly=147.0u
+habove= 0.6u hbelow = 100u
+kmx= 146 kmy= 146 kmz= 170 kild = 46 kbulk = 46 rho = 5320 cbulk = 350
isource:ib300 3007 0 idc= 0

ThermalBlock3:b301 3011 2 3013 3003 3015 2015 3017 lx=162.4u ly=147.0u
+habove= 0.6u hbelow = 100u
+kmx= 146 kmy= 146 kmz= 170 kild = 46 kbulk = 46 rho = 5320 cbulk = 350
isource:ib301 3017 0 idc= 0

ThermalBlock3:b302 3021 2 3023 3013 3025 2025 3027 lx=162.4u ly=147.0u
+habove= 0.6u hbelow = 100u
+kmx= 146 kmy= 146 kmz= 170 kild = 46 kbulk = 46 rho = 5320 cbulk = 350
isource:ib302 3027 0 idc= 0

ThermalBlock3:b303 3031 2 3033 3023 3035 2035 3037 lx=162.4u ly=147.0u
+habove= 0.6u hbelow = 100u
+kmx= 146 kmy= 146 kmz= 170 kild = 46 kbulk = 46 rho = 5320 cbulk = 350
*isource:ib303 3037 0 iac= 0.00 idc=0.00 f=10e9 phase=-90

```

ThermalBlock3:b304 3041 2 3043 3033 3045 2045 3047 lx=162.4u ly=147.0u
+habove= 0.6u hbelow = 100u
+kmx= 146 kmy= 146 kmz= 170 kild = 46 kbulk = 46 rho = 5320 cbulk = 350
*isource:ib304 3047 0 idc= 0.00 iac=0.00 f=10e9 phase=-90

ThermalBlock3:b305 3051 2 3053 3043 3055 2055 3057 lx=162.4u ly=147.0u
+habove= 0.6u hbelow = 100u
+kmx= 146 kmy= 146 kmz= 170 kild = 46 kbulk = 46 rho = 5320 cbulk = 350
isource:ib305 3057 0 idc= 0

ThermalBlock3:b306 3061 2 3063 3053 3065 2065 3067 lx=162.4u ly=147.0u
+habove= 0.6u hbelow = 100u
+kmx= 146 kmy= 146 kmz= 170 kild = 46 kbulk = 46 rho = 5320 cbulk = 350
isource:ib306 3067 0 idc= 0

ThermalBlock3:b307 3071 2 3073 3063 3075 2075 3077 lx=162.4u ly=147.0u
+habove= 0.6u hbelow = 100u
+kmx= 146 kmy= 146 kmz= 170 kild = 46 kbulk = 46 rho = 5320 cbulk = 350
isource:ib307 3077 0 idc= 0

ThermalBlock3:b308 3081 2 3083 3073 3085 2085 3087 lx=162.4u ly=147.0u
+habove= 0.6u hbelow = 100u
+kmx= 146 kmy= 146 kmz= 170 kild = 46 kbulk = 46 rho = 5320 cbulk = 350
isource:ib308 3087 0 idc= 0

ThermalBlock3:b309 3091 2 3 3083 3095 2095 3097 lx=162.4u ly=147.0u
+habove= 0.6u hbelow = 100u
+kmx= 146 kmy= 146 kmz= 170 kild = 46 kbulk = 46 rho = 5320 cbulk = 350
isource:ib309 3097 0 idc= 0

ThermalBlock3:b310 3101 3001 3103 4 3105 2105 3107 lx=162.4u ly=147.0u
+habove= 0.6u hbelow = 100u
+kmx= 146 kmy= 146 kmz= 170 kild = 46 kbulk = 46 rho = 5320 cbulk = 350
isource:ib310 3107 0 idc= 0

ThermalBlock3:b311 3111 3011 3113 3103 3115 2115 3117 lx=162.4u ly=147.0u
+habove= 0.6u hbelow = 100u
+kmx= 146 kmy= 146 kmz= 170 kild = 46 kbulk = 46 rho = 5320 cbulk = 350
isource:ib311 3117 0 idc= 0

ThermalBlock3:b312 3121 3021 3123 3113 3125 2125 3127 lx=162.4u ly=147.0u
+habove= 0.6u hbelow = 100u
+kmx= 146 kmy= 146 kmz= 170 kild = 46 kbulk = 46 rho = 5320 cbulk = 350

isource:ib312 3127 0 idc= 0

ThermalBlock3:b313 3131 3031 3133 3123 3135 2135 3137 lx=162.4u ly=147.0u
 +habove= 0.6u hbelow = 100u
 +kmx= 146 kmy= 146 kmz= 170 kild = 46 kbulk = 46 rho = 5320 cbulk = 350
 isource:ib313 3137 0 idc= 0

ThermalBlock3:b314 3141 3041 3143 3133 3145 2145 3147 lx=162.4u ly=147.0u
 +habove= 0.6u hbelow = 100u
 +kmx= 146 kmy= 146 kmz= 170 kild = 46 kbulk = 46 rho = 5320 cbulk = 350
 isource:ib314 3147 0 idc= 0

ThermalBlock3:b315 3151 3051 3153 3143 3155 2155 3157 lx=162.4u ly=147.0u
 +habove= 0.6u hbelow = 100u
 +kmx= 146 kmy= 146 kmz= 170 kild = 46 kbulk = 46 rho = 5320 cbulk = 350
 isource:ib315 3157 0 idc= 0

ThermalBlock3:b316 3161 3061 3163 3153 3165 2165 3167 lx=162.4u ly=147.0u
 +habove= 0.6u hbelow = 100u
 +kmx= 146 kmy= 146 kmz= 170 kild = 46 kbulk = 46 rho = 5320 cbulk = 350
 isource:ib316 3167 0 idc= 0

ThermalBlock3:b317 3171 3071 3173 3163 3175 2175 3177 lx=162.4u ly=147.0u
 +habove= 0.6u hbelow = 100u
 +kmx= 146 kmy= 146 kmz= 170 kild = 46 kbulk = 46 rho = 5320 cbulk = 350
 isource:ib317 3177 0 idc= 0

ThermalBlock3:b318 3181 3081 3183 3173 3185 2185 3187 lx=162.4u ly=147.0u
 +habove= 0.6u hbelow = 100u
 +kmx= 146 kmy= 146 kmz= 170 kild = 46 kbulk = 46 rho = 5320 cbulk = 350
 isource:ib318 3187 0 idc= 0

ThermalBlock3:b319 3191 3091 3 3183 3195 2195 3197 lx=162.4u ly=147.0u
 +habove= 0.6u hbelow = 100u
 +kmx= 146 kmy= 146 kmz= 170 kild = 46 kbulk = 46 rho = 5320 cbulk = 350
 isource:ib319 3197 0 idc= 0

ThermalBlock3:b320 3201 3101 3203 4 3205 2205 3207 lx=162.4u ly=147.0u
 +habove= 0.6u hbelow = 100u
 +kmx= 146 kmy= 146 kmz= 170 kild = 46 kbulk = 46 rho = 5320 cbulk = 350
 isource:ib320 3207 0 idc= 0

ThermalBlock3:b321 3211 3111 3213 3203 3215 2215 3217 lx=162.4u ly=147.0u
 +habove= 0.6u hbelow = 100u

+kmx= 146 kmy= 146 kmz= 170 kild = 46 kbulk = 46 rho = 5320 cbulk = 350
 isource:ib321 3217 0 idc= 0

ThermalBlock3:b322 3221 3121 3223 3213 3225 2225 3227 lx=162.4u ly=147.0u
 +habove= 0.6u hbelow = 100u
 +kmx= 146 kmy= 146 kmz= 170 kild = 46 kbulk = 46 rho = 5320 cbulk = 350
 isource:ib322 3227 0 idc= 0

ThermalBlock3:b323 3231 3131 3233 3223 3235 2235 3237 lx=162.4u ly=147.0u
 +habove= 0.6u hbelow = 100u
 +kmx= 146 kmy= 146 kmz= 170 kild = 46 kbulk = 46 rho = 5320 cbulk = 350
 isource:ib323 3237 0 idc= 0

ThermalBlock3:b324 3241 3141 3243 3233 3245 2245 3247 lx=162.4u ly=147.0u
 +habove= 0.6u hbelow = 100u
 +kmx= 146 kmy= 146 kmz= 170 kild = 46 kbulk = 46 rho = 5320 cbulk = 350
 isource:ib324 3247 0 idc= 0

ThermalBlock3:b325 3251 3151 3253 3243 3255 2255 3257 lx=162.4u ly=147.0u
 +habove= 0.6u hbelow = 100u
 +kmx= 146 kmy= 146 kmz= 170 kild = 46 kbulk = 46 rho = 5320 cbulk = 350
 isource:ib325 3257 0 idc= 0

ThermalBlock3:b326 3261 3161 3263 3253 3265 2265 3267 lx=162.4u ly=147.0u
 +habove= 0.6u hbelow = 100u
 +kmx= 146 kmy= 146 kmz= 170 kild = 46 kbulk = 46 rho = 5320 cbulk = 350
 isource:ib326 3267 0 idc= 0

ThermalBlock3:b327 3271 3171 3273 3263 3275 2275 3277 lx=162.4u ly=147.0u
 +habove= 0.6u hbelow = 100u
 +kmx= 146 kmy= 146 kmz= 170 kild = 46 kbulk = 46 rho = 5320 cbulk = 350
 isource:ib327 3277 0 idc= 0

ThermalBlock3:b328 3281 3181 3283 3273 3285 2285 3287 lx=162.4u ly=147.0u
 +habove= 0.6u hbelow = 100u
 +kmx= 146 kmy= 146 kmz= 170 kild = 46 kbulk = 46 rho = 5320 cbulk = 350
 isource:ib328 3287 0 idc= 0

ThermalBlock3:b329 3291 3191 3 3283 3295 2295 3297 lx=162.4u ly=147.0u
 +habove= 0.6u hbelow = 100u
 +kmx= 146 kmy= 146 kmz= 170 kild = 46 kbulk = 46 rho = 5320 cbulk = 350
 isource:ib329 3297 0 idc= 00

ThermalBlock3:b330 3301 3201 3303 4 3305 2305 3307 lx=162.4u ly=147.0u

+habove= 0.6u hbelow = 100u
+kmx= 146 kmy= 146 kmz= 170 kild = 46 kbulk = 46 rho = 5320 cbulk = 350
isource:ib330 3307 0 idc= 0.0

ThermalBlock3:b331 3311 3211 3313 3303 3315 2315 3317 lx=162.4u ly=147.0u
+habove= 0.6u hbelow = 100u
+kmx= 146 kmy= 146 kmz= 170 kild = 46 kbulk = 46 rho = 5320 cbulk = 350
isource:ib331 3317 0 idc= 0.0

ThermalBlock3:b332 3321 3221 3323 3313 3325 2325 3327 lx=162.4u ly=147.0u
+habove= 0.6u hbelow = 100u
+kmx= 146 kmy= 146 kmz= 170 kild = 46 kbulk = 46 rho = 5320 cbulk = 350
isource:ib332 3327 0 idc= 0.0

ThermalBlock3:b333 3331 3231 3333 3323 3335 2335 3337 lx=162.4u ly=147.0u
+habove= 0.6u hbelow = 100u
+kmx= 146 kmy= 146 kmz= 170 kild = 46 kbulk = 46 rho = 5320 cbulk = 350
isource:ib333 3337 0 idc= 0.0

ThermalBlock3:b334 3341 3241 3343 3333 3345 2345 3347 lx=162.4u ly=147.0u
+habove= 0.6u hbelow = 100u
+kmx= 146 kmy= 146 kmz= 170 kild = 46 kbulk = 46 rho = 5320 cbulk = 350
isource:ib334 3347 0 idc= 0.0

ThermalBlock3:b335 3351 3251 3353 3343 3355 2355 3357 lx=162.4u ly=147.0u
+habove= 0.6u hbelow = 100u
+kmx= 146 kmy= 146 kmz= 170 kild = 46 kbulk = 46 rho = 5320 cbulk = 350
isource:ib335 3357 0 idc= 0.0

ThermalBlock3:b336 3361 3261 3363 3353 3365 2365 3367 lx=162.4u ly=147.0u
+habove= 0.6u hbelow = 100u
+kmx= 146 kmy= 146 kmz= 170 kild = 46 kbulk = 46 rho = 5320 cbulk = 350
isource:ib336 3367 0 idc= 0.0

ThermalBlock3:b337 3371 3271 3373 3363 3375 2375 3377 lx=162.4u ly=147.0u
+habove= 0.6u hbelow = 100u
+kmx= 146 kmy= 146 kmz= 170 kild = 46 kbulk = 46 rho = 5320 cbulk = 350
isource:ib337 3377 0 idc= 0.0

ThermalBlock3:b338 3381 3281 3383 3373 3385 2385 3387 lx=162.4u ly=147.0u
+habove= 0.6u hbelow = 100u
+kmx= 146 kmy= 146 kmz= 170 kild = 46 kbulk = 46 rho = 5320 cbulk = 350
isource:ib338 3387 0 idc= 0.0

ThermalBlock3:b339 3391 3291 3 3383 3395 2395 3397 lx=162.4u ly=147.0u
+habove= 0.6u hbelow = 100u
+kmx= 146 kmy= 146 kmz= 170 kild = 46 kbulk = 46 rho = 5320 cbulk = 350
isource:ib339 3397 0 idc= 0.0

ThermalBlock3:b340 3401 3301 3403 4 3405 2405 3407 lx=162.4u ly=147.0u
+habove= 0.6u hbelow = 100u
+kmx= 146 kmy= 146 kmz= 170 kild = 46 kbulk = 46 rho = 5320 cbulk = 350
isource:ib340 3407 0 idc= 0.0

ThermalBlock3:b341 3411 3311 3413 3403 3415 2415 3417 lx=162.4u ly=147.0u
+habove= 0.6u hbelow = 100u
+kmx= 146 kmy= 146 kmz= 170 kild = 46 kbulk = 46 rho = 5320 cbulk = 350
isource:ib341 3417 0 idc= 0.0

ThermalBlock3:b342 3421 3321 3423 3413 3425 2425 3427 lx=162.4u ly=147.0u
+habove= 0.6u hbelow = 100u
+kmx= 146 kmy= 146 kmz= 170 kild = 46 kbulk = 46 rho = 5320 cbulk = 350
isource:ib342 3427 0 idc= 0.0

ThermalBlock3:b343 3431 3331 3433 3423 3435 2435 3437 lx=162.4u ly=147.0u
+habove= 0.6u hbelow = 100u
+kmx= 146 kmy= 146 kmz= 170 kild = 46 kbulk = 46 rho = 5320 cbulk = 350
isource:ib343 3437 0 idc= 0.0

ThermalBlock3:b344 3441 3341 3443 3433 3445 2445 3447 lx=162.4u ly=147.0u
+habove= 0.6u hbelow = 100u
+kmx= 146 kmy= 146 kmz= 170 kild = 46 kbulk = 46 rho = 5320 cbulk = 350
isource:ib344 3447 0 idc= 0.0

ThermalBlock3:b345 3451 3351 3453 3443 3455 2455 3457 lx=162.4u ly=147.0u
+habove= 0.6u hbelow = 100u
+kmx= 146 kmy= 146 kmz= 170 kild = 46 kbulk = 46 rho = 5320 cbulk = 350
isource:ib345 3457 0 idc= 0.0

ThermalBlock3:b346 3461 3361 3463 3453 3465 2465 3467 lx=162.4u ly=147.0u
+habove= 0.6u hbelow = 100u
+kmx= 146 kmy= 146 kmz= 170 kild = 46 kbulk = 46 rho = 5320 cbulk = 350
isource:ib346 3467 0 idc= 0.0

ThermalBlock3:b347 3471 3371 3473 3463 3475 2475 3477 lx=162.4u ly=147.0u
+habove= 0.6u hbelow = 100u
+kmx= 146 kmy= 146 kmz= 170 kild = 46 kbulk = 46 rho = 5320 cbulk = 350
isource:ib347 3477 0 idc= 0.0

ThermalBlock3:b348 3481 3381 3483 3473 3485 2485 3487 lx=162.4u ly=147.0u
 +habove= 0.6u hbelow = 100u
 +kmx= 146 kmy= 146 kmz= 170 kild = 46 kbulk = 46 rho = 5320 cbulk = 350
 isource:ib348 3487 0 idc= 0.0

ThermalBlock3:b349 3491 3391 3 3483 3495 2495 3497 lx=162.4u ly=147.0u
 +habove= 0.6u hbelow = 100u
 +kmx= 146 kmy= 146 kmz= 170 kild = 46 kbulk = 46 rho = 5320 cbulk = 350
 isource:ib349 3497 0 idc= 0.0

ThermalBlock3:b350 3501 3401 3503 4 3505 2505 3507 lx=162.4u ly=147.0u
 +habove= 0.6u hbelow = 100u
 +kmx= 146 kmy= 146 kmz= 170 kild = 46 kbulk = 46 rho = 5320 cbulk = 350
 isource:ib350 3507 0 idc= 0.0

ThermalBlock3:b351 3511 3411 3513 3503 3515 2515 3517 lx=162.4u ly=147.0u
 +habove= 0.6u hbelow = 100u
 +kmx= 146 kmy= 146 kmz= 170 kild = 46 kbulk = 46 rho = 5320 cbulk = 350
 isource:ib351 3517 0 idc= 0.0

ThermalBlock3:b352 3521 3421 3523 3513 3525 2525 3527 lx=162.4u ly=147.0u
 +habove= 0.6u hbelow = 100u
 +kmx= 146 kmy= 146 kmz= 170 kild = 46 kbulk = 46 rho = 5320 cbulk = 350
 isource:ib352 3527 0 idc= 0.0

ThermalBlock3:b353 3531 3431 3533 3523 3535 2535 3537 lx=162.4u ly=147.0u
 +habove= 0.6u hbelow = 100u
 +kmx= 146 kmy= 146 kmz= 170 kild = 46 kbulk = 46 rho = 5320 cbulk = 350
 *isource:ib353 3537 0 idc= 0.03696 iac=0 f=10e9 phase=-90

ThermalBlock3:b354 3541 3441 3543 3533 3545 2545 3547 lx=162.4u ly=147.0u
 +habove= 0.6u hbelow = 100u
 +kmx= 146 kmy= 146 kmz= 170 kild = 46 kbulk = 46 rho = 5320 cbulk = 350
 isource:ib354 3547 0 idc= 0.0

ThermalBlock3:b355 3551 3451 3553 3543 3555 2555 3557 lx=162.4u ly=147.0u
 +habove= 0.6u hbelow = 100u
 +kmx= 146 kmy= 146 kmz= 170 kild = 46 kbulk = 46 rho = 5320 cbulk = 350
 isource:ib355 3557 0 idc= 0.0

ThermalBlock3:b356 3561 3461 3563 3553 3565 2565 3567 lx=162.4u ly=147.0u
 +habove= 0.6u hbelow = 100u
 +dt=10.4 db=10.4 dn=2.77 ds=2.77 de=3 dw=3

+kmx= 146 kmy= 146 kmz= 170 kild = 46 kbulk = 46 rho = 5320 cbulk = 350
isource:ib356 3567 0 idc= 0.0

ThermalBlock3:b357 3571 3471 3573 3563 3575 2575 3577 lx=162.4u ly=147.0u
+habove= 0.6u hbelow = 100u
+kmx= 146 kmy= 146 kmz= 170 kild = 46 kbulk = 46 rho = 5320 cbulk = 350
isource:ib357 3577 0 idc= 0.0

ThermalBlock3:b358 3581 3481 3583 3573 3585 2585 3587 lx=162.4u ly=147.0u
+habove= 0.6u hbelow = 100u
+kmx= 146 kmy= 146 kmz= 170 kild = 46 kbulk = 46 rho = 5320 cbulk = 350
isource:ib358 3587 0 idc= 00

ThermalBlock3:b359 3591 3491 3 3583 3595 2595 3597 lx=162.4u ly=147.0u
+habove= 0.6u hbelow = 100u
+kmx= 146 kmy= 146 kmz= 170 kild = 46 kbulk = 46 rho = 5320 cbulk = 350
isource:ib359 3597 0 idc= 0

ThermalBlock3:b360 3601 3501 3603 4 3605 2605 3607 lx=162.4u ly=147.0u
+habove= 0.6u hbelow = 100u
+kmx= 146 kmy= 146 kmz= 170 kild = 46 kbulk = 46 rho = 5320 cbulk = 350
isource:ib360 3607 0 idc= 0

ThermalBlock3:b361 3611 3511 3613 3603 3615 2615 3617 lx=162.4u ly=147.0u
+habove= 0.6u hbelow = 100u
+kmx= 146 kmy= 146 kmz= 170 kild = 46 kbulk = 46 rho = 5320 cbulk = 350
isource:ib361 3617 0 idc= 0

ThermalBlock3:b362 3621 3521 3623 3613 3625 2625 3627 lx=162.4u ly=147.0u
+habove= 0.6u hbelow = 100u
+kmx= 146 kmy= 146 kmz= 170 kild = 46 kbulk = 46 rho = 5320 cbulk = 350
isource:ib362 3627 0 idc= 0

ThermalBlock3:b363 3631 3531 3633 3623 3635 2635 3637 lx=162.4u ly=147.0u
+habove= 0.6u hbelow = 100u
+kmx= 146 kmy= 146 kmz= 170 kild = 46 kbulk = 46 rho = 5320 cbulk = 350
isource:ib363 3637 0 idc= 0

ThermalBlock3:b364 3641 3541 3643 3633 3645 2645 3647 lx=162.4u ly=147.0u
+habove= 0.6u hbelow = 100u
+kmx= 146 kmy= 146 kmz= 170 kild = 46 kbulk = 46 rho = 5320 cbulk = 350
isource:ib364 3647 0 idc= 0

ThermalBlock3:b365 3651 3551 3653 3643 3655 2655 3657 lx=162.4u ly=147.0u

+habove= 0.6u hbelow = 100u
+kmx= 146 kmy= 146 kmz= 170 kild = 46 kbulk = 46 rho = 5320 cbulk = 350
isource:ib365 3657 0 idc= 0

ThermalBlock3:b366 3661 3561 3663 3653 3665 2665 3667 lx=162.4u ly=147.0u
+habove= 0.6u hbelow = 100u
+dn=2.77 ds=2.77 de=3 dw=3
+kmx= 146 kmy= 146 kmz= 170 kild = 46 kbulk = 46 rho = 5320 cbulk = 350
*isource:ib366 3667 0 idc= 0.120 iac=0 f=10e9 phase=-90

ThermalBlock3:b367 3671 3571 3673 3663 3675 2675 3677 lx=162.4u ly=147.0u
+habove= 0.6u hbelow = 100u
+kmx= 146 kmy= 146 kmz= 170 kild = 46 kbulk = 46 rho = 5320 cbulk = 350
isource:ib367 3677 0 idc= 0

ThermalBlock3:b368 3681 3581 3683 3673 3685 2685 3687 lx=162.4u ly=147.0u
+habove= 0.6u hbelow = 100u
+kmx= 146 kmy= 146 kmz= 170 kild = 46 kbulk = 46 rho = 5320 cbulk = 350
isource:ib368 3687 0 idc= 0

ThermalBlock3:b369 3691 3591 3 3683 3695 2695 3697 lx=162.4u ly=147.0u
+habove= 0.6u hbelow = 100u
+kmx= 146 kmy= 146 kmz= 170 kild = 46 kbulk = 46 rho = 5320 cbulk = 350
isource:ib369 3697 0 idc= 0

ThermalBlock3:b370 3701 3601 3703 4 3705 2705 3707 lx=162.4u ly=147.0u
+habove= 0.6u hbelow = 100u
+kmx= 146 kmy= 146 kmz= 170 kild = 46 kbulk = 46 rho = 5320 cbulk = 350
isource:ib370 3707 0 idc= 0

ThermalBlock3:b371 3711 3611 3713 3703 3715 2715 3717 lx=162.4u ly=147.0u
+habove= 0.6u hbelow = 100u
+kmx= 146 kmy= 146 kmz= 170 kild = 46 kbulk = 46 rho = 5320 cbulk = 350
isource:ib371 3717 0 idc= 0

ThermalBlock3:b372 3721 3621 3723 3713 3725 2725 3727 lx=162.4u ly=147.0u
+habove= 0.6u hbelow = 100u
+kmx= 146 kmy= 146 kmz= 170 kild = 46 kbulk = 46 rho = 5320 cbulk = 350
isource:ib372 3727 0 idc= 0

ThermalBlock3:b373 3731 3631 3733 3723 3735 2735 3737 lx=162.4u ly=147.0u
+habove= 0.6u hbelow = 100u
+kmx= 146 kmy= 146 kmz= 170 kild = 46 kbulk = 46 rho = 5320 cbulk = 350
isource:ib373 3737 0 idc= 0

ThermalBlock3:b374 3741 3641 3743 3733 3745 2745 3747 lx=162.4u ly=147.0u
 +habove= 0.6u hbelow = 100u
 +kmx= 146 kmy= 146 kmz= 170 kild = 46 kbulk = 46 rho = 5320 cbulk = 350
 isource:ib374 3747 0 idc= 0

ThermalBlock3:b375 3751 3651 3753 3743 3755 2755 3757 lx=162.4u ly=147.0u
 +habove= 0.6u hbelow = 100u
 +kmx= 146 kmy= 146 kmz= 170 kild = 46 kbulk = 46 rho = 5320 cbulk = 350
 isource:ib375 3757 0 idc= 0

ThermalBlock3:b376 3761 3661 3763 3753 3765 2765 3767 lx=162.4u ly=147.0u
 +habove= 0.6u hbelow = 100u
 +dt=10.4 db=10.4 dn=2.77 ds=2.77 de=3 dw=3
 +kmx= 146 kmy= 146 kmz= 170 kild = 46 kbulk = 46 rho = 5320 cbulk = 350
 isource:ib376 3767 0 idc= 0

ThermalBlock3:b377 3771 3671 3773 3763 3775 2775 3777 lx=162.4u ly=147.0u
 +habove= 0.6u hbelow = 100u
 +kmx= 146 kmy= 146 kmz= 170 kild = 46 kbulk = 46 rho = 5320 cbulk = 350
 isource:ib377 3777 0 idc= 0

ThermalBlock3:b378 3781 3681 3783 3773 3785 2785 3787 lx=162.4u ly=147.0u
 +habove= 0.6u hbelow = 100u
 +kmx= 146 kmy= 146 kmz= 170 kild = 46 kbulk = 46 rho = 5320 cbulk = 350
 isource:ib378 3787 0 idc= 0

ThermalBlock3:b379 3791 3691 3 3783 3795 2795 3797 lx=162.4u ly=147.0u
 +habove= 0.6u hbelow = 100u
 +kmx= 146 kmy= 146 kmz= 170 kild = 46 kbulk = 46 rho = 5320 cbulk = 350
 isource:ib379 3797 0 idc= 0

ThermalBlock3:b380 3801 3701 3803 4 3805 2805 3807 lx=162.4u ly=147.0u
 +habove= 0.6u hbelow = 100u
 +kmx= 146 kmy= 146 kmz= 170 kild = 46 kbulk = 46 rho = 5320 cbulk = 350
 isource:ib380 3807 0 idc= 0

ThermalBlock3:b381 3811 3711 3813 3803 3815 2815 3817 lx=162.4u ly=147.0u
 +habove= 0.6u hbelow = 100u
 +kmx= 146 kmy= 146 kmz= 170 kild = 46 kbulk = 46 rho = 5320 cbulk = 350
 isource:ib381 3817 0 idc= 0.

ThermalBlock3:b382 3821 3721 3823 3813 3825 2825 3827 lx=162.4u ly=147.0u
 +habove= 0.6u hbelow = 100u

+kmx= 146 kmy= 146 kmz= 170 kild = 46 kbulk = 46 rho = 5320 cbulk = 350
 isource:ib382 3827 0 idc= 0.

ThermalBlock3:b383 3831 3731 3833 3823 3835 2835 3837 lx=162.4u ly=147.0u
 +habove= 0.6u hbelow = 100u
 +kmx= 146 kmy= 146 kmz= 170 kild = 46 kbulk = 46 rho = 5320 cbulk = 350
 isource:ib383 3837 0 idc= 0

ThermalBlock3:b384 3841 3741 3843 3833 3845 2845 3847 lx=162.4u ly=147.0u
 +habove= 0.6u hbelow = 100u
 +kmx= 146 kmy= 146 kmz= 170 kild = 46 kbulk = 46 rho = 5320 cbulk = 350
 isource:ib384 3847 0 idc= 0

ThermalBlock3:b385 3851 3751 3853 3843 3855 2855 3857 lx=162.4u ly=147.0u
 +habove= 0.6u hbelow = 100u
 +kmx= 146 kmy= 146 kmz= 170 kild = 46 kbulk = 46 rho = 5320 cbulk = 350
 isource:ib385 3857 0 idc= 0

ThermalBlock3:b386 3861 3761 3863 3853 3865 2865 3867 lx=162.4u ly=147.0u
 +habove= 0.6u hbelow = 100u
 +kmx= 146 kmy= 146 kmz= 170 kild = 46 kbulk = 46 rho = 5320 cbulk = 350
 isource:ib386 3867 0 idc= 0

ThermalBlock3:b387 3871 3771 3873 3863 3875 2875 3877 lx=162.4u ly=147.0u
 +habove= 0.6u hbelow = 100u
 +kmx= 146 kmy= 146 kmz= 170 kild = 46 kbulk = 46 rho = 5320 cbulk = 350
 isource:ib387 3877 0 idc= 0

ThermalBlock3:b388 3881 3781 3883 3873 3885 2885 3887 lx=162.4u ly=147.0u
 +habove= 0.6u hbelow = 100u
 +kmx= 146 kmy= 146 kmz= 170 kild = 46 kbulk = 46 rho = 5320 cbulk = 350
 isource:ib388 3887 0 idc= 0

ThermalBlock3:b389 3891 3791 3 3883 3895 2895 3897 lx=162.4u ly=147.0u
 +habove= 0.6u hbelow = 100u
 +kmx= 146 kmy= 146 kmz= 170 kild = 46 kbulk = 46 rho = 5320 cbulk = 350
 isource:ib389 3897 0 idc= 0

ThermalBlock3:b390 1 3801 3903 4 3905 2905 3907 lx=162.4u ly=147.0u
 +habove= 0.6u hbelow = 100u
 +kmx= 146 kmy= 146 kmz= 170 kild = 46 kbulk = 46 rho = 5320 cbulk = 350
 isource:ib390 3907 0 idc= 0

ThermalBlock3:b391 1 3811 3913 3903 3915 2915 3917 lx=162.4u ly=147.0u

+habove= 0.6u hbelow = 100u
+kmx= 146 kmy= 146 kmz= 170 kild = 46 kbulk = 46 rho = 5320 cbulk = 350
isource:ib391 3917 0 idc= 0

ThermalBlock3:b392 1 3821 3923 3913 3925 2925 3927 lx=162.4u ly=147.0u
+habove= 0.6u hbelow = 100u
+kmx= 146 kmy= 146 kmz= 170 kild = 46 kbulk = 46 rho = 5320 cbulk = 350
isource:ib392 3927 0 idc= 0

ThermalBlock3:b393 1 3831 3933 3923 3935 2935 3937 lx=162.4u ly=147.0u
+habove= 0.6u hbelow = 100u
+kmx= 146 kmy= 146 kmz= 170 kild = 46 kbulk = 46 rho = 5320 cbulk = 350
isource:ib393 3937 0 idc= 00

ThermalBlock3:b394 1 3841 3943 3933 3945 2945 3947 lx=162.4u ly=147.0u
+habove= 0.6u hbelow = 100u
+kmx= 146 kmy= 146 kmz= 170 kild = 46 kbulk = 46 rho = 5320 cbulk = 350
isource:ib394 3947 0 idc= 0

ThermalBlock3:b395 1 3851 3953 3943 3955 2955 3957 lx=162.4u ly=147.0u
+habove= 0.6u hbelow = 100u
+kmx= 146 kmy= 146 kmz= 170 kild = 46 kbulk = 46 rho = 5320 cbulk = 350
isource:ib395 3957 0 idc= 0

ThermalBlock3:b396 1 3861 3963 3953 3965 2965 3967 lx=162.4u ly=147.0u
+habove= 0.6u hbelow = 100u
+kmx= 146 kmy= 146 kmz= 170 kild = 46 kbulk = 46 rho = 5320 cbulk = 350
isource:ib396 3967 0 idc= 0

ThermalBlock3:b397 1 3871 3973 3963 3975 2975 3977 lx=162.4u ly=147.0u
+habove= 0.6u hbelow = 100u
+kmx= 146 kmy= 146 kmz= 170 kild = 46 kbulk = 46 rho = 5320 cbulk = 350
isource:ib397 3977 0 idc= 0

ThermalBlock3:b398 1 3881 3983 3973 3985 2985 3987 lx=162.4u ly=147.0u
+habove= 0.6u hbelow = 100u
+kmx= 146 kmy= 146 kmz= 170 kild = 46 kbulk = 46 rho = 5320 cbulk = 350
isource:ib398 3987 0 idc= 0

ThermalBlock3:b399 1 3891 3 3983 3995 2995 3997 lx=162.4u ly=147.0u
+habove= 0.6u hbelow = 100u
+kmx= 146 kmy= 146 kmz= 170 kild = 46 kbulk = 46 rho = 5320 cbulk = 350
isource:ib399 3997 0 idc= 0

ThermalBlock3:b200 2001 2 2003 4 2005 1005 2007 lx=162.4u ly=147.0u
 +habove= 1.35u hbelow = 100u
 +kmx= 146 kmy= 146 kmz= 170 kild = 60 kbulk = 60 rho = 6700 cbulk = 500
 ource:ib200 2007 0 idc= 0

ThermalBlock3:b201 2011 2 2013 2003 2015 1015 2017 lx=162.4u ly=147.0u
 +habove= 1.35u hbelow = 100u
 +kmx= 146 kmy= 146 kmz= 170 kild = 60 kbulk = 60 rho = 6700 cbulk = 500
 ource:ib201 2017 0 idc= 0

ThermalBlock3:b202 2021 2 2023 2013 2025 1025 2027 lx=162.4u ly=147.0u
 +habove= 1.35u hbelow = 100u
 +kmx= 146 kmy= 146 kmz= 170 kild = 60 kbulk = 60 rho = 6700 cbulk = 500
 ource:ib202 2027 0 idc= 0

ThermalBlock3:b203 2031 2 2033 2023 2035 1035 2037 lx=162.4u ly=147.0u
 +habove= 1.35u hbelow = 100u
 +kmx= 146 kmy= 146 kmz= 170 kild = 60 kbulk = 60 rho = 6700 cbulk = 500
 ource:ib203 2037 0 idc= 0

ThermalBlock3:b204 2041 2 2043 2033 2045 1045 2047 lx=162.4u ly=147.0u
 +habove= 1.35u hbelow = 100u
 +kmx= 146 kmy= 146 kmz= 170 kild = 60 kbulk = 60 rho = 6700 cbulk = 500
 ource:ib204 2047 0 idc= 00

ThermalBlock3:b205 2051 2 2053 2043 2055 1055 2057 lx=162.4u ly=147.0u
 +habove= 1.35u hbelow = 100u
 +kmx= 146 kmy= 146 kmz= 170 kild = 60 kbulk = 60 rho = 6700 cbulk = 500
 ource:ib205 2057 0 idc= 00

ThermalBlock3:b206 2061 2 2063 2053 2065 1065 2067 lx=162.4u ly=147.0u
 +habove= 1.35u hbelow = 100u
 +kmx= 146 kmy= 146 kmz= 170 kild = 60 kbulk = 60 rho = 6700 cbulk = 500
 ource:ib206 2067 0 idc= 00

ThermalBlock3:b207 2071 2 2073 2063 2075 1075 2077 lx=162.4u ly=147.0u
 +habove= 1.35u hbelow = 100u
 +kmx= 146 kmy= 146 kmz= 170 kild = 60 kbulk = 60 rho = 6700 cbulk = 500
 ource:ib207 2077 0 idc= 0

ThermalBlock3:b208 2081 2 2083 2073 2085 1085 2087 lx=162.4u ly=147.0u
 +habove= 1.35u hbelow = 100u
 +kmx= 146 kmy= 146 kmz= 170 kild = 60 kbulk = 60 rho = 6700 cbulk = 500

isource:ib208 2087 0 idc= 0

ThermalBlock3:b209 2091 2 3 2083 2095 1095 2097 lx=162.4u ly=147.0u
 +habove= 1.35u hbelow = 100u
 +kmx= 146 kmy= 146 kmz= 170 kild = 60 kbulk = 60 rho = 6700 cbulk = 500
 isource:ib209 2097 0 idc= 0

ThermalBlock3:b210 2101 2001 2103 4 2105 1105 2107 lx=162.4u ly=147.0u
 +habove= 1.35u hbelow = 100u
 +kmx= 146 kmy= 146 kmz= 170 kild = 60 kbulk = 60 rho = 6700 cbulk = 500
 isource:ib210 2107 0 idc= 0

ThermalBlock3:b211 2111 2011 2113 2103 2115 1115 2117 lx=162.4u ly=147.0u
 +habove= 1.35u hbelow = 100u
 +kmx= 146 kmy= 146 kmz= 170 kild = 60 kbulk = 60 rho = 6700 cbulk = 500
 isource:ib211 2117 0 idc= 0

ThermalBlock3:b212 2121 2021 2123 2113 2125 1125 2127 lx=162.4u ly=147.0u
 +habove= 1.35u hbelow = 100u
 +kmx= 146 kmy= 146 kmz= 170 kild = 60 kbulk = 60 rho = 6700 cbulk = 500
 isource:ib212 2127 0 idc= 0.0

ThermalBlock3:b213 2131 2031 2133 2123 2135 1135 2137 lx=162.4u ly=147.0u
 +habove= 1.35u hbelow = 100u
 +kmx= 146 kmy= 146 kmz= 170 kild = 60 kbulk = 60 rho = 6700 cbulk = 500
 isource:ib213 2137 0 idc= 0

ThermalBlock3:b214 2141 2041 2143 2133 2145 1145 2147 lx=162.4u ly=147.0u
 +habove= 1.35u hbelow = 100u
 +kmx= 146 kmy= 146 kmz= 170 kild = 60 kbulk = 60 rho = 6700 cbulk = 500
 isource:ib214 2147 0 idc= 0

ThermalBlock3:b215 2151 2051 2153 2143 2155 1155 2157 lx=162.4u ly=147.0u
 +habove= 1.35u hbelow = 100u
 +kmx= 146 kmy= 146 kmz= 170 kild = 60 kbulk = 60 rho = 6700 cbulk = 500
 isource:ib215 2157 0 idc= 0

ThermalBlock3:b216 2161 2061 2163 2153 2165 1165 2167 lx=162.4u ly=147.0u
 +habove= 1.35u hbelow = 100u
 +kmx= 146 kmy= 146 kmz= 170 kild = 60 kbulk = 60 rho = 6700 cbulk = 500
 isource:ib216 2167 0 idc= 0

ThermalBlock3:b217 2171 2071 2173 2163 2175 1175 2177 lx=162.4u ly=147.0u
 +habove= 1.35u hbelow = 100u

+kmx= 146 kmy= 146 kmz= 170 kild = 60 kbulk = 60 rho = 6700 cbulk = 500
 ource:ib217 2177 0 idc= 0

ThermalBlock3:b218 2181 2081 2183 2173 2185 1185 2187 lx=162.4u ly=147.0u
 +habove= 1.35u hbelow = 100u
 +kmx= 146 kmy= 146 kmz= 170 kild = 60 kbulk = 60 rho = 6700 cbulk = 500
 ource:ib218 2187 0 idc= 0

ThermalBlock3:b219 2191 2091 3 2183 2195 1195 2197 lx=162.4u ly=147.0u
 +habove= 1.35u hbelow = 100u
 +kmx= 146 kmy= 146 kmz= 170 kild = 60 kbulk = 60 rho = 6700 cbulk = 500
 ource:ib219 2197 0 idc= 0

ThermalBlock3:b220 2201 2101 2203 4 2205 1205 2207 lx=162.4u ly=147.0u
 +habove= 1.35u hbelow = 100u
 +kmx= 146 kmy= 146 kmz= 170 kild = 60 kbulk = 60 rho = 6700 cbulk = 500
 ource:ib220 2207 0 idc= 0

ThermalBlock3:b221 2211 2111 2213 2203 2215 1215 2217 lx=162.4u ly=147.0u
 +habove= 1.35u hbelow = 100u
 +kmx= 146 kmy= 146 kmz= 170 kild = 60 kbulk = 60 rho = 6700 cbulk = 500
 ource:ib221 2217 0 idc= 0

ThermalBlock3:b222 2221 2121 2223 2213 2225 1225 2227 lx=162.4u ly=147.0u
 +habove= 1.35u hbelow = 100u
 +kmx= 146 kmy= 146 kmz= 170 kild = 60 kbulk = 60 rho = 6700 cbulk = 500
 ource:ib222 2227 0 idc= 0

ThermalBlock3:b223 2231 2131 2233 2223 2235 1235 2237 lx=162.4u ly=147.0u
 +habove= 1.35u hbelow = 100u
 +kmx= 146 kmy= 146 kmz= 170 kild = 60 kbulk = 60 rho = 6700 cbulk = 500
 ource:ib223 2237 0 idc= 0

ThermalBlock3:b224 2241 2141 2243 2233 2245 1245 2247 lx=162.4u ly=147.0u
 +habove= 1.35u hbelow = 100u
 +kmx= 146 kmy= 146 kmz= 170 kild = 60 kbulk = 60 rho = 6700 cbulk = 500
 ource:ib224 2247 0 idc= 0

ThermalBlock3:b225 2251 2151 2253 2243 2255 1255 2257 lx=162.4u ly=147.0u
 +habove= 1.35u hbelow = 100u
 +kmx= 146 kmy= 146 kmz= 170 kild = 60 kbulk = 60 rho = 6700 cbulk = 500
 ource:ib225 2257 0 idc= 0

ThermalBlock3:b226 2261 2161 2263 2253 2265 1265 2267 lx=162.4u ly=147.0u

+habove= 1.35u hbelow = 100u
+kmx= 146 kmy= 146 kmz= 170 kild = 60 kbulk = 60 rho = 6700 cbulk = 500
isource:ib226 2267 0 idc= 0

ThermalBlock3:b227 2271 2171 2273 2263 2275 1275 2277 lx=162.4u ly=147.0u
+habove= 1.35u hbelow = 100u
+kmx= 146 kmy= 146 kmz= 170 kild = 60 kbulk = 60 rho = 6700 cbulk = 500
isource:ib227 2277 0 idc= 0

ThermalBlock3:b228 2281 2181 2283 2273 2285 1285 2287 lx=162.4u ly=147.0u
+habove= 1.35u hbelow = 100u
+kmx= 146 kmy= 146 kmz= 170 kild = 60 kbulk = 60 rho = 6700 cbulk = 500
isource:ib228 2287 0 idc= 0

ThermalBlock3:b229 2291 2191 3 2283 2295 1295 2297 lx=162.4u ly=147.0u
+habove= 1.35u hbelow = 100u
+kmx= 146 kmy= 146 kmz= 170 kild = 60 kbulk = 60 rho = 6700 cbulk = 500
isource:ib229 2297 0 idc= 0

ThermalBlock3:b230 2301 2201 2303 4 2305 1305 2307 lx=162.4u ly=147.0u
+habove= 1.35u hbelow = 100u
+kmx= 146 kmy= 146 kmz= 170 kild = 60 kbulk = 60 rho = 6700 cbulk = 500
isource:ib230 2307 0 idc= 0

ThermalBlock3:b231 2311 2211 2313 2303 2315 1315 2317 lx=162.4u ly=147.0u
+habove= 1.35u hbelow = 100u
+kmx= 146 kmy= 146 kmz= 170 kild = 60 kbulk = 60 rho = 6700 cbulk = 500
isource:ib231 2317 0 idc= 0

ThermalBlock3:b232 2321 2221 2323 2313 2325 1325 2327 lx=162.4u ly=147.0u
+habove= 1.35u hbelow = 100u
+kmx= 146 kmy= 146 kmz= 170 kild = 60 kbulk = 60 rho = 6700 cbulk = 500
isource:ib232 2327 0 idc= 0

ThermalBlock3:b233 2331 2231 2333 2323 2335 1335 2337 lx=162.4u ly=147.0u
+habove= 1.35u hbelow = 100u
+kmx= 146 kmy= 146 kmz= 170 kild = 60 kbulk = 60 rho = 6700 cbulk = 500
isource:ib233 2337 0 idc= 0

ThermalBlock3:b234 2341 2241 2343 2333 2345 1345 2347 lx=162.4u ly=147.0u
+habove= 1.35u hbelow = 100u
+kmx= 146 kmy= 146 kmz= 170 kild = 60 kbulk = 60 rho = 6700 cbulk = 500
isource:ib234 2347 0 idc= 0

ThermalBlock3:b235 2351 2251 2353 2343 2355 1355 2357 lx=162.4u ly=147.0u
+habove= 1.35u hbelow = 100u
+kmx= 146 kmy= 146 kmz= 170 kild = 60 kbulk = 60 rho = 6700 cbulk = 500
isource:ib235 2357 0 idc= 0

ThermalBlock3:b236 2361 2261 2363 2353 2365 1365 2367 lx=162.4u ly=147.0u
+habove= 1.35u hbelow = 100u
+kmx= 146 kmy= 146 kmz= 170 kild = 60 kbulk = 60 rho = 6700 cbulk = 500
isource:ib236 2367 0 idc= 0

ThermalBlock3:b237 2371 2271 2373 2363 2375 1375 2377 lx=162.4u ly=147.0u
+habove= 1.35u hbelow = 100u
+kmx= 146 kmy= 146 kmz= 170 kild = 60 kbulk = 60 rho = 6700 cbulk = 500
isource:ib237 2377 0 idc= 0

ThermalBlock3:b238 2381 2281 2383 2373 2385 1385 2387 lx=162.4u ly=147.0u
+habove= 1.35u hbelow = 100u
+kmx= 146 kmy= 146 kmz= 170 kild = 60 kbulk = 60 rho = 6700 cbulk = 500
isource:ib238 2387 0 idc= 0

ThermalBlock3:b239 2391 2291 3 2383 2395 1395 2397 lx=162.4u ly=147.0u
+habove= 1.35u hbelow = 100u
+kmx= 146 kmy= 146 kmz= 170 kild = 60 kbulk = 60 rho = 6700 cbulk = 500
isource:ib239 2397 0 idc= 00

ThermalBlock3:b240 2401 2301 2403 4 2405 1405 2407 lx=162.4u ly=147.0u
+habove= 1.35u hbelow = 100u
+kmx= 146 kmy= 146 kmz= 170 kild = 60 kbulk = 60 rho = 6700 cbulk = 500
isource:ib240 2407 0 idc= 00

ThermalBlock3:b241 2411 2311 2413 2403 2415 1415 2417 lx=162.4u ly=147.0u
+habove= 1.35u hbelow = 100u
+kmx= 146 kmy= 146 kmz= 170 kild = 60 kbulk = 60 rho = 6700 cbulk = 500
isource:ib241 2417 0 idc= 0

ThermalBlock3:b242 2421 2321 2423 2413 2425 1425 2427 lx=162.4u ly=147.0u
+habove= 1.35u hbelow = 100u
+kmx= 146 kmy= 146 kmz= 170 kild = 60 kbulk = 60 rho = 6700 cbulk = 500
isource:ib242 2427 0 idc= 0

ThermalBlock3:b243 2431 2331 2433 2423 2435 1435 2437 lx=162.4u ly=147.0u
+habove= 1.35u hbelow = 100u
+kmx= 146 kmy= 146 kmz= 170 kild = 60 kbulk = 60 rho = 6700 cbulk = 500
isource:ib243 2437 0 idc= 0

ThermalBlock3:b244 2441 2341 2443 2433 2445 1445 2447 lx=162.4u ly=147.0u
 +habove= 1.35u hbelow = 100u
 +kmx= 146 kmy= 146 kmz= 170 kild = 60 kbulk = 60 rho = 6700 cbulk = 500
 ource:ib244 2447 0 idc=0

ThermalBlock3:b245 2451 2351 2453 2443 2455 1455 2457 lx=162.4u ly=147.0u
 +habove= 1.35u hbelow = 100u
 +kmx= 146 kmy= 146 kmz= 170 kild = 60 kbulk = 60 rho = 6700 cbulk = 500
 ource:ib245 2457 0 idc= 0

ThermalBlock3:b246 2461 2361 2463 2453 2465 1465 2467 lx=162.4u ly=147.0u
 +habove= 1.35u hbelow = 100u
 +kmx= 146 kmy= 146 kmz= 170 kild = 60 kbulk = 60 rho = 6700 cbulk = 500
 ource:ib246 2467 0 idc= 0

ThermalBlock3:b247 2471 2371 2473 2463 2475 1475 2477 lx=162.4u ly=147.0u
 +habove= 1.35u hbelow = 100u
 +kmx= 146 kmy= 146 kmz= 170 kild = 60 kbulk = 60 rho = 6700 cbulk = 500
 ource:ib247 2477 0 idc= 0

ThermalBlock3:b248 2481 2381 2483 2473 2485 1485 2487 lx=162.4u ly=147.0u
 +habove= 1.35u hbelow = 100u
 +kmx= 146 kmy= 146 kmz= 170 kild = 60 kbulk = 60 rho = 6700 cbulk = 500
 ource:ib248 2487 0 idc= 0

ThermalBlock3:b249 2491 2391 3 2483 2495 1495 2497 lx=162.4u ly=147.0u
 +habove= 1.35u hbelow = 100u
 +kmx= 146 kmy= 146 kmz= 170 kild = 60 kbulk = 60 rho = 6700 cbulk = 500
 ource:ib249 2497 0 idc= 0

ThermalBlock3:b250 2501 2401 2503 4 2505 1505 2507 lx=162.4u ly=147.0u
 +habove= 1.35u hbelow = 100u
 +kmx= 146 kmy= 146 kmz= 170 kild = 60 kbulk = 60 rho = 6700 cbulk = 500
 ource:ib250 2507 0 idc= 0

ThermalBlock3:b251 2511 2411 2513 2503 2515 1515 2517 lx=162.4u ly=147.0u
 +habove= 1.35u hbelow = 100u
 +kmx= 146 kmy= 146 kmz= 170 kild = 60 kbulk = 60 rho = 6700 cbulk = 500
 ource:ib251 2517 0 idc= 0

ThermalBlock3:b252 2521 2421 2523 2513 2525 1525 2527 lx=162.4u ly=147.0u
 +habove= 1.35u hbelow = 100u
 +kmx= 146 kmy= 146 kmz= 170 kild = 60 kbulk = 60 rho = 6700 cbulk = 500

isource:ib252 2527 0 idc= 0

ThermalBlock3:b253 2531 2431 2533 2523 2535 1535 2537 lx=162.4u ly=147.0u
 +habove= 1.35u hbelow = 100u
 +kmx= 146 kmy= 146 kmz= 170 kild = 60 kbulk = 60 rho = 6700 cbulk = 500
 isource:ib253 2537 0 idc= 00

ThermalBlock3:b254 2541 2441 2543 2533 2545 1545 2547 lx=162.4u ly=147.0u
 +habove= 1.35u hbelow = 100u
 +kmx= 146 kmy= 146 kmz= 170 kild = 60 kbulk = 60 rho = 6700 cbulk = 500
 isource:ib254 2547 0 idc= 0.0

ThermalBlock3:b255 2551 2451 2553 2543 2555 1555 2557 lx=162.4u ly=147.0u
 +habove= 1.35u hbelow = 100u
 +kmx= 146 kmy= 146 kmz= 170 kild = 60 kbulk = 60 rho = 6700 cbulk = 500
 isource:ib255 2557 0 idc= 0.0

ThermalBlock3:b256 2561 2461 2563 2553 2565 1565 2567 lx=162.4u ly=147.0u
 +habove= 1.35u hbelow = 100u
 +kmx= 146 kmy= 146 kmz= 170 kild = 60 kbulk = 60 rho = 6700 cbulk = 500
 isource:ib256 2567 0 idc= 0.

ThermalBlock3:b257 2571 2471 2573 2563 2575 1575 2577 lx=162.4u ly=147.0u
 +habove= 1.35u hbelow = 100u
 +kmx= 146 kmy= 146 kmz= 170 kild = 60 kbulk = 60 rho = 6700 cbulk = 500
 isource:ib257 2577 0 idc= 0

ThermalBlock3:b258 2581 2481 2583 2573 2585 1585 2587 lx=162.4u ly=147.0u
 +habove= 1.35u hbelow = 100u
 +kmx= 146 kmy= 146 kmz= 170 kild = 60 kbulk = 60 rho = 6700 cbulk = 500
 isource:ib258 2587 0 idc= 0

ThermalBlock3:b259 2591 2491 3 2583 2595 1595 2597 lx=162.4u ly=147.0u
 +habove= 1.35u hbelow = 100u
 +kmx= 146 kmy= 146 kmz= 170 kild = 60 kbulk = 60 rho = 6700 cbulk = 500
 isource:ib259 2597 0 idc= 0

ThermalBlock3:b260 2601 2501 2603 4 2605 1605 2607 lx=162.4u ly=147.0u
 +habove= 1.35u hbelow = 100u
 +kmx= 146 kmy= 146 kmz= 170 kild = 60 kbulk = 60 rho = 6700 cbulk = 500
 isource:ib260 2607 0 idc= 0

ThermalBlock3:b261 2611 2511 2613 2603 2615 1615 2617 lx=162.4u ly=147.0u
 +habove= 1.35u hbelow = 100u

+kmx= 146 kmy= 146 kmz= 170 kild = 60 kbulk = 60 rho = 6700 cbulk = 500
 isource:ib261 2617 0 idc= 0

ThermalBlock3:b262 2621 2521 2623 2613 2625 1625 2627 lx=162.4u ly=147.0u
 +habove= 1.35u hbelow = 100u
 +kmx= 146 kmy= 146 kmz= 170 kild = 60 kbulk = 60 rho = 6700 cbulk = 500
 isource:ib262 2627 0 idc= 0

ThermalBlock3:b263 2631 2531 2633 2623 2635 1635 2637 lx=162.4u ly=147.0u
 +habove= 1.35u hbelow = 100u
 +kmx= 146 kmy= 146 kmz= 170 kild = 60 kbulk = 60 rho = 6700 cbulk = 500
 isource:ib263 2637 0 idc= 0

ThermalBlock3:b264 2641 2541 2643 2633 2645 1645 2647 lx=162.4u ly=147.0u
 +habove= 1.35u hbelow = 100u
 +kmx= 146 kmy= 146 kmz= 170 kild = 60 kbulk = 60 rho = 6700 cbulk = 500
 isource:ib264 2647 0 idc= 0

ThermalBlock3:b265 2651 2551 2653 2643 2655 1655 2657 lx=162.4u ly=147.0u
 +habove= 1.35u hbelow = 100u
 +kmx= 146 kmy= 146 kmz= 170 kild = 60 kbulk = 60 rho = 6700 cbulk = 500
 isource:ib265 2657 0 idc= 0

ThermalBlock3:b266 2661 2561 2663 2653 2665 1665 2667 lx=162.4u ly=147.0u
 +habove= 1.35u hbelow = 100u
 +kmx= 146 kmy= 146 kmz= 170 kild = 60 kbulk = 60 rho = 6700 cbulk = 500
 isource:ib266 2667 0 idc= 0

ThermalBlock3:b267 2671 2571 2673 2663 2675 1675 2677 lx=162.4u ly=147.0u
 +habove= 1.35u hbelow = 100u
 +kmx= 146 kmy= 146 kmz= 170 kild = 60 kbulk = 60 rho = 6700 cbulk = 500
 isource:ib267 2677 0 idc= 0

ThermalBlock3:b268 2681 2581 2683 2673 2685 1685 2687 lx=162.4u ly=147.0u
 +habove= 1.35u hbelow = 100u
 +kmx= 146 kmy= 146 kmz= 170 kild = 60 kbulk = 60 rho = 6700 cbulk = 500
 isource:ib268 2687 0 idc= 0

ThermalBlock3:b269 2691 2591 3 2683 2695 1695 2697 lx=162.4u ly=147.0u
 +habove= 1.35u hbelow = 100u
 +kmx= 146 kmy= 146 kmz= 170 kild = 60 kbulk = 60 rho = 6700 cbulk = 500
 isource:ib269 2697 0 idc= 0

ThermalBlock3:b270 2701 2601 2703 4 2705 1705 2707 lx=162.4u ly=147.0u

+habove= 1.35u hbelow = 100u
 +kmx= 146 kmy= 146 kmz= 170 kild = 60 kbulk = 60 rho = 6700 cbulk = 500
 ource:ib270 2707 0 idc= 0

ThermalBlock3:b271 2711 2611 2713 2703 2715 1715 2717 lx=162.4u ly=147.0u
 +habove= 1.35u hbelow = 100u
 +kmx= 146 kmy= 146 kmz= 170 kild = 60 kbulk = 60 rho = 6700 cbulk = 500
 ource:ib271 2717 0 idc= 0

ThermalBlock3:b272 2721 2621 2723 2713 2725 1725 2727 lx=162.4u ly=147.0u
 +habove= 1.35u hbelow = 100u
 +kmx= 146 kmy= 146 kmz= 170 kild = 60 kbulk = 60 rho = 6700 cbulk = 500
 ource:ib272 2727 0 idc=0

ThermalBlock3:b273 2731 2631 2733 2723 2735 1735 2737 lx=162.4u ly=147.0u
 +habove= 1.35u hbelow = 100u
 +kmx= 146 kmy= 146 kmz= 170 kild = 60 kbulk = 60 rho = 6700 cbulk = 500
 ource:ib273 2737 0 idc= 0

ThermalBlock3:b274 2741 2641 2743 2733 2745 1745 2747 lx=162.4u ly=147.0u
 +habove= 1.35u hbelow = 100u
 +kmx= 146 kmy= 146 kmz= 170 kild = 60 kbulk = 60 rho = 6700 cbulk = 500
 ource:ib274 2747 0 idc= 0

ThermalBlock3:b275 2751 2651 2753 2743 2755 1755 2757 lx=162.4u ly=147.0u
 +habove= 1.35u hbelow = 100u
 +kmx= 146 kmy= 146 kmz= 170 kild = 60 kbulk = 60 rho = 6700 cbulk = 500
 ource:ib275 2757 0 idc= 0

ThermalBlock3:b276 2761 2661 2763 2753 2765 1765 2767 lx=162.4u ly=147.0u
 +habove= 1.35u hbelow = 100u
 +kmx= 146 kmy= 146 kmz= 170 kild = 60 kbulk = 60 rho = 6700 cbulk = 500
 ource:ib276 2767 0 idc= 0

ThermalBlock3:b277 2771 2671 2773 2763 2775 1775 2777 lx=162.4u ly=147.0u
 +habove= 1.35u hbelow = 100u
 +kmx= 146 kmy= 146 kmz= 170 kild = 60 kbulk = 60 rho = 6700 cbulk = 500
 ource:ib277 2777 0 idc= 0

ThermalBlock3:b278 2781 2681 2783 2773 2785 1785 2787 lx=162.4u ly=147.0u
 +habove= 1.35u hbelow = 100u
 +kmx= 146 kmy= 146 kmz= 170 kild = 60 kbulk = 60 rho = 6700 cbulk = 500
 ource:ib278 2787 0 idc= 0

ThermalBlock3:b279 2791 2691 3 2783 2795 1795 2797 lx=162.4u ly=147.0u
+habove= 1.35u hbelow = 100u
+kmx= 146 kmy= 146 kmz= 170 kild = 60 kbulk = 60 rho = 6700 cbulk = 500
isource:ib279 2797 0 idc= 0

ThermalBlock3:b280 2801 2701 2803 4 2805 1805 2807 lx=162.4u ly=147.0u
+habove= 1.35u hbelow = 100u
+kmx= 146 kmy= 146 kmz= 170 kild = 60 kbulk = 60 rho = 6700 cbulk = 500
isource:ib280 2807 0 idc= 0

ThermalBlock3:b281 2811 2711 2813 2803 2815 1815 2817 lx=162.4u ly=147.0u
+habove= 1.35u hbelow = 100u
+kmx= 146 kmy= 146 kmz= 170 kild = 60 kbulk = 60 rho = 6700 cbulk = 500
isource:ib281 2817 0 idc= 0

ThermalBlock3:b282 2821 2721 2823 2813 2825 1825 2827 lx=162.4u ly=147.0u
+habove= 1.35u hbelow = 100u
+kmx= 146 kmy= 146 kmz= 170 kild = 60 kbulk = 60 rho = 6700 cbulk = 500
isource:ib282 2827 0 idc= 0

ThermalBlock3:b283 2831 2731 2833 2823 2835 1835 2837 lx=162.4u ly=147.0u
+habove= 1.35u hbelow = 100u
+kmx= 146 kmy= 146 kmz= 170 kild = 60 kbulk = 60 rho = 6700 cbulk = 500
isource:ib283 2837 0 idc= 0

ThermalBlock3:b284 2841 2741 2843 2833 2845 1845 2847 lx=162.4u ly=147.0u
+habove= 1.35u hbelow = 100u
+kmx= 146 kmy= 146 kmz= 170 kild = 60 kbulk = 60 rho = 6700 cbulk = 500
isource:ib284 2847 0 idc= 0

ThermalBlock3:b285 2851 2751 2853 2843 2855 1855 2857 lx=162.4u ly=147.0u
+habove= 1.35u hbelow = 100u
+kmx= 146 kmy= 146 kmz= 170 kild = 60 kbulk = 60 rho = 6700 cbulk = 500
isource:ib285 2857 0 idc= 0

ThermalBlock3:b286 2861 2761 2863 2853 2865 1865 2867 lx=162.4u ly=147.0u
+habove= 1.35u hbelow = 100u
+kmx= 146 kmy= 146 kmz= 170 kild = 60 kbulk = 60 rho = 6700 cbulk = 500
isource:ib286 2867 0 idc= 0

ThermalBlock3:b287 2871 2771 2873 2863 2875 1875 2877 lx=162.4u ly=147.0u
+habove= 1.35u hbelow = 100u
+kmx= 146 kmy= 146 kmz= 170 kild = 60 kbulk = 60 rho = 6700 cbulk = 500
isource:ib287 2877 0 idc= 0

ThermalBlock3:b288 2881 2781 2883 2873 2885 1885 2887 lx=162.4u ly=147.0u
 +habove= 1.35u hbelow = 100u
 +kmx= 146 kmy= 146 kmz= 170 kild = 60 kbulk = 60 rho = 6700 cbulk = 500
 isource:ib288 2887 0 idc=0

ThermalBlock3:b289 2891 2791 3 2883 2895 1895 2897 lx=162.4u ly=147.0u
 +habove= 1.35u hbelow = 100u
 +kmx= 146 kmy= 146 kmz= 170 kild = 60 kbulk = 60 rho = 6700 cbulk = 500
 isource:ib289 2897 0 idc= 0

ThermalBlock3:b290 1 2801 2903 4 2905 1905 2907 lx=162.4u ly=147.0u
 +habove= 1.35u hbelow = 100u
 +kmx= 146 kmy= 146 kmz= 170 kild = 60 kbulk = 60 rho = 6700 cbulk = 500
 isource:ib290 2907 0 idc= 00

ThermalBlock3:b291 1 2811 2913 2903 2915 1915 2917 lx=162.4u ly=147.0u
 +habove= 1.35u hbelow = 100u
 +kmx= 146 kmy= 146 kmz= 170 kild = 60 kbulk = 60 rho = 6700 cbulk = 500
 isource:ib291 2917 0 idc= 0

ThermalBlock3:b292 1 2821 2923 2913 2925 1925 2927 lx=162.4u ly=147.0u
 +habove= 1.35u hbelow = 100u
 +kmx= 146 kmy= 146 kmz= 170 kild = 60 kbulk = 60 rho = 6700 cbulk = 500
 isource:ib292 2927 0 idc= 0

ThermalBlock3:b293 1 2831 2933 2923 2935 1935 2937 lx=162.4u ly=147.0u
 +habove= 1.35u hbelow = 100u
 +kmx= 146 kmy= 146 kmz= 170 kild = 60 kbulk = 60 rho = 6700 cbulk = 500
 isource:ib293 2937 0 idc= 0

ThermalBlock3:b294 1 2841 2943 2933 2945 1945 2947 lx=162.4u ly=147.0u
 +habove= 1.35u hbelow = 100u
 +kmx= 146 kmy= 146 kmz= 170 kild = 60 kbulk = 60 rho = 6700 cbulk = 500
 isource:ib294 2947 0 idc= 0

ThermalBlock3:b295 1 2851 2953 2943 2955 1955 2957 lx=162.4u ly=147.0u
 +habove= 1.35u hbelow = 100u
 +kmx= 146 kmy= 146 kmz= 170 kild = 60 kbulk = 60 rho = 6700 cbulk = 500
 isource:ib295 2957 0 idc= 0

ThermalBlock3:b296 1 2861 2963 2953 2965 1965 2967 lx=162.4u ly=147.0u
 +habove= 1.35u hbelow = 100u
 +kmx= 146 kmy= 146 kmz= 170 kild = 60 kbulk = 60 rho = 6700 cbulk = 500

isource:ib296 2967 0 idc= 0

ThermalBlock3:b297 1 2871 2973 2963 2975 1975 2977 lx=162.4u ly=147.0u
 +habove= 1.35u hbelow = 100u
 +kmx= 146 kmy= 146 kmz= 170 kild = 60 kbulk = 60 rho = 6700 cbulk = 500
 isource:ib297 2977 0 idc= 0

ThermalBlock3:b298 1 2881 2983 2973 2985 1985 2987 lx=162.4u ly=147.0u
 +habove= 1.35u hbelow = 100u
 +kmx= 146 kmy= 146 kmz= 170 kild = 60 kbulk = 60 rho = 6700 cbulk = 500
 isource:ib298 2987 0 idc= 0

ThermalBlock3:b299 1 2891 3 2983 2995 1995 2997 lx=162.4u ly=147.0u
 +habove= 1.35u hbelow = 100u
 +kmx= 146 kmy= 146 kmz= 170 kild = 60 kbulk = 60 rho = 6700 cbulk = 500
 isource:ib299 2997 0 idc= 0

ThermalBlock3:b100 1001 2 1003 4 1005 6 1007 lx=162.4u ly=147.0u
 +habove= 0.4u hbelow = 381u
 +kmx= 146 kmy= 146 kmz= 170 kild = 17.3 kbulk = 17.3 rho = 8359 cbulk = 502
 isource:ib100 1007 0 idc= 0

ThermalBlock3:b101 1011 2 1013 1003 1015 6 1017 lx=162.4u ly=147.0u
 +habove= 0.4u hbelow = 381u
 +kmx= 146 kmy= 146 kmz= 170 kild = 17.3 kbulk = 17.3 rho = 8359 cbulk = 502
 isource:ib101 1017 0 idc= 0.

ThermalBlock3:b102 1021 2 1023 1013 1025 6 1027 lx=162.4u ly=147.0u
 +habove= 0.4u hbelow = 381u
 +kmx= 146 kmy= 146 kmz= 170 kild = 17.3 kbulk = 17.3 rho = 8359 cbulk = 502
 isource:ib102 1027 0 idc= 0.

ThermalBlock3:b103 1031 2 1033 1023 1035 6 1037 lx=162.4u ly=147.0u
 +habove= 0.4u hbelow = 381u
 +kmx= 146 kmy= 146 kmz= 170 kild = 17.3 kbulk = 17.3 rho = 8359 cbulk = 502
 isource:ib103 1037 0 idc= 0.

ThermalBlock3:b104 1041 2 1043 1033 1045 6 1047 lx=162.4u ly=147.0u
 +habove= 0.4u hbelow = 381u
 +kmx= 146 kmy= 146 kmz= 170 kild = 17.3 kbulk = 17.3 rho = 8359 cbulk = 502
 isource:ib104 1047 0 idc= 0.

ThermalBlock3:b105 1051 2 1053 1043 1055 6 1057 lx=162.4u ly=147.0u
 +habove= 0.4u hbelow = 381u

+kmx= 146 kmy= 146 kmz= 170 kild = 17.3 kbulk = 17.3 rho = 8359 cbulk = 502
isource:ib105 1057 0 idc= 0

ThermalBlock3:b106 1061 2 1063 1053 1065 6 1067 lx=162.4u ly=147.0u
+habove= 0.4u hbelow = 381u
+kmx= 146 kmy= 146 kmz= 170 kild = 17.3 kbulk = 17.3 rho = 8359 cbulk = 502
isource:ib106 1067 0 idc= 0

ThermalBlock3:b107 1071 2 1073 1063 1075 6 1077 lx=162.4u ly=147.0u
+habove= 0.4u hbelow = 381u
+kmx= 146 kmy= 146 kmz= 170 kild = 17.3 kbulk = 17.3 rho = 8359 cbulk = 502
isource:ib107 1077 0 idc= 0

ThermalBlock3:b108 1081 2 1083 1073 1085 6 1087 lx=162.4u ly=147.0u
+habove= 0.4u hbelow = 381u
+kmx= 146 kmy= 146 kmz= 170 kild = 17.3 kbulk = 17.3 rho = 8359 cbulk = 502
isource:ib108 1087 0 idc= 0

ThermalBlock3:b109 1091 2 3 1083 1095 6 1097 lx=162.4u ly=147.0u
+habove= 0.4u hbelow = 381u
+kmx= 146 kmy= 146 kmz= 170 kild = 17.3 kbulk = 17.3 rho = 8359 cbulk = 502
isource:ib109 1097 0 idc= 0

ThermalBlock3:b110 1101 1001 1103 4 1105 6 1107 lx=162.4u ly=147.0u
+habove= 0.4u hbelow = 381u
+kmx= 146 kmy= 146 kmz= 170 kild = 17.3 kbulk = 17.3 rho = 8359 cbulk = 502
isource:ib110 1107 0 idc= 0

ThermalBlock3:b111 1111 1011 1113 1103 1115 6 1117 lx=162.4u ly=147.0u
+habove= 0.4u hbelow = 381u
+kmx= 146 kmy= 146 kmz= 170 kild = 17.3 kbulk = 17.3 rho = 8359 cbulk = 502
isource:ib111 1117 0 idc= 0

ThermalBlock3:b112 1121 1021 1123 1113 1125 6 1127 lx=162.4u ly=147.0u
+habove= 0.4u hbelow = 381u
+kmx= 146 kmy= 146 kmz= 170 kild = 17.3 kbulk = 17.3 rho = 8359 cbulk = 502
isource:ib112 1127 0 idc= 0

ThermalBlock3:b113 1131 1031 1133 1123 1135 6 1137 lx=162.4u ly=147.0u
+habove= 0.4u hbelow = 381u
+kmx= 146 kmy= 146 kmz= 170 kild = 17.3 kbulk = 17.3 rho = 8359 cbulk = 502
isource:ib113 1137 0 idc= 0

ThermalBlock3:b114 1141 1041 1143 1133 1145 6 1147 lx=162.4u ly=147.0u

+habove= 0.4u hbelow = 381u
 +kmx= 146 kmy= 146 kmz= 170 kild = 17.3 kbulk = 17.3 rho = 8359 cbulk = 502
 isource:ib114 1147 0 idc= 0

ThermalBlock3:b115 1151 1051 1153 1143 1155 6 1157 lx=162.4u ly=147.0u
 +habove= 0.4u hbelow = 381u
 +kmx= 146 kmy= 146 kmz= 170 kild = 17.3 kbulk = 17.3 rho = 8359 cbulk = 502
 isource:ib115 1157 0 idc= 0

ThermalBlock3:b116 1161 1061 1163 1153 1165 6 1167 lx=162.4u ly=147.0u
 +habove= 0.4u hbelow = 381u
 +kmx= 146 kmy= 146 kmz= 170 kild = 17.3 kbulk = 17.3 rho = 8359 cbulk = 502
 isource:ib116 1167 0 idc= 0

ThermalBlock3:b117 1171 1071 1173 1163 1175 6 1177 lx=162.4u ly=147.0u
 +habove= 0.4u hbelow = 381u
 +kmx= 146 kmy= 146 kmz= 170 kild = 17.3 kbulk = 17.3 rho = 8359 cbulk = 502
 isource:ib117 1177 0 idc= 0

ThermalBlock3:b118 1181 1081 1183 1173 1185 6 1187 lx=162.4u ly=147.0u
 +habove= 0.4u hbelow = 381u
 +kmx= 146 kmy= 146 kmz= 170 kild = 17.3 kbulk = 17.3 rho = 8359 cbulk = 502
 isource:ib118 1187 0 idc= 0.0

ThermalBlock3:b119 1191 1091 3 1183 1195 6 1197 lx=162.4u ly=147.0u
 +habove= 0.4u hbelow = 381u
 +kmx= 146 kmy= 146 kmz= 170 kild = 17.3 kbulk = 17.3 rho = 8359 cbulk = 502
 isource:ib119 1197 0 idc= 0

ThermalBlock3:b120 1201 1101 1203 4 1205 6 1207 lx=162.4u ly=147.0u
 +habove= 0.4u hbelow = 381u
 +kmx= 146 kmy= 146 kmz= 170 kild = 17.3 kbulk = 17.3 rho = 8359 cbulk = 502
 isource:ib120 1207 0 idc= 0

ThermalBlock3:b121 1211 1111 1213 1203 1215 6 1217 lx=162.4u ly=147.0u
 +habove= 0.4u hbelow = 381u
 +kmx= 146 kmy= 146 kmz= 170 kild = 17.3 kbulk = 17.3 rho = 8359 cbulk = 502
 isource:ib121 1217 0 idc= 0

ThermalBlock3:b122 1221 1121 1223 1213 1225 6 1227 lx=162.4u ly=147.0u
 +habove= 0.4u hbelow = 381u
 +kmx= 146 kmy= 146 kmz= 170 kild = 17.3 kbulk = 17.3 rho = 8359 cbulk = 502
 isource:ib122 1227 0 idc= 0

ThermalBlock3:b123 1231 1131 1233 1223 1235 6 1237 lx=162.4u ly=147.0u
+habove= 0.4u hbelow = 381u
+kmx= 146 kmy= 146 kmz= 170 kild = 17.3 kbulk = 17.3 rho = 8359 cbulk = 502
isource:ib123 1237 0 idc= 0

ThermalBlock3:b124 1241 1141 1243 1233 1245 6 1247 lx=162.4u ly=147.0u
+habove= 0.4u hbelow = 381u
+kmx= 146 kmy= 146 kmz= 170 kild = 17.3 kbulk = 17.3 rho = 8359 cbulk = 502
isource:ib124 1247 0 idc= 0

ThermalBlock3:b125 1251 1151 1253 1243 1255 6 1257 lx=162.4u ly=147.0u
+habove= 0.4u hbelow = 381u
+kmx= 146 kmy= 146 kmz= 170 kild = 17.3 kbulk = 17.3 rho = 8359 cbulk = 502
isource:ib125 1257 0 idc= 0

ThermalBlock3:b126 1261 1161 1263 1253 1265 6 1267 lx=162.4u ly=147.0u
+habove= 0.4u hbelow = 381u
+kmx= 146 kmy= 146 kmz= 170 kild = 17.3 kbulk = 17.3 rho = 8359 cbulk = 502
isource:ib126 1267 0 idc= 1.2389e-3

ThermalBlock3:b127 1271 1171 1273 1263 1275 6 1277 lx=162.4u ly=147.0u
+habove= 0.4u hbelow = 381u
+kmx= 146 kmy= 146 kmz= 170 kild = 17.3 kbulk = 17.3 rho = 8359 cbulk = 502
isource:ib127 1277 0 idc= 0

ThermalBlock3:b128 1281 1181 1283 1273 1285 6 1287 lx=162.4u ly=147.0u
+habove= 0.4u hbelow = 381u
+kmx= 146 kmy= 146 kmz= 170 kild = 17.3 kbulk = 17.3 rho = 8359 cbulk = 502
isource:ib128 1287 0 idc= 0

ThermalBlock3:b129 1291 1191 3 1283 1295 6 1297 lx=162.4u ly=147.0u
+habove= 0.4u hbelow = 381u
+kmx= 146 kmy= 146 kmz= 170 kild = 17.3 kbulk = 17.3 rho = 8359 cbulk = 502
isource:ib129 1297 0 idc= 0

ThermalBlock3:b130 1301 1201 1303 4 1305 6 1307 lx=162.4u ly=147.0u
+habove= 0.4u hbelow = 381u
+kmx= 146 kmy= 146 kmz= 170 kild = 17.3 kbulk = 17.3 rho = 8359 cbulk = 502
isource:ib130 1307 0 idc= 0

ThermalBlock3:b131 1311 1211 1313 1303 1315 6 1317 lx=162.4u ly=147.0u
+habove= 0.4u hbelow = 381u
+kmx= 146 kmy= 146 kmz= 170 kild = 17.3 kbulk = 17.3 rho = 8359 cbulk = 502
isource:ib131 1317 0 idc= 0

ThermalBlock3:b132 1321 1221 1323 1313 1325 6 1327 lx=162.4u ly=147.0u
 +habove= 0.4u hbelow = 381u
 +kmx= 146 kmy= 146 kmz= 170 kild = 17.3 kbulk = 17.3 rho = 8359 cbulk = 502
 isource:ib132 1327 0 idc= 0

ThermalBlock3:b133 1331 1231 1333 1323 1335 6 1337 lx=162.4u ly=147.0u
 +habove= 0.4u hbelow = 381u
 +kmx= 146 kmy= 146 kmz= 170 kild = 17.3 kbulk = 17.3 rho = 8359 cbulk = 502
 isource:ib133 1337 0 idc= 0

ThermalBlock3:b134 1341 1241 1343 1333 1345 6 1347 lx=162.4u ly=147.0u
 +habove= 0.4u hbelow = 381u
 +kmx= 146 kmy= 146 kmz= 170 kild = 17.3 kbulk = 17.3 rho = 8359 cbulk = 502
 isource:ib134 1347 0 idc= 0

ThermalBlock3:b135 1351 1251 1353 1343 1355 6 1357 lx=162.4u ly=147.0u
 +habove= 0.4u hbelow = 381u
 +kmx= 146 kmy= 146 kmz= 170 kild = 17.3 kbulk = 17.3 rho = 8359 cbulk = 502
 isource:ib135 1357 0 idc= 0

ThermalBlock3:b136 1361 1261 1363 1353 1365 6 1367 lx=162.4u ly=147.0u
 +habove= 0.4u hbelow = 381u
 +kmx= 146 kmy= 146 kmz= 170 kild = 17.3 kbulk = 17.3 rho = 8359 cbulk = 502
 isource:ib136 1367 0 idc= 0

ThermalBlock3:b137 1371 1271 1373 1363 1375 6 1377 lx=162.4u ly=147.0u
 +habove= 0.4u hbelow = 381u
 +kmx= 146 kmy= 146 kmz= 170 kild = 17.3 kbulk = 17.3 rho = 8359 cbulk = 502
 isource:ib137 1377 0 idc= 0

ThermalBlock3:b138 1381 1281 1383 1373 1385 6 1387 lx=162.4u ly=147.0u
 +habove= 0.4u hbelow = 381u
 +kmx= 146 kmy= 146 kmz= 170 kild = 17.3 kbulk = 17.3 rho = 8359 cbulk = 502
 isource:ib138 1387 0 idc= 0

ThermalBlock3:b139 1391 1291 3 1383 1395 6 1397 lx=162.4u ly=147.0u
 +habove= 0.4u hbelow = 381u
 +kmx= 146 kmy= 146 kmz= 170 kild = 17.3 kbulk = 17.3 rho = 8359 cbulk = 502
 isource:ib139 1397 0 idc= 0

ThermalBlock3:b140 1401 1301 1403 4 1405 6 1407 lx=162.4u ly=147.0u
 +habove= 0.4u hbelow = 381u
 +kmx= 146 kmy= 146 kmz= 170 kild = 17.3 kbulk = 17.3 rho = 8359 cbulk = 502

isource:ib140 1407 0 idc= 0

ThermalBlock3:b141 1411 1311 1413 1403 1415 6 1417 lx=162.4u ly=147.0u
 +habove= 0.4u hbelow = 381u
 +kmx= 146 kmy= 146 kmz= 170 kild = 17.3 kbulk = 17.3 rho = 8359 cbulk = 502
 isource:ib141 1417 0 idc= 0

ThermalBlock3:b142 1421 1321 1423 1413 1425 6 1427 lx=162.4u ly=147.0u
 +habove= 0.4u hbelow = 381u
 +kmx= 146 kmy= 146 kmz= 170 kild = 17.3 kbulk = 17.3 rho = 8359 cbulk = 502
 isource:ib142 1427 0 idc= 0

ThermalBlock3:b143 1431 1331 1433 1423 1435 6 1437 lx=162.4u ly=147.0u
 +habove= 0.4u hbelow = 381u
 +kmx= 146 kmy= 146 kmz= 170 kild = 17.3 kbulk = 17.3 rho = 8359 cbulk = 502
 isource:ib143 1437 0 idc= 0

ThermalBlock3:b144 1441 1341 1443 1433 1445 6 1447 lx=162.4u ly=147.0u
 +habove= 0.4u hbelow = 381u
 +kmx= 146 kmy= 146 kmz= 170 kild = 17.3 kbulk = 17.3 rho = 8359 cbulk = 502
 isource:ib144 1447 0 idc= 0

ThermalBlock3:b145 1451 1351 1453 1443 1455 6 1457 lx=162.4u ly=147.0u
 +habove= 0.4u hbelow = 381u
 +kmx= 146 kmy= 146 kmz= 170 kild = 17.3 kbulk = 17.3 rho = 8359 cbulk = 502
 isource:ib145 1457 0 idc= 0

ThermalBlock3:b146 1461 1361 1463 1453 1465 6 1467 lx=162.4u ly=147.0u
 +habove= 0.4u hbelow = 381u
 +kmx= 146 kmy= 146 kmz= 170 kild = 17.3 kbulk = 17.3 rho = 8359 cbulk = 502
 isource:ib146 1467 0 idc= 0

ThermalBlock3:b147 1471 1371 1473 1463 1475 6 1477 lx=162.4u ly=147.0u
 +habove= 0.4u hbelow = 381u
 +kmx= 146 kmy= 146 kmz= 170 kild = 17.3 kbulk = 17.3 rho = 8359 cbulk = 502
 isource:ib147 1477 0 idc= 0

ThermalBlock3:b148 1481 1381 1483 1473 1485 6 1487 lx=162.4u ly=147.0u
 +habove= 0.4u hbelow = 381u
 +kmx= 146 kmy= 146 kmz= 170 kild = 17.3 kbulk = 17.3 rho = 8359 cbulk = 502
 isource:ib148 1487 0 idc= 0

ThermalBlock3:b149 1491 1391 3 1483 1495 6 1497 lx=162.4u ly=147.0u
 +habove= 0.4u hbelow = 381u

+kmx= 146 kmy= 146 kmz= 170 kild = 17.3 kbulk = 17.3 rho = 8359 cbulk = 502
 ource:ib149 1497 0 idc= 0

ThermalBlock3:b150 1501 1401 1503 4 1505 6 1507 lx=162.4u ly=147.0u
 +habove= 0.4u hbelow = 381u
 +kmx= 146 kmy= 146 kmz= 170 kild = 17.3 kbulk = 17.3 rho = 8359 cbulk = 502
 ource:ib150 1507 0 idc= 0

ThermalBlock3:b151 1511 1411 1513 1503 1515 6 1517 lx=162.4u ly=147.0u
 +habove= 0.4u hbelow = 381u
 +kmx= 146 kmy= 146 kmz= 170 kild = 17.3 kbulk = 17.3 rho = 8359 cbulk = 502
 ource:ib151 1517 0 idc= 0

ThermalBlock3:b152 1521 1421 1523 1513 1525 6 1527 lx=162.4u ly=147.0u
 +habove= 0.4u hbelow = 381u
 +kmx= 146 kmy= 146 kmz= 170 kild = 17.3 kbulk = 17.3 rho = 8359 cbulk = 502
 ource:ib152 1527 0 idc=0

ThermalBlock3:b153 1531 1431 1533 1523 1535 6 1537 lx=162.4u ly=147.0u
 +habove= 0.4u hbelow = 381u
 +kmx= 146 kmy= 146 kmz= 170 kild = 17.3 kbulk = 17.3 rho = 8359 cbulk = 502
 ource:ib153 1537 0 idc= 0

ThermalBlock3:b154 1541 1441 1543 1533 1545 6 1547 lx=162.4u ly=147.0u
 +habove= 0.4u hbelow = 381u
 +kmx= 146 kmy= 146 kmz= 170 kild = 17.3 kbulk = 17.3 rho = 8359 cbulk = 502
 ource:ib154 1547 0 idc= 0

ThermalBlock3:b155 1551 1451 1553 1543 1555 6 1557 lx=162.4u ly=147.0u
 +habove= 0.4u hbelow = 381u
 +kmx= 146 kmy= 146 kmz= 170 kild = 17.3 kbulk = 17.3 rho = 8359 cbulk = 502
 ource:ib155 1557 0 idc= 00

ThermalBlock3:b156 1561 1461 1563 1553 1565 6 1567 lx=162.4u ly=147.0u
 +habove= 0.4u hbelow = 381u
 +kmx= 146 kmy= 146 kmz= 170 kild = 17.3 kbulk = 17.3 rho = 8359 cbulk = 502
 ource:ib156 1567 0 idc= 0

ThermalBlock3:b157 1571 1471 1573 1563 1575 6 1577 lx=162.4u ly=147.0u
 +habove= 0.4u hbelow = 381u
 +kmx= 146 kmy= 146 kmz= 170 kild = 17.3 kbulk = 17.3 rho = 8359 cbulk = 502
 ource:ib157 1577 0 idc= 0

ThermalBlock3:b158 1581 1481 1583 1573 1585 6 1587 lx=162.4u ly=147.0u

+habove= 0.4u hbelow = 381u
+kmx= 146 kmy= 146 kmz= 170 kild = 17.3 kbulk = 17.3 rho = 8359 cbulk = 502
isource:ib158 1587 0 idc= 0

ThermalBlock3:b159 1591 1491 3 1583 1595 6 1597 lx=162.4u ly=147.0u
+habove= 0.4u hbelow = 381u
+kmx= 146 kmy= 146 kmz= 170 kild = 17.3 kbulk = 17.3 rho = 8359 cbulk = 502
isource:ib159 1597 0 idc=0

ThermalBlock3:b160 1601 1501 1603 4 1605 6 1607 lx=162.4u ly=147.0u
+habove= 0.4u hbelow = 381u
+kmx= 146 kmy= 146 kmz= 170 kild = 17.3 kbulk = 17.3 rho = 8359 cbulk = 502
isource:ib160 1607 0 idc= 0

ThermalBlock3:b161 1611 1511 1613 1603 1615 6 1617 lx=162.4u ly=147.0u
+habove= 0.4u hbelow = 381u
+kmx= 146 kmy= 146 kmz= 170 kild = 17.3 kbulk = 17.3 rho = 8359 cbulk = 502
isource:ib161 1617 0 idc= 0

ThermalBlock3:b162 1621 1521 1623 1613 1625 6 1627 lx=162.4u ly=147.0u
+habove= 0.4u hbelow = 381u
+kmx= 146 kmy= 146 kmz= 170 kild = 17.3 kbulk = 17.3 rho = 8359 cbulk = 502
isource:ib162 1627 0 idc= 0

ThermalBlock3:b163 1631 1531 1633 1623 1635 6 1637 lx=162.4u ly=147.0u
+habove= 0.4u hbelow = 381u
+kmx= 146 kmy= 146 kmz= 170 kild = 17.3 kbulk = 17.3 rho = 8359 cbulk = 502
isource:ib163 1637 0 idc= 0

ThermalBlock3:b164 1641 1541 1643 1633 1645 6 1647 lx=162.4u ly=147.0u
+habove= 0.4u hbelow = 381u
+kmx= 146 kmy= 146 kmz= 170 kild = 17.3 kbulk = 17.3 rho = 8359 cbulk = 502
isource:ib164 1647 0 idc= 0

ThermalBlock3:b165 1651 1551 1653 1643 1655 6 1657 lx=162.4u ly=147.0u
+habove= 0.4u hbelow = 381u
+kmx= 146 kmy= 146 kmz= 170 kild = 17.3 kbulk = 17.3 rho = 8359 cbulk = 502
isource:ib165 1657 0 idc= 0

ThermalBlock3:b166 1661 1561 1663 1653 1665 6 1667 lx=162.4u ly=147.0u
+habove= 0.4u hbelow = 381u
+kmx= 146 kmy= 146 kmz= 170 kild = 17.3 kbulk = 17.3 rho = 8359 cbulk = 502
isource:ib166 1667 0 idc= 0

ThermalBlock3:b167 1671 1571 1673 1663 1675 6 1677 lx=162.4u ly=147.0u
+habove= 0.4u hbelow = 381u
+kmx= 146 kmy= 146 kmz= 170 kild = 17.3 kbulk = 17.3 rho = 8359 cbulk = 502
isource:ib167 1677 0 idc= 0

ThermalBlock3:b168 1681 1581 1683 1673 1685 6 1687 lx=162.4u ly=147.0u
+habove= 0.4u hbelow = 381u
+kmx= 146 kmy= 146 kmz= 170 kild = 17.3 kbulk = 17.3 rho = 8359 cbulk = 502
isource:ib168 1687 0 idc= 0

ThermalBlock3:b169 1691 1591 3 1683 1695 6 1697 lx=162.4u ly=147.0u
+habove= 0.4u hbelow = 381u
+kmx= 146 kmy= 146 kmz= 170 kild = 17.3 kbulk = 17.3 rho = 8359 cbulk = 502
isource:ib169 1697 0 idc= 0

ThermalBlock3:b170 1701 1601 1703 4 1705 6 1707 lx=162.4u ly=147.0u
+habove= 0.4u hbelow = 381u
+kmx= 146 kmy= 146 kmz= 170 kild = 17.3 kbulk = 17.3 rho = 8359 cbulk = 502
isource:ib170 1707 0 idc= 0

ThermalBlock3:b171 1711 1611 1713 1703 1715 6 1717 lx=162.4u ly=147.0u
+habove= 0.4u hbelow = 381u
+kmx= 146 kmy= 146 kmz= 170 kild = 17.3 kbulk = 17.3 rho = 8359 cbulk = 502
isource:ib171 1717 0 idc= 0

ThermalBlock3:b172 1721 1621 1723 1713 1725 6 1727 lx=162.4u ly=147.0u
+habove= 0.4u hbelow = 381u
+kmx= 146 kmy= 146 kmz= 170 kild = 17.3 kbulk = 17.3 rho = 8359 cbulk = 502
isource:ib172 1727 0 idc= 0

ThermalBlock3:b173 1731 1631 1733 1723 1735 6 1737 lx=162.4u ly=147.0u
+habove= 0.4u hbelow = 381u
+kmx= 146 kmy= 146 kmz= 170 kild = 17.3 kbulk = 17.3 rho = 8359 cbulk = 502
isource:ib173 1737 0 idc= 0

ThermalBlock3:b174 1741 1641 1743 1733 1745 6 1747 lx=162.4u ly=147.0u
+habove= 0.4u hbelow = 381u
+kmx= 146 kmy= 146 kmz= 170 kild = 17.3 kbulk = 17.3 rho = 8359 cbulk = 502
isource:ib174 1747 0 idc= 0

ThermalBlock3:b175 1751 1651 1753 1743 1755 6 1757 lx=162.4u ly=147.0u
+habove= 0.4u hbelow = 381u
+kmx= 146 kmy= 146 kmz= 170 kild = 17.3 kbulk = 17.3 rho = 8359 cbulk = 502
isource:ib175 1757 0 idc= 0

ThermalBlock3:b176 1761 1661 1763 1753 1765 6 1767 lx=162.4u ly=147.0u
+habove= 0.4u hbelow = 381u
+kmx= 146 kmy= 146 kmz= 170 kild = 17.3 kbulk = 17.3 rho = 8359 cbulk = 502
isource:ib176 1767 0 idc= 0

ThermalBlock3:b177 1771 1671 1773 1763 1775 6 1777 lx=162.4u ly=147.0u
+habove= 0.4u hbelow = 381u
+kmx= 146 kmy= 146 kmz= 170 kild = 17.3 kbulk = 17.3 rho = 8359 cbulk = 502
isource:ib177 1777 0 idc= 0

ThermalBlock3:b178 1781 1681 1783 1773 1785 6 1787 lx=162.4u ly=147.0u
+habove= 0.4u hbelow = 381u
+kmx= 146 kmy= 146 kmz= 170 kild = 17.3 kbulk = 17.3 rho = 8359 cbulk = 502
isource:ib178 1787 0 idc= 0

ThermalBlock3:b179 1791 1691 3 1783 1795 6 1797 lx=162.4u ly=147.0u
+habove= 0.4u hbelow = 381u
+kmx= 146 kmy= 146 kmz= 170 kild = 17.3 kbulk = 17.3 rho = 8359 cbulk = 502
isource:ib179 1797 0 idc= 0

ThermalBlock3:b180 1801 1701 1803 4 1805 6 1807 lx=162.4u ly=147.0u
+habove= 0.4u hbelow = 381u
+kmx= 146 kmy= 146 kmz= 170 kild = 17.3 kbulk = 17.3 rho = 8359 cbulk = 502
isource:ib180 1807 0 idc=0

ThermalBlock3:b181 1811 1711 1813 1803 1815 6 1817 lx=162.4u ly=147.0u
+habove= 0.4u hbelow = 381u
+kmx= 146 kmy= 146 kmz= 170 kild = 17.3 kbulk = 17.3 rho = 8359 cbulk = 502
isource:ib181 1817 0 idc= 0

ThermalBlock3:b182 1821 1721 1823 1813 1825 6 1827 lx=162.4u ly=147.0u
+habove= 0.4u hbelow = 381u
+kmx= 146 kmy= 146 kmz= 170 kild = 17.3 kbulk = 17.3 rho = 8359 cbulk = 502
isource:ib182 1827 0 idc= 0

ThermalBlock3:b183 1831 1731 1833 1823 1835 6 1837 lx=162.4u ly=147.0u
+habove= 0.4u hbelow = 381u
+kmx= 146 kmy= 146 kmz= 170 kild = 17.3 kbulk = 17.3 rho = 8359 cbulk = 502
isource:ib183 1837 0 idc= 0

ThermalBlock3:b184 1841 1741 1843 1833 1845 6 1847 lx=162.4u ly=147.0u
+habove= 0.4u hbelow = 381u
+kmx= 146 kmy= 146 kmz= 170 kild = 17.3 kbulk = 17.3 rho = 8359 cbulk = 502

isource:ib184 1847 0 idc= 0

ThermalBlock3:b185 1851 1751 1853 1843 1855 6 1857 lx=162.4u ly=147.0u
 +habove= 0.4u hbelow = 381u
 +kmx= 146 kmy= 146 kmz= 170 kild = 17.3 kbulk = 17.3 rho = 8359 cbulk = 502
 isource:ib185 1857 0 idc= 0

ThermalBlock3:b186 1861 1761 1863 1853 1865 6 1867 lx=162.4u ly=147.0u
 +habove= 0.4u hbelow = 381u
 +kmx= 146 kmy= 146 kmz= 170 kild = 17.3 kbulk = 17.3 rho = 8359 cbulk = 502
 isource:ib186 1867 0 idc= 0

ThermalBlock3:b187 1871 1771 1873 1863 1875 6 1877 lx=162.4u ly=147.0u
 +habove= 0.4u hbelow = 381u
 +kmx= 146 kmy= 146 kmz= 170 kild = 17.3 kbulk = 17.3 rho = 8359 cbulk = 502
 isource:ib187 1877 0 idc= 0

ThermalBlock3:b188 1881 1781 1883 1873 1885 6 1887 lx=162.4u ly=147.0u
 +habove= 0.4u hbelow = 381u
 +kmx= 146 kmy= 146 kmz= 170 kild = 17.3 kbulk = 17.3 rho = 8359 cbulk = 502
 isource:ib188 1887 0 idc= 0

ThermalBlock3:b189 1891 1791 3 1883 1895 6 1897 lx=162.4u ly=147.0u
 +habove= 0.4u hbelow = 381u
 +kmx= 146 kmy= 146 kmz= 170 kild = 17.3 kbulk = 17.3 rho = 8359 cbulk = 502
 isource:ib189 1897 0 idc= 0

ThermalBlock3:b190 1 1801 1903 4 1905 6 1907 lx=162.4u ly=147.0u
 +habove= 0.4u hbelow = 381u
 +kmx= 146 kmy= 146 kmz= 170 kild = 17.3 kbulk = 17.3 rho = 8359 cbulk = 502
 isource:ib190 1907 0 idc= 0

ThermalBlock3:b191 1 1811 1913 1903 1915 6 1917 lx=162.4u ly=147.0u
 +habove= 0.4u hbelow = 381u
 +kmx= 146 kmy= 146 kmz= 170 kild = 17.3 kbulk = 17.3 rho = 8359 cbulk = 502
 isource:ib191 1917 0 idc=0

ThermalBlock3:b192 1 1821 1923 1913 1925 6 1927 lx=162.4u ly=147.0u
 +habove= 0.4u hbelow = 381u
 +kmx= 146 kmy= 146 kmz= 170 kild = 17.3 kbulk = 17.3 rho = 8359 cbulk = 502
 isource:ib192 1927 0 idc= 0

ThermalBlock3:b193 1 1831 1933 1923 1935 6 1937 lx=162.4u ly=147.0u
 +habove= 0.4u hbelow = 381u

+kmx= 146 kmy= 146 kmz= 170 kild = 17.3 kbulk = 17.3 rho = 8359 cbulk = 502
 ource:ib193 1937 0 idc= 0

ThermalBlock3:b194 1 1841 1943 1933 1945 6 1947 lx=162.4u ly=147.0u
 +habove= 0.4u hbelow = 381u
 +kmx= 146 kmy= 146 kmz= 170 kild = 17.3 kbulk = 17.3 rho = 8359 cbulk = 502
 ource:ib194 1947 0 idc= 0

ThermalBlock3:b195 1 1851 1953 1943 1955 6 1957 lx=162.4u ly=147.0u
 +habove= 0.4u hbelow = 381u
 +kmx= 146 kmy= 146 kmz= 170 kild = 17.3 kbulk = 17.3 rho = 8359 cbulk = 502
 ource:ib195 1957 0 idc=0

ThermalBlock3:b196 1 1861 1963 1953 1965 6 1967 lx=162.4u ly=147.0u
 +habove= 0.4u hbelow = 381u
 +kmx= 146 kmy= 146 kmz= 170 kild = 17.3 kbulk = 17.3 rho = 8359 cbulk = 502
 ource:ib196 1967 0 idc= 0

ThermalBlock3:b197 1 1871 1973 1963 1975 6 1977 lx=162.4u ly=147.0u
 +habove= 0.4u hbelow = 381u
 +kmx= 146 kmy= 146 kmz= 170 kild = 17.3 kbulk = 17.3 rho = 8359 cbulk = 502
 ource:ib197 1977 0 idc= 0

ThermalBlock3:b198 1 1881 1983 1973 1985 6 1987 lx=162.4u ly=147.0u
 +habove= 0.4u hbelow = 381u
 +kmx= 146 kmy= 146 kmz= 170 kild = 17.3 kbulk = 17.3 rho = 8359 cbulk = 502
 ource:ib198 1987 0 idc= 0

ThermalBlock3:b199 1 1891 3 1983 1995 6 1997 lx=162.4u ly=147.0u
 +habove= 0.4u hbelow = 381u
 +kmx= 146 kmy= 146 kmz= 170 kild = 17.3 kbulk = 17.3 rho = 8359 cbulk = 502
 ource:ib199 1997 0 idc= 0

*sidewalls

ource:v1 1 0 idc=0
 ource:v2 2 0 idc=0
 ource:v3 3 0 idc=0
 ource:v4 4 0 idc=0

*surface discretization of top layer connected to zero power

*sources

ource:v3005 3005 0 idc=0
 ource:v3015 3015 0 idc=0

isource:v3025 3025 0 idc=0
isource:v3035 3035 0 idc=0
isource:v3045 3045 0 idc=0
isource:v3055 3055 0 idc=0
isource:v3065 3065 0 idc=0
isource:v3075 3075 0 idc=0
isource:v3085 3085 0 idc=0
isource:v3095 3095 0 idc=0
isource:v3105 3105 0 idc=0
isource:v3115 3115 0 idc=0
isource:v3125 3125 0 idc=0
isource:v3135 3135 0 idc=0
isource:v3145 3145 0 idc=0
isource:v3155 3155 0 idc=0
isource:v3165 3165 0 idc=0
isource:v3175 3175 0 idc=0
isource:v3185 3185 0 idc=0
isource:v3195 3195 0 idc=0
isource:v3205 3205 0 idc=0
isource:v3215 3215 0 idc=0
isource:v3225 3225 0 idc=0
isource:v3235 3235 0 idc=0
isource:v3245 3245 0 idc=0
isource:v3255 3255 0 idc=0
isource:v3265 3265 0 idc=0
isource:v3275 3275 0 idc=0
isource:v3285 3285 0 idc=0
isource:v3295 3295 0 idc=0
isource:v3305 3305 0 idc=0
isource:v3315 3315 0 idc=0
isource:v3325 3325 0 idc=0
isource:v3335 3335 0 idc=0
isource:v3345 3345 0 idc=0
isource:v3355 3355 0 idc=0
isource:v3365 3365 0 idc=0
isource:v3375 3375 0 idc=0
isource:v3385 3385 0 idc=0
isource:v3395 3395 0 idc=0
isource:v3405 3405 0 idc=0
isource:v3415 3415 0 idc=0
isource:v3425 3425 0 idc=0
isource:v3435 3435 0 idc=0
isource:v3445 3445 0 idc=0
isource:v3455 3455 0 idc=0

isource:v3465 3465 0 idc=0
isource:v3475 3475 0 idc=0
isource:v3485 3485 0 idc=0
isource:v3495 3495 0 idc=0
isource:v3505 3505 0 idc=0
isource:v3515 3515 0 idc=0
isource:v3525 3525 0 idc=0
isource:v3535 3535 0 idc=0
isource:v3545 3545 0 idc=0
isource:v3555 3555 0 idc=0
isource:v3565 3565 0 idc=0
isource:v3575 3575 0 idc=0
isource:v3585 3585 0 idc=0
isource:v3595 3595 0 idc=0
isource:v3605 3605 0 idc=0
isource:v3615 3615 0 idc=0
isource:v3625 3625 0 idc=0
isource:v3635 3635 0 idc=0
isource:v3645 3645 0 idc=0
isource:v3655 3655 0 idc=0
isource:v3665 3665 0 idc=0
isource:v3675 3675 0 idc=0
isource:v3685 3685 0 idc=0
isource:v3695 3695 0 idc=0
isource:v3705 3705 0 idc=0
isource:v3715 3715 0 idc=0
isource:v3725 3725 0 idc=0
isource:v3735 3735 0 idc=0
isource:v3745 3745 0 idc=0
isource:v3755 3755 0 idc=0
isource:v3765 3765 0 idc=0
isource:v3775 3775 0 idc=0
isource:v3785 3785 0 idc=0
isource:v3795 3795 0 idc=0
isource:v3805 3805 0 idc=0
isource:v3815 3815 0 idc=0
isource:v3825 3825 0 idc=0
isource:v3835 3835 0 idc=0
isource:v3845 3845 0 idc=0
isource:v3855 3855 0 idc=0
isource:v3865 3865 0 idc=0
isource:v3875 3875 0 idc=0
isource:v3885 3885 0 idc=0
isource:v3895 3895 0 idc=0

```

isource:v3905 3905 0 idc=0
isource:v3915 3915 0 idc=0
isource:v3925 3925 0 idc=0
isource:v3935 3935 0 idc=0
isource:v3945 3945 0 idc=0
isource:v3955 3955 0 idc=0
isource:v3965 3965 0 idc=0
isource:v3975 3975 0 idc=0
isource:v3985 3985 0 idc=0
isource:v3995 3995 0 idc=0

```

```

*heat sink temperature
vsource:v6 6 0 vdc=333

```

```

.tran3 tstep=3ps tstop=4ns out_steps=400 cm=0 reltol=0.01 im=1
.out plot term 3037 vt in "macro_r1_rf_308_coupled_p00001.temp"
.out plot term 3047 vt in "macro_r2_rf_308_coupled_p00001.temp"
.out plot term 3537 vt in "macro_t1_rf_308_coupled_p00001.temp"
.out plot term 3667 vt in "macro_t2_rf_308_coupled_p00001.temp"
.out plot term 51 vt in "macro_m1_rf_308_coupled_p00001.d"
.out plot term 192 vt in "macro_m2_rf_333_coupled_p00001.d"
.out plot element "mesfetct:m2" 1 it in
+"macro_m2_rf_308_coupled_p00001.di"
.out plot element "mesfetct:m1" 1 it in
+"macro_m1_rf_308_coupled_p00001.di"
.out plot element "mesfetct:m2" 2 it in
+"macro_m2_rf_308_coupled_p00001.pow"
.out plot element "mesfetct:m1" 2 it in
+"macro_m1_rf_308_coupled_p00001.pow"
.out plot term 26 vt in
+"macro_mmic_rf_308_coupled_p00001.out"
.end

```

B.10 Netlist For The Thermal Macromodel of the 3DIC

The netlist to study the temperature profile in a 3DIC discussed in the Chapter 5 is given below. This netlist uses the thermal macromodel developed in Section 5.5.

```

****Thermal netlist for the 3DIC with the thermal macromodel.

```

```

*Tier 1

```

```

ThermalBlock3:b100 1001 2 1003 4 1005 6 1007 lx=246.7u ly=261.915u
+habove= 0.4u hbelow = 6.24u

```

+dn= 2.1406 ds= 0.0000 de= 2.3902 dw= 0.0000 dt= 0.0000 db= 0.0000
 +kmx= 146 kmy= 146 kmz= 170 kild= 1.1 kbulk= 1.1 rho = 2300 cbulk = 710
 isource:ib100 1007 0 idc= 0.2062e-3

ThermalBlock3:b101 1011 2 1013 1003 1015 6 1017 lx=246.7u ly=261.915u
 +habove= 0.4u hbelow = 6.24u
 +dn= 1.6585 ds= 0.0000 de= 2.1811 dw= 2.3902 dt= 0.0000 db= 0.0000
 +kmx= 146 kmy= 146 kmz= 170 kild= 1.1 kbulk= 1.1 rho = 2300 cbulk = 710
 isource:ib101 1017 0 idc= 0.2143e-3

ThermalBlock3:b102 1021 2 1023 1013 1025 6 1027 lx=246.7u ly=261.915u
 +habove= 0.4u hbelow = 6.24u
 +dn= 1.7356 ds= 0.0000 de= 2.0903 dw= 2.1811 dt= 0.0095 db= 0.0000
 +kmx= 146 kmy= 146 kmz= 170 kild= 1.1 kbulk= 1.1 rho = 2300 cbulk = 710
 isource:ib102 1027 0 idc= 0.2577e-3

ThermalBlock3:b103 1031 2 1033 1023 1035 6 1037 lx=246.7u ly=261.915u
 +habove= 0.4u hbelow = 6.24u
 +dn= 1.7452 ds= 0.0000 de= 2.6083 dw= 2.0903 dt= 0.0095 db= 0.0000
 +kmx= 146 kmy= 146 kmz= 170 kild= 1.1 kbulk= 1.1 rho = 2300 cbulk = 710
 isource:ib103 1037 0 idc= 0.1883e-3

ThermalBlock3:b104 1041 2 1043 1033 1045 6 1047 lx=246.7u ly=261.915u
 +habove= 0.4u hbelow = 6.24u
 +dn= 1.8513 ds= 0.0000 de= 1.9903 dw= 2.6083 dt= 0.0237 db= 0.0000
 +kmx= 146 kmy= 146 kmz= 170 kild= 1.1 kbulk= 1.1 rho = 2300 cbulk = 710
 isource:ib104 1047 0 idc= 0.2145e-3

ThermalBlock3:b105 1051 2 1053 1043 1055 6 1057 lx=246.7u ly=261.915u
 +habove= 0.4u hbelow = 6.24u
 +dn= 1.8127 ds= 0.0000 de= 2.4356 dw= 1.9903 dt= 0.1043 db= 0.0000
 +kmx= 146 kmy= 146 kmz= 170 kild= 1.1 kbulk= 1.1 rho = 2300 cbulk = 710
 isource:ib105 1057 0 idc= 1.0417e-3

ThermalBlock3:b106 1061 2 1063 1053 1065 6 1067 lx=246.7u ly=261.915u
 +habove= 0.4u hbelow = 6.24u
 +dn= 1.4367 ds= 0.0000 de= 1.9903 dw= 2.4356 dt= 0.0190 db= 0.0000
 +kmx= 146 kmy= 146 kmz= 170 kild= 1.1 kbulk= 1.1 rho = 2300 cbulk = 710
 isource:ib106 1067 0 idc= 1.1965e-3

ThermalBlock3:b107 1071 2 1073 1063 1075 6 1077 lx=246.7u ly=261.915u
 +habove= 0.4u hbelow = 6.24u
 +dn= 1.5813 ds= 0.0000 de= 2.3447 dw= 1.9903 dt= 0.0237 db= 0.0000
 +kmx= 146 kmy= 146 kmz= 170 kild= 1.1 kbulk= 1.1 rho = 2300 cbulk = 710

isource:ib107 1077 0 idc= 0.3385e-3

ThermalBlock3:b108 1081 2 1083 1073 1085 6 1087 lx=246.7u ly=261.915u
+habove= 0.4u hbelow = 6.24u
+dn= 1.6295 ds= 0.0000 de= 2.2266 dw= 2.3447 dt= 0.1138 db= 0.0000
+kmx= 146 kmy= 146 kmz= 170 kild= 1.1 kbulk= 1.1 rho = 2300 cbulk = 710
isource:ib108 1087 0 idc= 0.2174e-3

ThermalBlock3:b109 1091 2 3 1083 1095 6 1097 lx=246.7u ly=261.915u
+habove= 0.4u hbelow = 6.24u
+dn= 2.4395 ds= 0.0000 de= 0.0000 dw= 2.2266 dt= 0.0000 db= 0.0000
+kmx= 146 kmy= 146 kmz= 170 kild= 1.1 kbulk= 1.1 rho = 2300 cbulk = 710
isource:ib109 1097 0 idc= 0.2314e-3

ThermalBlock3:b110 1101 1001 1103 4 1105 6 1107 lx=246.7u ly=261.915u
+habove= 0.4u hbelow = 6.24u
+dn= 2.1599 ds= 2.1406 de= 1.4759 dw= 0.0000 dt= 0.0379 db= 0.0000
+kmx= 146 kmy= 146 kmz= 170 kild= 1.1 kbulk= 1.1 rho = 2300 cbulk = 710
isource:ib110 1107 0 idc= 0.2663e-3

ThermalBlock3:b111 1111 1011 1113 1103 1115 6 1117 lx=246.7u ly=261.915u
+habove= 0.4u hbelow = 6.24u
+dn= 1.4560 ds= 1.6585 de= 1.5123 dw= 1.4759 dt= 0.0427 db= 0.0000
+kmx= 146 kmy= 146 kmz= 170 kild= 1.1 kbulk= 1.1 rho = 2300 cbulk = 710
isource:ib111 1117 0 idc= 0.4352e-3

ThermalBlock3:b112 1121 1021 1123 1113 1125 6 1127 lx=246.7u ly=261.915u
+habove= 0.4u hbelow = 6.24u
+dn= 1.4367 ds= 1.7356 de= 1.4305 dw= 1.5123 dt= 0.0474 db= 0.0000
+kmx= 146 kmy= 146 kmz= 170 kild= 1.1 kbulk= 1.1 rho = 2300 cbulk = 710
isource:ib112 1127 0 idc= 0.5513e-3

ThermalBlock3:b113 1131 1031 1133 1123 1135 6 1137 lx=246.7u ly=261.915u
+habove= 0.4u hbelow = 6.24u
+dn= 0.9931 ds= 1.7452 de= 1.7485 dw= 1.4305 dt= 0.0521 db= 0.0000
+kmx= 146 kmy= 146 kmz= 170 kild= 1.1 kbulk= 1.1 rho = 2300 cbulk = 710
isource:ib113 1137 0 idc= 0.2810e-3

ThermalBlock3:b114 1141 1041 1143 1133 1145 6 1147 lx=246.7u ly=261.915u
+habove= 0.4u hbelow = 6.24u
+dn= 1.4849 ds= 1.8513 de= 1.2305 dw= 1.7485 dt= 0.0853 db= 0.0000
+kmx= 146 kmy= 146 kmz= 170 kild= 1.1 kbulk= 1.1 rho = 2300 cbulk = 710
isource:ib114 1147 0 idc= 0.6385e-3

ThermalBlock3:b115 1151 1051 1153 1143 1155 6 1157 lx=246.7u ly=261.915u
+habove= 0.4u hbelow = 6.24u
+dn= 1.3885 ds= 1.8127 de= 1.9757 dw= 1.2305 dt= 0.0995 db= 0.0000
+kmx= 146 kmy= 146 kmz= 170 kild= 1.1 kbulk= 1.1 rho = 2300 cbulk = 710
isource:ib115 1157 0 idc= 1.2744e-3

ThermalBlock3:b116 1161 1061 1163 1153 1165 6 1167 lx=246.7u ly=261.915u
+habove= 0.4u hbelow = 6.24u
+dn= 1.6006 ds= 1.4367 de= 1.4759 dw= 1.9757 dt= 0.1517 db= 0.0000
+kmx= 146 kmy= 146 kmz= 170 kild= 1.1 kbulk= 1.1 rho = 2300 cbulk = 710
isource:ib116 1167 0 idc= 1.7565e-3

ThermalBlock3:b117 1171 1071 1173 1163 1175 6 1177 lx=246.7u ly=261.915u
+habove= 0.4u hbelow = 6.24u
+dn= 1.7549 ds= 1.5813 de= 1.6395 dw= 1.4759 dt= 0.2702 db= 0.0000
+kmx= 146 kmy= 146 kmz= 170 kild= 1.1 kbulk= 1.1 rho = 2300 cbulk = 710
isource:ib117 1177 0 idc= 1.2404e-3

ThermalBlock3:b118 1181 1081 1183 1173 1185 6 1187 lx=246.7u ly=261.915u
+habove= 0.4u hbelow = 6.24u
+dn= 1.2053 ds= 1.6295 de= 1.4396 dw= 1.6395 dt= 0.1327 db= 0.0000
+kmx= 146 kmy= 146 kmz= 170 kild= 1.1 kbulk= 1.1 rho = 2300 cbulk = 710
isource:ib118 1187 0 idc= 0.3530e-3

ThermalBlock3:b119 1191 1091 3 1183 1195 6 1197 lx=246.7u ly=261.915u
+habove= 0.4u hbelow = 6.24u
+dn= 2.1695 ds= 2.4395 de= 0.0000 dw= 1.4396 dt= 0.0190 db= 0.0000
+kmx= 146 kmy= 146 kmz= 170 kild= 1.1 kbulk= 1.1 rho = 2300 cbulk = 710
isource:ib119 1197 0 idc= 0.3438e-3

ThermalBlock3:b120 1201 1101 1203 4 1205 6 1207 lx=246.7u ly=261.915u
+habove= 0.4u hbelow = 6.24u
+dn= 2.6323 ds= 2.1599 de= 1.8013 dw= 0.0000 dt= 0.0237 db= 0.0000
+kmx= 146 kmy= 146 kmz= 170 kild= 1.1 kbulk= 1.1 rho = 2300 cbulk = 710
isource:ib120 1207 0 idc= 0.6334e-3

ThermalBlock3:b121 1211 1111 1213 1203 1215 6 1217 lx=246.7u ly=261.915u
+habove= 0.4u hbelow = 6.24u
+dn= 1.5042 ds= 1.4560 de= 1.7286 dw= 1.8013 dt= 0.0190 db= 0.0000
+kmx= 146 kmy= 146 kmz= 170 kild= 1.1 kbulk= 1.1 rho = 2300 cbulk = 710
isource:ib121 1217 0 idc= 0.9131e-3

ThermalBlock3:b122 1221 1121 1223 1213 1225 6 1227 lx=246.7u ly=261.915u
+habove= 0.4u hbelow = 6.24u

+dn= 1.9188 ds= 1.4367 de= 1.9830 dw= 1.7286 dt= 0.0237 db= 0.0000
 +kmx= 146 kmy= 146 kmz= 170 kild= 1.1 kbulk= 1.1 rho = 2300 cbulk = 710
 isource:ib122 1227 0 idc= 0.5074e-3

ThermalBlock3:b123 1231 1131 1233 1223 1235 6 1237 lx=246.7u ly=261.915u
 +habove= 0.4u hbelow = 6.24u
 +dn= 1.8127 ds= 0.9931 de= 1.8921 dw= 1.9830 dt= 0.0332 db= 0.0000
 +kmx= 146 kmy= 146 kmz= 170 kild= 1.1 kbulk= 1.1 rho = 2300 cbulk = 710
 isource:ib123 1237 0 idc= 0.8529e-3

ThermalBlock3:b124 1241 1141 1243 1233 1245 6 1247 lx=246.7u ly=261.915u
 +habove= 0.4u hbelow = 6.24u
 +dn= 1.6585 ds= 1.4849 de= 1.4014 dw= 1.8921 dt= 0.1659 db= 0.0000
 +kmx= 146 kmy= 146 kmz= 170 kild= 1.1 kbulk= 1.1 rho = 2300 cbulk = 710
 isource:ib124 1247 0 idc= 0.8324e-3

ThermalBlock3:b125 1251 1151 1253 1243 1255 6 1257 lx=246.7u ly=261.915u
 +habove= 0.4u hbelow = 6.24u
 +dn= 1.6970 ds= 1.3885 de= 1.9467 dw= 1.4014 dt= 0.1138 db= 0.0000
 +kmx= 146 kmy= 146 kmz= 170 kild= 1.1 kbulk= 1.1 rho = 2300 cbulk = 710
 isource:ib125 1257 0 idc= 1.0139e-3

ThermalBlock3:b126 1261 1161 1263 1253 1265 6 1267 lx=246.7u ly=261.915u
 +habove= 0.4u hbelow = 6.24u
 +dn= 1.7260 ds= 1.6006 de= 1.1924 dw= 1.9467 dt= 0.0806 db= 0.0000
 +kmx= 146 kmy= 146 kmz= 170 kild= 1.1 kbulk= 1.1 rho = 2300 cbulk = 710
 isource:ib126 1267 0 idc= 1.2389e-3

ThermalBlock3:b127 1271 1171 1273 1263 1275 6 1277 lx=246.7u ly=261.915u
 +habove= 0.4u hbelow = 6.24u
 +dn= 2.1502 ds= 1.7549 de= 2.1375 dw= 1.1924 dt= 0.0853 db= 0.0000
 +kmx= 146 kmy= 146 kmz= 170 kild= 1.1 kbulk= 1.1 rho = 2300 cbulk = 710
 isource:ib127 1277 0 idc= 0.8455e-3

ThermalBlock3:b128 1281 1181 1283 1273 1285 6 1287 lx=246.7u ly=261.915u
 +habove= 0.4u hbelow = 6.24u
 +dn= 2.0634 ds= 1.2053 de= 1.4196 dw= 2.1375 dt= 0.1517 db= 0.0000
 +kmx= 146 kmy= 146 kmz= 170 kild= 1.1 kbulk= 1.1 rho = 2300 cbulk = 710
 isource:ib128 1287 0 idc= 0.5865e-3

ThermalBlock3:b129 1291 1191 3 1283 1295 6 1297 lx=246.7u ly=261.915u
 +habove= 0.4u hbelow = 6.24u
 +dn= 2.2177 ds= 2.1695 de= 0.0000 dw= 1.4196 dt= 0.0569 db= 0.0000
 +kmx= 146 kmy= 146 kmz= 170 kild= 1.1 kbulk= 1.1 rho = 2300 cbulk = 710

isource:ib129 1297 0 idc= 0.8918e-3

ThermalBlock3:b130 1301 1201 1303 4 1305 6 1307 lx=246.7u ly=261.915u
 +habove= 0.4u hbelow = 6.24u
 +dn= 2.3527 ds= 2.6323 de= 1.7304 dw= 0.0000 dt= 0.0190 db= 0.0000
 +kmx= 146 kmy= 146 kmz= 170 kild= 1.1 kbulk= 1.1 rho = 2300 cbulk = 710
 isource:ib130 1307 0 idc= 0.6940e-3

ThermalBlock3:b131 1311 1211 1313 1303 1315 6 1317 lx=246.7u ly=261.915u
 +habove= 0.4u hbelow = 6.24u
 +dn= 1.8031 ds= 1.5042 de= 1.7667 dw= 1.7304 dt= 0.0664 db= 0.0000
 +kmx= 146 kmy= 146 kmz= 170 kild= 1.1 kbulk= 1.1 rho = 2300 cbulk = 710
 isource:ib131 1317 0 idc= 0.7565e-3

ThermalBlock3:b132 1321 1221 1323 1313 1325 6 1327 lx=246.7u ly=261.915u
 +habove= 0.4u hbelow = 6.24u
 +dn= 2.1695 ds= 1.9188 de= 1.5940 dw= 1.7667 dt= 0.0569 db= 0.0000
 +kmx= 146 kmy= 146 kmz= 170 kild= 1.1 kbulk= 1.1 rho = 2300 cbulk = 710
 isource:ib132 1327 0 idc= 0.5307e-3

ThermalBlock3:b133 1331 1231 1333 1323 1335 6 1337 lx=246.7u ly=261.915u
 +habove= 0.4u hbelow = 6.24u
 +dn= 1.6199 ds= 1.8127 de= 1.7849 dw= 1.5940 dt= 0.0521 db= 0.0000
 +kmx= 146 kmy= 146 kmz= 170 kild= 1.1 kbulk= 1.1 rho = 2300 cbulk = 710
 isource:ib133 1337 0 idc= 0.6781e-3

ThermalBlock3:b134 1341 1241 1343 1333 1345 6 1347 lx=246.7u ly=261.915u
 +habove= 0.4u hbelow = 6.24u
 +dn= 1.8127 ds= 1.6585 de= 1.1215 dw= 1.7849 dt= 0.0853 db= 0.0000
 +kmx= 146 kmy= 146 kmz= 170 kild= 1.1 kbulk= 1.1 rho = 2300 cbulk = 710
 isource:ib134 1347 0 idc= 0.5689e-3

ThermalBlock3:b135 1351 1251 1353 1343 1355 6 1357 lx=246.7u ly=261.915u
 +habove= 0.4u hbelow = 6.24u
 +dn= 1.8706 ds= 1.6970 de= 2.0666 dw= 1.1215 dt= 0.1138 db= 0.0000
 +kmx= 146 kmy= 146 kmz= 170 kild= 1.1 kbulk= 1.1 rho = 2300 cbulk = 710
 isource:ib135 1357 0 idc= 0.8361e-3

ThermalBlock3:b136 1361 1261 1363 1353 1365 6 1367 lx=246.7u ly=261.915u
 +habove= 0.4u hbelow = 6.24u
 +dn= 1.5524 ds= 1.7260 de= 1.6122 dw= 2.0666 dt= 0.2180 db= 0.0000
 +kmx= 146 kmy= 146 kmz= 170 kild= 1.1 kbulk= 1.1 rho = 2300 cbulk = 710
 isource:ib136 1367 0 idc= 0.8731e-3

ThermalBlock3:b137 1371 1271 1373 1363 1375 6 1377 lx=246.7u ly=261.915u
 +habove= 0.4u hbelow = 6.24u
 +dn= 1.9092 ds= 2.1502 de= 1.9848 dw= 1.6122 dt= 0.0521 db= 0.0000
 +kmx= 146 kmy= 146 kmz= 170 kild= 1.1 kbulk= 1.1 rho = 2300 cbulk = 710
 isource:ib137 1377 0 idc= 0.9202e-3

ThermalBlock3:b138 1381 1281 1383 1373 1385 6 1387 lx=246.7u ly=261.915u
 +habove= 0.4u hbelow = 6.24u
 +dn= 1.8320 ds= 2.0634 de= 1.5213 dw= 1.9848 dt= 0.0569 db= 0.0000
 +kmx= 146 kmy= 146 kmz= 170 kild= 1.1 kbulk= 1.1 rho = 2300 cbulk = 710
 isource:ib138 1387 0 idc= 0.6198e-3

ThermalBlock3:b139 1391 1291 3 1383 1395 6 1397 lx=246.7u ly=261.915u
 +habove= 0.4u hbelow = 6.24u
 +dn= 2.3527 ds= 2.2177 de= 0.0000 dw= 1.5213 dt= 0.0521 db= 0.0000
 +kmx= 146 kmy= 146 kmz= 170 kild= 1.1 kbulk= 1.1 rho = 2300 cbulk = 710
 isource:ib139 1397 0 idc= 0.6497e-3

ThermalBlock3:b140 1401 1301 1403 4 1405 6 1407 lx=246.7u ly=261.915u
 +habove= 0.4u hbelow = 6.24u
 +dn= 1.7452 ds= 2.3527 de= 1.7849 dw= 0.0000 dt= 0.0237 db= 0.0000
 +kmx= 146 kmy= 146 kmz= 170 kild= 1.1 kbulk= 1.1 rho = 2300 cbulk = 710
 isource:ib140 1407 0 idc= 0.7837e-3

ThermalBlock3:b141 1411 1311 1413 1403 1415 6 1417 lx=246.7u ly=261.915u
 +habove= 0.4u hbelow = 6.24u
 +dn= 1.7067 ds= 1.8031 de= 1.7849 dw= 1.7849 dt= 0.1374 db= 0.0000
 +kmx= 146 kmy= 146 kmz= 170 kild= 1.1 kbulk= 1.1 rho = 2300 cbulk = 710
 isource:ib141 1417 0 idc= 0.8654e-3

ThermalBlock3:b142 1421 1321 1423 1413 1425 6 1427 lx=246.7u ly=261.915u
 +habove= 0.4u hbelow = 6.24u
 +dn= 2.1695 ds= 2.1695 de= 2.0030 dw= 1.7849 dt= 0.0521 db= 0.0000
 +kmx= 146 kmy= 146 kmz= 170 kild= 1.1 kbulk= 1.1 rho = 2300 cbulk = 710
 isource:ib142 1427 0 idc= 0.6638e-3

ThermalBlock3:b143 1431 1331 1433 1423 1435 6 1437 lx=246.7u ly=261.915u
 +habove= 0.4u hbelow = 6.24u
 +dn= 1.6392 ds= 1.6199 de= 1.6668 dw= 2.0030 dt= 0.0237 db= 0.0000
 +kmx= 146 kmy= 146 kmz= 170 kild= 1.1 kbulk= 1.1 rho = 2300 cbulk = 710
 isource:ib143 1437 0 idc= 0.7687e-3

ThermalBlock3:b144 1441 1341 1443 1433 1445 6 1447 lx=246.7u ly=261.915u
 +habove= 0.4u hbelow = 6.24u

+dn= 2.2659 ds= 1.8127 de= 1.3941 dw= 1.6668 dt= 0.1848 db= 0.0000
 +kmx= 146 kmy= 146 kmz= 170 kild= 1.1 kbulk= 1.1 rho = 2300 cbulk = 710
 isource:ib144 1447 0 idc= 0.8712e-3

ThermalBlock3:b145 1451 1351 1453 1443 1455 6 1457 lx=246.7u ly=261.915u
 +habove= 0.4u hbelow = 6.24u
 +dn= 2.1695 ds= 1.8706 de= 1.7667 dw= 1.3941 dt= 0.2133 db= 0.0000
 +kmx= 146 kmy= 146 kmz= 170 kild= 1.1 kbulk= 1.1 rho = 2300 cbulk = 710
 isource:ib145 1457 0 idc= 0.7027e-3

ThermalBlock3:b146 1461 1361 1463 1453 1465 6 1467 lx=246.7u ly=261.915u
 +habove= 0.4u hbelow = 6.24u
 +dn= 1.5138 ds= 1.5524 de= 1.5940 dw= 1.7667 dt= 0.2702 db= 0.0000
 +kmx= 146 kmy= 146 kmz= 170 kild= 1.1 kbulk= 1.1 rho = 2300 cbulk = 710
 isource:ib146 1467 0 idc= 0.6726e-3

ThermalBlock3:b147 1471 1371 1473 1463 1475 6 1477 lx=246.7u ly=261.915u
 +habove= 0.4u hbelow = 6.24u
 +dn= 1.6681 ds= 1.9092 de= 1.6304 dw= 1.5940 dt= 0.0995 db= 0.0000
 +kmx= 146 kmy= 146 kmz= 170 kild= 1.1 kbulk= 1.1 rho = 2300 cbulk = 710
 isource:ib147 1477 0 idc= 0.6056e-3

ThermalBlock3:b148 1481 1381 1483 1473 1485 6 1487 lx=246.7u ly=261.915u
 +habove= 0.4u hbelow = 6.24u
 +dn= 1.9284 ds= 1.8320 de= 1.4305 dw= 1.6304 dt= 0.0711 db= 0.0000
 +kmx= 146 kmy= 146 kmz= 170 kild= 1.1 kbulk= 1.1 rho = 2300 cbulk = 710
 isource:ib148 1487 0 idc= 0.1874e-3

ThermalBlock3:b149 1491 1391 3 1483 1495 6 1497 lx=246.7u ly=261.915u
 +habove= 0.4u hbelow = 6.24u
 +dn= 2.7191 ds= 2.3527 de= 0.0000 dw= 1.4305 dt= 0.1517 db= 0.0000
 +kmx= 146 kmy= 146 kmz= 170 kild= 1.1 kbulk= 1.1 rho = 2300 cbulk = 710
 isource:ib149 1497 0 idc= 0.3512e-3

ThermalBlock3:b150 1501 1401 1503 4 1505 6 1507 lx=246.7u ly=261.915u
 +habove= 0.4u hbelow = 6.24u
 +dn= 2.5455 ds= 1.7452 de= 1.5032 dw= 0.0000 dt= 0.0190 db= 0.0000
 +kmx= 146 kmy= 146 kmz= 170 kild= 1.1 kbulk= 1.1 rho = 2300 cbulk = 710
 isource:ib150 1507 0 idc= 0.7049e-3

ThermalBlock3:b151 1511 1411 1513 1503 1515 6 1517 lx=246.7u ly=261.915u
 +habove= 0.4u hbelow = 6.24u
 +dn= 2.1309 ds= 1.7067 de= 1.8758 dw= 1.5032 dt= 0.1848 db= 0.0000
 +kmx= 146 kmy= 146 kmz= 170 kild= 1.1 kbulk= 1.1 rho = 2300 cbulk = 710

isource:ib151 1517 0 idc= 0.6487e-3

ThermalBlock3:b152 1521 1421 1523 1513 1525 6 1527 lx=246.7u ly=261.915u
 +habove= 0.4u hbelow = 6.24u
 +dn= 2.0249 ds= 2.1695 de= 1.7122 dw= 1.8758 dt= 0.1185 db= 0.0000
 +kmx= 146 kmy= 146 kmz= 170 kild= 1.1 kbulk= 1.1 rho = 2300 cbulk = 710
 isource:ib152 1527 0 idc= 0.7707e-3

ThermalBlock3:b153 1531 1431 1533 1523 1535 6 1537 lx=246.7u ly=261.915u
 +habove= 0.4u hbelow = 6.24u
 +dn= 1.9477 ds= 1.6392 de= 1.9394 dw= 1.7122 dt= 0.0332 db= 0.0000
 +kmx= 146 kmy= 146 kmz= 170 kild= 1.1 kbulk= 1.1 rho = 2300 cbulk = 710
 isource:ib153 1537 0 idc= 0.8873e-3

ThermalBlock3:b154 1541 1441 1543 1533 1545 6 1547 lx=246.7u ly=261.915u
 +habove= 0.4u hbelow = 6.24u
 +dn= 2.2466 ds= 2.2659 de= 1.3396 dw= 1.9394 dt= 0.1991 db= 0.0000
 +kmx= 146 kmy= 146 kmz= 170 kild= 1.1 kbulk= 1.1 rho = 2300 cbulk = 710
 isource:ib154 1547 0 idc= 0.5716e-3

ThermalBlock3:b155 1551 1451 1553 1543 1555 6 1557 lx=246.7u ly=261.915u
 +habove= 0.4u hbelow = 6.24u
 +dn= 2.3334 ds= 2.1695 de= 1.8667 dw= 1.3396 dt= 0.2228 db= 0.0000
 +kmx= 146 kmy= 146 kmz= 170 kild= 1.1 kbulk= 1.1 rho = 2300 cbulk = 710
 isource:ib155 1557 0 idc= 0.6298e-3

ThermalBlock3:b156 1561 1461 1563 1553 1565 6 1567 lx=246.7u ly=261.915u
 +habove= 0.4u hbelow = 6.24u
 +dn= 1.7742 ds= 1.5138 de= 1.3668 dw= 1.8667 dt= 0.1943 db= 0.0000
 +kmx= 146 kmy= 146 kmz= 170 kild= 1.1 kbulk= 1.1 rho = 2300 cbulk = 710
 isource:ib156 1567 0 idc= 1.1627e-3

ThermalBlock3:b157 1571 1471 1573 1563 1575 6 1577 lx=246.7u ly=261.915u
 +habove= 0.4u hbelow = 6.24u
 +dn= 1.9188 ds= 1.6681 de= 1.4759 dw= 1.3668 dt= 0.0427 db= 0.0000
 +kmx= 146 kmy= 146 kmz= 170 kild= 1.1 kbulk= 1.1 rho = 2300 cbulk = 710
 isource:ib157 1577 0 idc= 0.7054e-3

ThermalBlock3:b158 1581 1481 1583 1573 1585 6 1587 lx=246.7u ly=261.915u
 +habove= 0.4u hbelow = 6.24u
 +dn= 2.0152 ds= 1.9284 de= 1.5304 dw= 1.4759 dt= 0.0853 db= 0.0000
 +kmx= 146 kmy= 146 kmz= 170 kild= 1.1 kbulk= 1.1 rho = 2300 cbulk = 710
 isource:ib158 1587 0 idc= 0.2670e-3

ThermalBlock3:b159 1591 1491 3 1583 1595 6 1597 lx=246.7u ly=261.915u
+habove= 0.4u hbelow = 6.24u
+dn= 2.7962 ds= 2.7191 de= 0.0000 dw= 1.5304 dt= 0.0427 db= 0.0000
+kmx= 146 kmy= 146 kmz= 170 kild= 1.1 kbulk= 1.1 rho = 2300 cbulk = 710
isource:ib159 1597 0 idc= 0.2224e-3

ThermalBlock3:b160 1601 1501 1603 4 1605 6 1607 lx=246.7u ly=261.915u
+habove= 0.4u hbelow = 6.24u
+dn= 2.3816 ds= 2.5455 de= 1.5850 dw= 0.0000 dt= 0.0284 db= 0.0000
+kmx= 146 kmy= 146 kmz= 170 kild= 1.1 kbulk= 1.1 rho = 2300 cbulk = 710
isource:ib160 1607 0 idc= 0.8160e-3

ThermalBlock3:b161 1611 1511 1613 1603 1615 6 1617 lx=246.7u ly=261.915u
+habove= 0.4u hbelow = 6.24u
+dn= 2.1020 ds= 2.1309 de= 1.9576 dw= 1.5850 dt= 0.1138 db= 0.0000
+kmx= 146 kmy= 146 kmz= 170 kild= 1.1 kbulk= 1.1 rho = 2300 cbulk = 710
isource:ib161 1617 0 idc= 0.8576e-3

ThermalBlock3:b162 1621 1521 1623 1613 1625 6 1627 lx=246.7u ly=261.915u
+habove= 0.4u hbelow = 6.24u
+dn= 2.1213 ds= 2.0249 de= 1.7395 dw= 1.9576 dt= 0.0853 db= 0.0000
+kmx= 146 kmy= 146 kmz= 170 kild= 1.1 kbulk= 1.1 rho = 2300 cbulk = 710
isource:ib162 1627 0 idc= 0.8939e-3

ThermalBlock3:b163 1631 1531 1633 1623 1635 6 1637 lx=246.7u ly=261.915u
+habove= 0.4u hbelow = 6.24u
+dn= 1.8031 ds= 1.9477 de= 1.9303 dw= 1.7395 dt= 0.0379 db= 0.0000
+kmx= 146 kmy= 146 kmz= 170 kild= 1.1 kbulk= 1.1 rho = 2300 cbulk = 710
isource:ib163 1637 0 idc= 1.3748e-3

ThermalBlock3:b164 1641 1541 1643 1633 1645 6 1647 lx=246.7u ly=261.915u
+habove= 0.4u hbelow = 6.24u
+dn= 2.0538 ds= 2.2466 de= 1.6940 dw= 1.9303 dt= 0.1185 db= 0.0000
+kmx= 146 kmy= 146 kmz= 170 kild= 1.1 kbulk= 1.1 rho = 2300 cbulk = 710
isource:ib164 1647 0 idc= 0.7110e-3

ThermalBlock3:b165 1651 1551 1653 1643 1655 6 1657 lx=246.7u ly=261.915u
+habove= 0.4u hbelow = 6.24u
+dn= 1.9092 ds= 2.3334 de= 1.9121 dw= 1.6940 dt= 0.2417 db= 0.0000
+kmx= 146 kmy= 146 kmz= 170 kild= 1.1 kbulk= 1.1 rho = 2300 cbulk = 710
isource:ib165 1657 0 idc= 0.5971e-3

ThermalBlock3:b166 1661 1561 1663 1653 1665 6 1667 lx=246.7u ly=261.915u
+habove= 0.4u hbelow = 6.24u

+dn= 1.9670 ds= 1.7742 de= 1.3123 dw= 1.9121 dt= 0.0806 db= 0.0000
 +kmx= 146 kmy= 146 kmz= 170 kild= 1.1 kbulk= 1.1 rho = 2300 cbulk = 710
 isource:ib166 1667 0 idc= 0.9792e-3

ThermalBlock3:b167 1671 1571 1673 1663 1675 6 1677 lx=246.7u ly=261.915u
 +habove= 0.4u hbelow = 6.24u
 +dn= 1.9959 ds= 1.9188 de= 1.2305 dw= 1.3123 dt= 0.0427 db= 0.0000
 +kmx= 146 kmy= 146 kmz= 170 kild= 1.1 kbulk= 1.1 rho = 2300 cbulk = 710
 isource:ib167 1677 0 idc= 1.2196e-3

ThermalBlock3:b168 1681 1581 1683 1673 1685 6 1687 lx=246.7u ly=261.915u
 +habove= 0.4u hbelow = 6.24u
 +dn= 1.7549 ds= 2.0152 de= 1.4396 dw= 1.2305 dt= 0.0521 db= 0.0000
 +kmx= 146 kmy= 146 kmz= 170 kild= 1.1 kbulk= 1.1 rho = 2300 cbulk = 710
 isource:ib168 1687 0 idc= 0.6434e-3

ThermalBlock3:b169 1691 1591 3 1683 1695 6 1697 lx=246.7u ly=261.915u
 +habove= 0.4u hbelow = 6.24u
 +dn= 2.1406 ds= 2.7962 de= 0.0000 dw= 1.4396 dt= 0.0332 db= 0.0000
 +kmx= 146 kmy= 146 kmz= 170 kild= 1.1 kbulk= 1.1 rho = 2300 cbulk = 710
 isource:ib169 1697 0 idc= 0.3955e-3

ThermalBlock3:b170 1701 1601 1703 4 1705 6 1707 lx=246.7u ly=261.915u
 +habove= 0.4u hbelow = 6.24u
 +dn= 2.6130 ds= 2.3816 de= 1.3578 dw= 0.0000 dt= 0.0427 db= 0.0000
 +kmx= 146 kmy= 146 kmz= 170 kild= 1.1 kbulk= 1.1 rho = 2300 cbulk = 710
 isource:ib170 1707 0 idc= 0.7344e-3

ThermalBlock3:b171 1711 1611 1713 1703 1715 6 1717 lx=246.7u ly=261.915u
 +habove= 0.4u hbelow = 6.24u
 +dn= 1.9188 ds= 2.1020 de= 1.9212 dw= 1.3578 dt= 0.0284 db= 0.0000
 +kmx= 146 kmy= 146 kmz= 170 kild= 1.1 kbulk= 1.1 rho = 2300 cbulk = 710
 isource:ib171 1717 0 idc= 0.9756e-3

ThermalBlock3:b172 1721 1621 1723 1713 1725 6 1727 lx=246.7u ly=261.915u
 +habove= 0.4u hbelow = 6.24u
 +dn= 2.0249 ds= 2.1213 de= 1.7485 dw= 1.9212 dt= 0.0332 db= 0.0000
 +kmx= 146 kmy= 146 kmz= 170 kild= 1.1 kbulk= 1.1 rho = 2300 cbulk = 710
 isource:ib172 1727 0 idc= 1.0033e-3

ThermalBlock3:b173 1731 1631 1733 1723 1735 6 1737 lx=246.7u ly=261.915u
 +habove= 0.4u hbelow = 6.24u
 +dn= 2.0442 ds= 1.8031 de= 1.7667 dw= 1.7485 dt= 0.0284 db= 0.0000
 +kmx= 146 kmy= 146 kmz= 170 kild= 1.1 kbulk= 1.1 rho = 2300 cbulk = 710

isource:ib173 1737 0 idc= 1.1193e-3

ThermalBlock3:b174 1741 1641 1743 1733 1745 6 1747 lx=246.7u ly=261.915u
 +habove= 0.4u hbelow = 6.24u
 +dn= 2.2370 ds= 2.0538 de= 1.7304 dw= 1.7667 dt= 0.1138 db= 0.0000
 +kmx= 146 kmy= 146 kmz= 170 kild= 1.1 kbulk= 1.1 rho = 2300 cbulk = 710
 isource:ib174 1747 0 idc= 1.1893e-3

ThermalBlock3:b175 1751 1651 1753 1743 1755 6 1757 lx=246.7u ly=261.915u
 +habove= 0.4u hbelow = 6.24u
 +dn= 2.0056 ds= 1.9092 de= 1.5850 dw= 1.7304 dt= 0.1564 db= 0.0000
 +kmx= 146 kmy= 146 kmz= 170 kild= 1.1 kbulk= 1.1 rho = 2300 cbulk = 710
 isource:ib175 1757 0 idc= 1.2210e-3

ThermalBlock3:b176 1761 1661 1763 1753 1765 6 1767 lx=246.7u ly=261.915u
 +habove= 0.4u hbelow = 6.24u
 +dn= 1.7260 ds= 1.9670 de= 1.3305 dw= 1.5850 dt= 0.0190 db= 0.0000
 +kmx= 146 kmy= 146 kmz= 170 kild= 1.1 kbulk= 1.1 rho = 2300 cbulk = 710
 isource:ib176 1767 0 idc= 0.9869e-3

ThermalBlock3:b177 1771 1671 1773 1763 1775 6 1777 lx=246.7u ly=261.915u
 +habove= 0.4u hbelow = 6.24u
 +dn= 2.0538 ds= 1.9959 de= 1.5759 dw= 1.3305 dt= 0.0284 db= 0.0000
 +kmx= 146 kmy= 146 kmz= 170 kild= 1.1 kbulk= 1.1 rho = 2300 cbulk = 710
 isource:ib177 1777 0 idc= 0.8777e-3

ThermalBlock3:b178 1781 1681 1783 1773 1785 6 1787 lx=246.7u ly=261.915u
 +habove= 0.4u hbelow = 6.24u
 +dn= 1.8802 ds= 1.7549 de= 1.1487 dw= 1.5759 dt= 0.0190 db= 0.0000
 +kmx= 146 kmy= 146 kmz= 170 kild= 1.1 kbulk= 1.1 rho = 2300 cbulk = 710
 isource:ib178 1787 0 idc= 1.0280e-3

ThermalBlock3:b179 1791 1691 3 1783 1795 6 1797 lx=246.7u ly=261.915u
 +habove= 0.4u hbelow = 6.24u
 +dn= 2.7288 ds= 2.1406 de= 0.0000 dw= 1.1487 dt= 0.0190 db= 0.0000
 +kmx= 146 kmy= 146 kmz= 170 kild= 1.1 kbulk= 1.1 rho = 2300 cbulk = 710
 isource:ib179 1797 0 idc= 0.9841e-3

ThermalBlock3:b180 1801 1701 1803 4 1805 6 1807 lx=246.7u ly=261.915u
 +habove= 0.4u hbelow = 6.24u
 +dn= 2.5841 ds= 2.6130 de= 1.2469 dw= 0.0000 dt= 0.0190 db= 0.0000
 +kmx= 146 kmy= 146 kmz= 170 kild= 1.1 kbulk= 1.1 rho = 2300 cbulk = 710
 isource:ib180 1807 0 idc= 0.6427e-3

ThermalBlock3:b181 1811 1711 1813 1803 1815 6 1817 lx=246.7u ly=261.915u
 +habove= 0.4u hbelow = 6.24u
 +dn= 1.7067 ds= 1.9188 de= 1.6740 dw= 1.2469 dt= 0.0190 db= 0.0000
 +kmx= 146 kmy= 146 kmz= 170 kild= 1.1 kbulk= 1.1 rho = 2300 cbulk = 710
 isource:ib181 1817 0 idc= 0.9570e-3

ThermalBlock3:b182 1821 1721 1823 1813 1825 6 1827 lx=246.7u ly=261.915u
 +habove= 0.4u hbelow = 6.24u
 +dn= 2.0442 ds= 2.0249 de= 1.2469 dw= 1.6740 dt= 0.0427 db= 0.0000
 +kmx= 146 kmy= 146 kmz= 170 kild= 1.1 kbulk= 1.1 rho = 2300 cbulk = 710
 isource:ib182 1827 0 idc= 0.9458e-3

ThermalBlock3:b183 1831 1731 1833 1823 1835 6 1837 lx=246.7u ly=261.915u
 +habove= 0.4u hbelow = 6.24u
 +dn= 1.5813 ds= 2.0442 de= 1.6377 dw= 1.2469 dt= 0.0284 db= 0.0000
 +kmx= 146 kmy= 146 kmz= 170 kild= 1.1 kbulk= 1.1 rho = 2300 cbulk = 710
 isource:ib183 1837 0 idc= 1.1265e-3

ThermalBlock3:b184 1841 1741 1843 1833 1845 6 1847 lx=246.7u ly=261.915u
 +habove= 0.4u hbelow = 6.24u
 +dn= 2.0924 ds= 2.2370 de= 1.6740 dw= 1.6377 dt= 0.0427 db= 0.0000
 +kmx= 146 kmy= 146 kmz= 170 kild= 1.1 kbulk= 1.1 rho = 2300 cbulk = 710
 isource:ib184 1847 0 idc= 1.0444e-3

ThermalBlock3:b185 1851 1751 1853 1843 1855 6 1857 lx=246.7u ly=261.915u
 +habove= 0.4u hbelow = 6.24u
 +dn= 1.9477 ds= 2.0056 de= 1.6104 dw= 1.6740 dt= 0.0379 db= 0.0000
 +kmx= 146 kmy= 146 kmz= 170 kild= 1.1 kbulk= 1.1 rho = 2300 cbulk = 710
 isource:ib185 1857 0 idc= 0.9061e-3

ThermalBlock3:b186 1861 1761 1863 1853 1865 6 1867 lx=246.7u ly=261.915u
 +habove= 0.4u hbelow = 6.24u
 +dn= 1.9574 ds= 1.7260 de= 1.1560 dw= 1.6104 dt= 0.0237 db= 0.0000
 +kmx= 146 kmy= 146 kmz= 170 kild= 1.1 kbulk= 1.1 rho = 2300 cbulk = 710
 isource:ib186 1867 0 idc= 0.6226e-3

ThermalBlock3:b187 1871 1771 1873 1863 1875 6 1877 lx=246.7u ly=261.915u
 +habove= 0.4u hbelow = 6.24u
 +dn= 2.1791 ds= 2.0538 de= 2.0285 dw= 1.1560 dt= 0.0284 db= 0.0000
 +kmx= 146 kmy= 146 kmz= 170 kild= 1.1 kbulk= 1.1 rho = 2300 cbulk = 710
 isource:ib187 1877 0 idc= 1.2216e-3

ThermalBlock3:b188 1881 1781 1883 1873 1885 6 1887 lx=246.7u ly=261.915u
 +habove= 0.4u hbelow = 6.24u

+dn= 1.8127 ds= 1.8802 de= 1.3923 dw= 2.0285 dt= 0.0190 db= 0.0000
 +kmx= 146 kmy= 146 kmz= 170 kild= 1.1 kbulk= 1.1 rho = 2300 cbulk = 710
 isource:ib188 1887 0 idc= 1.0037e-3

ThermalBlock3:b189 1891 1791 3 1883 1895 6 1897 lx=246.7u ly=261.915u
 +habove= 0.4u hbelow = 6.24u
 +dn= 2.6130 ds= 2.7288 de= 0.0000 dw= 1.3923 dt= 0.0190 db= 0.0000
 +kmx= 146 kmy= 146 kmz= 170 kild= 1.1 kbulk= 1.1 rho = 2300 cbulk = 710
 isource:ib189 1897 0 idc= 0.6130e-3

ThermalBlock3:b190 1 1801 1903 4 1905 6 1907 lx=246.7u ly=261.915u
 +habove= 0.4u hbelow = 6.24u
 +dn= 0.0000 ds= 2.5841 de= 1.2941 dw= 0.0000 dt= 0.0000 db= 0.0000
 +kmx= 146 kmy= 146 kmz= 170 kild= 1.1 kbulk= 1.1 rho = 2300 cbulk = 710
 isource:ib190 1907 0 idc= 0.2720e-3

ThermalBlock3:b191 1 1811 1913 1903 1915 6 1917 lx=246.7u ly=261.915u
 +habove= 0.4u hbelow = 6.24u
 +dn= 0.0000 ds= 1.7067 de= 1.5123 dw= 1.2941 dt= 0.0047 db= 0.0000
 +kmx= 146 kmy= 146 kmz= 170 kild= 1.1 kbulk= 1.1 rho = 2300 cbulk = 710
 isource:ib191 1917 0 idc= 0.3363e-3

ThermalBlock3:b192 1 1821 1923 1913 1925 6 1927 lx=246.7u ly=261.915u
 +habove= 0.4u hbelow = 6.24u
 +dn= 0.0000 ds= 2.0442 de= 1.6395 dw= 1.5123 dt= 0.0000 db= 0.0000
 +kmx= 146 kmy= 146 kmz= 170 kild= 1.1 kbulk= 1.1 rho = 2300 cbulk = 710
 isource:ib192 1927 0 idc= 0.4773e-3

ThermalBlock3:b193 1 1831 1933 1923 1935 6 1937 lx=246.7u ly=261.915u
 +habove= 0.4u hbelow = 6.24u
 +dn= 0.0000 ds= 1.5813 de= 1.4123 dw= 1.6395 dt= 0.0047 db= 0.0000
 +kmx= 146 kmy= 146 kmz= 170 kild= 1.1 kbulk= 1.1 rho = 2300 cbulk = 710
 isource:ib193 1937 0 idc= 0.4779e-3

ThermalBlock3:b194 1 1841 1943 1933 1945 6 1947 lx=246.7u ly=261.915u
 +habove= 0.4u hbelow = 6.24u
 +dn= 0.0000 ds= 2.0924 de= 1.5213 dw= 1.4123 dt= 0.0000 db= 0.0000
 +kmx= 146 kmy= 146 kmz= 170 kild= 1.1 kbulk= 1.1 rho = 2300 cbulk = 710
 isource:ib194 1947 0 idc= 0.4513e-3

ThermalBlock3:b195 1 1851 1953 1943 1955 6 1957 lx=246.7u ly=261.915u
 +habove= 0.4u hbelow = 6.24u
 +dn= 0.0000 ds= 1.9477 de= 2.1848 dw= 1.5213 dt= 0.0142 db= 0.0000
 +kmx= 146 kmy= 146 kmz= 170 kild= 1.1 kbulk= 1.1 rho = 2300 cbulk = 710

isource:ib195 1957 0 idc= 0.1748e-3

ThermalBlock3:b196 1 1861 1963 1953 1965 6 1967 lx=246.7u ly=261.915u
 +habove= 0.4u hbelow = 6.24u
 +dn= 0.0000 ds= 1.9574 de= 1.7849 dw= 2.1848 dt= 0.0000 db= 0.0000
 +kmx= 146 kmy= 146 kmz= 170 kild= 1.1 kbulk= 1.1 rho = 2300 cbulk = 710
 isource:ib196 1967 0 idc= 0.2116e-3

ThermalBlock3:b197 1 1871 1973 1963 1975 6 1977 lx=246.7u ly=261.915u
 +habove= 0.4u hbelow = 6.24u
 +dn= 0.0000 ds= 2.1791 de= 1.6849 dw= 1.7849 dt= 0.0000 db= 0.0000
 +kmx= 146 kmy= 146 kmz= 170 kild= 1.1 kbulk= 1.1 rho = 2300 cbulk = 710
 isource:ib197 1977 0 idc= 0.3539e-3

ThermalBlock3:b198 1 1881 1983 1973 1985 6 1987 lx=246.7u ly=261.915u
 +habove= 0.4u hbelow = 6.24u
 +dn= 0.0000 ds= 1.8127 de= 1.2669 dw= 1.6849 dt= 0.0000 db= 0.0000
 +kmx= 146 kmy= 146 kmz= 170 kild= 1.1 kbulk= 1.1 rho = 2300 cbulk = 710
 isource:ib198 1987 0 idc= 0.3644e-3

ThermalBlock3:b199 1 1891 3 1983 1995 6 1997 lx=246.7u ly=261.915u
 +habove= 0.4u hbelow = 6.24u
 +dn= 0.0000 ds= 2.6130 de= 0.0000 dw= 1.2669 dt= 0.0000 db= 0.0000
 +kmx= 146 kmy= 146 kmz= 170 kild= 1.1 kbulk= 1.1 rho = 2300 cbulk = 710
 isource:ib199 1997 0 idc= 0.2031e-3

*Tier 2

ThermalBlock3:b200 2001 2 2003 4 2005 1005 2007 lx=246.7u ly=261.915u
 +habove= 1.35u hbelow = 6.24u
 +dn= 1.8811 ds= 0.0000 de= 2.1069 dw= 0.0000 dt= 0.0000 db= 0.0000
 +kmx= 146 kmy= 146 kmz= 170 kild= 1.1 kbulk= 1.1 rho = 2300 cbulk = 710
 isource:ib200 2007 0 idc= 0.7441e-3

ThermalBlock3:b201 2011 2 2013 2003 2015 1015 2017 lx=246.7u ly=261.915u
 +habove= 1.35u hbelow = 6.24u
 +dn= 1.4593 ds= 0.0000 de= 1.8922 dw= 2.1069 dt= 0.0000 db= 0.0000
 +kmx= 146 kmy= 146 kmz= 170 kild= 1.1 kbulk= 1.1 rho = 2300 cbulk = 710
 isource:ib201 2017 0 idc= 0.7650e-3

ThermalBlock3:b202 2021 2 2023 2013 2025 1025 2027 lx=246.7u ly=261.915u
 +habove= 1.35u hbelow = 6.24u
 +dn= 1.4171 ds= 0.0000 de= 2.3693 dw= 1.8922 dt= 0.0095 db= 0.0332
 +kmx= 146 kmy= 146 kmz= 170 kild= 1.1 kbulk= 1.1 rho = 2300 cbulk = 710

isource:ib202 2027 0 idc= 0.5712e-3

ThermalBlock3:b203 2031 2 2033 2023 2035 1035 2037 lx=246.7u ly=261.915u
 +habove= 1.35u hbelow = 6.24u
 +dn= 1.2906 ds= 0.0000 de= 1.9479 dw= 2.3693 dt= 0.0095 db= 0.0474
 +kmx= 146 kmy= 146 kmz= 170 kild= 1.1 kbulk= 1.1 rho = 2300 cbulk = 710
 isource:ib203 2037 0 idc= 0.4179e-3

ThermalBlock3:b204 2041 2 2043 2033 2045 1045 2047 lx=246.7u ly=261.915u
 +habove= 1.35u hbelow = 6.24u
 +dn= 1.2990 ds= 0.0000 de= 1.9081 dw= 1.9479 dt= 0.0237 db= 0.0995
 +kmx= 146 kmy= 146 kmz= 170 kild= 1.1 kbulk= 1.1 rho = 2300 cbulk = 710
 isource:ib204 2047 0 idc= 0.7104e-3

ThermalBlock3:b205 2051 2 2053 2043 2055 1055 2057 lx=246.7u ly=261.915u
 +habove= 1.35u hbelow = 6.24u
 +dn= 1.3665 ds= 0.0000 de= 2.2421 dw= 1.9081 dt= 0.1043 db= 0.3128
 +kmx= 146 kmy= 146 kmz= 170 kild= 1.1 kbulk= 1.1 rho = 2300 cbulk = 710
 isource:ib205 2057 0 idc= 0.7558e-3

ThermalBlock3:b206 2061 2 2063 2053 2065 1065 2067 lx=246.7u ly=261.915u
 +habove= 1.35u hbelow = 6.24u
 +dn= 1.1810 ds= 0.0000 de= 2.4170 dw= 2.2421 dt= 0.0190 db= 0.0521
 +kmx= 146 kmy= 146 kmz= 170 kild= 1.1 kbulk= 1.1 rho = 2300 cbulk = 710
 isource:ib206 2067 0 idc= 0.5940e-3

ThermalBlock3:b207 2071 2 2073 2063 2075 1075 2077 lx=246.7u ly=261.915u
 +habove= 1.35u hbelow = 6.24u
 +dn= 1.4256 ds= 0.0000 de= 1.7253 dw= 2.4170 dt= 0.0237 db= 0.0664
 +kmx= 146 kmy= 146 kmz= 170 kild= 1.1 kbulk= 1.1 rho = 2300 cbulk = 710
 isource:ib207 2077 0 idc= 0.5432e-3

ThermalBlock3:b208 2081 2 2083 2073 2085 1085 2087 lx=246.7u ly=261.915u
 +habove= 1.35u hbelow = 6.24u
 +dn= 1.4171 ds= 0.0000 de= 1.8286 dw= 1.7253 dt= 0.1138 db= 0.2275
 +kmx= 146 kmy= 146 kmz= 170 kild= 1.1 kbulk= 1.1 rho = 2300 cbulk = 710
 isource:ib208 2087 0 idc= 0.2432e-3

ThermalBlock3:b209 2091 2 3 2083 2095 1095 2097 lx=246.7u ly=261.915u
 +habove= 1.35u hbelow = 6.24u
 +dn= 1.7799 ds= 0.0000 de= 0.0000 dw= 1.8286 dt= 0.0000 db= 0.0000
 +kmx= 146 kmy= 146 kmz= 170 kild= 1.1 kbulk= 1.1 rho = 2300 cbulk = 710
 isource:ib209 2097 0 idc= 0.2361e-3

ThermalBlock3:b210 2101 2001 2103 4 2105 1105 2107 lx=246.7u ly=261.915u
+habove= 1.35u hbelow = 6.24u
+dn= 1.8642 ds= 1.8811 de= 1.2673 dw= 0.0000 dt= 0.0379 db= 0.0758
+kmx= 146 kmy= 146 kmz= 170 kild= 1.1 kbulk= 1.1 rho = 2300 cbulk = 710
isource:ib210 2107 0 idc= 0.5772e-3

ThermalBlock3:b211 2111 2011 2113 2103 2115 1115 2117 lx=246.7u ly=261.915u
+habove= 1.35u hbelow = 6.24u
+dn= 1.1556 ds= 1.4593 de= 1.5853 dw= 1.2673 dt= 0.0427 db= 0.1611
+kmx= 146 kmy= 146 kmz= 170 kild= 1.1 kbulk= 1.1 rho = 2300 cbulk = 710
isource:ib211 2117 0 idc= 0.6462e-3

ThermalBlock3:b212 2121 2021 2123 2113 2125 1125 2127 lx=246.7u ly=261.915u
+habove= 1.35u hbelow = 6.24u
+dn= 1.4509 ds= 1.4171 de= 1.6410 dw= 1.5853 dt= 0.0474 db= 0.2275
+kmx= 146 kmy= 146 kmz= 170 kild= 1.1 kbulk= 1.1 rho = 2300 cbulk = 710
isource:ib212 2127 0 idc= 0.8379e-3

ThermalBlock3:b213 2131 2031 2133 2123 2135 1135 2137 lx=246.7u ly=261.915u
+habove= 1.35u hbelow = 6.24u
+dn= 1.0713 ds= 1.2906 de= 1.4740 dw= 1.6410 dt= 0.0521 db= 0.4503
+kmx= 146 kmy= 146 kmz= 170 kild= 1.1 kbulk= 1.1 rho = 2300 cbulk = 710
isource:ib213 2137 0 idc= 0.6563e-3

ThermalBlock3:b214 2141 2041 2143 2133 2145 1145 2147 lx=246.7u ly=261.915u
+habove= 1.35u hbelow = 6.24u
+dn= 1.2063 ds= 1.2990 de= 1.3786 dw= 1.4740 dt= 0.0853 db= 0.4645
+kmx= 146 kmy= 146 kmz= 170 kild= 1.1 kbulk= 1.1 rho = 2300 cbulk = 710
isource:ib214 2147 0 idc= 0.9588e-3

ThermalBlock3:b215 2151 2051 2153 2143 2155 1155 2157 lx=246.7u ly=261.915u
+habove= 1.35u hbelow = 6.24u
+dn= 1.3412 ds= 1.3665 de= 1.5456 dw= 1.3786 dt= 0.0995 db= 0.4882
+kmx= 146 kmy= 146 kmz= 170 kild= 1.1 kbulk= 1.1 rho = 2300 cbulk = 710
isource:ib215 2157 0 idc= 1.0471e-3

ThermalBlock3:b216 2161 2061 2163 2153 2165 1165 2167 lx=246.7u ly=261.915u
+habove= 1.35u hbelow = 6.24u
+dn= 1.4256 ds= 1.1810 de= 1.3230 dw= 1.5456 dt= 0.1517 db= 0.4977
+kmx= 146 kmy= 146 kmz= 170 kild= 1.1 kbulk= 1.1 rho = 2300 cbulk = 710
isource:ib216 2167 0 idc= 0.7942e-3

ThermalBlock3:b217 2171 2071 2173 2163 2175 1175 2177 lx=246.7u ly=261.915u
+habove= 1.35u hbelow = 6.24u

+dn= 1.3665 ds= 1.4256 de= 1.4263 dw= 1.3230 dt= 0.2702 db= 0.7109
 +kmx= 146 kmy= 146 kmz= 170 kild= 1.1 kbulk= 1.1 rho = 2300 cbulk = 710
 isource:ib217 2177 0 idc= 0.8131e-3

ThermalBlock3:b218 2181 2081 2183 2173 2185 1185 2187 lx=246.7u ly=261.915u
 +habove= 1.35u hbelow = 6.24u
 +dn= 1.2906 ds= 1.4171 de= 1.4104 dw= 1.4263 dt= 0.1327 db= 0.4218
 +kmx= 146 kmy= 146 kmz= 170 kild= 1.1 kbulk= 1.1 rho = 2300 cbulk = 710
 isource:ib218 2187 0 idc= 0.4843e-3

ThermalBlock3:b219 2191 2091 3 2183 2195 1195 2197 lx=246.7u ly=261.915u
 +habove= 1.35u hbelow = 6.24u
 +dn= 1.6786 ds= 1.7799 de= 0.0000 dw= 1.4104 dt= 0.0190 db= 0.0379
 +kmx= 146 kmy= 146 kmz= 170 kild= 1.1 kbulk= 1.1 rho = 2300 cbulk = 710
 isource:ib219 2197 0 idc= 0.2137e-3

ThermalBlock3:b220 2201 2101 2203 4 2205 1205 2207 lx=246.7u ly=261.915u
 +habove= 1.35u hbelow = 6.24u
 +dn= 1.8136 ds= 1.8642 de= 1.4327 dw= 0.0000 dt= 0.0237 db= 0.0474
 +kmx= 146 kmy= 146 kmz= 170 kild= 1.1 kbulk= 1.1 rho = 2300 cbulk = 710
 isource:ib220 2207 0 idc= 0.3674e-3

ThermalBlock3:b221 2211 2111 2213 2203 2215 1215 2217 lx=246.7u ly=261.915u
 +habove= 1.35u hbelow = 6.24u
 +dn= 1.6702 ds= 1.1556 de= 1.2816 dw= 1.4327 dt= 0.0190 db= 0.0995
 +kmx= 146 kmy= 146 kmz= 170 kild= 1.1 kbulk= 1.1 rho = 2300 cbulk = 710
 isource:ib221 2217 0 idc= 0.5184e-3

ThermalBlock3:b222 2221 2121 2223 2213 2225 1225 2227 lx=246.7u ly=261.915u
 +habove= 1.35u hbelow = 6.24u
 +dn= 1.5268 ds= 1.4509 de= 1.7030 dw= 1.2816 dt= 0.0237 db= 0.1422
 +kmx= 146 kmy= 146 kmz= 170 kild= 1.1 kbulk= 1.1 rho = 2300 cbulk = 710
 isource:ib222 2227 0 idc= 0.7115e-3

ThermalBlock3:b223 2231 2131 2233 2223 2235 1235 2237 lx=246.7u ly=261.915u
 +habove= 1.35u hbelow = 6.24u
 +dn= 1.6365 ds= 1.0713 de= 1.5917 dw= 1.7030 dt= 0.0332 db= 0.1280
 +kmx= 146 kmy= 146 kmz= 170 kild= 1.1 kbulk= 1.1 rho = 2300 cbulk = 710
 isource:ib223 2237 0 idc= 0.6698e-3

ThermalBlock3:b224 2241 2141 2243 2233 2245 1245 2247 lx=246.7u ly=261.915u
 +habove= 1.35u hbelow = 6.24u
 +dn= 1.6280 ds= 1.2063 de= 1.4406 dw= 1.5917 dt= 0.1659 db= 0.2133
 +kmx= 146 kmy= 146 kmz= 170 kild= 1.1 kbulk= 1.1 rho = 2300 cbulk = 710

isource:ib224 2247 0 idc= 0.8221e-3

ThermalBlock3:b225 2251 2151 2253 2243 2255 1255 2257 lx=246.7u ly=261.915u
 +habove= 1.35u hbelow = 6.24u
 +dn= 1.5943 ds= 1.3412 de= 1.8938 dw= 1.4406 dt= 0.1138 db= 0.3318
 +kmx= 146 kmy= 146 kmz= 170 kild= 1.1 kbulk= 1.1 rho = 2300 cbulk = 710
 isource:ib225 2257 0 idc= 1.0163e-3

ThermalBlock3:b226 2261 2161 2263 2253 2265 1265 2267 lx=246.7u ly=261.915u
 +habove= 1.35u hbelow = 6.24u
 +dn= 1.5015 ds= 1.4256 de= 1.4327 dw= 1.8938 dt= 0.0806 db= 0.3792
 +kmx= 146 kmy= 146 kmz= 170 kild= 1.1 kbulk= 1.1 rho = 2300 cbulk = 710
 isource:ib226 2267 0 idc= 0.7090e-3

ThermalBlock3:b227 2271 2171 2273 2263 2275 1275 2277 lx=246.7u ly=261.915u
 +habove= 1.35u hbelow = 6.24u
 +dn= 1.7714 ds= 1.3665 de= 1.3850 dw= 1.4327 dt= 0.0853 db= 0.2702
 +kmx= 146 kmy= 146 kmz= 170 kild= 1.1 kbulk= 1.1 rho = 2300 cbulk = 710
 isource:ib227 2277 0 idc= 0.5873e-3

ThermalBlock3:b228 2281 2181 2283 2273 2285 1285 2287 lx=246.7u ly=261.915u
 +habove= 1.35u hbelow = 6.24u
 +dn= 1.7377 ds= 1.2906 de= 1.1703 dw= 1.3850 dt= 0.1517 db= 0.2986
 +kmx= 146 kmy= 146 kmz= 170 kild= 1.1 kbulk= 1.1 rho = 2300 cbulk = 710
 isource:ib228 2287 0 idc= 0.2769e-3

ThermalBlock3:b229 2291 2191 3 2283 2295 1295 2297 lx=246.7u ly=261.915u
 +habove= 1.35u hbelow = 6.24u
 +dn= 1.9907 ds= 1.6786 de= 0.0000 dw= 1.1703 dt= 0.0569 db= 0.1138
 +kmx= 146 kmy= 146 kmz= 170 kild= 1.1 kbulk= 1.1 rho = 2300 cbulk = 710
 isource:ib229 2297 0 idc= 0.2252e-3

ThermalBlock3:b230 2301 2201 2303 4 2305 1305 2307 lx=246.7u ly=261.915u
 +habove= 1.35u hbelow = 6.24u
 +dn= 2.3872 ds= 1.8136 de= 1.2912 dw= 0.0000 dt= 0.0190 db= 0.0379
 +kmx= 146 kmy= 146 kmz= 170 kild= 1.1 kbulk= 1.1 rho = 2300 cbulk = 710
 isource:ib230 2307 0 idc= 0.4868e-3

ThermalBlock3:b231 2311 2211 2313 2303 2315 1315 2317 lx=246.7u ly=261.915u
 +habove= 1.35u hbelow = 6.24u
 +dn= 1.8220 ds= 1.6702 de= 1.6092 dw= 1.2912 dt= 0.0664 db= 0.0853
 +kmx= 146 kmy= 146 kmz= 170 kild= 1.1 kbulk= 1.1 rho = 2300 cbulk = 710
 isource:ib231 2317 0 idc= 0.4777e-3

ThermalBlock3:b232 2321 2221 2323 2313 2325 1325 2327 lx=246.7u ly=261.915u
+habove= 1.35u hbelow = 6.24u
+dn= 1.7124 ds= 1.5268 de= 1.8080 dw= 1.6092 dt= 0.0569 db= 0.2275
+kmx= 146 kmy= 146 kmz= 170 kild= 1.1 kbulk= 1.1 rho = 2300 cbulk = 710
isource:ib232 2327 0 idc= 0.6623e-3

ThermalBlock3:b233 2331 2231 2333 2323 2335 1335 2337 lx=246.7u ly=261.915u
+habove= 1.35u hbelow = 6.24u
+dn= 1.3834 ds= 1.6365 de= 1.8477 dw= 1.8080 dt= 0.0521 db= 0.2085
+kmx= 146 kmy= 146 kmz= 170 kild= 1.1 kbulk= 1.1 rho = 2300 cbulk = 710
isource:ib233 2337 0 idc= 0.4997e-3

ThermalBlock3:b234 2341 2241 2343 2333 2345 1345 2347 lx=246.7u ly=261.915u
+habove= 1.35u hbelow = 6.24u
+dn= 1.4003 ds= 1.6280 de= 1.4502 dw= 1.8477 dt= 0.0853 db= 0.1754
+kmx= 146 kmy= 146 kmz= 170 kild= 1.1 kbulk= 1.1 rho = 2300 cbulk = 710
isource:ib234 2347 0 idc= 1.1476e-3

ThermalBlock3:b235 2351 2251 2353 2343 2355 1355 2357 lx=246.7u ly=261.915u
+habove= 1.35u hbelow = 6.24u
+dn= 1.8136 ds= 1.5943 de= 1.7046 dw= 1.4502 dt= 0.1138 db= 0.3507
+kmx= 146 kmy= 146 kmz= 170 kild= 1.1 kbulk= 1.1 rho = 2300 cbulk = 710
isource:ib235 2357 0 idc= 1.0800e-3

ThermalBlock3:b236 2361 2261 2363 2353 2365 1365 2367 lx=246.7u ly=261.915u
+habove= 1.35u hbelow = 6.24u
+dn= 1.1810 ds= 1.5015 de= 1.2594 dw= 1.7046 dt= 0.2180 db= 0.4645
+kmx= 146 kmy= 146 kmz= 170 kild= 1.1 kbulk= 1.1 rho = 2300 cbulk = 710
isource:ib236 2367 0 idc= 0.7025e-3

ThermalBlock3:b237 2371 2271 2373 2363 2375 1375 2377 lx=246.7u ly=261.915u
+habove= 1.35u hbelow = 6.24u
+dn= 1.5690 ds= 1.7714 de= 1.9193 dw= 1.2594 dt= 0.0521 db= 0.1043
+kmx= 146 kmy= 146 kmz= 170 kild= 1.1 kbulk= 1.1 rho = 2300 cbulk = 710
isource:ib237 2377 0 idc= 0.3400e-3

ThermalBlock3:b238 2381 2281 2383 2373 2385 1385 2387 lx=246.7u ly=261.915u
+habove= 1.35u hbelow = 6.24u
+dn= 1.1219 ds= 1.7377 de= 1.3627 dw= 1.9193 dt= 0.0569 db= 0.1138
+kmx= 146 kmy= 146 kmz= 170 kild= 1.1 kbulk= 1.1 rho = 2300 cbulk = 710
isource:ib238 2387 0 idc= 0.2543e-3

ThermalBlock3:b239 2391 2291 3 2383 2395 1395 2397 lx=246.7u ly=261.915u
+habove= 1.35u hbelow = 6.24u

+dn= 1.7799 ds= 1.9907 de= 0.0000 dw= 1.3627 dt= 0.0521 db= 0.1043
+kmx= 146 kmy= 146 kmz= 170 kild= 1.1 kbulk= 1.1 rho = 2300 cbulk = 710
isource:ib239 2397 0 idc= 0.1937e-3

ThermalBlock3:b240 2401 2301 2403 4 2405 1405 2407 lx=246.7u ly=261.915u
+habove= 1.35u hbelow = 6.24u
+dn= 2.4294 ds= 2.3872 de= 1.2753 dw= 0.0000 dt= 0.0237 db= 0.0427
+kmx= 146 kmy= 146 kmz= 170 kild= 1.1 kbulk= 1.1 rho = 2300 cbulk = 710
isource:ib240 2407 0 idc= 0.5441e-3

ThermalBlock3:b241 2411 2311 2413 2403 2415 1415 2417 lx=246.7u ly=261.915u
+habove= 1.35u hbelow = 6.24u
+dn= 2.1341 ds= 1.8220 de= 1.5376 dw= 1.2753 dt= 0.1374 db= 0.1659
+kmx= 146 kmy= 146 kmz= 170 kild= 1.1 kbulk= 1.1 rho = 2300 cbulk = 710
isource:ib241 2417 0 idc= 0.7506e-3

ThermalBlock3:b242 2421 2321 2423 2413 2425 1425 2427 lx=246.7u ly=261.915u
+habove= 1.35u hbelow = 6.24u
+dn= 1.8220 ds= 1.7124 de= 1.6012 dw= 1.5376 dt= 0.0521 db= 0.1232
+kmx= 146 kmy= 146 kmz= 170 kild= 1.1 kbulk= 1.1 rho = 2300 cbulk = 710
isource:ib242 2427 0 idc= 0.4084e-3

ThermalBlock3:b243 2431 2331 2433 2423 2435 1435 2437 lx=246.7u ly=261.915u
+habove= 1.35u hbelow = 6.24u
+dn= 1.4762 ds= 1.3834 de= 1.7682 dw= 1.6012 dt= 0.0237 db= 0.0901
+kmx= 146 kmy= 146 kmz= 170 kild= 1.1 kbulk= 1.1 rho = 2300 cbulk = 710
isource:ib243 2437 0 idc= 0.2644e-3

ThermalBlock3:b244 2441 2341 2443 2433 2445 1445 2447 lx=246.7u ly=261.915u
+habove= 1.35u hbelow = 6.24u
+dn= 1.4340 ds= 1.4003 de= 1.1322 dw= 1.7682 dt= 0.1848 db= 0.2939
+kmx= 146 kmy= 146 kmz= 170 kild= 1.1 kbulk= 1.1 rho = 2300 cbulk = 710
isource:ib244 2447 0 idc= 0.3606e-3

ThermalBlock3:b245 2451 2351 2453 2443 2455 1455 2457 lx=246.7u ly=261.915u
+habove= 1.35u hbelow = 6.24u
+dn= 1.6618 ds= 1.8136 de= 1.9511 dw= 1.1322 dt= 0.2133 db= 0.4740
+kmx= 146 kmy= 146 kmz= 170 kild= 1.1 kbulk= 1.1 rho = 2300 cbulk = 710
isource:ib245 2457 0 idc= 0.3178e-3

ThermalBlock3:b246 2461 2361 2463 2453 2465 1465 2467 lx=246.7u ly=261.915u
+habove= 1.35u hbelow = 6.24u
+dn= 1.8473 ds= 1.1810 de= 1.0447 dw= 1.9511 dt= 0.2702 db= 0.5782
+kmx= 146 kmy= 146 kmz= 170 kild= 1.1 kbulk= 1.1 rho = 2300 cbulk = 710

isource:ib246 2467 0 idc= 0.2646e-3

ThermalBlock3:b247 2471 2371 2473 2463 2475 1475 2477 lx=246.7u ly=261.915u
 +habove= 1.35u hbelow = 6.24u
 +dn= 1.8558 ds= 1.5690 de= 1.8477 dw= 1.0447 dt= 0.0995 db= 0.2038
 +kmx= 146 kmy= 146 kmz= 170 kild= 1.1 kbulk= 1.1 rho = 2300 cbulk = 710
 isource:ib247 2477 0 idc= 0.2364e-3

ThermalBlock3:b248 2481 2381 2483 2473 2485 1485 2487 lx=246.7u ly=261.915u
 +habove= 1.35u hbelow = 6.24u
 +dn= 1.5099 ds= 1.1219 de= 0.9652 dw= 1.8477 dt= 0.0711 db= 0.1469
 +kmx= 146 kmy= 146 kmz= 170 kild= 1.1 kbulk= 1.1 rho = 2300 cbulk = 710
 isource:ib248 2487 0 idc= 0.2488e-3

ThermalBlock3:b249 2491 2391 3 2483 2495 1495 2497 lx=246.7u ly=261.915u
 +habove= 1.35u hbelow = 6.24u
 +dn= 1.5774 ds= 1.7799 de= 0.0000 dw= 0.9652 dt= 0.1517 db= 0.3033
 +kmx= 146 kmy= 146 kmz= 170 kild= 1.1 kbulk= 1.1 rho = 2300 cbulk = 710
 isource:ib249 2497 0 idc= 0.2240e-3

ThermalBlock3:b250 2501 2401 2503 4 2505 1505 2507 lx=246.7u ly=261.915u
 +habove= 1.35u hbelow = 6.24u
 +dn= 2.2607 ds= 2.4294 de= 1.4502 dw= 0.0000 dt= 0.0190 db= 0.0379
 +kmx= 146 kmy= 146 kmz= 170 kild= 1.1 kbulk= 1.1 rho = 2300 cbulk = 710
 isource:ib250 2507 0 idc= 0.5049e-3

ThermalBlock3:b251 2511 2411 2513 2503 2515 1515 2517 lx=246.7u ly=261.915u
 +habove= 1.35u hbelow = 6.24u
 +dn= 1.5521 ds= 2.1341 de= 1.4502 dw= 1.4502 dt= 0.1848 db= 0.3270
 +kmx= 146 kmy= 146 kmz= 170 kild= 1.1 kbulk= 1.1 rho = 2300 cbulk = 710
 isource:ib251 2517 0 idc= 0.4271e-3

ThermalBlock3:b252 2521 2421 2523 2513 2525 1525 2527 lx=246.7u ly=261.915u
 +habove= 1.35u hbelow = 6.24u
 +dn= 1.8895 ds= 1.8220 de= 1.5297 dw= 1.4502 dt= 0.1185 db= 0.2607
 +kmx= 146 kmy= 146 kmz= 170 kild= 1.1 kbulk= 1.1 rho = 2300 cbulk = 710
 isource:ib252 2527 0 idc= 0.3460e-3

ThermalBlock3:b253 2531 2431 2533 2523 2535 1535 2537 lx=246.7u ly=261.915u
 +habove= 1.35u hbelow = 6.24u
 +dn= 1.7546 ds= 1.4762 de= 1.7762 dw= 1.5297 dt= 0.0332 db= 0.0901
 +kmx= 146 kmy= 146 kmz= 170 kild= 1.1 kbulk= 1.1 rho = 2300 cbulk = 710
 isource:ib253 2537 0 idc= 0.2888e-3

ThermalBlock3:b254 2541 2441 2543 2533 2545 1545 2547 lx=246.7u ly=261.915u
 +habove= 1.35u hbelow = 6.24u
 +dn= 1.5268 ds= 1.4340 de= 1.3389 dw= 1.7762 dt= 0.1991 db= 0.2749
 +kmx= 146 kmy= 146 kmz= 170 kild= 1.1 kbulk= 1.1 rho = 2300 cbulk = 710
 isource:ib254 2547 0 idc= 0.4077e-3

ThermalBlock3:b255 2551 2451 2553 2543 2555 1555 2557 lx=246.7u ly=261.915u
 +habove= 1.35u hbelow = 6.24u
 +dn= 1.9486 ds= 1.6618 de= 1.6330 dw= 1.3389 dt= 0.2228 db= 0.4787
 +kmx= 146 kmy= 146 kmz= 170 kild= 1.1 kbulk= 1.1 rho = 2300 cbulk = 710
 isource:ib255 2557 0 idc= 0.3590e-3

ThermalBlock3:b256 2561 2461 2563 2553 2565 1565 2567 lx=246.7u ly=261.915u
 +habove= 1.35u hbelow = 6.24u
 +dn= 1.6112 ds= 1.8473 de= 1.3627 dw= 1.6330 dt= 0.1943 db= 0.3887
 +kmx= 146 kmy= 146 kmz= 170 kild= 1.1 kbulk= 1.1 rho = 2300 cbulk = 710
 isource:ib256 2567 0 idc= 0.2630e-3

ThermalBlock3:b257 2571 2471 2573 2563 2575 1575 2577 lx=246.7u ly=261.915u
 +habove= 1.35u hbelow = 6.24u
 +dn= 1.8052 ds= 1.8558 de= 1.7285 dw= 1.3627 dt= 0.0427 db= 0.0901
 +kmx= 146 kmy= 146 kmz= 170 kild= 1.1 kbulk= 1.1 rho = 2300 cbulk = 710
 isource:ib257 2577 0 idc= 0.3058e-3

ThermalBlock3:b258 2581 2481 2583 2573 2585 1585 2587 lx=246.7u ly=261.915u
 +habove= 1.35u hbelow = 6.24u
 +dn= 1.3244 ds= 1.5099 de= 1.0050 dw= 1.7285 dt= 0.0853 db= 0.1706
 +kmx= 146 kmy= 146 kmz= 170 kild= 1.1 kbulk= 1.1 rho = 2300 cbulk = 710
 isource:ib258 2587 0 idc= 0.2594e-3

ThermalBlock3:b259 2591 2491 3 2583 2595 1595 2597 lx=246.7u ly=261.915u
 +habove= 1.35u hbelow = 6.24u
 +dn= 1.7461 ds= 1.5774 de= 0.0000 dw= 1.0050 dt= 0.0427 db= 0.0901
 +kmx= 146 kmy= 146 kmz= 170 kild= 1.1 kbulk= 1.1 rho = 2300 cbulk = 710
 isource:ib259 2597 0 idc= 0.2656e-3

ThermalBlock3:b260 2601 2501 2603 4 2605 1605 2607 lx=246.7u ly=261.915u
 +habove= 1.35u hbelow = 6.24u
 +dn= 2.0498 ds= 2.2607 de= 1.2912 dw= 0.0000 dt= 0.0284 db= 0.0569
 +kmx= 146 kmy= 146 kmz= 170 kild= 1.1 kbulk= 1.1 rho = 2300 cbulk = 710
 isource:ib260 2607 0 idc= 0.2966e-3

ThermalBlock3:b261 2611 2511 2613 2603 2615 1615 2617 lx=246.7u ly=261.915u
 +habove= 1.35u hbelow = 6.24u

+dn= 1.4424 ds= 1.5521 de= 1.5297 dw= 1.2912 dt= 0.1138 db= 0.1754
 +kmx= 146 kmy= 146 kmz= 170 kild= 1.1 kbulk= 1.1 rho = 2300 cbulk = 710
 isource:ib261 2617 0 idc= 0.2799e-3

ThermalBlock3:b262 2621 2521 2623 2613 2625 1625 2627 lx=246.7u ly=261.915u
 +habove= 1.35u hbelow = 6.24u
 +dn= 1.8052 ds= 1.8895 de= 1.5456 dw= 1.5297 dt= 0.0853 db= 0.1611
 +kmx= 146 kmy= 146 kmz= 170 kild= 1.1 kbulk= 1.1 rho = 2300 cbulk = 710
 isource:ib262 2627 0 idc= 0.4895e-3

ThermalBlock3:b263 2631 2531 2633 2623 2635 1635 2637 lx=246.7u ly=261.915u
 +habove= 1.35u hbelow = 6.24u
 +dn= 1.7292 ds= 1.7546 de= 1.5774 dw= 1.5456 dt= 0.0379 db= 0.0711
 +kmx= 146 kmy= 146 kmz= 170 kild= 1.1 kbulk= 1.1 rho = 2300 cbulk = 710
 isource:ib263 2637 0 idc= 0.3561e-3

ThermalBlock3:b264 2641 2541 2643 2633 2645 1645 2647 lx=246.7u ly=261.915u
 +habove= 1.35u hbelow = 6.24u
 +dn= 1.9486 ds= 1.5268 de= 1.5694 dw= 1.5774 dt= 0.1185 db= 0.1422
 +kmx= 146 kmy= 146 kmz= 170 kild= 1.1 kbulk= 1.1 rho = 2300 cbulk = 710
 isource:ib264 2647 0 idc= 0.7212e-3

ThermalBlock3:b265 2651 2551 2653 2643 2655 1655 2657 lx=246.7u ly=261.915u
 +habove= 1.35u hbelow = 6.24u
 +dn= 1.7124 ds= 1.9486 de= 1.5853 dw= 1.5694 dt= 0.2417 db= 0.4645
 +kmx= 146 kmy= 146 kmz= 170 kild= 1.1 kbulk= 1.1 rho = 2300 cbulk = 710
 isource:ib265 2657 0 idc= 0.6190e-3

ThermalBlock3:b266 2661 2561 2663 2653 2665 1665 2667 lx=246.7u ly=261.915u
 +habove= 1.35u hbelow = 6.24u
 +dn= 1.4256 ds= 1.6112 de= 1.4184 dw= 1.5853 dt= 0.0806 db= 0.1896
 +kmx= 146 kmy= 146 kmz= 170 kild= 1.1 kbulk= 1.1 rho = 2300 cbulk = 710
 isource:ib266 2667 0 idc= 0.3664e-3

ThermalBlock3:b267 2671 2571 2673 2663 2675 1675 2677 lx=246.7u ly=261.915u
 +habove= 1.35u hbelow = 6.24u
 +dn= 1.8220 ds= 1.8052 de= 1.8398 dw= 1.4184 dt= 0.0427 db= 0.0853
 +kmx= 146 kmy= 146 kmz= 170 kild= 1.1 kbulk= 1.1 rho = 2300 cbulk = 710
 isource:ib267 2677 0 idc= 0.2403e-3

ThermalBlock3:b268 2681 2581 2683 2673 2685 1685 2687 lx=246.7u ly=261.915u
 +habove= 1.35u hbelow = 6.24u
 +dn= 1.8136 ds= 1.3244 de= 1.0686 dw= 1.8398 dt= 0.0521 db= 0.1043
 +kmx= 146 kmy= 146 kmz= 170 kild= 1.1 kbulk= 1.1 rho = 2300 cbulk = 710

isource:ib268 2687 0 idc= 0.2541e-3

ThermalBlock3:b269 2691 2591 3 2683 2695 1695 2697 lx=246.7u ly=261.915u
 +habove= 1.35u hbelow = 6.24u
 +dn= 1.9654 ds= 1.7461 de= 0.0000 dw= 1.0686 dt= 0.0332 db= 0.0664
 +kmx= 146 kmy= 146 kmz= 170 kild= 1.1 kbulk= 1.1 rho = 2300 cbulk = 710
 isource:ib269 2697 0 idc= 0.2320e-3

ThermalBlock3:b270 2701 2601 2703 4 2705 1705 2707 lx=246.7u ly=261.915u
 +habove= 1.35u hbelow = 6.24u
 +dn= 1.9486 ds= 2.0498 de= 1.5138 dw= 0.0000 dt= 0.0427 db= 0.0853
 +kmx= 146 kmy= 146 kmz= 170 kild= 1.1 kbulk= 1.1 rho = 2300 cbulk = 710
 isource:ib270 2707 0 idc= 0.2268e-3

ThermalBlock3:b271 2711 2611 2713 2703 2715 1715 2717 lx=246.7u ly=261.915u
 +habove= 1.35u hbelow = 6.24u
 +dn= 1.1050 ds= 1.4424 de= 1.5615 dw= 1.5138 dt= 0.0284 db= 0.0569
 +kmx= 146 kmy= 146 kmz= 170 kild= 1.1 kbulk= 1.1 rho = 2300 cbulk = 710
 isource:ib271 2717 0 idc= 0.2629e-3

ThermalBlock3:b272 2721 2621 2723 2713 2725 1725 2727 lx=246.7u ly=261.915u
 +habove= 1.35u hbelow = 6.24u
 +dn= 1.8136 ds= 1.8052 de= 1.5853 dw= 1.5615 dt= 0.0332 db= 0.0664
 +kmx= 146 kmy= 146 kmz= 170 kild= 1.1 kbulk= 1.1 rho = 2300 cbulk = 710
 isource:ib272 2727 0 idc= 0.3107e-3

ThermalBlock3:b273 2731 2631 2733 2723 2735 1735 2737 lx=246.7u ly=261.915u
 +habove= 1.35u hbelow = 6.24u
 +dn= 1.6702 ds= 1.7292 de= 1.7285 dw= 1.5853 dt= 0.0284 db= 0.0569
 +kmx= 146 kmy= 146 kmz= 170 kild= 1.1 kbulk= 1.1 rho = 2300 cbulk = 710
 isource:ib273 2737 0 idc= 0.4162e-3

ThermalBlock3:b274 2741 2641 2743 2733 2745 1745 2747 lx=246.7u ly=261.915u
 +habove= 1.35u hbelow = 6.24u
 +dn= 1.7377 ds= 1.9486 de= 1.5615 dw= 1.7285 dt= 0.1138 db= 0.1374
 +kmx= 146 kmy= 146 kmz= 170 kild= 1.1 kbulk= 1.1 rho = 2300 cbulk = 710
 isource:ib274 2747 0 idc= 0.7308e-3

ThermalBlock3:b275 2751 2651 2753 2743 2755 1755 2757 lx=246.7u ly=261.915u
 +habove= 1.35u hbelow = 6.24u
 +dn= 1.8305 ds= 1.7124 de= 1.5376 dw= 1.5615 dt= 0.1564 db= 0.2844
 +kmx= 146 kmy= 146 kmz= 170 kild= 1.1 kbulk= 1.1 rho = 2300 cbulk = 710
 isource:ib275 2757 0 idc= 0.9469e-3

ThermalBlock3:b276 2761 2661 2763 2753 2765 1765 2767 lx=246.7u ly=261.915u
+habove= 1.35u hbelow = 6.24u
+dn= 1.6955 ds= 1.4256 de= 1.2355 dw= 1.5376 dt= 0.0190 db= 0.0521
+kmx= 146 kmy= 146 kmz= 170 kild= 1.1 kbulk= 1.1 rho = 2300 cbulk = 710
isource:ib276 2767 0 idc= 0.3035e-3

ThermalBlock3:b277 2771 2671 2773 2763 2775 1775 2777 lx=246.7u ly=261.915u
+habove= 1.35u hbelow = 6.24u
+dn= 1.7799 ds= 1.8220 de= 1.8159 dw= 1.2355 dt= 0.0284 db= 0.0853
+kmx= 146 kmy= 146 kmz= 170 kild= 1.1 kbulk= 1.1 rho = 2300 cbulk = 710
isource:ib277 2777 0 idc= 0.1966e-3

ThermalBlock3:b278 2781 2681 2783 2773 2785 1785 2787 lx=246.7u ly=261.915u
+habove= 1.35u hbelow = 6.24u
+dn= 1.7208 ds= 1.8136 de= 1.2673 dw= 1.8159 dt= 0.0190 db= 0.0569
+kmx= 146 kmy= 146 kmz= 170 kild= 1.1 kbulk= 1.1 rho = 2300 cbulk = 710
isource:ib278 2787 0 idc= 0.2801e-3

ThermalBlock3:b279 2791 2691 3 2783 2795 1795 2797 lx=246.7u ly=261.915u
+habove= 1.35u hbelow = 6.24u
+dn= 2.3619 ds= 1.9654 de= 0.0000 dw= 1.2673 dt= 0.0190 db= 0.0379
+kmx= 146 kmy= 146 kmz= 170 kild= 1.1 kbulk= 1.1 rho = 2300 cbulk = 710
isource:ib279 2797 0 idc= 0.1796e-3

ThermalBlock3:b280 2801 2701 2803 4 2805 1805 2807 lx=246.7u ly=261.915u
+habove= 1.35u hbelow = 6.24u
+dn= 2.1088 ds= 1.9486 de= 1.6076 dw= 0.0000 dt= 0.0190 db= 0.0379
+kmx= 146 kmy= 146 kmz= 170 kild= 1.1 kbulk= 1.1 rho = 2300 cbulk = 710
isource:ib280 2807 0 idc= 0.1877e-3

ThermalBlock3:b281 2811 2711 2813 2803 2815 1815 2817 lx=246.7u ly=261.915u
+habove= 1.35u hbelow = 6.24u
+dn= 1.7799 ds= 1.1050 de= 1.6871 dw= 1.6076 dt= 0.0190 db= 0.0379
+kmx= 146 kmy= 146 kmz= 170 kild= 1.1 kbulk= 1.1 rho = 2300 cbulk = 710
isource:ib281 2817 0 idc= 0.2025e-3

ThermalBlock3:b282 2821 2721 2823 2813 2825 1825 2827 lx=246.7u ly=261.915u
+habove= 1.35u hbelow = 6.24u
+dn= 1.8305 ds= 1.8136 de= 1.4247 dw= 1.6871 dt= 0.0427 db= 0.0853
+kmx= 146 kmy= 146 kmz= 170 kild= 1.1 kbulk= 1.1 rho = 2300 cbulk = 710
isource:ib282 2827 0 idc= 0.3662e-3

ThermalBlock3:b283 2831 2731 2833 2823 2835 1835 2837 lx=246.7u ly=261.915u
+habove= 1.35u hbelow = 6.24u

+dn= 1.5774 ds= 1.6702 de= 1.4327 dw= 1.4247 dt= 0.0284 db= 0.0569
 +kmx= 146 kmy= 146 kmz= 170 kild= 1.1 kbulk= 1.1 rho = 2300 cbulk = 710
 isource:ib283 2837 0 idc= 0.3743e-3

ThermalBlock3:b284 2841 2741 2843 2833 2845 1845 2847 lx=246.7u ly=261.915u
 +habove= 1.35u hbelow = 6.24u
 +dn= 1.8642 ds= 1.7377 de= 1.6315 dw= 1.4327 dt= 0.0427 db= 0.0853
 +kmx= 146 kmy= 146 kmz= 170 kild= 1.1 kbulk= 1.1 rho = 2300 cbulk = 710
 isource:ib284 2847 0 idc= 0.4890e-3

ThermalBlock3:b285 2851 2751 2853 2843 2855 1855 2857 lx=246.7u ly=261.915u
 +habove= 1.35u hbelow = 6.24u
 +dn= 1.6196 ds= 1.8305 de= 1.2339 dw= 1.6315 dt= 0.0379 db= 0.0806
 +kmx= 146 kmy= 146 kmz= 170 kild= 1.1 kbulk= 1.1 rho = 2300 cbulk = 710
 isource:ib285 2857 0 idc= 0.9347e-3

ThermalBlock3:b286 2861 2761 2863 2853 2865 1865 2867 lx=246.7u ly=261.915u
 +habove= 1.35u hbelow = 6.24u
 +dn= 1.7208 ds= 1.6955 de= 1.0590 dw= 1.2339 dt= 0.0237 db= 0.0664
 +kmx= 146 kmy= 146 kmz= 170 kild= 1.1 kbulk= 1.1 rho = 2300 cbulk = 710
 isource:ib286 2867 0 idc= 0.2337e-3

ThermalBlock3:b287 2871 2771 2873 2863 2875 1875 2877 lx=246.7u ly=261.915u
 +habove= 1.35u hbelow = 6.24u
 +dn= 1.6955 ds= 1.7799 de= 1.6394 dw= 1.0590 dt= 0.0284 db= 0.0569
 +kmx= 146 kmy= 146 kmz= 170 kild= 1.1 kbulk= 1.1 rho = 2300 cbulk = 710
 isource:ib287 2877 0 idc= 0.2068e-3

ThermalBlock3:b288 2881 2781 2883 2873 2885 1885 2887 lx=246.7u ly=261.915u
 +habove= 1.35u hbelow = 6.24u
 +dn= 1.4846 ds= 1.7208 de= 1.0829 dw= 1.6394 dt= 0.0190 db= 0.0474
 +kmx= 146 kmy= 146 kmz= 170 kild= 1.1 kbulk= 1.1 rho = 2300 cbulk = 710
 isource:ib288 2887 0 idc= 0.3070e-3

ThermalBlock3:b289 2891 2791 3 2883 2895 1895 2897 lx=246.7u ly=261.915u
 +habove= 1.35u hbelow = 6.24u
 +dn= 2.2860 ds= 2.3619 de= 0.0000 dw= 1.0829 dt= 0.0190 db= 0.0379
 +kmx= 146 kmy= 146 kmz= 170 kild= 1.1 kbulk= 1.1 rho = 2300 cbulk = 710
 isource:ib289 2897 0 idc= 0.1718e-3

ThermalBlock3:b290 1 2801 2903 4 2905 1905 2907 lx=246.7u ly=261.915u
 +habove= 1.35u hbelow = 6.24u
 +dn= 0.0000 ds= 2.1088 de= 1.2832 dw= 0.0000 dt= 0.0000 db= 0.0000
 +kmx= 146 kmy= 146 kmz= 170 kild= 1.1 kbulk= 1.1 rho = 2300 cbulk = 710

isource:ib290 2907 0 idc= 0.0653e-3

ThermalBlock3:b291 1 2811 2913 2903 2915 1915 2917 lx=246.7u ly=261.915u
 +habove= 1.35u hbelow = 6.24u
 +dn= 0.0000 ds= 1.7799 de= 1.4820 dw= 1.2832 dt= 0.0047 db= 0.0095
 +kmx= 146 kmy= 146 kmz= 170 kild= 1.1 kbulk= 1.1 rho = 2300 cbulk = 710
 isource:ib291 2917 0 idc= 0.0581e-3

ThermalBlock3:b292 1 2821 2923 2913 2925 1925 2927 lx=246.7u ly=261.915u
 +habove= 1.35u hbelow = 6.24u
 +dn= 0.0000 ds= 1.8305 de= 1.2594 dw= 1.4820 dt= 0.0000 db= 0.0000
 +kmx= 146 kmy= 146 kmz= 170 kild= 1.1 kbulk= 1.1 rho = 2300 cbulk = 710
 isource:ib292 2927 0 idc= 0.1471e-3

ThermalBlock3:b293 1 2831 2933 2923 2935 1935 2937 lx=246.7u ly=261.915u
 +habove= 1.35u hbelow = 6.24u
 +dn= 0.0000 ds= 1.5774 de= 1.4820 dw= 1.2594 dt= 0.0047 db= 0.0095
 +kmx= 146 kmy= 146 kmz= 170 kild= 1.1 kbulk= 1.1 rho = 2300 cbulk = 710
 isource:ib293 2937 0 idc= 0.1138e-3

ThermalBlock3:b294 1 2841 2943 2933 2945 1945 2947 lx=246.7u ly=261.915u
 +habove= 1.35u hbelow = 6.24u
 +dn= 0.0000 ds= 1.8642 de= 1.3468 dw= 1.4820 dt= 0.0000 db= 0.0000
 +kmx= 146 kmy= 146 kmz= 170 kild= 1.1 kbulk= 1.1 rho = 2300 cbulk = 710
 isource:ib294 2947 0 idc= 0.0838e-3

ThermalBlock3:b295 1 2851 2953 2943 2955 1955 2957 lx=246.7u ly=261.915u
 +habove= 1.35u hbelow = 6.24u
 +dn= 0.0000 ds= 1.6196 de= 1.4502 dw= 1.3468 dt= 0.0142 db= 0.0379
 +kmx= 146 kmy= 146 kmz= 170 kild= 1.1 kbulk= 1.1 rho = 2300 cbulk = 710
 isource:ib295 2957 0 idc= 0.1341e-3

ThermalBlock3:b296 1 2861 2963 2953 2965 1965 2967 lx=246.7u ly=261.915u
 +habove= 1.35u hbelow = 6.24u
 +dn= 0.0000 ds= 1.7208 de= 1.4422 dw= 1.4502 dt= 0.0000 db= 0.0000
 +kmx= 146 kmy= 146 kmz= 170 kild= 1.1 kbulk= 1.1 rho = 2300 cbulk = 710
 isource:ib296 2967 0 idc= 0.0766e-3

ThermalBlock3:b297 1 2871 2973 2963 2975 1975 2977 lx=246.7u ly=261.915u
 +habove= 1.35u hbelow = 6.24u
 +dn= 0.0000 ds= 1.6955 de= 1.4422 dw= 1.4422 dt= 0.0000 db= 0.0095
 +kmx= 146 kmy= 146 kmz= 170 kild= 1.1 kbulk= 1.1 rho = 2300 cbulk = 710
 isource:ib297 2977 0 idc= 0.0678e-3

ThermalBlock3:b298 1 2881 2983 2973 2985 1985 2987 lx=246.7u ly=261.915u
 +habove= 1.35u hbelow = 6.24u
 +dn= 0.0000 ds= 1.4846 de= 1.1004 dw= 1.4422 dt= 0.0000 db= 0.0047
 +kmx= 146 kmy= 146 kmz= 170 kild= 1.1 kbulk= 1.1 rho = 2300 cbulk = 710
 isource:ib298 2987 0 idc= 0.0800e-3

ThermalBlock3:b299 1 2891 3 2983 2995 1995 2997 lx=246.7u ly=261.915u
 +habove= 1.35u hbelow = 6.24u
 +dn= 0.0000 ds= 2.2860 de= 0.0000 dw= 1.1004 dt= 0.0000 db= 0.0000
 +kmx= 146 kmy= 146 kmz= 170 kild= 1.1 kbulk= 1.1 rho = 2300 cbulk = 710
 isource:ib299 2997 0 idc= 0.0680e-3

*Tier 3

ThermalBlock3:b300 3001 2 3003 4 5 2005 3007 lx=246.7u ly=261.915u
 +habove= 0.6u hbelow = 5.11u
 +dn= 2.2313 ds= 0.0000 de= 2.4941 dw= 0.0000 dt= 0.0000 db= 0.0000
 +kmx= 146 kmy= 146 kmz= 170 kild= 1.1 kbulk= 1.1 rho = 2300 cbulk = 710
 isource:ib300 3007 0 idc= 0.7740e-3

ThermalBlock3:b301 3011 2 3013 3003 5 2015 3017 lx=246.7u ly=261.915u
 +habove= 0.6u hbelow = 5.11u
 +dn= 2.1977 ds= 0.0000 de= 2.8217 dw= 2.4941 dt= 0.0000 db= 0.0000
 +kmx= 146 kmy= 146 kmz= 170 kild= 1.1 kbulk= 1.1 rho = 2300 cbulk = 710
 isource:ib301 3017 0 idc= 0.4986e-3

ThermalBlock3:b302 3021 2 3023 3013 5 2025 3027 lx=246.7u ly=261.915u
 +habove= 0.6u hbelow = 5.11u
 +dn= 1.9510 ds= 0.0000 de= 2.5787 dw= 2.8217 dt= 0.0237 db= 0.0237
 +kmx= 146 kmy= 146 kmz= 170 kild= 1.1 kbulk= 1.1 rho = 2300 cbulk = 710
 isource:ib302 3027 0 idc= 0.2552e-3

ThermalBlock3:b303 3031 2 3033 3023 5 2035 3037 lx=246.7u ly=261.915u
 +habove= 0.6u hbelow = 5.11u
 +dn= 1.6146 ds= 0.0000 de= 2.9803 dw= 2.5787 dt= 0.0379 db= 0.0379
 +kmx= 146 kmy= 146 kmz= 170 kild= 1.1 kbulk= 1.1 rho = 2300 cbulk = 710
 isource:ib303 3037 0 idc= 0.2390e-3

ThermalBlock3:b304 3041 2 3043 3033 5 2045 3047 lx=246.7u ly=261.915u
 +habove= 0.6u hbelow = 5.11u
 +dn= 1.5698 ds= 0.0000 de= 2.5998 dw= 2.9803 dt= 0.0758 db= 0.0758
 +kmx= 146 kmy= 146 kmz= 170 kild= 1.1 kbulk= 1.1 rho = 2300 cbulk = 710
 isource:ib304 3047 0 idc= 0.2398e-3

ThermalBlock3:b305 3051 2 3053 3043 5 2055 3057 lx=246.7u ly=261.915u
+habove= 0.6u hbelow = 5.11u
+dn= 1.4801 ds= 0.0000 de= 2.4201 dw= 2.5998 dt= 0.2085 db= 0.2085
+kmx= 146 kmy= 146 kmz= 170 kild= 1.1 kbulk= 1.1 rho = 2300 cbulk = 710
isource:ib305 3057 0 idc= 0.2107e-3

ThermalBlock3:b306 3061 2 3063 3053 5 2065 3067 lx=246.7u ly=261.915u
+habove= 0.6u hbelow = 5.11u
+dn= 1.4576 ds= 0.0000 de= 2.0925 dw= 2.4201 dt= 0.0332 db= 0.0332
+kmx= 146 kmy= 146 kmz= 170 kild= 1.1 kbulk= 1.1 rho = 2300 cbulk = 710
isource:ib306 3067 0 idc= 0.2438e-3

ThermalBlock3:b307 3071 2 3073 3063 5 2075 3077 lx=246.7u ly=261.915u
+habove= 0.6u hbelow = 5.11u
+dn= 1.7828 ds= 0.0000 de= 2.5047 dw= 2.0925 dt= 0.0427 db= 0.0427
+kmx= 146 kmy= 146 kmz= 170 kild= 1.1 kbulk= 1.1 rho = 2300 cbulk = 710
isource:ib307 3077 0 idc= 0.2890e-3

ThermalBlock3:b308 3081 2 3083 3073 5 2085 3087 lx=246.7u ly=261.915u
+habove= 0.6u hbelow = 5.11u
+dn= 1.6258 ds= 0.0000 de= 2.4518 dw= 2.5047 dt= 0.1138 db= 0.1138
+kmx= 146 kmy= 146 kmz= 170 kild= 1.1 kbulk= 1.1 rho = 2300 cbulk = 710
isource:ib308 3087 0 idc= 0.3830e-3

ThermalBlock3:b309 3091 2 3 3083 5 2095 3097 lx=246.7u ly=261.915u
+habove= 0.6u hbelow = 5.11u
+dn= 2.9826 ds= 0.0000 de= 0.0000 dw= 2.4518 dt= 0.0000 db= 0.0000
+kmx= 146 kmy= 146 kmz= 170 kild= 1.1 kbulk= 1.1 rho = 2300 cbulk = 710
isource:ib309 3097 0 idc= 0.3376e-3

ThermalBlock3:b310 3101 3001 3103 4 5 2105 3107 lx=246.7u ly=261.915u
+habove= 0.6u hbelow = 5.11u
+dn= 2.3322 ds= 2.2313 de= 2.0333 dw= 0.0000 dt= 0.0379 db= 0.0379
+kmx= 146 kmy= 146 kmz= 170 kild= 1.1 kbulk= 1.1 rho = 2300 cbulk = 710
isource:ib310 3107 0 idc= 0.7140e-3

ThermalBlock3:b311 3111 3011 3113 3103 5 2115 3117 lx=246.7u ly=261.915u
+habove= 0.6u hbelow = 5.11u
+dn= 2.0295 ds= 2.1977 de= 2.2341 dw= 2.0333 dt= 0.1185 db= 0.1185
+kmx= 146 kmy= 146 kmz= 170 kild= 1.1 kbulk= 1.1 rho = 2300 cbulk = 710
isource:ib311 3117 0 idc= 0.6737e-3

ThermalBlock3:b312 3121 3021 3123 3113 5 2125 3127 lx=246.7u ly=261.915u
+habove= 0.6u hbelow = 5.11u

+dn= 1.8277 ds= 1.9510 de= 1.9382 dw= 2.2341 dt= 0.1801 db= 0.1801
 +kmx= 146 kmy= 146 kmz= 170 kild= 1.1 kbulk= 1.1 rho = 2300 cbulk = 710
 isource:ib312 3127 0 idc= 0.2801e-3

ThermalBlock3:b313 3131 3031 3133 3123 5 2135 3137 lx=246.7u ly=261.915u
 +habove= 0.6u hbelow = 5.11u
 +dn= 1.3007 ds= 1.6146 de= 1.8325 dw= 1.9382 dt= 0.3981 db= 0.3981
 +kmx= 146 kmy= 146 kmz= 170 kild= 1.1 kbulk= 1.1 rho = 2300 cbulk = 710
 isource:ib313 3137 0 idc= 0.1215e-3

ThermalBlock3:b314 3141 3041 3143 3133 5 2145 3147 lx=246.7u ly=261.915u
 +habove= 0.6u hbelow = 5.11u
 +dn= 1.4016 ds= 1.5698 de= 1.7586 dw= 1.8325 dt= 0.3792 db= 0.3792
 +kmx= 146 kmy= 146 kmz= 170 kild= 1.1 kbulk= 1.1 rho = 2300 cbulk = 710
 isource:ib314 3147 0 idc= 0.2252e-3

ThermalBlock3:b315 3151 3051 3153 3143 5 2155 3157 lx=246.7u ly=261.915u
 +habove= 0.6u hbelow = 5.11u
 +dn= 1.4913 ds= 1.4801 de= 1.9277 dw= 1.7586 dt= 0.3887 db= 0.3887
 +kmx= 146 kmy= 146 kmz= 170 kild= 1.1 kbulk= 1.1 rho = 2300 cbulk = 710
 isource:ib315 3157 0 idc= 0.1797e-3

ThermalBlock3:b316 3161 3061 3163 3153 5 2165 3167 lx=246.7u ly=261.915u
 +habove= 0.6u hbelow = 5.11u
 +dn= 1.2446 ds= 1.4576 de= 1.4415 dw= 1.9277 dt= 0.3460 db= 0.3460
 +kmx= 146 kmy= 146 kmz= 170 kild= 1.1 kbulk= 1.1 rho = 2300 cbulk = 710
 isource:ib316 3167 0 idc= 0.2899e-3

ThermalBlock3:b317 3171 3071 3173 3163 5 2175 3177 lx=246.7u ly=261.915u
 +habove= 0.6u hbelow = 5.11u
 +dn= 1.5249 ds= 1.7828 de= 1.8008 dw= 1.4415 dt= 0.4408 db= 0.4408
 +kmx= 146 kmy= 146 kmz= 170 kild= 1.1 kbulk= 1.1 rho = 2300 cbulk = 710
 isource:ib317 3177 0 idc= 0.1972e-3

ThermalBlock3:b318 3181 3081 3183 3173 5 2185 3187 lx=246.7u ly=261.915u
 +habove= 0.6u hbelow = 5.11u
 +dn= 1.5810 ds= 1.6258 de= 1.8325 dw= 1.8008 dt= 0.2891 db= 0.2891
 +kmx= 146 kmy= 146 kmz= 170 kild= 1.1 kbulk= 1.1 rho = 2300 cbulk = 710
 isource:ib318 3187 0 idc= 0.3014e-3

ThermalBlock3:b319 3191 3091 3 3183 5 2195 3197 lx=246.7u ly=261.915u
 +habove= 0.6u hbelow = 5.11u
 +dn= 2.5789 ds= 2.9826 de= 0.0000 dw= 1.8325 dt= 0.0190 db= 0.0190
 +kmx= 146 kmy= 146 kmz= 170 kild= 1.1 kbulk= 1.1 rho = 2300 cbulk = 710

isource:ib319 3197 0 idc= 0.4639e-3

ThermalBlock3:b320 3201 3101 3203 4 5 2205 3207 lx=246.7u ly=261.915u
 +habove= 0.6u hbelow = 5.11u
 +dn= 2.9489 ds= 2.3322 de= 2.1369 dw= 0.0000 dt= 0.0237 db= 0.0237
 +kmx= 146 kmy= 146 kmz= 170 kild= 1.1 kbulk= 1.1 rho = 2300 cbulk = 710
 isource:ib320 3207 0 idc= 0.4029e-3

ThermalBlock3:b321 3211 3111 3213 3203 5 2215 3217 lx=246.7u ly=261.915u
 +habove= 0.6u hbelow = 5.11u
 +dn= 2.1528 ds= 2.0295 de= 2.4857 dw= 2.1369 dt= 0.0806 db= 0.0806
 +kmx= 146 kmy= 146 kmz= 170 kild= 1.1 kbulk= 1.1 rho = 2300 cbulk = 710
 isource:ib321 3217 0 idc= 0.5255e-3

ThermalBlock3:b322 3221 3121 3223 3213 5 2225 3227 lx=246.7u ly=261.915u
 +habove= 0.6u hbelow = 5.11u
 +dn= 2.4107 ds= 1.8277 de= 2.4222 dw= 2.4857 dt= 0.1185 db= 0.1185
 +kmx= 146 kmy= 146 kmz= 170 kild= 1.1 kbulk= 1.1 rho = 2300 cbulk = 710
 isource:ib322 3227 0 idc= 0.4607e-3

ThermalBlock3:b323 3231 3131 3233 3223 5 2235 3237 lx=246.7u ly=261.915u
 +habove= 0.6u hbelow = 5.11u
 +dn= 1.8837 ds= 1.3007 de= 2.4222 dw= 2.4222 dt= 0.0948 db= 0.0948
 +kmx= 146 kmy= 146 kmz= 170 kild= 1.1 kbulk= 1.1 rho = 2300 cbulk = 710
 isource:ib323 3237 0 idc= 0.4514e-3

ThermalBlock3:b324 3241 3141 3243 3233 5 2245 3247 lx=246.7u ly=261.915u
 +habove= 0.6u hbelow = 5.11u
 +dn= 2.2089 ds= 1.4016 de= 1.7247 dw= 2.4222 dt= 0.0474 db= 0.0474
 +kmx= 146 kmy= 146 kmz= 170 kild= 1.1 kbulk= 1.1 rho = 2300 cbulk = 710
 isource:ib324 3247 0 idc= 0.5002e-3

ThermalBlock3:b325 3251 3151 3253 3243 5 2255 3257 lx=246.7u ly=261.915u
 +habove= 0.6u hbelow = 5.11u
 +dn= 2.1753 ds= 1.4913 de= 1.7459 dw= 1.7247 dt= 0.2180 db= 0.2180
 +kmx= 146 kmy= 146 kmz= 170 kild= 1.1 kbulk= 1.1 rho = 2300 cbulk = 710
 isource:ib325 3257 0 idc= 0.2036e-3

ThermalBlock3:b326 3261 3161 3263 3253 5 2265 3267 lx=246.7u ly=261.915u
 +habove= 0.6u hbelow = 5.11u
 +dn= 1.7604 ds= 1.2446 de= 1.3971 dw= 1.7459 dt= 0.2986 db= 0.2986
 +kmx= 146 kmy= 146 kmz= 170 kild= 1.1 kbulk= 1.1 rho = 2300 cbulk = 710
 isource:ib326 3267 0 idc= 0.2258e-3

ThermalBlock3:b327 3271 3171 3273 3263 5 2275 3277 lx=246.7u ly=261.915u
+habove= 0.6u hbelow = 5.11u
+dn= 2.3098 ds= 1.5249 de= 2.2637 dw= 1.3971 dt= 0.1848 db= 0.1848
+kmx= 146 kmy= 146 kmz= 170 kild= 1.1 kbulk= 1.1 rho = 2300 cbulk = 710
isource:ib327 3277 0 idc= 0.2997e-3

ThermalBlock3:b328 3281 3181 3283 3273 5 2285 3287 lx=246.7u ly=261.915u
+habove= 0.6u hbelow = 5.11u
+dn= 2.3659 ds= 1.5810 de= 1.8410 dw= 2.2637 dt= 0.1469 db= 0.1469
+kmx= 146 kmy= 146 kmz= 170 kild= 1.1 kbulk= 1.1 rho = 2300 cbulk = 710
isource:ib328 3287 0 idc= 0.3221e-3

ThermalBlock3:b329 3291 3191 3 3283 5 2295 3297 lx=246.7u ly=261.915u
+habove= 0.6u hbelow = 5.11u
+dn= 2.8480 ds= 2.5789 de= 0.0000 dw= 1.8410 dt= 0.0569 db= 0.0569
+kmx= 146 kmy= 146 kmz= 170 kild= 1.1 kbulk= 1.1 rho = 2300 cbulk = 710
isource:ib329 3297 0 idc= 0.4242e-3

ThermalBlock3:b330 3301 3201 3303 4 5 2305 3307 lx=246.7u ly=261.915u
+habove= 0.6u hbelow = 5.11u
+dn= 2.6462 ds= 2.9489 de= 1.7480 dw= 0.0000 dt= 0.0190 db= 0.0190
+kmx= 146 kmy= 146 kmz= 170 kild= 1.1 kbulk= 1.1 rho = 2300 cbulk = 710
isource:ib330 3307 0 idc= 0.5950e-3

ThermalBlock3:b331 3311 3211 3313 3303 5 2315 3317 lx=246.7u ly=261.915u
+habove= 0.6u hbelow = 5.11u
+dn= 2.1977 ds= 2.1528 de= 2.4032 dw= 1.7480 dt= 0.0190 db= 0.0190
+kmx= 146 kmy= 146 kmz= 170 kild= 1.1 kbulk= 1.1 rho = 2300 cbulk = 710
isource:ib331 3317 0 idc= 0.6133e-3

ThermalBlock3:b332 3321 3221 3323 3313 5 2325 3327 lx=246.7u ly=261.915u
+habove= 0.6u hbelow = 5.11u
+dn= 2.0183 ds= 2.4107 de= 2.2236 dw= 2.4032 dt= 0.1706 db= 0.1706
+kmx= 146 kmy= 146 kmz= 170 kild= 1.1 kbulk= 1.1 rho = 2300 cbulk = 710
isource:ib332 3327 0 idc= 0.3950e-3

ThermalBlock3:b333 3331 3231 3333 3323 5 2335 3337 lx=246.7u ly=261.915u
+habove= 0.6u hbelow = 5.11u
+dn= 2.0295 ds= 1.8837 de= 2.3610 dw= 2.2236 dt= 0.1564 db= 0.1564
+kmx= 146 kmy= 146 kmz= 170 kild= 1.1 kbulk= 1.1 rho = 2300 cbulk = 710
isource:ib333 3337 0 idc= 0.2917e-3

ThermalBlock3:b334 3341 3241 3343 3333 5 2345 3347 lx=246.7u ly=261.915u
+habove= 0.6u hbelow = 5.11u

+dn= 2.2089 ds= 2.2089 de= 1.8114 dw= 2.3610 dt= 0.0901 db= 0.0901
 +kmx= 146 kmy= 146 kmz= 170 kild= 1.1 kbulk= 1.1 rho = 2300 cbulk = 710
 isource:ib334 3347 0 idc= 0.3045e-3

ThermalBlock3:b335 3351 3251 3353 3343 5 2355 3357 lx=246.7u ly=261.915u
 +habove= 0.6u hbelow = 5.11u
 +dn= 2.3771 ds= 2.1753 de= 1.9805 dw= 1.8114 dt= 0.2370 db= 0.2370
 +kmx= 146 kmy= 146 kmz= 170 kild= 1.1 kbulk= 1.1 rho = 2300 cbulk = 710
 isource:ib335 3357 0 idc= 0.1528e-3

ThermalBlock3:b336 3361 3261 3363 3353 5 2365 3367 lx=246.7u ly=261.915u
 +habove= 0.6u hbelow = 5.11u
 +dn= 2.2874 ds= 1.7604 de= 1.6423 dw= 1.9805 dt= 0.2465 db= 0.2465
 +kmx= 146 kmy= 146 kmz= 170 kild= 1.1 kbulk= 1.1 rho = 2300 cbulk = 710
 isource:ib336 3367 0 idc= 0.2565e-3

ThermalBlock3:b337 3371 3271 3373 3363 5 2375 3377 lx=246.7u ly=261.915u
 +habove= 0.6u hbelow = 5.11u
 +dn= 2.2537 ds= 2.3098 de= 2.4349 dw= 1.6423 dt= 0.0521 db= 0.0521
 +kmx= 146 kmy= 146 kmz= 170 kild= 1.1 kbulk= 1.1 rho = 2300 cbulk = 710
 isource:ib337 3377 0 idc= 0.3924e-3

ThermalBlock3:b338 3381 3281 3383 3373 5 2385 3387 lx=246.7u ly=261.915u
 +habove= 0.6u hbelow = 5.11u
 +dn= 2.0183 ds= 2.3659 de= 1.8114 dw= 2.4349 dt= 0.0569 db= 0.0569
 +kmx= 146 kmy= 146 kmz= 170 kild= 1.1 kbulk= 1.1 rho = 2300 cbulk = 710
 isource:ib338 3387 0 idc= 0.4762e-3

ThermalBlock3:b339 3391 3291 3 3383 5 2395 3397 lx=246.7u ly=261.915u
 +habove= 0.6u hbelow = 5.11u
 +dn= 3.1956 ds= 2.8480 de= 0.0000 dw= 1.8114 dt= 0.0521 db= 0.0521
 +kmx= 146 kmy= 146 kmz= 170 kild= 1.1 kbulk= 1.1 rho = 2300 cbulk = 710
 isource:ib339 3397 0 idc= 0.3529e-3

ThermalBlock3:b340 3401 3301 3403 4 5 2405 3407 lx=246.7u ly=261.915u
 +habove= 0.6u hbelow = 5.11u
 +dn= 3.0611 ds= 2.6462 de= 1.5366 dw= 0.0000 dt= 0.0190 db= 0.0190
 +kmx= 146 kmy= 146 kmz= 170 kild= 1.1 kbulk= 1.1 rho = 2300 cbulk = 710
 isource:ib340 3407 0 idc= 0.2774e-3

ThermalBlock3:b341 3411 3311 3413 3403 5 2415 3417 lx=246.7u ly=261.915u
 +habove= 0.6u hbelow = 5.11u
 +dn= 2.0631 ds= 2.1977 de= 2.4032 dw= 1.5366 dt= 0.0284 db= 0.0284
 +kmx= 146 kmy= 146 kmz= 170 kild= 1.1 kbulk= 1.1 rho = 2300 cbulk = 710

isource:ib341 3417 0 idc= 0.4572e-3

ThermalBlock3:b342 3421 3321 3423 3413 5 2425 3427 lx=246.7u ly=261.915u
 +habove= 0.6u hbelow = 5.11u
 +dn= 2.5229 ds= 2.0183 de= 2.4455 dw= 2.4032 dt= 0.0711 db= 0.0711
 +kmx= 146 kmy= 146 kmz= 170 kild= 1.1 kbulk= 1.1 rho = 2300 cbulk = 710
 isource:ib342 3427 0 idc= 0.2755e-3

ThermalBlock3:b343 3431 3331 3433 3423 5 2435 3437 lx=246.7u ly=261.915u
 +habove= 0.6u hbelow = 5.11u
 +dn= 2.4780 ds= 2.0295 de= 2.4244 dw= 2.4455 dt= 0.0664 db= 0.0664
 +kmx= 146 kmy= 146 kmz= 170 kild= 1.1 kbulk= 1.1 rho = 2300 cbulk = 710
 isource:ib343 3437 0 idc= 0.1445e-3

ThermalBlock3:b344 3441 3341 3443 3433 5 2445 3447 lx=246.7u ly=261.915u
 +habove= 0.6u hbelow = 5.11u
 +dn= 2.6013 ds= 2.2089 de= 1.9699 dw= 2.4244 dt= 0.1090 db= 0.1090
 +kmx= 146 kmy= 146 kmz= 170 kild= 1.1 kbulk= 1.1 rho = 2300 cbulk = 710
 isource:ib344 3447 0 idc= 0.2122e-3

ThermalBlock3:b345 3451 3351 3453 3443 5 2455 3457 lx=246.7u ly=261.915u
 +habove= 0.6u hbelow = 5.11u
 +dn= 2.4107 ds= 2.3771 de= 2.0862 dw= 1.9699 dt= 0.2607 db= 0.2607
 +kmx= 146 kmy= 146 kmz= 170 kild= 1.1 kbulk= 1.1 rho = 2300 cbulk = 710
 isource:ib345 3457 0 idc= 0.1741e-3

ThermalBlock3:b346 3461 3361 3463 3453 5 2465 3467 lx=246.7u ly=261.915u
 +habove= 0.6u hbelow = 5.11u
 +dn= 2.1416 ds= 2.2874 de= 1.9488 dw= 2.0862 dt= 0.3081 db= 0.3081
 +kmx= 146 kmy= 146 kmz= 170 kild= 1.1 kbulk= 1.1 rho = 2300 cbulk = 710
 isource:ib346 3467 0 idc= 0.1192e-3

ThermalBlock3:b347 3471 3371 3473 3463 5 2475 3477 lx=246.7u ly=261.915u
 +habove= 0.6u hbelow = 5.11u
 +dn= 2.2201 ds= 2.2537 de= 2.1813 dw= 1.9488 dt= 0.1043 db= 0.1043
 +kmx= 146 kmy= 146 kmz= 170 kild= 1.1 kbulk= 1.1 rho = 2300 cbulk = 710
 isource:ib347 3477 0 idc= 0.3514e-3

ThermalBlock3:b348 3481 3381 3483 3473 5 2485 3487 lx=246.7u ly=261.915u
 +habove= 0.6u hbelow = 5.11u
 +dn= 1.8165 ds= 2.0183 de= 1.5049 dw= 2.1813 dt= 0.0758 db= 0.0758
 +kmx= 146 kmy= 146 kmz= 170 kild= 1.1 kbulk= 1.1 rho = 2300 cbulk = 710
 isource:ib348 3487 0 idc= 0.5182e-3

ThermalBlock3:b349 3491 3391 3 3483 5 2495 3497 lx=246.7u ly=261.915u
+habove= 0.6u hbelow = 5.11u
+dn= 2.9714 ds= 3.1956 de= 0.0000 dw= 1.5049 dt= 0.1517 db= 0.1517
+kmx= 146 kmy= 146 kmz= 170 kild= 1.1 kbulk= 1.1 rho = 2300 cbulk = 710
isource:ib349 3497 0 idc= 0.1703e-3

ThermalBlock3:b350 3501 3401 3503 4 5 2505 3507 lx=246.7u ly=261.915u
+habove= 0.6u hbelow = 5.11u
+dn= 3.3302 ds= 3.0611 de= 1.7269 dw= 0.0000 dt= 0.0190 db= 0.0190
+kmx= 146 kmy= 146 kmz= 170 kild= 1.1 kbulk= 1.1 rho = 2300 cbulk = 710
isource:ib350 3507 0 idc= 0.2028e-3

ThermalBlock3:b351 3511 3411 3513 3503 5 2515 3517 lx=246.7u ly=261.915u
+habove= 0.6u hbelow = 5.11u
+dn= 2.2874 ds= 2.0631 de= 1.8854 dw= 1.7269 dt= 0.1422 db= 0.1422
+kmx= 146 kmy= 146 kmz= 170 kild= 1.1 kbulk= 1.1 rho = 2300 cbulk = 710
isource:ib351 3517 0 idc= 0.3724e-3

ThermalBlock3:b352 3521 3421 3523 3513 5 2525 3527 lx=246.7u ly=261.915u
+habove= 0.6u hbelow = 5.11u
+dn= 2.4107 ds= 2.5229 de= 2.2870 dw= 1.8854 dt= 0.1422 db= 0.1422
+kmx= 146 kmy= 146 kmz= 170 kild= 1.1 kbulk= 1.1 rho = 2300 cbulk = 710
isource:ib352 3527 0 idc= 0.2312e-3

ThermalBlock3:b353 3531 3431 3533 3523 5 2535 3537 lx=246.7u ly=261.915u
+habove= 0.6u hbelow = 5.11u
+dn= 2.0743 ds= 2.4780 de= 2.3398 dw= 2.2870 dt= 0.0569 db= 0.0569
+kmx= 146 kmy= 146 kmz= 170 kild= 1.1 kbulk= 1.1 rho = 2300 cbulk = 710
isource:ib353 3537 0 idc= 0.2564e-3

ThermalBlock3:b354 3541 3441 3543 3533 5 2545 3547 lx=246.7u ly=261.915u
+habove= 0.6u hbelow = 5.11u
+dn= 2.1528 ds= 2.6013 de= 2.1390 dw= 2.3398 dt= 0.0758 db= 0.0758
+kmx= 146 kmy= 146 kmz= 170 kild= 1.1 kbulk= 1.1 rho = 2300 cbulk = 710
isource:ib354 3547 0 idc= 0.2969e-3

ThermalBlock3:b355 3551 3451 3553 3543 5 2555 3557 lx=246.7u ly=261.915u
+habove= 0.6u hbelow = 5.11u
+dn= 2.4780 ds= 2.4107 de= 1.9805 dw= 2.1390 dt= 0.2559 db= 0.2559
+kmx= 146 kmy= 146 kmz= 170 kild= 1.1 kbulk= 1.1 rho = 2300 cbulk = 710
isource:ib355 3557 0 idc= 0.2207e-3

ThermalBlock3:b356 3561 3461 3563 3553 5 2565 3567 lx=246.7u ly=261.915u
+habove= 0.6u hbelow = 5.11u

+dn= 2.3883 ds= 2.1416 de= 1.6317 dw= 1.9805 dt= 0.1943 db= 0.1943
 +kmx= 146 kmy= 146 kmz= 170 kild= 1.1 kbulk= 1.1 rho = 2300 cbulk = 710
 isource:ib356 3567 0 idc= 0.2666e-3

ThermalBlock3:b357 3571 3471 3573 3563 5 2575 3577 lx=246.7u ly=261.915u
 +habove= 0.6u hbelow = 5.11u
 +dn= 2.8144 ds= 2.2201 de= 2.5935 dw= 1.6317 dt= 0.0474 db= 0.0474
 +kmx= 146 kmy= 146 kmz= 170 kild= 1.1 kbulk= 1.1 rho = 2300 cbulk = 710
 isource:ib357 3577 0 idc= 0.4108e-3

ThermalBlock3:b358 3581 3481 3583 3573 5 2585 3587 lx=246.7u ly=261.915u
 +habove= 0.6u hbelow = 5.11u
 +dn= 2.6910 ds= 1.8165 de= 1.6529 dw= 2.5935 dt= 0.0853 db= 0.0853
 +kmx= 146 kmy= 146 kmz= 170 kild= 1.1 kbulk= 1.1 rho = 2300 cbulk = 710
 isource:ib358 3587 0 idc= 0.4212e-3

ThermalBlock3:b359 3591 3491 3 3583 5 2595 3597 lx=246.7u ly=261.915u
 +habove= 0.6u hbelow = 5.11u
 +dn= 3.1283 ds= 2.9714 de= 0.0000 dw= 1.6529 dt= 0.0474 db= 0.0474
 +kmx= 146 kmy= 146 kmz= 170 kild= 1.1 kbulk= 1.1 rho = 2300 cbulk = 710
 isource:ib359 3597 0 idc= 0.1658e-3

ThermalBlock3:b360 3601 3501 3603 4 5 2605 3607 lx=246.7u ly=261.915u
 +habove= 0.6u hbelow = 5.11u
 +dn= 2.3883 ds= 3.3302 de= 1.9699 dw= 0.0000 dt= 0.0284 db= 0.0284
 +kmx= 146 kmy= 146 kmz= 170 kild= 1.1 kbulk= 1.1 rho = 2300 cbulk = 710
 isource:ib360 3607 0 idc= 0.2049e-3

ThermalBlock3:b361 3611 3511 3613 3603 5 2615 3617 lx=246.7u ly=261.915u
 +habove= 0.6u hbelow = 5.11u
 +dn= 1.6707 ds= 2.2874 de= 1.9488 dw= 1.9699 dt= 0.0616 db= 0.0616
 +kmx= 146 kmy= 146 kmz= 170 kild= 1.1 kbulk= 1.1 rho = 2300 cbulk = 710
 isource:ib361 3617 0 idc= 0.4308e-3

ThermalBlock3:b362 3621 3521 3623 3613 5 2625 3627 lx=246.7u ly=261.915u
 +habove= 0.6u hbelow = 5.11u
 +dn= 1.9622 ds= 2.4107 de= 2.0228 dw= 1.9488 dt= 0.0758 db= 0.0758
 +kmx= 146 kmy= 146 kmz= 170 kild= 1.1 kbulk= 1.1 rho = 2300 cbulk = 710
 isource:ib362 3627 0 idc= 0.2767e-3

ThermalBlock3:b363 3631 3531 3633 3623 5 2635 3637 lx=246.7u ly=261.915u
 +habove= 0.6u hbelow = 5.11u
 +dn= 2.0856 ds= 2.0743 de= 2.1602 dw= 2.0228 dt= 0.0332 db= 0.0332
 +kmx= 146 kmy= 146 kmz= 170 kild= 1.1 kbulk= 1.1 rho = 2300 cbulk = 710

isource:ib363 3637 0 idc= 0.3545e-3

ThermalBlock3:b364 3641 3541 3643 3633 5 2645 3647 lx=246.7u ly=261.915u
 +habove= 0.6u hbelow = 5.11u
 +dn= 2.4444 ds= 2.1528 de= 2.1179 dw= 2.1602 dt= 0.0237 db= 0.0237
 +kmx= 146 kmy= 146 kmz= 170 kild= 1.1 kbulk= 1.1 rho = 2300 cbulk = 710
 isource:ib364 3647 0 idc= 0.4643e-3

ThermalBlock3:b365 3651 3551 3653 3643 5 2655 3657 lx=246.7u ly=261.915u
 +habove= 0.6u hbelow = 5.11u
 +dn= 2.0071 ds= 2.4780 de= 2.0439 dw= 2.1179 dt= 0.2228 db= 0.2228
 +kmx= 146 kmy= 146 kmz= 170 kild= 1.1 kbulk= 1.1 rho = 2300 cbulk = 710
 isource:ib365 3657 0 idc= 0.3307e-3

ThermalBlock3:b366 3661 3561 3663 3653 5 2665 3667 lx=246.7u ly=261.915u
 +habove= 0.6u hbelow = 5.11u
 +dn= 2.1640 ds= 2.3883 de= 1.8431 dw= 2.0439 dt= 0.1090 db= 0.1090
 +kmx= 146 kmy= 146 kmz= 170 kild= 1.1 kbulk= 1.1 rho = 2300 cbulk = 710
 isource:ib366 3667 0 idc= 0.4653e-3

ThermalBlock3:b367 3671 3571 3673 3663 5 2675 3677 lx=246.7u ly=261.915u
 +habove= 0.6u hbelow = 5.11u
 +dn= 1.9510 ds= 2.8144 de= 2.2236 dw= 1.8431 dt= 0.0427 db= 0.0427
 +kmx= 146 kmy= 146 kmz= 170 kild= 1.1 kbulk= 1.1 rho = 2300 cbulk = 710
 isource:ib367 3677 0 idc= 0.4360e-3

ThermalBlock3:b368 3681 3581 3683 3673 5 2685 3687 lx=246.7u ly=261.915u
 +habove= 0.6u hbelow = 5.11u
 +dn= 1.5922 ds= 2.6910 de= 1.6846 dw= 2.2236 dt= 0.0521 db= 0.0521
 +kmx= 146 kmy= 146 kmz= 170 kild= 1.1 kbulk= 1.1 rho = 2300 cbulk = 710
 isource:ib368 3687 0 idc= 0.5824e-3

ThermalBlock3:b369 3691 3591 3 3683 5 2695 3697 lx=246.7u ly=261.915u
 +habove= 0.6u hbelow = 5.11u
 +dn= 2.3434 ds= 3.1283 de= 0.0000 dw= 1.6846 dt= 0.0332 db= 0.0332
 +kmx= 146 kmy= 146 kmz= 170 kild= 1.1 kbulk= 1.1 rho = 2300 cbulk = 710
 isource:ib369 3697 0 idc= 0.2050e-3

ThermalBlock3:b370 3701 3601 3703 4 5 2705 3707 lx=246.7u ly=261.915u
 +habove= 0.6u hbelow = 5.11u
 +dn= 2.7471 ds= 2.3883 de= 2.1284 dw= 0.0000 dt= 0.0427 db= 0.0427
 +kmx= 146 kmy= 146 kmz= 170 kild= 1.1 kbulk= 1.1 rho = 2300 cbulk = 710
 isource:ib370 3707 0 idc= 0.2989e-3

ThermalBlock3:b371 3711 3611 3713 3703 5 2715 3717 lx=246.7u ly=261.915u
 +habove= 0.6u hbelow = 5.11u
 +dn= 1.4240 ds= 1.6707 de= 1.3675 dw= 2.1284 dt= 0.0284 db= 0.0284
 +kmx= 146 kmy= 146 kmz= 170 kild= 1.1 kbulk= 1.1 rho = 2300 cbulk = 710
 isource:ib371 3717 0 idc= 0.3036e-3

ThermalBlock3:b372 3721 3621 3723 3713 5 2725 3727 lx=246.7u ly=261.915u
 +habove= 0.6u hbelow = 5.11u
 +dn= 2.1528 ds= 1.9622 de= 1.9171 dw= 1.3675 dt= 0.0332 db= 0.0332
 +kmx= 146 kmy= 146 kmz= 170 kild= 1.1 kbulk= 1.1 rho = 2300 cbulk = 710
 isource:ib372 3727 0 idc= 0.2549e-3

ThermalBlock3:b373 3731 3631 3733 3723 5 2735 3737 lx=246.7u ly=261.915u
 +habove= 0.6u hbelow = 5.11u
 +dn= 2.2762 ds= 2.0856 de= 2.6252 dw= 1.9171 dt= 0.0284 db= 0.0284
 +kmx= 146 kmy= 146 kmz= 170 kild= 1.1 kbulk= 1.1 rho = 2300 cbulk = 710
 isource:ib373 3737 0 idc= 0.2784e-3

ThermalBlock3:b374 3741 3641 3743 3733 5 2745 3747 lx=246.7u ly=261.915u
 +habove= 0.6u hbelow = 5.11u
 +dn= 2.0071 ds= 2.4444 de= 2.0545 dw= 2.6252 dt= 0.0237 db= 0.0237
 +kmx= 146 kmy= 146 kmz= 170 kild= 1.1 kbulk= 1.1 rho = 2300 cbulk = 710
 isource:ib374 3747 0 idc= 0.3276e-3

ThermalBlock3:b375 3751 3651 3753 3743 5 2755 3757 lx=246.7u ly=261.915u
 +habove= 0.6u hbelow = 5.11u
 +dn= 2.1304 ds= 2.0071 de= 2.6146 dw= 2.0545 dt= 0.1280 db= 0.1280
 +kmx= 146 kmy= 146 kmz= 170 kild= 1.1 kbulk= 1.1 rho = 2300 cbulk = 710
 isource:ib375 3757 0 idc= 0.4419e-3

ThermalBlock3:b376 3761 3661 3763 3753 5 2765 3767 lx=246.7u ly=261.915u
 +habove= 0.6u hbelow = 5.11u
 +dn= 2.1304 ds= 2.1640 de= 1.6952 dw= 2.6146 dt= 0.0332 db= 0.0332
 +kmx= 146 kmy= 146 kmz= 170 kild= 1.1 kbulk= 1.1 rho = 2300 cbulk = 710
 isource:ib376 3767 0 idc= 0.4631e-3

ThermalBlock3:b377 3771 3671 3773 3763 5 2775 3777 lx=246.7u ly=261.915u
 +habove= 0.6u hbelow = 5.11u
 +dn= 1.9846 ds= 1.9510 de= 1.8008 dw= 1.6952 dt= 0.0569 db= 0.0569
 +kmx= 146 kmy= 146 kmz= 170 kild= 1.1 kbulk= 1.1 rho = 2300 cbulk = 710
 isource:ib377 3777 0 idc= 0.3461e-3

ThermalBlock3:b378 3781 3681 3783 3773 5 2785 3787 lx=246.7u ly=261.915u
 +habove= 0.6u hbelow = 5.11u

+dn= 1.9174 ds= 1.5922 de= 1.4732 dw= 1.8008 dt= 0.0379 db= 0.0379
 +kmx= 146 kmy= 146 kmz= 170 kild= 1.1 kbulk= 1.1 rho = 2300 cbulk = 710
 isource:ib378 3787 0 idc= 0.3186e-3

ThermalBlock3:b379 3791 3691 3 3783 5 2795 3797 lx=246.7u ly=261.915u
 +habove= 0.6u hbelow = 5.11u
 +dn= 2.2537 ds= 2.3434 de= 0.0000 dw= 1.4732 dt= 0.0190 db= 0.0190
 +kmx= 146 kmy= 146 kmz= 170 kild= 1.1 kbulk= 1.1 rho = 2300 cbulk = 710
 isource:ib379 3797 0 idc= 0.2878e-3

ThermalBlock3:b380 3801 3701 3803 4 5 2805 3807 lx=246.7u ly=261.915u
 +habove= 0.6u hbelow = 5.11u
 +dn= 3.1171 ds= 2.7471 de= 1.7142 dw= 0.0000 dt= 0.0190 db= 0.0190
 +kmx= 146 kmy= 146 kmz= 170 kild= 1.1 kbulk= 1.1 rho = 2300 cbulk = 710
 isource:ib380 3807 0 idc= 0.2348e-3

ThermalBlock3:b381 3811 3711 3813 3803 5 2815 3817 lx=246.7u ly=261.915u
 +habove= 0.6u hbelow = 5.11u
 +dn= 1.4801 ds= 1.4240 de= 1.5239 dw= 1.7142 dt= 0.0190 db= 0.0190
 +kmx= 146 kmy= 146 kmz= 170 kild= 1.1 kbulk= 1.1 rho = 2300 cbulk = 710
 isource:ib381 3817 0 idc= 0.3534e-3

ThermalBlock3:b382 3821 3721 3823 3813 5 2825 3827 lx=246.7u ly=261.915u
 +habove= 0.6u hbelow = 5.11u
 +dn= 2.1865 ds= 2.1528 de= 1.9995 dw= 1.5239 dt= 0.0427 db= 0.0427
 +kmx= 146 kmy= 146 kmz= 170 kild= 1.1 kbulk= 1.1 rho = 2300 cbulk = 710
 isource:ib382 3827 0 idc= 0.2426e-3

ThermalBlock3:b383 3831 3731 3833 3823 5 2835 3837 lx=246.7u ly=261.915u
 +habove= 0.6u hbelow = 5.11u
 +dn= 2.1080 ds= 2.2762 de= 2.4857 dw= 1.9995 dt= 0.0284 db= 0.0284
 +kmx= 146 kmy= 146 kmz= 170 kild= 1.1 kbulk= 1.1 rho = 2300 cbulk = 710
 isource:ib383 3837 0 idc= 0.2958e-3

ThermalBlock3:b384 3841 3741 3843 3833 5 2845 3847 lx=246.7u ly=261.915u
 +habove= 0.6u hbelow = 5.11u
 +dn= 2.1080 ds= 2.0071 de= 2.2109 dw= 2.4857 dt= 0.0427 db= 0.0427
 +kmx= 146 kmy= 146 kmz= 170 kild= 1.1 kbulk= 1.1 rho = 2300 cbulk = 710
 isource:ib384 3847 0 idc= 0.2969e-3

ThermalBlock3:b385 3851 3751 3853 3843 5 2855 3857 lx=246.7u ly=261.915u
 +habove= 0.6u hbelow = 5.11u
 +dn= 2.0071 ds= 2.1304 de= 2.4011 dw= 2.2109 dt= 0.0427 db= 0.0427
 +kmx= 146 kmy= 146 kmz= 170 kild= 1.1 kbulk= 1.1 rho = 2300 cbulk = 710

isource:ib385 3857 0 idc= 0.4924e-3

ThermalBlock3:b386 3861 3761 3863 3853 5 2865 3867 lx=246.7u ly=261.915u
 +habove= 0.6u hbelow = 5.11u
 +dn= 2.1080 ds= 2.1304 de= 1.6719 dw= 2.4011 dt= 0.0427 db= 0.0427
 +kmx= 146 kmy= 146 kmz= 170 kild= 1.1 kbulk= 1.1 rho = 2300 cbulk = 710
 isource:ib386 3867 0 idc= 0.2792e-3

ThermalBlock3:b387 3871 3771 3873 3863 5 2875 3877 lx=246.7u ly=261.915u
 +habove= 0.6u hbelow = 5.11u
 +dn= 2.2201 ds= 1.9846 de= 1.7353 dw= 1.6719 dt= 0.0284 db= 0.0284
 +kmx= 146 kmy= 146 kmz= 170 kild= 1.1 kbulk= 1.1 rho = 2300 cbulk = 710
 isource:ib387 3877 0 idc= 0.2699e-3

ThermalBlock3:b388 3881 3781 3883 3873 5 2885 3887 lx=246.7u ly=261.915u
 +habove= 0.6u hbelow = 5.11u
 +dn= 2.1528 ds= 1.9174 de= 1.8304 dw= 1.7353 dt= 0.0284 db= 0.0284
 +kmx= 146 kmy= 146 kmz= 170 kild= 1.1 kbulk= 1.1 rho = 2300 cbulk = 710
 isource:ib388 3887 0 idc= 0.2993e-3

ThermalBlock3:b389 3891 3791 3 3883 5 2895 3897 lx=246.7u ly=261.915u
 +habove= 0.6u hbelow = 5.11u
 +dn= 3.0274 ds= 2.2537 de= 0.0000 dw= 1.8304 dt= 0.0190 db= 0.0190
 +kmx= 146 kmy= 146 kmz= 170 kild= 1.1 kbulk= 1.1 rho = 2300 cbulk = 710
 isource:ib389 3897 0 idc= 0.2612e-3

ThermalBlock3:b390 1 3801 3903 4 5 2905 3907 lx=246.7u ly=261.915u
 +habove= 0.6u hbelow = 5.11u
 +dn= 0.0000 ds= 3.1171 de= 1.4309 dw= 0.0000 dt= 0.0000 db= 0.0000
 +kmx= 146 kmy= 146 kmz= 170 kild= 1.1 kbulk= 1.1 rho = 2300 cbulk = 710
 isource:ib390 3907 0 idc= 0.0888e-3

ThermalBlock3:b391 1 3811 3913 3903 5 2915 3917 lx=246.7u ly=261.915u
 +habove= 0.6u hbelow = 5.11u
 +dn= 0.0000 ds= 1.4801 de= 1.3675 dw= 1.4309 dt= 0.0047 db= 0.0047
 +kmx= 146 kmy= 146 kmz= 170 kild= 1.1 kbulk= 1.1 rho = 2300 cbulk = 710
 isource:ib391 3917 0 idc= 0.0937e-3

ThermalBlock3:b392 1 3821 3923 3913 5 2925 3927 lx=246.7u ly=261.915u
 +habove= 0.6u hbelow = 5.11u
 +dn= 0.0000 ds= 2.1865 de= 1.6317 dw= 1.3675 dt= 0.0000 db= 0.0000
 +kmx= 146 kmy= 146 kmz= 170 kild= 1.1 kbulk= 1.1 rho = 2300 cbulk = 710
 isource:ib392 3927 0 idc= 0.0852e-3

```

ThermalBlock3:b393 1 3831 3933 3923 5 2935 3937 lx=246.7u ly=261.915u
+habove= 0.6u hbelow = 5.11u
+dn= 0.0000 ds= 2.1080 de= 1.5789 dw= 1.6317 dt= 0.0047 db= 0.0047
+kmx= 146 kmy= 146 kmz= 170 kild= 1.1 kbulk= 1.1 rho = 2300 cbulk = 710
isource:ib393 3937 0 idc= 0.1069e-3

```

```

ThermalBlock3:b394 1 3841 3943 3933 5 2945 3947 lx=246.7u ly=261.915u
+habove= 0.6u hbelow = 5.11u
+dn= 0.0000 ds= 2.1080 de= 1.8325 dw= 1.5789 dt= 0.0000 db= 0.0000
+kmx= 146 kmy= 146 kmz= 170 kild= 1.1 kbulk= 1.1 rho = 2300 cbulk = 710
isource:ib394 3947 0 idc= 0.0731e-3

```

```

ThermalBlock3:b395 1 3851 3953 3943 5 2955 3957 lx=246.7u ly=261.915u
+habove= 0.6u hbelow = 5.11u
+dn= 0.0000 ds= 2.0071 de= 1.5472 dw= 1.8325 dt= 0.0237 db= 0.0237
+kmx= 146 kmy= 146 kmz= 170 kild= 1.1 kbulk= 1.1 rho = 2300 cbulk = 710
isource:ib395 3957 0 idc= 0.1124e-3

```

```

ThermalBlock3:b396 1 3861 3963 3953 5 2965 3967 lx=246.7u ly=261.915u
+habove= 0.6u hbelow = 5.11u
+dn= 0.0000 ds= 2.1080 de= 8.4335 dw= 1.5472 dt= 0.0000 db= 0.0000
+kmx= 146 kmy= 146 kmz= 170 kild= 1.1 kbulk= 1.1 rho = 2300 cbulk = 710
isource:ib396 3967 0 idc= 0.0773e-3

```

```

ThermalBlock3:b397 1 3871 3973 3963 5 2975 3977 lx=246.7u ly=261.915u
+habove= 0.6u hbelow = 5.11u
+dn= 0.0000 ds= 2.2201 de= 1.3147 dw= 8.4335 dt= 0.0095 db= 0.0095
+kmx= 146 kmy= 146 kmz= 170 kild= 1.1 kbulk= 1.1 rho = 2300 cbulk = 710
isource:ib397 3977 0 idc= 0.0740e-3

```

```

ThermalBlock3:b398 1 3881 3983 3973 5 2985 3987 lx=246.7u ly=261.915u
+habove= 0.6u hbelow = 5.11u
+dn= 0.0000 ds= 2.1528 de= 1.6106 dw= 1.3147 dt= 0.0047 db= 0.0047
+kmx= 146 kmy= 146 kmz= 170 kild= 1.1 kbulk= 1.1 rho = 2300 cbulk = 710
isource:ib398 3987 0 idc= 0.0863e-3

```

```

ThermalBlock3:b399 1 3891 3 3983 5 2995 3997 lx=246.7u ly=261.915u
+habove= 0.6u hbelow = 5.11u
+dn= 0.0000 ds= 3.0274 de= 0.0000 dw= 1.6106 dt= 0.0000 db= 0.0000
+kmx= 146 kmy= 146 kmz= 170 kild= 1.1 kbulk= 1.1 rho = 2300 cbulk = 710
isource:ib399 3997 0 idc= 0.0798e-3

```

```

*Resistors to sidewalls
res:r1 1 11 r=0.1e9

```

```
res:r2 2 22 r=0.1e9
res:r3 3 33 r=0.1e9
res:r4 4 44 r=0.1e9
res:r6 5 55 r=0.1e9
***adding epoxy Rth and Handle Si Rth
**Si Handle is 675um thick and has a thermal conductivity of 146 Wm/K
res:rsi 6 7 r=0.73
res:rsix1 6 1 r=5.5
res:rsix2 6 2 r=5.5
res:rsix3 6 3 r=5.5
res:rsix4 6 4 r=5.5
**Epoxy is 200um thick and has a thermal conductivity of 1 Wm/K
res:re 7 8 r=15.425
res:re1 8 1 r=2354.9
res:re2 8 2 r=2354.9
res:re3 8 3 r=2354.9
res:re4 8 4 r=2354.9
res:rev 8 9 r=15.425

vsource:v1 11 0 vdc=300
vsource:v2 22 0 vdc=300
vsource:v3 33 0 vdc=300
vsource:v4 44 0 vdc=300
vsource:v5 55 0 vdc=300
*Heat sink
vsource:v6 9 0 vdc=300

.dc
.out plot term 7 vt in "tepoxy.out"
.out plot term 1007 vt in "temperature1007.out"
.out plot term 1017 vt in "temperature1017.out"
.out plot term 1027 vt in "temperature1027.out"
.out plot term 1037 vt in "temperature1037.out"
.out plot term 1047 vt in "temperature1047.out"
.out plot term 1057 vt in "temperature1057.out"
.out plot term 1067 vt in "temperature1067.out"
.out plot term 1077 vt in "temperature1077.out"
.out plot term 1087 vt in "temperature1087.out"
.out plot term 1097 vt in "temperature1097.out"
.out plot term 1107 vt in "temperature1107.out"
.out plot term 1117 vt in "temperature1117.out"
.out plot term 1127 vt in "temperature1127.out"
.out plot term 1137 vt in "temperature1137.out"
.out plot term 1147 vt in "temperature1147.out"
```

.out plot term 1157 vt in "temperature1157.out"
.out plot term 1167 vt in "temperature1167.out"
.out plot term 1177 vt in "temperature1177.out"
.out plot term 1187 vt in "temperature1187.out"
.out plot term 1197 vt in "temperature1197.out"
.out plot term 1207 vt in "temperature1207.out"
.out plot term 1217 vt in "temperature1217.out"
.out plot term 1227 vt in "temperature1227.out"
.out plot term 1237 vt in "temperature1237.out"
.out plot term 1247 vt in "temperature1247.out"
.out plot term 1257 vt in "temperature1257.out"
.out plot term 1267 vt in "temperature1267.out"
.out plot term 1277 vt in "temperature1277.out"
.out plot term 1287 vt in "temperature1287.out"
.out plot term 1297 vt in "temperature1297.out"
.out plot term 1307 vt in "temperature1307.out"
.out plot term 1317 vt in "temperature1317.out"
.out plot term 1327 vt in "temperature1327.out"
.out plot term 1337 vt in "temperature1337.out"
.out plot term 1347 vt in "temperature1347.out"
.out plot term 1357 vt in "temperature1357.out"
.out plot term 1367 vt in "temperature1367.out"
.out plot term 1377 vt in "temperature1377.out"
.out plot term 1387 vt in "temperature1387.out"
.out plot term 1397 vt in "temperature1397.out"
.out plot term 1407 vt in "temperature1407.out"
.out plot term 1417 vt in "temperature1417.out"
.out plot term 1427 vt in "temperature1427.out"
.out plot term 1437 vt in "temperature1437.out"
.out plot term 1447 vt in "temperature1447.out"
.out plot term 1457 vt in "temperature1457.out"
.out plot term 1467 vt in "temperature1467.out"
.out plot term 1477 vt in "temperature1477.out"
.out plot term 1487 vt in "temperature1487.out"
.out plot term 1497 vt in "temperature1497.out"
.out plot term 1507 vt in "temperature1507.out"
.out plot term 1517 vt in "temperature1517.out"
.out plot term 1527 vt in "temperature1527.out"
.out plot term 1537 vt in "temperature1537.out"
.out plot term 1547 vt in "temperature1547.out"
.out plot term 1557 vt in "temperature1557.out"
.out plot term 1567 vt in "temperature1567.out"
.out plot term 1577 vt in "temperature1577.out"
.out plot term 1587 vt in "temperature1587.out"

.out plot term 1597 vt in "temperature1597.out"
.out plot term 1607 vt in "temperature1607.out"
.out plot term 1617 vt in "temperature1617.out"
.out plot term 1627 vt in "temperature1627.out"
.out plot term 1637 vt in "temperature1637.out"
.out plot term 1647 vt in "temperature1647.out"
.out plot term 1657 vt in "temperature1657.out"
.out plot term 1667 vt in "temperature1667.out"
.out plot term 1677 vt in "temperature1677.out"
.out plot term 1687 vt in "temperature1687.out"
.out plot term 1697 vt in "temperature1697.out"
.out plot term 1707 vt in "temperature1707.out"
.out plot term 1717 vt in "temperature1717.out"
.out plot term 1727 vt in "temperature1727.out"
.out plot term 1737 vt in "temperature1737.out"
.out plot term 1747 vt in "temperature1747.out"
.out plot term 1757 vt in "temperature1757.out"
.out plot term 1767 vt in "temperature1767.out"
.out plot term 1777 vt in "temperature1777.out"
.out plot term 1787 vt in "temperature1787.out"
.out plot term 1797 vt in "temperature1797.out"
.out plot term 1807 vt in "temperature1807.out"
.out plot term 1817 vt in "temperature1817.out"
.out plot term 1827 vt in "temperature1827.out"
.out plot term 1837 vt in "temperature1837.out"
.out plot term 1847 vt in "temperature1847.out"
.out plot term 1857 vt in "temperature1857.out"
.out plot term 1867 vt in "temperature1867.out"
.out plot term 1877 vt in "temperature1877.out"
.out plot term 1887 vt in "temperature1887.out"
.out plot term 1897 vt in "temperature1897.out"
.out plot term 1907 vt in "temperature1907.out"
.out plot term 1917 vt in "temperature1917.out"
.out plot term 1927 vt in "temperature1927.out"
.out plot term 1937 vt in "temperature1937.out"
.out plot term 1947 vt in "temperature1947.out"
.out plot term 1957 vt in "temperature1957.out"
.out plot term 1967 vt in "temperature1967.out"
.out plot term 1977 vt in "temperature1977.out"
.out plot term 1987 vt in "temperature1987.out"
.out plot term 1997 vt in "temperature1997.out"
.out plot term 2007 vt in "temperature2007.out"
.out plot term 2017 vt in "temperature2017.out"
.out plot term 2027 vt in "temperature2027.out"

.out plot term 2037 vt in "temperature2037.out"
.out plot term 2047 vt in "temperature2047.out"
.out plot term 2057 vt in "temperature2057.out"
.out plot term 2067 vt in "temperature2067.out"
.out plot term 2077 vt in "temperature2077.out"
.out plot term 2087 vt in "temperature2087.out"
.out plot term 2097 vt in "temperature2097.out"
.out plot term 2107 vt in "temperature2107.out"
.out plot term 2117 vt in "temperature2117.out"
.out plot term 2127 vt in "temperature2127.out"
.out plot term 2137 vt in "temperature2137.out"
.out plot term 2147 vt in "temperature2147.out"
.out plot term 2157 vt in "temperature2157.out"
.out plot term 2167 vt in "temperature2167.out"
.out plot term 2177 vt in "temperature2177.out"
.out plot term 2187 vt in "temperature2187.out"
.out plot term 2197 vt in "temperature2197.out"
.out plot term 2207 vt in "temperature2207.out"
.out plot term 2217 vt in "temperature2217.out"
.out plot term 2227 vt in "temperature2227.out"
.out plot term 2237 vt in "temperature2237.out"
.out plot term 2247 vt in "temperature2247.out"
.out plot term 2257 vt in "temperature2257.out"
.out plot term 2267 vt in "temperature2267.out"
.out plot term 2277 vt in "temperature2277.out"
.out plot term 2287 vt in "temperature2287.out"
.out plot term 2297 vt in "temperature2297.out"
.out plot term 2307 vt in "temperature2307.out"
.out plot term 2317 vt in "temperature2317.out"
.out plot term 2327 vt in "temperature2327.out"
.out plot term 2337 vt in "temperature2337.out"
.out plot term 2347 vt in "temperature2347.out"
.out plot term 2357 vt in "temperature2357.out"
.out plot term 2367 vt in "temperature2367.out"
.out plot term 2377 vt in "temperature2377.out"
.out plot term 2387 vt in "temperature2387.out"
.out plot term 2397 vt in "temperature2397.out"
.out plot term 2407 vt in "temperature2407.out"
.out plot term 2417 vt in "temperature2417.out"
.out plot term 2427 vt in "temperature2427.out"
.out plot term 2437 vt in "temperature2437.out"
.out plot term 2447 vt in "temperature2447.out"
.out plot term 2457 vt in "temperature2457.out"
.out plot term 2467 vt in "temperature2467.out"

.out plot term 2477 vt in "temperature2477.out"
.out plot term 2487 vt in "temperature2487.out"
.out plot term 2497 vt in "temperature2497.out"
.out plot term 2507 vt in "temperature2507.out"
.out plot term 2517 vt in "temperature2517.out"
.out plot term 2527 vt in "temperature2527.out"
.out plot term 2537 vt in "temperature2537.out"
.out plot term 2547 vt in "temperature2547.out"
.out plot term 2557 vt in "temperature2557.out"
.out plot term 2567 vt in "temperature2567.out"
.out plot term 2577 vt in "temperature2577.out"
.out plot term 2587 vt in "temperature2587.out"
.out plot term 2597 vt in "temperature2597.out"
.out plot term 2607 vt in "temperature2607.out"
.out plot term 2617 vt in "temperature2617.out"
.out plot term 2627 vt in "temperature2627.out"
.out plot term 2637 vt in "temperature2637.out"
.out plot term 2647 vt in "temperature2647.out"
.out plot term 2657 vt in "temperature2657.out"
.out plot term 2667 vt in "temperature2667.out"
.out plot term 2677 vt in "temperature2677.out"
.out plot term 2687 vt in "temperature2687.out"
.out plot term 2697 vt in "temperature2697.out"
.out plot term 2707 vt in "temperature2707.out"
.out plot term 2717 vt in "temperature2717.out"
.out plot term 2727 vt in "temperature2727.out"
.out plot term 2737 vt in "temperature2737.out"
.out plot term 2747 vt in "temperature2747.out"
.out plot term 2757 vt in "temperature2757.out"
.out plot term 2767 vt in "temperature2767.out"
.out plot term 2777 vt in "temperature2777.out"
.out plot term 2787 vt in "temperature2787.out"
.out plot term 2797 vt in "temperature2797.out"
.out plot term 2807 vt in "temperature2807.out"
.out plot term 2817 vt in "temperature2817.out"
.out plot term 2827 vt in "temperature2827.out"
.out plot term 2837 vt in "temperature2837.out"
.out plot term 2847 vt in "temperature2847.out"
.out plot term 2857 vt in "temperature2857.out"
.out plot term 2867 vt in "temperature2867.out"
.out plot term 2877 vt in "temperature2877.out"
.out plot term 2887 vt in "temperature2887.out"
.out plot term 2897 vt in "temperature2897.out"
.out plot term 2907 vt in "temperature2907.out"

.out plot term 2917 vt in "temperature2917.out"
.out plot term 2927 vt in "temperature2927.out"
.out plot term 2937 vt in "temperature2937.out"
.out plot term 2947 vt in "temperature2947.out"
.out plot term 2957 vt in "temperature2957.out"
.out plot term 2967 vt in "temperature2967.out"
.out plot term 2977 vt in "temperature2977.out"
.out plot term 2987 vt in "temperature2987.out"
.out plot term 2997 vt in "temperature2997.out"
.out plot term 3007 vt in "temperature3007.out"
.out plot term 3017 vt in "temperature3017.out"
.out plot term 3027 vt in "temperature3027.out"
.out plot term 3037 vt in "temperature3037.out"
.out plot term 3047 vt in "temperature3047.out"
.out plot term 3057 vt in "temperature3057.out"
.out plot term 3067 vt in "temperature3067.out"
.out plot term 3077 vt in "temperature3077.out"
.out plot term 3087 vt in "temperature3087.out"
.out plot term 3097 vt in "temperature3097.out"
.out plot term 3107 vt in "temperature3107.out"
.out plot term 3117 vt in "temperature3117.out"
.out plot term 3127 vt in "temperature3127.out"
.out plot term 3137 vt in "temperature3137.out"
.out plot term 3147 vt in "temperature3147.out"
.out plot term 3157 vt in "temperature3157.out"
.out plot term 3167 vt in "temperature3167.out"
.out plot term 3177 vt in "temperature3177.out"
.out plot term 3187 vt in "temperature3187.out"
.out plot term 3197 vt in "temperature3197.out"
.out plot term 3207 vt in "temperature3207.out"
.out plot term 3217 vt in "temperature3217.out"
.out plot term 3227 vt in "temperature3227.out"
.out plot term 3237 vt in "temperature3237.out"
.out plot term 3247 vt in "temperature3247.out"
.out plot term 3257 vt in "temperature3257.out"
.out plot term 3267 vt in "temperature3267.out"
.out plot term 3277 vt in "temperature3277.out"
.out plot term 3287 vt in "temperature3287.out"
.out plot term 3297 vt in "temperature3297.out"
.out plot term 3307 vt in "temperature3307.out"
.out plot term 3317 vt in "temperature3317.out"
.out plot term 3327 vt in "temperature3327.out"
.out plot term 3337 vt in "temperature3337.out"
.out plot term 3347 vt in "temperature3347.out"

.out plot term 3357 vt in "temperature3357.out"
.out plot term 3367 vt in "temperature3367.out"
.out plot term 3377 vt in "temperature3377.out"
.out plot term 3387 vt in "temperature3387.out"
.out plot term 3397 vt in "temperature3397.out"
.out plot term 3407 vt in "temperature3407.out"
.out plot term 3417 vt in "temperature3417.out"
.out plot term 3427 vt in "temperature3427.out"
.out plot term 3437 vt in "temperature3437.out"
.out plot term 3447 vt in "temperature3447.out"
.out plot term 3457 vt in "temperature3457.out"
.out plot term 3467 vt in "temperature3467.out"
.out plot term 3477 vt in "temperature3477.out"
.out plot term 3487 vt in "temperature3487.out"
.out plot term 3497 vt in "temperature3497.out"
.out plot term 3507 vt in "temperature3507.out"
.out plot term 3517 vt in "temperature3517.out"
.out plot term 3527 vt in "temperature3527.out"
.out plot term 3537 vt in "temperature3537.out"
.out plot term 3547 vt in "temperature3547.out"
.out plot term 3557 vt in "temperature3557.out"
.out plot term 3567 vt in "temperature3567.out"
.out plot term 3577 vt in "temperature3577.out"
.out plot term 3587 vt in "temperature3587.out"
.out plot term 3597 vt in "temperature3597.out"
.out plot term 3607 vt in "temperature3607.out"
.out plot term 3617 vt in "temperature3617.out"
.out plot term 3627 vt in "temperature3627.out"
.out plot term 3637 vt in "temperature3637.out"
.out plot term 3647 vt in "temperature3647.out"
.out plot term 3657 vt in "temperature3657.out"
.out plot term 3667 vt in "temperature3667.out"
.out plot term 3677 vt in "temperature3677.out"
.out plot term 3687 vt in "temperature3687.out"
.out plot term 3697 vt in "temperature3697.out"
.out plot term 3707 vt in "temperature3707.out"
.out plot term 3717 vt in "temperature3717.out"
.out plot term 3727 vt in "temperature3727.out"
.out plot term 3737 vt in "temperature3737.out"
.out plot term 3747 vt in "temperature3747.out"
.out plot term 3757 vt in "temperature3757.out"
.out plot term 3767 vt in "temperature3767.out"
.out plot term 3777 vt in "temperature3777.out"
.out plot term 3787 vt in "temperature3787.out"

```

.out plot term 3797 vt in "temperature3797.out"
.out plot term 3807 vt in "temperature3807.out"
.out plot term 3817 vt in "temperature3817.out"
.out plot term 3827 vt in "temperature3827.out"
.out plot term 3837 vt in "temperature3837.out"
.out plot term 3847 vt in "temperature3847.out"
.out plot term 3857 vt in "temperature3857.out"
.out plot term 3867 vt in "temperature3867.out"
.out plot term 3877 vt in "temperature3877.out"
.out plot term 3887 vt in "temperature3887.out"
.out plot term 3897 vt in "temperature3897.out"
.out plot term 3907 vt in "temperature3907.out"
.out plot term 3917 vt in "temperature3917.out"
.out plot term 3927 vt in "temperature3927.out"
.out plot term 3937 vt in "temperature3937.out"
.out plot term 3947 vt in "temperature3947.out"
.out plot term 3957 vt in "temperature3957.out"
.out plot term 3967 vt in "temperature3967.out"
.out plot term 3977 vt in "temperature3977.out"
.out plot term 3987 vt in "temperature3987.out"
.out plot term 3997 vt in "temperature3997.out"
.end

```

B.11 BSIMSOI Extracted Model Parameters

The model parameters to verify the BSIMSOI model developed in *fREEDA*[™] are given in Table B.3. These parameters were received from MIT Lincoln Labs.

B.12 Netlist To Verify The BSIMSOI Model

The netlist to verify the electrothermal BSIMSOI model developed in *fREEDA*[™] is given below. This netlist is used to simulate the results in Section 6.3

```

** BSIMSOI mosfet dc characteristic ****
.dc sweep="vsource:vd" start=0 stop=2.0 step=0.1
.model nf_soi nmos
+tsi=4.2e-8 nch = 5.8e17
+TOX = 4.2E-9 TOXM = 4.2e-9
+TBOX = 4.0E-7 XJ = 1E-7
+NSUB = 2E13 VTH0 = 0.61 K1 = 0.56

```

Table B.3: Model parameters of the FDSOI MOSFET from MIT Lincoln Labs.

A0	-0.3	K2	0	TCJSWG	0.0005	RSHG	1.6
A1	0	K2B	0.25	TII	-0.2264	RTH0	0.1
A2	0.99	K3	0	TNOM	22	SHMOD	1
ACDE	0.11	K3B	0	TOX	4.2E-09	SIIO	2
AELY	0	KB1	0	TSI	4.2E-08	SI1	0
AGIDL	4E-09	KETA	0	TT	3E-10	SI2	0
AGS	0	KETAS	0	U0	370	SIID	0
AHLI	1E-15	KT1	-0.16	UA	0	SOIMOD	1
ALPHA0	8E-09	KT1L	0	UA1	0	TBOX	4E-07
ASD	0.3	KT2	-0.0646	UB	1E-18	FBJTII	0
AT	34000	LBJT0	9E-08	UB1	0	RHALO	1E+15
B0	0	LDIF0	0.001	UC	0	ETAB	0
B1	0	LEVEL	33	UC1	0	RGATEM	1
BETA0	0	LII	-1E-08	UTE	-1.8	ETA0	0.05
BETA1	0	LINT	4E-08	VABJT	10	RDSW	320
BETA2	0.15	LL	0	VBSA	0.16	K1W2	0
BGIDL	2E+09	LLN	2	VDSATII0	0.5		
CAPMOD	2	LN	7E-07	VERSION	3.2		
CDSC	0.01	LW	0	VOFF	-0.16		
CDSCB	-0.01	LWL	2E-28	VOFFFD	0		
CDSCD	0	LWN	1	VREC0	0.05		
CF	0	MJSWG	0.5	VSAT	75000		
CGDL	0	MOBMOD	1	VSDFB	-0.8		
CGDO	6E-10	MOIN	15	VSDTH	-0.3		
CGEO	0	MOINFD	1000000	VTH0	0.61		
CGSL	0	NBJT	2.5	VTUN0	0		
CGSO	2.5E-10	NCH	5.8E+17	W0	0		
CIT	0	NDIF	-1	WINT	0		
CJSWG	8E-10	NDIODE	1	WL	0		
CKAPPA	0.6	NFACTOR	1	WLN	1		
CLC	5E-08	NGATE	1.5E+20	WR	0.82		
CLE	0.6	NGCON	1	WTH0	0.000004		
CSDESW	0	NGIDL	0.5	WW	0		
CSDMIN	0.000016	NLX	0	WWL	0		
CTH0	0.00001	NOFFFD	1	WWN	1		
DELTA	0.01	NRB	1	XBJT	1.15		
DELVT	0	NRECF0	1.8	XDIF	1.11		
DK2B	0.4	NRECF0	10	XGL	0		
DLBG	0	NSUB	2E+13	XGW	0		
DLCB	0	NTRECF	-0.3	XJ	1E-07		
DROUT	0.4	NTRECR	10	XPART	0		
DSUB	0.2	NTUN	10	XRCRG1	12		
DVBD0	2.4	PBSWG	0.9	XRCRG2	1		
DVBD1	0.5	PCLM	0.8	XREC	0.9		
DVT0	2.4	PDIBLC1	0.1	XTUN	0		
DVT0W	-1.3	PDIBLC2	0	FBODY	1		
DVT1	0.5	PDIBLCB	0	ISBJT	0.000002		
DVT1W	500000	PRT	10	ISDIF	4E-08		
DVT2	0	PRWB	0	ISREC	0.003		
DVT2W	0	PRWG	0	ISTUN	0.00001		
DWB	0	PVAG	0	K1	0.56		
DWG	-4E-08	RBODY	10	K1B	0.8		
ESATII	4.00E+06	RBSH	100	K1W1	0		

```

+K2 = 0 K3 = 0 K3B = 0
+K1W1 = 0 K1W2 = 0 KB1 = 0
+W0 = 0 NLX = 0 DVTOW = -1.3
+AGIDL = 4E-9 BGIDL = 2E9 NGIDL = 0.5
+DVT1W = 5E5 DVT2W = 0 DVTO = 2.4
+DVT1 = 0.5 DVT2 = 0 UO = 0.037
+UA = 0 UB = 1E-18 UC = 0
+VSAT = 7.5E4 AO = -0.3 AGS = 0
+B0 = 0 B1 = 0 FBJTII = 0
+ESATII = 4E6 SII0 = 2 SII1 = 0
+SII2 = 0 SIID = 0 KETA = 0
+KETAS = 0 RTHO = 0.1 A1 = 0
+A2 = 0.99 RDSW = 320 PRWG = 0
+PRWB = 0 WR = 0.82
+LINT = 4E-8 DWG = 0 DWB = 0
+VOFF = -0.16 NFACTOR = 1 CIT = 0
+CDSC = 0.01 CDSCD = 0 CDSCB = -0.01
+BETA0 = 0 BETA1 = 0 BETA2 = 0.15
+ETA0 = 0.05 ETAB = 0 DSUB = 0.2
+PCLM = 0.8 PDIBLC1 = 0.1 PDIBLC2 = 0
+PDIBLCB = 0 DROUT = 0.4 PVAG = 0
+DELTA = 0.01 NGATE = 1.5E20 ALPHA0 = 8E-9
+VDSATII0 = 0.5 MOBMOD = 1 TII = -0.2264
+PRT = 10 UTE = -1.8 KT1 = -0.16
+KT1L = 0 LII = 1E-8 KT2 = -0.0646
+UA1 = 0 UB1 = 0
+AT = 3.4E4 TCJSWG = 5E-4 WL = 0
+WLN = 1 WVN = 0.7
+WWL = 0 LL = 0 LLN = 2
+LW = 0 LWN = 1 LWL = 2e-28
+CAPMOD = 2 XPART = 0 CJSWG = 8E-10
+PBSWG = 0.9 MJSWG = 0.5 CSDESW = 0
+CSDMIN = 1.6e-5 CGDO = 6E-10 CGSO = 2.5E-10
+CGEO = 0 CGSL = 0 CGDL = 0
+CKAPPA = 0.6 CF = 0 CLC = 5E-8
+CLE = 0.6 DLC = 0 DWC = 0
+SHMOD = 1 RBODY = 10 RBSH = 100
+CTHO = 1E-5 NDIODE = 1 NTUN = 10
+VTUNO = 5 ISBJT = 2E-6 NBJT = 2.5
+LBJTO = 9E-8 VABJT = 10 AELY = 0
+AHLI = 1E-15 ISDIF = 4E-8 ISREC = 0.003
+ISTUN = 1E-5 XBJT = 1.15 XDIF = 1.11
+XREC = 0.8 XTUN = 0 NTRECF = -0.3
+NTRECR = 10 TT = 3E-10 LN = 7E-7

```

```

+NRECFO = 1.8 NRECRO = 10 VRECO = 0.05
+VSDTH = -0.3 VSDFB = -0.8 ASD = 0.3
+DLBG = 0 DELVT = 0 FBODY = 1
+ACDE = 0.11 MOIN = 15 LDIFO = 1E-3
+NDIF = -1 SOIMOD = 1 VBSA = 0.16
+DVBD0 = 2.4 DVBD1 = 0.5 NOFFFD = 1
+VOFFFD = 0 MOINFD = 1E6 DK2B = 0.4
+K2B = 0.25 WTH0 = 4E-6 RHALO = 1E15
+K1B = 0.8 temp=300
.ref "tref"
*bsim3nsoitest:m1 d g s b model="nf_soi" w=200e-6 l=0.2e-6
bsim3nsoitestt:m1 d g s b 1000 "tref" model="nf_soi" w=200e-6 l=0.2e-6
res:rth 1000 1001 r=300
vsource:vt 1001 "tref" vdc=300
cap:cd d 0 c=5e-12
vsource:vd d 0 vdc=1.0
vsource:vs s 0 vdc=0.0
vsource:vb b 0 vdc=0.0
*Gate bias
vsource:vg g 0 vdc=1.8
*Plot drain current
.out plot element "bsim3nsoitestt:m1" 0 it in "tsoi_idc_vg_1p8_300K.dc"
*Plot temperature
.out plot element "bsim3nsoitestt:m1" 3 ut in "tsoi_temp_vg_1p8_300K.dc"
.end

```

B.13 Measured BSIMSOI I/V Curves

The measured I/V curves of the FDSOI MOSFET used to verify the BSIMSOI model developed in *fREEDA*TM are shown in Table B.4. These measurements were received from the Air Force Research Lab, Dayton, Ohio.

Table B.4: Measured drain current (A) of the FDSOI MOSFET.

VDS	Vg=0.0	Vg=0.2	Vg=0.4	Vg=0.6	Vg=0.8	Vg=1.0	Vg=1.2	Vg=1.4	Vg=1.6	Vg=1.8	Vg=2.0
0	-1.60E-06	-1.06E-06	5.69E-07	-8.18E-05	-8.58E-05	-8.58E-05	-8.75E-05	-8.87E-05	-8.95E-05	-9.00E-05	-9.03E-05
0.1	-1.17E-06	8.53E-05	0.00127	0.004998	0.007962	0.009839	0.011087	0.011997	0.012599	0.01309	0.013388
0.2	-8.59E-07	3.62E-05	0.001806	0.008397	0.014958	0.019675	0.022835	0.02494	0.026418	0.027517	0.028336
0.3	3.57E-06	9.15E-05	0.002105	0.010051	0.019677	0.027213	0.032297	0.035859	0.038419	0.040254	0.041615
0.4	-2.96E-07	0.000174	0.002381	0.011095	0.022554	0.032524	0.039949	0.045273	0.049091	0.051887	0.053966
0.5	-1.04E-06	0.000198	0.002816	0.011925	0.024234	0.035996	0.045634	0.052908	0.058275	0.062215	0.065164
0.6	1.75E-06	0.000103	0.003175	0.01269	0.025447	0.038194	0.049594	0.05874	0.065746	0.071021	0.075042
0.7	2.35E-06	0.00013	0.00353	0.013394	0.026457	0.03973	0.052205	0.062931	0.07158	0.07827	0.083458
0.8	1.80E-07	0.000186	0.003886	0.01408	0.027349	0.040887	0.053964	0.065817	0.075857	0.083985	0.090378
0.9	8.61E-07	0.000189	0.004263	0.014733	0.028194	0.041878	0.055271	0.067784	0.078905	0.088261	0.095921
1	4.26E-08	0.00026	0.00468	0.0154	0.028967	0.042759	0.056291	0.069194	0.081005	0.091362	0.10012
1.1	1.90E-06	0.000333	0.005186	0.016134	0.02973	0.043554	0.05718	0.070242	0.082505	0.093573	0.10324
1.2	4.03E-07	0.000447	0.005796	0.01692	0.030488	0.044305	0.057925	0.071101	0.08359	0.095117	0.10547
1.3	2.58E-06	0.000603	0.006503	0.01784	0.031307	0.045039	0.05864	0.071809	0.084407	0.096223	0.10708
1.4	3.73E-06	0.000811	0.007305	0.018855	0.03222	0.045811	0.059319	0.072438	0.085078	0.097046	0.10819
1.5	1.50E-05	0.001088	0.008182	0.019962	0.033199	0.046642	0.06001	0.073015	0.085618	0.09766	0.10899
1.6	2.13E-05	0.001448	0.009153	0.021336	0.0343	0.047566	0.060745	0.073628	0.086132	0.098127	0.10959
1.7	6.91E-05	0.001928	0.010258	0.022519	0.03551	0.048591	0.061566	0.074267	0.086613	0.09855	0.11001
1.8	7.55E-05	0.002423	0.011554	0.023991	0.036876	0.049791	0.062519	0.074969	0.087147	0.098959	0.11035
1.9	0.000167	0.003449	0.013133	0.02571	0.03847	0.051154	0.063642	0.075841	0.087788	0.099413	0.1107
2	0.000392	0.004762	0.015088	0.027808	0.040399	0.052802	0.064958	0.076899	0.088552	0.099974	0.11107

B.14 BSIMSOI Model Parameters

Model parameters of the BSIMSOI model are listed in the tables below. These model parameters are taken from the UCB BSIMSOI users manual.

This manual is available with the UCB BSIMSOI model code and can be downloaded at <http://www-device.eecs.berkeley.edu/~bsimsoi/>.

Table B.5: BSIMSOI Built-In Potential Lowering (ΔV_{bi}) Model Parameters

Symbol used in equation	Symbol used in SPICE	Description	Unit	Default
$SoiMod$	soiMod	SOI model selector. SoiMod=0: BSIMPD. SoiMod=1: unified model for PD&FD. SoiMod=2: ideal FD.	-	0
$V_{nonideal}$	vbsa	Offset voltage due to non-idealities	V	0
$N_{OFF,FD}$	nofffd	Smoothing parameter in FD module	-	1
$V_{OFF,FD}$	vofffd	Smoothing parameter in FD module	V	0
K_{1b}	K1b	First backgate body effect parameter	-	1
K_{2b}	K2b	Second backgate body effect parameter for short channel effect	-	0
D_{k2b}	dk2b	Third backgate body effect parameter for short channel effect	-	0
D_{vbd0}	dvbd0	First short channel effect parameter in FD module	-	0
D_{vbd1}	dvbd1	Second short channel effect parameter in FD module	-	0
$MoinFD$	moinfd	Gate bias dependence coefficient of surface potential in FD module	-	1e3

Table B.6: BSIMSOI BSIMPD Model Control Parameters

Symbol used in equation	Symbol used in SPICE	Description	Unit	Default	Notes (below the table)
None	level	Level 9 for BSIM3SOI	-	9	-
<i>Shmod</i>	shMod	Flag for self-heating 0 - no self-heating, 1 - self-heating	-	0	
<i>Mobmod</i>	mobmod	Mobility model selector	-	1	-
<i>Capmod</i>	capmod	Flag for the short channel capacitance model	-	2	nI-1
<i>Noimod</i>	noimod	Flag for Noise model	-	1	-
<i>RgateMod</i>	rgateMod	Gate resistance model selector	-	0	-

Table B.7: Process Parameters

Symbol used in equation	Symbol used in SPICE	Description	Unit	Default	Notes (below the table)
t_{si}	Tsi	Silicon film thickness	m	10^{-7}	-
t_{box}	Tbox	Buried oxide thickness	m	3×10^{-7}	-
t_{ox}	Tox	Gate oxide thickness	m	1×10^{-8}	-
X_j	Xj	S/D junction depth	m	nI-2	-
n_{ch}	Nch	Channel doping concentration	$1/\text{cm}^3$	1.7×10^{17}	-
n_{sub}	Nsub	Substrate doping concentration	$1/\text{cm}^3$	6×10^{16}	nI-3
N_{gate}	ngate	poly gate doping concentration	$1/\text{cm}^3$	0	-

Table B.8: DC Parameters

Symbol used in equation	Symbol used in SPICE	Description	Unit	Default	Notes (below the table)
V_{th0}	vth0	Threshold voltage @ $V_{bs}=0$ for long and wide device	-	0.7	-
K_1	k1	First order body effect coefficient	$V^{1/2}$	0.6	-
K_{1w1}	k1w1	First body effect width dependent parameter	m	0	-
K_{1w2}	k1w2	Second body effect width dependent parameter	m	0	-
K_2	k2	Second order body effect coefficient	-	0	-
K_3	k3	Narrow width coefficient	-	0	-
K_{3b}	k3b	Body effect coefficient of k3	1/V	0	-
K_{b1}	Kb1	Backgate body charge coefficient	-	1	-
W_0	w0	Narrow width parameter	m	0	-
N_{LX}	nlx	Lateral non-uniform doping parameter	m	1.74e-7	-
D_{vt0}	Dvt0	first coefficient of short-channel effect on Vth	-	2.2	-
D_{vt1}	dvt1	Second coefficient of short-channel effect on Vth	-	0.53	-
D_{vt2}	dvt2	Body-bias coefficient of short-channel effect on Vth	1/V	-0.032	-
D_{vt0w}	dvt0w	first coefficient of narrow width effect on Vth for small channel length	-	0	-
D_{vt1w}	dvt1w	Second coefficient of narrow width effect on Vth for small channel length	-	5.3e6	-
D_{vt2w}	dvt2w	Body-bias coefficient of narrow width effect on Vth for small channel length	1/V	-0.032	-

μ_0	u0	Mobility at Temp = Tnom NMOSFET PMOSFET	cm ² /(V-sec)	670 250	-
U_a	ua	First-order mobility degradation coefficient	m/V	2.25e-9	-
U_b	ub	Second-order mobility degradation coefficient	(m/V) 2	5.9e-19	-
U_c	uc	Body-effect of mobility degradation coefficient	1/V	-.0465	-
v_{sat}	vsat	Saturation velocity at Temp=Tnom	m/sec	8e4	-
$A0$	a0	Bulk charge effect coefficient for channel length	-	1.0	-
A_{gs}	ags	Gate bias coefficient of A_{bulk}	1/V	0.0	-
$B0$	b0	Bulk charge effect coefficient for channel width	m	0.0	-
$B1$	b1	Bulk charge effect width offset	m	0.0	-
$Keta$	keta	Body-bias coefficient of bulk charge effect	V ⁻¹	0	-
$Ketas$	Ketas	Surface potential adjustment for bulk charge effect	V	0	-
A_1	A1	First non-saturation effect parameter	1/V	0.0	-
A_2	A2	Second non-saturation effect parameter	0	1.0	-
R_{dsw}	rdsw	Parasitic resistance per unit width	Ω - μm^{wr}	100	-
Prw_b	prwb	Body effect coefficient of R _{dsw}	1/V	0	-
Prw_g	prwg	Gate bias effect coefficient of R _{dsw}	1/V ^{1/2}	0	-
Wr	wr	Width offset from Weff for R _d s calculation	-	1	-
$Nfactor$	nfactor	Subthreshold swing factor	-	1	-

W_{int}	wint	Width offset fitting parameter from I-V without bias	m	0.0	-
L_{int}	lint	Length offset fitting parameter from I-V without bias	m	0.0	-
DW_g	dwg	Coefficient of W_{eff} 's gate dependence	m/V	0.0	
DW_b	dwb	Coefficient of W_{eff} 's substrate body bias dependence	m/V ^{1/2}	0.0	
DW_{bc}	Dwbc	Width offset for body contact isolation edge	m	0.0	
V_{off}	voff	Offset voltage in the subthreshold region for large W and L	V	-0.08	-
η_{0}	eta0	DIBL coefficient in subthreshold region	-	0.08	-
η_{ab}	etab	Body-bias coefficient for the subthreshold DIBL effect	1/V	-0.07	-
D_{sub}	dsub	DIBL coefficient exponent	-	0.56	-
C_{it}	cit	Interface trap capacitance	F/m ²	0.0	-
C_{dsc}	cdsc	Drain/Source to channel coupling capacitance	F/m ²	2.4e-4	-
C_{dscb}	cdscb	Body-bias sensitivity of C_{dsc}	F/m ²	0	-
C_{dscd}	cdscd	Drain-bias sensitivity of C_{dsc}	F/m ²	0	-
P_{clm}	pclm	Channel length modulation parameter	-	1.3	-
P_{dibl1}	pdibl1	First output resistance DIBL effect correction parameter	-	.39	-
P_{dibl2}	pdibl2	Second output resistance DIBL effect correction parameter	-	0.086	-
D_{rout}	drout	L dependence coefficient of the DIBL correction parameter in R_{out}	-	0.56	-
P_{vag}	pvag	Gate dependence of Early voltage	-	0.0	-
δ	delta	Effective V_{ds} parameter	-	0.01	-

α_0	alpha0	The first parameter of impact ionization current	m/V	0.0	-
F_{bjtiii}	fbjtiii	Fraction of bipolar current affecting the impact ionization	-	0.0	-
β_0	beta0	First V_{ds} dependent parameter of impact ionization current	V^{-1}	0	-
β_1	beta1	Second V_{ds} dependent parameter of impact ionization current	-	0	-
β_2	beta2	Third V_{ds} dependent parameter of impact ionization current	V	0.1	-
$V_{dsatiii0}$	vdsatiii0	Nominal drain saturation voltage at threshold for impact ionization current	V	0.9	-
T_{ii}	tii	Temperature dependent parameter for impact ionization current	-	0	-
L_{ii}	lii	Channel length dependent parameter at threshold for impact ionization current	-	0	-
E_{satiii}	esatiii	Saturation channel electric field for impact ionization current	V/m	1e7	-
S_{iii0}	siii0	First V_{gs} dependent parameter for impact ionization current	V^{-1}	0.5	-
S_{iii1}	siii1	Second V_{gs} dependent parameter for impact ionization current	V^{-1}	0.1	-
S_{iii2}	siii2	Third V_{gs} dependent parameter for impact ionization current	-	0	-
S_{iid}	siid	V_{ds} dependent parameter of drain saturation voltage for impact ionization current	V^{-1}	0	-
α_{gidl}	Agidl	GIDL constant	Ω^{-1}	0.0	-

β_{gidl}	Bgidl	GIDL exponential coefficient	V/m	0.0	-
χ	Ngidl	GIDL V_{ds} enhancement coefficient	V	1.2	-
n_{tun}	Ntun	Reverse tunneling non-ideality factor	-	10.0	-
n_{diode}	Ndio	Diode non-ideality factor	-	1.0	-
n_{recf0}	Nrecf0	Recombination non-ideality factor at forward bias	-	2.0	-
n_{recr0}	Nrecr0	Recombination non-ideality factor at reversed bias	-	10	-
i_{sbjt}	Isbjt	BJT injection saturation current	A/m ²	1e-6	-
i_{sdif}	Isdif	Body to source/drain injection saturation current	A/m ²	1e-7	-
i_{srec}	Isrec	Recombination in depletion saturation current	A/m ²	1e-5	-
i_{stun}	Istun	Reverse tunneling saturation current	A/m ²	0.0	-
Ln	Ln	Electron/hole diffusion length	m	2e-6	-
V_{rec0}	Vrec0	Voltage dependent parameter for recombination current	V	0	-
V_{tun0}	Vtun0	Voltage dependent parameter for tunneling current	V	0	-
N_{bjt}	Nbjt	Power coefficient of channel length dependency for bipolar current	-	1	-
L_{bjt0}	Lbjt0	Reference channel length for bipolar current	m	0.20e-6	-
V_{abjt}	Vabjt	Early voltage for bipolar current	V	10	-
A_{ely}	Aely	Channel length dependency of early voltage for bipolar current	V/m	0	-
A_{hli}	Ahli	High level injection parameter for bipolar current	-	0	-
R_{body}	Rbody	Intrinsic body contact sheet resistance	ohm/square	0.0	-

<i>Rbsh</i>	Rbsh	Extrinsic body contact sheet resistance	ohm/square	0.0	-
<i>Rsh</i>	rsh	Source drain sheet resistance in ohm per square	ohm/square	0.0	-
<i>Rhalo</i>	rhalo	Body halo sheet resistance	ohm/m	1e15	-

Table B.9: Gate-to-body Tunneling Parameters

Symbol used in equation	Symbol used in SPICE	Description	Unit	Default
I_{gMod}	igMod	Gate current model selector	-	0
$Toxqm$	toxqm	Oxide thickness for I_{gb} calculation	m	Tox
$Ntox$	ntox	Power term of gate current	-	1
$Toxref$	toxref	Target oxide thickness	m	2.5e-9
φ_g	ebg	Effective bandgap in gate current calculation	V	1.2
α_{gb1}	alphaGB1	First V_{ox} dependent parameter for gate current in inversion	1/V	.35
β_{gb1}	betaGB1	Second V_{ox} dependent parameter for gate current in inversion	1/V ²	.03
V_{gb1}	vgb1	Third V_{ox} dependent parameter for gate current in inversion	V	300
V_{EVB}	vevb	Vaux parameter for valence band electron tunneling	-	0.075
α_{gb2}	alphaGB2	First V_{ox} dependent parameter for gate current in accumulation	1/V	.43
β_{gb2}	betaGB2	Second V_{ox} dependent parameter for gate current in accumulation	1/V ²	.05
V_{gb2}	vgb2	Third V_{ox} dependent parameter for gate current in accumulation	V	17
V_{ECB}	vecb	Vaux parameter for conduction band electron tunneling	-	.026

Table B.10: AC and Capacitance Parameters

Symbol used in equation	Symbol used in SPICE	Description	Unit	Default	Notes (below the table)
X_{part}	xpart	Charge partitioning rate flag	-	0	
$CGSO$	cgso	Non LDD region source-gate overlap capacitance per channel length	F/m	calculated	nC-1
$CGDO$	cgdo	Non LDD region drain-gate overlap capacitance per channel length	F/m	calculated	nC-2
$CGEO$	cgeo	Gate substrate overlap capacitance per unit channel length	F/m	0.0	-
C_{jswg}	cjswg	Source/Drain (gate side) sidewall junction capacitance per unit width (normalized to 100nm T_{si})	F/m ²	1e-10	-
P_{bswg}	pbswg	Source/Drain (gate side) sidewall junction capacitance built in potential	V	.7	-
M_{jswg}	mjswg	Source/Drain (gate side) sidewall junction capacitance grading coefficient	V	0.5	-
t_t	tt	Diffusion capacitance transit time coefficient	second	1e-12	-
N_{dif}	Ndif	Power coefficient of channel length dependency for diffusion capacitance	-	-1	-
L_{dif0}	Ldif0	Channel-length dependency coefficient of diffusion cap.	-	1	-
V_{sdfb}	vsdfb	Source/drain bottom diffusion capacitance flatband voltage	V	calculated	nC-3
V_{sdth}	vsdth	Source/drain bottom diffusion	V	calcu-	nC-4

		capacitance threshold voltage		lated	
C_{sdmin}	csdmin	Source/drain bottom diffusion minimum capacitance	V	calculated	nC-5
A_{sd}	asd	Source/drain bottom diffusion smoothing parameter	-	0.3	-
C_{sdesw}	csdesw	Source/drain sidewall fringing capacitance per unit length	F/m	0.0	-
$CGSl$	cgsl	Light doped source-gate region overlap capacitance	F/m	0.0	-
$CGDl$	cgdl	Light doped drain-gate region overlap capacitance	F/m	0.0	-
$CKAPPA$	ckappa	Coefficient for lightly doped region overlap capacitance fringing field capacitance	F/m	0.6	-
C_f	cf	Gate to source/drain fringing field capacitance	F/m	calculated	nC-6
CLC	clc	Constant term for the short channel model	m	0.1×10^{-7}	-
CLE	cle	Exponential term for the short channel model	none	0.0	-
DLC	dlc	Length offset fitting parameter for gate charge	m	lint	-
$DLCB$	dlcb	Length offset fitting parameter for body charge	m	0	-
$DLBG$	dlbg	Length offset fitting parameter for backgate charge	m	0.0	-
DWC	dwc	Width offset fitting parameter from C-V	m	wint	-
$DelVt$	delvt	Threshold voltage adjust for C-V	V	0.0	-
F_{body}	fbody	Scaling factor for body charge	-	1.0	-
$acde$	acde	Exponential coefficient for charge	m/V	1.0	-

		thickness in capMod=3 for accumulation and depletion regions.			
<i>moin</i>	moin	Coefficient for the gate-bias dependent surface potential.	$V^{1/2}$	15.0	-

Table B.11: Temperature Parameters

Symbol used in equation	Symbol used in SPICE	Description	Unit	Default	Note
T_{nom}	tnom	Temperature at which parameters are expected	°C	27	-
μ_{te}	ute	Mobility temperature exponent	none	-1.5	-
K_{t1}	kt1	Temperature coefficient for threshold voltage	V	-0.11	-
K_{t11}	kt11	Channel length dependence of the temperature coefficient for threshold voltage	V*m	0.0	
K_{t2}	kt2	Body-bias coefficient of the V_{th} temperature effect	none	0.022	-
U_{a1}	ua1	Temperature coefficient for U_a	m/V	4.31e-9	-
U_{b2}	ub1	Temperature coefficient for U_b	(m/V) ²	-7.61e-18	-
U_{c1}	uc1	Temperature coefficient for U_c	1/V	-0.056	nT-1
A_t	at	Temperature coefficient for saturation velocity	m/sec	3.3e4	-
T_{cjswg}	tcjswg	Temperature coefficient of C_{jswg}	1/K	0	-
T_{pbswg}	tpbswg	Temperature coefficient of P_{bswg}	V/K	0	-
C_{th0}	cth0	Normalized thermal capacity	(W*sec) / m°C	1e-5	-
P_{rt}	prt	Temperature coefficient for R_{dsw}	Ω - μ m	0	-
R_{th0}	rth0	Normalized thermal resistance	m°C/W	0	-
N_{tref}	Ntref	Temperature coefficient for N_{ref}	-	0	-
N_{trecr}	Ntrecr	Temperature coefficient for N_{recr}	-	0	-
X_{bjt}	xbjt	Power dependence of j_{bjt} on temperature	-	1	-
X_{dif}	xdif	Power dependence of j_{dif} on temperature	-	X_{bjt}	-
X_{rec}	xrec	Power dependence of j_{rec} on temperature	-	1	-
X_{tun}	xtun	Power dependence of j_{tun} on temperature	-	0	-
W_{th0}	Wth0	Minimum width for thermal resistance calculation	m	0	-

Table B.12: RF Parameters

Symbol used in equation	Symbol used in SPICE	Description	Unit	Default
RgateMod	rgateMod	Gate resistance model selector rgateMod = 0 No gate resistance rgateMod = 1 Constant gate resistance rgateMod = 2 Rii model with variable resistance rgateMod = 3 Rii model with two nodes	-	0
XRCRG1	xrcrg1	Parameter for distributed channel-resistance effect for intrinsic input resistance	-	12.0
<i>XRCRG2</i>	xrcrg2	Parameter to account for the excess channel diffusion resistance for intrinsic input resistance	-	1.0
<i>NGCON</i>	ngcon	Number of gate contacts	-	1
<i>XGW</i>	xgw	Distance from the gate contact to the channel edge	m	0.0
<i>XGL</i>	xgl	Offset of the gate length due to variations in patterning	m	0.0

B.15 BSIMSOI Model Equations

Device equations of the BSIMSOI model are presented in this section. These model equations are taken from the UCB BSIMSOI users manual.

This manual is available with the UCB BSIMSOI model code and can be downloaded at <http://www-device.eecs.berkeley.edu/~bsimsoi/>.

Equation List for BSIMSOI Built-In Potential Lowering

Calculation

$$V_{bs0} = \frac{C_{Si}}{C_{Si} + C_{BOX}} \cdot \left(\phi_i - \frac{qN_{ch}}{2\epsilon_{Si}} \cdot T_{Si}^2 + V_{nonideal} + \Delta V_{DIBL} \right) + \eta_e \frac{C_{BOX}}{C_{Si} + C_{BOX}} \cdot (V_{es} - V_{FBb})$$

$$\text{where } C_{Si} = \frac{\epsilon_{Si}}{T_{Si}}, C_{BOX} = \frac{\epsilon_{OX}}{T_{BOX}}, C_{OX} = \frac{\epsilon_{OX}}{T_{OX}}$$

$$\Delta V_{DIBL} = D_{vbd0} \left(\exp\left(-D_{vbd1} \frac{L_{eff}}{2l}\right) + 2 \exp\left(-D_{vbd1} \frac{L_{eff}}{l}\right) \right) \cdot (V_{bi} - 2\Phi_B)$$

$$\eta_e = K_{1b} - K_{2b} \cdot \left(\exp\left(-D_{k2b} \frac{L_{eff}}{2l}\right) + 2 \exp\left(-D_{k2b} \frac{L_{eff}}{l}\right) \right)$$

$$\phi_i = \phi_{iON} - \frac{C_{OX}}{C_{OX} + (C_{Si}^{-1} + C_{BOX}^{-1})^{-1}} \cdot N_{OFF,FD} V_t \cdot \ln \left(1 + \exp\left(\frac{V_{th,FD} - V_{gs_eff} - V_{OFF,FD}}{N_{OFF,FD} V_t}\right) \right)$$

$$\phi_{iON} = 2\Phi_B + V_t \ln \left(1 + \frac{V_{gsteff,FD} (V_{gsteff,FD} + 2K_1 \sqrt{2\Phi_B})}{MoinFD \cdot K_1 \cdot V_t^2} \right),$$

$$V_{gsteff,FD} = N_{OFF,FD} V_t \cdot \ln \left(1 + \exp\left(\frac{V_{gs_eff} - V_{th,FD} - V_{OFF,FD}}{N_{OFF,FD} V_t}\right) \right)$$

$$V_{bsmos} = V_{bs} - \frac{C_{Si}}{2qN_{ch}T_{Si}} (V_{bs0}(T_{OX} \rightarrow \infty) - V_{bs})^2 \quad \text{if } V_{bs} \leq V_{bs0}(T_{OX} \rightarrow \infty)$$

$$= V_{bs} \quad \text{else}$$

Equation List for BSIMSOI IV

Body Voltages

V_{bsh} is equal to the V_{bs} bounded between (V_{bsc}, ϕ_{s1}) . V_{bsh} is used in V_{th} and

Abulk calculation

$$T_1 = V_{bsc} + 0.5 \left[V_{bs} - V_{bsc} - \delta + \sqrt{(V_{bs} - V_{bsc} - \delta)^2 - 4\delta V_{bsc}} \right], \quad V_{bsc} = -5V$$

$$V_{bsh} = \phi_{s1} - 0.5 \left[\phi_{s1} - T_1 - \delta + \sqrt{(\phi_{s1} - T_1 - \delta)^2 + 4\delta T_1} \right], \quad \phi_{s1} = 1.5V$$

V_{bsh} is further limited to $0.95\phi_s$ to give V_{bseff} .

$$V_{bseff} = \phi_{s0} - 0.5 \left[\phi_{s0} - V_{bsh} - \delta + \sqrt{(\phi_{s0} - V_{bsh} - \delta)^2 + 4\delta V_{bsh}} \right], \quad \phi_{s0} = 0.95\phi_s$$

Effective Channel Length and Width

$$dW' = W_{int} + \frac{W_l}{L^{L_{ln}}} + \frac{W_w}{W^{L_{wn}}} + \frac{W_{wl}}{L^{L_{ln}} W^{L_{wn}}}$$

$$dW = dW' + dW_g V_{gseff} + dW_b \left(\sqrt{\Phi_s - V_{bseff}} - \sqrt{\Phi_s} \right)$$

$$dL = L_{int} + \frac{L_l}{L^{L_{ln}}} + \frac{L_w}{W^{L_{wn}}} + \frac{L_{wl}}{L^{L_{ln}} W^{L_{wn}}}$$

$$L_{eff} = L_{drawn} - 2dL$$

$$W_{eff} = W_{drawn} - N_{bc} dW_{bc} - (2 - N_{bc}) dW \quad W_{eff}' = W_{drawn} - N_{bc} dW_{bc} - (2 - N_{bc}) dW'$$

$$W_{diod} = \frac{W_{eff}'}{N_{seg}} + P_{dbcp}$$

$$W_{dios} = \frac{W_{eff}'}{N_{seg}} + P_{sbcp}$$

Threshold Voltage

$$\begin{aligned}
 V_{th} &= V_{th0} + K_{1eff} (sqrtPhisExt - \sqrt{\Phi_s}) - K_2 V_{bseff} \\
 &+ K_{1eff} \left(\sqrt{1 + \frac{N_{LK}}{L_{eff}}} - 1 \right) \sqrt{\Phi_s} + (K_3 + K_{3b} V_{bseff}) \frac{T_{ox}}{W_{eff}' + W_o} \Phi_s \\
 &- D_{VT0w} \left(\exp\left(-D_{VT1w} \frac{W_{eff}' L_{eff}}{2l_{tw}}\right) + 2 \exp\left(-D_{VT1w} \frac{W_{eff}' L_{eff}}{l_{tw}}\right) \right) (V_{bi} - \Phi_s) \\
 &- D_{VT0} \left(\exp\left(-D_{VT1} \frac{L_{eff}}{2l_t}\right) + 2 \exp\left(-D_{VT1} \frac{L_{eff}}{l_t}\right) \right) (V_{bi} - \Phi_s) \\
 &- \left(\exp\left(-D_{sub} \frac{L_{eff}}{2l_{to}}\right) + 2 \exp\left(-D_{sub} \frac{L_{eff}}{l_{to}}\right) \right) (E_{tao} + E_{tab} V_{bseff}) V_{ds} \\
 l_t &= \sqrt{\epsilon_{si} X_{dep} / C_{ox}} (1 + D_{VT2} V_{bseff})
 \end{aligned}$$

$$sqrtPhisExt = \sqrt{\phi_s - V_{bseff}} + s(V_{bsh} - V_{bseff}), \quad s = -\frac{1}{2\sqrt{\phi_s - \phi_{s0}}}$$

$$K_{1eff} = K_1 \left(1 + \frac{K_{1w1}}{W_{eff}' + K_{1w2}} \right)$$

$$l_{tw} = \sqrt{\epsilon_{si} X_{dep} / C_{ox}} (1 + D_{VT2w} V_{bseff}) \quad l_{to} = \sqrt{\epsilon_{si} X_{dep0} / C_{ox}}$$

$$X_{dep} = \sqrt{\frac{2\epsilon_{si} (\Phi_s - V_{bseff})}{qN_{ch}}} \quad X_{dep0} = \sqrt{\frac{2\epsilon_{si} \Phi_s}{qN_{ch}}}$$

$$V_{bi} = v_t \ln\left(\frac{N_{ch} N_{DS}}{n_i^2}\right)$$

Poly depletion effect

$$V_{poly} + \frac{1}{2} X_{poly} E_{poly} = \frac{qN_{gate} X_{poly}^2}{2\epsilon_{si}}$$

$$\epsilon_{ox} E_{ox} = \epsilon_{si} E_{poly} = \sqrt{2q\epsilon_{si} N_{gate} V_{poly}}$$

$$V_{gs} - V_{FB} - \phi_s = V_{poly} + V_{ox}$$

$$a(V_{gs} - V_{FB} - \phi_s - V_{poly})^2 - V_{poly} = 0$$

$$a = \frac{\epsilon_{ox}^2}{2q\epsilon_{si} N_{gate} T_{ox}^2}$$

$$V_{gs_eff} = V_{FB} + \phi_s + \frac{q\epsilon_{si} N_{gate} T_{ox}^2}{\epsilon_{ox}^2} \left[\sqrt{1 + \frac{2\epsilon_{ox}^2 (V_{gs} - V_{FB} - \phi_s)}{q\epsilon_{si} N_{gate} T_{ox}^2}} - 1 \right]$$

Effective V_{gst} for all region (with Polysilicon Depletion Effect)

$$V_{gst_eff} = \frac{2nv_t \ln \left[1 + \exp\left(\frac{V_{gs_eff} - V_{th}}{2nv_t}\right) \right]}{1 + 2nC_{ox} \sqrt{\frac{2\Phi_s}{q\epsilon_{si} N_{ch}}} \exp\left(-\frac{V_{gs_eff} - V_{th} - 2V_{off}}{2nv_t}\right)}$$

$$n = 1 + N_{factor} \frac{\epsilon_{si} / X_{dep}}{C_{ox}} +$$

$$\frac{(C_{dsc} + C_{dscd} V_{ds} + C_{dscb} V_{bseff}) \left[\exp(-D_{VT1} \frac{L_{eff}}{2l_t}) + 2 \exp(-D_{VT1} \frac{L_{eff}}{l_t}) \right]}{C_{ox}} + \frac{C_{it}}{C_{ox}}$$

Effective Bulk Charge Factor

$$A_{bulk} = 1 + \left(\frac{K_{1eff}}{2\sqrt{(\phi_s + Ketas) - \frac{V_{bsh}}{1 + Keta \cdot V_{bsh}}}} \left(\frac{A_0 L_{eff}}{L_{eff} + 2\sqrt{T_{si} X_{dep}}} \right) \right. \\ \left. \left(1 - A_{gs} V_{gs1eff} \left(\frac{L_{eff}}{L_{eff} + 2\sqrt{T_{si} X_{dep}}} \right)^2 \right) + \frac{B_0}{W'_{eff} + B_1} \right) \\ A_{bulk0} = A_{bulk}(V_{gs1eff} = 0)$$

Mobility and Saturation Velocity

For Mobmod=1

$$\mu_{eff} = \frac{\mu_o}{1 + (U_a + U_c V_{bseff}) \left(\frac{V_{gsteff} + 2V_{th}}{T_{ox}} \right) + U_b \left(\frac{V_{gsteff} + 2V_{th}}{T_{ox}} \right)^2}$$

For Mobmod=2

$$\mu_{eff} = \frac{\mu_o}{1 + (U_a + U_c V_{bseff}) \left(\frac{V_{gsteff}}{T_{ox}} \right) + U_b \left(\frac{V_{gsteff}}{T_{ox}} \right)^2}$$

For Mobmod=3

$$\mu_{eff} = \frac{\mu_o}{1 + \left[U_a \left(\frac{V_{gstef} + 2V_{th}}{T_{ox}} \right) + U_b \left(\frac{V_{gsteff} + 2V_{th}}{T_{ox}} \right)^2 \right] (1 + U_c V_{bseff})}$$

Drain Saturation Voltage

For $R_{ds} > 0$ or $\lambda \neq 1$:

$$V_{dsat} = \frac{-b - \sqrt{b^2 - 4ac}}{2a}$$

$$a = A_{bulk}^2 W_{eff} v_{sat} C_{ox} R_{ds} + \left(\frac{1}{\lambda} - 1\right) A_{bulk}$$

$$b = - \left[(V_{gsteff} + 2v_t) \left(\frac{2}{\lambda} - 1\right) + A_{bulk} E_{sat} L_{eff} + 3A_{bulk} (V_{gsteff} + 2v_t) W_{eff} v_{sat} C_{ox} R_{ds} \right]$$

$$c = (V_{gsteff} + 2v_t) E_{sat} L_{eff} + 2(V_{gsteff} + 2v_t)^2 W_{eff} v_{sat} C_{ox} R_{ds}$$

$$\lambda = A_1 V_{gsteff} + A_2$$

For $R_{ds} = 0$, $\lambda = 1$:

$$V_{dsat} = \frac{E_{sat} L_{eff} (V_{gsteff} + 2v_t)}{A_{bulk} E_{sat} L_{eff} + (V_{gsteff} + 2v_t)}$$

$$E_{sat} = \frac{2v_{sat}}{\mu_{eff}}$$

V_{dseff}

$$V_{dseff} = V_{dsat} - \frac{1}{2} \left[V_{dsat} - V_{ds} - \delta + \sqrt{(V_{dsat} - V_{ds} - \delta)^2 + 4\delta V_{dsat}} \right]$$

Drain current expression

$$I_{ds,MOSFET} = \frac{1}{N_{seg}} \frac{I_{dso}(V_{dseff})}{1 + \frac{R_{ds} I_{dso}(V_{dseff})}{V_{dseff}}} \left(1 + \frac{V_{ds} - V_{dseff}}{V_A}\right)$$

$$\beta = \mu_{eff} C_{ox} \frac{W_{eff}}{L_{eff}}$$

$$I_{dso} = \frac{\beta V_{gsteff} \left(1 - A_{bulk} \frac{V_{dseff}}{2(V_{gsteff} + 2v_t)}\right) V_{dseff}}{1 + \frac{V_{dseff}}{E_{sat} L_{eff}}}$$

$$V_A = V_{Asat} + \left(1 + \frac{P_{vag} V_{gsteff}}{E_{sat} L_{eff}}\right) \left(\frac{1}{V_{ACLM}} + \frac{1}{V_{ADIBLC}}\right)^{-1}$$

$$V_{ACLM} = \frac{A_{bulk} E_{sat} L_{eff} + V_{gsteff}}{P_{clm} A_{bulk} E_{sat} litl} (V_{ds} - V_{dseff})$$

$$V_{ADIBLC} = \frac{(V_{gsteff} + 2v_t)}{\theta_{rout} (1 + P_{DIBLCB} V_{bseff})} \left(1 - \frac{A_{bulk} V_{dsat}}{A_{bulk} V_{dsat} + 2v_t}\right)$$

$$\theta_{rout} = P_{DIBLC1} \left[\exp(-D_{ROUT} \frac{L_{eff}}{2l_{t0}}) + 2 \exp(-D_{ROUT} \frac{L_{eff}}{l_{t0}})\right] + P_{DIBLC2}$$

$$V_{Asat} = \frac{E_{sat} L_{eff} + V_{dsat} + 2R_{ds} v_{sat} C_{ox} W_{eff} V_{gsteff} \left[1 - \frac{A_{bulk} V_{dsat}}{2(V_{gsteff} + 2v_t)}\right]}{2/\lambda - 1 + R_{ds} v_{sat} C_{ox} W_{eff} A_{bulk}}$$

$$litl = \sqrt{\frac{\epsilon_{Si} T_{ox} T_{Si}}{\epsilon_{ox}}}$$

Drain/Source Resistance

$$R_{ds} = R_{dsw} \frac{1 + P_{rwg} V_{gsteff} + P_{rwb} (\sqrt{\phi_s - V_{bseff}} - \sqrt{\phi_s})}{(10^6 W_{eff}')^{Wr}}$$

Impact Ionization Current

$$I_{ii} = \alpha_0 (I_{ds, MOSFET} + F_{bjii} I_c) \exp\left(\frac{V_{diff}}{\beta_2 + \beta_1 V_{diff} + \beta_0 V_{diff}^2}\right)$$

$$V_{diff} = V_{ds} - V_{dsatii}$$

$$V_{dsatii} = V_{gsStep} + \left[V_{dsatii0} \left(1 + T_{ii} \left(\frac{T}{T_{nom}} - 1 \right) \right) - \frac{L_{ii}}{L_{eff}} \right]$$

$$V_{gsStep} = \left(\frac{E_{satii} L_{eff}}{1 + E_{satii} L_{eff}} \right) \left(\frac{1}{1 + S_{ii1} V_{gsteff}} + S_{ii2} \right) \left(\frac{S_{ii0} V_{gst}}{1 + S_{iid} V_{ds}} \right)$$

Gate-Induced-Drain-Leakage (GIDL)

$$\text{At drain, } I_{dgidl} = W_{diod} \alpha_{gidl} E_s \exp\left(-\frac{\beta_{gidl}}{E_s}\right), \quad E_s = \frac{V_{ds} - V_{gs} - \chi}{3T_{ox}}$$

$$\text{At source, } I_{sgidl} = W_{dios} \alpha_{gidl} E_s \exp\left(-\frac{\beta_{gidl}}{E_s}\right), \quad E_s = \frac{-V_{gs} - \chi}{3T_{ox}}$$

If E_s is negative, I_{gidl} is set to zero for both drain and source.

Oxide tunneling current

In inversion,

$$J_{gb} = A \frac{V_{gb} V_{aux}}{I_{ox}^2} \left(\frac{I_{oxref}}{I_{oxqm}} \right)^{N_{ox}} \exp \left(\frac{-B(\hat{a}_{gb1} - \hat{a}_{gb1} |V_{ox}|) I_{ox}}{1 - |V_{ox}|/V_{gb1}} \right)$$

$$V_{aux} = V_{EVB} \ln \left(1 + \exp \left(\frac{|V_{ox}| - \bar{\phi}_g}{V_{EVB}} \right) \right)$$

$$A = \frac{q^3}{8\pi h \phi_b}$$

$$B = \frac{8\pi \sqrt{2m_{ox}} \phi_b^{3/2}}{3hq}$$

$$\phi_b = 4.2eV$$

$$m_{ox} = 0.3m_0$$

In accumulation,

$$J_{gb} = A \frac{V_{gb} V_{aux}}{I_{ox}^2} \left(\frac{I_{oxref}}{I_{oxqm}} \right)^{N_{ox}} \exp \left(\frac{-B(\hat{a}_{gb2} - \hat{a}_{gb2} |V_{ox}|) I_{ox}}{1 - |V_{ox}|/V_{gb2}} \right)$$

$$V_{aux} = V_{ECB} V_t \ln \left(1 + \exp \left(-\frac{V_{gb} - V_{fb}}{V_{ECB}} \right) \right)$$

$$A = \frac{q^3}{8\pi h \phi_b}$$

$$B = \frac{8\pi \sqrt{2m_{ox}} \phi_b^{3/2}}{3hq}$$

$$\phi_b = 3.1eV$$

$$m_{ox} = 0.4m_0$$

Body contact current

$$R_{bp} = \left(R_{body} \frac{W'_{eff} / N_{seg}}{L_{eff}} \right) \parallel \left(R_{halo} \frac{W'_{eff} / N_{seg}}{2} \right), \quad R_{bodyext} = R_{bsh} N_{rb}$$

For 4-T device, $I_{bp} = 0$

For 5-T device,

$$I_{bp} = \frac{V_{bp}}{R_{bp} + R_{bodyext}}$$

Diode and BJT currents

Bipolar Transport Factor

$$\alpha_{bjt} = \exp\left[-0.5\left(\frac{L_{eff}}{L_n}\right)^2\right]$$

Body-to-Source/drain diffusion

$$I_{bs1} = W_{dios} T_{si} j_{sdif} \left(\exp\left(\frac{V_{bs}}{n_{dio} V_t}\right) - 1 \right)$$

$$I_{bd1} = W_{dioid} T_{si} j_{sdif} \left(\exp\left(\frac{V_{bd}}{n_{dio} V_t}\right) - 1 \right)$$

Recombination/trap-assisted tunneling current in depletion region

$$I_{bs2} = W_{dios} T_{si} j_{srec} \left(\exp\left(\frac{V_{bs}}{0.026 n_{recf}}\right) - \exp\left(\frac{V_{sb}}{0.026 n_{recr}} \frac{V_{rec0}}{V_{rec0} + V_{sb}}\right) \right)$$

$$I_{bd2} = W_{dioid} T_{si} j_{srec} \left(\exp\left(\frac{V_{bd}}{0.026 n_{recf}}\right) - \exp\left(\frac{V_{db}}{0.026 n_{recr}} \frac{V_{rec0}}{V_{rec0} + V_{db}}\right) \right)$$

Reversed bias tunneling leakage

$$I_{bs4} = W_{dios} T_{si} j_{stun} \left(1 - \exp\left(\frac{V_{sb}}{0.026 n_{tun}} \frac{V_{tun0}}{V_{tun0} + V_{sb}}\right) \right)$$

$$I_{bd4} = W_{dioid} T_{si} j_{stun} \left(1 - \exp\left(\frac{V_{db}}{0.026 n_{tun}} \frac{V_{tun0}}{V_{tun0} + V_{db}}\right) \right)$$

Recombination current in neutral body

$$I_{bs3} = (1 - \alpha_{bjt}) I_{en} \left[\exp\left(\frac{V_{bs}}{n_{dio} V_t}\right) - 1 \right] \frac{1}{\sqrt{E_{hli3} + 1}}$$

$$I_{bd3} = (1 - \alpha_{bjt}) I_{en} \left[\exp\left(\frac{V_{bd}}{n_{dio} V_t}\right) - 1 \right] \frac{1}{\sqrt{E_{hli4} + 1}}$$

$$I_{en} = \frac{W'_{eff}}{N_{seg}} T_{si} j_{sbjt} \left[L_{bjt0} \left(\frac{1}{L_{eff}} + \frac{1}{L_n} \right) \right]^{N_{bjt}}$$

$$E_{hli3} = A_{hli_eff} \left[\exp\left(\frac{V_{bs}}{n_{dio} V_t}\right) - 1 \right]$$

$$E_{hli4} = A_{hli_eff} \left[\exp\left(\frac{V_{bd}}{n_{dio} V_t}\right) - 1 \right]$$

$$A_{hli_eff} = A_{hli} \exp\left[\frac{-E_g(300K)}{n_{dio} V_t} X_{bjt} \left(1 - \frac{T}{T_{nom}} \right) \right]$$

BJT collector current

$$I_c = \alpha_{bjt} I_{en} \left\{ \exp\left[\frac{V_{bs}}{n_{dio} V_t}\right] - \exp\left[\frac{V_{bd}}{n_{dio} V_t}\right] \right\} \frac{1}{E_{2nd}}$$

$$E_{2nd} = \frac{E_{ely} + \sqrt{E_{ely}^2 + 4E_{hli}}}{2}$$

$$E_{ely} = 1 + \frac{V_{bs} + V_{bd}}{V_{Abjt} + A_{ely} L_{eff}}$$

$$E_{hli} = E_{hli3} + E_{hli4}$$

Total body-source/drain current

$$I_{bs} = I_{bs1} + I_{bs2} + I_{bs3} + I_{bs4}$$

$$I_{bd} = I_{bd1} + I_{bd2} + I_{bd3} + I_{bd4}$$

Total body current

$$I_{ii} + I_{dgidl} + I_{sgidl} + I_{gb} - I_{bs} - I_{bd} - I_{bp} = 0$$

Temperature effects

$$V_{th(T)} = V_{th(Tnom)} + (K_{T1} + K_{r1l} / L_{eff} + K_{T2} V_{bseff})(T / T_{nom} - 1)$$

$$\mu_{o(T)} = \mu_{o(Tnom)} \left(\frac{T}{T_{nom}}\right)^{\mu_{te}}, \quad v_{sat(T)} = v_{sat(Tnom)} - A_T(T / T_{nom} - 1)$$

$$R_{dsw(T)} = R_{dsw(Tnom)} + P_{rt} \left(\frac{T}{T_{nom}} - 1\right)$$

$$U_{a(T)} = U_{a(Tnom)} + U_{a1}(T / T_{nom} - 1)$$

$$U_{b(T)} = U_{b(Tnom)} + U_{b1}(T / T_{nom} - 1)$$

$$U_{c(T)} = U_{c(Tnom)} + U_{c1}(T / T_{nom} - 1)$$

$$R_{th} = \frac{R_{th0}}{(W'_{eff} + W_{th0}) / N_{seg}}, \quad C_{th} = C_{th0} \frac{W'_{eff} + W_{th0}}{N_{seg}}$$

$$j_{sbjt} = j_{sbjt0} \exp \left[\frac{-E_g(300K)}{n_{dio}V_t} X_{bjt} \left(1 - \frac{T}{T_{nom}} \right) \right]$$

$$j_{sdif} = j_{sdif0} \exp \left[\frac{-E_g(300K)}{n_{dio}V_t} X_{dif} \left(1 - \frac{T}{T_{nom}} \right) \right]$$

$$j_{srec} = j_{srec0} \exp \left[\frac{-E_g(300K)}{n_{recf0}V_t} X_{rec} \left(1 - \frac{T}{T_{nom}} \right) \right]$$

$$j_{stun} = j_{stun0} \exp \left[X_{tun} \left(\frac{T}{T_{nom}} - 1 \right) \right]$$

$$n_{recf} = n_{recf0} \left[1 + nt_{recf} \left(\frac{T}{T_{nom}} - 1 \right) \right]$$

$$n_{recl} = n_{recl0} \left[1 + nt_{recl} \left(\frac{T}{T_{nom}} - 1 \right) \right]$$

E_g is the energy gap energy.

Gate-to-channel current (I_{gc}) and gate-to-S/D current (I_{gs} and I_{gd})

I_{gc} –gate to channel tunneling current

$$I_{gc} = W_{eff} L_{eff} \cdot A \cdot T_{oxRatio} \cdot V_{gs_eff} \cdot V_{aux} \cdot \exp\left[-B \cdot T_{oxqm} (a_{igc} - b_{igc} \cdot V_{oxdepinv}) \cdot (1 + c_{igc} \cdot V_{oxdepinv})\right]$$

Note here I_{gc} is the gate to channel current with $V_{ds}=0$

$$V_{aux} = n_{igc} \cdot V_m \cdot \log\left(1 + \exp\left(\frac{V_{gs_eff} - V_{th0}}{n_{igc} \cdot V_m}\right)\right)$$

$$T_{oxRatio} = \left(\frac{T_{oxref}}{T_{oxqm}}\right)^{ntox} \cdot \frac{1}{T_{oxqm}^2}$$

I_{gs} and I_{gd} –gate tunneling current between the gate and the source/drain diffusion region

$$I_{gs} = W_{eff} Dlcig \cdot A \cdot T_{oxRatioEdge} \cdot V_{gs} \cdot V'_{gs} \cdot \exp\left[-B \cdot T_{oxqm} \cdot Poxedge \cdot (a_{igsd} - b_{igsd} \cdot V'_{gs}) \cdot (1 + c_{igsd} \cdot V'_{gs})\right]$$

$$I_{gd} = W_{eff} Dlcig \cdot A \cdot T_{oxRatioEdge} \cdot V_{gd} \cdot V'_{gd} \cdot \exp\left[-B \cdot T_{oxqm} \cdot Poxedge \cdot (a_{igsd} - b_{igsd} \cdot V'_{gd}) \cdot (1 + c_{igsd} \cdot V'_{gd})\right]$$

$$T_{oxRatioEdge} = \left(\frac{T_{oxref}}{T_{oxqm} \cdot Poxedge}\right)^{ntox} \cdot \frac{1}{(T_{oxqm} \cdot Poxedge)^2}$$

$$V'_{gs} = \sqrt{(V_{gs} - V_{fbcd})^2 + 1.0e-4} \quad , \quad V'_{gd} = \sqrt{(V_{gd} - V_{fbcd})^2 + 1.0e-4} .$$

Partition of I_{gc}

$$I_{gc} = I_{gcs} + I_{gcd}$$

$$I_{gcs} = I_{gc} \cdot \frac{\pi \text{ gcd} \cdot V_{ds} + \exp(-\pi \text{ gcd} \cdot V_{ds}) - 1 + 1.0e-4}{\pi \text{ gcd}^2 \cdot V_{ds}^2 + 2.0e-4}$$

$$I_{gcd} = I_{gc} \cdot \frac{1 - (\pi \text{ gcd} \cdot V_{ds} + 1) \cdot \exp(-\pi \text{ gcd} \cdot V_{ds}) + 1.0e-4}{\pi \text{ gcd}^2 \cdot V_{ds}^2 + 2.0e-4}$$

Equation List for BSIMSOI CV

Dimension Dependence

$$\delta W_{\text{eff}} = DWC + \frac{W_{lc}}{L^{W_{lc}}} + \frac{W_{wc}}{W^{W_{wc}}} + \frac{W_{wlc}}{L^{W_{lc}} W^{W_{wc}}}$$

$$\delta L_{\text{eff}} = DLC + \frac{L_{lc}}{L^{L_{lc}}} + \frac{L_{wc}}{W^{L_{wc}}} + \frac{L_{wlc}}{L^{L_{lc}} W^{L_{wc}}}$$

$$L_{\text{active}} = L_{\text{drawn}} - 2\delta L_{\text{eff}}$$

$$L_{\text{activeB}} = L_{\text{active}} - DLCB$$

$$L_{\text{activeBG}} = L_{\text{activeB}} + 2\delta L_{\text{bg}}$$

$$W_{\text{active}} = W_{\text{drawn}} - N_{bc} dW_{bc} - (2 - N_{bc})\delta W_{\text{eff}}$$

$$W_{\text{diodCV}} = \frac{W_{\text{active}}}{N_{\text{seg}}} + P_{\text{sbcP}}$$

$$W_{\text{diodCV}} = \frac{W_{\text{active}}}{N_{\text{seg}}} + P_{\text{dbcP}}$$

Charge Conservation

$$Q_{\text{Bf}} = Q_{\text{acc}} + Q_{\text{sub0}} + Q_{\text{subs}}$$

$$Q_{\text{inv}} = Q_{\text{inv},s} + Q_{\text{inv},d}$$

$$Q_g = -(Q_{\text{inv}} + Q_{\text{Bf}})$$

$$Q_b = Q_{\text{Bf}} - Q_e + Q_{js} + Q_{jd}$$

$$Q_s = Q_{\text{inv},s} - Q_{js}$$

$$Q_d = Q_{\text{inv},d} - Q_{jd}$$

$$Q_g + Q_e + Q_b + Q_s + Q_d = 0$$

Intrinsic Charges

(1) capMod = 2

Front Gate Body Charge

Accumulation Charge

$$V_{FB\text{eff}} = V_{fb} - 0.5 \left((V_{fb} - V_{gb} - \delta) + \sqrt{(V_{fb} - V_{gb} - \delta)^2 + \delta^2} \right)$$

where $V_{gb} = V_{gs} - V_{b\text{seff}}$

$$V_{fb} = V_{th} - \phi_s - K_{1\text{eff}} \sqrt{\phi_s - V_{b\text{seff}}} + \text{delvt}$$

$$V_{g\text{steff}CV} = n v_t \ln \left(1 + \exp \left[\frac{V_{gs} - V_{th}}{n v_t} \right] \cdot \exp \left[- \frac{\text{delvt}}{n v_t} \right] \right)$$

$$Q_{acc} = -F_{\text{body}} \left(\frac{W_{\text{active}} L_{\text{active}B}}{N_{\text{seg}}} + A_{\text{gbcp}} \right) C_{\text{ox}} (V_{FB\text{eff}} - V_{fb})$$

Gate Induced Depletion Charge

$$Q_{\text{sub}0} = -F_{\text{body}} \left(\frac{W_{\text{active}} L_{\text{active}B}}{N_{\text{seg}}} + A_{\text{gbcp}} \right) C_{\text{ox}} \frac{K_{1\text{eff}}^2}{2}$$

$$\left(-1 + \sqrt{1 + \frac{4(V_{gs} - V_{FB\text{eff}} - V_{g\text{steff}CV} - V_{b\text{seff}})}{K_{1\text{eff}}^2}} \right)$$

Drain Induced Depletion Charge

$$V_{dsatCV} = V_{gsteffCV} / A_{bulkCV}, \quad A_{bulkCV} = A_{bulk0} \left[1 + \left(\frac{CLC}{L_{activeB}} \right)^{CLE} \right]$$

$$V_{dsCV} = V_{dsatCV} - \frac{1}{2} (V_{dsatCV} - V_{ds} - \delta + \sqrt{(V_{dsatCV} - V_{ds} - \delta)^2 + 4\delta V_{dsatCV}})$$

$$Q_{subs} = F_{body} \left(\frac{W_{active} L_{activeB}}{N_{seg}} + A_{gbcp} \right) C_{ox}$$

$$(A_{bulkCV} - 1) \left[\frac{V_{dsCV}}{2} - \frac{A_{bulkCV} V_{dsCV}^2}{12(V_{gsteffCV} - A_{bulkCV} V_{dsCV} / 2)} \right]$$

Back Gate Body Charge

$$Q_e = k_{b1} F_{body} \left(\frac{W_{active} L_{activeBG}}{N_{seg}} + A_{ebcp} \right) C_{box} (V_{es} - V_{fbb} - V_{bseff})$$

Inversion Charge

$$V_{cveff} = V_{dsat,CV} - 0.5 \left(V_4 + \sqrt{V_4^2 + 4\delta_4 V_{dsat,CV}} \right) \text{ where } V_4 = V_{dsat,CV} - V_{ds} - \delta_4; \delta_4 = 0.02$$

$$Q_{inv} = - \left(\frac{W_{active} L_{active}}{N_{seg}} + A_{gbcp} \right) C_{ox}$$

$$\left(\left(V_{gsteffCV} - \frac{A_{bulkCV}}{2} V_{cveff} \right) + \frac{A_{bulkCV}^2 V_{cveff}^2}{12 \left(V_{gsteffCV} - \frac{A_{bulkCV}}{2} V_{cveff} \right)} \right)$$

50/50 Charge Partition

$$Q_{inv,s} = Q_{inv,d} = 0.5Q_{inv}$$

40/60 Charge Partition

$$Q_{inv,s} = -\frac{\left(\frac{W_{active}L_{active}}{N_{seg}} + A_{gbcp}\right)C_{ox}}{2\left(V_{gsteffCV} - \frac{A_{bulkCV}}{2}V_{cveff}\right)^2}\left(V_{gsteffCV}^3 - \frac{4}{3}V_{gsteffCV}^2\left(A_{bulkCV}V_{cveff}\right)\right)$$

$$+ \frac{2}{3}V_{gsteff}\left(A_{bulkCV}V_{cveff}\right)^2 - \frac{2}{15}\left(A_{bulkCV}V_{cveff}\right)^3$$

$$Q_{inv,d} = -\frac{\left(\frac{W_{active}L_{active}}{N_{seg}} + A_{gbcp}\right)C_{ox}}{2\left(V_{gsteffCV} - \frac{A_{bulkCV}}{2}V_{cveff}\right)^2}\left(V_{gsteffCV}^3 - \frac{5}{3}V_{gsteffCV}^2\left(A_{bulkCV}V_{cveff}\right)\right)$$

$$+ V_{gsteff}\left(A_{bulkCV}V_{cveff}\right)^2 - \frac{1}{5}\left(A_{bulkCV}V_{cveff}\right)^3$$

0/100 Charge Partition

$$Q_{inv,s} = -\frac{W_{active}L_{active} + A_{gbcp}}{N_{seg}}C_{ox}\left(\frac{V_{gsteffCV}}{2} + \frac{A_{bulkCV}V_{cveff}}{4} - \frac{\left(A_{bulkCV}V_{cveff}\right)^2}{24\left(V_{gsteffCV} - \frac{A_{bulkCV}}{2}V_{cveff}\right)}\right)$$

$$Q_{inv,d} = -\frac{W_{active}L_{active} + A_{gbcp}}{N_{seg}}C_{ox}\left(\frac{V_{gsteffCV}}{2} - \frac{3A_{bulkCV}V_{cveff}}{4} + \frac{\left(A_{bulkCV}V_{cveff}\right)^2}{8\left(V_{gsteffCV} - \frac{A_{bulkCV}}{2}V_{cveff}\right)}\right)$$

(2) capMod = 3 (Charge-Thickness Model)

Front Gate Body Charge

Accumulation Charge

$$V_{FB\text{eff}} = V_{fb} - 0.5 \left((V_{fb} - V_{gb} - \delta) + \sqrt{(V_{fb} - V_{gb} - \delta)^2 + \delta^2} \right)$$

where $V_{gb} = V_{gs} - V_{b\text{seff}}$

$$V_{fb} = V_{th} - \phi_s - K_{1\text{eff}} \sqrt{\phi_s - V_{b\text{seff}}}$$

$$Q_{\text{acc}} = -F_{\text{body}} \left(\frac{W_{\text{active}} L_{\text{activeB}}}{N_{\text{seg}}} + A_{\text{gbcp}} \right) C_{\text{oxeff}} V_{\text{gbacc}}$$

$$V_{\text{gbacc}} = 0.5 \left(V_0 + \sqrt{V_0^2 + 4\delta V_{fb}} \right)$$

$$V_0 = V_{fb} + V_{b\text{seff}} - V_{gs} - \delta$$

$$C_{\text{oxeff}} = \frac{C_{\text{ox}} C_{\text{cen}}}{C_{\text{ox}} + C_{\text{cen}}}$$

$$C_{\text{cen}} = \epsilon_{\text{Si}} / X_{\text{DC}}$$

Gate Induced Depletion Charge

$$Q_{\text{sub0}} = -F_{\text{body}} \left(\frac{W_{\text{active}} L_{\text{activeB}}}{N_{\text{seg}}} + A_{\text{gbcp}} \right) C_{\text{oxeff}} \frac{K_{1\text{eff}}^2}{2} \left(-1 \right. \\ \left. + \sqrt{1 + \frac{4(V_{gs} - V_{FB\text{eff}} - V_{\text{gsteffCV}} - V_{b\text{seff}})}{K_{1\text{eff}}^2}} \right)$$

Drain Induced Depletion Charge

$$V_{dsatCV} = (V_{gsteffCV} - \Phi_\delta) / A_{bulkCV}$$

$$\Phi_\delta = \Phi_s - 2\Phi_B = v_t \ln \left[1 + \frac{V_{gsteffCV} (V_{gsteffCV} + 2K_{1eff} \sqrt{2\Phi_B})}{moinK_{1eff} v_t^2} \right]$$

$$V_{dsCV} = V_{dsatCV} - \frac{1}{2} (V_{dsatCV} - V_{ds} - \delta + \sqrt{(V_{dsatCV} - V_{ds} - \delta)^2 + 4\delta V_{dsatCV}})$$

$$Q_{subs} = F_{body} \left(\frac{W_{active} L_{activeB}}{N_{seg}} + A_{gbcP} \right) C_{oxeff} (A_{bulkCV} - 1) \left[\frac{V_{dsCV}}{2} - \frac{A_{bulkCV} V_{dsCV}^2}{12(V_{gsteffCV} - \Phi_\delta - A_{bulkCV} V_{dsCV} / 2)} \right]$$

Back Gate Body Charge

$$Q_e = k_{b1} F_{body} \left(\frac{W_{active} L_{activeBG}}{N_{seg}} + A_{ebcP} \right) C_{box} (V_{es} - V_{fbb} - V_{bseff})$$

Inversion Charge

$$V_{cveff} = V_{dsat,CV} - 0.5 \left(V_4 + \sqrt{V_4^2 + 4\delta_4 V_{dsat,CV}} \right) \text{ where } V_4 = V_{dsat,CV} - V_{ds} - \delta_4;$$

$$\delta_4 = 0.02$$

$$Q_{inv} = - \left(\frac{W_{active} L_{active}}{N_{seg}} + A_{gbcp} \right) C_{oxeff} \left(V_{gsteffCV} - \Phi_{\delta} - \frac{A_{bulkCV}}{2} V_{cveff} \right) + \frac{A_{bulkCV}^2 V_{cveff}^2}{12 \left(V_{gsteffCV} - \Phi_{\delta} - \frac{A_{bulkCV}}{2} V_{cveff} \right)}$$

50/50 Charge Partition

$$Q_{inv,s} = Q_{inv,d} = 0.5 Q_{inv}$$

40/60 Charge Partition

$$Q_{inv,s} = - \frac{\left(\frac{W_{active} L_{active}}{N_{seg}} + A_{gbcp} \right) C_{oxeff}}{2 \left(V_{gsteffCV} - \Phi_{\delta} - \frac{A_{bulkCV}}{2} V_{cveff} \right)^2} \left((V_{gsteffCV} - \Phi_{\delta})^3 - \frac{4}{3} (V_{gsteffCV} - \Phi_{\delta})^2 \right)$$

$$\left(A_{bulkCV} V_{cveff} \right) + \frac{2}{3} (V_{gsteff} - \Phi_{\delta}) \left(A_{bulkCV} V_{cveff} \right)^2 - \frac{2}{15} \left(A_{bulkCV} V_{cveff} \right)$$

$$Q_{inv,d} = - \frac{\left(\frac{W_{active} L_{active}}{N_{seg}} + A_{gbcp} \right) C_{oxeff}}{2 \left(V_{gsteffCV} - \Phi_{\delta} - \frac{A_{bulkCV}}{2} V_{cveff} \right)^2} \left((V_{gsteffCV} - \Phi_{\delta})^3 - \frac{5}{3} (V_{gsteffCV} - \Phi_{\delta})^2 \left(A_{bulkCV} V_{cveff} \right) \right)$$

$$+ (V_{gsteffCV} - \Phi_{\delta}) \left(A_{bulkCV} V_{cveff} \right)^2 - \frac{1}{5} \left(A_{bulkCV} V_{cveff} \right)^3$$

0/100 Charge Partition

$$Q_{inv,s} = -\frac{W_{active}L_{active} + A_{gbc}C_{oxeff}}{N_{seg}} \left(\frac{V_{gstieffCV} - \Phi_{\delta}}{2} + \frac{A_{bulkCV}V_{cveff}}{4} - \frac{(A_{bulkCV}V_{cveff})^2}{24 \left(V_{gstieffCV} - \Phi_{\delta} - \frac{A_{bulkCV}V_{cveff}}{2} \right)} \right)$$

$$Q_{inv,d} = -\frac{W_{active}L_{active} + A_{gbc}C_{oxeff}}{N_{seg}} \left(\frac{V_{gstieffCV} - \Phi_{\delta}}{2} - \frac{3A_{bulkCV}V_{cveff}}{4} + \frac{(A_{bulkCV}V_{cveff})^2}{8 \left(V_{gstieffCV} - \Phi_{\delta} - \frac{A_{bulkCV}V_{cveff}}{2} \right)} \right)$$

Overlap Capacitance

Source Overlap Charge

$$V_{gs_overlap} = \frac{1}{2} \left\{ (V_{gs} + \delta) + \sqrt{(V_{gs} + \delta)^2 + 4\delta} \right\}$$

$$\frac{Q_{overlap,s}}{W_{diosCV}} = CGS0 \cdot V_{gs} + CGS1 \left\{ V_{gs} - V_{gs_overlap} + \frac{CKAPPA}{2} \left(-1 + \sqrt{1 + \frac{4V_{gs_overlap}}{CKAPPA}} \right) \right\}$$

Drain Overlap Charge

$$V_{gd_overlap} = \frac{1}{2} \left\{ (V_{gd} + \delta) + \sqrt{(V_{gd} + \delta)^2 + 4\delta} \right\}$$

$$\frac{Q_{overlap,d}}{W_{diod}CV} = CGD0 \cdot V_{gd} + CGD1 \left\{ V_{gd} - V_{gd_overlap} + \frac{CKAPPA}{2} \left(-1 + \sqrt{1 + \frac{4V_{gd_overlap}}{CKAPPA}} \right) \right\}$$

Gate Overlap Charge

$$Q_{overlap,g} = -(Q_{overlap,s} + Q_{overlap,d})$$

Source/Drain Junction Charge

For $V_{bs} < 0.95\phi_s$

$$Q_{jswg} = Q_{bsdep} + Q_{bsdif}$$

else

$$Q_{jswg} = C_{bsdep} (0.95\phi_s) (V_{bs} - 0.95\phi_s) + Q_{bsdif}$$

For $V_{bd} < 0.95\phi_s$

$$Q_{jdwg} = Q_{bddep} + Q_{bddif}$$

else

$$Q_{jdwg} = C_{bddep} (0.95\phi_s) (V_{bd} - 0.95\phi_s) + Q_{bddif}$$

where

$$Q_{bsdep} = W_{diosCV} C_{jswg} \frac{T_{si}}{10^{-7}} \frac{P_{bswg}}{1 - M_{jswg}} \left[1 - \left(1 - \frac{V_{bs}}{P_{bswg}} \right)^{1 - M_{jswg}} \right]$$

$$Q_{bddep} = W_{diodCV} C_{jswg} \frac{T_{si}}{10^{-7}} \frac{P_{bswg}}{1 - M_{jswg}} \left[1 - \left(1 - \frac{V_{bd}}{P_{bswg}} \right)^{1 - M_{jswg}} \right]$$

$$Q_{bsdif} = \tau \frac{W_{eff}'}{N_{seg}} T_{si} J_{sbit} \left[1 + L_{dif0} \left(L_{bj0} \left(\frac{1}{L_{eff}} + \frac{1}{L_n} \right)^{N_{dif}} \right) \right] \left[\exp \left(\frac{V_{bs}}{n_{dio} V_t} \right) - 1 \right] \frac{1}{\sqrt{E_{hlis} + 1}}$$

$$Q_{bddif} = \tau \frac{W_{eff}'}{N_{seg}} T_{si} J_{sbit} \left[1 + L_{dif0} \left(L_{bj0} \left(\frac{1}{L_{eff}} + \frac{1}{L_n} \right)^{N_{dif}} \right) \right] \left[\exp \left(\frac{V_{bd}}{n_{dio} V_t} \right) - 1 \right] \frac{1}{\sqrt{E_{hlid} + 1}}$$

$$C_{jswg} = C_{jswg0} [1 + t_{cjswg} (T - T_{nom})]$$

$$P_{bswg} = P_{bswg0} - t_{pbswg} (T - T_{nom})$$

Extrinsic Capacitance

Bottom S/D to Substrate Capacitance (per unit area)

$$C_{esb} = \begin{cases} C_{box} & \text{if } V_{s/d,e} < V_{sdfb} \\ C_{box} - \frac{1}{A_{sd}} (C_{box} - C_{min}) \left(\frac{V_{s/d,e} - V_{sdfb}}{V_{sdth} - V_{sdfb}} \right)^2 & \text{elseif } V_{s/d,e} < V_{sdfb} + A_{sd} (V_{sdth} - V_{sdfb}) \\ C_{min} + \frac{1}{1 - A_{sd}} (C_{box} - C_{min}) \left(\frac{V_{s/d,e} - V_{sdth}}{V_{sdth} - V_{sdfb}} \right)^2 & \text{elseif } V_{s/d,e} < V_{sdth} \\ C_{min} & \text{else} \end{cases}$$

Sidewall S/D to Substrate Capacitance (per unit length)

$$C_{s/d,esw} = C_{sdesw} \log \left(1 + \frac{T_{si}}{T_{box}} \right)$$

B.16 BSIMSOI fREEDA™ Model Code

BSIMSOI Header File:

```
// Bsim3nsoitest MOSFET MODEL
//
//          Drain 1
//          o
//          |
//          |
//          |---+
//          |
// Gate 2 o-----|-----o 4 Bulk
//          |
//          |---+
//          |
//          |
//          o
//          Source 3
//
//
//
// Author: Sonali Luniya and Ramya Mohan

#ifndef Bsim3nsoitestT_h
#define Bsim3nsoitestT_h 1

class Bsim3nsoitestT:public AdolcElement2
{
public:

    Bsim3nsoitestT(const string& iname);

    ~Bsim3nsoitestT() {}

    static const char* getNetlistName()
    {
        return einfo.name;
    }

    // Do some local initialization
    virtual void init() throw(string&);

private:
```

```

// Generic state variable evaluation routine
virtual void eval1(adoublev& x, adoublev& xt,
adoublev& y1, adoublev& z1);
virtual void eval2(adoublev& dy1, adoublev& z1,
adoublev& y2, adoublev& z2);
virtual void getLocalRefIdx(UnsignedVector& local_ref_vec,
TerminalVector& term_list);
// Element information
static ItemInfo einfo;

// Number of parameters of this element
static const unsigned n_par;

// Parameter variables

double l, w, dtocv, llc, lwc, lwlc, wlc, wwc, wwlc, tsi,
tox, toxref, tbox, tnom, rbody;
double rbsh, rsh, rhalo, wint, lint, wth0, ll, wl, lln, wln,
lw, ww, lwn, wwn, lw1, ww1, ln;
double xpart, xj, k1b, k2b, dk2b, vbsa, aigc, bigc, cigc,
aigsd, bigsd, cigsd, nigc;
double pioxedge, pigcd, k1w1, k1w2, k3, k3b, kb1, w0,
nlx, nsub, ngate;
double dvt0, dvt1, dvt2, dvt0w, dvt1w, dvt2w, eta0, etab,
dsub, voff, nfactor, cdsc, cdsbc, cdsd;
double cit, u0, prwg, prwb, wr, rds, a0, ags, a1, a2, b0,
b1, vsat, keta, ketas;
double dwg, dwb, dwbc, pclm, pdibl1, pdibl2, pdiblb, drout,
pvag, delta, alpha0, beta0;
double beta1, beta2, fbjtii, vdsatii0, tii, lii, esatii,
sii0, sii1, sii2, siid, agidl;
double bgidl, ngidl, ebg, vgb1, vgb2, voxh, deltax, ntox,
ntun, ndiode, nrecf0, nrecr0;
double isbjt, isdif, isrec, istun, vrec0, vtun0, nbjt, lbjt0,
vabjt, aely, vevb, vecb;
double cjswg, mjswg, pbswg, tt, ldif0, cgeo, cgso, cgdo, dlc,
dwc, dlcb, dlbg, fbody, clc;
double cle, cf, csdmin, asd, csdesw, vsdth, delvt, acde,
moin, ckappa, cgdl, cgsl;
double ndif, rth0, cth0, tpbswg, tcjswg, kt1, kt1l, kt2,
ute, ua1, ub1, uc1, prt, at, nrecf;
double nrecr, xbjt, xdif, xrec, xtun, dlcig, nbc, nseg,
pdbc, psbc, toxqm, type, toxm;
double xt1, dvbd0, dvbd1, temp, npeak, capMod, vbm, nofffd,

```

```

vofffd,moinFD,shmod ;
double ahli,ua,ub,uc,vsdfb,k2,k1,vth0,nch;
//bool pmos;

// Parameter information
static ParmInfo pinfo[];

};

#endif

BSIMSOI C++ File:

/*Model code for BSIMSOI*/
#include "../network/CircuitManager.h"
#include "../network/Element.h"
#include "../network/AdolcElement2.h"
#include "Bsim3nsoitestT.h"

//Static members
const unsigned Bsim3nsoitestT::n_par = 206;

//Element information
ItemInfo Bsim3nsoitestT::einfo = {
    "bsim3nsoitestt",
    "Mosfet model using Bsim3nsoitestT level, version 3.2.4",
    "Sonali Luniya and Ramya Mohan",
    DEFAULT_ADDRESS"elements/Bsim3nsoitestT.h.html",
    "2005_07_07"
};

//Parameters
ParmInfo Bsim3nsoitestT::pinfo[] = {
    {"l", "Length (m)", TR_DOUBLE, false},
    {"w", "Width (m)", TR_DOUBLE, false},
    {"dtoxcv", "---", TR_DOUBLE, false},
    {"llc", "Length reduction parameter for CV", TR_DOUBLE, false},
    {"lwc", "Length reduction parameter for CV", TR_DOUBLE, false},
    {"lwlc", "Length reduction parameter for CV", TR_DOUBLE, false},
    {"wlc", "Width reduction parameter for CV", TR_DOUBLE, false},
    {"wwc", "Width reduction parameter for CV", TR_DOUBLE, false},
    {"wwlc", "Width reduction parameter for CV", TR_DOUBLE, false},
    {"tsi", "Silicon film thickness (m)", TR_DOUBLE, false},
    {"tox", "Gate oxide thickness (m)", TR_DOUBLE, false},
    {"toxref", "---Target Oxide Thickness", TR_DOUBLE, false},
    {"tbox", "Buried Oxide thickness (m)", TR_DOUBLE, false},

```

```

{"tnom", "Parameter measurement temperature (K)", TR_DOUBLE, false},
{"rbody", "Intrinsic body contact sheet resistance (ohm/square)",
TR_DOUBLE, false},
{"rbsh", "Extrinsic body contact sheet resistance (ohm/square)",
TR_DOUBLE, false},
{"rsh", "S-D sheet resistancde (ohm/square)", TR_DOUBLE, false},
{"rhalo", "Body halo sheet resistance (ohm/m)", TR_DOUBLE, false},
{"wint", "Width offset fitting parameter from I-V without bias (m)",
TR_DOUBLE, false},
{"lint", "Length offset fitting parameter from I-V without bias (m)",
TR_DOUBLE, false},
{"wth0", "-----", TR_DOUBLE, false},
{"ll", "Length reduction parameter", TR_DOUBLE, false},
{"wl", "Width reduction parameter", TR_DOUBLE, false},
{"lln", "Length reduction parameter", TR_DOUBLE, false},
{"wln", "Width reduction parameter", TR_DOUBLE, false},
{"lw", "Length reduction parameter", TR_DOUBLE, false},
{"ww", "Width reduction parameter", TR_DOUBLE, false},
{"lwn", "Length reduction parameter", TR_DOUBLE, false},
{"wwn", "Width reduction parameter", TR_DOUBLE, false},
{"lwl", "Length reduction parameter", TR_DOUBLE, false},
{"wwl", "Width reduction parameter", TR_DOUBLE, false},
{"ln", "Electron/hole diffusion length (m)", TR_DOUBLE, false},
{"xpart", "-----Channel charge partititoning", TR_DOUBLE, false},
{"xj", "S/DJunction depth (m)", TR_DOUBLE, false},
{"k1b", "k1b", TR_DOUBLE, false},
{"k2b", "k2b", TR_DOUBLE, false},
{"dk2b", "dk2b", TR_DOUBLE, false},
{"vbsa", "vbsa", TR_DOUBLE, false},
{"aigc", "---", TR_DOUBLE, false},
{"bigc", "-----", TR_DOUBLE, false},
{"cigc", "-----", TR_DOUBLE, false},
{"aigsd", "-----", TR_DOUBLE, false},
{"bigsd", "-----", TR_DOUBLE, false},
{"cigsd", "-----", TR_DOUBLE, false},
{"nigc", "-----", TR_DOUBLE, false},
{"poxedge", "-----", TR_DOUBLE, false},
{"pigcd", "-----", TR_DOUBLE, false},
{"vth0", "Threshold voltage @Vbs=0 for long and wide device",
TR_DOUBLE, false},
{"k1", "First order body effect coefficient ( $V^{0.5}$ )",
TR_DOUBLE, false},
{"k1w1", "First body effect width dependent parameter (m)",
TR_DOUBLE, false},

```

```

{"k1w2", "Second body effect width dependent parameter (m)",
TR_DOUBLE, false},
{"k2", "Second order body effect coefficient", TR_DOUBLE, false},
{"k3", "Narrow width effect coefficient", TR_DOUBLE, false},
{"k3b", "Body effect coefficient of k3 (1/V)", TR_DOUBLE, false},
{"kb1", "Backgate body charge coefficient", TR_DOUBLE, false},
{"w0", "Narrow width effect parameter (m)", TR_DOUBLE, false},
{"nlx", "Lateral non-uniform doping parameter (m)", TR_DOUBLE, false},
{"nch", "Channel doping concentration (1/cm^3)",TR_DOUBLE, false},
{"nsub", "Substrate doping concentration (1/cm^3)",TR_DOUBLE, false},
{"ngate", "Poly-gate doping concentration (1/cm^3)",TR_DOUBLE, false},
{"dvt0", "First coefficient of short-channel effect on Vth", T
R_DOUBLE, false},
{"dvt1", "Second coefficient of short-channel effect on Vth",
TR_DOUBLE, false},
{"dvt2", "Body-bias coefficient of short-channel effect on Vth (1/V)",
TR_DOUBLE, false},
{"dvt0w", "First coefficient of narrow width effect on
Vth for small channel length", TR_DOUBLE, false},
{"dvt1w", "Second coefficient of narrow width effect on
Vth for small channel length", TR_DOUBLE, false},
{"dvt2w", "Body-bias coefficient of narrow width effect on
Vth for small channel length (1/V)", TR_DOUBLE, false},
{"eta0", "DIBL coefficeint subthreshold region", TR_DOUBLE, false},
{"etab", "Body bias coefficeint for the subthreshold DIBL effect
(1/V)", TR_DOUBLE, false},
{"dsub", "DIBL coefficient in the subthreshold region",
TR_DOUBLE, false},
{"voff", "Offset voltage in the threshold region for large W
and L (V)", TR_DOUBLE, false},
{"nfactor", "Subthreshold swing factor", TR_DOUBLE, false},
{"cdsc", "Drain/Source to channel coupling capacitance (F/m^2)",
TR_DOUBLE, false},
{"cdscb", "Body-bias sensitivity of cdsc (F/m^2)", TR_DOUBLE, false},
{"cdscd", "Drain-bias sensitivity of cdsc (F/m^2)",TR_DOUBLE, false},
{"cit", "Interface trap capacitance (F/m^2)", TR_DOUBLE, false},
{"u0", "Mobility at Temp=Tnom (cm^2/V-sec)", TR_DOUBLE, false},
{"ua", "First-oreder mobility degradation coefficient (m/V)",
TR_DOUBLE, false},
{"ub", "Second-order mobility degradation coefficient (m/V)^2",
TR_DOUBLE, false},
{"uc", "Body-effect of mobility degradation coefficient (1/V)",
TR_DOUBLE, false},
{"prwg", "Gate-bias effect coefficient of rdsw", TR_DOUBLE, false},

```

```

{"prwb", "Body effect coefficient of rds (1/V)", TR_DOUBLE, false},
{"wr", "Width offset from Weff for Rds calculation",
TR_DOUBLE, false},
{"rds", "Parasitic resistance per unit width (ohm-um)",
TR_DOUBLE, false},
{"a0", "Bulk charge effect coefficient for channel length",
TR_DOUBLE, false},
{"ags", "Gate bias coefficient of Abulk (1/V)", TR_DOUBLE, false},
{"a1", "First non-saturation effect parameter (1/V)", TR_DOUBLE, false},
{"a2", "Second non-saturation effect parameter", TR_DOUBLE, false},
{"b0", "Bulk charge effect coefficient for channel width (m)",
TR_DOUBLE, false},
{"b1", "Bulk charge effect width offset (m)", TR_DOUBLE, false},
{"vsat", "Saturation velocity at Temp=Tnom (m/sec)", TR_DOUBLE, false},
{"keta", "Body-bias coefficient of bulk charge effect (1/V)",
TR_DOUBLE, false},
{"ketas", "Surface potential adjustment for bulk charge effect (V)",
TR_DOUBLE, false},
{"dwg", "Coefficient of Weff's gate dependence (m/V)", TR_DOUBLE, false},
{"dwb", "Coefficient of Weff's substrate body bias dependence
(m/V)^0.5", TR_DOUBLE, false},
{"dwbc", "Width offset for body contact isolation edge (m)",
TR_DOUBLE, false},
{"pclm", "Channel length modulation parameter", TR_DOUBLE, false},
{"pdibl1", "First output resistance DIBL effect correction parameter",
TR_DOUBLE, false},
{"pdibl2", "Second output resistance DIBL effect correction parameter",
TR_DOUBLE, false},
{"pdiblb", "Body-effect on drain induced barrier lowering",
TR_DOUBLE, false},
{"drout", "----listed in the pgm", TR_DOUBLE, false},
{"pvag", "Gate dependence of Early voltage", TR_DOUBLE, false},
{"delta", "Effective Vds parameter", TR_DOUBLE, false},
{"alpha0", "The first parameter of impact ionization current (m/V)",
TR_DOUBLE, false},
{"beta0", "First Vds dependent parameter of impact ionization current
(1/V)", TR_DOUBLE, false},
{"beta1", "Second Vds dependent parameter of impact ionization current",
TR_DOUBLE, false},
{"beta2", "Third Vds dependent parameter of impact ionization current
(V)", TR_DOUBLE, false},
{"fbjtii", "----", TR_DOUBLE, false},
{"vdsatii0", "Nominal drain saturation voltage at threshold for
impact ionization current (V)", TR_DOUBLE, false},

```

```

{"tii", "Temperature dependent parameter for impact
ionization current", TR_DOUBLE, false},
{"lii", "Channel length dependent parameter at threshold
for impact ionization current", TR_DOUBLE, false},
{"esatii", "Saturation channel electric field
for impact ionization current (V/m)", TR_DOUBLE, false},
{"sii0", "First Vgs dependent parameter for impact
ionization current ( $V^{-1}$ )", TR_DOUBLE, false},
{"sii1", "Second Vgs dependent parameter for impact
ionization current ( $V^{-1}$ )", TR_DOUBLE, false},
{"sii2", "Third Vgs dependent parameter for impact
ionization current", TR_DOUBLE, false},
{"siid", "Vds dependent parameter of drain voltage
for impact ionization current ( $V^{-1}$ )", TR_DOUBLE, false},
{"agidl", "GIDL constant ( $\text{ohm}^{-1}$ )", TR_DOUBLE, false},
{"bgidl", "GIDL Exponential coefficient (V/m)", TR_DOUBLE, false},
{"ngidl", "GIDL Vds enhancement coefficient (V)", TR_DOUBLE, false},
{"ebg", "-----", TR_DOUBLE, false},
{"vgb1", "-----", TR_DOUBLE, false},
{"vgb2", "-----", TR_DOUBLE, false},
{"voxh", "----", TR_DOUBLE, false},
{"deltavox", "-----", TR_DOUBLE, false},
{"ntox", "-----", TR_DOUBLE, false},
{"ntun", "Reverse tunneling non-ideality factor", TR_DOUBLE, false},
{"ndiode", " Diode non-ideality factor", TR_DOUBLE, false},
{"nrecf0", "Recombination non-ideality factor at forward bias",
TR_DOUBLE, false},
{"nrecr0", "Recombination non-ideality factor at reversed bias",
TR_DOUBLE, false},
{"isbjt", "BJT Injection saturation current ( $\text{A}/\text{m}^2$ )", TR_DOUBLE, false},
{"isdif", "Body to source/drain injection saturation current
( $\text{A}/\text{m}^2$ )", TR_DOUBLE, false},
{"isrec", "Recombination in depletion saturation current
( $\text{A}/\text{m}^2$ )", TR_DOUBLE, false},
{"istun", "Reverse tunneling saturation current ( $\text{A}/\text{m}^2$ )",
TR_DOUBLE, false},
{"vrec0", "Voltage dependent parameter for recombination current (V)",
TR_DOUBLE, false},
{"vtun0", "Voltage dependent parameter for tunneling current (V)",
TR_DOUBLE, false},
{"nbjt", "Power coefficient of channel length dependency for
bipolar current", TR_DOUBLE, false},
{"lbjt0", "Reference channel length for bipolar current (m)",
TR_DOUBLE, false},

```

```

{"vabjt", "Early Voltage for bipolar current (V)", TR_DOUBLE, false},
{"aely", "Channel length dependency of early voltage
for bipolar current (V/m)",
TR_DOUBLE, false},
{"ahli", "High level injection parameter for bipolar current",
TR_DOUBLE, false},
{"vevb", "----", TR_DOUBLE, false},
{"vecb", "-----", TR_DOUBLE, false},
{"cjswg", "Source/Drain (gate side) sidewall junction capacitance
per unit width (normalized to 100nm tsi) (F/m^2)",
TR_DOUBLE, false},
{"mjswg", "Source/Drain (gate side) sidewall junction capacitance
grading coefficient (V)", TR_DOUBLE, false},
{"pbswg", "Source/Drain (gate side) sidewall junction capacitance
built in potential (V)", TR_DOUBLE, false},
{"tt", "Diffusion capacitance transit time coefficient (sec)",
TR_DOUBLE, false},
{"ldif0", "ldif0", TR_DOUBLE, false},
{"cgeo", "Gate substrate overlap capacitance per unit channel
length (F/m)", TR_DOUBLE, false},
{"cgso", "-----", TR_DOUBLE, false},
{"cgdo", "-----", TR_DOUBLE, false},
{"dlc", "Length offset fitting parameter for gate charge (m)",
TR_DOUBLE, false},
{"dwc", "Width offset fitting parameter from C-V (m)",
TR_DOUBLE, false},
{"dlcb", "Length offset fitting parameter for body charge (m)",
TR_DOUBLE, false},
{"dlbg", "Length offset fitting parameter for backgate charge (m)",
TR_DOUBLE, false},
{"fbody", "Scaling factor for body charge", TR_DOUBLE, false},
{"clc", "Constant term for the short channel model (m)",
TR_DOUBLE, false},
{"cle", "Exponential term for the short channel model",
TR_DOUBLE, false},
{"cf", "---in the pgm", TR_DOUBLE, false},
{"csdmin", "-----", TR_DOUBLE, false},
{"asd", "-----", TR_DOUBLE, false},
{"csdesw", "S/D sidewall fringing capacitance per unit length
(F/m)", TR_DOUBLE, false},
{"vsdfb", "-----", TR_DOUBLE, false},
{"vsdth", "-----", TR_DOUBLE, false},
{"delvt", "Threshold voltage adjust for C-V (V)", TR_DOUBLE, false},
{"acde", "---in the pghm", TR_DOUBLE, false},

```

```

{"moin", "Coefficient for the gate-bias dependent surface potential
V0.5", TR_DOUBLE, false},
{"ckappa", "Coefficient for lightly doped region overlap
capacitance fringing field capacitance (F/m)", TR_DOUBLE, false},
{"cgdl", "Light doped drain-gate region overlap
capacitance (F/m)", TR_DOUBLE, false},
{"cgsl", "Light doped source-gate region overlap
capacitance (F/m)", TR_DOUBLE, false},
{"ndif", "ndif", TR_DOUBLE, false},
{"rth0", "-----", TR_DOUBLE, false},
{"cth0", "-----", TR_DOUBLE, false},
{"tpbswg", "-----", TR_DOUBLE, false},
{"tcjswg", "-----", TR_DOUBLE, false},
{"kt1", "Temperature coefficient of Vth (V)", TR_DOUBLE, false},
{"kt1l", "Channel length dependence of the
temperature coefficient of Vth (V*m)", TR_DOUBLE, false},
{"kt2", "Body-bias coefficient of the
Vth temperature effect", TR_DOUBLE, false},
{"ute", "Temperature coefficient of mobility", TR_DOUBLE, false},
{"ua1", "Temperature coefficient for ua
(m/V)", TR_DOUBLE, false},
{"ub1", "Temperature coefficient for ub
((m/V)2)", TR_DOUBLE, false},
{"uc1", "Temperature coefficient for uc (1/V)", TR_DOUBLE, false},
{"prt", "Temperature coefficient of rdsw (ohm-um)",
TR_DOUBLE, false},
{"at", "Temperature coefficient of vsat (m/sec)",
TR_DOUBLE, false},
{"ntrecf", "Temperature coefficient for Nrecf", TR_DOUBLE, false},
{"ntrecr", "Temperature coefficient for Nrecr", TR_DOUBLE, false},
{"xbjt", "xbjt", TR_DOUBLE, false},
{"xdif", "xdif", TR_DOUBLE, false},
{"xrec", "xrec", TR_DOUBLE, false},
{"xtun", "xtun", TR_DOUBLE, false},
{"dlcig", "----", TR_DOUBLE, false},
{"nbc", "----", TR_DOUBLE, false},
{"nseg", "----", TR_DOUBLE, false},
{"pdbcpc", "-----", TR_DOUBLE, false},
{"psbcpc", "-----", TR_DOUBLE, false},
{"toxqm", "Effective oxide thickness considering
quantum effect", TR_DOUBLE, false},
{"type", "-----", TR_DOUBLE, false},
{"toxm", "=-----", TR_DOUBLE, false},
{"xt1", "Doping depth", TR_DOUBLE, false},

```

```

{"dvbd0", "dvbd0", TR_DOUBLE, false},
{"dvbd1", "dvbd1", TR_DOUBLE, false},
{"temp", "Circuit temperature", TR_DOUBLE, false},
{"npeak", "--", TR_DOUBLE, false},
{"capMod", "Capacitance model ", TR_DOUBLE, false},
{"vbm", "Maximum body voltage", TR_DOUBLE, false},
{"nofffd", "nofffd", TR_DOUBLE, false},
{"vofffd", "vofffd", TR_DOUBLE, false},
{"moinFD", "moinfd", TR_DOUBLE, false},
{"shmod", "self heat - shmod", TR_DOUBLE, false}
};

```

```

Bsim3nsoitestT::Bsim3nsoitestT(const string& iname)
    : AdolcElement2(&einfo, pinfo, n_par, iname)
{
    //Set default parameter values
    paramvalue[0] = &(l = 0.25e-6);
    paramvalue[1] = &(w = 10.0e-6);
    paramvalue[2] = &(dtoxcv = 0);
    paramvalue[3] = &(llc = 0);
    paramvalue[4] = &(lwc = 0);
    paramvalue[5] = &(lwlc = 0);
    paramvalue[6] = &(wlc = 0);
    paramvalue[7] = &(wwc = 0);
    paramvalue[8] = &(wwlc = 0);
    paramvalue[9] = &(tsi = 1e-07);
    paramvalue[10] = &(tox = 5e-09);
    paramvalue[11] = &(toxref = 5e-09);
    paramvalue[12] = &(tbox = 5e-07);
    paramvalue[13] = &(tnom = 293.15);
    paramvalue[14] = &(rbody = 1);
    paramvalue[15] = &(rbsh = 0);
    paramvalue[16] = &(rsh = 0);
    paramvalue[17] = &(rhalo = 1e+015);
    paramvalue[18] = &(wint = 0);
    paramvalue[19] = &(lint = 0);
    paramvalue[20] = &(wth0 = 0);
    paramvalue[21] = &(ll = 0);
    paramvalue[22] = &(wl = 0);
    paramvalue[23] = &(lln = 1);
    paramvalue[24] = &(wln = 1);
    paramvalue[25] = &(lw = 0);
    paramvalue[26] = &(ww = 0);
}

```

```
paramvalue[27] = &(lwn = 1);
paramvalue[28] = &(wnn = 1);
paramvalue[29] = &(lwl = 0);
paramvalue[30] = &(wwl = 0);
paramvalue[31] = &(ln = 2e-06);
paramvalue[32] = &(xpart = 1);
paramvalue[33] = &(xj = 1e-07);
paramvalue[34] = &(k1b = 0);
paramvalue[35] = &(k2b = 0);
paramvalue[36] = &(dk2b = 0);
paramvalue[37] = &(vbsa = 0.0);
paramvalue[38] = &(aigc = 1);
paramvalue[39] = &(bigc = 1);
paramvalue[40] = &(cigc = 1);
paramvalue[41] = &(aigsd = 1);
paramvalue[42] = &(bigsd = 1);
paramvalue[43] = &(cigsd = 1);
paramvalue[44] = &(nigc = 1);
paramvalue[45] = &(pioxedge = 1);
paramvalue[46] = &(pigcd = 1);
paramvalue[47] = &(vth0 = 0.53);
paramvalue[48] = &(k1 = 0.56);
paramvalue[49] = &(k1w1 = 0);
paramvalue[50] = &(k1w2 = 0);
paramvalue[51] = &(k2 = 0);
paramvalue[52] = &(k3 = -2);
paramvalue[53] = &(k3b = 0);
paramvalue[54] = &(kb1 = 1);
paramvalue[55] = &(w0 = 0);
paramvalue[56] = &(nlx = 0);
paramvalue[57] = &(nch = 8e+17);
paramvalue[58] = &(nsub = 5e+15);
paramvalue[59] = &(ngate = 2e+20);
paramvalue[60] = &(dvt0 = 1);
paramvalue[61] = &(dvt1 = 0.15);
paramvalue[62] = &(dvt2 = 0);
paramvalue[63] = &(dvt0w = 0);
paramvalue[64] = &(dvt1w = 2000000);
paramvalue[65] = &(dvt2w = -0.032);
paramvalue[66] = &(eta0 = 0.5);
paramvalue[67] = &(etab = 0);
paramvalue[68] = &(dsub = 0.35);
paramvalue[69] = &(voff = -0.15);
paramvalue[70] = &(nfactor = 0.4);
```

```
paramvalue[71] = &(cdsc = 0.005);
paramvalue[72] = &(cdscb = -0.01);
paramvalue[73] = &(cdscd = 0);
paramvalue[74] = &(cit = 0);
paramvalue[75] = &(u0 = 0.05);
paramvalue[76] = &(ua = 0);
paramvalue[77] = &(ub = 1.2e-18);
paramvalue[78] = &(uc = 0);
paramvalue[79] = &(prwg = 0);
paramvalue[80] = &(prwb = 0);
paramvalue[81] = &(wr = 1);
paramvalue[82] = &(rdsw = 100);
paramvalue[83] = &(a0 = 0);
paramvalue[84] = &(ags = 0);
paramvalue[85] = &(a1 = 0);
paramvalue[86] = &(a2 = 0.99);
paramvalue[87] = &(b0 = 0);
paramvalue[88] = &(b1 = 0);
paramvalue[89] = &(vsat = 80000);
paramvalue[90] = &(keta = 0);
paramvalue[91] = &(ketas = 0);
paramvalue[92] = &(dwg = 0);
paramvalue[93] = &(dwb = 0);
paramvalue[94] = &(dwbc = 0);
paramvalue[95] = &(pclm = 1);
paramvalue[96] = &(pdibl1 = 0.1);
paramvalue[97] = &(pdibl2 = 0);
paramvalue[98] = &(pdiblb = 0);
paramvalue[99] = &(drout = 0.4);
paramvalue[100] = &(pvag = 0);
paramvalue[101] = &(delta = 0.001);
paramvalue[102] = &(alpha0 = 8e-09);
paramvalue[103] = &(beta0 = 0);
paramvalue[104] = &(beta1 = 0);
paramvalue[105] = &(beta2 = 0.05);
paramvalue[106] = &(fbjtii = 0);
paramvalue[107] = &(vdsatii0 = 0.8);
paramvalue[108] = &(tii = -0.2);
paramvalue[109] = &(lii = 5e-08);
paramvalue[110] = &(esatii = 1e+08);
paramvalue[111] = &(sii0 = 0.5);
paramvalue[112] = &(sii1 = 0);
paramvalue[113] = &(sii2 = 0);
paramvalue[114] = &(siid = 0);
```

```
paramvalue[115] = &(agidl = 2e-09);
paramvalue[116] = &(bgidl = 2e+09);
paramvalue[117] = &(ngidl = 0.5);
paramvalue[118] = &(ebg = 1.2);
paramvalue[119] = &(vgb1 = 300);
paramvalue[120] = &(vgb2 = 17);
paramvalue[121] = &(voxh = 5);
paramvalue[122] = &(deltavox = 0.005);
paramvalue[123] = &(ntox = 1);
paramvalue[124] = &(ntun = 3.6);
paramvalue[125] = &(ndiode = 1);
paramvalue[126] = &(nrecf0 = 1.8);
paramvalue[127] = &(nrecr0 = 1);
paramvalue[128] = &(isbjt = 3e-07);
paramvalue[129] = &(isdif = 3e-08);
paramvalue[130] = &(isrec = 0.0005);
paramvalue[131] = &(istun = 1e-08);
paramvalue[132] = &(vrec0 = 0.05);
paramvalue[133] = &(vtun0 = 5);
paramvalue[134] = &(nbjt = 1);
paramvalue[135] = &(lbjt0 = 2e-07);
paramvalue[136] = &(vabjt = 10);
paramvalue[137] = &(aely = 0);
paramvalue[138] = &(ahli = 1e-15);
paramvalue[139] = &(vevb = 0.075);
paramvalue[140] = &(vecb = 0.026);
paramvalue[141] = &(cjswg = 5e-10);
paramvalue[142] = &(mjswg = 0.5);
paramvalue[143] = &(pbswg = 0.8);
paramvalue[144] = &(tt = 5e-10);
paramvalue[145] = &(ldif0 = 0.001);
paramvalue[146] = &(cgeo = 0);
paramvalue[147] = &(cgso = 6.5e-10);
paramvalue[148] = &(cgdo = 6e-10);
paramvalue[149] = &(dlc = 0);
paramvalue[150] = &(dwc = 0);
paramvalue[151] = &(dlcb = 0);
paramvalue[152] = &(dlbg = 0);
paramvalue[153] = &(fbody = 1);
paramvalue[154] = &(clc = 1e-07);
paramvalue[155] = &(cle = 0.6);
paramvalue[156] = &(cf = 0);
paramvalue[157] = &(csdmin = 2.5e-05);
paramvalue[158] = &(asd = 0.5);
```

```
paramvalue[159] = &(csdesw = 0);
paramvalue[160] = &(vsdfb = -0.8);
paramvalue[161] = &(vsdth = -0.3);
paramvalue[162] = &(delvt = 0);
paramvalue[163] = &(acde = 0);
paramvalue[164] = &(moin = 15);
paramvalue[165] = &(ckappa = 0.6);
paramvalue[166] = &(cgdl = 0);
paramvalue[167] = &(cgsl = 0);
paramvalue[168] = &(ndif = -1);
paramvalue[169] = &(rth0 = 0.09);
paramvalue[170] = &(cth0 = 1e-05);
paramvalue[171] = &(tpbswg = 0);
paramvalue[172] = &(tcjswg = 0.0005);
paramvalue[173] = &(kt1 = -0.2);
paramvalue[174] = &(kt11 = 8e-09);
paramvalue[175] = &(kt2 = -0.06);
paramvalue[176] = &(ute = -1.5);
paramvalue[177] = &(ua1 = 3e-10);
paramvalue[178] = &(ub1 = -3e-18);
paramvalue[179] = &(uc1 = -6e-11);
paramvalue[180] = &(prt = 10);
paramvalue[181] = &(at = 65000);
paramvalue[182] = &(ntrecf = 0.1);
paramvalue[183] = &(ntrecl = -1);
paramvalue[184] = &(xbjt = 1e-20);
paramvalue[185] = &(xdif = 1.6);
paramvalue[186] = &(xrec = 0.8);
paramvalue[187] = &(xtun = 6);
paramvalue[188] = &(dlcig = lint);
paramvalue[189] = &(nbc = 0);
paramvalue[190] = &(nseg = 1);
paramvalue[191] = &(pdbcpl = 0);
paramvalue[192] = &(psbcpl = 0);
paramvalue[193] = &(toxqm = tox);
paramvalue[194] = &(type = 1);
paramvalue[195] = &(toxm = tox);
paramvalue[196] = &(xt1 = 1.55e-7);
paramvalue[197] = &(dvbd0 = 0.0);
paramvalue[198] = &(dvbd1 = 0.0);
paramvalue[199] = &(temp = 300.15);
paramvalue[200] = &(npeak = 5.8e+17);
paramvalue[201] = &(capMod = 2.0);
paramvalue[202] = &(vbm = 0.0);
```

```

paramvalue[203] = &(nofffd = 1.0);
paramvalue[204] = &(vofffd = 0.0);
paramvalue[205] = &(moinFD = 1e6);
paramvalue[206] = &(shmod = 1.0);

//Set flags
setFlags(NONLINEAR | MULTI_REF | TR_TIME_DOMAIN);
}

void Bsim3nsoitestT::init() throw(string&)
{
//Set number of terminals
setNumTerms(6);

//Set number of state variables
setNumberOfStates(4);

//create tape
IntVector var(4);
var[0] = 0; //Vds
var[1] = 1; //temp
var[2] = 2; //Vbs
var[3] = 3; //Vgs

IntVector novar;
DoubleVector nodelay;
createTape1(var, novar, nodelay, 4, 8);
createTape2();
}

void Bsim3nsoitestT::getLocalRefIdx(UnsignedVector& local_ref_vec,
TerminalVector& term_list)
{
// Make sure the vectors are empty
term_list.erase(term_list.begin(), term_list.end());
local_ref_vec.erase(local_ref_vec.begin(), local_ref_vec.end());

// Insert vector elements
term_list.push_back(getTerminal(0));
term_list.push_back(getTerminal(1));
term_list.push_back(getTerminal(2));
term_list.push_back(getTerminal(3)); // Local reference terminal
term_list.push_back(getTerminal(4));
}

```

```

term_list.push_back(getTerminal(5)); // Local reference terminal

local_ref_vec.push_back(3); // Local reference index
local_ref_vec.push_back(5); // Local reference index
}

void Bsim3nsoitestT::eval1(adoublev& x, adoublev& xt,
adoublev& y1, adoublev& z1)
{

    adouble Vgs_eff, Vbsmos, Vbp, Vbsh, Vbseff, Phis,
    sqrtPhis, Xdep, lt1, ltw;
    adouble DeltVthtemp, DIBL_Sft;
    adouble sqrtPhisExt, Vth, n, Vgst, VgstNVt, ExpArg,
    Vgsteff, Vgst2Vtm, Weff, Rds;
    adouble Abulk, Abulk0, Denomi, ueff, WVCox, WVCoxRds, AbovVgst2Vtm;
    adouble Vdsat, Vdseff, diffVds, Vasat, VACLM, VADIBL, Va,
    CoxWovL, beta, fgche1, fgche2;
    adouble gche, Vfb, V3, Vfbeff, Qac0, Qsub0, AbulkCV,
    VdsatCV, V4, VdseffCV, qbulk;
    adouble qinv, qsrc, qgate, qbody, qsub, qdrn;
    adouble T0, T1, T2, T3, T4, T5, T6, T7, T8, T9, T10, T
    11, T12, T13, T14, TMP, TMP3, TMP4, TMP11, TMP12, TMP13;
    adouble t0, t1, t2, t3, t4, t5, t6, t7, t8, t9, t10, tmp,
    tmp1, tmp2, tmp3, tmp4, vbsc, V0, T00, TT0;
    adouble Esat, EsatL;
    adouble cjsbs, dcjsbs_dT, cjdbs, dcjdbs_dT, DioMax,arg,
    PhiBSWG,MJSWG,dT3_dVb, qjs, qjd;
    adouble SDphi, qse, qde,qgd, qgs, qge;
    adouble vfbb, vearly;
    adouble sdt1, st1, st2, st3, st4, dt2, dt3, dt4;
    adouble Ahli = ahli;
    adouble Ua = ua;
    adouble Ub = ub;
    adouble Uc = uc;
    adouble Vsdfb = vsdfb;
    adouble K2 = k2;
    adouble K1 = k1;
    adouble Vth0 = vth0;
    adouble Nch = nch;

    int soiMod = 1 ;

```

```

int rgateMod = 0;
int selfheat = ((shmod ==1) && (rth0 !=0.0));

#define EPSOX 3.453133e-11
#define EPSSI 1.03594e-10
#define PI 3.141592654
#define Charge_q 1.60219e-19
#define Kb 1.3806226e-23
#define KboQ 8.617087e-5 /* Kb / q */
#define Eg300 1.115 /* energy gap at 300K */
#define DELTA_1 0.02
#define DELTA_2 0.02
#define DELTA_3 0.02
/* Original is 0.02, for matching IBM model, change to 0.08 */
#define DELTA_3_SOI 0.08
#define DELTA_4 0.02
#define DELT_Vbseff 0.005
#define DELTA_VFB 0.02
#define OFF_Vbsitf 0.02 /* v3.1*/
#define CONST_20V3 0.6666666666
#define MAX_EXPL 2.688117142e+43
#define MIN_EXPL 3.720075976e-44
#define EXPL_THRESHOLD 100.0
#define DEXP(A,B,C) {
    if (A > EXPL_THRESHOLD) {
        B = MAX_EXPL*(1.0+(A)-EXPL_THRESHOLD);
        C = MAX_EXPL;
    } else if (A < -EXPL_THRESHOLD) {
        B = MIN_EXPL;
        C = 0;
    } else {
        B = exp(A);
        C = B;
    }
}

#define DEXP1(D,E) {
    if (D > EXPL_THRESHOLD) {
        E = MAX_EXPL*(1.0+(D)-EXPL_THRESHOLD);
    } else if (D < -EXPL_THRESHOLD) {
        E = MIN_EXPL;
    } else {
        E = exp(D);
    }
}

```

```

    }
}

//double vcrit = vt0 * log(vt0 / (root2 * 1e-14));
double factor1 = sqrt(EPSSI / EPSOX * tox);
double cox = 3.453133e-11 / tox;
double ldrn = l;
double wdrn = w;

t0 = pow(ldrn, lln);
t1 = pow(wdrn, lwn);
tmp1 = ll / t0 + lw / t1 + lwl / (t0 * t1);
adouble dl = lint + tmp1;
tmp1 = llc / t0 + lwc / t1 + lwlc / (t0 * t1);
adouble Dlc = dlc + tmp1;
adouble DLCIG = dlcig + tmp1;
t2 = pow(ldrn, wln);
t3 = pow(wdrn, wwn);
tmp2 = wl / t2 + ww / t3 + ww1 / (t2 * t3);
adouble dw = wint + tmp2;
tmp2 = wlc / t2 + wwc / t3 + wwlc / (t2 * t3);
adouble Dwc = dwc + tmp2;
double nbc = 0.0;
adouble leff = 1 - 2.0 * dl;
adouble weff = w - nbc * dwbc - (2.0 - nbc) * dw;
double pdbc = 0;
double psbc = 0;

adouble wdiod = weff / nseg + pdbc;
adouble wdios = weff / nseg + psbc;

adouble leffCV = 1 - 2.0 * Dlc;

adouble weffCV = w - nbc * dwbc - (2.0 - nbc) * Dwc;
adouble wdiodCV = weffCV / nseg + pdbc;
adouble wdiosCV = weffCV / nseg + psbc;
adouble leffCVb = 1 - 2.0 * Dlc - dlcb;
adouble leffCVbg = leffCVb + 2 * dlbg;
adouble abulkCVfactor = 1.0 + pow((clc / leff), cle);
adouble uatemp = ua;
adouble ubtemp = ub;

```

```

adouble uctemp = uc;
adouble rds0denom = pow(weff * 1e6, wr);
adouble rth = rth0 / (weff + wth0) * nseg;
adouble cth = cth0 * (weff + wth0) / nseg;

adouble frbody = 1.0;

adouble Rbody = frbody * rbody * rhalo / (2 * rbody + rhalo * leff)
* weff / nseg;

adouble oxideRatio = pow(toxref/toxqm, ntox) / toxqm / toxqm;
adouble GatesidewallJctPotential = 0.9;
adouble bodyJctGateSideGradingCoeff = 0.5;
adouble unitLengthGateSidewallJctCap = 8.0e-10;
adouble tt = 1e-12;
adouble sourceArea = 0.0;
adouble drainArea = 0.0;
adouble Cbox = 3.453133e-11 / tbox; //---Check
adouble csbox = Cbox * sourceArea;
adouble cdbox = Cbox * drainArea;
adouble csmin = Cbox * sourceArea;
adouble cdmin = Cbox * drainArea;
double Vtm0 = KboQ * tnom;
double Eg0 = 1.16 - 7.02e-4 * tnom * tnom / (tnom + 1108.0);
double ni0 = 1.45e10 * (tnom / 300.15) * sqrt(tnom / 300.15) *
exp(21.5565981 - Eg0 / (2.0 * Vtm0));/* ni is in cm^-3 */

// double phi = 2.0 * Vtm0 * log(npeak / ni0);
adouble Temp=0.0;
adouble TempRatio=0.0;
if(selfheat)
{
    Temp = x[1] +temp;
    TempRatio = Temp / tnom; /* calulcatedtemp/tnom */
}
else
{
    Temp = temp;
    TempRatio = Temp / tnom; /* ckt temp/tnom */
}
adouble Vtm = KboQ * Temp;
adouble Eg = 1.16 - 7.02e-4 * Temp * Temp / (Temp + 1108.0);
t1 = ((7.02e-4 * t5) - t0 * (14.04e-4 * Temp)) / t0 / t0;
/* T1 = dEg / dT */

```

```

t2 = 1.9230584e-4;
/* T2 = 1 / 300.15^(3/2) */
t5 = sqrt(Temp);
t3 = 1.45e10 * Temp * t5 * t2;
t4 = exp(21.5565981 - Eg / (2.0 * Vtm));
adouble ni = t3 * t4;
t0 = log(1.0e20 * Nch / (ni * ni));
adouble vbi = Vtm * t0;
adouble phi = 2.0 * Vtm * log(npeak / ni);
if (nsub > 0)
  {
    t0 = log(Nch / nsub);
    vfbb = -type * Vtm * t0;
  }
else
  {
    t0 = log(-Nch * nsub / ni / ni);
    vfbb = -type * Vtm * t0;
  }

adouble sqrtPhi = sqrt(phi);
adouble Xdep0 = sqrt(2.0 * EPSSI / (Charge_q * npeak * 1.0e6))
* sqrtPhi;
t3 = TempRatio - 1.0;
t8 = 1/ tnom;
t4 = Eg300 / Vtm * t3;
t7 = xbjt * t4 / ndiode;
DEXP1(t7,t0)

  if (xbjt == xdif) {
    t1 = t0;
  }
  else {
    t7 = xdif * t4 / ndiode;
    DEXP1(t7,t1);
  }
t7 = xrec * t4 / nrecf0;
DEXP1(t7,t2);
/* high level injection */
Ahli = ahli * t0;
adouble jbjt = isbjt * t0;
adouble jdif = isdif * t1;
adouble jrec = isrec * t2;
t7 = xtun * t3;

```

```

DEXP1(t7,t0);
adouble jtun = istun * t0;
adouble u0temp = u0 * pow(TempRatio, ute);
adouble vsattemp = vsat -at * t3;
adouble rds0 = (rdsW + prt * t3) / rds0denom;

if(selfheat)
{
    Ua = uatemp + ua1 * t3;
    Ub = ubtemp + ub1 * t3;
    Uc = uctemp + uc1 * t3;
}
else
{
    Ua = ua;
    Ub = ub;
    Uc = uc;
}

adouble TempRatioMinus1 = Temp / tnom - 1.0;
adouble vtm = Vtm;

/* v2.2.2 bug fix */

if (Vsdfb==0)
{
    if (nsub > 0)
        Vsdfb = -type * (vtm*log(1e20 * nsub / ni /ni) - 0.3);
    else if (nsub < 0)
        Vsdfb = -type * (vtm*log(-1e20 / nsub) + 0.3);
}

adouble gamma1 = 5.753e-12 * sqrt(Nch) / cox;
adouble gamma2 = 5.753e-12 * sqrt(nsub) / cox;
adouble cf = 2.0 * EPSOX / PI * log(1.0 + 0.4e-6 / tox);
adouble Cgdo = (cgdo + cf) * wdiodCV;
adouble Cgso = (cgso + cf) * wdiosCV;
adouble Cgeo = cgeo * leffCV;

if ((Nch==0) && (gamma1!=0))
{

```

```

    T0 = gamma1 * cox;
    Nch = 3.021E22 * TempRatioMinus1 * TempRatioMinus1;
}

if (u0 > 1.0)
    u0 = u0 / 1.0e4;

adouble phis3 = sqrtPhi * phi;
adouble sqrtXdep0 = sqrt(Xdep0);
adouble lit1 = sqrt(3.0 * xj * tox);
adouble cdep0 = sqrt(Charge_q * EPSSI * npeak * 1.0e6 / 2.0 / phi);

/* v3.0 */
adouble vfbsd;
if (ngate > 0.0)
    { vfbsd = Vtm0 * log(ngate / 1.0e20);
    }
else
    vfbsd = 0.0;

adouble poxedge = 1.0;
adouble ToxRatio = exp(ntax * log(toxref / toxqm)) / toxqm / toxqm;
adouble ToxRatioEdge = exp(ntax * log(toxref / (toxqm * poxedge)))
/ toxqm / toxqm / poxedge / poxedge;
adouble Aechvb = (type == 1.0) ? 4.97232e-7 : 3.42537e-7;
adouble Bechvb = (type == 1.0) ? 7.45669e11 : 1.16645e12;
adouble AechvbEdge = Aechvb * weff/nseg * DLCIG * ToxRatioEdge;
/* v3.1 bug fix DLCIG*/
adouble BechvbEdge = -Bechvb * toxqm * poxedge;
Aechvb *= weff/nseg * leff * ToxRatio; /* v3.1 bug fix */
Bechvb *= -toxqm;

/* v3.0 */

/*Fix this k1 k2 problem */
/* figure out a way to find out if K1 , K2 are given are not */
adouble vbx;
/* if( k1 || k2 )
{
    if (K1 ==0)
    {cout << "Warning: k1 should be specified with k2.\n" << endl;

```

```

K1 = 0.53;
}
  if (K2 ==0)
  {cout << "Warning: k2 should be specified with k1.\n" << endl;
  K2 = -0.0186;
  }
  if (xt1)
cout << "Warning: xt is ignored because k1 or k2 is given." << endl;
  if (vbx !=0)
cout<<"Warning: vbx is ignored because k1 or k2 is given."<< endl;
  if (vbm !=0)
cout<<"Warning: vbm is ignored because k1 or k2 is given."<< endl;
  if (gamma1!=0)
cout<<"Warning: gamma1 is ignored because k1 or k2 is given."<< endl;
  if (gamma2!=0)
cout<<"Warning: gamma2 is ignored because k1 or k2 is given."<< endl;
  }
else
  {
  */
  if (vbx==0)
vbx = phi - 7.7348e-4 * Nch * xt1 * xt1;
  if (vbx > 0.0)
vbx = -vbx;
  if (vbm > 0.0)
vbm = -vbm;

  if (gamma1==0)
gamma1 = 5.753e-12 * sqrt(Nch) / cox;
  if (gamma2==0)
gamma2 = 5.753e-12 * sqrt(nsub) / cox;

  t0 = gamma1 - gamma2;
  t1 = sqrt(phi - vbx) - sqrtPhi;
  t2 = sqrt(phi * (phi - vbm)) - phi;
  K2 = t0 * t1 / (2.0 * t2 + vbm);
  K1 = gamma2 - 2.0 * K2 * sqrt(phi - vbm);
  //}

if (K2 < 0.0)
  {
  t0 = 0.5 * K1 / K2;
  vbsc = 0.9 * (phi - t0 * t0);
  if (vbsc > -3.0)

```

```

        vbsc = -3.0;
    else if (vbsc < -30.0)
        vbsc = -30.0;
    }
else
    vbsc = -30.0;

if (vbsc > vbm)
    vbsc = vbm;

if ((t0 = weff + k1w2) < 1e-8)
    t0 = 1e-8;

K1 = 0.56;
adouble kleff = K1 * (1 + k1w1/t0);
adouble vfb;

if (Vth0!=0)
    {
        vfb = type * Vth0 - phi - kleff * sqrtPhi;
    }
else
    {
        vfb = -1.0;
        Vth0 = type * (vfb + phi + kleff * sqrtPhi);
    }

kleff *= tox / toxm;
K2 *= tox / toxm;

t1 = sqrt(EPSSI / EPSOX * tox * Xdep0);
t0 = exp(-0.5 * dsub * leff / t1);
adouble theta0vb0 = (t0 + 2.0 * t0 * t0);

t0 = exp(-0.5 * drout * leff / t1);
t2 = (t0 + 2.0 * t0 * t0);
adouble thetaRout = pdibl1 * t2 + pdibl2;

//until pg 15 of b3soitemp.c - adding it below:

if ( ((nsub > 0) && (type > 0)) ||((nsub < 0) && (type < 0)) )

```

```

{
  t0 = vsdth - Vsdfb;
  sdt1 = Vsdfb + asd * t0;
  t1 = csbox - csmin;
  t2 = t1 / t0 / t0;
  st2 = t2 / asd;
  st3 = t2 / ( 1 - asd);
  st4 = t0 * t1 * ( 1 + asd) / 3 - csmin * Vsdfb;

  t1 = cdbox - cadmin;
  t2 = t1 / t0 / t0;
  dt2 = t2 / asd;
  dt3 = t2 / ( 1 - asd);
  dt4 = t0 * t1 * ( 1 + asd) / 3 - cadmin * Vsdfb;
} else
  {
  t0 = Vsdfb - vsdth;
  sdt1 = vsdth + asd * t0;
  t1 = csmin - csbox;
  t2 = t1 / t0 / t0;
  st2 = t2 / asd;
  st3 = t2 / ( 1 - asd);
  st4 = t0 * t1 * ( 1 + asd) / 3 - csbox * vsdth;

  t1 = cadmin - cdbox;
  t2 = t1 / t0 / t0;
  dt2 = t2 / asd;
  dt3 = t2 / ( 1 - asd);
  dt4 = t0 * t1 * ( 1 + asd) / 3 - cdbox * vsdth;
  }

/* v2.0 release */
if (ln < 1e-15) ln = 1e-15;
t0 = -0.5 * leff * leff / ln / ln;
DEXP1(t0,t1);
adouble arfabjt = t1;

t0 = lbjt0 * (1.0 / leff + 1.0 / ln);
adouble lratio = pow(t0,nbjt);
adouble lratiodif = 1.0 + ldif0 * pow(t0,ndif);

if ((vearly = vabjt + aely * leff) < 1)
  vearly = 1;

```

```

adouble qsi = Charge_q * npeak * (1.0 + nlx / leff) * 1e6 * tsi;

adouble ldeb = sqrt(EPSSI * Vtm0 / (Charge_q * Nch * 1.0e6)) / 3.0;

adouble csi = 1.03594e-10 / tsi;

adouble Vesfb = x[2] - vfb;

//*****Bsim3nsoitestT*****//
/* Poly Gate Si DEpeleration Effect */
t0 = vfb + phi;
if((ngate > 1.e18) && (ngate < 1.e25) && (x[3] > t0))
{
    t1 = 1.0e6 * Charge_q * EPSSI * ngate / (cox * cox);
    T4 = sqrt(1.0 + 2.0 * (x[3] - t0) / t1);
    cout<<"t1 "<<t1<<endl;
    cout<<"T4 ="<<T4<<endl;
    T2 = t1 * (T4 - 1.0);
    T3 = 0.5 * T2 * T2 / t1;
    T7 = 1.12 - T3 - 0.05;
    T6 = sqrt(T7 * T7 + 0.224);
    T5 = 1.12 - 0.5 * (T7 + T6);
    Vgs_eff = x[3] - T5;

}
else
{
    Vgs_eff = x[3];
}

adouble Leff = leff;
V0 = vbi - phi;

/* begin of v3.0 block addition */
/* B/S built-in potential lowering calculation */
//or 0 for FD module
/* Prepare Vbs0 & Vbs0mos for VthFD calculation */
t0 = - dvbd1 * leff / litl;
t1 = dvbd0 * (exp(0.5 * t0) + 2 * exp(t0));
t2 = t1 * (vbi - phi);
t3 = 0.5 * qsi / csi;
adouble Vbs0t = phi - t3 + vbsa + t2;
t0 = 1 + csi / Cbox;

```

```

t3 = -dk2b * leff / lit1;
t5 = k2b * (exp(0.5 * t3) + 2 * exp(t3));
t1 = (k1b - t5) / t0;
T2 = t1 * Vesfb;
t4 = 1.0 / (1 + Cbox / csi);
adouble Vbs0 = t4 * Vbs0t + T2;
/* Zero field body potential cal. */

//Vbs0 is adouble
T1 = Vbs0t - Vbs0 - 0.005;
T2 = sqrt(T1 * T1 + (2.5e-5));
T3 = 0.5 * (T1 + T2);
T4 = T3 * csi / qsi;
adouble Vbs0mos = Vbs0 - 0.5 * T3 * T4;
T5 = 0.5 * T4 * (1 + T1 / T2);

/* Set the upper bound of Vbs0mos to be phi for square root calc*/

t1 = phi - 0.02;
T2 = t1 - Vbs0mos - 0.005;
T3 = sqrt(T2 * T2 + 4.0 * 0.005);
Vbs0mos = t1 - 0.5 * (T2 + T3);
T4 = 0.5 * (1 + T2 / T3);

/* VthFD calculation */

adouble Theta0, thetavth, Delt_vth, DeltVthw;
Phis = phi - Vbs0mos;
sqrtPhis = sqrt(Phis);
Xdep = Xdep0 * sqrtPhis / sqrtPhi;
T3 = sqrt(Xdep);
T0 = dvt2 * Vbs0mos;
if (T0 >= -0.5)
{
    T1 = 1.0 + T0;
    t2 = dvt2;
}
else
{
    T4 = 1.0 / (3.0 + 8.0 * T0);
    T1 = (1.0 + 3.0 * T0) * T4;
    T2 = dvt2 * T4 * T4;
}

```

```

lt1 = factor1 * T3 * T1;
T0 = dvt2w * Vbs0mos;
if (T0 >= -0.5)
  {
    T1 = 1.0 + T0;
    t2 = dvt2w;
  }
else
  {
    T4 = 1.0 / (3.0 + 8.0 * T0);
    T1 = (1.0 + 3.0 * T0) * T4;
    T2 = dvt2w * T4 * T4;
  }
ltw = factor1 * T3 * T1;

T0 = -0.5 * dvt1 * Leff / lt1;
if (T0 > -EXPL_THRESHOLD)
  {
    T1 = exp(T0);
    Theta0 = T1 * (1.0 + 2.0 * T1);
  }
else
  {
    T1 = MIN_EXPL;
    Theta0 = T1 * (1.0 + 2.0 * T1);
  }
thetavth = dvt0 * Theta0;
Delt_vth = thetavth * V0;

T0 = -0.5 * dvt1w * weff * Leff / ltw;
if (T0 > -EXPL_THRESHOLD)
  {
    T1 = exp(T0);
    T2 = T1 * (1.0 + 2.0 * T1);
  }
else
  {
    T1 = MIN_EXPL;
    T2 = T1 * (1.0 + 2.0 * T1);
  }

T0 = dvt0w * T2;
DeltVthw = T0 * V0; //DeltVthw is T2 in Bsim3 code
t0 = sqrt(1.0 + nlx / Leff);

```

```

T1 = (kt1 + kt11 / Leff + kt2 * Vbs0mos);
DeltVthtemp = k1eff * (t0 - 1.0) * sqrtPhi + T1 * TempRatioMinus1;
tmp2 = tox * phi / (weff + w0);
T3 = eta0 + etab * Vbs0mos;
condassign(T3, -T3 + 1.0e-4, (2.0e-4 - T3) / (3.0 - 2.0e4 * T3), T3);
/--Not changed to if..else
DIBL_Sft = T3 * theta0vb0 * x[0];
K2=0.0;
adouble VthFD = type * Vth0 + k1eff * (sqrtPhis - sqrtPhi) - K2 *
Vbs0mos - Delt_vth - DeltVthw + (k3+ k3b * Vbs0mos) * tmp2 +
DeltVthtemp - DIBL_Sft; /--Not changed '1.0' to "type" parameter

/* VtgseffFD calculation for PhiFD */

adouble VtgsFD, ExpVtgsFD, VtgseffFD;
VtgsFD = VthFD - Vgs_eff;
t10 = nofffd * Vtm;
DEXP((VtgsFD - vofffd) / t10, ExpVtgsFD, T0);
VtgseffFD = t10 * log(1.0 + ExpVtgsFD);
T0 /= (1.0 + ExpVtgsFD);

/* Surface potential modeling at strong inversion: PhiON */

adouble VgstFD, ExpVgstFD, VgsteffFD;
VgstFD = Vgs_eff - VthFD;
adouble A,B,C;
A = (VgstFD - vofffd) / t10;
B = ExpVgstFD;
C = T0;
if (A > EXPL_THRESHOLD) {
    B = MAX_EXPL*(1.0 + (A)-EXPL_THRESHOLD);
    C = MAX_EXPL;
} else if (A < -EXPL_THRESHOLD) {
    B = MIN_EXPL;
    T0 = 0;
} else {
    B = exp(A);
    C = B;
}

ExpVgstFD = B;
T0 = C;
VgsteffFD = t10 * log(1.0 + ExpVgstFD);
T0 /= (1.0 + ExpVgstFD);

```

```

T1 = moinFD * k1eff * Vtm * Vtm;
T2 = VgsteffFD + 2 * k1eff * sqrt(phi);
T0 = 1 + VgsteffFD * T2 / T1;
adouble PhiON = phi + Vtm * log(T0);

/* Surface potential from subthreshold to inversion: PhiFD */

t0 = cox / (cox + 1.0 / (1.0 / csi + 1.0 / Cbox));
adouble PhiFD = PhiON - t0 * VtgseffFD;

/* built-in potential lowering: Vbs0 */
t0 = -dvbd1 * leff / lit1;
t1 = dvbd0 * (exp(0.5 * t0) + 2 * exp(t0));
t2 = t1 * (vbi - phi);
t3 = 0.5 * qsi / csi;
Vbs0t = PhiFD - t3 + vbsa + t2;
t0 = 1 + csi / Cbox;
t3 = -dk2b * leff / lit1;
t5 = k2b * (exp(0.5 * t3) + 2 * exp(t3));
t1 = (k1b - t5) / t0;
T2 = t1 * Vesfb;
t0 = 1.0 / (1 + Cbox / csi);
Vbs0 = t0 * Vbs0t + T2;

/*set lowerbound for Vbs to VBS0: Vbsitf */

/* soiMod = 1 */

T1 = 0.0 - (Vbs0 + OFF_Vbsitf) - 0.01; //Vbs=0.0
T2 = sqrt(T1 * T1 + 0.0001);
T3 = 0.5 * (1 + T1/T2);
adouble Vbsitf = (Vbs0 + OFF_Vbsitf) + 0.5 * (T1 + T2);

//Based on Vbsitf,calculate zero-field body potential for MOS:Vbsmos

T1 = Vbs0t - Vbsitf - 0.005;
T2 = sqrt(T1 * T1 + (2.5e-5));
T3 = 0.5 * (T1 + T2);
T4 = T3 * csi / qsi;
Vbsmos = Vbsitf - 0.5 * T3 * T4;
/* end of v3.0 block edition */

/* v3.0 modification */
/* T2 is Vbsmos limited above Vbsc=-5 */

```

```

T0 = Vbsmos + 5 - 0.001;
T1 = sqrt(T0 * T0 - 0.004 * (-5));
T2 = (-5) + 0.5 * (T0 + T1);

/* Vbsh is T2 limited below 1.5 */

t0 = 1.5;
T1 = t0 - T2 - 0.002;
T3 = sqrt(T1 * T1 + 0.008 * t0);
Vbsh = t0 - 0.5 * (T1 + T3);

/* Vbseff is Vbsh limited to 0.95*phi */

t0 = 0.95 * phi;
T1 = t0 - Vbsh - 0.002;
T2 = sqrt(T1 * T1 + 0.008 * t0);
Vbseff = t0 - 0.5 * (T1 + T2);
/* END OF MODIFICATION */

Phis = phi - Vbseff;
sqrtPhis = sqrt(Phis);

Xdep = Xdep0 * sqrtPhis / sqrtPhi;
//*****
//From here I am going to add lines of Bsim3 code
//*****

/* Vth Calculation */

T3 = sqrt(Xdep);

/* condassign(T1, dvt2 * Vbseff + 0.5, 1.0 + dvt2 * Vbseff,
(1.0 + 3.0 * dvt2 * Vbseff) / (3.0 + 8.0 * dvt2 * Vbseff));
*/

T0 = dvt2 * Vbseff;
if (T0 >= - 0.5)
{
  T1 = 1.0 + T0;
  T2 = dvt2 ;
}
else /* Added to avoid any discontinuity problems caused by dvt2 */
{
  T4 = 1.0 / (3.0 + 8.0 * T0);
  T1 = (1.0 + 3.0 * T0) * T4;
}

```

```

    T2 = dvt2 * T4 * T4 ;
}
lt1 = factor1 * T3 * T1;
/* condassign(T1, dvt2w * Vbseff + 0.5, 1.0 + dvt2w * Vbseff,
(1.0 + 3.0 * dvt2w * Vbseff) / (3.0 + 8.0 * dvt2w * Vbseff));
*/

T0 = dvt2w * Vbseff;
if (T0 >= - 0.5)
{   T1 = 1.0 + T0;
    T2 = dvt2w;
}
else /* Added to avoid any discontinuity problems caused by dvt2w */
{   T4 = 1.0 / (3.0 + 8.0 * T0);
    T1 = (1.0 + 3.0 * T0) * T4;
    T2 = dvt2w * T4 * T4 ;
}

ltw = factor1 * T3 * T1;

T0 = -0.5 * dvt1 * Leff / lt1;
if (T0 > -EXPL_THRESHOLD)
{   T1 = exp(T0);
    Theta0 = T1 * (1.0 + 2.0 * T1);
}
else
{   T1 = MIN_EXPL;
    Theta0 = T1 * (1.0 + 2.0 * T1);
}
thetavth = dvt0 * Theta0;
Delt_vth = thetavth * V0;

T0 = -0.5 * dvt1w * weff * Leff / ltw;
if (T0 > -EXPL_THRESHOLD)
{   T1 = exp(T0);
    T2 = T1 * (1.0 + 2.0 * T1);
}
else
{   T1 = MIN_EXPL;
    T2 = T1 * (1.0 + 2.0 * T1);
}

T0 = dvt0w * T2;
DeltVthw = T0 * V0; //DeltVthw is T2 in Bsim3 code

```

```

T0 = sqrt(1.0 + nlx / Leff);

T1 = (kt1 + kt1l / Leff + kt2 * Vbseff);
DeltVthtemp = kleff * (T0 - 1.0) * sqrtPhi + T1 * TempRatioMinus1;
tmp2 = tox * phi / (weff + w0);
T3 = eta0 + etab * Vbseff;
DIBL_Sft = T3 * theta0vb0 * x[0];
T9 = 2.2361 / sqrtPhi;
sqrtPhisExt = sqrtPhi - T9 * (Vbsh - Vbseff);
Vth = 1.0 * Vth0 + kleff * (sqrtPhisExt - sqrtPhi) - K2 * Vbseff -
Delt_vth - DeltVthw + (k3 + k3b * Vbseff) * tmp2 + DeltVthtemp - DIBL_Sft;
adouble von = Vth;

/* Calculate n */

T2 = nfactor * EPSSI / Xdep;
T3 = cdsb + cdsb * Vbseff + cdsd * x[0];
T4 = (T2 + T3 * Theta0 + cit) / cox;

// condassign(n, T4 + 0.5, 1.0 + T4, (1.0 + 3.0 * T4) * (1.0 /
//(3.0 + 8.0 * T4)));

if (T4 >= -0.5)
{
  n = 1.0 + T4;
}/* avoid discontinuity problems caused by T4 */

else
{
  T0 = 1.0 / (3.0 + 8.0 * T4);
  n = (1.0 + 3.0 * T4) * T0;
  T0 *= T0;
}

/* Poly Gate Si effect is already discussed in the very beginning */

/* Effective Vgst (Vgsteff) Calculation */

Vgst = Vgs_eff - Vth;
T10 = 2.0 * n * Vtm;
VgstNVt = Vgst / T10;
ExpArg = (2.0 * voff - Vgst) / T10;
adouble ExpVgst, dT2_dVg;
if (VgstNVt > EXPL_THRESHOLD)
{
  Vgsteff = Vgst;
}

```

```

}
else if (ExpArg > EXPL_THRESHOLD)
{   T0 = (Vgst - voff) / (n * Vtm);
    ExpVgst = exp(T0);
    Vgsteff = Vtm * cdep0 / cox * ExpVgst;
    T3 = Vgsteff / (n * Vtm) ;
}
else
{   ExpVgst = exp(VgstNVt);
    T1 = T10 * log(1.0 + ExpVgst);

    dT2_dVg = -cox / (Vtm * cdep0)
              * exp(ExpArg);
    T2 = 1.0 - T10 * dT2_dVg;
    Vgsteff = T1 / T2;
}

Vgst2Vtm = Vgsteff + 2.0 * Vtm;

/* Calculate Effective Channel Geometry */

T9 = sqrtPhis - sqrtPhi;
Weff = weff - (2.0 - nbc) * (dwg * Vgsteff + dwb * T9);

if (Weff < 2.0e-8) /* to avoid the discontinuity problem due to Weff*/
{   T0 = 1.0 / (6.0e-8 - 2.0 * Weff);
    Weff = 2.0e-8 * (4.0e-8 - Weff) * T0;
}

T0 = prwg * Vgsteff + prwb * T9;
if (T0 >= -0.9)
{   Rds = rds0 * (1.0 + T0);
}
else
/* to avoid the discontinuity problem due to prwg and prwb*/
{   T1 = 1.0 / (17.0 + 20.0 * T0);
    Rds = rds0 * (0.8 + T0) * T1;
}

/* Calculate Abulk */

if (a0 == 0.0)
Abulk0 = Abulk = 1.0;
else

```

```

{
  T10 = keta * Vbsh;
  if (T10 >= -0.9) {
    T11 = 1.0 / (1.0 + T10);
  }
  else { /* added to avoid the problems caused by Keta */
    T12 = 1.0 / (0.8 + T10);
    T11 = (17.0 + 20.0 * T10) * T12;
  }

  T10 = phi + ketas;
  T13 = (Vbsh * T11) / T10;

  if(T13 < 0.96)
  {
    T14 = 1/ sqrt(1-T13);
    T10 = 0.5 * T14 / (1-T13);
  }
  else
  {
    T11 = 1.0 / (1.0 - 1.043406 * T13);
    T14 = (6.00167 - 6.26044 * T13) * T11;
    T10 = 0.001742 * T11 * T11;
  }
  t10 = 0.5 * kleff / sqrt(phi + ketas);
  T1 = t10 * T14;
  T9 = sqrt(xj * Xdep);
  TMP11 = Leff + 2.0 * T9;
  T5 = Leff / TMP11;
  TMP12 = a0 * T5;
  tmp3 = weff + b1;
  tmp4 = b0 / tmp3;
  T2 = TMP12 + tmp4;
  T6 = T5 * T5;
  T7 = T5 * T6;
  Abulk0 = 1 + T1 * T2;
  T8 = ags * a0 * T7;
  Abulk = Abulk0 + (-T1 * T8) * Vgsteff;
}

if (Abulk0 < 0.01)
{
  T9 = 1.0 / (3.0 - 200.0 * Abulk0);
}

```

```

    Abulk0 = (0.02 - Abulk0) * T9;
}

if (Abulk < 0.01)
{
    T9 = 1.0 / (3.0 - 200.0 * Abulk);
    Abulk = (0.02 - Abulk) * T9;
}

/* Mobility calculation */
//check the following
// mobMod == 1 (default)

T0 = Vgsteff + Vth + Vth;//cout << "Vgsteff is " << Vgsteff << endl;
T2 = Ua + Uc * Vbseff;
T3 = T0 / tox;
T5 = T3 * (T2 + Ub * T3);

if (T5 >= -0.8)
{
    Denomi = 1.0 + T5;
}
else /*Added to avoid the discontinuity problem caused by ua and ub*/
{
    T9 = 1.0 / (7.0 + 10.0 * T5);
    Denomi = (0.6 + T5) * T9;
    T9 *= T9;
}

ueff = u0temp / Denomi;

/* Saturation Drain Voltage Vdsat*/

WVCox = Weff * vsattemp * cox;
WVCoxRds = WVCox * Rds;

Esat = 2.0 * vsattemp / ueff;
EsatL = Esat * Leff;
/* Sqrt() */
// a1 = a1;
adouble Lambda, dLambda_dVg;
if (a1 == 0.0)
{
    Lambda = a2;
    dLambda_dVg = 0.0;
}

```

```

AbovVgst2Vtm = Abulk / Vgst2Vtm;
if ((Rds == 0.0) && (Lambda == 1.0))
{
    T0 = 1.0 / (Abulk * EsatL + Vgst2Vtm);
    tmp1 = 0.0;
    T1 = T0 * T0;
    T2 = Vgst2Vtm * T0;
    T3 = EsatL * Vgst2Vtm;
    Vdsat = T3 * T0;
}
else
{
    tmp1 = dLambda_dVg / (Lambda * Lambda);
    T9 = Abulk * WVCoxRds;
    T8 = Abulk * T9;
    T7 = Vgst2Vtm * T9;
    T6 = Vgst2Vtm * WVCoxRds;
    T0 = 2.0 * Abulk * (T9 - 1.0 + 1.0 / Lambda);

    T1 = Vgst2Vtm * (2.0 / Lambda - 1.0) + Abulk * EsatL + 3.0 * T7;

    T2 = Vgst2Vtm * (EsatL + 2.0 * T6);

    T3 = sqrt(T1 * T1 - 2.0 * T0 * T2);
    Vdsat = (T1 - T3) / T0;
}

/* Effective Vds (Vdseff) Calculation */
T1 = Vdsat - x[0] - delta;
T2 = sqrt(T1 * T1 + 4.0 * delta * Vdsat);
T0 = T1 / T2;
T3 = 2.0 * delta / T2;

Vdseff = Vdsat - 0.5 * (T1 + T2);
if (Vdseff > x[0])
    Vdseff = x[0];

diffVds = x[0] - Vdseff;
/* Calculate VAsat */

TMP4 = 1.0 - 0.5 * Abulk * Vdsat / Vgst2Vtm;
T9 = WVCoxRds * Vgsteff;//expanded
T8 = T9 / Vgst2Vtm;
T0 = EsatL + Vdsat + 2.0 * T9 * TMP4;

```

```

T9 = WVCoxRds * Abulk;
T1 = 2.0 / Lambda - 1.0 + T9;
Vasat = T0 / T1;
/* Calculate VACLM */
if ((pclm > 0.0) && (diffVds > 1.0e-10))
{
    T0 = 1.0 / (pclm * Abulk * litl);

    T2 = Vgsteff / EsatL;
    T1 = Leff * (Abulk + T2);

    T9 = T0 * T1;
    VACLM = T9 * diffVds;
}
else
{
    VACLM = MAX_EXPL;
}

//cout << "VACLM is " << VACLM << endl;

/* Calculate VADIBL */

/*
T1 = sqrt(EPSSI / EPSOX * tox * Xdep0);

if (thetaRout > 0.0)
{
    T8 = Abulk * Vdsat;
    T0 = Vgst2Vtm * T8;
    T1 = Vgst2Vtm + T8;

    T9 = T1 * T1;
    T2 = thetaRout;
    VADIBL = (Vgst2Vtm - T0 / T1) / T2;

    T7 = pdiblb * Vbseff;
    if (T7 >= -0.9)
    {
        T3 = 1.0 / (1.0 + T7);
        VADIBL *= T3;
    }
    else
/* Added to avoid the discontinuity problem caused by pdiblcb */
    {
        T4 = 1.0 / (0.8 + T7);
        T3 = (17.0 + 20.0 * T7) * T4;
        VADIBL *= T3;
    }
}

```

```

}
else
{  VADIBL = MAX_EXPL;
}

//cout << "VADIBL is " << VADIBL << endl;

/* Calculate VA */

T8 = pvag / EsatL;
T9 = T8 * Vgsteff;

if (T9 > -0.9)
{  T0 = 1.0 + T9;
}
else /* Added to avoid the discontinuity problems caused by pvag */
{  T1 = 1.0 / (17.0 + 20.0 * T9);
   T0 = (0.8 + T9) * T1;
   T1 *= T1;

   T9 *= T1 / EsatL;
}

TMP11 = VACLM * VACLM;
TMP12 = VADIBL * VADIBL;
TMP13 = VACLM + VADIBL;

T1 = VACLM * VADIBL / TMP13;
Va = Vasat + T0 * T1;
/* Calculate Ids */

CoxWovL = cox * Weff / Leff;
beta = ueff * CoxWovL;
T0 = 1.0 - 0.5 * Abulk * Vdseff / Vgst2Vtm;
fgche1 = Vgsteff * T0;
T9 = Vdseff / EsatL;
fgche2 = 1.0 + T9;
gche = beta * fgche1 / fgche2;
T0 = 1.0 + gche * Rds;
T9 = Vdseff / T0;
adouble Idl = gche * T9;
T9 = diffVds / Va;
T0 = 1.0 + T9;
adouble Ids = Idl * T0 / nseg;

```

```

// /*****
// /* all the extra currents */
// /* soiMod != 2 v3.2*/
//
// /* Calculate GIDL current */
//
//
adouble Idgidl, Isgidl;

T0 = 3 * tox;
// /* For drain side */
T1 = (x[0] - Vgs_eff - ngidl) / t0;
if ((agidl <= 0.0) || (bgidl <= 0.0) || (T1 <= 0.0))
    Idgidl = 0.0;
else
{
    T2 = bgidl / T1;
    if (T2 < EXPL_THRESHOLD)
    {
        Idgidl = wdiod * agidl * T1 * exp(-T2);
        T3 = Idgidl / T1 * (T2 + 1.0);
    }
    else
    {
        T3 = wdiod * agidl * MIN_EXPL;
        Idgidl = T3 * T1;
    }
}

// /* For source side */
T1 = (- Vgs_eff - ngidl) / T0;

if ((agidl <= 0.0) || (bgidl <= 0.0) || (T1 <= 0.0))
    Isgidl = 0.0;
else
{
    T2 = bgidl / T1;
    if (T2 < EXPL_THRESHOLD)
    {
        Isgidl = wdios * agidl * T1 * exp(-T2);
        T3 = Isgidl / T1 * (T2 + 1.0);
    }
    else

```

```

    {
        T3 = wdios * agidl * MIN_EXPL;
        Isgidl = T3 * T1;
    }
}

/* calculate diode and BJT current */

adouble ExpVbsNVtm, ExpVbdNVtm;

adouble WsTsi = wdios * tsi;
adouble WdTsi = wdiod * tsi;

adouble NVtm1 = Vtm * ndiode;
adouble E2ndFactor , ic, Ic;

T0 = x[2] / NVtm1;
DEXP(T0,ExpVbsNVtm,T1) ;
T0 = (x[2] - x[0]) / NVtm1;

DEXP(T0, ExpVbdNVtm, T1);

/*****/

/* Ibs1 / Ibd1 : diffusion current */

adouble Ibs1, Ibd1, Ibs2, Ibd2;
        // adouble Ahli,jbjt, jdif, jrec, jtun;

bjjt = isbjt;
jdif = isdif;
jrec = isrec;
jtun = istun;

if (jdif == 0.0)
    Ibs1 = Ibd1 = 0.0;
else
{
    T0 = WsTsi * jdif;
    Ibs1 = T0 * (ExpVbsNVtm - 1.0);

    T0 = WdTsi * jdif;
    Ibd1 = T0 * (ExpVbdNVtm - 1.0);
}

```

```

}

/* Ibs2 : recombination/trap-assisted tunneling current */

adouble NVtmf = 0.026 * nrecf0 * (1 + ntrecf * (TempRatio - 1));
adouble NVtmr = 0.026 * nrecr0 * (1 + ntrecr * (TempRatio - 1));

if (jrec == 0.0)
  Ibs2 = Ibd2 = 0.0;
else
{
  T0 = x[2] / NVtmf; //T0 = Vbs / NVtm1;

  DEXP(T0, T10, T2);

  T4 = 1 / NVtmf;

  if ((vrec0 - x[2]) < 1e-3) //Vbs
  {
    T1 = 1e3;
    T0 = -x[2] / NVtmr * vrec0 * T1; //Vbs
    T11 = -exp(T0);
  }
  else
  {
    T1 = 1 / (vrec0 - x[2]+x[0]);
    T0 = -x[2] / NVtmr * vrec0 * T1;

    DEXP(T0, T11, T2);
    T11 = -T11;
  }
  T3 = WsTsi * jrec;
  Ibs2 = T3 * (T10 + T11);

  // /* Ibd2 */

  T0 = (x[2] - x[0]) / NVtmf; //Vbd

  DEXP(T0, T10, T2);
  T4 = 1 / NVtmf;

  if ((vrec0 - (x[2] - x[0])) < 1e-3)
  {

```

```

        T1 = 1e3;
        T0 = -(x[2] - x[0]) / NVtmr * vrec0 * T1;
        T11 = -exp(T0);
    }
else
    {
        T1 = 1 / (vrec0 - (x[2] - x[0]));
        T0 = (x[0] - x[2]) / NVtmr * vrec0 * T1;

        DEXP(T0, T11, T2);
        T11 = -T11;
    }
T3 = WdTsi * jrec;
Ibd2 = T3 * (T10 + T11);
}

// /* Ibs3/Ibd3 : recombination current in neutral body */
//
adouble Ibs3, Ibd3, Ibs4, Ibd4, Ehli, EhliFactor;
adouble Ehli, EhliFactor, Ibsdif, Ibddif;
adouble Ien;
//
t0 = lbjt0 * (1.0 / leff + 1.0 / ln);
lratio = pow(t0, nbjt);
lratiodif = 1.0 + ldif0 * pow(t0, ndif);

adouble WTsi = weff / nseg * tsi;
if (jbjt == 0.0)
    Ibs3 = Ibd3 = Ibsdif = Ibddif = 0.0;
else
    {
        Ien = WTsi * jbjt * lratio;
        if ((Ehli = Ahli * (ExpVbsNVtm - 1)) < 1e-5)
            {
                Ehli = 0.0;
                EhliFactor = 1.0;
            }
        else
            {
                EhliFactor = 1.0 / sqrt(1 + Ehli);
            }

        if ((Ehli = Ahli * (ExpVbdNVtm - 1)) < 1e-5)
            {

```

```

        Ehlid = 0.0;
        EhlidFactor = 1.0;
    }
else{
    EhlidFactor = 1.0 / sqrt(1 + Ehlid);
}

/* Ibjt(L) */
if (ln < 1e-15)
    ln = 1e-15;
t0 = -0.5 * leff * leff / ln / ln;
// // //define DEXP(A,B) {
if (t0 > EXPL_THRESHOLD)
    t1 = MAX_EXPL*(1.0+(t0)-EXPL_THRESHOLD);
else if (t0 < -EXPL_THRESHOLD)
    t1 = MIN_EXPL;
else
    t1 = exp(t0);

adouble arfabjt = t1;
t0 = 1 - arfabjt;
t1 = t0 * Ien;
Ibs3 = t1 * (ExpVbsNVtm - 1) * EhliFactor;
Ibd3 = t1 * (ExpVbdNVtm - 1) * EhlidFactor;

/* Effective diffusion current for capacitance calculation */
adouble Iendif = WTsi * jbjt * lratiodif;
adouble Ibsdif = Iendif * (ExpVbsNVtm - 1) * EhliFactor;
adouble Ibddif = Iendif * (ExpVbdNVtm - 1) * EhlidFactor;
//}

/* Ic: Bjt collector current */
int bjtoff =0;

if ((bjtoff == 1) || (x[0] == 0.0)) {
    ic = Ic = 0.0;
}
else {
    //      /* second order effects */
    T0 = 1 + (x[2] + (x[2]-x[0])) / vearly;
    T1 = Ehli + Ehlid;
    T3 = sqrt(T0 * T0 + 4 * T1);
    T2 = (T0 + T3) / 2.0;
}

```

```

if (T2 < .1)
  {
    E2ndFactor = 10.0;
  }
else {
  E2ndFactor = 1.0 / T2;
}
T0 = arfabjt * Ien;
ic = Ic = T0 * (ExpVbsNVtm - ExpVbdNVtm) * E2ndFactor;
}
}

// /* Ibs4/Ibd4 : tunneling currents */
//
adouble NVtm2 = 0.026 * ntun;
if (jtun == 0.0)
  Ibs4 = Ibd4 = 0.0;
else
  {
    if ((vtun0 - x[2] < 1e-3))
      {
        T1 = 1e3;
        T0 = -x[2] / NVtm2 * vtun0 * T1;
        T1 = exp(T0);
        T3 = WsTsi * jtun;
        Ibs4 = T3 * (1 - T1);
      }
    else
      {
        T1 = 1 / (vtun0 - x[2]);
        T0 = -x[2] / NVtm2 * vtun0 * T1;
        DEXP(T0, T1, T2);
        T3 = WsTsi * jtun;
        Ibs4 = T3 * (1 - T1);
      }
  }

if ((vtun0 - (x[2] - x[0])) < 1e-3)
  {
    T1 = 1e3;
    T0 = - (x[2] - x[0]) / NVtm2 * vtun0 * T1;
    T1 = exp(T0);
    T3 = WdTsi * jtun;
    Ibd4 = T3 * (1 - T1);
  }

```

```

else
{
    T1 = 1 / (vtun0 - (x[2] - x[0]));
    T0 = - (x[2] - x[0]) / NVtm2 * vtun0 * T1;
    DEXP(T0, T1, T2);

    T3 = WdTsi * jtun;
    Ibd4 = T3 * (1 - T1);
}
}

adouble itun = - Ibd3 - Ibd4;
adouble Ibs = Ibs1 + Ibs2 + Ibs3 + Ibs4;
adouble Ibd = Ibd1 + Ibd2 + Ibd3 + Ibd4;

/*Neglecting gate-tunneling from page 40 to page 47 */

/* v3.0: gate-tunneling */
double igbMod = 0;
double igcMod = 0;
adouble Vgb, Voxacc, Voxdepinv, Vaux, vgs_eff, vgd_eff, Vox, Voxeff;
adouble Igc, Igcs, Igcd, Igs, Igb, Igd, Igb1, Igb2;
adouble VxNVt, ExpVxNVt;
if ((igbMod != 0) || (igcMod != 0))
{
    Vgb = Vgs_eff - x[2];

    /* Calculate Vox first */
    Vfb = type * Vth0 - phi - k1eff * sqrtPhi;

    T3 = Vfb - Vgs_eff + x[2] - DELTA_3;

    if (Vfb <= 0.0)
        T0 = sqrt(T3 * T3 - 4.0 * DELTA_3 * Vfb);
    else
        T0 = sqrt(T3 * T3 + 4.0 * DELTA_3 * Vfb);

    Vfbeff = Vfb - 0.5 * (T3 + T0);

    Voxacc = Vfb - Vfbeff;

    if (Voxacc < 0.0)
        Voxacc = 0.0;
}

```

```

T0 = Vgs_eff - Vgsteff - Vfbeff - Vbseff;
cout<<"Vfb = "<<Vfb<<" Vgs_eff "<<Vgs_eff<<endl;

if (k1eff == 0.0)
    Voxdepinv = 0.0;
else {
    if (T0 < 0.0)
        T1 = T0/k1eff;
    else {
        T1 = k1eff/2*(-1 + sqrt(1 + 4*T0/k1eff/k1eff));
        T2 = k1eff/2 *0.5/sqrt(1 + 4*T0/k1eff/k1eff) *4/k1eff/k1eff;
    }
    Voxdepinv = Vgs_eff - (T1*T1 + x[2]) - Vfb;
}
}

/* gate-channel tunneling component */
if (igcMod)
{
    T0 = Vtm * n1gc;
    VxNVt = (Vgs_eff - type * Vth0) / T0;
    /* Vth instead of Vth0 may be used */
    if (VxNVt > EXPL_THRESHOLD)
        Vaux = Vgs_eff - type * Vth0;
    else if (VxNVt < -EXPL_THRESHOLD)
        Vaux = T0 * log(1.0 + MIN_EXPL);
    else
    {
        ExpVxNVt = exp(VxNVt);
        Vaux = T0 * log(1.0 + ExpVxNVt);
    }

    T2 = Vgs_eff * Vaux;
    T11 = Aechvb;
    T12 = Bechvb;
    T3 = a1gc * c1gc - b1gc;
    T4 = b1gc * c1gc;
    T5 = T12 * (a1gc + T3 * Voxdepinv - T4 * Voxdepinv * Voxdepinv);

    if (T5 > EXPL_THRESHOLD)
        T6 = MAX_EXPL;
    else if (T5 < -EXPL_THRESHOLD)

```

```

    T6 = MIN_EXPL;
else
    T6 = exp(T5);

Igc = T11 * T2 * T6;

T7 = -pigcd * x[0];
T8 = T7 * T7 + 2.0e-4;

if (T7 > EXPL_THRESHOLD)
    T9 = MAX_EXPL;
else if (T7 < -EXPL_THRESHOLD)
    T9 = MIN_EXPL;
else
    T9 = exp(T7);

T0 = T8 * T8;
T1 = T9 - 1.0 + 1.0e-4;
T10 = (T1 - T7) / T8;

Igcds = Igc * T10;

T1 = T9 - 1.0 - 1.0e-4;
T10 = (T7 * T9 - T1) / T8;

Igcd = Igc * T10;
Igcds = Igcds;
Igcd = Igcd;

T0 = x[3] - vfbsd;
vgs_eff = sqrt(T0 * T0 + 1.0e-4);

T2 = x[3] * vgs_eff;
T11 = AechvbEdge;
T12 = BechvbEdge;
T3 = aigsd * cigsd - bigsd;
T4 = bigsd * cigsd;
T5 = T12 * (aigsd + T3 * vgs_eff - T4 * vgs_eff * vgs_eff);

if (T5 > EXPL_THRESHOLD)
    T6 = MAX_EXPL;
else if (T5 < -EXPL_THRESHOLD)

```

```

    T6 = MIN_EXPL;
else
    T6 = exp(T5);

Igs = T11 * T2 * T6;

T0 = (x[3] - x[0]) - vfbsd;
vgd_eff = sqrt(T0 * T0 + 1.0e-4);

T2 = (x[3] - x[0]) * vgd_eff;

T5 = T12 * (aigsd + T3 * vgd_eff - T4 * vgd_eff * vgd_eff);

if (T5 > EXPL_THRESHOLD)
    T6 = MAX_EXPL;
else if (T5 < -EXPL_THRESHOLD)
    T6 = MIN_EXPL;
else
    T6 = exp(T5);

Igd = T11 * T2 * T6;

}
else
{
    Igs = 0.0;
    Igd = 0.0;
}

/* gate-body tunneling component */
adouble alphaGB1 = 0.35;
adouble betaGB1 = 0.03;
adouble alphaGB2 = 0.43;
adouble betaGB2 = 0.05;
if ( soiMod != 2) /* v3.2 */
/* v3.1: the Igb calculation is skipped for the ideal FD mode */
{

    Vox = Voxdepinv;
    /* Voxeff is Vox limited below Voxh */
    T0 = voxh;
    T1 = T0 - Vox - deltavox;
    T3 = sqrt(T1 * T1 + 4* deltavox * T0);
    Voxeff = T0 - 0.5 * (T1 + T3);
}

```

```

Vox = Voxeff;

T0 = (Vox - ebg)/ vevb;
DEXP(T0, T1, T2); /* T1=exp(T0), T2=dT1_dT0 */
Vaux = vevb * log(1 + T1);

if ( vgb1 != 0) {
    T0 = 1 - Vox / vgb1;
}
else
    T0 = 1;

if (T0 < 0.01) {
    T0 = 0.01;
}

/* v2.2.3 bug fix */
T1 = Leff * Weff * 3.7622e-7 * oxideRatio / nseg;

T2 = -3.1051e10 * toxqm;
T3 = alphaGB1;
T4 = betaGB1;
T6 = T2*(T3 - T4 * Vox) / T0;

DEXP(T6, T5, T7); /* T5=exp(T6), T7=dT5_dT6 */
Igb1 = T1 * Vgb * Vaux * T5;

Vox = Voxacc;
/* Voxeff is Vox limited below Voxh */
T0 = voxh;
T1 = T0 - Vox - deltax;
T3 = sqrt(T1 * T1 + 4* deltax * T0);
Voxeff = T0 - 0.5 * (T1 + T3);
Vox = Voxeff;
T0 = (-Vgb+(Vfb))/ vecb;
DEXP(T0, T1, T2); /* T1=exp(T0), T2=dT1_dT0 */
Vaux = vecb* log(1 + T1);
if ( vgb2 != 0) {
    T0 = 1 - Vox / vgb2;
}
else
    T0 = 1;

```

```

if (T0 < 0.01) {
    T0 = 0.01;
}

/* v2.2.3 bug fix */
T1 = Leff * Weff * 4.9758e-7 * oxideRatio / nseg;

T2 = -2.357e10 * toxqm;
T3 = alphaGB2;
T4 = betaGB2;

T6 = T2*(T3 - T4 * Vox) / T0;
DEXP(T6, T5, T7); /* T5=exp(T6), T7=dT5_dT6 */

Igb2 = T1 * (x[3]-x[2]) * Vaux * T5;

// Igb1 dominates in inversion region,
//while Igb2 doninates in accumulation */
// v2.2.3 bug fix for residue at low Vgb */

if (Vgb >= 0)
    Igb = Igb1;
else
    Igb = Igb2;
}
else {
    Igb = 0.0;
}

/* end of gate-body tunneling */
/* end of v3.0 gate-tunneling */
/* v3.1 on page 47 */
/* Calculate substrate current Iii */
adouble Iii, VgsStep, Vdsatii, Ratio, Vdiff;
adouble Vdsatii0;

if (alpha0 <= 0.0)
    Iii = 0.0;
else
{

```

```

Vdsatii0 = vdsatii0 * (1 + tii * (TempRatio - 1.0)) - lii / Leff;
/* Calculate VgsStep */
T0 = esatii * Leff;
T1 = sii0 * T0 / (1 + T0);
T0 = 1 / (1 + sii1 * Vgsteff);
T3 = T0 + sii2;
T4 = Vgst * sii1 * T0 * T0;
T2 = Vgst * T3;
T3 = 1 / (1 + siid * x[0]);
VgsStep = T1 * T2 * T3;
Vdsatii = Vdsatii0 + VgsStep;
Vdiff = x[0] - Vdsatii;
T0 = beta2 + beta1 * Vdiff + beta0 * Vdiff * Vdiff;
if (T0 < 1e-5)
    T0 = 1e-5;
else
    T1 = beta1 + 2 * beta0 * Vdiff;

if ((T0 < Vdiff / EXPL_THRESHOLD) && (Vdiff > 0.0))
    Ratio = alpha0 * MAX_EXPL;
else if ((T0 < -Vdiff / EXPL_THRESHOLD) && (Vdiff < 0.0))
    Ratio = alpha0 * MIN_EXPL;
else
    Ratio = alpha0 * exp(Vdiff / T0);
/* Avoid too high ratio */
if (Ratio > 10.0)
    Ratio = 10.0;
T0 = Ids + fbjtii * Ic; //For the time being put Ic = 0
Iii = Ratio * T0;
}
/*****/
/* C-V Model for capMod=2 */

if (capMod == 2)
{
    Vfb = Vth - phi - kleff * sqrtPhis + delvt;
    V3 = Vfb - Vgs_eff + Vbseff - DELTA_3_SOI;
    if (Vfb <= 0.0)
    {
        T0 = sqrt(V3 * V3 - 4.0 * DELTA_3_SOI * Vfb);
        T2 = -DELTA_3_SOI / T0;
    }
    else

```

```

    {
        T0 = sqrt(V3 * V3 + 4.0 * DELTA_3_SOI * Vfb);
        T2 = DELTA_3_SOI / T0;
    }
T1 = 0.5 * (1.0 + V3 / T0);
Vfbeff = Vfb - 0.5 * (V3 + T0);
adouble CoxWL, CoxWLb;
adouble agbcp = 0.0;
adouble aebcp = 0.0;
CoxWL = cox * (weffCV / nseg * leffCV + agbcp);
CoxWLb = fbody * cox * (weffCV / nseg * leffCVb + agbcp);
Qac0 = CoxWLb * (Vfbeff - Vfb);

t0 = 0.5 * K1;
T3 = Vgs_eff - Vfbeff - Vbseff - Vgsteff;
if (kleff == 0.0)
    {
        T1 = 0.0;
        T2 = 0.0;
    }
else if (T3 < 0.0)
    {
        T1 = t0 + T3 / kleff;
        T2 = CoxWLb;
    }
else
    {
        T1 = sqrt(t0 * t0 + T3);
        T2 = CoxWLb * T0 / T1;
    }

Qsub0 = CoxWLb * K1 * (T1 - t0);
AbulkCV = Abulk0 * abulkCVfactor;
VdsatCV = Vgsteff / AbulkCV;
V4 = VdsatCV - x[0] - DELTA_4;
T0 = sqrt(V4 * V4 + 4.0 * DELTA_4 * VdsatCV);
VdseffCV = VdsatCV - 0.5 * (V4 + T0);
T1 = 0.5 * (1.0 + V4 / T0);
T2 = DELTA_4 / T0;
T3 = (1.0 - T1 - T2) / AbulkCV;
T0 = AbulkCV * VdseffCV;
T1 = 12.0 * (Vgsteff - 0.5 * T0 + 1e-20);
T2 = VdseffCV / T1;
T3 = T0 * T2;

```

```

T4 = (1.0 - 12.0 * T2 * T2 * AbulkCV);
T5 = (6.0 * T0 * (4.0 * Vgsteff - T0) / (T1 * T1) - 0.5);
T6 = 12.0 * T2 * T2 * Vgsteff;
T7 = 1.0 - AbulkCV;
qbulk = CoxWLb * T7 * (0.5 * VdseffCV - T3);
T4 = -T7 * (T4 - 1.0);
T5 = -T7 * T5;
T6 = -(T7 * T6 + (0.5 * VdseffCV - T3));
/* Total inversion charge */
T0 = AbulkCV * VdseffCV;
T1 = 12.0 * (Vgsteff - 0.5 * T0 + 1e-20);
T2 = T0 / T1;
T3 = T0 * T2;

T4 = (1.0 - 12.0 * T2 * T2);
T7 = T2 * (2.0 + 6.0 * T2) - 0.5;

T5 = T7 * AbulkCV;
T6 = T7 * VdseffCV;

qinv = CoxWL * (Vgsteff - 0.5 * T0 + T3);

/* Inversion charge partitioning into S / D */
if (xpart > 0.5)
{ /* 0/100 Charge partition model */
  T1 = T1 + T1;
  qsrc = -CoxWL * (0.5 * Vgsteff + 0.25 * T0 - T0 * T0 / T1);
}
else if (xpart < 0.5)
{ /* 40/60 Charge partition model */
  T1 = T1 / 12.0;
  T2 = 0.5 * CoxWL / (T1 * T1);
  T3 = Vgsteff * (2.0 * T0 * T0 / 3.0 + Vgsteff *
(Vgsteff - 4.0 * T0 / 3.0))
- 2.0 * T0 * T0 * T0 / 15.0;
  cout<<"T1 "<<T1<<" T2 "<<T2<<" T3 "<<T3<<endl;
  qsrc = -T2 * T3;
}
else
{ /* 50/50 Charge partition model */
  qsrc = - 0.5 * (qinv + qbulk);
}

```

```

/* Backgate charge */

adouble CboxWL = kb1 * fbody * Cbox * (weffCV / nseg *
leffCVbg + aebcp);
adouble Qe1 = CboxWL * (Vesfb - 0.0);

qgate = qinv + Qac0 + Qsub0;
qbody = (qbulk - Qac0 - Qsub0 - Qe1);
qsub = Qe1;
qdrn = -(qgate + qsrc + qbody + qsub);

cout<<"Qgate "<<qgate<<endl;
cout<<"Qbody ="<<qbody<<endl;
cout<<"Qsub ="<<qsub<<endl;
cout<<"Qsrc ="<<qsrc<<endl;
cout<<"Qdrn = "<<qdrn<<endl;

} /* End of Capmod ==2 */
/*****/
/* C-V Model for capMod=3 */
if(capMod==3)
{
adouble dtoxcv = 0.0;
adouble Cox = 3.453133e-11 / (tox - dtoxcv);
adouble agbcp = 0.0;
adouble CoxWL = cox * (weffCV / nseg *leffCV + agbcp);
CoxWL = CoxWL * tox / (tox- dtoxcv);
adouble CoxWlb = CoxWlb * tox / (tox - dtoxcv);
adouble Tox = 1.0e8 * (tox - dtoxcv);

/* vfbzb calculation for capMod 3 */

adouble k1ox = K1;
adouble noff = 1.0;
adouble voffcv = 0.0;

T0 = -0.5 * dvt1w * weff * leff / (factor1 * sqrt(Xdep0));

condassign(T2, T0 + EXPL_THRESHOLD, exp(T0) * (1.0 + 2.0 * exp(t0)),
MIN_EXPL * (1.0 + 2.0 * MIN_EXPL));

T0 = dvt0w * T2;
T2 = T0 * (vbi - phi);

```

```

T0 = -0.5 * dvt1 * leff / (factor1 * sqrt(Xdep0));

condassign(T3, T0 + EXPL_THRESHOLD, exp(T0) * (1.0 + 2.0 * exp(T0)),
MIN_EXPL * (1.0 + 2.0 * MIN_EXPL));

T3 = dvt0 * T3 * (vbi - phi);
T4 = tox * phi / (weff + w0);
T0 = sqrt(1.0 + nlx / leff);
T5 = k1ox * (T0 - 1.0) * sqrtPhi + (kt1 + kt11 / leff) *
(Temp/tnom - 1.0);
T6 = Vth0 - T2 - T3 + k3 * T4 + T5;
adouble vfbzb = T6 - phi - K1 * sqrtPhi;
adouble tmp = sqrt(Xdep0);
tmp1 = vbi - phi;
tmp2 = factor1 * tmp;

T0 = -0.5 * dvt1w * weff * leff / tmp2;
if (T0 > -EXPL_THRESHOLD)
  { T1 = exp(T0);
    T2 = T1 * (1.0 + 2.0 * T1);
  }
else
  { T1 = MIN_EXPL;
    T2 = T1 * (1.0 + 2.0 * T1);
  }
T0 = dvt0w * T2;
T2 = T0 * tmp1;

T0 = -0.5 * dvt1 * leff / tmp2;
if (T0 > -EXPL_THRESHOLD)
  { T1 = exp(T0);
    T3 = T1 * (1.0 + 2.0 * T1);
  }
else
  { T1 = MIN_EXPL;
    T3 = T1 * (1.0 + 2.0 * T1);
  }
T3 = dvt0 * T3 * tmp1;

T4 = (tox - dtoxv) * phi / (weff + w0);

T0 = sqrt(1.0 + nlx / leff);

```

```

T5 = k1eff * (T0 - 1.0) * sqrtPhi + (kt1 + kt11 / leff) *
(TempRatio - 1.0);

TMP3 = type * Vth0 - T2 - T3 + k3 * T4 + T5;
vfbzb = TMP3 - phi - k1eff * sqrtPhi;
/* End of vfbzb */

//Calculation for VbseffCV

adouble VbseffCV;

condassign(VbseffCV, Vbseff, phi - Phis, Vbseff);

//Calculation for VgsteffCV

T0 = n * noff * Vtm0;
T1 = (Vgs_eff - Vth) / T0;

condassign(Vgsteff, T1 - EXPL_THRESHOLD, Vgs_eff - Vth - voffcv, T0
* log(1.0 + exp(T1)));
condassign(Vgsteff, -T1 - EXPL_THRESHOLD, T0 * log(1.0 + MIN_EXPL), T0
* log(1.0 + exp(T1)));
//Calculation for Vfbeff

V3 = vfbzb - Vgs_eff + Vbseff - 0.02;
condassign(T0, vfbzb, sqrt(V3 * V3 + 4.0 * 0.02 * vfbzb),
sqrt(V3 * V3 - 4.0 * 0.02 * vfbzb));
//adouble Vfbeff;
Vfbeff = vfbzb - 0.5 * (V3 + T0);
Tox = 1.0e8 * tox;
T0 = (Vgs_eff - VbseffCV - vfbzb) / Tox;

//Calculation for Tcen

ldeb = sqrt(EPSSI * Vtm0 / (Charge_q * Nch * 1.0e6)) / 3.0;
adouble acde = 1.0;
adouble Tcen;
T1 = T0 * acde;

if ((-EXPL_THRESHOLD < T1) && (T1 < EXPL_THRESHOLD))
    Tcen = ldeb * exp(T1);
else if (T1 <= -EXPL_THRESHOLD)
    Tcen = ldeb * MIN_EXPL;

```

```

else
    Tcen = ldeb * MAX_EXPL;

V3 = ldeb - Tcen - (1.0e-3 * Tox);

//adouble V4;
V4 = sqrt(V3 * V3 + 4.0 * (1.0e-3 * Tox) * ldeb);

Tcen = ldeb - 0.5 * (V3 + V4);
adouble Ccen;
Ccen = EPSSI / Tcen;

adouble Coxeff;
Coxeff = Ccen * cox / (Ccen + cox);
//Calculation for QoverlapCox

//adouble QovCox, Qac0, CoxWLCen, Qsub0;

adouble CoxWLCen = cox * Weff * leff * Coxeff / cox;
//cout << "CoxWLCen = " << CoxWLCen << endl;
Qac0 = CoxWLCen * (Vfbeff - vfbzb);
adouble QovCox = Qac0 / Coxeff;

T0 = 0.5 * k1ox;
T3 = Vgs_eff - Vfbeff - VbseffCV - Vgsteff;
T1 = sqrt(T0 * T0 + T3);
T2 = CoxWLCen * T0 / T1;

condassign(T1, -T3, (T0 + T3 / k1ox), (sqrt(T0 * T0 + T3)));
condassign(T2, -T3, CoxWLCen, (CoxWLCen * T0 / T1));

Qsub0 = CoxWLCen * k1ox * (T1 - T0);
QovCox = Qsub0 / Coxeff;
//Calculation for Delta_phi

condassign(t2, k1ox, moin * Vtm0 * k1ox * k1ox, 0.25 * moin * Vtm0);
condassign(t0, k1ox, k1ox * sqrt(phi), 0.5 * sqrt(phi));

adouble DeltaPhi;

T1 = 2.0 * t0 + Vgsteff;

DeltaPhi = Vtm0 * log(1.0 + T1 * Vgsteff / t2);
T3 = 4.0 * (Vth - vfbzb - phi);

```

```

Tox = Tox + Tox;
condassign(T0, T3, (Vgsteff + T3) / Tox, (Vgsteff + 1.0e-20) / Tox);
TMP = exp(0.7 * log(T0));
T1 = 1.0 + TMP;
T2 = 0.7 * TMP / (T0 * Tox);
Tcen = 1.9e-9 / T1;

Ccen = EPSSI / Tcen;
Coxeff = Ccen * cox / (Ccen + cox);
CoxWLCen = cox * Weff * leff * Coxeff / cox;

//adouble AbulkCV;
AbulkCV = Abulk0 * (1.0 + pow((clc/leff),cle));

//adouble VdsatCV;
VdsatCV = (Vgsteff - DeltaPhi) / AbulkCV;

T0 = VdsatCV - x[0] - 0.02;
T1 = sqrt(T0 * T0 + 4.0 * 0.02 * VdsatCV);

//adouble VdseffCV;
condassign(VdseffCV, T0, VdsatCV - 0.5 * (T0 + T1), VdsatCV *
(1.0 - 0.04/(T1-T0)));

if (x[0] == 0.0)
    VdseffCV = 0.0;

T0 = AbulkCV * VdseffCV;
T1 = Vgsteff - DeltaPhi;
T2 = 12.0 * (T1 - 0.5 * T0 + 1.0e-20);
T3 = T0 / T2;
T4 = 1.0 - 12.0 * T3 * T3;
T5 = AbulkCV * (6.0 * T0 * (4.0 * T1 - T0) / (T2 * T2) - 0.5);
T6 = T5 * VdseffCV / AbulkCV;
qgate = CoxWLCen * (T1 - T0 * (0.5 - T3));

//adouble qbulk;
qbulk = CoxWLCen * (1.0 - AbulkCV) * (0.5*VdseffCV - T0*VdseffCV/T2);
QovCox = qbulk / Coxeff;

T2 = T2 / 12.0;
T3 = 0.5 * CoxWLCen / (T2 * T2);
T4 = T1 * (2.0 * T0 * T0 / 3.0 + T1 * (T1 - 4.0 * T0 / 3.0)) -

```

```

2.0 * T0 * T0 * T0 / 15.0;

//adouble qsrc;
qsrc = -T3 * T4;
//cout << "COXWLCEN = " << CoxWLCen << endl;

/* Backgate charge */

adouble aebcp = 0.0;
adouble tbox = 3e-7;

adouble CboxWL = kb1 * fbody * Cbox * (weffCV/nseg*leffCVbg+aebcp);
adouble Qe1 = CboxWL * (Vesfb - 0.0);
qgate = qgate + Qac0 + Qsub0 - qbulk;
//qbulk -= (Qac0 + Qsub0);
qbody = qbulk - Qac0 - Qsub0 - Qe1;
qsub = Qe1;
qdrn = -(qgate + qbody + qsub + qsrc);

} /* End of Capmod==3 */

if(soiMod<2)
{
/* Intrinsic S/D charge */
PhiBSWG = GatesidewallJctPotential;
MJSWG = bodyJctGateSideGradingCoeff;
cjsbs = unitLengthGateSidewallJctCap * wdiosCV * tsi / 1e-7;
dcjsbs_dT = cjsbs * tcjswg;
cjsbs += dcjsbs_dT * (Temp - tnom);
cjdbbs = unitLengthGateSidewallJctCap * wdiodCV * tsi / 1e-7;
dcjdbbs_dT = cjdbbs * tcjswg;
cjdbbs += dcjdbbs_dT * (Temp - tnom);
adouble DioMax = 0.9 * (PhiBSWG);

adouble argtemp=0.0;
arg = 1.0 - x[2] / PhiBSWG;

if (MJSWG == 0.5)
    dT3_dVb = 1.0 / sqrt(arg);
else
    dT3_dVb = exp(-MJSWG * log(arg));
T3 = (1.0 - arg * dT3_dVb) * PhiBSWG / (1.0 - MJSWG);
qjs = cjsbs * T3 + tt * Ibsdif;
arg = 1.0 - ((x[2]-x[0]) > DioMax ? DioMax : (x[2]-x[0]))/PhiBSWG;

```

```

if (MJSWG == 0.5)
    dT3_dVb = 1.0 / sqrt(arg);
else
    dT3_dVb = exp(-MJSWG * log(arg));
T3 = (1.0 - arg * dT3_dVb) * PhiBSWG / (1.0 - MJSWG);
if ((x[2]-x[0]) > DioMax)
    T3 += dT3_dVb * ((x[2]-x[0]) - DioMax);
qjd = cjdb * T3 + tt * Ibddif;
}/* End of Intrinsic S/D charge */

qdrn -= qjd;
qbody += (qjs + qjd);
qsrc = -(qgate + qbody + qdrn + qsub);

/* Extrinsic Bottom S/D to substrate charge */
//T10 = -model->B3S0Itype * ves;
T10 = 0.0;
/* T10 is vse without type conversion */
//T11 = model->B3S0Itype * (vds - ves);
T11 = x[0] - T10;
/* T11 is vde without type conversion */
SDphi = 2.0*vtm*log(fabs(nsub) / ni);
adouble tmp = sqrt(2.0*EPSSI*SDphi/(Charge_q * abs(nsub) * 1.0e6));
adouble tmp1p = EPSSI / tmp;
//csdmin = tmp1p * Cbox /(tmp1p + Cbox);
if (csdmin != 0.0)
{
    if ( ((nsub > 0) && (type > 0)) ||((nsub < 0) && (type < 0)))
    {
        if (Vsdfb > T10)
            qse = csbox * (T10 - Vsdfb);
        else if (T10 < sdt1)
        {
            T0 = T10 - Vsdfb;
            T1 = T0 * T0;
            qse = T0 * (csbox - st2 / 3 * T1) ;
        }
        else if (T10 < vsdth)
        {
            T0 = T10 - vsdth;
            T1 = T0 * T0;
            qse = csmin * T10 + st4 + st3 / 3 * T0 * T1;
        }
    }
}

```

```

        else
            qse = csmin * T10 + st4;
        }
    else
    {
        if (T10 < vsdth)
            qse = csmin * (T10 - vsdth);

            else if (T10 < sdt1)
            {
                T0 = T10 - vsdth;
                T1 = T0 * T0;
                qse = T0 * (csmin - st2 / 3 * T1) ;
            }
            else if (T10 < Vsdfb)
            {
                T0 = T10 - Vsdfb;
                T1 = T0 * T0;
                qse = csbox * T10 + st4 + st3 / 3 * T0 * T1;
            }
            else
                qse = csbox * T10 + st4;

        }

    if ( ((nsub > 0) && (type > 0)) || ((nsub < 0) && (type < 0)))
    {
        if (Vsdfb > T11)
            qde = cdbox * (T11 - Vsdfb);
            else if (T11 < sdt1)
            {
                T0 = T10 - Vsdfb;
                T1 = T0 * T0;
                qde = T0 * (csbox - st2 / 3 * T1) ;
            }
            else if (T11 < vsdth)
            {
                T0 = T11 - vsdth;
                T1 = T0 * T0;
                qde = cadmin * T11 + dt4 + dt3 / 3 * T0 * T1;
            }
            else
                qde = cadmin * T11 + dt4;
        }
    else

```

```

{
    if (T11 < vsdth)
qde = cadmin * (T11 - vsdth);

        else if (T11 < sdt1)
        {
            T0 = T11 - vsdth;
            T1 = T0 * T0;
            qde = T0 * (cadmin - dt2 / 3 * T1) ;
        }
        else if (T11 < Vsdfb)
        {
            T0 = T11 - Vsdfb;
            T1 = T0 * T0;
            qde = cdbox * T11 + dt4 + dt3 / 3 * T0 * T1;
        }
        else
qde = cdbox * T11 + st4;

    }

}
else
{
    qse = csbox * T10;
    qde = cdbox * T11;
} /*end of Extrinsic Bottom S/D charge */
//qse += csesw * T10;
//qde += cdesw * T11;
T0 = x[3]-x[2] + DELTA_1;
T1 = sqrt(T0 * T0 + 4.0 * DELTA_1);
T2 = 0.5 * (T0 - T1);
/* v2.2.3 bug fix */
T3 = wdiodCV * cgd1;
/* v3.1 bug fix */
T4 = sqrt(1.0 - 4.0 * T2 / ckappa);
adouble dcgdo = Cgdo + T3 - T3 * (1.0 - 1.0 / T4) *
(0.5 - 0.5 * T0 / T1);
adouble qgdo = (dcgdo + T3) * (x[3] - x[2]) - T3 *
(T2+ 0.5 * ckappa * (T4 - 1.0));

//if (rgateMod == 3) {
// qgdo = (cgdo + T3) * vgmd - T3 * (T2 + 0.5 * ckappa * (T4 - 1.0));
//} /* v3.2 bug fix */

```

```

T0 = x[3] + DELTA_1;
//if (rgateMod == 3)
// T0 = vgms + DELTA_1; /* v3.2 bug fix */

T1 = sqrt(T0 * T0 + 4.0 * DELTA_1);
T2 = 0.5 * (T0 - T1);
T3 = wdiosCV * cgs1; /* v3.1 bug fix */
T4 = sqrt(1.0 - 4.0 * T2 / ckappa);
adouble dcgso = Cgso + T3 - T3 * (1.0 - 1.0 / T4)*
(0.5 - 0.5 * T0 / T1);
adouble qgso = (dcgso + T3) * x[3] - T3 *
(T2 + 0.5 * ckappa * (T4 - 1.0));

//if (rgateMod == 3) {
//qgso = (cgso + T3) * vgms - T3 * (T2+ 0.5 * ckappa * (T4 - 1.0));
//}

if (soiMod > 0)
{
  /* v3.1 wanh added for RF */
  if (rgateMod == 3)
  {
    qgd = qgdo;
    qgs = qgso;
    qge = 0; /* v3.1 wanh changed */
    qgate += qge;
    qbody -= 0;
    qdrn += qde - qgd;
    qsub -= qse + qde;
    qsrc = -(qgate + qbody + qdrn + qsub);
  }
  else
  {
    qgd = qgdo;
    qgs = qgso;
    qgate += qgd + qgs + qge;
    qdrn += qde - qgd;
    qsub -= qge + qse + qde;
    qsrc = -(qgate + qbody + qdrn + qsub);
  }
}
y1[0] = qdrn;
y1[1] = qgate;

```

```
y1[2] = qsrc;
y1[3] = temp;
adouble Icjd = Ibd - Iii - Idgidl;
adouble Icjs = Ibs - Isgidl;
z1[0] = Ids + Ic -Icjd + Igd ;
z1[1] = Igd + Igs + Igb;
z1[2] = -Ids - Ic + -Icjs + Igs;
z1[3]= - Ids * (x[0]-x[2]);
z1[4] = x[0] - x[2];//Vdb
z1[5] = x[3] - x[2];//Vgb
z1[6] = - x[2];//Vsb
z1[7] = x[1] + temp;
}

void Bsim3nsoitestT::eval2(adoublev& dy1, adoublev& z1,
adoublev& vp, adoublev& ip)
{
    vp[0] = z1[4];
    vp[1] = z1[5];
    vp[2] = z1[6];
    vp[3] = z1[7];
    ip[0] = z1[0] + dy1[0];
    ip[1] = z1[1] + dy1[1];
    ip[2] = z1[2] + dy1[2];
    ip[3] = z1[3] + dy1[0];
}
```